A Versatile Electrochemical Protocol for the Synthesis of Transition Metal Complexes

Michael Richard Chapman

Submitted in accordance with the requirements for the degree of

Doctor of Philosophy

The University of Leeds

School of Chemistry

October 2016

The candidate confirms that the work submitted is his/her own, except where work which has formed part of jointly-authored publications has been included. The contribution of the candidate and the other authors to this work has been explicitly indicated below. The candidate confirms that appropriate credit has been given within the thesis where reference has been made to the work of others.

References for jointly-authored publications:

1. M. R. Chapman, Y. M Shafi, N. Kapur, B. N. Nguyen[*], C. E. Willans[*], 'Electrochemical flow-reactor for expedient synthesis of copper-*N*-heterocyclic carbene complexes', *Chem. Commun.* **2015**, *51*, 1282-1284.

The work reported within this publication is presented in Chapter 2 of this thesis. Reactor design and construction were performed by Dr Bao Nguyen, Dr Charlotte Willans, Prof Nikil Kapur and the candidate, with preliminary optimisation studies conducted by Mr Yarseen Shafi. All other work was performed by the candidate.

2. M. R. Chapman, S. E. Henkelis, N. Kapur, B. N. Nguyen[*], C. E. Willans[*], 'A straightforward electrochemical approach to imine- and amine-bisphenolate metal complexes with facile control over metal oxidation state', *ChemistryOpen* **2016**, *5*, 351-356.

The research described within this publication is presented in Chapter 4 of this thesis. Eight compounds were prepared by Ms Susan Henkelis. Dr Bao Nguyen, Dr Charlotte Willans and Prof Nikil Kapur were primary investigators. All other work was performed by the candidate.

3. M. R. Chapman, B. R. M. Lake, C. M. Pask, B. N. Nguyen, C. E. Willans[*], 'Solid-state structure, solution-state behaviour and catalytic activity of electronically divergent C,N-chelating palladium-*N*-heterocyclic carbene complexes', *Dalton Trans.* **2015**, *44*, 15938-15948.

The work reported within this publication is presented in Chapter 5 of this thesis. Underlying findings, including the preparation of one compound, were conducted by Dr Benjamin Lake. Assistance with X-ray crystallographic analysis was provided by Dr Christopher Pask. Dr Bao Nguyen and Dr Charlotte Willans were primary investigators. All other work was performed by the candidate.

4. M. R. Chapman, C. M. Pask, A. Ariafard[*], C. E. Willans[*], 'σ-Alkenyl *endo*-palladacycle formation *via* regiospecific functionalisation of an unreactive NHC-tethered $C(sp^2)$-H bond', *Chem. Commun.* **2015**, *51*, 5513-5515.

The research described within this publication is presented in Chapter 6 of this thesis. Assistance with X-ray crystallographic analysis was provided by Dr Christopher Pask. Theoretical calculations were conducted by Dr Alireza Ariafard. Dr Charlotte Willans was the primary investigator. All other work was performed by the candidate.

Abstract

This thesis concerns the application of a versatile electrochemical procedure to prepare organometallic compounds. Primarily, the method is employed to produce various transition metal complexes of *N*-heterocyclic carbenes (NHCs) from the electrochemical reduction of azolium salts. Importantly, the method generates hydrogen gas as the only side-product and takes place under mild and ambient conditions. The research focuses on the translation of this methodology into a continuous-flow protocol, improving the efficiency and widening the applications associated with the procedure. Using novel reaction engineering, the design and construction of a versatile and modular copper-plate reactor is presented which is capable of producing pure copper(I)-NHCs in flow.

It was found that the method could be extended towards several iron(II)-NHC complexes, through dissolution of a metallic iron electrode. Under these conditions, a family of *N*-pyridyl substituted imidazolium salts were electrochemically reduced and coordinated to iron, producing a variety of octahedral, low-spin iron(II)-NHCs in high yield. By adjusting the electronic properties of the ligand, an ammonia-bound iron(II)-NHC adduct was observed for the first time. Through tuning ligand denticity, the first example of a dinuclear iron(II)-NHC helicate complex was also prepared.

A wide array of Schiff base metal complexes have also been prepared using the same synthetic methodology. Performing an overall two-electron reduction of salen ligand precursors in the presence of metallic copper, nickel or zinc leads directly to their metal(II)-salen products in good yield. Synthetic practicality was demonstrated by the use of hydrous and aerobic reaction conditions, coupled with a straightforward isolation procedure. By modification of reaction conditions, further versatility was showcased in the selective synthesis of either iron(II)- or iron(III)-salen products from an iron(0) metal source. Using a bimetallic anodic alloy comprised of elemental manganese and nickel, selective liberation of Mn^{2+} ions was achieved to exclusively afford a number of manganese(II)- and manganese(IV)-salen complexes.

A family of novel palladium(II)-NHC complexes bearing electronically diverse *N*-pyridyl wingtip substituents are described. A combination of spectroscopic and crystallographic analyses have been used to affiliate dynamic solution-state behaviour with the solid-state structure of these compounds, with a view to design robust catalysts for challenging C-C bond forming reactions.

Amongst the scope of palladium(II)-NHC complexes explored, an unusual example of non-innocent ligand behaviour was observed for one electronically unique example. Modifying reaction conditions, this behaviour could be accentuated to selectively yield a σ-alkenyl palladacyclic product, which was investigated using a combined experimental and theoretical approach.

Table of Contents

Chapter 1:

Introduction

Chapter 2:

Design, construction and optimisation of an electrochemical flow-reactor for expedient synthesis of copper(I) N-heterocyclic carbene complexes

Chapter 3:

Exploitation of a synthetically clean electrochemical route to iron(II) N-heterocyclic carbene complexes

Chapter 4:

A synthetically versatile electrochemical approach towards imine- and amine-bis(phenolate) base metal complexes

Chapter 5:

Relating solid-state structure, solution-state behaviour and catalytic activity of C,N-chelating palladium(II) N-heterocyclic carbene complexes

Chapter 6:

Experimental and theoretical approach to rationalise a rare cyclometalation at palladium

List of Figures

Chapter 6:

Chapter 6:

List of Abbreviations

Å	Angstrom, 1.0×10^{-10} metres
Ar*H*	Protons attached to an aromatic ring
ax	Axial
br	Broad
Br^-	Bromide
C_{A0}	Initial concentration of A
$^{13}C\{^{1}H\}$	Proton-decoupled carbon (NMR)
˚C	Degrees Celcius
Δ	Chemical shift
COSY	Correlation spectroscopy
CSTR	Continuous stirred-tank reactor
DCM	Dichloromethane
Deg	Degrees
d	Doublet resonance (NMR)
dept	Distortionless enhancement by polarisation transfer
DFT	Density functional theory
DMF	*N,N'*-Dimethyl formamide
DMSO	Dimethyl sulfoxide
e.g.	*Exempli gratia* (for the sake of example)
eq	Equatorial
ESI	Electrospray ionisation
e.s.d	Estimated standard deviation
et al.	*et alia* (and others)
fac	Facial
Fc	Ferrocene
G	Gibbs free energy
H	Height
HCl	Hydrochloric acid
HOMO	Highest occupied molecular orbital
HRMS	High resolution mass spectrometry
I	Current
i.e.	*id est* (that is)
im*H*	Protons attached to C4 or C5 carbon atoms of an imidazole ring
IR	Infrared
Hz	Hertz
J	Coupling constant (NMR)

K	Kelvin
kcal	Kilocalorie
L	Ligand
LUMO	Lowest unoccupied molecular orbital
NHC	*N*-Heterocyclic carbene
NMR	Nuclear magnetic resonance
m	Multiplet resonance (NMR)
m/z	Mass to charge ratio
mA	Milliamperes
mer	Meridional
mes*H*	Protons attached to a mesityl ring
MHz	Megahertz
MS	Mass spectrometry
m/z	Mass-to-charge ratio
P	Primitive
PFR	Plug-flow reactor
PF_6^-	Hexafluorophosphate
pm	Picometres, 1.0×10^{-12} metres
ppm	Parts per million
py*H*	Protons attached to a pyridyl ring
Q_c	Consumed coulombic charge
Q_e	Delivered coulombic charge
rt	Room temperature
s	Singlet resonance (NMR)
sept	Septet resonance (NMR)
t	Triplet resonance (NMR)
τ	Residence time/space time
THF	Tetrahydrofuran
U	Feed velocity
v_o	Volumetric flow-rate
V	Voltage
VT	Variable temperature
W	Width

Compounds are labelled throughout this thesis as follows: **IX.X** = imidazole, **PX.X** = precursor, **MX.X** = monomer form, **AX.X** = ammonia-bound.

Chapter 1

Introduction

1.1 Overview

The work presented in this thesis details a versatile electrochemical route to transition metal *N*-heterocyclic carbenes (NHCs). The methodology provides atom-efficient access to a broad variety of organometallic products, eliminating hydrogen gas as the only stoichiometric side-product. Working directly at the interface between chemistry and engineering has allowed translation of the method into the only known continuous-flow electrochemical protocol for the synthesis of organometallic compounds to date. This chapter will introduce the reader to the chemistry of transition metal-NHCs, outline the core principles of their syntheses and describe their development based on current, topical literature. It will aim to place the relevance of the work into context and express the significance of the research within the field of synthetic organometallic chemistry.

1.2 Organometallic chemistry

The field of organometallic chemistry combines aspects of traditional inorganic and organic chemistry, in the study of compounds containing at least one bond between a carbon atom and a metal. Undoubtedly longstanding, the field arguably emerged in 1760 where Louis Claude Cadet de Gassicourt reported on the extraction of cacodyl (tetramethyldiarsine) from cobalt minerals, whilst investigating their application as inks and dyes.[1]

The following two hundred years saw numerous landmark discoveries in the field, with William Ziese uncovering the first platinum-ethylene complex,[2] Edward Frankland synthesising dimethyl zinc[3,4] and Victor Grignard preparing various reactive organomagnesium compounds.[5] Alongside Grignard, the Nobel committee have recognised organometallic chemistry as a distinct subfield for which the Nobel prize in Chemistry has also been awarded to Ernst Fischer and Geoffrey Wilkinson for their pioneering work on metallocenes,[6] and more recently shared between Robert Grubbs, Yves Chauvin and Richard Schrock for their revolutionary development of metal-catalysed alkene metathesis reactions.[7] True to the latter, is perhaps the most distinguished example of a transition metal-NHC complex, for which the unique properties of the carbenic ligand are essential to the reactivity of the organometallic catalyst (**Figure 1.1**).
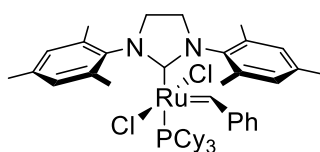
Figure 1.1 Archetypal ruthenium-NHC complex, prepared by Grubbs and co-workers.[7]

1.3   Carbenes

Introduced by Hine and Doering into organic chemistry in 1954, and by Fischer into the organometallic domain ten years later, carbenes originated as intriguing chemical phenomena which have played important roles as both ephemeral intermediates and well-defined compounds over the last six decades.[8,9]

A carbene is a neutral compound housing a divalent carbon atom with only six valence electrons; the carbene centre itself is able to adopt either a linear or bent geometry which may be described by a particular degree of hybridisation.[10] A carbene possessing a linear geometry implies an sp-hybridised carbon centre with triplet state multiplicity, where two non-bonding electrons occupy two independent, degenerate p-orbitals (p_x and p_y), (**Figure 1.2**, **A**). However, bending the motif removes such degeneracy and instead the carbene adopts an sp^2-type hybridisation, which is able to exist as either a spin-paired singlet (**B**), spin-unpaired triplet (**C**) or spin-unpaired singlet state (**D**).

Further, a bent geometry renders the p_y orbital effectively unchanged and is commonly coined p_π, whilst the orbital which originates as pure p_x is stabilised through acquisition of some s-character and is typically termed σ. Indeed, carbenes naturally adopt a bent configuration where linear geometry is an extreme case, therefore their frontier orbitals are systematically referred to as p_π and σ.[11]
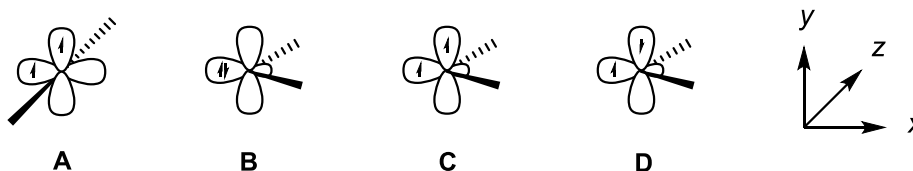
Figure 1.2 Representative singlet and triplet carbene electronic structures.

The ground state spin multiplicity of bent carbenes is a fundamental feature which governs their reactivity.[12] Singlet carbenes maintain a filled and a vacant p-orbital for which they may be viewed to have ambiphilic character, whilst triplet carbenes comprise two singly occupied p-orbitals and can be described as diradicals. The true reactivity is strongly dependent upon the nature of the two α-substituents adjacent to the carbenic centre, with inductive and mesomeric effects regulating the magnitude of the energy gap between p_π and σ for both ground states. The singlet ground state is favoured by a large p_π − σ separation, whereas existence of a triplet ground state requires a small p_π − σ energy gap (in fact, Hoffmann and co-workers have calculated a minimum energy value of 2.0 eV is essential to induce a singlet ground state, where any value below 1.5 eV exclusively results in formation of a triplet ground state).[13]

1.3.1 Electronic effects

The electronegativity of groups adjacent to the carbenic centre are known to influence the multiplicity of the ground state through inductive effects.[14,15] Exemplifying this, Harrison and colleagues have shown that it is possible to flip the carbene ground state from a triplet to a singlet by sequentially modifying the substituents from electropositive lithium, to 'standard' hydrogen and finally to electronegative fluorine, as shown in **Figure 1.3**.[16]
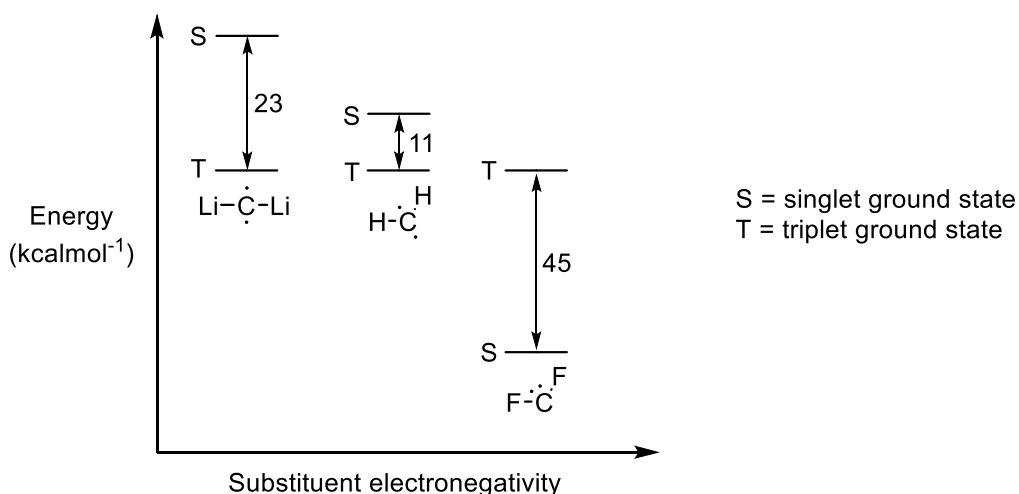
***Figure 1.3** Influence of substituent electronegativity on ground state spin multiplicity.[16]*

Since this report, it has been confirmed that σ-electron withdrawing groups α to the carbene favour the singlet state by stabilising the filled non-bonding σ-orbital, expanding the $p_\pi - \sigma$ energy gap. Similarly, π-donor groups (for example, -F, -Cl, -Br, -I, -NR$_2$, -PR$_2$) are also able to promote formation of the singlet carbene by destabilising the p_π orbital which also increases the $p_\pi - \sigma$ energy difference (**Figure 1.4**, **a**). Conversely, π-withdrawing α-substituents (such as -COR, -CN, -CF$_3$, -BR$_2$, -PR$_3^+$) are able to reduce the energy of the p_π orbital, minimising the $p_\pi - \sigma$ energy separation which promotes formation of the triplet carbene. It is also possible for σ-donating moieties to destabilise the σ-orbital, raising its energy closer to that of p_π to lessen the energy barrier (**b**).

(a) Singlet multiplicity   **(b)** Triplet multiplicity
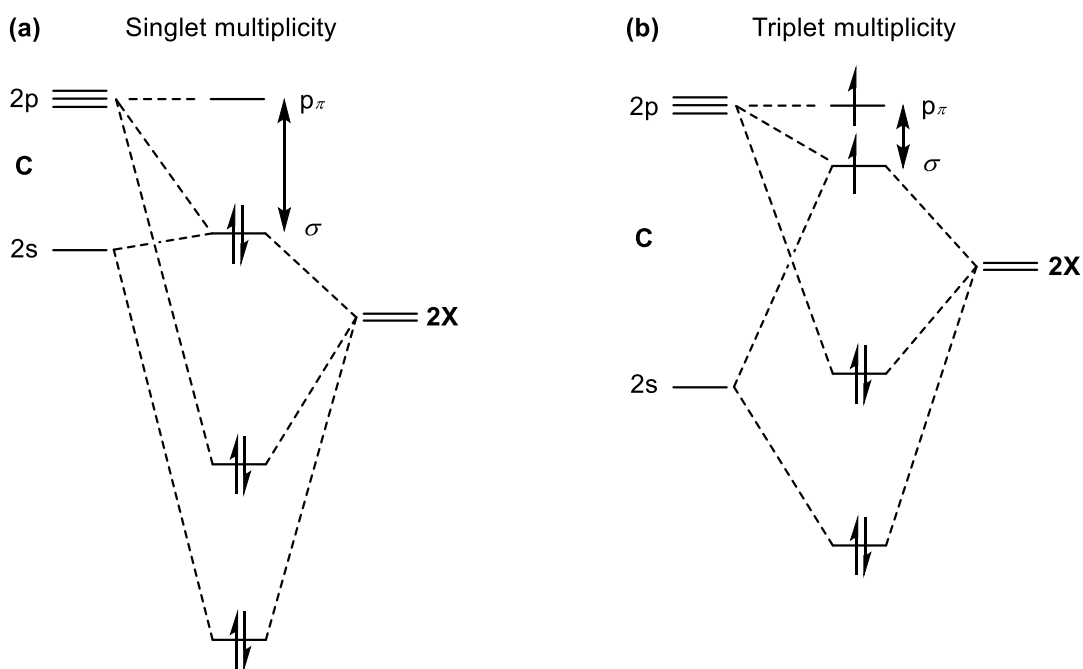
Figure 1.4 *Orbital energy level diagram illustrating: (**a**) a large $p_\pi - \sigma$ energy gap favours a spin-paired σ-orbital to afford a singlet state, (**b**) a small $p_\pi - \sigma$ energy gap allows promotion of one electron to p_π to deliver a spin-unpaired triplet state (X = α-substituent).*

Due to the intrinsic high energy of the p_π spin-unpaired electron involved in a triplet state electronic structure, it is often less problematic to access a substitution pattern which stabilises a singlet carbene. In fact, early work conducted by Pauling suggests that ideal substituents which stabilise a singlet carbene should aim to protect electroneutrality of the carbenic centre.[17] Oversimplifying this model, three methods can be identified to accomplish an ideally stabilised singlet state carbene (**Figure 1.5**).

a) Two neighbouring π-donor/σ-withdrawing α-substituents, generating a push-push mesomeric/pull-pull inductive pattern (as observed for diaminocarbenes).

b) Two neighbouring σ-donor α-substituents, forming a pull-pull mesomeric/push-push inductive pattern (such as diborylcarbenes).

c) One π-donor and one π-acceptor α-substituent, creating a push-pull mesomeric pattern (akin to phosphinophosphoniocarbenes and phosphinosilylcarbenes).

(a) Diaminocarbene   **(b) Diborylcarbene**   **(c) Phosphinosilylcarbene**
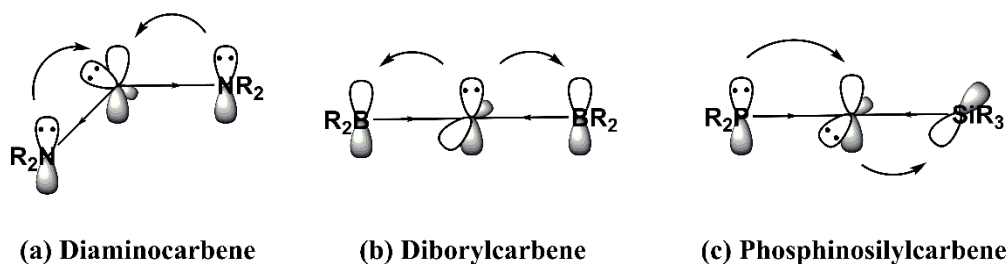
Figure 1.5 *Ideal singlet state substituent patterns, as outlined by Pauling.*

1.3.2 Steric effects

In cases where electronic effects are remote, steric factors are able to govern the ground state spin multiplicity of a carbene. Instances where the parent carbene bond angle resides below 90° (for example, cyclopropylidene = 60°)[18] allow the energy of the singlet imidazolylidene to drop below that of the triplet state.[17] However, by positioning sterically bulky substituents adjacent to the carbenic centre, the motif is forced to adopt a more linear configuration (*i.e.* carbene bond angle > 90°) which inherently stabilises a triplet over the corresponding singlet state. As a result, the use of large substituents to exploit the stabilisation of linear carbenes remains the only known method of isolating triplet carbenes on account of their high reactivity (**Figure 1.6**).[11]

Figure 1.6 Exemplar bulky substituents to give rise to kinetically stable triplet carbenes.[11]

1.4 *N*-Heterocyclic carbenes

Heteroatom donor groups attached to a carbene centre render the originally degenerate orbitals unequal in energy, amplifying the nucleophilicity of the carbon atom and strengthening its thermodynamic stability. As mentioned above, the singlet-triplet state splitting is dependent upon the electronegativities of the π-donor substituents X and Y in carbenes of the type :CXY. Though a scope of heteroatoms are available (*e.g.* O, S, P, N), only singlet carbenes containing two nitrogen donor atoms have been isolated as crystalline solids.[19] As preparative chemistry is heavily reliant upon kinetic stability, *N*-heterocyclic carbenes have been developed as a solution to many intrinsic problems associated with isolating stable free carbenes.

N-Heterocyclic carbenes (NHCs) are mono-, di- or triaminocarbenes which hold a bent geometry (typical NCN bond angle between 100 - 110°),[11] housing an sp^2-hybridised carbenic centre and exclusively exist with singlet state multiplicity.[20] The nitrogen atoms adjacent to the carbene are relatively electronegative, allowing electron density to be removed from the carbene to stabilise a non-bonding lone pair (σ). Simultaneously, the nitrogen groups are able to supply electron density from their sp^2-hybridised lone pairs into an empty carbenic p-orbital, destabilising p_π to overall assist formation of the singlet state (**Figure 1.7**).

Donation to p_π

Withdrawal from σ
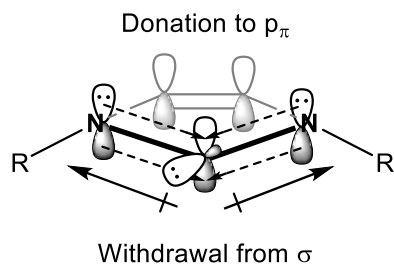
Figure 1.7 Representative N-heterocyclic carbene frontier orbital diagram.

Furthermore, NHCs comprise a cyclic 6π electronic system which obeys Hückel's rules, providing aromatic character to supplement their stability. However, according to Frenking and Boehme, the aromaticity of NHCs is not as pronounced as should be expected, and is therefore not the main contributor to their stability.[21] Nevertheless, Heinemann and co-workers have performed *ab initio* calculations which suggest *ca.* 113 kcalmol^{-1} thermodynamic stabilisation energy difference between an acyclic, non-conjugated methylene unit and an NHC group (**Figure 1.8**).

Transient
methylene carbene

- 87 kcalmol^{-1}

Acyclic
diaminocarbene

- 6 kcalmol^{-1}

Cyclic
diaminocarbene

- 20 kcalmol^{-1}

N-heterocyclic carbene
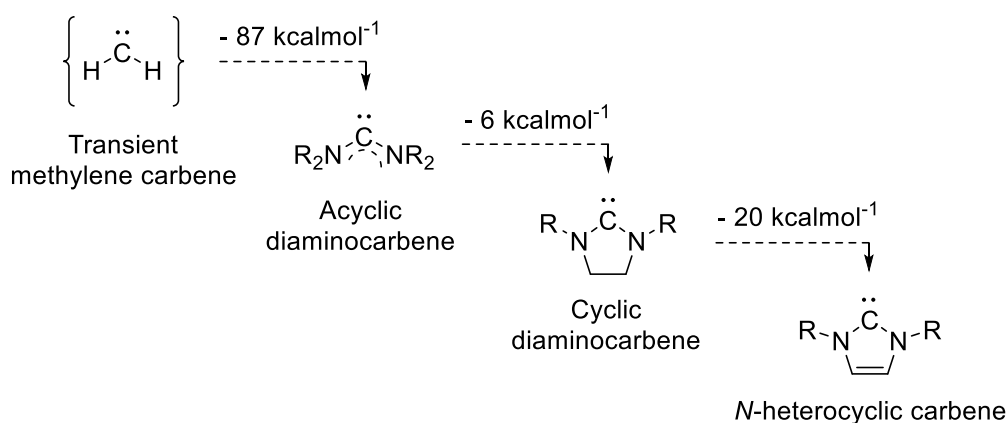
Figure 1.8 Downhill energy pathway from methylenic to N-heterocyclic carbene.

1.5 Metal-carbene bonding

Carbenes complexed with metals are often divided into two distinct groups: Fischer-type and Schrock-type carbenes. This classification is based upon the nature of the interaction between the metal and carbon atom (*i.e.* the M-C bond).

Fischer-type carbenes are generally found on low oxidation state, electron-rich metal complexes (for example, zero-valent iron, molybdenum or chromium)[22] containing electrophilic, π-acceptor ligands. The chemical bonding within this model is based upon σ-type electron donation of the filled lone pair orbital of the carbene to an empty metal d-orbital, with concomitant π-backbonding of a filled metal d-orbital to an empty p-orbital on carbon (see **Figure 1.9** for an illustration of Fischer-type carbene orbital interactions).
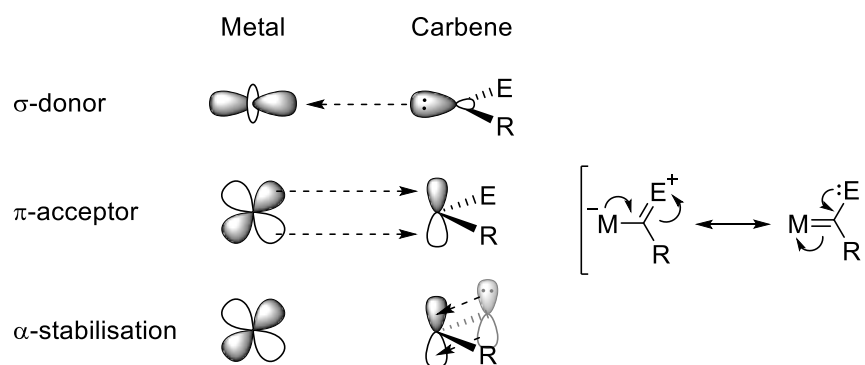
Figure 1.9 Orbital diagram to represent bonding interactions within Fischer-type metal-carbene complexes and their associated resonance structures.

In comparison, Schrock-type carbenes are generally found coordinated to higher oxidation state metals (for example, titanium(IV) or tantalum(V)),[23] and do not possess an α-heteroatom to stabilise their carbocationic character. Carbenes of this type polarise π-electron density towards carbon, generating a nucleophilic carbenic centre (see **Figure 1.10** for an illustration of Schrock-type carbene orbital interactions).
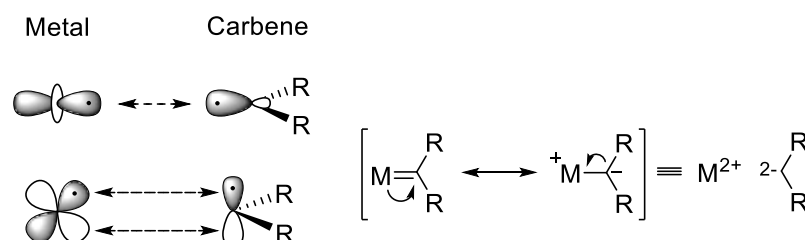
Figure 1.10 Orbital diagram to represent bonding interactions within Schrock-type metal-carbene complexes and their associated resonance structures.

Unlike Fischer and Schrock carbenes, *N*-heterocyclic carbenes are relatively stable and may be assembled in the absence of a metal coordination sphere. In terms of electronic structure, metal-NHC bonding is most comparable to that of Fischer-type carbene complexes, albeit energetically unequal.[23] Each α-substituent of an NHC possesses a lone-pair of electrons, which act to provide a positive mesomeric effect through donation of π-electron density toward each empty p_π-orbital of the carbenic centre. In doing so, the energy of p_π (*i.e.* LUMO) is increased beyond that of each metal d-orbital, decreasing the π-backbonding capability from M → C.[20] The overall result is a metal-carbene bonding interaction largely composed of σ-donation (*i.e.* C → M dominates the electronic structure, see **Figure 1.11**). It is possible however, to reorganise the HOMO-LUMO energy difference and improve π-backbonding within metal-NHCs. For example, Hor and Young have shown that annulation of pyrimidine to the backbone of a 5-membered NHC markedly increases their π-acceptor capability, whilst Whittlesey and colleagues have developed a series of carbonyl substituted, ring-expanded diamidocarbenes which serve the same purpose.[24–26]
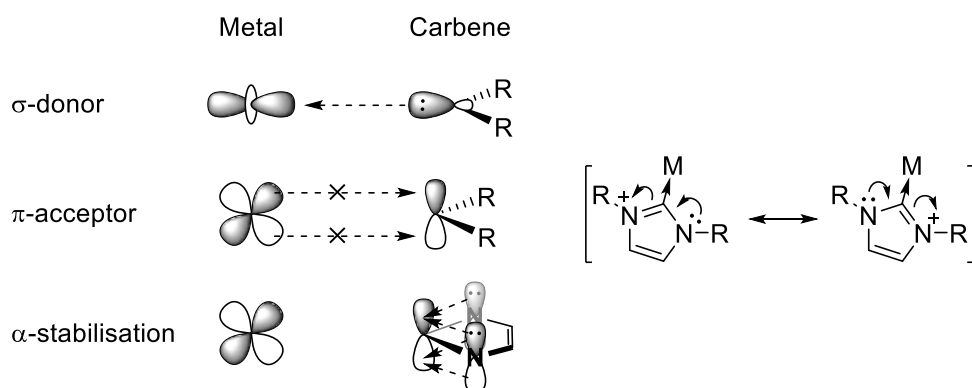
Figure 1.11 Orbital diagram to represent bonding interactions within metal-NHC complexes and their associated resonance structures.

The strong nucleophilicity of NHC ligands often leads to their comparison with tertiary phosphines.[27] A primary difference between these ligands derives from the electronic structures displayed in **Figure 1.11**, insofar as NHCs display poor π-backbonding to generally produce stronger σ-bound metal complexes than those of phosphines. The upshot of such strong donation is increased electron density at the metal centre, often generating complexes with improved thermal stability and higher reactivity than their phosphine counterparts.[28]

1.6   Synthetic strategies to metal-NHC complexes

Since Arduengo and co-workers reported on the isolation of the first stable free NHC (1,3-*bis*(1-adamantyl)imidazol-2-ylidene), academic interest in the synthesis and reactivity of transition metal-NHC complexes has grown exponentially.[29] Undoubtedly, Arduengo's discovery was built upon the foundations established by Öfele and Wanzlick, who independently described the synthesis of the first transition metal-NHC complexes over four decades ago.[30,31]

Commensurate with the growing interest, are the number of reports on synthetic routes to access these compounds. However, the development of new methodology has been and remains vital. The following discussion aims to guide the reader through current synthetic strategies to metal-NHC complexes, deconstructing their mode of action whilst considering potential drawbacks in the context of preparative chemistry.

1.6.1   *N*-Heterocyclic carbene precursors

Without question, azolium salts represent the most frequently employed class of NHC ligand precursor. From a retrosynthetic standpoint, azolium ions offer a convenient path to transition metal-NHC complexes, through direct coordination of a metal to the heterocyclic ring scaffold. In order to do so, a relatively acidic 'C2-proton' of the salt must first be removed – usually through direct interaction with an appropriate source of base (see **Figure 1.12** for common azolium

cations, and their respective aqueous pK_a values as recorded by Amyes and Diver).[32] Due to their versatile synthetic utility, intensive research has been focused on efficient methods to construct azolium salts, shaping the subject of a recent review article by César and Lavigne.[33]

| 23.8 | 23.0 | 21.6 | 19.5 |
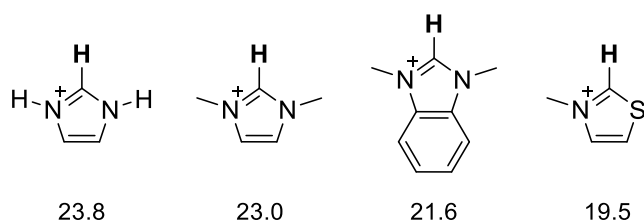
Figure 1.12 *Carbon acid pK_a values (recorded in water) of common azolium cations. Each acidic 'C2-proton' is represented by bold text.[32]*

Surprisingly, the symmetric synthesis of *N*-substituted imidazolium salts was first reported by Wallach in 1925, which logically assembles the heterocyclic scaffold through a one-pot condensation of glyoxal, formaldehyde and two equivalents of primary amine (**Scheme 1.1**).[34]
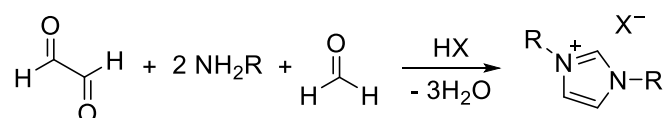
Scheme 1.1 *Wallach's original route to symmetrical imidazolium salts.[34]*

Provided that the desired primary amine is available, Wallach's synthetic route remains the most commonly employed method of forming symmetrical imidazolium ions to date. For instances where an unsymmetrical analogue is required, a modified two-step procedure is often employed *via* alkylation of an imidazole intermediate (**Scheme 1.2**).[35,36]
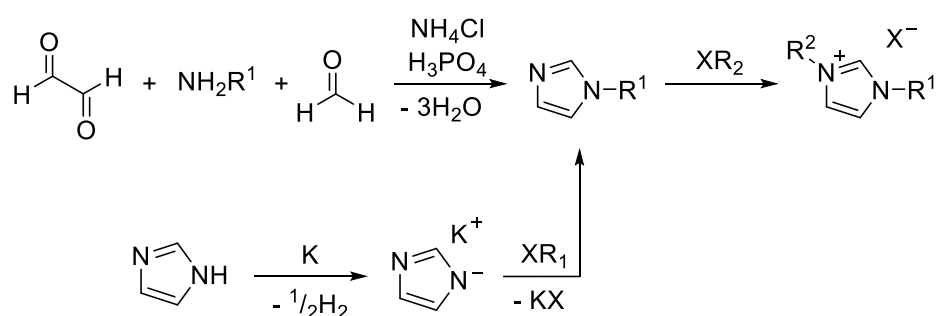
Scheme 1.2 *Complementary routes to unsymmetrical imidazolium salts.[35,36]*

1.6.2 Interaction of a free NHC with a metal precursor

Perhaps the most widely adopted method of preparing transition metal-NHC complexes is by way of their corresponding free NHC, itself generated through reaction of an azolium salt with a strong base (*e.g.* NaH or ^{n}BuLi).[27] Once formed, the highly reactive free carbene may be isolated, characterised and added to an appropriate metal source to furnish a metal-NHC complex.

Given in **Scheme 1.3** is an example of this technique described by Nolan and Bantreil, in the synthesis of a ruthenium-NHC complex.[37] Following deprotonation of IMesH.Cl (IMes = 1,3-*bis*-(2,4,6-trimethylphenyl)imidazol-2-ylidene) with a slight excess of base, the corresponding free NHC is obtained in 81 % yield. Subsequent treatment of Grubbs' first-generation catalyst with the free NHC leads to phosphine displacement, affording the desired ruthenium-NHC complex in 77 % isolated yield. Notably, the authors record the total time to synthesise the free NHC as 56 hours, followed by an additional 4 hours incorporation time to produce the organometallic product.
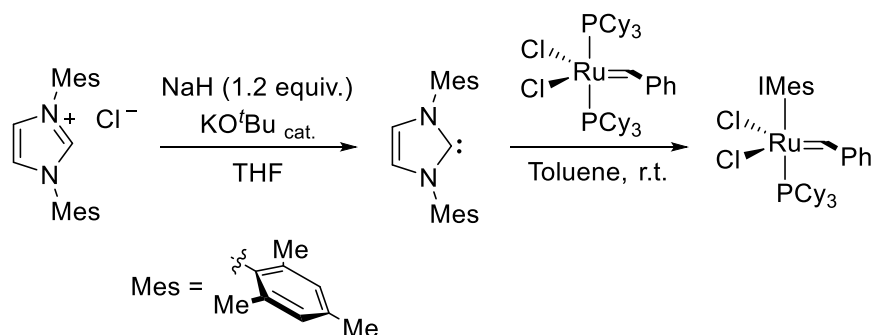
***Scheme 1.3** Phosphine-displacement route to ruthenium-NHC complex, described by Nolan.[37]*

Nucleophilic NHCs have also been shown to cleave a range of dimeric metal complexes containing bridging ligands, such as halides, carbon monoxide or acetonitrile. For example, Herrmann and Köcher have described the reaction of $[(\eta^2,\eta^2\text{-COD})MCl]_2$ or $[Cp^*MCl_2]_2$ (where M = Ir, Rh) with one or two equivalents of free NHC to produce a range of mononuclear metal-NHC complexes.[38,39] The authors employ 1,3-dimethylimidazol-2-ylidene as a sterically unencumbered and reactive free ligand, to split a series of coordinatively diverse dinuclear metal precursors in forming various metal-NHC complexes in high yield – with each unambiguously characterised through single-crystal X-ray diffraction (SCXRD) methods (a summary is supplied in **Scheme 1.4**). The same authors (amongst others)[40] have also demonstrated that dimer cleavage and NHC incorporation also occurs with $[(\eta^6\text{-cymene})RuCl_2]_2$ and $[Os(CO)_3Cl_2]_2$,[38,39] with Nolan *et al.* using this approach to break even higher order nuclear clusters such as $[Cp^*RuCl]_4$ to afford $Cp^*Ru(NHC)Cl$-type complexes.[41]
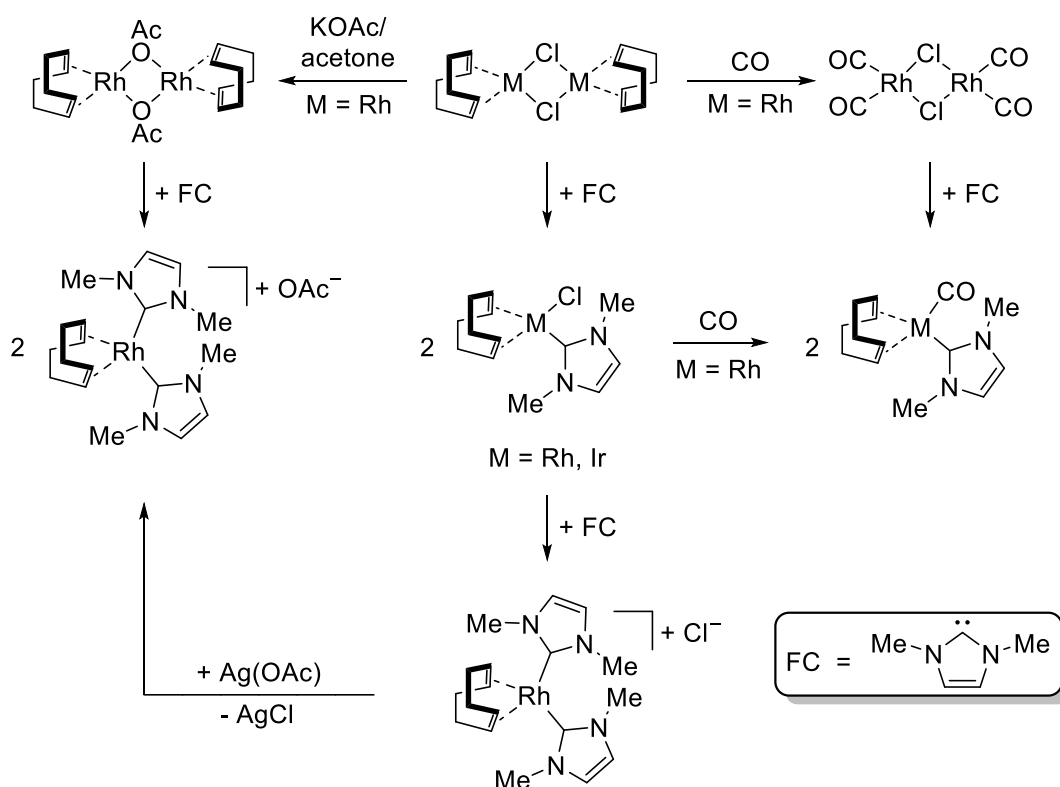
Scheme 1.4 Herrmann's rhodium(I) and iridium(I)-NHC synthesis via dimeric metal precursors.[38]

Though widely adopted, the use of free carbenes in organometallic synthesis is undoubtedly challenging. In particular, free NHCs are renowned for their reactivity toward traces of moisture, with the resulting hydrolysed products highly dependent upon the ratio of NHC to water present within the reaction mixture, according to a detailed study by Mourgas and Gudat.[42] Typically, reprotonation of the C2 carbon atom is to be expected, replenishing the original imidazolium cation with a hydroxide counteranion. However, Denk and colleagues have also shown that a binary mixture of NHC/water causes rapid hydrolysis of a free NHC to produce a ring-opened formamide product in high yield.[43]

Nevertheless, the interaction of a metal precursor with a pre-formed free NHC is currently one of the most popular methods of forming a transition metal-NHC complex. Generally, there is little requirement on the metal centre with respect to coordination environment or oxidation state to allow its reaction with a free NHC to occur.[44] However, base-sensitive groups are not well-tolerated with this method, which restricts the level of functionality to be incorporated within the ligand template. Moreover, select examples of free NHCs have been seen to undergo rearrangement reactions involving the deprotonated C2 carbon atom of the heterocyclic ring. An example of this was published by Kawaguchi and co-workers, who found that allowing a solution of a *bis*(phenoxide)-substituted NHC to reach room temperature led to an unusual 1,2-benzyl migration reaction, effectively quenching the free carbene to afford a C2-functionalised

imidazole.[45] For these reasons, deprotonation of an azolium ion is typically followed by metalation *in situ*, without isolating or even observing the carbenic intermediate.

1.6.3 *In situ* deprotonation and metalation

To avoid isolating and handling a reactive free carbene, a transition metal-NHC complex may be prepared through *in situ* deprotonation and subsequent metalation of an azolium salt. A key advantage of this approach is the inclusion of relatively weak bases to perform the deprotonation step (*e.g.* NEt_3 or K_2CO_3), with all reagents combined in a single pot. Once formed, the free NHC is trapped by interaction with a suitable metal source to produce the desired complex, which may be isolated and purified by straightforward recrystallisation steps.

However, in certain cases the addition of external base may give rise to different products compared to the use of metal salts with basic anions. For example, Teles and Enders found that employment of potassium *tert*-butoxide with an imidazolium perchlorate and one equivalent of palladium(II) acetate in the presence of sodium iodide forms a dimeric palladium(II) *mono*-NHC complex (shown in **Scheme 1.5**).[46] Nonetheless, singly ligated, dinuclear complexes of this type are valuable precursors to the introduction of other ligands through dimer cleavage (*e.g.* phosphines or other NHC groups).[47,48]
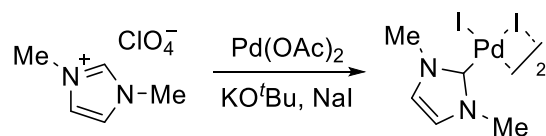
***Scheme 1.5** One-pot preparation of dimeric palladium(II)-NHC.[46]*

Along similar lines, Herrmann and Spiegler have also used lithium *tert*-butoxide as an *in situ* deprotonation agent with imidazolium salts, in the presence of $[(\eta^2,\eta^2\text{-COD})RhCl]_2$ in THF solvent at room temperature.[47] The resulting rhodium(I)-NHC complexes were analogous to those obtained through reaction with much stronger bases, such as NaH. This being said, Fehlhammer and co-workers have added strong bases such as *n*-butyl lithium to a mixture of 1,1'-methylene-3,3'-dimethylimidazolium iodide in the presence of suspended palladium(II) iodide, successfully producing the corresponding $Pd(NHC)_4I_2$ complex, albeit in poor yield (12 %, which may be improved by deprotonation with acetate anions – see below).[49]

In 1997, Lin and co-workers devised an elegant route to gold(I)-NHC complexes containing long alkyl chain *N*-substituents (up to C_{16}), which falls within the bracket of *in situ* deprotonation.[50] By employing Bu_4NBr as phase-transfer catalyst, the authors were able to generate gold(I)-NHC complexes with a diluted, aqueous solution of sodium hydroxide as source of base, in the presence of a DCM biphase containing $(Me_2S)AuCl$ (the molecular structure of Lin's gold(I) complex is

provided in **Figure 1.13**). Not only does this example represent a novel synthetic route to transition metal-NHC complexes through phase-transfer catalysis, but also showcases the ability for a weak base such as sodium hydroxide (pK_a *ca.* 14)[51] to deprotonate a benzimidazolium salt (pK_a *ca.* 22)[52,53] when in the presence of a suitable metal source.
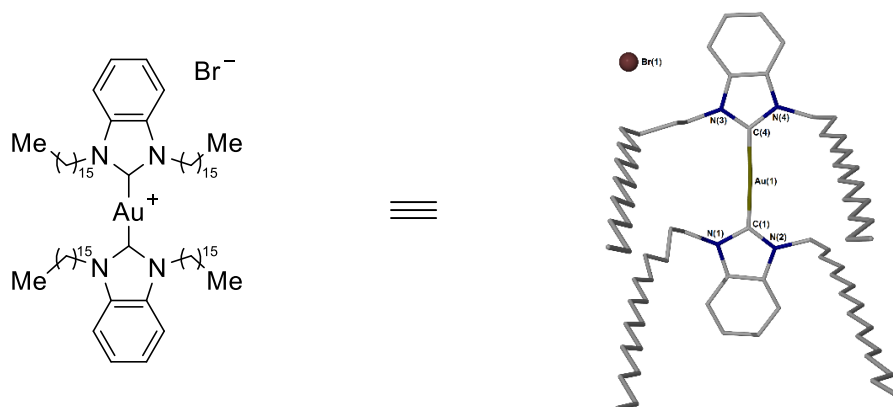
Figure 1.13 Left: Lin's gold(I) bis-NHC complex, prepared through NaOH deprotonation and phase-transfer catalysed Au metalation. Right: the molecular structure of Lin's gold(I) complex, represented as a stick-diagram for clarity.[50]

In a more recent example by Slawin and Cazin, a variety of copper(I)-NHC complexes comprising sterically bulky *N*-substituents were prepared by treatment of an imidazolium halide with copper(I) chloride, in the presence of two equivalents of potassium *tert*-butoxide (**Scheme 1.6**).[54] Under these reaction conditions, good to high yields were achieved (50 - 90 %) of the desired copper(I)-NHC complexes under relatively mild conditions (60 ˚C, 24 hours reaction time, 10 examples).
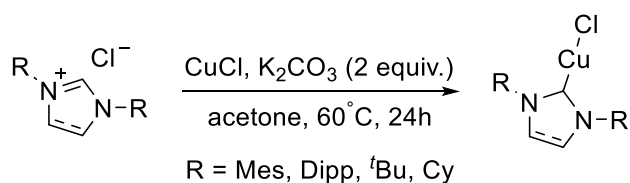
Scheme 1.6 In situ deprotonation/metalation route to copper(I)-NHCs, outlined by Cazin.[54]

Within the correct setting, this methodology provides clean access to a variety of metal-NHC complexes. However, a pitfall becomes evident where strong bases are applied in the presence of sensitive functional groups. For instance, Willans and Lake have reported on the treatment of an allyl tethered imidazolium ion with copper(I) bromide, using potassium *tert*-butoxide as source of base. The authors discovered that a base-catalysed background reaction had taken place, to rearrange the terminal allyl group and provide an inseparable mixture of three copper(I)-NHC isomers.[55] On the other hand, Crabtree and Peris have noted that in some cases the use of mild

bases simply proves ineffective in deprotonating the azolium starting material entirely – presenting a significant problem when incorporating acidic functions into the ligand assembly.[56]

1.6.4 Deprotonation by Brønsted basic anions

Employment of Brønsted basic anions either at the metal precursor or connected to the azolium component offers a convenient means of both generating and metalating a desired ligand in a single step. For this purpose, commercially available metal acetate salts or alkoxides are frequently used as both deprotonation agent and metal source.

In 1968, Wanzlick introduced this concept by reacting mercury(II) acetate with two equivalents of 1,3-*bis*-phenylimidazolium perchlorate, affording the first mercury(II) *bis*-NHC complex, as shown in **Scheme 1.7**.[31] Here, deprotonation of the imidazolium salt occurs *via* the acetate anion, producing a short-lived free NHC which is trapped by coordination to the mercury ion.
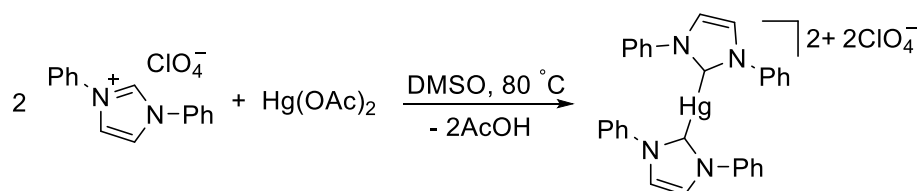
Scheme 1.7 Wanzlick's original route to the first mercury(II) bis-NHC complex.[31]

Over the subsequent three decades, this methodology has proven especially valuable for the synthesis of palladium(II) and nickel(II)-NHC complexes, from their corresponding metal(II) diacetates and imidazolium or triazolium salts. With respect to palladium, examples are known whereby *in situ* deprotonation may even occur under solvent-free conditions, though use of polar solvents are often reported to enhance product yield.[39,57–59]

Herrmann and Schwarz have prepared a variety of palladium and nickel complexes bearing methylene-bridged chelating NHC groups, which at the time were only accessible by this route.[59] In this publication, the authors treat 1,1'-di-*tert*-butyl-3,3'-methylenediimidazolium diiodide with one equivalent of palladium(II) acetate, in DMSO solvent at 50 ˚C (see **Scheme 1.8**). Following the reaction after four hours, the authors were able to trap and crystallographically authenticate palladium(II) *mono*-NHC intermediate **A**, which subsequently continues to form fully chelated analogue **B** after 20 minutes of further heating at 150 ˚C. These observations – particularly through single crystal X-ray analysis – provide key insight into the reaction mechanism. From the molecular structure of intermediate **A**, it is clear to see how *in situ* deprotonation is able to lead to rapid metalation using basic metal precursors, based on proximity alone.
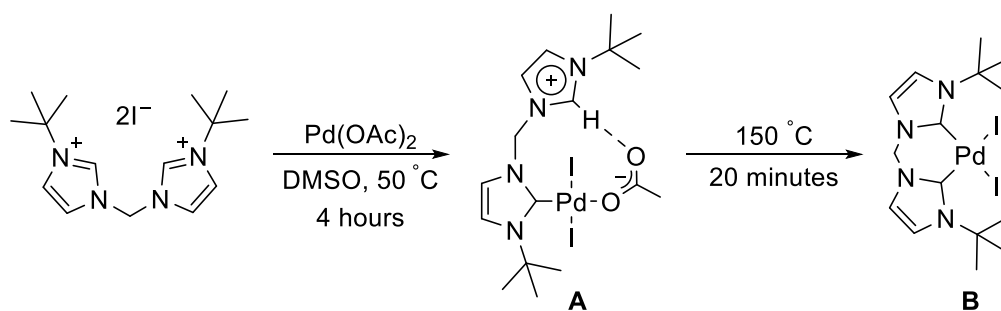
Scheme 1.8 *Herrmann's synthetic route to palladium(II) bis-NHC complexes, via basic metal acetate precursor.[59]*

For rhodium(I) and iridium(I) compounds, μ-alkoxo ligands play the role of basic anion. Employment of μ-alkoxo complexes of (η^2,η^2-COD)-rhodium(I) and iridium(I) (themselves generated *in situ* through reaction of their μ-chloro bridged analogues with sodium alkoxide) with imidazolium salts, affords the corresponding metal-carbene complexes under ambient conditions (as shown in **Scheme 1.9**).[39] The method itself is operationally practical, as an ethanolic slurry of [Rh(η^2,η^2-COD)Cl]$_2$ is simply treated with both sodium ethoxide and azolium salt in a single pot, at room temperature. In this example, the *in situ* forted rhodium (or iridium) ethoxide complex acts as deprotonating agent.[60]
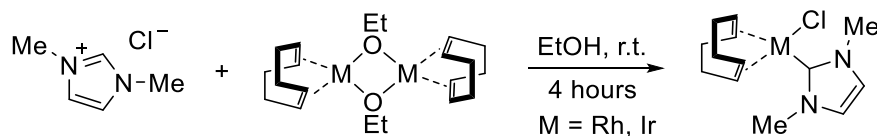
Scheme 1.9 *Synthetic route to Rh(I) and Ir(I)-NHC complexes, pioneered by Köcher.[39]*

Following this protocol, it is also possible to prepare benzimidazolin-2-ylidene complexes of rhodium(I), and equally extend the methodology to triazolium or even tetrazolium salts.[44]

Interestingly, Tilset and Voges have also shown loosely bound η^5-cyclopentadienyl anions to serve as source of base in the deprotonation of imidazolium salts.[61] Treatment of chromocene with 1,3-dimesitylimidazolium chloride in THF solvent affords CpCrCl(1,3-dimesitylimidazol-2-ylidene) as reaction product, which represents a rare example of a CpCr(II) complex containing four unpaired electrons (*i.e.* a 14-electron complex).

Deprotonation and subsequent metalation in this manner offers similar benefits to those described in section **1.6.3** (see above), in terms of synthetic practicality. However, many basic metal precursors are not readily available. By way of just one example, Cu$_2$O and Ag$_2$O are both commercially available and have been shown to react with various azolium ions to produce copper(I) and silver(I)-NHC complexes.[62,63] However, the corresponding basic oxide of their direct group 11 neighbour, 'Au$_2$O', does not exist due to instability, making this route incompatible in producing gold(I)-NHCs.

1.6.5 Transmetalation from silver(I)

Perhaps one of the most widely adopted methods of forming transition metal-NHC complexes is by way of transmetalation of the NHC group from a silver(I)-NHC complex to a suitable metal source. Under these circumstances, the silver(I)-NHC complex is acting as a masked free NHC, from which transmetalation of the organic component is thermodynamically favourable due to (i) the low bond strength of the Ag-$C_{carbene}$ bond, and (ii) the formation of silver(I) halide byproduct. The typically high lattice energy of silver(I) halide formation makes the latter of these most important, and gives rise to a strong driving force for transmetalation to occur.

The first example of a silver(I)-NHC complex was reported by Arduengo *et al.* in 1993.[64] In this communication, the authors react 1,3-*bis*-(2,4,6-trimethylphenyl)imidazol-2-ylidene with half an equivalent of silver(I) triflate to produce the corresponding homoleptic silver(I) *bis*-NHC complex, in 80 % isolated yield.

However, employment of these complexes as carbene-transfer agents did not occur until 1998, where Lin and colleagues accidentally used Ag_2O to deprotonate an imidazolium salt whilst in the presence of a gold(I) precursor, isolating only the corresponding gold(I)-NHC complex.[65,66] The authors noted that significant quantities of silver(I)-NHC were formed exclusively in absence of a gold(I) source, indicating a discrete transmetalation step was indeed involved and not simply deprotonation and metalation of a free NHC (see **Scheme 1.10**).
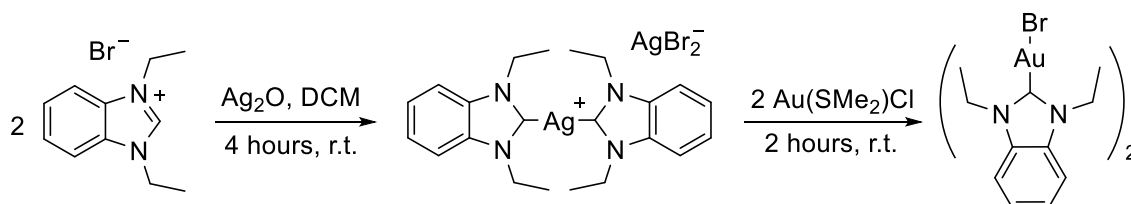
Scheme 1.10 *Formation of a gold(I)-NHC complex via transmetalation from silver(I).*[65]

Following on from Lin's original findings, transmetalation from silver(I) has become a popular method of synthesising various transition metal-NHC complexes. In a comprehensive study, Cramer and Jenkins recently demonstrated the transmetalation of a macrocyclic *tetra*-NHC ligand from a dimeric silver(I) complex to a broad range of metals, including platinum(II), palladium(II), nickel(II), rhodium(III), cobalt(II) and ruthenium(II).[67] Further canvassing the periodic table, the authors also exploited this route to obtain rare examples of transmetalation to chromium(III) and iron(II), with preparation of the first gold(III) *tetra*-carbene complex in 47 % isolated yield (see **Scheme 1.11**). Above all else, these findings underscore the generality and versatility of transmetalation from silver.
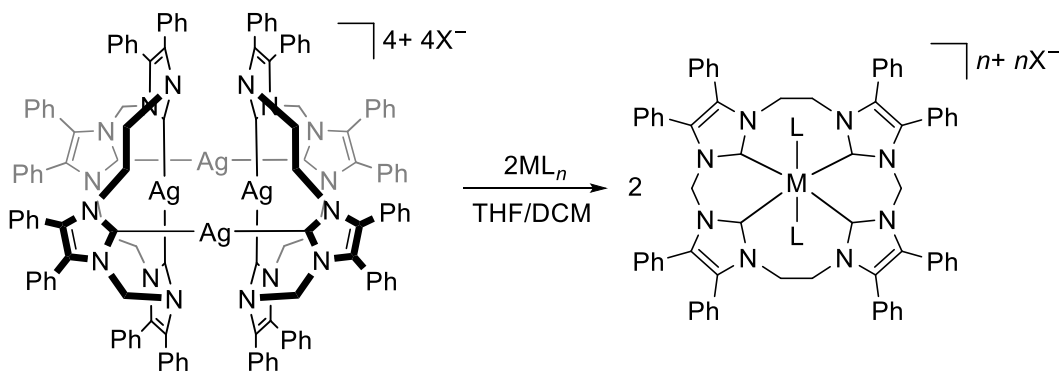
Scheme 1.11 *Versatile transmetalation of tetra-NHC from silver(I), reported by Cramer.*[67]

Recently, Crabtree and co-workers have demonstrated a stepwise transmetalation approach to mixed monodentate *bis*-NHC complexes of iridium(I), employing silver(I)-NHC compounds as transfer agents.[68] Reaction of $[Ir(\eta^2,\eta^2\text{-COD})Cl]_2$ with a silver(I)-NHC (NHC = 1,3-dimethylimidazol-2-ylidene) first produced the corresponding $[Ir(\eta^2,\eta^2\text{-COD})(NHC)Cl]$ compound, which upon further treatment with a preformed $[Ag(NHC)_2][PF_6]$ complex (NHC = 1,3-dimethyltriazol-5-ylidene) afforded a mixed imidazol-2-ylidene/triazol-5-ylidene iridium(I)-NHC product (as shown in **Scheme 1.12**).
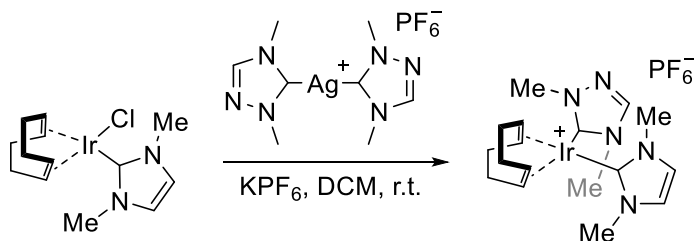
Scheme 1.12 *Stepwise silver(I)-carbene transfer to iridium(I), described by Crabtree.*[68]

In fact, work-up and isolation of the silver(I)-NHC transfer agent is not always essential. In a recent publication by Albrecht and co-workers, a series of iridium(III), ruthenium(II) and palladium(II) complexes were prepared containing mesoionic (commonly referred to as 'abnormal') imidazolylidenes.[69] Within these findings, one pot is charged with two equivalents of *N*-methylimidazo[1,2-*a*]pyridinium iodide (as source of carbene), followed by one equivalent of Ag_2O and an equal amount of $[IrCp^*Cl_2]_2$. The solids are stirred as a slurry in DCM solvent at room temperature, producing the corresponding $[IrCp^*(a\text{NHC})Cl]$ in a single step, without even observing the silver(I)-*a*NHC intermediate.

The concept of driving ligand transfer by disconnecting a relatively weak M-C$_{carbene}$ bond to produce one that is much stronger is not limited to silver(I), though is undoubtedly most practiced.[66] A number of research groups have described the transmetalation of NHCs from

various metal centres, including copper(I), nickel(II) and zirconium(IV).[70–72] In a well-argued publication by Albrecht and Neels, the authors describe transmetalation of NHC groups from copper(I) to ruthenium(II), and justify their motivation to do so based on the reduced cost of copper over silver.[73] It may be put across however, that this is something of a false economy, given that each copper(I)-NHC complex must be prepared through use of expensive bases. In response, Cazin and Furst have combined the use of Cu_2O as *in situ* deprotonation/metalation agent with imidazolium salts, to which a suitable metal source may be added to provide clean, inexpensive access to transition metal-NHC complexes.[74]

In many cases, transmetalation of an NHC group from silver(I) (or other appropriate transition metals) is a suitable and efficient method of producing transition metal-NHC compounds. The route benefits from a strong driving force, avoids strong bases and is often synthetically practical. However, in terms of reaction economy this route is poor. For every molecule of desired product, one molecule of silver(I) halide is formed as side-product which is typically removed through filtration and discarded. Indeed, the inherent low solubility of silver(I) halides in common laboratory solvents provides a simple means of its removal from small scale reactions (*i.e.* milligrams or grams), though presents a problem where scale up is concerned. As an oversimplified example, in order to produce 1 mmol of any compound containing a single M-$C_{carbene}$ bond, an equimolar quantity of silver(I) halide is generated; in the case of AgCl this equates to 142 mg of side product, which is valued in the order of *ca.* £7 (Sigma-Aldrich, 2016). Therefore, a strong push remains to develop synthetically clean, atom efficient and scalable methods of forming transition metal-NHC complexes.

1.6.6 Elimination of small molecules from neutral precursors

In 1961, Wanzlick and Kleiner described the synthesis and thermal elimination of chloroform from a cyclic trichloromethyl substituted heterocycle (**Scheme 1.13**, **A**), which led to sole isolation of an electron-rich dimeric tetraaminoethylene derivative (**C**).[75–77] At the time, Wanzlick proposed that the reaction mechanism must occur *via* two equivalents of free carbene (**B**), which was later confirmed and shown to be a dynamic equilibrium mixture of the two by Denk and co-workers, by entrapment of free carbene through its protonation with hydrochloric acid (**D**).[78] In fact, the same authors used these findings to demonstrate that a mixture of two different tetraaminoethylene molecules could readily exchange their carbene units upon heating (*i.e.* A=A + B=B → 2 A=B), further supporting Wanzlick's argument (**E**).
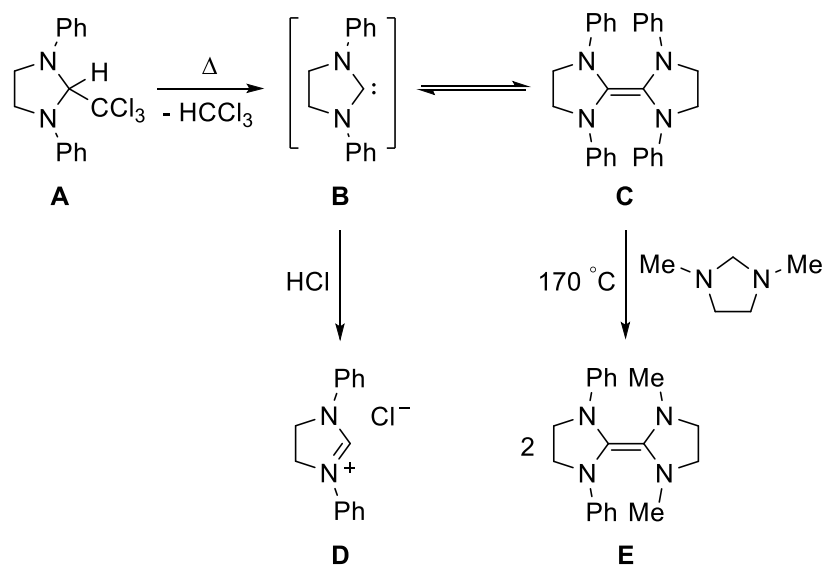
Scheme 1.13 Wanzlick's thermal elimination strategy to free NHCs, which was confirmed 38 years later by Denk and Hatano.[75,78]

Perhaps the most notable example of this method was presented by Grubbs and co-workers, in a modified synthesis of Grubbs' second-generation catalyst.[79] Here, the authors build upon the original research of Lappert and colleagues, who themselves had employed NHC-chloroform and -amine adducts to access [Pt(NHC)(PEt$_3$)Cl$_2$] and [Pt(NHC)$_2$Cl$_2$] complexes through thermal elimination.[80] In place of a trichloromethyl substituent (as shown in **Scheme 1.13**, compound **A**), a methoxide group is employed to give an 'alcohol-protected' version of the NHC, which is simply removed under high vacuum to produce a free NHC. The presence of [Ru=CHPh(PCy$_3$)$_2$(Cl)$_2$] within the reaction mixture allows rapid entrapment of the free carbene, affording the desired ruthenium-NHC complex in 59 % yield.

1.6.7 Oxidative addition

Perhaps underutilised, is transition metal-NHC formation through oxidative addition of a low valent metal source to a C-X bond (X = carbon, halide or hydrogen).

In 2011, Hahn and co-workers exploited this route to prepare several palladium(II) and platinum(II)-NHC complexes, from their corresponding 2-halogenazoles.[81] The authors realised that not only azolium cations, but also neutral 2-halo-substituted benzimidazoles oxidatively add to transition metal precursors. Reaction of 2-chloro-*N*-methylbenzimidazole with one equivalent of [Pd(PPh$_3$)$_4$], followed by subsequent protonation with NH$_4$BF$_4$, yields the corresponding [Pd(NHC)(Cl)(PPh$_3$)$_2$] complex, exclusively in the *trans* isomeric form (see **Scheme 1.14**). The same group have more recently reported a similar oxidative addition reaction on unsubstituted 2-chlorobenzimidazole, producing the corresponding C2-metalated complex bearing two protic nitrogen atoms.[82]
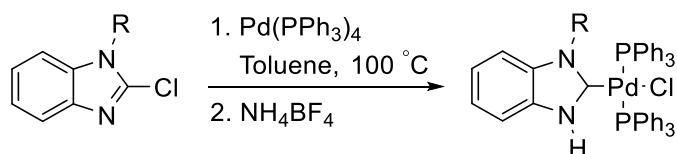
Scheme 1.14 Hahn's oxidative addition approach to palladium(II)-NHC complexes.
R = methyl[81] or hydrogen.[82]

An interesting example communicated by Baker *et al.* describes the formation of a cyclophanyl-NHC complex of palladium(II) *via* oxidative addition of a C-C bond within a bridged diimidazolium ion (as illustrated in **Scheme 1.15**).[83] Treatment of diimidazolium dibromide **A** with [Pd(PPh₃)₄] in DMSO solvent at 90 °C affords the palladium(II)-NHC complex, **B**. The authors note that upon addition of one equivalent of CuBr (a known PPh₃ scavenger), the isolated yield of **B** could be significantly improved from 40 to 80 %, with a corresponding reduction in reaction time from 3 days to 18 hours.
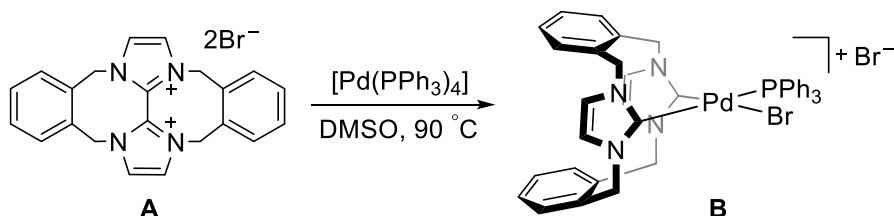
Scheme 1.15 Synthesis of a palladium(II)-NHC through oxidative cleavage of a C-C bond.[83]

In a related example, Crabtree and Peris have described the treatment of a ferrocenyl-tethered diimidazolium salt with [Ir(η^2,η^2-COD)Cl]₂ in the presence of triethylamine, to originally afford an iridium(I) *mono*-NHC complex (see **Scheme 1.16**, **A**).[56] Following characterisation, an NMR tube containing **A** was allowed to stand at room temperature for two hours, in the absence of external base, leading to spontaneous and quantitative formation of iridium(III) *bis*-NHC hydride complex, **B**. Here, the authors suggest that metalation of the imidazolium ring proceeds through oxidative addition of the C2-H bond, though are not able to fully rationalise the role of base throughout each metalation step.
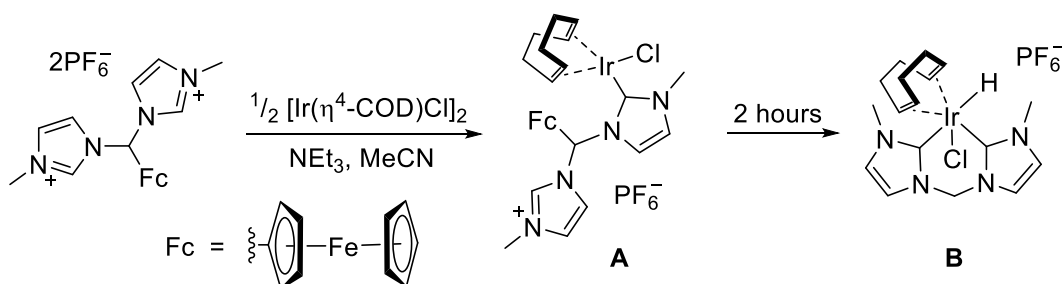
Scheme 1.16 Crabtree's iridium(III) bis-NHC hydride complex, formed through unexpected oxidative addition of an imidazolium C2-H bond to iridium(I).[56]

20

Tactical employment of oxidative addition allows access to unusual transition metal-NHC complexes. The method is often performed in a single pot, and does not rely on relative acidity of protons bound to the imidazolium ring. However, a great deal of retrosynthetic foresight is required to incorporate specific carbon-halogen bonds into a heterocyclic substrate, and are therefore not always trivial to prepare. Consequently, NHC precursors of this type are rare and limit the scope of this methodology.

1.6.8 Electrochemical methodology

In contrast to popular synthetic strategies, Chen, Liu and Xia developed an elegant synthetic protocol toward coinage metal-NHC complexes which avoids handling reactive free carbenes by direct reaction of zero-valent metal powders with imidazolium salts in common aerobic laboratory solvent.[84] The method represents a major landmark in metal-NHC synthesis, as the procedure is operationally simple and the complexes formed are isolated as air-stable solids.

However, in 2011 the same authors developed an electrochemical procedure for the isolation of metal-NHC complexes, which equally bypasses handling of reactive intermediates by employment of an appropriate metal as sacrificial anode, with a Pt counter-electrode as cathode.[85] The electrochemical mechanism underpinning the overall reaction is given in **Scheme 1.17**, and builds upon the original research of Feroci and Inesi regarding the electrogeneration of carbenes from ionic liquids.[86]
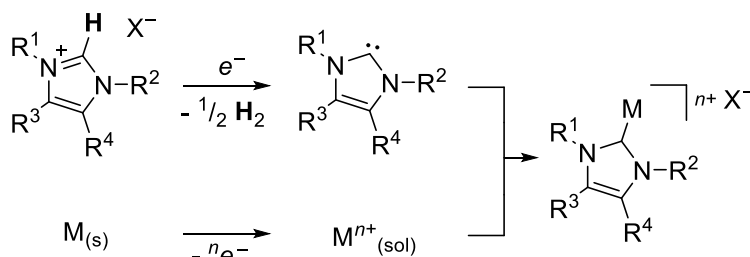
Scheme 1.17 *Overall electrochemical reaction concerning the formation of metal-NHC complexes, using metal plate electrodes and imidazolium salts. Top reaction: cathodic reduction of imidazolium ion, releasing molecular hydrogen to form a free-NHC. Bottom reaction: anodic oxidation of zero-valent metal source, liberating metal ions into solution.*

A solution of imidazolium salt in acetonitrile is used as source of carbene, which acquires an electron from the cathode to supply free NHCs whilst releasing molecular hydrogen as the only byproduct. The production of free NHCs was simply monitored by the generation of hydrogen gas and subsequent formation of the metal-NHC complexes were observed by colouration of the reaction mixture. Spectroscopically pure complexes were obtained by crystallisation after passing 1.0 Fmol^{-1} electricity at constant current, which enabled access to a scope of transition metal-NHC complexes in moderate yield, including isolation of a notable trinuclear copper(I)-NHC

complex, consisting of a triangular Cu_3 core bridged by three NHCs to represent a rare example of a copper(I) complex with 3c-2e bridging NHC ligands (see **Figure 1.14**).[87,88]
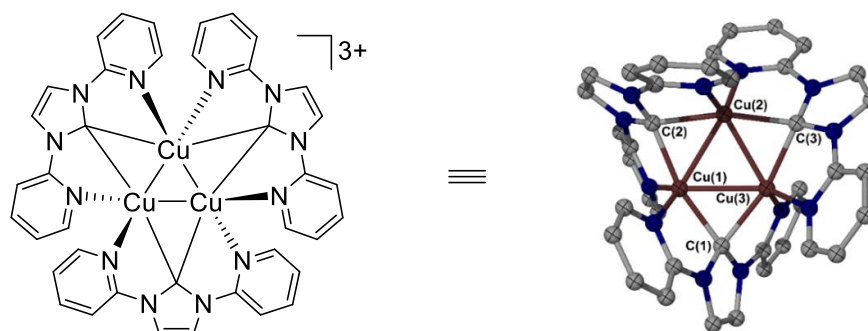
Figure 1.14 *Taken from the crystal structure of Chen's trinuclear Cu_3 complex, displaying the cationic portion of the asymmetric unit.[87]*

Despite Chen's electrochemical procedure representing a new mode of access to metal-NHCs, only ligand precursors bearing *N*-pyridine or pyrimidine substituents were found to deliver stable complexes under aerobic conditions. In addition, use of non-coordinating counteranions led only to production of cationic complexes, with no further investigation of neutral analogues or ligands bearing previously "inaccessible" *N*-substituents (*i.e.* base-sensitive groups).

In response, our group reported a valuable extension to Chen's model which allows controlled access to copper(I)-NHC complexes in which the carbenic ligand does not bear a pendant donor arm (**Figure 1.15**).[89] Furthermore, the electrolytic protocol is suitable for the preparation of both neutral Cu(NHC)X (**A**) and cationic [Cu(NHC)$_2$]X (**B**) complexes (where X = halide), through simple counteranion modification.
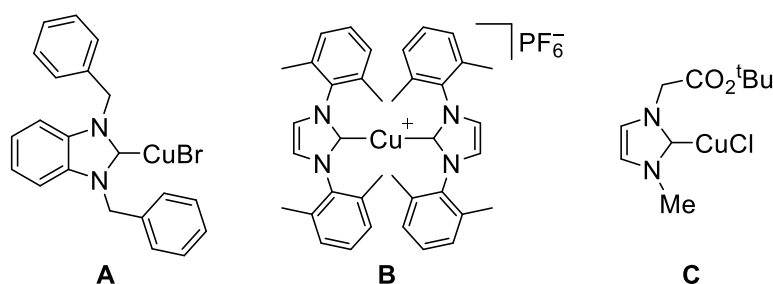
Figure 1.15 *Electrochemically derived copper(I)-NHC complexes, including overall neutral (**A**), cationic (**B**) and base sensitive (**C**) examples.[89]*

A leading advantage of the electrochemical system is the circumvention of strongly basic reaction conditions. This improvement is demonstrated by the extension of imidazolium substrates now suitable for selective metalation at their corresponding C2 position (*i.e.* N*C*N of the imidazolium ring), whilst in the presence of functionality containing acidic hydrogen atoms susceptible to deprotonation by strong bases, such as formation of unsymmetrical *N-tert*-butylacetate substituted copper(I)-NHC complex **C**, in high purity.

The electrochemical synthesis of metal-NHC complexes exemplifies a synthetically clean, chemoselective route which is highly atom economical, as lightweight molecular H_2 is the only side-product. However, in terms of reaction engineering, the net efficiency of the electrochemical cell is poor. Primarily, the batch reactor suffers low rates of mass and charge transfer as a result of inefficient mixing throughout the bulk volume element. Moreover, a relatively large interelectrodic distance separates each metal plate (*ca.* 30 mm at the minimum point), combined with a low interfacial area (*ca.* 8.0 cm^2 electrode contact area, 20 mL solvent) contacting the electrode surface and weak ionic liquid. These design issues lead to the application of high overpotentials (*ca.* 30 V applied to maintain 50 mA current) in order to generate sufficient current density to perform electrochemical work, leading to a large coulombic waste and long average residence time (low space-time-yield) to achieve acceptable conversion.

1.7   Project outline

The original and principal target of this research involves the translation of current electrochemical synthetic methods of preparing transition metal-NHC complexes from static batch into a continuous-flow protocol. For this purpose, a suitable electrochemical flow-reactor is to be designed and constructed, capable of eliminating the physical drawbacks of design associated with previous electrochemical batch procedures, including current continuous chemical routes.[90] State-of-the-art reactor design will seek to address physical chemical phenomena, such as (i) reaction mixing, (ii) multiphasic mass (and charge) transfer, and (iii) scalability. To do so, research will be conducted at the interface between chemistry and engineering to produce a rare example of organometallic synthesis in continuous-flow.

Using a design-of-experiment approach, reaction engineering will be employed to maximise electrochemical and synthetic output of the reactor for a number of benchmark examples. Following, it should be possible to configure the reactor to produce a variety of functionally diverse transition metal-NHC complexes, predetermined by choice of anodic metal and carbene precursor.

In addition to azolium salts, the electrochemical reduction and subsequent coordination of various other protic precursors is to be investigated throughout the course of research. Overlapping this idea with the electrochemical oxidation of assorted metals, it is envisaged that a broad range of organometallic products may be prepared by means of a single comprehensive reaction.

An overarching goal of the research lies in the post-synthetic applications of these organometallic products. The electrochemical protocol occurs under exceptionally mild conditions, lending itself to the synthesis of previously inaccessible metal compounds. From a fundamental angle, this will be exploited to rationally design and isolate transition metal complexes with highly desirable properties. Following their synthesis, the employment of continuous-flow methodology should provide a platform to directly dispense these metal complexes into reaction media for catalytic study.

1.8 Bibliography

1. (a) D. Seyferth, *Organometallics* **2001**, *20*, 1488–1498; (b) T. D. Sideris, G. M. Tsivgoulis, D. G. Vachliotis, P. V. Ioannou, *Main Group Chemistry* **2009**, *8*, 163–176; (c) H. C. Marsmann, J. R. Vanwazer, *J. Am. Chem. Soc.* **1970**, *92*, 969–972.

2. W. C. Ziese, *Ann. Phys.* **1831**, *97*, 497–541.

3. E. Frankland, *Q. J. Chem. Soc.* **1850**, *2*, 263–296.

4. D. Seyferth, *Organometallics* **2001**, *20*, 2940–2955.

5. The Nobel Prize in Chemistry **1912**, *Nobelprize.org*, *Nobel Media AB 2013*, Web. 15 Jun 2014. http://www.nobelprize.org/nobel_prizes/chemistry/laureates/1912/.

6. The Nobel Prize in Chemistry **1973**, *Nobelprize.org*, *Nobel Media AB 2013*, Web. 15 Jun 2014. http://www.nobelprize.org/nobel_prizes/chemistry/laureates/1973/.

7. The Nobel Prize in Chemistry **2005**, *Nobelprize.org*, *Nobel Media AB 2013*, Web. 15 Jun 2014. http://www.nobelprize.org/nobel_prizes/chemistry/laureates/2005/.

8. (a) W. von E. Doering, A. K. Hoffmann, *J. Am. Chem. Soc.* **1954**, *76*, 6162–6165; (b) A. Nasr, A. Winkler, M. Tamm, *Coord. Chem. Rev.* **2016**, *316*, 68–124.

9. (a) E. O. Fischer, A. Maasböl, *Angew. Chem. Int. Ed.* **1964**, *3*, 580–581; (b) S. B. Wang, X. C. Wang, *Angew. Chem. Int. Ed.* **2016**, *55*, 2308–2320; (c) C. I. Ezugwu, N. A. Kabir, M. Yusubov, F. Verpoort, *Coord. Chem. Rev.* **2016**, *307*, 188–210.

10. (a) S. T. Liddle, I. S. Edworthy, P. L. Arnold, *Chem. Soc. Rev.* **2007**, *36*, 1732–1744; (b) E. Baba, T. R. Cundari, I. Firkin, *Inorg. Chim. Acta* **2005**, *358*, 2867–2875; (c) R. Weiss, S. Reichel, M. Handke, F. Hampel, *Angew. Chem. Int. Ed.* **1998**, *3*, 344–347.

11. (a) D. Bourissou, O. Guerret, F. P. Gabbaï, G. Bertrand, *Chem. Rev.* **2000**, *100*, 39–92; (b) J. L. G-Lopez, D. Chavez, M. P.-Hake, A. T. Royappa, A. L. Rheingold, D. B. Grotjahn, V. M.-Soto, *Organometallics* **2016**, *35*, 3148–3153.

12. G. B. Schuster, *Adv. Phys. Org. Chem.* **1986**, *22*, 311–361.

13. R. Hoffmann, *J. Am. Chem. Soc.* **1968**, *90*, 1475–1485.

14. W. W. Schoeller, *J. Chem. Soc. Chem. Commun.* **1980**, 124–125.

15. (a) L. Pauling, *J. Chem. Soc. Chem. Commun.* **1980**, 688–689; (b) A. J. Arduengo, R. Dias, R. L. Harlow, M. Kline, *J. Am. Chem. Soc.* **1992**, *114*, 5530–5534.

16. (a) J. F. Harrison, *J. Am. Chem. Soc.* **1971**, *93*, 4112–4119; (b) R. M.-Barrios, F. L. Cozens, N. P. Schepp, *J. Org. Chem.* **2009**, *74*, 1148–1155; (c) Y. Canac, S. Conejero, B. Donnadieu, W. W. Schoeller, G. Bertrand, *J. Am. Chem. Soc.* **2005**, *127*, 7312–7313; (d) T. Itoh, Y. Nakata, K. Hirai, H. Tomioka, *J. Am. Chem. Soc.* **2006**, *128*, 957–967.

17. R. Hoffmann, G. D. Zeiss, G. W. Van Dine, *J. Am. Chem. Soc.* **1968**, *90*, 1485–1499.

18. X. Tan, W. Wang, P. Li, *J. Saudi Chem. Soc.* **2016**, *20*, 321–329.

19. A. J. Arduengo, H. Bock, H. Chen, M. Denk, D. A. Dixon, J. C. Green, W. A. Herrmann, N. L. Jones, M. Wagner, R. West, *J. Am. Chem. Soc.* **1994**, *116*, 6641–6649.

20. (a) W. A. Herrmann, C. Köcher, *Angew. Chem. Int. Ed.* **1997**, *36*, 2162–2187; (b) S. W.-Pietsch, U. Radius, T. B. Marder, *Dalton Trans.* **2016**, *45*, 5880–5895.

21. C. Boehme, G. Frenking, *J. Am. Chem. Soc.* **1996**, *118*, 2039–2046.

22. H. G. Raubenheimer, *Dalton Trans.* **2014**, *43*, 16959–16973.

23. (a) P. de Frémont, N. Marion, S. P. Nolan, *Coord. Chem. Rev.* **2009**, *253*, 862–892; (b) C. A. Main, S. S. Rahman, R. C. Hartley, *Tetrahedron Lett.* **2008**, *49*, 4771–4774; (c) C. Macleod, G. J. McKieran, E. J. Guthrie, L. J. Farrugia, D. W. Hamprecht, J. Macritchie, R. C. Hartley, *J. Org. Chem.* **2003**, *68*, 387–401; (d) J. Ito, M. G. Crestani, B. C. Bailey, X. F. Gao, D. J. Mindiola, *Polyhedron* **2014**, *84*, 177–181; (e) Z. H. Wei, W. B. Zhang, G. M. Luo, F. Xu, Y. X. Mei, H. Cai, *J. Organomet. Chem.* **2016**, *808*, 104–108; (f) M. Bortoluzzi, E. Ferretti, F. Marchetti, G. Pampaloni, S. Zacchini, *Dalton Trans.* **2016**, *45*, 6939–6948.

24. J. J. Hu, S.-Q. Bai, H. H. Yeh, D. J. Young, Y. Chi, T. S. A. Hor, *Dalton Trans.* **2011**, *40*, 4402–4406.

25. L. R. Collins, G. Hierlmeier, M. F. Mahon, I. M. Riddlestone, M. K. Whittlesey, *Chem. Eur. J.* **2015**, *21*, 3215–3218.

26. L. R. Collins, T. M. Rookes, M. F. Mahon, I. M. Riddlestone, M. K. Whittlesey, *Organometallics* **2014**, *33*, 5882–5887.

27. (a) P. L. Arnold, S. Pearson, *Coord. Chem. Rev.* **2007**, *251*, 596–609; (b) D. Patel, S. T. Liddle, S. A. Mungur, M. Rodden, A. J. Blake, P. L. Arnold, *Chem. Commun.* **2006**, 1124–1126; (c) E. Peris, R. H. Crabtree, *Coord. Chem. Rev.* **2004**, *248*, 2239–2246; (d) T. Jensen, L. Breyfogle, M. Hillmyer, W. Tolman, *Chem. Commun.* **2004**, 2504–2505.

28. (a) D. J. D. Wilson, S. A. Couchman, J. L. Dutton, *Inorg. Chem.* **2012**, *51*, 7657–7668; (b) T. M. Trnka, R. H. Grubbs, *Acc. Chem. Res.* **2001**, *34*, 18–29.

29. (a) A. J. Arduengo, R. L. Harlow, M. Kline, *J. Am. Chem. Soc.* **1991**, *113*, 361–363; (b) A. J. Arduengo, *U.S. Patent 5, 077, 414* **1991**; (c) A. J. Arduengo, R. Krafczyk, R. Schmutzler, H. A. Craig, J. R. Goerlich, W. J. Marshall, M. Unverzagt, *Tetrahedron* **1999**, *55*, 14523–14534.

30. K. Öfele, *J. Organomet. Chem.* **1968**, *12*, 42–43.

31. H.-W. Wanzlick, H.-J. Schönherr, *Angew. Chem. Int. Ed.* **1968**, *7*, 141–142.

32. T. L. Amyes, S. T. Diver, J. P. Richard, F. M. Rivas, K. Toth, *J. Am. Chem. Soc.* **2004**, *126*, 4366–4374.

33. L. Benhamou, E. Chardon, G. Lavigne, S. Bellemin-Laponnaz, V. César, *Chem. Rev.* **2011**, *111*, 2705–2733.

34. (a) J. Wallach, *Ber. Dtsch. Chem. Ges.* **1925**, *15*, 645; (b) L. Hintermann, *Beilstein J. Org. Chem.* **2007**, *3*, 22.

35. A. A. Gridnev, I. M. Mihaltseva, *Synth. Commun.* **1994**, *24*, 1547–1555.

36. I. Nieto, F. Cervantes-Lee, J. M. Smith, *Chem. Commun.* **2005**, *125*, 3811–3813.

37. (a) X. Bantreil, S. P. Nolan, *Nat. Protoc.* **2011**, *6*, 69–77; (b) S. P. Nolan, J. Huang, *U.S. Patent 7, 622, 590* **2009**; (c) L. Jafarpour, H.-J. Schanz, E. D. Stevens, S. P. Nolan, *Organometallics* **1999**, *18*, 5416–5419.

38. W. A. Herrmann, C. Köcher, L. J. Gooßen, G. R. J. Artus, *Chem. Eur. J.* **1996**, *2*, 1627–1636.

39. W. A. Herrmann, M. Elison, J. Fischer, C. Köcher, G. R. J. Artus, *Chem. Eur. J.* **1996**, *2*, 772–780.

40. L. Jafarpour, J. Huang, E. D. Stevens, S. P. Nolan, *Organometallics* **1999**, *18*, 3760–3763.

41. J. Huang, E. D. Stevens, S. P. Nolan, J. L. Petersen, *J. Am. Chem. Soc.* **1999**, *121*, 2674–2678.

42. O. Hollóczki, P. Terleczky, D. Szieberth, G. Mourgas, D. Gudat, L. Nyulászi, *J. Am. Chem. Soc.* **2011**, *133*, 780–789.

43. M. K. Denk, J. M. Rodezno, S. Gupta, A. J. Lough, *J. Organomet. Chem.* **2001**, *617*, 242–253.

44. (a) T. Weskamp, V. P. W. Böhm, W. A. Herrmann, *J. Organomet. Chem.* **2000**, *600*, 12–22; (b) M. Henrion, M. J. Chetcuti, V. Ritleng, *Chem. Commun.* **2014**, *50*, 4624–4627; (c) R. J. Lowry, M. T. Jan, K. A. Abboud, I. Ghiviriga, A. S. Veige, *Polyhedron* **2010**, *29*, 553–563; (d) D. R. Armstrong, S. E. Baillie, V. L. Blair, N. G. Chabloz, J. Diez, J. G.-Alvarez, A. R. Kennedy, S. D. Robertson, E. Hevia, *Chem. Sci.* **2013**, *4*, 4259–4266.

45. H. Aihara, T. Matsuo, H. Kawaguchi, *Chem. Commun.* **2003**, *41*, 2204–2205.

46. (a) D. Enders, H. Gielen, G. Raabe, J. Runsink, J. H. Teles, *Chem. Ber.* **1996**, *129*, 1483–1488; (b) W. A. Herrmann, M. Elison, J. Fischer, C. Köcher, G. R. J. Artus, *Angew. Chem.* **1995**, *107*, 2602–2605.

47. W. A. Herrmann, L. J. Gooβen, M. Spiegler, *J. Organomet. Chem.* **1997**, *547*, 357–366.

48. T. Weskamp, V. P. Böhm, W. A. Herrmann, *J. Organomet. Chem.* **1999**, *585*, 348–352.

49. W. P. Fehlhammer, T. Bliss, U. Kernbach, I. Brüdgam, *J. Organomet. Chem.* **1995**, *490*, 149–153.

50. K. M. Lee, C. K. Lee, I. J. B. Lin, *Angew. Chem. Int. Ed.* **1997**, *36*, 1850–1852.

51. J. Reijenga, A. van Hoof, A. van Loon, B. Teunissen, *Anal. Chem. Insights* **2013**, *8*, 53–71.

52. (a) J. Ruiz, L. García, M. Vivanco, Á. Berros, J. F. Van der Maelen, *Angew. Chem. Int. Ed. Engl.* **2015**, *54*, 4212–4216; (b) G. Jerez, G. Kaufman, M. Prystai, S. Schenkeveld, K. K. Donkor, *J. Sep. Sci.* **2009**, *32*, 1087–1095; (c) E. M. Higgins, J. A. Sherwood, A. G. Lindsay, J. Armstrong, R. S. Massey, R. W. Alder, A. C. O'Donoghue, *Chem. Commun.* **2011**, *47*, 1559–1561.

53. M. W. Washabaugh, W. P. Jencks, *Biochemistry* **1988**, *27*, 5044–5053.

54. O. Santoro, A. Collado, A. M. Z. Slawin, S. P. Nolan, C. S. J. Cazin, *Chem. Commun.* **2013**, *49*, 10483–10485.

55. B. R. M. Lake, C. E. Willans, *Chem. Eur. J.* **2013**, *19*, 16780–16790.

56. M. Viciano, E. Mas-Marzá, M. Poyatos, M. Sanaú, R. H. Crabtree, E. Peris, *Angew. Chem. Int. Ed. Engl.* **2005**, *44*, 444–447.

57. W. A. Herrmann, M. Elison, J. Fischer, C. Köcher, G. R. J. Artus, *Angew. Chem. Int. Ed. Engl.* **1995**, *34*, 2371–2374.

58. W. A. Herrmann, G. Gerstberger, M. Spiegler, *Organometallics* **1997**, *16*, 2209–2212.

59. W. A. Herrmann, J. Schwarz, M. G. Gardiner, *Organometallics* **1999**, *18*, 4082–4089.

60. C. Köcher, W. A. Herrmann, *J. Organomet. Chem.* **1997**, *532*, 261–265.

61. M. H. Voges, C. Rømming, M. Tilset, *Organometallics* **1999**, *18*, 529–533.

62. D. C. F. Monteiro, R. M. Phillips, B. D. Crossley, J. Fielden, C. E. Willans, *Dalton Trans.* **2012**, *41*, 3720–3725.

63. (a) B. R. M. Lake, C. E. Willans, *Organometallics* **2014**, *33*, 2027–2038; (b) J. Dupont, *J. Braz. Chem. Soc.* **2004**, *15*, 341–350; (c) V. J. Catalano, M. A. Malwitz, A. O. Etogo, *Inorg. Chem.* **2004**, *43*, 5714–5724.

64. A. J. Arduengo, H. V. R. Dias, J. C. Calabrese, F. Davidson, *Organometallics* **1993**, *12*, 3405–3409.

65. H. M. J. Wang, I. J. B. Lin, *Organometallics* **1998**, *17*, 972–975.

66. (a) J. C. Y. Lin, R. T. W. Huang, C. S. Lee, A. Bhattacharyya, W. S. Hwang, I. J. B. Lin, *Chem. Rev.* **2009**, *109*, 3561–3598; (b) D. Krishnamurthy, M. R. Karver, E. Fiorillo, V. Orru, S. M. Stanford, N. Bottini, A. M. Barrios, *J. Med. Chem.* **2008**, *51*, 4790–4795; (c) S. Ray, R. Mohan, J. K. Singh, M. K. Samantaray, M. M. Shaikh, D. Panda, P. Ghosh, *J. Am. Chem. Soc.* **2007**, *129*, 15042–15053.

67. For ruthenium(II), see: (a) Z. Lu, S. A. Cramer, D. M. Jenkins, *Chem. Sci.* **2012**, *3*, 3081–3087; (b) P. Csabai, F. Joo, *Organometallics* **2004**, *23*, 5640–5643; (c) P. L. Chiu, H. M. Lee, *Organometallics* **2005**, *24*, 1692–1702. For ruthenium(III), see: (d) P. L. Arnold, A. C. Scarisbrick, *Organometallics* **2004**, *23*, 2519–2521. For ruthenium(IV), see: (e) J. J. van Veldhuizen, S. B. Garber, J. S. Kingsbury, A. H. Hoveyda, *J. Am. Chem. Soc.* **2002**, *124*, 4954–4955; (f) J. J. van Veldhuizen, J. E. Campbell, R. E. Giudici, A. H. Hoveyda, *J. Am. Chem. Soc.* **2005**, *127*, 6877–6882.

68. L. N. Appelhans, C. D. Incarvito, R. H. Crabtree, *J. Organomet. Chem.* **2008**, *693*, 2761–2766.

69. (a) A. Petronilho, H. Mueller-Bunz, M. Albrecht, *J. Organomet. Chem.* **2014**, *775*, 117–123; (b) A. R. Chianese, A. Kovacevic, B. M. Zeglis, J. W. Faller, R. H. Crabtree, *Organometallics* **2004**, *23*, 2461–2468.

70. (a) C. Chen, H. Qiu, W. Chen, *J. Organomet. Chem.* **2012**, *696*, 4166–4172; (b) J. Pytkowicz, S. Roland, P. Mangeney, *Tetrahedron: Asymmetry* **2001**, *631*, 157–163; (c) A. Alexakis, C. L. Winn, F. Guillen, J. Pytkowicz, S. Roland, P. Mangeney, *Adv. Synth. Catal.* **2003**, *345*, 345–348.

71. (a) B. Liu, X. Liu, C. Chen, C. Chen, W. Chen, *Organometallics* **2012**, *31*, 282–288; (b) X. Wang, S. Liu, G.-X. Jin, *Organometallics* **2004**, *45*, 299–309; (c) S. Winston, N. Stylianides, A. A. D. Tulloch, J. A. Wright, A. A. Danoloulos, *Polyhedron* **2004**, *23*, 2813–2820.

72. (a) G. T. S. Andavan, E. B. Bauer, C. S. Letko, T. K. Hollis, F. S. Tham, *J. Organomet. Chem.* **2005**, *690*, 5938–5947; (b) D. J. Nielsen, K. J. Cavell, B. W. Skelton, A. H. White, *Inorg. Chim. Acta* **2003**, *352*, 143–150.

73. (a) G. Venkatachalam, M. Heckenroth, A. Neels, M. Albrecht, *Helv. Chim. Acta* **2009**, *92*, 1034–1045; (b) Z. Wang, H. Dong, Y. Zou, Q. Zhao, J. Tan, J. Liu, X. Lu, J. Xiao, Q. Zhang, W. Hu, *ACS Appl. Mater. Interfaces* **2016**, *8*, 7919–7927.

74. M. R. L. Furst, C. S. J. Cazin, *Chem. Commun.* **2010**, *46*, 6924–6925.

75. (a) H.-W. Wanzlick, H. J. Kleiner, *Angew. Chem. Int. Ed.* **1961**, *73*, 493–495; (b) H.-W. Wanzlick, *Angew. Chem. Int. Ed. Engl.* **1962**, *1*, 75–80.

76. (a) H.-W. Wanzlick, F. Esser, H.-J. Kleiner, *Chem. Ber.* **1963**, *96*, 1208–1212; (b) D. M. Lemal, R. A. Lovald, K. I. Kawano, *J. Am. Chem. Soc.* **1964**, *86*, 2518–2519; (c) H. E. Winberg, J. E. Carnahan, D. D. Coffman, M. Brown, *J. Am. Chem. Soc.* **1965**, *87*, 2055–2056.

77. H.-W. Wanzlick, E. Schikora, *Angew. Chem. Int. Ed.* **1960**, *72*, 494.

78. M. K. Denk, K. Hatano, M. Ma, *Tetrahedron Lett.* **1999**, *40*, 2057–2060.

79.   T. M. Trnka, J. P. Morgan, M. S. Sanford, T. E. Wilhelm, M. Scholl, T.-L. Choi, S. Ding, M. W. Day, R. H. Grubbs, *J. Am. Chem. Soc.* **2003**, *125*, 2546–2558.

80.   D. J. Cardin, B. Cetinkaya, E. Cetinkaya, M. F. Lappert, *J. Chem. Soc. Dalton Trans.* **1973**, 514–522.

81.   T. Kösterke, T. Pape, F. E. Hahn, *J. Am. Chem. Soc.* **2011**, *133*, 2112–2115.

82.   R. Das, A. Hepp, C. G. Daniliuc, F. E. Hahn, *Organometallics* **2014**, *33*, 6975–6987.

83.   M. V. Baker, D. H. Brown, V. J. Hesler, B. W. Skelton, A. H. White, *Organometallics* **2007**, *26*, 250–252.

84.   B. Liu, Q. Xia, W. Chen, *Angew. Chem. Int. Ed.* **2009**, *48*, 5513–5516.

85.   B. Liu, Y. Zhang, D. Xu, W. Chen, *Chem. Commun.* **2011**, *47*, 2883–2885.

86.   M. Feroci, I. Chiarotto, M. Orsini, G. Sotgiu, A. Inesi, *Adv. Synth. Catal.* **2008**, *350*, 1355–1359.

87.   S. Gischig, A. Togni, *Organometallics* **2005**, *24*, 203–205.

88.   Z. Xi, X. Zhang, W. Chen, S. Fu, D. Wang, *Organometallics* **2007**, *26*, 6636–6642.

89.   B. R. M. Lake, E. K. Bullough, T. J. Williams, A. C. Whitwood, M. A. Little, C. E. Willans, *Chem. Commun.* **2012**, *48*, 4887–4889.

90.   S. M. Opalka, J. K. Park, A. R. Longstreet, D. T. McQuade, *Org. Lett.* **2013**, *15*, 996–999.

Chapter 2

Design, construction and optimisation of an electrochemical flow-reactor for expedient synthesis of copper(I) *N*-heterocyclic carbene complexes

2.1 Introduction

The growth in copper-catalysed organic reactions has been driven by numerous factors. The ability of copper to readily access Cu^0, Cu^I, Cu^{II} and Cu^{III} oxidation states to regulate processes involving one- and two-electron (*i.e.* radical and polar) mechanisms has led to incredibly rich and diverse chemistry.[1–3] Moreover, the different oxidation states of copper associate well with a large number of different functional groups through Lewis acid interactions or π-coordination. Overall, these features confer a broad range of activities which allow copper to catalyse the union of many organic substrates along various mechanisms (*e.g.* Ullmann coupling,[4] Diels-Alder reaction,[5] Castro-Stevens coupling,[6] Kharasch-Sosnovsky reaction[7] and Huisgen cycloaddition[8]), provoking such interest that it has been the topic of a number of recent review articles.[9–11]

The push to replace critical materials with those that are abundant, particularly in applications which use large quantities of catalysts, poses many benefits. Earth-abundant materials are generally inexpensive, less susceptible to supply fluctuation and more environmentally benign. On a per mole basis, Pt is approximately 4,000 times more expensive than Ni, and 10,000 times that of Fe, with Pd 3,000-fold more costly than Cu.[12] However, employment of these metals as catalysts (*i.e.* the first-row transition metals) often leads to lower functional group tolerance and subdued chemical selectivity, requiring a more expensive ligand choice to upgrade reactivity. Nonetheless, in certain cases copper catalysts have been shown to construct C-C and C-N bonds with similar efficiency as their palladium counterparts.[13]

2.1.1 Synthesis of copper(I) *N*-heterocyclic carbenes

Monocationic copper (*i.e.* Cu^I) is a soft transition metal ion which interacts strongly with soft donor groups, such as *N*-heterocyclic carbenes (NHCs). This favourable interaction has led to numerous synthetic reports regarding the synthesis and isolation of copper(I)-NHCs, with the first example documented by Arduengo and co-workers in 1993.[14] The copper(I) *bis*-NHC complex was prepared *via* treatment of two equivalents of the free NHC (IMes = 1,3-*bis*(2,4,6-trimethylphenyl)imidazol-2-ylidene) with one equivalent of the benzene solvate of $Cu(CF_3SO_3)$ in THF solvent.

Since Arduengo's influential findings, a broad range of structurally diverse copper-NHC complexes have been published, which may be prepared along a number of common synthetic routes and have been reviewed through Chapter 1 of this thesis.

Recently, McQuade and co-workers have developed the idea of using continuous-flow to synthesise copper(I)-NHCs and avoid use of Schlenk line or glovebox techniques.[15] The method involves flowing a solution of a soluble ligand precursor over a packed-bed of insoluble Cu_2O, suspended within molecular sieves. Employing a Vapourtec R-series reactor system equipped with a heated Omnifit column, the authors found that a flow-rate of 0.80 mLmin^{-1} (residence time = 2 minutes) and a column temperature of 110 ˚C allowed high conversion (>90 %) of numerous substrates to their corresponding copper complexes. In many cases, however, the employment of high reaction temperatures led to significant leaching of the solid support, coupled with difficult product purification from the high boiling reaction solvent (toluene). As outlined in Chapter 1, our ability to electrochemically generate these complexes under neutral and ambient conditions using low boiling solvent represents a significant edge over McQuade's synthesis, and may similarly be achieved using a suitable electrochemical flow-reactor.

2.1.2 Continuous-flow technology

The past two decades have seen far-reaching progress in the development of microfluidic systems for use in chemical synthesis, with the field continuing to mature exponentially.[16] Continuous-flow reactors are able to manipulate and control fluids that are geometrically constrained within environments having internal dimensions, or hydrodynamic diameters, within the micro- or millimeter region. Operating chemical synthesis in this manner offers a variety of advantages over "conventional" batch processing, particularly with respect to reactions requiring rapid heat, mass or photon transfer.[17–20]

The concept of continuous synthesis has been applied extensively as a useful tool towards the process intensification of numerous active pharmaceutical ingredients (APIs). For example, Jamison and Snead recently reported a "three-minute synthesis" of high purity ibuprofen (equating to 8.09 gh^{-1}, or 70.8 kgy^{-1}), involving three bond-forming steps, one work-up and one in-line liquid-liquid (L-L) extraction, using equipment with an overall footprint of half the size of a standard laboratory fumehood.[21] This represents a paragon of continuous-flow processing, comprising a Friedel-Crafts acylation under neat conditions, an exothermic in-line quench of the subsequent unreacted $AlCl_3$, use of aggressive iodine monochloride oxidant along with L-L separations run at or above 200 psi to deliver solvent-free product.

In 2012, Seeberger and co-workers described the continuous synthesis of artemisinin (anti-malaria drug) from dihydroartemisinic acid, which itself is readily available from the fermentation of artemisinic acid in engineered yeast.[20] Central to the reaction is a continuous photochemical transformation, involving a singlet-oxygen-induced ene reaction followed by the addition of triplet oxygen, triggering a cascade sequence to install an endoperoxide motif essential to the final

product. The employment of a low-inventory immersed-well photoreactor bypasses many of the shortcomings associated with use of singlet oxygen on a process scale (*e.g.* chemical runaway, explosion risk, mass transfer, heat dissipation). Moreover, the relatively small reactor volume allows for a high degree of light penetration throughout the reaction mixture, enabling a residence time of two minutes to achieve pure product, with the authors extrapolating a value of 200 g of API per day under these conditions.

Further typical benefits of continuous-flow processing include (i) enhanced mixing, (ii) increased chemical selectivity, (iii) improved green metrics and (iv) versatile scalability. However, in a well-argued publication, Jensen and McMullen have outlined conditions in which the use of flow chemistry "makes sense", relative to batch.[22] The authors underline that the rate of chemical reaction must be rapid when compared with the rate of mass transfer of the system – providing this criterion is met, there is clear justification to translate a chemical process into flow.

Taking consideration of the intrinsic bottlenecks associated with the electrochemical batch synthesis of copper(I)-NHCs developed within our group (see Chapter 1), it was sought to design a flow-reactor capable of overcoming these drawbacks. Wirth and Yoshida have independently shown that the distance between electrodes in electrochemical microreactors can be sufficiently small such that the two diffusion layers of each electrode may overlap to become coupled.[23,24] In turn, high conductivities may be reached using relatively low applied potentials, leading to improved cell-efficiency to maximise chemical conversion. Likewise, the prospect of scaling out through multiple small-scale electrochemical reactors is attractive, as low quantities of hydrogen gas side-product could be simply managed whilst substantially increasing output scale.

2.2   Prototypical copper flow-reactor: 'proof-of-concept'

The design of a chemical reactor deals with multiple aspects of chemical engineering. For example, a typical approach to a final design would usually consider: (i) kinetic/thermodynamic data, (ii) physical properties of the feedstock, intermediates and products and (iii) requisite for mass and heat transfer. From here, a reasonable estimate can be produced regarding optimal reaction conditions for a desired output parameter (*e.g.* yield, cost, E-factor). Using semi-empirical methods, the reactor size and performance can be approximated, and further used to optimise a set of conditions for a specific chemical reaction.

2.2.1   Reactor design and construction

In terms of electrochemical flow-reactors, much research has been devoted to continuous-flow stirred-tank electrochemical reactors (CSTER), whereby spatial variations of the process variables may be ignored. By comparison, much less attention has been paid to the plug-flow

electrochemical reactor (PFER) model, in which "a flow of fluid passes, with no element overtaking nor mixing with that preceding or following it".[25] With respect to the electrochemical synthesis of metal-NHCs, operating under PFER conditions would be appropriate, as low reactor volumes are possible which maximise the electrode/solution interface, allowing a solution of imidazolium salt to act as both reagent feed and supporting electrolyte.

An oversimplified model may be derived to describe the performance of such a reactor, given a fixed input feed of electrolytic solution enters the reactor element of initial concentration C_{A0} and exits at equal flow-rate of concentration C_A (as shown in **Figure 2.1**).
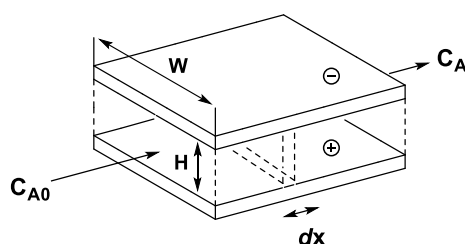
Figure 2.1 Parallel-plate electrochemical flow-reactor model.

The principle axis of the tubular reactor is linear (*x*-coordinate), with cross-sectional area (WH) and electrode area held constant. The fraction of the feed-rate with respect to reactor cross-section is equal to the feed-velocity, and the overall reactor performance may be evaluated based on registered current. The model is based on the primary assumption that electrolyte velocity, temperature and concentration possess a flat profile across the interelectrode distance (*i.e.* reactor channel), hence they vary only along the axial distance measured from the reactor entrance, and not along any direction transverse to this axis. The fluid flowing through the reactor may then be considered as a series of infinitely thin 'coherent plugs', each with uniform composition that differs from those before and after it.

Taking account of this model, an original reactor prototype was designed (**Figure 2.2**), comprising a linear PTFE flow-channel ($190.0 \times 4.0 \times 3.5$ mm, image **A**) which supports two monopolar copper electrodes ($190.0 \times 4.0 \times 0.5$ mm, image **B**) held at an interelectrodic separation of 2.5 mm, providing an overall void volume of 1.90 cm^3 and total electrode surface area of 15.2 cm^2. The electrodes are positioned with non-conducting rubber gaskets and encased by a pair of steel plates (image **C**). The inner portion of the finalised construct is given in image **D**.

A   **B**   **C**

D
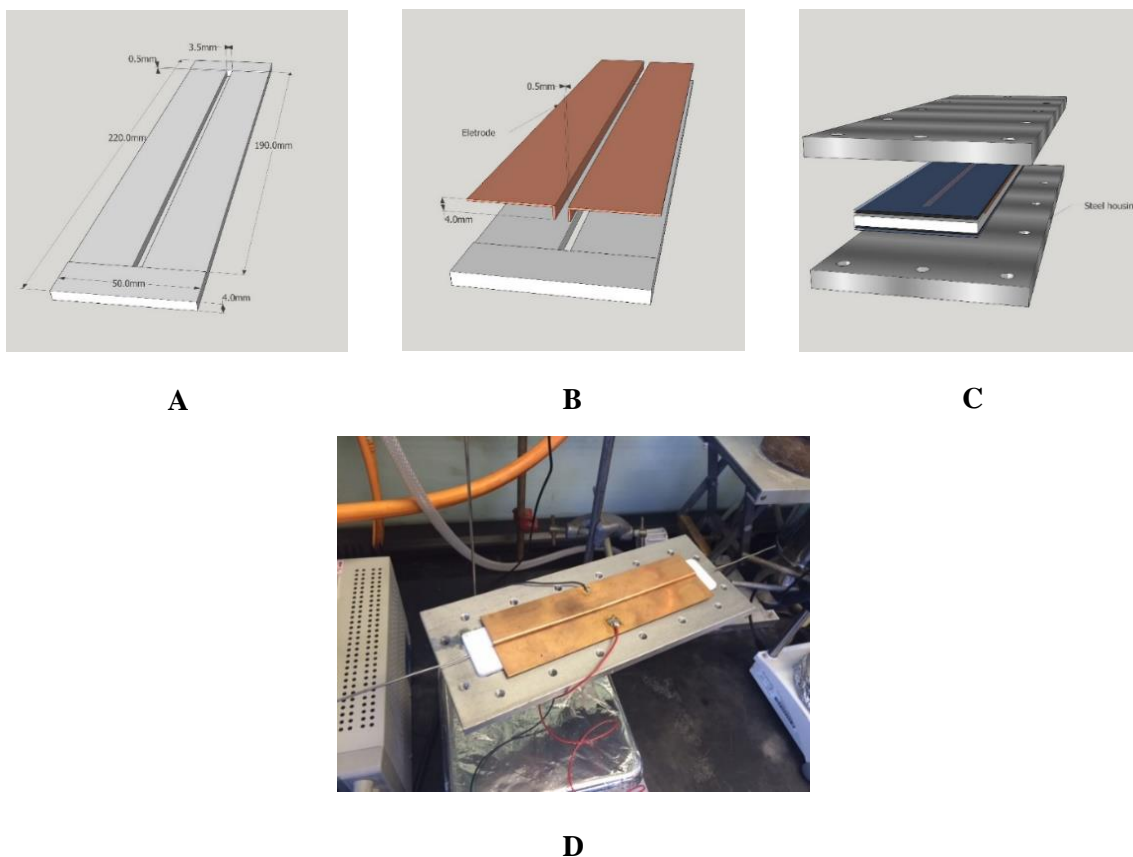
Figure 2.2 *'First-generation' electrochemical flow-reactor prototype. Images **A**, **B** and **C** are simulated.*

In order to establish an electrical potential between the two electrodes, an external power supply was connected to each copper plate *via* a positive and negative terminal, which were subsequently linked to an ammeter in-series.

2.2.2 Reaction optimisation studies

With the electrochemical flow-reactor in-hand, it was decided to optimise key process variables such as residence time and current density, by evaluating the cell efficiency over a range of applied potentials and volumetric flow-rates. For this purpose, a benchmark reaction was selected in which the ubiquitous imidazolium salt IMesH.Cl (**P2.1**) was employed to be converted to its corresponding copper(I) complex, IMesCuCl (**2.1**), as illustrated in **Scheme 2.1**. The suitability of the reaction was determined by the ability to prepare carbene precursor **P2.1** on a multigram scale by simple reaction of *N,N'*-dimesityl diazabutadiene and paraformaldehyde in the presence of acid,[26] with the corresponding copper(I) complex (**2.1**) known to be both bench-stable and diamagnetic, to enable reaction monitoring by NMR spectroscopy.[27]
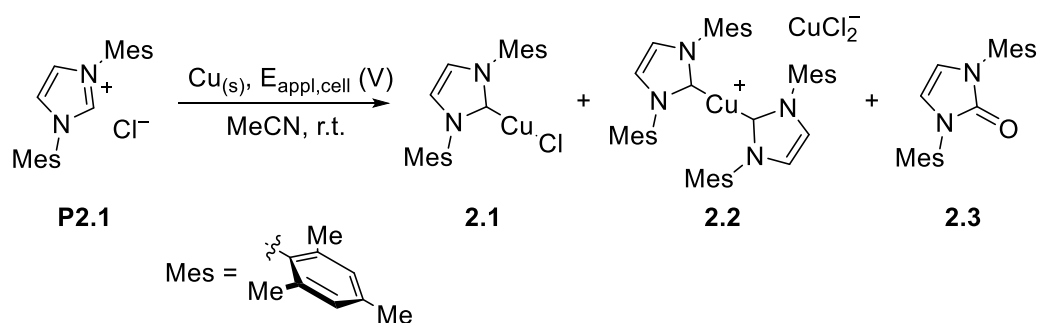
*Scheme 2.1 Benchmark synthesis of IMesCuCl (**2.1**) employed for optimisation study.*

To date, few studies have been reported on the electrochemical behaviour of azolium salts, with specific noteworthy examples from Pichon,[28] Clyburne,[29] Coughlin[30] and Sun.[31] More recently, a comprehensive list of the redox properties of a broad series of azolium ions was documented by Boydston and Ogawa, using cyclic voltammetry to record their half-wave potentials ($E_{1/2}$) in MeCN solvent (using an undivided cell composed of a glassy carbon working electrode, Pt basket counter electrode and a $Ag/AgNO_3$ reference electrode).[32] Whilst the series comprises several commonly used classes of azolium species for direct comparison, IMesH.Cl is not included. However, the formal reduction potential of the saturated analogue, SIMesH.Cl, is measured to be -2.4 V, with closely related structural analogue, IPrH.Cl, recorded at -2.23 V under the stated conditions.

In a similar manner, it was decided to employ cyclic voltammetry to measure the potentiometric work required to reduce IMesH.Cl to its corresponding free NHC. An undivided cell housing a Pt disk working electrode, inert Pt rod auxiliary electrode and a Ag/AgCl reference electrode were utilised, recording the measurement in anhydrous acetonitrile to mimic the reaction solvent. Under these conditions, and using the ferrocene/ferrocenium redox couple as an internal standard, the formal reduction potential of IMesH.Cl was observed at -2.32 V (for full experimental details, copies of cyclic voltammograms and data extrapolation, see Experimental).

A positive displacement pump capable of recirculating the reaction mixture was connected to the input feed (containing a 6.6 mM solution of **P2.1** in anhydrous, degassed MeCN) and reactor inlet, with a collection flask situated at the reactor outlet *via* transparent Teflon tubing ($^1/_8$" I.D.), as shown in **Figure 2.3**.
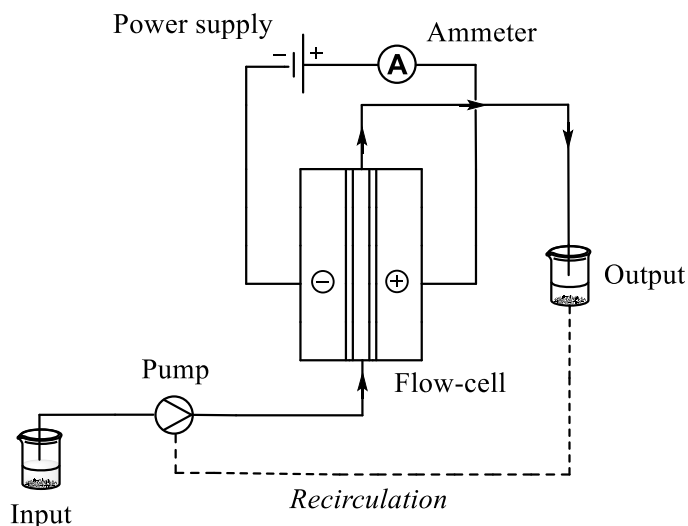
Figure 2.3 *Schematic of continuous configuration for the electrochemical synthesis of copper(I)-NHCs.*

Preliminary results involving flow of an MeCN solution of IMesH.Cl (**P2.1**) through the electrochemical reactor at a range of flow-rates and applied potentials indicated that a significant quantity of [Cu(IMes)$_2$][CuCl$_2$], **2.2**, was produced as a side-product (verified by ^{1}H NMR spectroscopy). It was deemed that the relatively large interelectrodic distance, alongside poor mixing of the *in situ* generated carbene with [Cu(NCMe)$_4$]$^+$, were the origin of low chemical selectivity. In an early report, Tarbell and Mehta have previously studied the effect of turbulent mixing on the selectivity of competing chemical reactions, with the authors underscoring the importance of high Reynolds numbers within microfluidic channels to generally minimise side-reactions.[33] Consequently, soda-lime glass beads (2.0 mm O.D.) were packed into the flow-channel in a staggered arrangement to reduce the effective volume of the reactor to 1.05 mL and subsequently increase flow-velocity (reactor volume calculations were performed through both a direct and indirect method, which provided strong agreement and are detailed in the Experimental). As a result, overall residence time associated with the reactor was reduced and formation of copper(I) *bis*-NHC **2.2** was completely supressed. All subsequent data using this prototypical reactor were recorded with the use of glass beads.

A stock solution of **P2.1** (6.6 mM) in anhydrous MeCN was prepared and pumped through the flow-reactor in a single pass at a range of flow-rates, whilst systematically subject to varying applied potential. The resulting output phase for each condition was collected and solvent removed *in vacuo* to deliver crude reaction mixtures, which were directly analysed by ^{1}H NMR spectroscopy (summarised in **Table 2.1**).

Entry	Flow-rate (mLmin^{-1})	τ_r (min)	$E_{appl,}$ (V)	Current (mA)^a	Current density (mAcm^{-2})	Conversion (P2.1:2.1)^b
1	0.50	2.10	1.50	0.82	0.11	82:18
2	0.50	2.10	2.00	1.27	0.17	70:30
3	0.50	2.10	2.50	2.70	0.36	64:36
4	0.75	1.40	1.50	0.92	0.12	90:10
5	0.75	1.40	2.00	1.31	0.17	77:23
6	0.75	1.40	1.50	2.81	0.37	70:30
7	1.00	1.05	1.50	1.01	0.13	93:7
8	1.00	1.05	2.00	1.47	0.19	79:21
9	1.00	1.05	2.50	2.90	0.38	73:27
10^c	0.50	2.10	2.50	7.15	0.94	75:25

Table 2.1 *Conversion ratio of **P2.1:2.1** at variable flow-rates/applied electrical potential.* *^{a}Registered at steady-state, ^{b}determined by ^{1}H NMR spectroscopy, ^{c}[**P2.1**] = 33.0 mM. Average reactor residence time is represented by τ_r.*

Of the conditions outlined, a residence time of 2.1 minutes and an applied electrical potential of 2.50 V (entry 3) provided topmost conversion of **P2.1** in a single pass (forming **2.1** in 36 %). It was found that applying a cell potential $\geq$ 3.0 V led to formation of an insoluble Cu-containing species (unidentified green precipitate) which caused reactor blockage. Comparably, increasing residence time above 2.10 minutes was avoided, as the required low flow-rates were anticipated to lead to poor mixing within the flow-channel (*i.e.* negating the effect of glass beads).

The coulombic efficiency of the flow-cell can be estimated from the theoretical amount of charge (Q) required to reduce 36 % of a 6.6 mM solution of **P2.1**, evaluated against the observed quantity of charge passed through the cell (which may be indirectly calculated from the steady-state current value over a fixed residence time). Under the 'optimum' conditions (*i.e.* entry 3), the coulombic efficiency of the flow-cell reaches 67 %, demonstrating a notable improvement on the original batch-cell (*ca.* 50 %).[34] However, a five-fold increase in concentration of **P2.1** (33.0 mM stock reagent feed, entry 10) provided a decrease in overall conversion (forming **2.1** in 25 %), indicative of a mass transfer-limited regime.

Despite low yielding in the first instance, recirculation of the reactor output phase containing a mixture of IMesH.Cl **P2.1** and IMesCuCl **2.1** through the cell allowed further consumption of imidazolium over time. Under these conditions, electrolytic recirculation of a 6.6 mM solution (20 cm^3, 0.132 mmol) of **P2.1** allowed full conversion to deliver complex **2.1** in 92 % yield after 80 minutes process time (a graphical representation is provided in **Figure 2.4**).
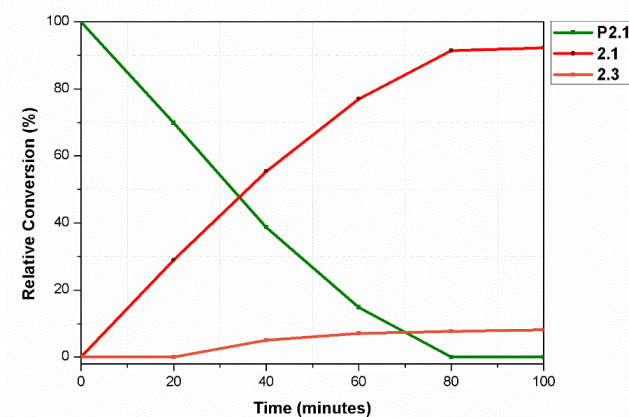
Figure 2.4 *Conversion versus time plot for the formation of IMesCuCl (**2.1**, red trace) from parent imidazolium precursor IMesH.Cl (**P2.1**, green trace), under recirculatory conditions. Relative product distribution measured by ^{1}H NMR spectroscopy, with imidazolinone side-product (**2.3**) represented by an orange trace.*

In addition to copper(I)-NHC **2.1**, ^{1}H NMR spectroscopy highlighted formation and accumulation of a related species over time, which was separated from the crude reaction mixture and confirmed to be **2.3** (8 % yield, see **Scheme 2.1**). It is well-reported that free NHCs are able to react with molecular oxygen, terminating in imidazolinones of the type **2.3**.[35] Presumably, this side-product is observed as a consequence of air being introduced into the reactor channel during recirculation, and is not a result of poor chemical selectivity.

2.2.3   Down-stream copper(I)-NHC catalysed hydrosilylation reactions

The reduction of carbonyl bonds to their corresponding alcohol functionality by hydride transfer is a fundamental and widely used transformation in organic synthesis.[36–42] Transition-metal catalysis has been successfully employed to effect the reduction of carbonyl compounds *via* hydrogenation or hydrosilylation, with the former often proceeding in good yield when under the caveat of high pressure or elevated temperature. By comparison, the 'softer' reaction conditions of hydrosilylation generally allow for good functional group tolerance, alongside a reduction/protection sequence which occurs in a single, atom-efficient step.

Nagai and Kagan independently reported the first Rh-based catalytic hydrosilylation systems in the early 1970's,[43,44] and since there have been numerous publications involving other precious metals (*e.g.* Re, Ru, and Ir) which are able to catalyse this transformation.[45–49] Over the last two decades however, efforts have been aimed toward finding alternative, efficient systems which centre around less expensive and abundant metals such as Ti,[50] Fe,[51] Mn[52] and Zn.[53] Brunner and Miehling first described a highly active copper diphosphine catalyst in 1984 which is able to catalyse the hydrosilylation of acetophenone with modest enantioselectivity (up to 100 % conversion, 39 % *e.e.*), with the active species postulated to be a Cu^I-hydride.[54]

38

Lipshutz and co-workers have previously described the formation of a CuH species in a system combining a catalytic quantity of CuCl/NaO^{t}Bu/diphosphine with a stoichiometric amount of hydrosilylating agent,[55] with Riant and Carreira independently reporting CuF$_2$ to also act as a useful precursor to CuH.[56,57]

Copper-NHCs have been exposed as interesting alternatives to copper diphosphines in the catalytic hydrosilylation of carbonyl compounds. It is generally accepted that the strong electron-donating properties of the NHC ligand leads to more robust metal-ligand bonding, with superior steric protection of the metal active site from each exocyclic *N*-substituent to act as a more effective 'shield' than even a tertiary phosphine ligand. With this in mind, Nolan and colleagues have previously illustrated that IPrCuCl (IPr = *N,N'-bis*(2,6-diisopropylphenyl)imidazol-2-ylidene), ICyCuCl (ICy = *N,N'-bis*(cyclohexyl)imidazol-2-ylidene) and IMesCuCl (**2.2**) are highly efficient copper(I)-NHC catalysts for the hydrosilylation of functionalised ketones.[58] The authors underline that these well-defined complexes perform the reaction with higher activity than their *in situ*-generated versions, though purification steps are required to isolate the well-defined derivatives from their original copper source (*i.e.* Cu^I-halide).

It was speculated that our electrochemical flow-reactor may complement this reaction system, insofar as providing the capability to dispense small quantities of well-defined, high-purity copper(I)-NHC catalyst without requirement for work-up, isolation and purification. Longstreet and McQuade have previously demonstrated the use of an insoluble Cu$_2$O packed-bed reactor for the generation of soluble copper(I)-NHCs, and their subsequent down-stream deployment in the *β*-borylation of ethyl crotonate.[15] However, high temperatures are required to synthesise the original copper(I)-NHC catalysts, eventually leading to leaching of Cu$_2$O to potentially pollute the effluent stream. As our electrochemical approach is only able to produce Cu$^+$ ions and carbenes in a precise stoichiometric ratio, metal leaching is not foreseen to be feasible.

Therein, it was decided to compare the catalytic performance of electrochemically-derived IMesCuCl (**P2.1**) with that of its purified analogue, in the hydrosilylation of sterically diverse ketones (**Scheme 2.2**). A freshly prepared solution of **P2.1** (0.13 mmol in 20 mL MeCN) was recirculated continuously through the flow-reactor at 0.50 mLmin^{-1} under a fixed applied potential of 2.50 V (i_{init} = 3.00 mA, at steady-state), at room temperature for 80 minutes (giving an average residence time of 252 seconds per reactor volume). Following, an aliquot of the solution (5.0 mL, 0.03 mmol) was dispensed directly into a pre-formed hydrosilylation mixture (the results of which are summarised in **Table 2.2**).

$$\underset{R\quad R'}{\overset{O}{\|}} \xrightarrow[\substack{NaO^tBu\ (20\ mol\%)\\PhMe,\ 80\ °C}]{\substack{\textbf{2.1}\ (3\ mol\%)\\HSiEt_3\ (5\ equiv.)}} \underset{R\quad R'}{\overset{O^{-SiEt_3}}{\|}}$$
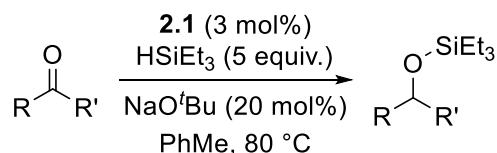
Scheme 2.2 General hydrosilylation reaction catalysed by 2.1.

Entry	R	R'	Time (h)[a]	Yield (%)[a,b]	Time (h)[c]	Yield (%)[b,c]
1	cyclohexyl	cyclohexyl	2	97	2	98
2	2-furyl	methyl	6	95	6	94
3	2-thiophenyl	methyl	6	97	6	97
4	2-pyridyl	methyl	6	94	6.5	90
5	2-chlorophenyl	methyl	5	97	6	98

Table 2.2 *Evaluation of IMesCuCl (**2.1**) in catalytic hydrosilylation of ketones. Conditions: ketone substrate (1.0 mmol), triethylsilane (5.07 mmol), NaO^tBu (0.20 mmol), anhydrous toluene (10 mL). [a]Using **2.1** from electrochemical flow-reactor in MeCN (5.0 mL, 0.03 mmol aliquot), [b]isolated yield, [c]using isolated and purified **2.1** (3 mol%).*

The reactions were monitored by ^{1}H NMR spectroscopy, as each features a diagnostic signal between 5.22 – 3.14 ppm (300 MHz, CDCl$_3$, 298K), corroborating with the instalment of a proton adjacent to the silyl enol group (*H*COSi). Near-quantitative isolated yields, comparable to those reported by Nolan using pure IMesCuCl were achieved.[58] To confirm these findings, identical reaction conditions using electrogenerated **2.1** were reproduced in our laboratory using isolated/purified **2.1**, to provide very similar yields (see **Table 2.2**, columns 5 and 6). It is noteworthy that transfer of **2.1** from the flow-reactor *via* MeCN is well-tolerated, as toluene provides good miscibility to give a monophasic reaction mixture. These results demonstrate the potential of the electrochemical flow-reactor to act as an 'on-demand dispenser' of high purity catalyst, directly into reaction media without additional purification steps.

2.3   Stacked-disk electrochemical copper flow-reactor

The philosophy of scaling-up a chemical process requires matching several 'similarity criteria', such as geometric, kinematic and thermal similarities between reactors. In the case of electrochemical reactors, an additional criterion is necessary to define scale-up which describes current and potential similarity. Typically, this provides difficulty in meeting geometric similarity as simply increasing the interelectrodic gap (*i.e.* larger flow-channels) generates a large ohmic drop to reduce overall cell-efficiency. However, this problem is usually tackled by using multiple cells and reactor units (*i.e.* reactor scale-out). Kinematic similarity is concerned with flow-velocities within a system. In any microfluidic device, Reynolds number (*i.e.* flow-regime)

generally governs pressure drop, fluid hold-up and mass transfer capacity, therefore it is desirable to maintain an optimum fluid flow-rate at all reactor scales. Lastly, it is important to consider total current density of the reactor *via* current/potential similarity. Upgrading this criterion is usually achieved by fixing a minimum distance between electrodes, and maximising interfacial area between electrolyte and electrode surface.

On account of our 'first generation' electrochemical flow-reactor prototype delivering a 20 % increase in coulombic efficiency compared with the original batch protocol, it was sought to construct a more versatile reactor which is able to further improve synthetic performance and remove obligation for reaction recycling.

2.3.1   Reactor design, construction and optimisation

The concept of a 'voltaic pile' was first introduced in 1800 by Alessandro Volta, which paved-the-way to a series of discoveries including electrical decomposition of H_2O to H_2 and O_2 (*i.e.* electrolysis), and subsequently the discovery or isolation of chemical elements (including Na, K, Ca, B, Ba, Sr and Mg) by Humphry Davy.[59] Since, the idea of assembling electrodes into a stacked array has been widely adopted in synthetic electrochemical reactors, as a means of maximising the electrode surface/electrolyte volume interface and extend overall current density. However, the notion of combining this reactor template with the 'dissolving electrode' model has not previously been considered. It was postulated that our continuous electrochemical procedure could be adapted into a parallel-plate design, whereby the metal ion source is now incorporated into a stack of electrodes separated by electrolytic solution.

A modular reactor was designed (**Figure 2.5**) comprising a sequence of six square copper plates ($50 \times 50 \times 1$ mm), separated by five PTFE spacers (1 mm thickness) which each house a winding flow-channel (4×200 mm, total volume per channel of 0.8 cm^3, images **A** and **B**). The electrodes alternate between anode and cathode to provide five consecutive parallel-plate electrochemical flow-reactors, with an overall void volume of 4.0 cm^3 and interfacial area of 80 cm^2. The whole assembly is positioned with a pair of steel plates (image **C**), and the final construct is presented in image **D**.

A

B

C

D
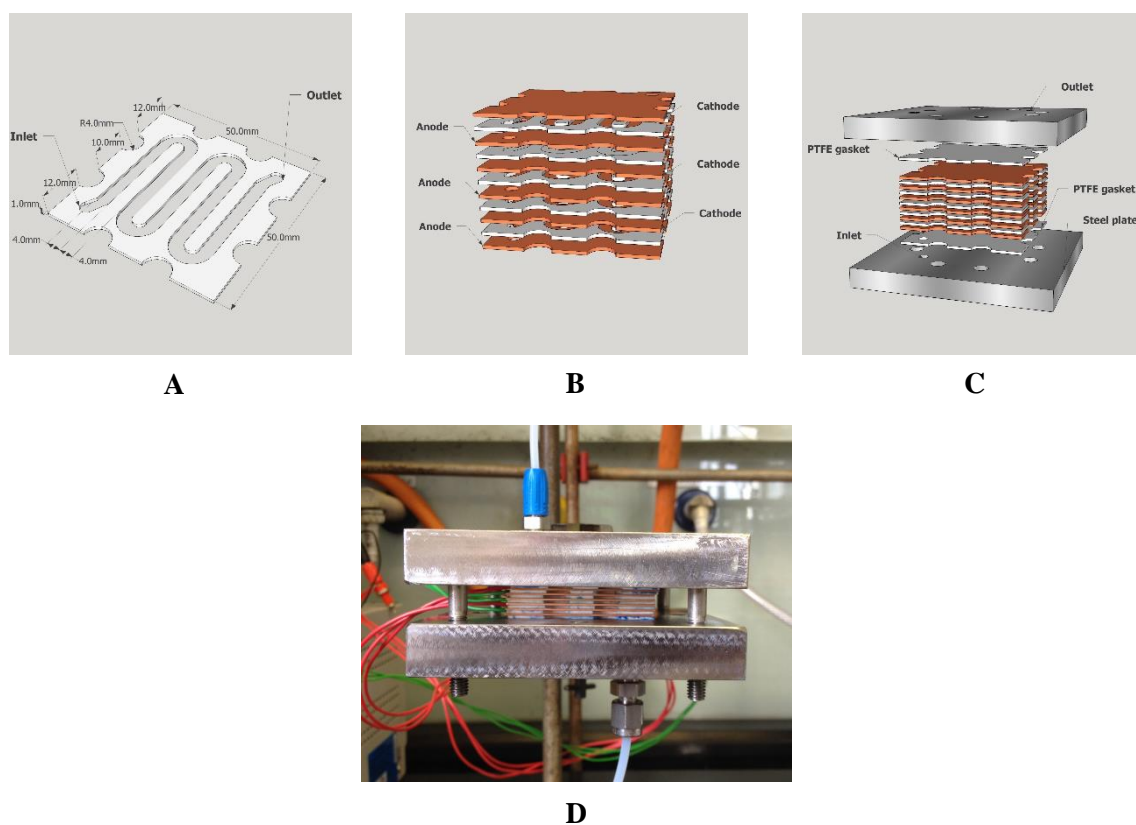
Figure 2.5 *Revised electrochemical flow-reactor. Images **A**, **B** and **C** are simulated.*

To assess the revised flow-reactor, a solution of IMesH.Cl **P2.1** (0.13 mmol in 20 mL MeCN) was electrochemically converted to IMesCuCl **2.1** (using a similar design-of-experiment as described in section **2.2.2**), the results of which are summarised in **Table 2.3**.

Entry	Flow-rate (mLmin^{-1})	τ_r (min)	E_{appl} (V)	Current (mA)[a]	Conversion (P2.1:2.1)[b]
1	0.67	6.0	1.37	1.79	80:20
2	0.67	6.0	1.70	5.89	37:63
3	0.67	6.0	1.94	10.00	3:97
4	1.00	4.0	1.16	2.01	84:16
5	1.00	4.0	1.30	2.88	74:26
6	1.00	4.0	1.59	6.13	51:49
7	1.00	4.0	1.88	10.00	23:77
8	1.33	3.0	1.10	2.20	85:15
9	1.33	3.0	1.24	3.21	78:22
10	1.33	3.0	1.41	6.33	59:41

Table 2.3 *Conversion ratio of **P2.1:2.1** at variable flow-rates/applied electrical potential.*
[a]Registered at steady-state, [b]determined by ^{1}H NMR spectroscopy. Average reactor residence time is represented by τ_r.

Experimental evaluation provided a clear improvement on both electrochemical output and product selectivity. It was found that applying a cell potential to maintain an observed current ≥ 11 mA (at any given flow-rate) precipitated significant quantities of insoluble (Cu-containing) byproducts, leading to reactor fouling. This problem could be suppressed by controlling cell potential to limit steady-state current to 10 mA. Under this condition, and applying a potential of 1.94 V with an average residence time of 6 minutes (entry 3), complex **2.1** was formed in 97 % yield in single-pass mode. Formation of imidazolinone **2.3** was reduced to 3 %, presumably due to an increased rate of formation of IMesCuCl (**2.1**) by shortening the diffusive path between electrodes. A comparison between the proton NMR spectra of authentic imidazolium salt **P2.1** with the crude output phase is given in **Figure 2.6**, following a simple evaporative work-up.
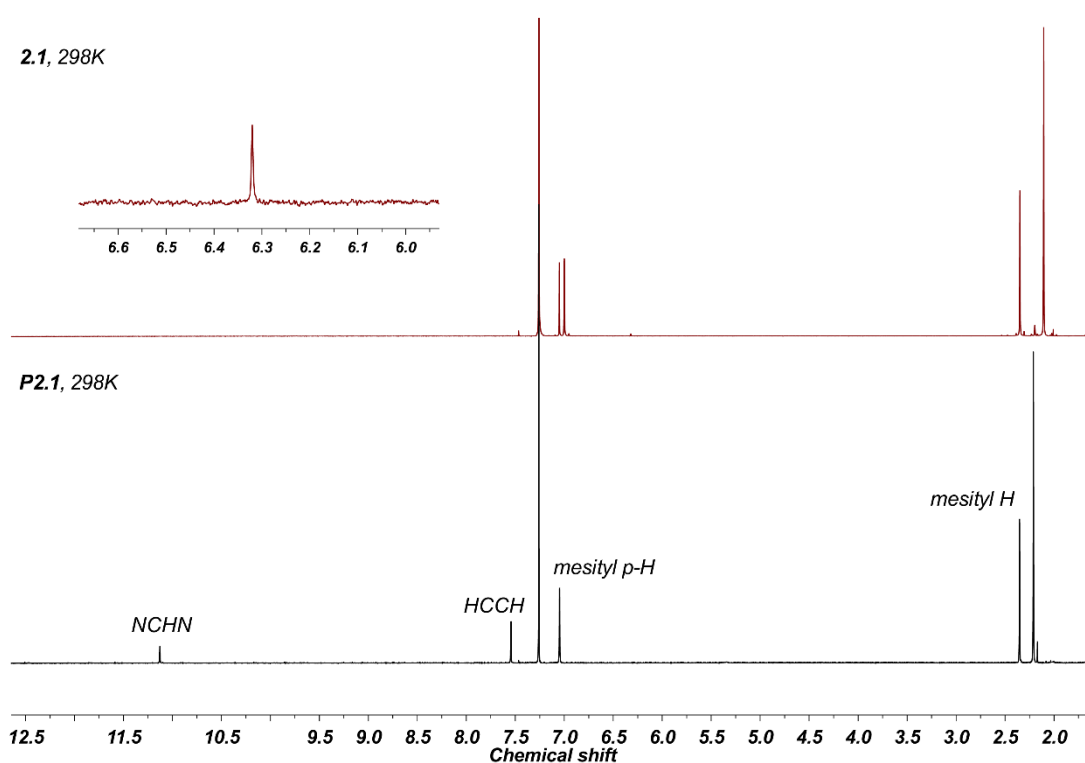
Figure 2.6 *^{1}H NMR spectrum of ligand precursor **P2.1** (black trace, 500 MHz, CDCl$_3$, 298K), noting original imidazolium NCHN singlet at 11.13 ppm. ^{1}H NMR spectrum of Cu-NHC **2.1** (red trace, 500 MHz, CDCl$_3$, 298K), following evaporation of reaction solvent. Inset: diagnostic singlet (6.32 ppm) of imidazolinone side-product **2.3** (3 %, relative).*

The overall time to convert 0.13 mmol of IMesH.Cl **P2.1** to complex **2.1** was reduced to 29.9 minutes (20 mL, 0.67 mLmin^{-1}, single pass). Under these conditions, it is possible to produce 100 mg of IMesCuCl per hour (which may be extrapolated to 0.91 kgy^{-1}), with theoretical calculations suggesting anode replacement to take place after 89 days continuous processing (5×0.8 cm^2 anodic surfaces, 1 mm thickness, providing 35.8 g Cu to be liberated at 298 K). From an engineering perspective, upscaling this process could be performed simply through (i) increasing channel dimensions in accordance with reactor-stack (*i.e.* reactor volume),

and (ii) scaling out *via* numerous identical reactors. A direct comparison between the performance of each flow-reactor described within is summarised in **Table 2.4**.

	Prototypical flow-reactor	Stacked-disk flow-reactor
Single electrode surface (cm^2)	7.6	40
Interelectrodic distance (mm)	2.5	1.0
Applied potential (V)	2.50	1.94
Observed current (mA)^a	2.7	10.0
Residence time (s)	126	360
Time to process 0.13 mmol of **P2.1** to **2.1** (min)	80.0 (92 %)^b	29.9 (97 %)^c

Table 2.4 *Comparison between the electrochemical synthesis of IMesCuCl (**2.1**) using first- and second-generation flow-reactors. ^{a}Registered at steady-state, ^{b}in recirculation mode, ^{c}in single pass mode.*

2.3.2 Complex scope

Not only does the low applied potential (1.94 V *versus* 2.50 V from the original cell prototype) used in the optimised conditions (**Table 2.3**, entry 3) highlight the improved Faradaic efficiency of the flow-reactor (with a voltaic efficiency of 93 %), it also represents a capacity to selectively form desired metal complexes in the presence of redox sensitive functional groups. It was next decided to examine the versatility of the optimised flow-reactor by synthesising a range of copper(I)-NHC complexes from various imidazolium salts, using a single reactor assembly (**Scheme 2.3**). In particular, complexes comprising base-sensitive ligand substituents were targeted, including examples which proved challenging under electrochemical batch conditions (**Table 2.5**).
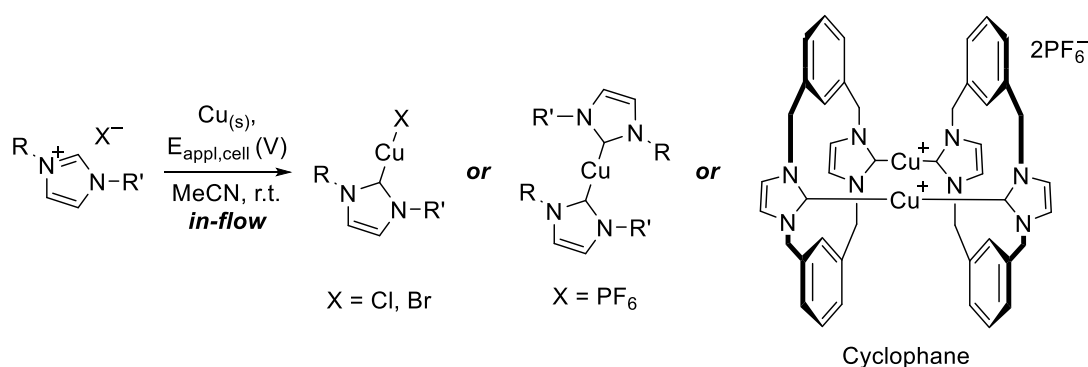
Scheme 2.3 *General synthesis of various copper(I)-NHC complexes under continuous electrochemical conditions.*

Entry	Complex (precursor)	R	R'	X⁻	E_{appl} (V)	I (mA)[c]	τ_P (min)[d]	Yield (%)[e]
1	**2.1 (P2.1)**	mesityl[a]	mesityl	Cl	1.94	10.0	29.9	94
2	**2.4 (P2.2)**	mesityl[a]	mesityl	PF_6	2.54	20.1	20.0	93
3	**2.5 (P2.3)**	picolyl[a]	allyl	Br	2.20	19.3	6.7	91
4	**2.6 (P2.4)**	methyl[a]	$CH_2CO_2{}^tBu$	Cl	2.40	31.0	13.3	95
5	**2.7 (P2.5)**	benzyl[a]	benzyl	PF_6	2.95	28.7	20.0	94
6	**2.8 (P2.6)**	cyclophanyl[b]		PF_6	4.90	74.4	300	95

Table 2.5 *Scope of Cu^I-NHC complexes prepared under continuous electrochemical conditions, using the stacked-disk flow-reactor. [a]In single pass mode, [b]in recirculation mode, [c]registered at steady-state, [d]process time required to convert 0.13 mmoles imidazolium precursor (6.6 mM), [e]determined by ¹H NMR spectroscopy.*

Ionic solutions of imidazolium cations associated with weakly coordinating counteranions (*e.g.* BF_4, PF_6, SbF_6) have been shown to provide poor conductivity when subject to an applied potential.[34] As our electrochemical method relies on the imidazolium salt solution to play the role as both reagent and electrolyte, a poorly conducting ionic solution can lead to extensive residence times under batch conditions (*i.e.* hours or even days), to achieve acceptable conversion to desired product.

From the outset, the hexafluorophosphate congener of complex **2.1** was targeted (entry 1), [(IMes)₂Cu⁺][PF_6^-] (**2.4**), from precursor IMesH.PF_6 (**P2.2**). Applying a potential of 2.54 V generated a steady-state current of 20.1 mA at room temperature – a notable improvement on batch mode (35 V applied to generate 100 mA).[34] Under this condition, an optimised residence time was found to be 240 seconds to deliver the homoleptic copper(I) *bis*-NHC complex (**2.4**) in 93 % yield (maximum yield in batch mode = 74 %, τ_r = 220 minutes). Based on relative conversion, the production of **2.4** using the continuous electrochemical protocol reaches a Faradaic efficiency of 52 %, compared with previous batch synthesis unable to surpass 7 %.

Selective metalation of imidazolium ions at the C2 ring-position whilst in the presence of base-sensitive *N*-substituents remains a challenge, as discussed within Chapter 1 of this thesis. In particular, flexible picolyl *N*-donors are useful groups to incorporate within this template, as their ability to coordinate to a metal centre may provide a complex with additional stability. In our laboratory, the adjacent methylenic-bridge between these groups has demonstrated susceptibility to deprotonation, and therefore selective chemical synthesis of copper-NHCs containing this fragment can be problematic. Therefore, *N*-picolyl, *N'*-allyl substituted imidazolium bromide precursor (**P2.3**) was prepared and the selective electrochemical synthesis of its corresponding copper(I)-NHC complex (**2.5**) optimised using the flow-reactor (entry 2). Under an applied

potential of 2.20 V with an average residence time of 80 seconds, complex **2.5** was produced in 91 % yield (mass production rate of 1.83 gh^{-1}), with full selectivity to coordinate at the C2 ring position. The product was analysed and confirmed by multinuclear NMR spectroscopy, with the electrospray mass spectrum featuring a dominant mass peak (*m/z*) 262.0397, attributable to an [M – Br]$^{+}$ molecular fragment.

Along a similar vein, selective C2-complexation of *N*-ester substituted imidazolium salts is difficult to achieve under traditional chemical conditions (*i.e.* basic). The pK_a value of a methylene group directly attached to an ester is typically quoted between 23 – 25,[60] which is estimated to be even lower when jointly connected to a nitrogen atom (*i.e.* imidazole), bringing the acidity of this position within a similar range to that of the imidazolium C2 proton (pK_a estimated around 19 – 21).[61] As a result, few copper-NHC complexes are known which comprise *N*-ester functionality.[34] Flowing a freshly prepared solution of *N*-methyl, *N'*-*tert*-butylacetate substituted imidazolium chloride (**P2.4**) through the electrochemical reactor at 1.5 mLmin^{-1} (average residence time = 160 seconds), whilst subject to an applied potential of 2.40 V (generating 31.0 mA current) delivered the corresponding C2 metalated [(NHC)CuCl]-type complex (**2.6**) in 95 % yield (entry 3). A comparison between the proton NMR spectra of authentic imidazolium precursor **P2.4** with the reactor output phase containing **2.6** is given in **Figure 2.7**, following an evaporative work-up under an inert atmosphere.
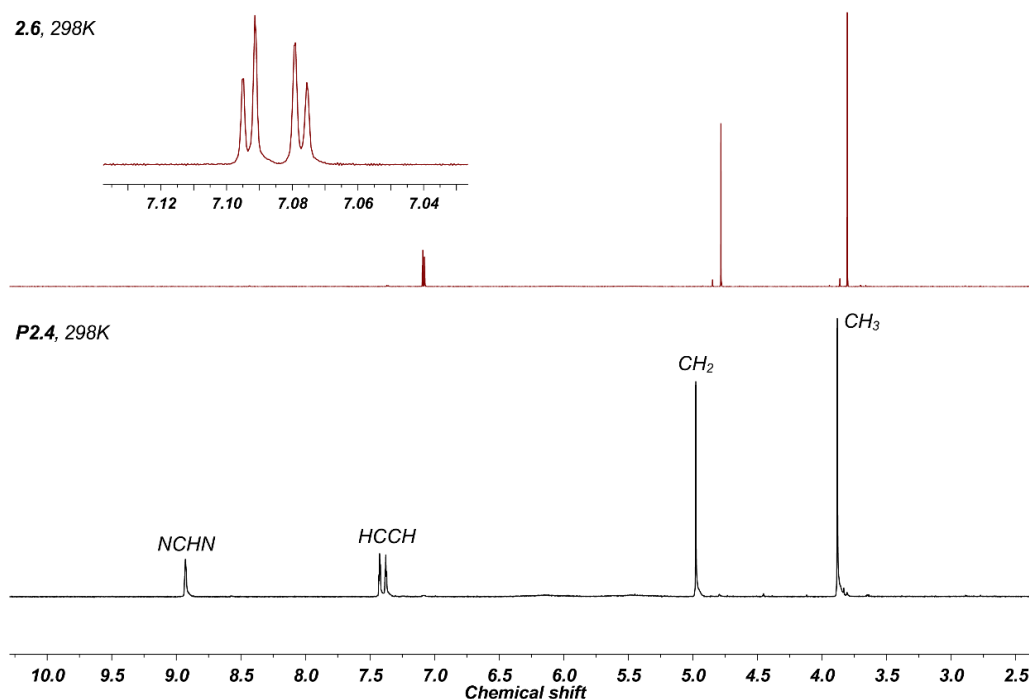
Figure 2.7 *^{1}H NMR spectrum of ligand precursor **P2.4** (black trace, 300 MHz, CD$_3$CN, 298K), noting original imidazolium NCHN singlet at 8.93 ppm. ^{1}H NMR spectrum of Cu-NHC **2.6** (red trace, 500 MHz, CD$_3$CN, 298K), following evaporation of reaction solvent (signal attributed to ^{t}Bu omitted for clarity). Inset: magnified spectrum of **2.6** (7.13 – 7.03 ppm region), highlighting two magnetically inequivalent NHC backbone doublet resonances.*

Employment of a weakly conducting solution containing *N,N'-bis*-benzyl substituted imidazolium hexafluorophosphate (**P2.5**), subject to an applied potential of 2.95 V for an average residence time of 4.0 minutes (flow-rate = 1.0 mLmin^{-1}) produced copper(I) *bis*-NHC complex **2.7** in 94 % yield (**Table 2.5**, entry 5).

Perhaps the most challenging example of copper-NHC complex formation under electrochemical batch conditions, is formation of dinuclear cyclophanyl copper(I) *bis*-NHC complex, **2.8**. In our hands, treatment of a 67 mM solution of macrocyclic *bis*-imidazolium hexafluorophosphate (**P2.6**) with an applied potential of 35 V generated a modest current amplitude of 10 mA in batch mode.[34] Limited by poor conductivity, a residence time of 15 hours was required to achieve 72 % yield of the desired complex, pertaining to 74 % of passing current wasted. Under the optimised electrochemical flow conditions, an applied potential of 4.90 V generates 74.4 mA current using a ten-fold more dilute solution of **P2.6** (6.6 mM sample), representing a significant improvement on batch. Recirculation of 20 mL of this solution for a total process time of 300 minutes (flow-rate = 1.0 mLmin^{-1}, 75 reactor volumes processed) provided access to **2.8** in 95 % yield, further underlining improved cell-efficiency. Notable, were the presence of two diastereotopic doublet resonances in the solution ^{1}H NMR spectrum of the product, characteristic of protons linked to each methylene bridging unit of the Cu$_2$L$_2$ cyclophanyl complex (see **Figure 2.8** for associated ^{1}H NMR spectra).
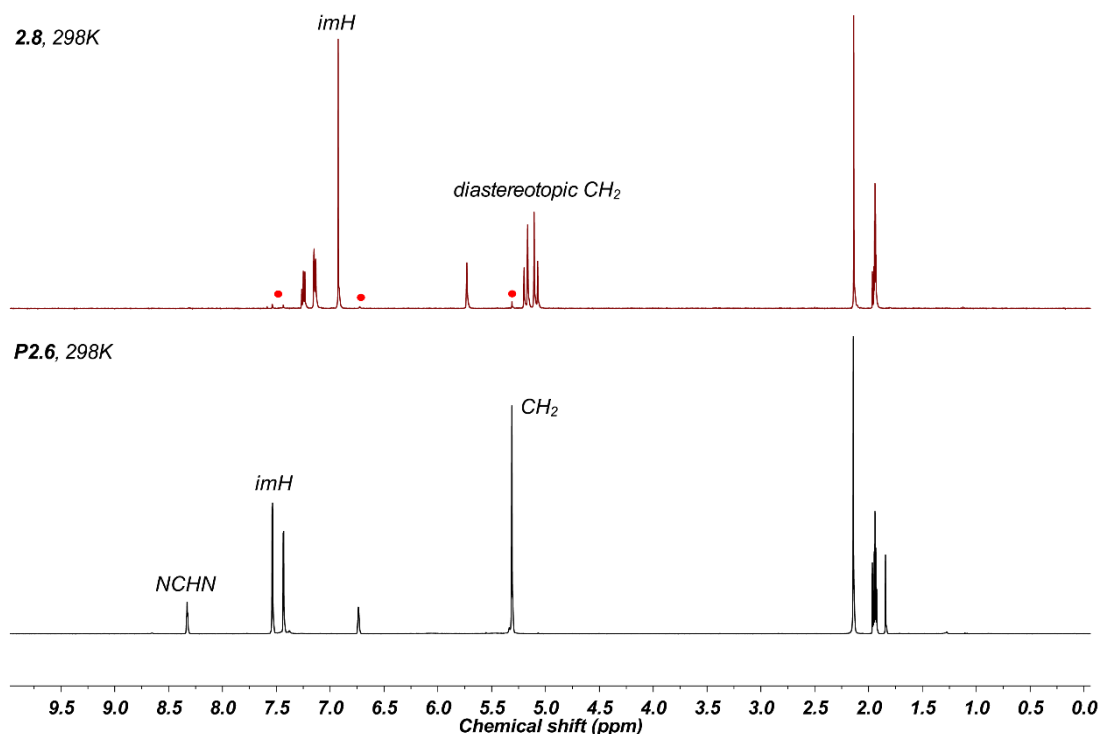
Figure 2.8 *^{1}H NMR spectrum of ligand precursor **P2.6** (black trace, 300 MHz, CD$_3$CN, 298K), noting original imidazolium NCHN singlet at 8.31 ppm. ^{1}H NMR spectrum of Cu$_2$L$_2$ complex **2.8** (red trace, 500 MHz, CD$_3$CN, 298K), following evaporation of reaction solvent. Red circles indicate unreacted starting material (5 % relative to product).*

2.4 Conclusions and future work

Although numerous methods exist for the synthesis of copper-NHC complexes, many employ strongly basic reaction conditions which narrow the scope of functionality built within the ligand scaffold. Likewise, these routes often accumulate stoichiometric quantities of metal-containing byproducts, reducing atom economy which cannot be sensibly managed on a multigram scale. An electrochemical protocol was developed under batch conditions, which is able to selectively produce copper(I)-NHC complexes under neutral and ambient conditions in good yield. Importantly, the procedure does not require external reagents and is able to utilise an imidazolium salt solution as both feedstock and electrolyte, providing a highly atom efficient route to metal complexes which is scalable.

This chapter discusses the design, construction and optimisation of two simple and effective electrochemical flow-reactors, capable of selectively synthesising copper(I)-NHC complexes under mild reaction conditions. As far as the author is aware, these reactors are the first of their type to combine the classical pure plug-flow reactor system (PFR) with the 'dissolving electrode' model. By translating the original protocol into continuous-flow, key reactor metrics may be optimised, such as (i) solid/solution interfacial area, (ii) interelectrodic distance, (iii) reactor mixing and (iv) current density. In doing so, the synthetic step can be condensed into a much lower residence time, and require an applied potential much closer to the measured reduction potential of the original carbene source. It is envisaged that under the optimised continuous conditions outlined within this chapter, a range of synthetically useful copper-NHC complexes may be prepared on a multigram scale following a trivial evaporative work-up procedure.

Not only is this strategy useful to produce gram quantities of complex for storage, but equally enables the generation of precise amounts of catalyst to be directly dispensed into reaction media, without isolation or further purification steps. The direct application of high purity copper(I)-NHC into the hydrosilylation of various ketones showed virtually no difference in catalytic activity when compared with its isolated version. The ability to not only bypass handling of free carbene, but also precise quantities of sensitive complexes themselves, poses numerous advantages when considering employment of those compounds in rapid catalytic screening, for example.

Finally, the synthetic utility of the continuous flow-cell was demonstrated through the preparation of various copper(I) *mono-* and *bis*-NHC complexes, each in high yield (> 90 %). Of note are examples comprising base-sensitive ligand *N*-substituents (*e.g.* benzylic, allylic, picolylic and acetyl), which are fully tolerated under the neutral reaction conditions. To the author's knowledge, this work represents the only example of synthesising metal-NHC complexes in continuous-flow

whereby reactor bed leaching is not a possibility, as non-stoichiometric metal liberation is forbidden (*i.e.* conservation of electroneutrality).

Future work is to be focussed towards use of alternative, cheap and abundant anodic metal sources, such as Fe, Co and Ni. Where the method has a significant edge on those pre-existing, is in formation of metal-NHCs composed of potentially reactive functionality (*e.g.* alcohols and amines). Tolerance of these groups may allow access to complexes of ligands with significant bifunctional character, which should be explored.

As a long-term goal, it could be envisaged that continuous reactors of this type may provide some solution to energy harvesting from renewable sources. For example, the ability to power a wide array of these reactors (*i.e.* generate electricity) from solar or wind energy, to ultimately capture this energy in the form of large quantities of high-value organometallic compounds may be viewed as an effective 'battery' for further chemical deployment.

2.5   Experimental

Where stated, manipulations were performed under an atmosphere of dry nitrogen by means of standard Schlenk line or glovebox techniques. Anhydrous solvents were prepared by passing the solvent over activated alumina to remove water, copper catalyst to remove oxygen and molecular sieves to remove any remaining water, *via* the Dow-Grubbs solvent system. Deuterated CD_3CN, $CDCl_3$ and $(CD_3)_2SO$ were dried over CaH_2, cannula filtered or distilled, and then freeze-pump-thaw degassed prior to use. All other chemicals were obtained from commercial sources and used as received. Cu foil (99.9 % purity) was used as electrode surface directly without further purification (purchased from Goodfellow Cambridge Ltd).

2.5.1   Instrumentation

^1H and ^{13}C NMR spectra were recorded by automated procedures on either a Bruker Avance (500/125 MHz) or DPX (300/75 MHz) NMR spectrometer, using the residual solvent as an internal standard. The values of chemical shift are reported in parts per million (ppm) with the multiplicities of the spectra assigned as follows: singlet (s), doublet (d), triplet (t), quartet (q), multiplet (m) and broad (br), values for coupling constants (*J*) are assigned in Hz. High-resolution electrospray mass spectra (ESI-MS) were measured on an open-access Bruker Daltonics (micro TOF) instrument operating in the electrospray mode. Samples for microanalysis were dried under vacuum prior to analysis and the elemental composition determined by Ms. Tanya Marinko-Covell of the University of Leeds Microanalytical Service using a Carlo Erba elemental analyser MOD 1106 spectrometer.

Electrochemical measurements were conducted using an Autolab PGSTAT20 voltammetric analyser under an argon atmosphere, solvated in pre-dried CH_3CN containing 0.10 M [$^nBu_4N$]BF_4 as supporting electrolyte. Voltammetric experiments utilised a Pt disk working electrode, a Pt rod auxiliary electrode and a Ag/AgCl reference electrode. All potentials quoted are referenced to an internal ferrocene/ferrocenium standard.

The original reactor prototype was designed in collaboration with Professor Frans Muller of the University of Leeds, School of Chemical and Process Engineering, and constructed by Mr Matthew Broadbent of the University of Leeds, mechanical workshop. The 'second-generation' reactor was designed and constructed in collaboration with Professor Nikil Kapur of the University of Leeds, School of Mechanical Engineering. Where stated, a recirculation sample-loop was fitted to these reactors using a Global FIA (milliGAT), self-priming positive displacement recirculation pump, operated by an external laptop computer. Calculated reactor images depicted within this chapter were simulated using the software package 'SketchUp'. A PSD 30/3B high performance digital power supply was used as potential source (CV mode), with current measurements recorded using a 15XP-B Amprobe digital multimeter, at a milliampere scale.

2.5.2 Preparation of imidazolium salt precursors

Synthesis of 1,3-*bis*(2,4,6-trimethylphenyl)imidazolium chloride (P2.1). A round-bottomed flask equipped with magnetic stir bar was charged with *N,N'*-dimesityl-1,4-diaza-1,3-butadiene (2.00 g, 6.84 mmol) and ethyl acetate (25 mL), and the mixture cooled to 0 ˚C. A separate solution of paraformaldehyde (0.27 g, 8.90 mmol) dissolved in hydrochloric acid (2.80 mL of a 4M solution in dioxane) was added dropwise over *ca.* 15 minutes, and the mixture allowed to stir at room temperature for a further 16 hours. The crude solid was collected by vacuum filtration and washed with cold ethyl acetate (3×20 mL). Recrystallisation from acetone/pentane afforded the title compound as a microcrystalline colourless solid. Yield: 1.57 g, 4.60 mmol, 67 %. Mp decomp. at >350 ˚C. ^{1}H NMR (300 MHz, CDCl$_3$) δ (ppm) 11.07 (br s, 1H, NC*H*N), 7.55 (s, 2H, im*H*), 7.05 (s, 4H, mesityl *m*-C*H*), 2.35 (s, 6H, mesityl *p*-CH_3), 2.21 (s, 12H, mesityl *o*-CH_3). ^{13}C{^{1}H} NMR (75 MHz, CDCl$_3$) δ (ppm) 141.1, 139.6, 134.2, 130.5, 129.8, 124.0, 21.1, 17.8. HR-MS (ESI$^+$) *m/z* 305.2028 [$C_{21}H_{25}N_2$]$^+$, calcd. [M − Cl]$^+$ 305.2012. All data are consistent with the literature.[62]

Figure 2.9 (see below) illustrates a full-sweep cyclic voltammogram of **P2.1**, with supplementary discussion provided below. All potentials quoted are referenced to an internal ferrocene/ferrocenium standard and were obtained at a scan rate (*v*) of 300 mVs^{-1}.

The ferrocene/ferrocenium couple under these conditions was observed at $+0.44 \leq E_{1/2} \leq 0.58$ V *vs* Ag/AgCl, providing an observed reduction potential of **P2.1** at -2.32 V (*vs* Fc/Fc$^+$).
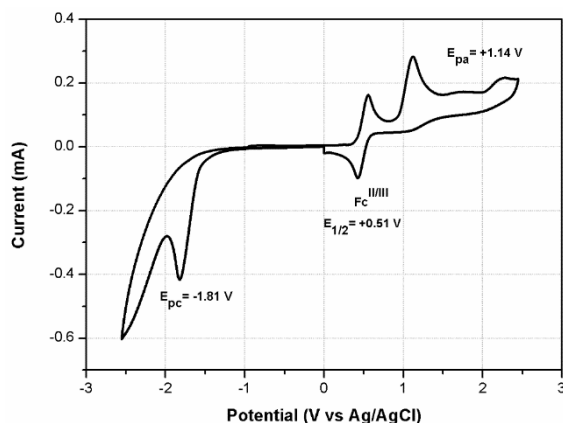
Figure 2.9 *Cyclic voltammogram of IMesH.Cl **P2.1** (1.0 mM) in non-aqueous media (CH$_3$CN/[^{n}Bu$_4$N]BF$_4$ 0.10 M), v = 300 mVs^{-1}, T = 298 K, [Fc] = 1.0 mM, E$_{pa}$ ascribed to counteranion oxidation band.*

The voltammogram features an irreversible reduction wave upon scanning toward an initial cathodic vertex at -1.81 V, corresponding to imidazolium reduction. The kinetic region associated with the cathodic peak is relatively small, implying a short-lived carbenic intermediate is formed *via* a one-electron reduction process followed by loss of hydrogen to produce a free NHC which is rapidly consumed (likely *via* oxidation or chemical decomposition). After the switching potential, an irreversible anodic band is observed at +1.55 V which is ascribed to chloride oxidation.

Synthesis of 1,3-*bis*(2,4,6-trimethylphenyl)imidazolium hexafluorophosphate (P2.2). Ammonium hexafluorophosphate (1.44 g, 8.81 mmol) and **P2.1** (1.00 g, 2.94 mmol) were dissolved in deionised water (50 mL) and stirred for 2 hours at room temperature. The colourless precipitate was collected by vacuum filtration and washed with cold water (3 × 30 mL). Recrystallisation from acetone/diethyl ether afforded the title compound as a microcrystalline colourless solid. Yield: 1.21 g, 2.68 mmol, 91 %. ^{1}H NMR (300 MHz, CDCl$_3$) δ (ppm) 8.65 (s, 1H, NC*H*N), 7.55 (s, 2H, im*H*), 7.07 (s, 4H, mesityl *m*-C*H*), 2.37 (s, 6H, mesityl *p*-C*H$_3$*), 2.13 (s, 12H, mesityl *o*-C*H$_3$*). ^{13}C{^{1}H} NMR (75 MHz, CDCl$_3$) δ (ppm) 141.7, 136.6, 134.1, 130.4, 130.1, 125.4, 21.3, 17.2. HR-MS (ESI$^+$) *m/z* 305.1721 [C$_{21}$H$_{25}$N$_2$]$^+$, calcd. [M − PF$_6$]$^+$ 305.2012. All data are consistent with the literature.[62]

Synthesis of 1-allyl-3-(2-methylpyridyl)imidazolium bromide (P2.3). 2-Bromomethylpyridine hydrobromide (0.51 g, 2.00 mmol), 1-allylimidazole (0.23 g, 2.1 mmol) and potassium carbonate (1.40 g, 10.00 mmol) were charged to a round-bottomed flask and stirred in acetonitrile (50 mL) at 60 °C for 18 hours. Following, the mixture was filtered (removing excess K_2CO_3) and concentrated *in vacuo* to give a pale orange oil. Dissolution of this oil into acetonitrile (10 mL), followed by reprecipitation with diethyl ether (50 mL) (process repeated two more times) delivered the pure product as a pale yellow oil. Yield: 0.25 g, 2.00 mmol, quantitative. ^{1}H NMR (400 MHz, CDCl$_3$) δ (ppm) 10.92 (s, 1H, NC*H*N), 8.55 (d, *J* = 4.0 Hz, 1H, im*H*), 7.87 (d, *J* = 8.0 Hz, 1H, *m*-C*H*), 7.76 (td, *J* = 8.0 Hz, 1H, *p*-C*H*), 7.63 (d, *J* = 4.0 Hz, 1H, im*H*), 7.30 (td, *J* = 8.0 Hz, 1H, *m'*-C*H*), 7.16 (d, *J* = 8.0 Hz, 1H, *o*-C*H*), 6.02 (m, 1H, CH$_2$=C*H*), 5.79 (s, 2H, C*H*$_2$), 5.49 (d, *J* = 12.0 Hz, 2H, C*H*$_2$=CH), 4.92 (d, *J* = 3.0 Hz, 2H, NC*H*$_2$). ^{13}C{^{1}H} NMR (100 MHz, CDCl$_3$) δ (ppm) 152.2, 150.0, 137.9, 137.6, 129.6, 124.3, 124.2, 123.1, 121.3, 110.1, 54.2, 52.4. HR-MS (ESI$^+$) *m/z* 200.1202 [C$_{12}$H$_{14}$N$_3$]$^+$, calcd. [M − Br]$^+$ 200.1182. Anal. calcd. (%) for C$_{12}$H$_{14}$N$_3$Br·(^{3}/$_4$H$_2$O): C 49.08, H 5.32, N 14.31; found C 48.70, H 5.10, N 14.90.

Synthesis of 1-methyl-3-(*tert*-butylacetate)imidazolium chloride (P2.4). 1-Methylimidazole (1.60 mL, 20.0 mmol) and *tert*-butyl chloroacetate (2.90 mL, 20.0 mmol) were added to a round-bottomed flask and stirred at room temperature for 18 hours. After this time, the reaction mixture solidified. The solid was dissolved in dichloromethane (20 mL) and reprecipitated using an excess of hexane. Recrystallisation of the colourless solid from dichloromethane/hexane, followed by washing with diethyl ether (3 × 30 mL) delivered the desired product as a hygroscopic colourless solid, which was subsequently dried under vacuum. Yield: 3.59 g, 15.4 mmol, 77 %. ^{1}H NMR (300 MHz, (CD$_3$)$_2$SO) δ (ppm) 9.31 (s, 1H, NC*H*N), 7.78 (br s, 2H, im*H*), 5.22 (s, 2H, C*H*$_2$), 3.91 (s, 3H, C*H*$_3$), 1.44 (s, 9H, 3C*H*$_3$). ^{13}C{^{1}H} NMR (75 MHz, (CD$_3$)$_2$SO) δ (ppm) 165.8, 137.7, 123.6, 123.1, 82.9, 49.5, 35.7, 27.6. HR-MS (ESI$^+$) *m/z* 197.1307 [C$_{10}$H$_{17}$N$_2$O$_2$]$^+$, calcd. [M − Cl]$^+$ 197.1285. All data are consistent with the literature.[63]

Synthesis of 1,3-(dibenzyl)imidazolium hexafluorophosphate (P2.5). 1*H*-Imidazole (0.79 g, 11.7 mmol) and potassium carbonate (2.42 g, 17.5 mmol) were stirred in acetonitrile (60 mL) for 15 minutes at room temperature. Benzyl bromide (2.77 mL, 23.36 mmol) was added in a single portion and stirring continued for a further 48 hours. After this time, the solvent was removed *in vacuo* and water (100 mL) was added. The aqueous phase was extracted with dichloromethane (4 × 40 mL), organic phases combined, dried over anhydrous magnesium sulfate and filtered under vacuum. Following concentration, the resultant solid was washed repeatedly with cold diethyl ether (3 × 30 mL) and dried under vacuum to afford the title compound as a colourless solid. Yield: 3.50 g, 10.62 mmol, 91 %. ^{1}H NMR (400 MHz, CDCl$_3$) δ (ppm) 10.79 (s, 1H, NC*H*N), 7.49 − 7.45 (m, 4H, 2C*H*$_2$), 7.38 − 7.35 (m, 6H, ar*H*), 7.25 (d, *J* = 1.5 Hz, 2H,

im*H*), 5.56 (s, 4H, C*H*$_2$). ^{13}C{^{1}H} NMR (100 MHz, CDCl$_3$) δ (ppm) 137.0, 132.7, 129.5, 129.4, 129.0, 121.8, 53.4. HR-MS (ESI$^+$) *m/z* 249.1420 [C$_{17}$H$_{17}$N$_2$]$^+$, calcd. [M − Br]$^+$ 249.1386. All data are consistent with the literature.[34]

1,3-(Dibenzyl)imidazolium bromide (1.00 g, 3.04 mmol) and ammonium hexafluorophosphate (2.48 g, 15.2 mmol) were stirred in water (50 mL) at room temperature for 2 hours. After this time, a colourless precipitate formed which was collected by vacuum filtration and washed with cold water (3 × 30 mL), followed by recrystallisation from acetone/diethyl ether to yield the title compound as a colourless microcrystalline solid. Yield: 1.14 g, 2.89 mmol, 95 %. ^{1}H NMR (300 MHz, CDCl$_3$) δ (ppm) 9.63 (s, 1H, NC*H*N), 7.30 – 7.40 (m, 10H, ar*H*), 7.24 (m, 2H, im*H*), 5.23 (s, 4H, NC*H*$_2$). ^{13}C{^{1}H} NMR (75 MHz, CDCl$_3$) δ (ppm) δ 136.2, 132.5, 129.3, 129.1, 128.6, 121.4, 53.2. HR-MS (ESI$^+$) *m/z* 249.1391 [C$_{17}$H$_{17}$N$_2$]$^+$, calcd. [M − PF$_6$]$^+$ 249.1386. All data are consistent with the literature.[34]

Synthesis of diimidazolium cyclophanyl dihexafluorophosphate (P2.6). 1,3-*Bis*(bromomethyl)benzene (2.50 g, 9.41 mmol) was dissolved in anhydrous acetone (100 mL). A solution of 1,3-*bis*(imidazole-1-ylmethyl)benzene (2.30 g, 9.41 mmol) in anhydrous acetone (100 mL) was added dropwise over 4 hours at room temperature. The mixture was further stirred for 18 hours, upon which a colourless precipitate had formed, which was collected by vacuum filtration and washed repeatedly with cold acetone (2 × 40 mL) and diethyl ether (2 × 40 mL) to deliver the diimidazolium bromide as a microcrystalline colourless solid. Yield: 2.70 g, 5.41 mmol, 57 %. ^{1}H NMR (300 MHz, (CD$_3$)$_2$SO) δ (ppm) 9.50 (s, 2H, NC*H*N), 7.86 (s, 4H, im*H*), 7.60 (d, *J* = 7.4 Hz, 4H, ar*H*), 7.54 − 7.45 (m, 2H, ar*H*), 7.17 (s, 2H, ar*H*), 5.46 (s, 8H, C*H*$_2$). ^{13}C{^{1}H} NMR (75 MHz, (CD$_3$)$_2$SO) δ (ppm) 136.3, 136.0, 129.4, 129.1, 126.0, 123.1, 51.7. HR-MS (ESI$^+$) *m/z* 421.1041 [C$_{22}$H$_{22}$N$_4$Br]$^+$, calcd. [M − Br]$^+$ 421.1028. All data are consistent with the literature.[34]

To a methanolic solution of diimidazolium cyclophanyl dibromide (1.20 g, 2.40 mmol), ammonium hexafluorophosphate (3.90 g, 24.1 mmol) in methanol was added in a single portion and allowed to stir for 2 hours. The resultant colourless precipitate was collected by vacuum filtration and washed repeatedly with cold methanol (3 × 30 mL) followed by diethyl ether (3 × 30 mL) and dried *in vacuo* to give the pure product as a microcrystalline colourless solid. Yield: 1.30 g, 2.00 mmol, 84 %. ^{1}H NMR (500 MHz, (CD$_3$)$_2$SO) δ (ppm) 9.22 (s, 2H, NC*H*N), 7.81 (d, *J* = 1.4 Hz, 4H, im*H*), 7.58 (d, *J* = 6.4 Hz, 4H, ar*H*), 7.56 − 7.50 (m, 2H, ar*H*), 6.94 (s, 2H, ar*H*), 5.43 (s, 8H, C*H*$_2$). ^{13}C{^{1}H} NMR (75 MHz, (CD$_3$)$_2$SO) δ (ppm) 136.2, 136.1, 129.5, 129.1, 125.5, 123.2, 51.8. All data are consistent with the literature.[34]

2.5.3 Preparation of copper(I)-NHC complexes

General procedure using electrochemical flow-reactor 2 (stacked-disk). A solution of appropriate imidazolium salt (**P2.1 – P2.6**, 6.6 mM, 20 mL anhydrous MeCN) was passed through the revised electrochemical flow-reactor (4.0 mL hold-up volume) *via* syringe pump[*], for the allocated residence time whilst subject to an applied potential (as outlined in **Table 2.5**). The resulting output phase was collected into a separate Schlenk tube under an atmosphere of N_2, and solvents removed *in vacuo* to provide a crude residue which was analysed directly by ^{1}H NMR spectroscopy, using a sealed J. Young NMR tube. Relative conversions of imidazolium salt precursors to copper(I) complexes were recorded by solution integration measurement, and are listed in **Table 2.5**. [*]A recirculation sample-loop was employed for example **2.8**.

Synthesis of [1,3-*bis*(2,4,6-trimethylphenyl)imidazol-2-ylidene]copper(I) chloride (2.1). Imidazolium chloride **P2.1** was reacted according to the general procedure. Relative conversion: 94 %, E_{appl}: 1.94 V, τ_{res}: 29.9 minutes. Signals attributed to product: ^{1}H NMR (300 MHz, CDCl$_3$) δ (ppm) 7.05 (s, 2H, im*H*), 7.00 (s, 4H, mesityl *m*-C*H*), 2.35 (s, 6H, mesityl *p*-C*H*$_3$), 2.11 (s, 12H, mesityl *o*-C*H*$_3$). All data are consistent with the literature.[34]

Synthesis of *bis*[1,3-*bis*(2,4,6-trimethylphenyl)imidazol-2-ylidene]copper(I) hexafluorophosphate (2.4). Imidazolium hexafluorophosphate **P2.2** was reacted according to the general procedure. Relative conversion: 93 %, E_{appl}: 2.54 V, τ_{res}: 20.0 minutes. Signals attributed to product: ^{1}H NMR (300 MHz, CDCl$_3$) δ (ppm) 7.01 (s, 4H, im*H*), 6.90 (s, 8H, mesityl *m*-C*H*), 2.43 (s, 12H, mesityl *p*-C*H*$_3$), 1.68 (s, 24H, mesityl *o*-C*H*$_3$). All data are consistent with the literature.[34]

Synthesis of [1-allyl-3-(2-methylpyridyl)imidazol-2-ylidene]copper(I) bromide (2.5). Imidazolium bromide **P2.3** was reacted according to the general procedure. Relative conversion: 91 %, E_{appl}: 2.20 V, τ_{res}: 6.7 minutes. Signals attributed to product: ^{1}H NMR (300 MHz, CD$_3$CN) δ (ppm) 8.57 (d, *J* = 5.4 Hz, 1H, py*H*), 7.80 (td, *J* = 5.4, 1.8 Hz, 1H, py*H*), 7.41 – 7.33 (m, 2H, py*H*), 7.19 (d, *J* = 1.8 Hz, 1H, im*H*), 7.08 (d, *J* = 1.8 Hz, 1H, im*H*), 6.00 (m, 1H, C=C*H*), 5.41 – 5.12 (m, 2H, alkenyl *H*), 4.69 (m, 2H, NC*H*$_2$). All data are consistent with the literature.[63]

Synthesis of [1-methyl-3-(*tert*-butylacetate)imidazol-2-ylidene]copper(I) chloride (2.6). Imidazolium chloride **P2.4** was reacted according to the general procedure. Relative conversion: 95 %, E_{appl}: 2.40 V, τ_{res}: 13.3 minutes. Signals attributed to product: ^{1}H NMR (300 MHz, CD$_3$CN) δ (ppm) 7.10 (d, *J* = 1.2 Hz, 1H, im*H*), 7.08 (d, *J* = 1.2 Hz, 1H, im*H*), 4.78 (s, 2H, NC*H*$_2$), 3.81 (s, 3H, C*H*$_3$), 1.47 (s, 9H, (C*H*$_3$)$_3$). All data are consistent with the literature.[34]

Synthesis of *bis*[(1,3-dibenzyl)imidazol-2-ylidene]copper(I) hexafluorophosphate (2.7). Imidazolium hexafluorophosphate **P2.5** was reacted according to the general procedure. Relative conversion: 94 %, E_{appl}: 2.95 V, τ_{res}: 20.0 minutes. Signals attributed to product: ^{1}H NMR (300 MHz, CD$_3$CN) δ (ppm) 7.72 (br s, 2H, im*H*), 7.40 – 7.24 (m, 20H, ar*H*), 6.94 (br s, 2H, im*H*), 5.30 (s, 4H, C*H$_2$*), 5.19 (s, 4H, C*H$_2$*'). All data are consistent with the literature.[34]

Synthesis of Cu$_2$L$_2$ cyclophanyl dihexafluorophosphate (2.8). Diimidazolium dihexafluorophosphate **P2.6** was reacted according to the general procedure. Relative conversion: 95 %, E_{appl}: 4.90 V, τ_{res}: 300 minutes. Signals attributed to product: ^{1}H NMR (300 MHz, CD$_3$CN) δ (ppm) 7.26 (t, J = 4.5 Hz, 4H, ar*H*), 7.15 (d, J = 4.5 Hz, 8H, ar*H*), 6.93 (s, 8H, im*H*), 5.73 (s, 4H, ar*H*), 5.20 (d, J = 9.9 Hz, 8H, C*H$_2$*), 5.11 (d, J = 9.9 Hz, 8H, C*H$_2$*'). All data are consistent with the literature.[34]

2.5.4 Preparation of silyl ethers

Hydrosilylation procedure of functionalised ketones *via* pre-defined catalyst.

Bis[1,3-*bis*(2,4,6-trimethylphenyl)imidazol-2-ylidene]copper(I) chloride **2.1** (31.2 mg, 0.0772 mmol) and sodium *tert*-butoxide (50.0 mg, 0.52 mmol) were stirred vigorously in anhydrous toluene (10 mL) for 10 minutes. To this solution, triethylsilane (2.05 mL, 12.9 mmol) was added dropwise by syringe and the solution stirred for a further 10 minutes, upon which ketone substrate (2.57 mmol) was added and the mixture heated to 80 ˚C for 2 hours under an inert atmosphere. After this time, the mixture was filtered through a Celite plug and rinsed with a portion of ethyl acetate (10 mL), which was concentrated under reduced pressure to afford spectroscopically pure silyl ether as a colourless oil. Yield: 94 % or above.[58]

Hydrosilylation procedure of functionalised ketones *via* electrogenerated catalyst.

A freshly prepared anhydrous solution of 1,3-*bis*(2,4,6-trimethylphenyl)imidazolium chloride **2.1** (45 mg, 0.13 mmol) in acetonitrile (20 mL) was recirculated through a continuous electrochemical flow reactor at 0.50 mLmin[-1], under a fixed applied potential of 2.50 V ($i_{init.}$ = 3.00 mA) at room temperature for 80 minutes. After this time (t$_{80}$), the an aliquot of this solution (5.0 mL, 0.03 mmol) was dispensed directly into a flame-dried Schlenk flask charged with sodium *tert*-butoxide (19.0 mg, 0.20 mmol) in anhydrous toluene (10 mL) and stirred vigorously at room temperature under an inert atmosphere for 10 minutes. To this solution, triethylsilane (0.81 mL, 5.07 mmol) was added dropwise by syringe and the solution stirred for a further 10 minutes at 80 ˚C, upon which ketone substrate (1.00 mmol) was added and the mixture stirred at 80 ˚C for 2 – 6.5 hours under an inert atmosphere. After this time, the mixture was filtered through a Celite

plug and rinsed with a portion of ethyl acetate (10 mL) which was concentrated under reduced pressure to afford spectroscopically pure silyl ether as a colourless oil. Yield: 94 % or above.

Synthesis of (dicyclohexylmethoxy)triethylsilane. Title compound isolated as a pale yellow oil. Yield: 0.78 g, 2.50 mmol, 97 % (98 % from pre-defined catalyst). ^{1}H NMR (300 MHz, CDCl$_3$) δ (ppm) 3.14 (t, J = 6.0 Hz, 1H, H_{α}OSi), 1.85 – 1.70 (m, 6H, cy$H$), 1.70 – 1.59 (m, 2H, cy$H$), 1.59 – 1.48 (m, 2H, cy$H$), 1.47 – 1.33 (m, 2H, cy$H$), 1.28 – 0.93 (m) and 0.97 (t, J = 8.1 Hz, 19H, SiCH_2), 0.61 (q, J = 8.1 Hz, 6H, CH$_2$CH_3). ^{13}C{^{1}H} NMR (75 MHz, CDCl$_3$) δ (ppm) 81.9, 41.1, 30.7, 28.1, 26.7, 7.2, 5.6. All data are consistent with the literature.[58]

Synthesis of [1-(furanyl-2-yl)ethoxy]triethylsilane. Title compound isolated as a pale yellow oil. Yield: 0.55 g, 2.44 mmol, 95 % (94 % from pre-defined catalyst). ^{1}H NMR (300 MHz, CDCl$_3$) δ (ppm) 7.34 (d, J = 2.6 Hz, 1H, fur$H$), 6.34 – 6.24 (m, 1H, fur$H$), 6.18 (d, J = 2.6 Hz, 1H, fur$H$), 4.88 (q, J = 6.4 Hz, 1H, H_{α}OSi), 1.50 (d, J = 6.4 Hz, 3H, CH_3), 0.94 (t, J = 8.0 Hz, 9H, CH$_2$CH_3), 0.61 (q, J = 8.0 Hz, 6H, CH_2CH$_3$). ^{13}C{^{1}H} NMR (75 MHz, CDCl$_3$) δ (ppm) 158.2, 141.2, 109.9, 104.7, 64.1, 22.9, 6.6, 4.6. All data are consistent with the literature.[58]

Synthesis of [1-(thien-2-yl)ethoxy]triethylsilane. Title compound isolated as a pale yellow oil. Yield: 0.60 g, 2.50 mmol, 97 % (97 % from pre-defined catalyst). ^{1}H NMR (300 MHz, CDCl$_3$) δ (ppm) 7.18 (d, J = 3.6 Hz, 1H, thien$H$), 6.95 – 6.87 (m, 1H, thien$H$), 6.88 (d, J = 3.6 Hz, 1H, thien$H$), 5.14 (q, J = 6.4 Hz, 1H, H_{α}OSi), 1.55 (d, J = 6.4 Hz, 3H, CH_3), 0.96 (t, J = 7.9 Hz, 9H, CH$_2$CH_3), 0.63 (q, J = 7.9 Hz, 6H, CH_2CH$_3$). ^{13}C{^{1}H} NMR (75 MHz, CDCl$_3$) δ (ppm) 151.5, 126.3, 123.6, 122.0, 66.9, 27.1, 6.8, 4.7. All data are consistent with the literature.[58]

Synthesis of [1-pyridin-2-yl)ethoxy]triethylsilane. Title compound isolated as a pale yellow oil. Yield: 0.57 g, 2.40 mmol, 94 % (90 % from pre-defined catalyst). ^{1}H NMR (300 MHz, CDCl$_3$) δ (ppm) 8.44 (d, J = 4.0 Hz, 1H, py$H$), 7.72 – 7.63 (m, 1H, py$H$), 7.51 (d, J = 4.0 Hz, 1H, py$H$), 7.17 – 7.06 (m, 1H, py$H$), 4.92 (q, J = 6.4 Hz, 1H, H_{α}OSi), 1.44 (d, J = 6.4 Hz, 3H, CH_3), 0.89 (t, J = 8.0 Hz, 9H, CH$_2$CH_3), 0.51 (q, J = 8.0 Hz, 6H, CH_2CH$_3$). ^{13}C{^{1}H} NMR (75 MHz, CDCl$_3$) δ (ppm) 165.8, 148.3, 136.5, 121.6, 119.2, 71.8, 25.5, 6.7, 4.7. All data are consistent with the literature.[58]

Synthesis of [1-(2-chlorophenyl)ethoxy]triethylsilane. Title compound isolated as a pale yellow oil. Yield: 0.15 g, 0.98 mmol, 97 % (98 % from pre-defined catalyst). ^{1}H NMR (300 MHz, CDCl$_3$) δ (ppm) 7.64 (d, J = 6.0 Hz, 1H, ar$H$), 7.26 (d, J = 6.0 Hz, 1H, ar$H$), 7.14 (t, J = 6.0 Hz, 2H, ar$H$), 5.22 (q, J = 6.4 Hz, 1H, H_{α}OSi), 1.40 (d, J = 6.4 Hz, 3H, CH_3), 0.90 (t, J = 6.0 Hz, 9H, CH$_2$CH_3), 0.51 (q, J = 6.0 Hz, 6H, CH_2CH$_3$). ^{13}C{^{1}H} NMR (75 MHz, CDCl$_3$) δ (ppm) 144.4, 130.6, 128.9, 127.8, 127.0, 126.9, 67.0, 25.2, 6.7, 4.4. All data are consistent with the literature.[58]

2.5.6 Flow-channel volume calculations

The volume of the flow channel, after packing with soda-lime glass beads (dia. 2 mm, Smith Scientific Ltd.) was determined indirectly by subtracting the volume of the glass beads.

The effective channel volume was therefore calculated by measuring the increase in volume of a known quantity of water (3.0 mL) upon the addition of the glass beads (measured to be 0.85 mL). An alternative method involved measuring the weight of the glass beads (2.155 g, using $d = 2.52$ g/mL, volume = 2.155/2.52 = 0.855 mL). Both methods provided strong agreement, therefore the average value for volume of glass beads was taken to be 0.85 mL.

2.6   Bibliography

1.   (a) C. Zhang, C. Tang, N. Jiao, *Chem. Soc. Rev.* **2012**, *41*, 3464–3484; (b) R. A. Sheldon, *Chem. Ind.* **1992**, 903–906; (c) D. J. C. Constable, P. J. Dunn, J. D. Hayler, G. R. Humphrey, J. L. Leazer Jr., R. J. Linderman, K. Lorenz, J. Manley, B. A. Pearlman, A. Wells, A. Zaks, T. Y. Zhang, *Green Chem.* **2007**, *9*, 411–420.

2.   (a) A. E. Wendlandt, A. M. Suess, S. S. Stahl, *Angew. Chem. Int. Ed. Engl.* **2011**, *50*, 11062–11087; (b) E. Roduner, W. Kaim, B. Sarkar, V. B. Urlacher, J. Pleiss, R. Gläser, W.-D. Einicke, G. A. Sprenger, U. Beifuß, E. Klemm, C. Liebner, H. Hieronymus, S.-F. Hsu, B. Pleitker, S. Sabine Laschat, *ChemCatChem* **2013**, *5*, 82–112.

3.   Z. Li, D. S. Bohle, C.-J. Li, *Proc. Natl. Acad. Sci. U. S. A.* **2006**, *103*, 8928–8933.

4.   (a) P. E. Fanta, *Chem. Rev.* **1946**, *38*, 139–196; (b) D. T. Ziegler, J. Choi, J. M. M.-Molina, A. C. Bissember, J. C. Peters, G. C. Fu, *J. Am. Chem. Soc.* **2013**, *135*, 13107–13112.

5.   (a) S. Reymond, J. Cossy, *Chem. Rev.* **2008**, *108*, 5359–5406; (b) U. Pinder, G. Lutz, C. Otto, *Chem. Rev.* **1993**, *93*, 741–761; (c) D. Carmona, M. P. Lamata, L. A. Oro, *Coord. Chem. Rev.* **1992**, *92*, 1007–1019.

6.   (a) W. Li, C. M. Schneider, G. I. Georg, *Org. Lett.* **2015**, *17*, 3902–3905; (b) G. Batu, R. Stevenson, *J. Org. Chem.* **1980**, *45*, 1532–1534.

7.   L. Aldea, J. I. García, J. A. Mayoral, *Dalton Trans.* **2012**, *41*, 8285–8289.

8.   (a) P. M. Diz, A. Coelho, A. El Maatougui, J. Azuaje, O. Caamaño, Á. Gil, E. Sotelo, *J. Org. Chem.* **2013**, *78*, 6540–6549; (b) F. Amblard, J. H. Cho, R. F. Schinazi, *Chem. Rev.* **2009**, *109*, 4207–4220.

9.   S. E. Allen, R. R. Walvoord, R. Padilla-Salinas, M. C. Kozlowski, *Chem. Rev.* **2013**, *113*, 6234–6458.

10.   S. Chiba, *Bull. Chem. Soc. Jpn.* **2013**, *86*, 1400–1411.

11.   X.-X. Guo, D.-W. Gu, Z. Wu, W. Zhang, *Chem. Rev.* **2015**, *115*, 1622–1651.

12.   *N. R. C. (U.S.) C. S. Roundtable Review* **2012**.

13.   (a) X. Xie, G. Cai, D. Ma, *Org. Lett.* **2005**, *7*, 4693–4695; (b) Z.-J. Liu, X. Lu, G. Wang, L. Li, W.-T. Jiang, Y.-D. Wang, B. Xiao, Y. Fu, *J. Am. Chem. Soc.* **2016**, *138*, 9714–9719; (c) C.-T. Yang, Z.-Q. Zhang, J. Liang, J.-H. Liu, X.-Y. Lu, H.-H. Chen, L. Liu, *J. Am. Chem. Soc.* **2012**, *134*, 11124–11127.

14.   A. J. Arduengo, H. V. R. Dias, J. C. Calabrese, F. Davidson, *Organometallics* **1993**, *12*, 3405–3409.

15.   S. M. Opalka, J. K. Park, A. R. Longstreet, D. T. McQuade, *Org. Lett.* **2013**, *15*, 996–999.

16.   K. S. Elvira, X. Casadevall i Solvas, R. C. R. Wootton, A. J. deMello, *Nat. Chem.* **2013**, *5*, 905–915.

17.   J. R. Goodell, J. P. McMullen, N. Zaborenko, J. R. Maloney, C.-X. Ho, K. F. Jensen, J. A. Porco, A. B. Beeler, *J. Org. Chem.* **2009**, *74*, 6169–6180.

18.   N. Zaborenko, M. W. Bedore, T. F. Jamison, K. F. Jensen, *Org. Process Res. Dev.* **2011**, *15*, 131–139.

19. A. Shimoyama, Y. Fujimoto, K. Fukase, *Synlett* **2011**, *16*, 2359–2362.

20. B. Pieber, C. O. Kappe, *Green Chem.* **2013**, *15*, 320–324.

21. D. R. Snead, T. F. Jamison, *Angew. Chem. Int. Ed.* **2014**, *53*, 14451–14455.

22. R. L. Hartman, J. P. McMullen, K. F. Jensen, *Angew. Chem. Int. Ed. Engl.* **2011**, *50*, 7502–7519.

23. K. Watts, W. Gattrell, T. Wirth, *Beilstein J. Org. Chem.* **2012**, *7*, 1108–1114.

24. K. Kataoka, Y. Hagiwara, K. Midorikawa, S. Suga, J. Yoshida, *Org. Process Res. Dev.* **2008**, *12*, 1130–1136.

25. O. Levenspiel, *Chemical Reaction Engineering*, Wiley **1999**, 3rd edition.

26. M. Süssner, H. Plenio, *Chem. Commun.* **2005**, *43*, 5417–5419.

27. J. D. Egbert, C. S. J. Cazin, S. P. Nolan, *Catal. Sci. Technol.* **2013**, *3*, 912–926.

28. I. Abdellah, B. Cassirame, S. Condon, J.-Y. Nédélec, C. Pichon, *Current Topics in Electrochemistry* **2011**, *16*, 81–91.

29. B. Gorodetsky, T. Ramnial, N. R. Branda, J. A. C. Clyburne, *Chem. Commun.* **2004**, *40*, 1972–1973.

30. S. Sanghi, E. Willett, C. Versek, M. Tuominen, E. B. Coughlin, *RSC Adv.* **2012**, *2*, 848–853.

31. C. Liao, N. Shao, K. S. Han, X.-G. Sun, D.-E. Jiang, E. W. Hagaman, S. Dai, *Phys. Chem. Chem. Phys.* **2011**, *13*, 21503–21510.

32. K. A. Ogawa, A. J. Boydston, *Chem. Lett.* **2014**, *43*, 907–909.

33. R. V. Mehta, J. M. Tarbell, *AIChE J.* **1987**, *33*, 1089–1101.

34. B. R. M. Lake, E. K. Bullough, T. J. Williams, A. C. Whitwood, M. A. Little, C. E. Willans, *Chem. Commun.* **2012**, *48*, 4887–4889.

35. S. S. Stahl, J. L. Thorman, R. C. Nelson, M. A. Kozee, *J. Am. Chem. Soc.* **2001**, *123*, 7188–7189.

36. M. B. Smith, J. March, *March's Advanced Organic Chemistry*, John Wiley & Sons, Inc., Hoboken, NJ, USA **2006**, 5th edition.

37. R. Noyori, T. Ohkuma, M. Kitamura, H. Takaya, N. Sayo, H. Kumobayashi, S. Akutagawa, *J. Am. Chem. Soc.* **1987**, *109*, 5856–5858.

38. K. Mashima, K. Kusano, N. Sato, Y. Matsumura, K. Nozaki, H. Kumobayashi, N. Sayo, Y. Hori, T. Ishizaki, *J. Org. Chem.* **1994**, *59*, 3064–3076.

39. R. Noyori, T. Ohkuma, *Angew. Chem. Int. Ed. Engl.* **2001**, *40*, 40–73.

40. R. Noyori, *Angew. Chem. Int. Ed.* **2002**, *41*, 2008–2022.

41. P. V. Ramachandran, H. C. Brown, *Reductions in Organic Synthesis*, A. F. Abdel-Magid (Ed.), American Chemical Society, Washington D.C. **1996**, 84–97.

42. J. Yang, T. D. Tilley, *Angew. Chem. Int. Ed.* **2010**, *49*, 10186–10188.

43. I. Ojima, M. Nihonyanagi, Y. Nagai, *J. Chem. Soc. Chem. Commun.* **1972**, 938.

44. W. Dumont, J. C. Poulin, T. P. Dang, H. B. Kagan, *J. Am. Chem. Soc.* **1973**, *95*, 8295–8299.

45. (a) G. Du, M. M. Abu-Omar, *Organometallics* **2006**, *25*, 4920–4923; (b) Y. Nakajima, S. Shimada, *RSC Adv.* **2015**, *5*, 20603–20616; (c) A. K. Roy, *Adv. Organomet. Chem.* **2007**, *55*, 1–59.

46. E. A. Ison, E. R. Trivedi, R. A. Corbin, M. M. Abu-Omar, *J. Am. Chem. Soc.* **2005**, *127*, 15374–15375.

47.   K. A. Nolin, J. R. Krumper, M. D. Pluth, R. G. Bergman, F. D. Toste, *J. Am. Chem. Soc.* **2007**, *129*, 14684–14696.

48.   L. H. Gade, V. César, S. Bellemin-Laponnaz, *Angew. Chem. Int. Ed.* **2004**, *43*, 1014–1017.

49.   B. Tao, G. C. Fu, *Angew. Chem. Int. Ed.* **2002**, *41*, 3892–3894.

50.   M. B. Carter, B. Schiott, A. Gutierrez, S. L. Buchwald, *J. Am. Chem. Soc.* **1994**, *116*, 11667–11670.

51.   N. S. Shaikh, S. Enthaler, K. Junge, M. Beller, *Angew. Chem. Int. Ed.* **2008**, *47*, 2497–2501.

52.   M. DiBiase Cavanaugh, B. T. Gregg, A. R. Cutler, *Organometallics* **1996**, *15*, 2764–2769.

53.   H. Mimoun, J. Y. de Saint Laumer, L. Giannini, R. Scopelliti, C. Floriani, *J. Am. Chem. Soc.* **1999**, *121*, 6158–6166.

54.   H. Brunner, W. Miehling, *J. Organomet. Chem.* **1984**, *7*, 275.

55.   B. H. Lipshutz, K. Noson, W. Chrisman, *J. Am. Chem. Soc.* **2001**, *123*, 12917–12918.

56.   S. Sirol, J. Courmarcel, N. Mostefai, O. Riant, *Org. Lett.* **2001**, *3*, 4111–4113.

57.   C. Czekelius, E. M. Carreira, *Org. Lett.* **2004**, *6*, 4575–4577.

58.   S. Díez-González, H. Kaur, F. K. Zinn, E. D. Stevens, S. P. Nolan, *J. Org. Chem.* **2005**, *70*, 4784–4796.

59.   P. Elliott, *Notes Rec. R. Soc.*, London press **1999**, *53*, 59–78.

60.   D. E. Levy, *Arrow Pushing in Organic Chemistry*, John Wiley & Sons, Inc., Hoboken, NJ, USA **2008**, 1st edition.

61.   M. W. Washabaugh, W. P. Jencks, *Biochemistry* **1988**, *27*, 5044–5053.

62.   M. Süßner, H. Plenio, *Chem. Commun.* **2005**, *41*, 5417–5419.

63.   B. R. M. Lake, C. E. Willans, *Organometallics* **2014**, *33*, 2027–2038.

Exploitation of a synthetically clean electrochemical route to iron(II) *N*-heterocyclic carbene complexes

3.1   Introduction

Over forty years ago, Öfele and Kreiter were first to describe the preparation of an iron *N*-heterocyclic carbene complex, which was indirectly isolated from an impure mixture of tetrazolium carbonylferrates.[1] However, amongst Lappert's landmark discoveries was the treatment of an electron-rich olefin with iron(0) pentacarbonyl to afford the first, well-characterised iron-NHC complex in 95 % yield (**Scheme 3.1**).[2]
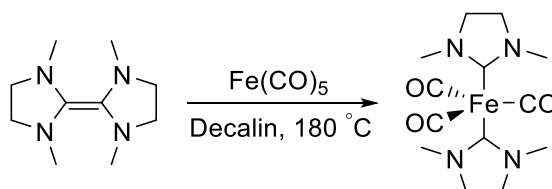
Scheme 3.1 High-yielding synthetic route to iron-NHCs, reported by Lappert in 1977.[2]

The chemistry of iron-NHCs remains in its relative infancy when compared with that of neighbouring transition metal complexes of carbenes. In fact, the majority of significant contributions to the field have only been realised over the last decade and have led synthetic chemists to re-evaluate the potential applications of these compounds, according to a timely review article by Layfield and Ingleson.[3]

Perhaps the most common approach to prepare iron-NHCs was developed by Fehlhammer and co-workers, by adding an iron halide to a solution of free carbene – itself generated through deprotonation of an imidazolium salt.[4] Without question, this technique widened the field of iron-NHC chemistry by allowing various combinations of free NHC and iron precursor to produce an assortment of complexes. Typically, butyl lithium or sodium hydride is chosen as source of base to supply free NHCs,[5] which inherently places limitation on this methodology, as discussed within Chapter 1.

Smith and colleagues described an elegant variation on transmetalation in 2005, by employing magnesium carbenes in the synthesis of scorpionate-type iron-NHCs.[6] The absolute structure of the magnesium carbene was unambiguously assigned through X-ray crystallographic analysis, and used directly to transfer the heterocyclic ligand to iron(II) dibromide (see **Scheme 3.2**). Along similar lines, Chen *et al.* have successfully transmetalated carbenes to iron from silver(I), with Braunstein and Monakhov adopting the same tactic using a lithium carbene adduct.[7,8]
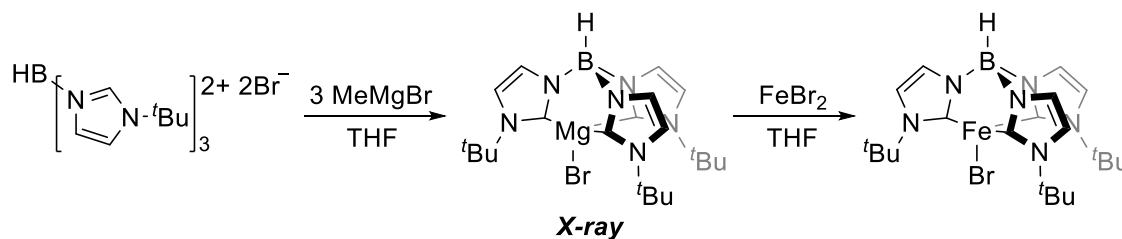
Scheme 3.2 *Transmetalation from a well-defined magnesium-NHC, by Smith.*[6]

The latest advance in terms of synthetic methodology was reported by Danopoulos in 2004, which again rests upon the original findings of Lappert and co-workers and is now considered the 'preferred path' to iron-NHC complexes.[5,9,10] The method relies on a highly Brønsted basic iron(II) precursor, [Fe{N(SiMe$_3$)$_2$}$_2$], bearing two equivalents of internal base to deprotonate imidazolium ions, whilst providing a halide-free iron(II) source to metalate the subsequent free carbenes *in situ*. Conveniently, the method by-produces two equivalents of volatile HN(SiMe$_3$)$_2$, which may be simply removed under vacuum and typically affords the desired iron(II)-NHC complex cleanly, in high yield.

Employment of [Fe{N(SiMe$_3$)$_2$}$_2$] has not only led to the predictable synthesis of various iron-NHC complexes, but also allowed access to unusual low-coordinate iron complexes of NHCs with broad fundamental impact. A notable example was recently published by Layfield and colleagues, who took full advantage of the 'steric pressure' imposed by bulky NHC ligands (for example, IMes, IPr and I^{t}Bu) to derive a route to the first three-coordinate NHC complexes of [Fe{N(SiMe$_3$)$_2$}$_2$].[11] Overlapping theoretical calculations with these complexes, the authors found that the Fe-C$_{carbene}$ bond energy decreases dramatically as the steric bulk of the NHC increases. Taking this idea forward, the group showed that for the sterically encumbered iron-NHC analogue, [Fe(IPr){N(SiMe$_3$)$_2$}$_2$] (IPr = 1,3-*bis*(diisopropylphenyl)imidazol-2-ylidene) (**A**), a remarkably facile thermal rearrangement is possible, to give the first three-coordinate abnormal iron carbene complex (**B**) (see **Scheme 3.3**).[12]
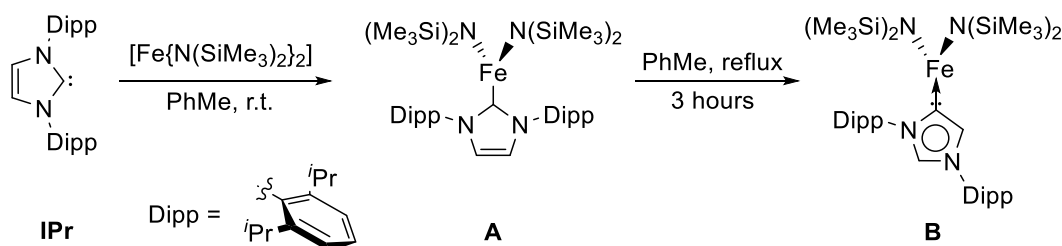
Scheme 3.3 *Layfield's synthetic route to low-coordinate iron-NHC complexes.*[11]

Despite representing an efficient reagent, a major drawback of using [Fe{N(SiMe$_3$)$_2$}$_2$] is its inherent sensitivity to both air and moisture. Likewise, the design of such an aggressive deprotonation agent makes this precursor relatively functional group-intolerant, especially when in proximity to base-sensitive groups. Moreover, the precursor itself must be prepared in-house from reaction of a suitable iron(II) halide with two equivalents of LiN(SiMe$_3$)$_2$, and subsequently purified by high vacuum distillation under rigorously inert conditions to give the highly reactive product as an oily green residue.

The established synthetic routes to iron-NHC complexes summarised above represent those most commonly employed to date. Whilst each allows controlled access to the organometallic products, all involve use of strongly basic conditions, or harsh iron precursors which possess low functional group compatibility. The requirement of these conditions typically limit product scale to milligrams and restrict functionality comprised within the ligand framework.

Described within Chapter 2 is a versatile and simple electrochemical protocol for the synthesis of copper(I)-NHC complexes, which obviates the use of strong bases or elevated temperatures whilst liberating gaseous H$_2$ as the only side-product. It was envisaged that this methodology could be translated to afford complexes of iron, by employment of a sacrificial iron anode as metal source, allowing access to previously inaccessible iron-NHCs in an efficient and scalable manner. Described within this chapter, are findings regarding the electrochemical synthesis of various novel iron(II)-NHC complexes, with detailed characterisation to assess their identity in both the solid and solution-state.

3.2   Pyridyl-substituted ligand precursor synthesis

In 2009, Chen and co-workers described the first example of an octahedral iron(II) complex containing a donor-substituted NHC ligand (1,3-*bis*(2-pyridyl)imidazol-2-ylidene), which was prepared from the electrochemical oxidation of iron(0) powder with concomitant reduction of an imidazolium salt.[13] Though low-yielding, the method underscored the stabilising effect of neutral hemilabile donor groups on the iron(II) centre, particularly with respect to air and moisture (one molecule of H$_2$O was even located within the crystalline lattice of the complex, by X-ray diffraction methods). Recent findings from our laboratory have equally exposed NHC/pyridine hybrids to be an effective class of ancillary ligand for the stabilisation of metal complexes, particularly those capable of adopting various oxidation states.[14] Taking note of these observations, it was sought to prepare several NHC ligand precursors by way of their corresponding imidazolium salt, with a view to incorporate chelating pyridyl functionality into the ligand template to further coordinate and stabilise an iron(II) metal centre, through various topologies and denticities.

Azolium hexafluorophosphates **P3.1** and **P3.2** were synthesised using modified literature procedures.[15,16] Independent reaction of freshly prepared 2-pyridylimidazole (**I3.1**) and *N*-mesitylimidazole (**I3.2**) with neat 2-bromopyridine at 160 ˚C cleanly afforded each *N*-pyridyl appended imidazolium bromide. Subsequent treatment of each salt with two equivalents of NH$_4$PF$_6$ under aqueous conditions provided their corresponding imidazolium hexafluorophosphate analogues, **P3.1** and **P3.2**, in 64 and 66 % overall yield, respectively (**Scheme 3.4**).

I3.1: R = 2-pyridyl
I3.2: R = mesityl

P3.1: R = 2-pyridyl
P3.2: R = mesityl
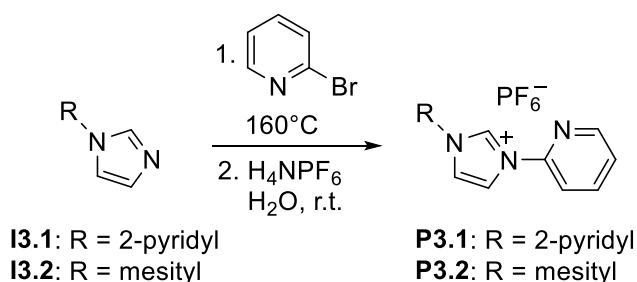
Scheme 3.4 Synthetic route to 2-pyridyl substituted imidazolium hexafluorophosphates, P3.1 and P3.2.

Both **P3.1** and **P3.2** were fully characterised using multinuclear NMR spectroscopy and high-resolution mass spectrometry. Of note, were the presence of diagnostic low-field resonances in both solution proton NMR spectra of **P3.1** and **P3.2**, observed at 9.89 and 9.41 ppm (300 MHz, CD$_3$CN) respectively, indicative of azolium ion formation (*i.e.* each NC*H*N signal). Further, mass peaks (*m/z*) 223.0988 and 264.1507 were noted in the electrospray mass spectra of **P3.1** and **P3.2**, respectively, attributable to each [M − PF$_6$]$^+$ mass fragment, with their bulk purities confirmed by combustion analysis.

Numerous synthetic reports have pointed out the benefits of a rigid ligand environment around an iron centre during catalysis.[17–20] Becoming more popular however, is the concept of using NHC ligands bearing flexible donor wingtip substituents. In a detailed solution NMR study by Herrmann and Kühn, it was illustrated that varying the chain length between a donor *N*-substituent and NHC unit has a marked effect on both coordination mode and geometry of octahedral iron(II) complexes, which the authors usefully exploited in catalyst design.[21] Therefore, a number of *N*-picolyl substituted imidazolium salts were prepared with a view to produce sterically fluid polydentate NHC ligands.

Reaction of imidazole with one equivalent of 2-bromomethylpyridine hydrobromide under basic conditions smoothly affords *N*-picolylimidazole (**I3.3**), which represents a useful synthetic building block for this class of compound. Treatment of **I3.3** with a second equivalent of 2-bromomethylpyridine hydrobromide produces a *C$_2$*-symmetric, *bis*-picolyl substituted imidazolium bromide (the X-ray crystal structure of which is illustrated in Chapter 5),

which undergoes rapid anion exchange with aqueous NH_4PF_6 to afford tridentate NHC precursor, **P3.3** in 59 % yield. Methylene-linked *bis*-NHC ligand precursor **P3.4** is accessed through reaction of **I3.3** with a ten-fold excess of dibromomethane, followed by a similar aqueous anion exchange reaction to that of **P3.3**, furnishing the C_2-symmetric tetradentate NHC precursor in 80 % overall yield. In addition, unsymmetrical *N*-ester substituted analogue, **P3.5**, was prepared by refluxing a solution of **I3.3** with *tert*-butyl chloroacetate (1.5 equivalents) in MeCN solvent, followed by subsequent anion exchange with NH_4PF_6, to cleanly give the product in 62 % isolated yield (see **Scheme 3.5** for each reaction pathway).
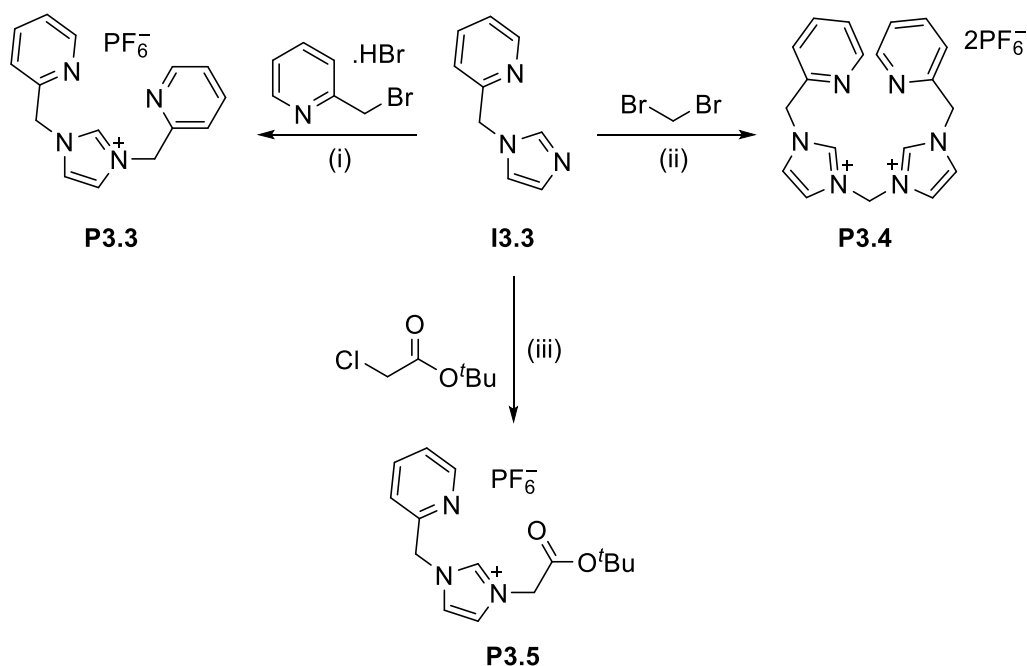
Scheme 3.5 *Synthetic routes to N-picolyl substituted imidazolium hexafluorophosphates,*
P3.3 – **P3.5**. *Conditions prior to anion exchange: (i) K_2CO_3 (3 equiv.), MeCN solvent, 60 ˚C, 18 hours; (ii) THF solvent, 80 ˚C, 18 hours; (iii) MeCN solvent, 60 ˚C, 16 hours.*

Imidazolium salts **P3.3** – **P3.5** were purified by recrystallisation and authenticated using multinuclear NMR spectroscopy, ESI mass spectrometry and elemental analysis. Both the ^1H and $^{13}C\{^1H\}$ NMR spectra of **P3.3** and **P3.4** illustrated the expected C_2-symmetric molecular environments, featuring low-field singlet resonances at 8.78 and 8.99 ppm (400 MHz, CD_3CN) respectively, corroborating their deshielded NC*H*N azolium protons. Electrospray mass spectrometry of **P3.3** and **P3.4** detected dominant mass collections at (*m/z*) 251.1304 and 477.1414, respectively, attributable to each of their $[M - PF_6]^+$ mass fragments. **P3.5** was analysed by similar methods, with all solution NMR spectroscopic analysis demonstrating a non C_2-symmetric molecular environment, and a $[M - PF_6]^+$ mass peak showcased in the ESI mass spectrum at 274.1562.

Previous findings from our group have shown *N*-allyl substituted NHCs containing electronically diverse pyridine rings to be an interesting class of ancillary ligand,[14,22] and will be discussed in detail through Chapters 5 and 6. In keeping with our interests, *N*-pyridyl, *N'*-allyl-substituted imidazolium bromides **P3.6** and **P3.7** were also synthesised. *N*-Pyridylimidazole (**I3.1**) was prepared from a well-documented Ullmann coupling procedure between imidazole and 2-bromopyridine, as previously reported within our group.[14] Novel 2-DMAP (DMAP = dimethylaminopyridine) substituted analogue, **I3.7**, was obtained through a modified two-step protocol *via* 2-bromo-4-dimethylaminopyridine. Initial reaction of DMAP with one equivalent BF₃(OEt)₂ at 0 ˚C produces the corresponding Lewis acid adduct *in situ*, which is able to direct an *ortho*-lithiation reaction at the pyridine ring upon addition of *n*-butyl lithium at -78 ˚C. Subsequent addition of carbon tetrabromide (one equivalent) to the lithiated intermediate affords *mono-o*-brominated DMAP, which can be further purified by column chromatography. Coupling of 2-bromo-4-dimethylaminopyridine with imidazole under analogous conditions to those producing **I3.1**, leads to formation of **I3.7**. Independent treatment of **I3.1** and **I3.7** with allyl bromide (four equivalents) allows clean access to *N*-pyridyl-*N'*-allyl substituted imidazolium bromides, **P3.6** and **P3.7**, in quantitative yield (see **Scheme 3.6** for each reaction pathway).
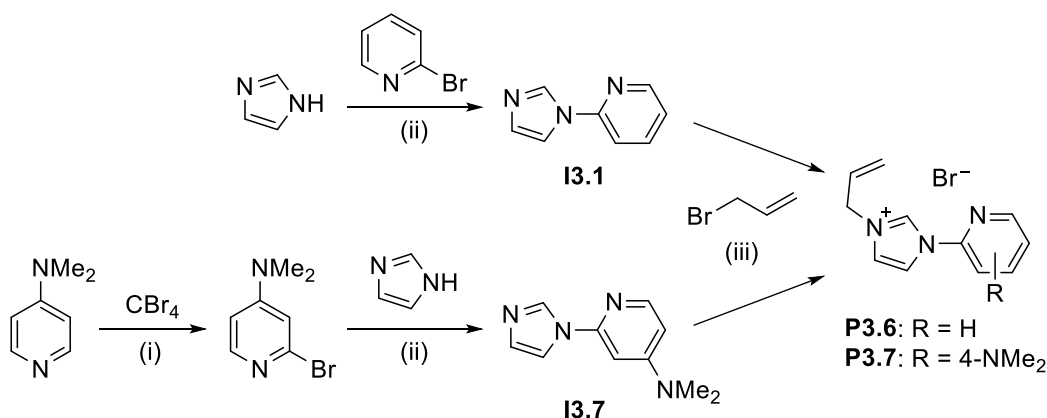
Scheme 3.6 *Synthetic routes to N-allyl substituted imidazolium bromides, **P3.6** and **P3.7**. Conditions: (i) BF₃(OEt)₂ (1 equiv.), THF solvent, 0 ˚C, 30 minutes, followed by ⁿBuLi (1 equiv.), -78 ˚C, 30 minutes, followed by CBr₄, room temperature, 14 hours; (ii) CuI/D-L proline (3 mol% each), K₂CO₃ (2 equiv.), DMSO solvent, 100 ˚C, 18 hours; (iii) MeCN solvent, 80 ˚C, 18 hours.*

Azolium bromides **P3.6** and **P3.7** were fully characterised by NMR spectroscopy, high-resolution mass spectrometry and combustion analysis. All acquired data supported the expected molecular environments, and do not require comment. In addition, colourless block crystals of **P3.7** suitable for X-ray crystallographic analysis were procured from the slow diffusion of diethyl ether vapours into an acetonitrile solution of the product, which further confirmed the absolute molecular structure of the novel salt (a structural solution is given in **Figure 3.1**).
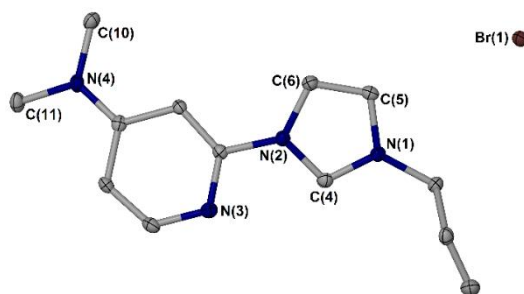
Figure 3.1 *Molecular structure of ligand precursor, **P3.7**. Atomic displacement parameters are drawn at the 50 % probability level, hydrogen atoms are omitted for clarity.*

C(4)-N(1)	1.325(4)	N(1)-C(4)-N(2)	108.5(2)
C(4)-N(2)	1.339(4)	N(2)-C(6)-C(5)	106.9(2)
C(5)-C(6)	1.352(4)	C(4)-N(1)-C(5)	108.8(2)

Table 3.1 *Selected bond lengths (Å) and angles (˚) from the crystal structure of **P3.7**.*

3.3   Pyridyl-bridged ligand precursor synthesis

The properties and catalytic applications of metal complexes comprising NHC-based pincer-type ligands were comprehensively reviewed by Danopoulos and Pugh in 2007.[23] Since, the groups of Peris and Crabtree have also audited the field, with all reports underlining the robustness of metal-ligand binding within these complexes – the upshot of which is thought to be suppression of ligand-centred catalyst deactivation pathways.[24–26]

Until recently, relatively few reports on the synthesis and applications of iron(II) *bis*(carbene)pyridine pincers were documented.[27] Nevertheless, in 2012 Chirik and co-workers proved this class of compound to be highly efficient in the hydrogenation of unactivated and essentially unfunctionalised alkenes.[28] Following on from these findings, the same authors recently published the employment of these complexes as highly active, site-selective catalysts for ^{3}H labelling of pharmaceutical drugs – rejuvenating interest in C,N,C-chelating iron(II) pincers of NHCs.[29]

In 2015, Harlang and Wärnmark reported on an iron(II) *tetra*-NHC complex comprising 2,6-pyridyl bridged carbene ligands, which acts as a highly potent sensitizer.[30] The complex demonstrates an excited-state lifetime one thousand-fold longer than its iron *bis*-NHC analogue, though the complex itself requires tedious and low-yielding synthetic preparation due to the obvious mismatch between metal/ligand stoichiometry. It was speculated that our methodology may provide a useful synthetic platform to produce these complexes.

The direct linkage of substituted imidazole to the 2- and 6-positions of a pyridine ring allows access to a ligand template for building C,N,C-chelating pincer NHC complexes, by way of their

corresponding *bis*-imidazolium salts. On account of these, four separate batches of freshly prepared 2,6-dibromomethylpyridine were independently treated with two equivalents of *N*-methylimidazole, *N*-allylimidazole, *N*-(2-methoxy)phenylimidazole and *N*-picolylimidazole to generate four functionally diverse pyridyl-bridged *bis*-NHC ligand precursors, **P3.8** – **P3.11** (see **Scheme 3.7** for reaction pathway).

P3.8: R = methyl, **71 %**
P3.9: R = allyl, **66 %**
P3.10: R = (2-OMe)Ph, **60 %**
P3.11: R = picolyl, **64 %**
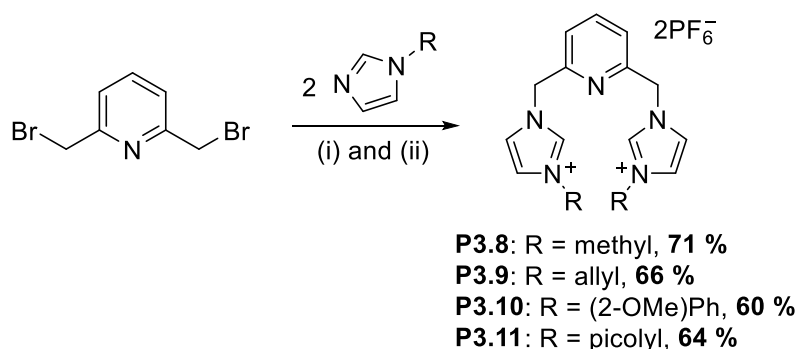
Scheme 3.7 *Synthetic route to 2,6-pyridyl-bridged bis-imidazolium salts, **P3.8** – **P3.11**. Conditions: (i) MeCN, 80 ˚C, 16 hours; (ii) H₄NPF₆ (2 equiv.), H₂O, r.t., 2 hours.*

P3.8 – **P3.11** were each fully characterised by multinuclear NMR spectroscopy, ESI mass spectrometry and combustion analysis. Common across all, were a diagnostic low-field singlet in both the ^{1}H (400 MHz, CD$_3$CN) and ^{13}C{^{1}H} (100 MHz, CD$_3$CN) NMR spectra, between 8.5 – 10.0 and 155 – 160 ppm, respectively, strongly indicative of C_2-symmetric *bis*-imidazolium ion formation (C2 environments). Descending the list, positive mass peaks (*m/z*) 414.1294, 160.5971, 227.1103 and 568.1852 were noted in each respective ESI mass spectrum, attributable to [**P3.8** – PF$_6$]$^+$, [**P3.9** – 2PF$_6$]$^{2+}$, [**P3.10** – 2PF$_6$]$^{2+}$ and [**P3.11** – PF$_6$]$^+$ molecular fragments.

In addition, single crystals of the novel *bis*-imidazolium dihexafluorophosphate, **P3.11**, were obtained through the slow diffusion of diethyl ether vapours into an acetonitrile solution of the product, which were amenable to X-ray diffraction analysis and confirmed the expected molecular structure of **P3.11**, with all bond metrics within the expected range (**Figure 3.2**).
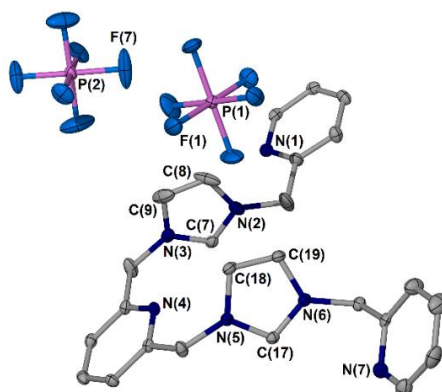
Figure 3.2 *Molecular structure of **P3.11**. Atomic displacement parameters are drawn at the 50 % probability level, hydrogen atoms are omitted for clarity.*

3.4 Synthesis and characterisation of *N*-donor substituted iron(II)-NHC complexes

In a detailed study, Meyer and Kühn have used Mössbauer spectroscopy to demonstrate that NHC/pyridine hybrid ligands impose a strong ligand field, imparting low-spin states (*i.e.* $S = 0$) on complexes of iron(II).[31] Befitting these predictions, Chen's original product of electrochemical oxidation of iron(0) powder whilst in the presence of an NHC/pyridine hybrid precursor, led to the sole isolation of a low-spin, octahedral iron(II) complex.[13] It was therefore envisaged that electrochemical reduction of ligand precursors **P3.1** – **P3.7** in the presence of Fe^{2+} ions would lead to octahedral iron(II) diamagnets of this type, allowing reaction monitoring by NMR spectroscopy.

3.4.1 Complexation of *N*-aryl, *N'*-pyridyl substituted imidazolium precursors

From the outset, a pair of dry iron foil electrodes (99.5 % purity, $13 \times 10 \times 1$ mm) were introduced to an anhydrous, N_2-purged MeCN solution of ligand precursor **P3.1** (33 mM solution), and a potential range applied (25 – 28 V) to maintain a constant steady-state current of 50 mA (measured by an in-series ammeter). Within the first ten minutes (30 C charge passed, under the stated conditions), the colourless reaction mixture became a deep red solution, indicative of complex formation. Likewise, gas evolution was observed from the electrochemical cathode, suggestive of H_2 production from imidazolium reduction. The composition of the reaction contents was monitored by ESI mass spectrometry, which provided a crude handle on reaction progress. After 90 minutes process time, the solution was filtered and product isolated by recrystallisation, affording the iron(II) *bis*-NHC complex, **3.1**, as a microcrystalline red powder in 82 % yield (**Scheme 3.8**).

P3.1: R = 2-pyridyl
P3.2: R = mesityl

3.1: R = 2-pyridyl, **82 %**
3.2: R = mesityl, **74 %**
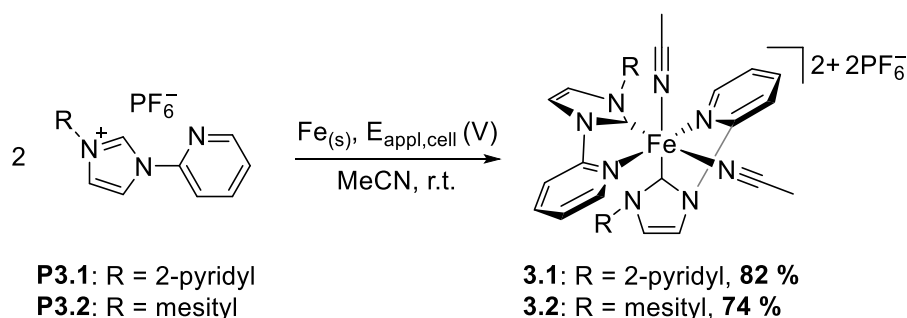
Scheme 3.8 *Electrochemical synthetic route to iron(II) bis-NHC complexes,* ***3.1*** *and* ***3.2***.

Following isolation, **3.1** was initially analysed by ^{1}H NMR spectroscopy, which clearly illustrated a sequence of sharp, well-resolved signals implicative of a diamagnetic iron(II) sample, adopting a low-spin d^6 electronic configuration. The same spectrum showcased removal of an original low-field NC*H*N imidazolium proton signal, alongside the presence of ten distinct ^{1}H environments, attributable to two coordinated NHC ligands which are magnetically related by C_2 symmetry, with

each chelated through only one *N*-pyridyl donor group. The product was also probed by $^{13}C\{^{1}H\}$ NMR spectroscopy, which featured twelve distinct singlet resonances in the aromatic region, with one remote low-field signal at 200.1 ppm (125 MHz, CD$_3$CN), corroborating with both C_2 equivalent carbenic nuclei. A comparison between the proton NMR spectra of azolium **P3.1** with iron(II) complex **3.1** is provided in **Figure 3.3**.
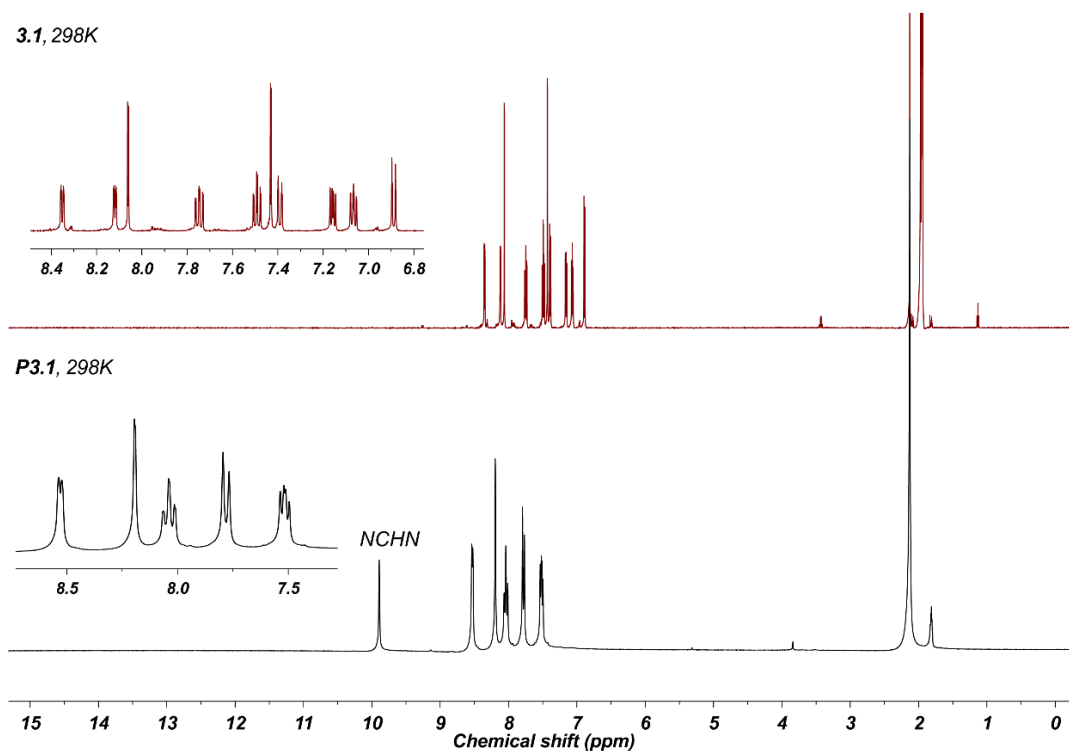
Figure 3.3 *^{1}H NMR spectrum of authentic ligand precursor **P3.1** (black trace, 300 MHz, CD$_3$CN, 298K), noting loss of original imidazolium signal at 9.89 ppm. ^{1}H NMR spectrum of Fe-NHC complex **3.1** (red trace, 500 MHz, CD$_3$CN, 298K).*

Iron(II) *bis*-NHC complex **3.1** was also analysed by high-resolution mass spectrometry, featuring a dominant dicationic mass cluster at (*m/z*) 250.0574, attributable to an [Fe(NHC)$_2$]$^{2+}$ molecular fragment, losing two molecules of labile MeCN and a pair of non-coordinating PF$_6$ counteranions prior to detection.

Bright red needles of **3.1** were obtained through the slow vapour diffusion of diethyl ether into a concentrated acetonitrile solution of the complex, and subsequently analysed by X-ray diffraction methods. The structural solution is provided in **Figure 3.4**.
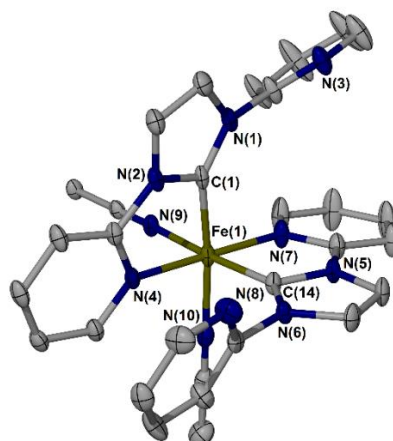
Figure 3.4 *Molecular structure of **3.1**. Atomic displacement parameters are drawn at the 40 % probability level, hydrogen atoms and two PF$_6$ counteranions are omitted for clarity.*

Fe(1)-C(1)	1.933(6)	C(1)-Fe(1)-C(14)	88.3(2)
Fe(1)-C(14)	1.912(5)	C(1)-Fe(1)-N(7)	98.5(2)
Fe(1)-N(4)	1.997(4)	C(1)-Fe(1)-N(10)	173.03(19)
Fe(1)-N(7)	2.000(5)	C(1)-Fe(1)-N(4)	81.3(2)

Table 3.2 *Selected bond lengths (Å) and angles (°) from the crystal structure of **3.1**.*

The solid-state structural elucidation of **3.1** illustrates an iron(II) metal centre coordinating two NHC ligands, in octahedral geometry. Each independent carbenic ligand is disposed mutually *cis* at a relative angle of 88.3(2)°, whilst both reside *trans* to a coordinating molecule of MeCN solvent. Only one pyridyl group of each ligand is able to coordinate to the iron(II) centre, leaving the other twisted orthogonal to the chelated plane (giving rise to ten magnetically inequivalent aromatic signals in the ^{1}H NMR spectrum). All contact distances pertaining to the inner coordination sphere of **3.1** agree with those previously reported.[3] All solution-state measurements support the observed solid-state molecular structure, including combustion analysis, implying that **3.1** does indeed exist as a [Fe(NHC)$_2$(MeCN)$_2$]2PF$_6$ complex in both physical states.

Electrochemical conversion of analogue **P3.2** in the same manner as **P3.1** demonstrated a sequence of similar physical observations during reaction, affording iron(II) *bis*-NHC complex **3.2** as a microcrystalline dark red powder, in 74 % yield. The product was assessed using similar methods to those outlined for **3.1**, with multinuclear NMR spectroscopy particularly informative (for comparison, a ^{1}H NMR recording is illustrated in **Figure 3.5**). Sharp, well-resolved signals were observed in all solution NMR spectroscopic measurements, suggestive of an iron(II) complex pertaining to a low-spin d^6 electronic configuration. Unexpectedly, a total of eight magnetically inequivalent aromatic signals were observed in the ^{1}H NMR spectrum of **3.2**, where only seven inequivalent protons exist within the ligand precursor (*i.e.* **P3.2**). Based on multiplicity

alone, singlet resonances observed at 6.68 and 6.53 ppm (500 MHz, CD$_3$CN, inset image of **Figure 3.5**) must pertain to those directly attached to each mesityl ring, which should maintain relation by symmetry. Likewise, three inequivalent binary methyl signals are observed in the same spectrum at 2.34, 2.14 and 1.61 ppm, further evidencing a break in symmetry of each mesityl ring within the product. Nonetheless, their apparent magnetic inequivalence is not obvious from NMR data alone.
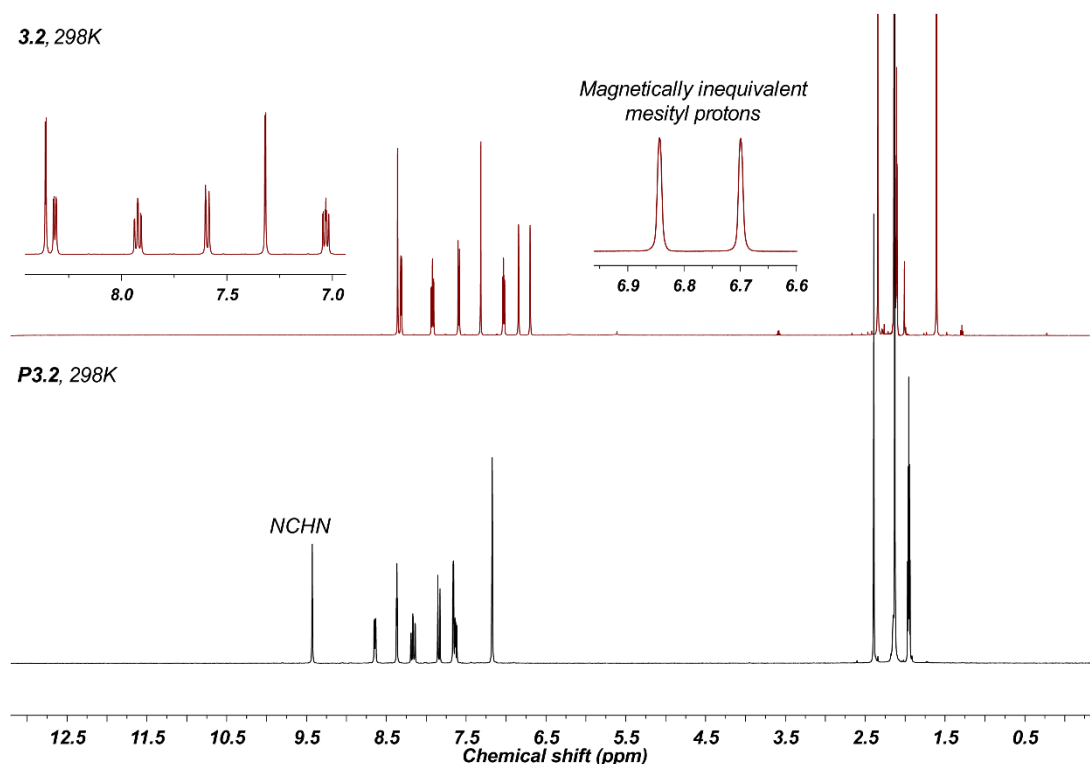
Figure 3.5 *^{1}H NMR spectrum of authentic ligand precursor **P3.2** (black trace, 300 MHz, CD$_3$CN, 298K), noting loss of original imidazolium signal at 9.45 ppm. ^{1}H NMR spectrum of Fe-NHC complex **3.2** (red trace, 500 MHz, CD$_3$CN, 298K), indicating magnetic inequivalence of aromatic mesityl signals upon complexation.*

The electrospray mass spectrum of **3.2** features a molecular ion peak at (*m/z*) 809.2356, attributable to a [Fe(NHC)$_2$(MeCN)$_2$PF$_6$]$^+$ cation, with a subsequent positive mass fragmentation pattern observed at 727.1842 and 291.1139, corroborating each [Fe(NHC)$_2$PF$_6$]$^+$ and [Fe(NHC)$_2$]$^{2+}$ species, respectively. Though little structural information may be extracted, all peaks observed in the ESI mass spectrum signify formation of an FeL$_2$-type complex.

Slowly diffusing diethyl ether vapours into an acetonitrile solution of **3.2** allowed isolation of single crystals of the product, which were subsequently analysed through X-ray crystallography (**Figure 3.6**).
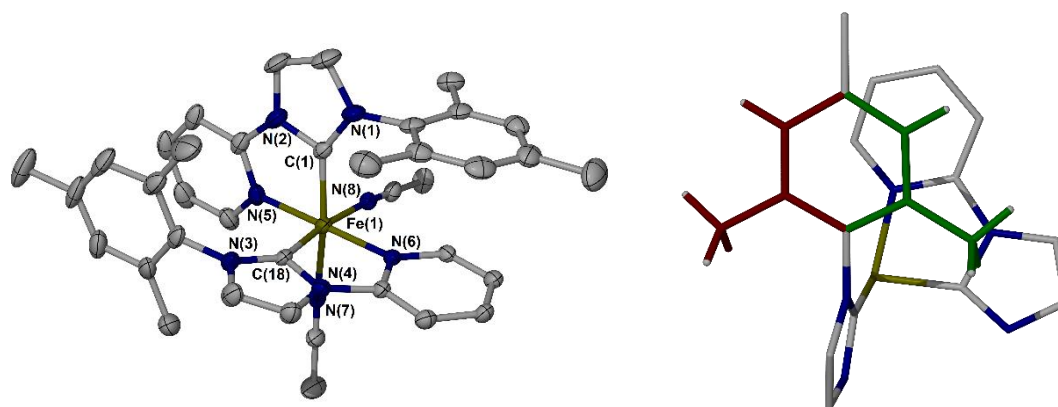
Figure 3.6 *Left: cationic portion of the asymmetric unit of* **3.2**. *Atomic displacement parameters are drawn at the 50 % probability level, hydrogen atoms and two PF₆ counteranions are omitted for clarity. Right: partial molecular structure of* **3.2**, *highlighting origin of magnetic inequivalence in each mesityl ring (red versus green bonds).*

Fe(1)-C(1)	1.910(5)	C(1)-Fe(1)-C(18)	90.7(2)
Fe(1)-C(18)	1.930(5)	C(1)-Fe(1)-N(5)	80.9(2)
Fe(1)-N(5)	1.984(4)	C(1)-Fe(1)-N(6)	98.41(19)
Fe(1)-N(6)	1.998(4)	C(1)-Fe(1)-N(7)	173.8(2)

Table 3.3 *Selected bond lengths (Å) and angles (˚) from the crystal structure of* **3.2**.

Verified through solid-state analysis, **3.2** forms as an [Fe(NHC)₂(MeCN)₂]2PF₆ complex, analogous to **3.1**. Disposed about an octahedral iron(II) centre, are two mutually *cis* NHC ligands which chelate to the metal through each *N*-pyridyl donor wingtip. Although unremarkable bond metrics are acquired, the crystal structure provides insight to the origin of magnetic inequivalence of each mesityl ring in solution NMR studies. Apparent in the solid-state, are the presence of π-π interactions between each mesityl and pyridyl ring of **3.2** (interplanar distance = 3.2 Å). Despite the ability to freely rotate, each mesityl ring appears conformationally locked to position one half of each mesityl group above a pyridine ring (**Figure 3.6**, green bonds), and the other half away from the ring current (red bonds), to generate inequivalence on an NMR timescale at room temperature. Akin to **3.1**, all solution-state analysis of **3.2** support the solid-state molecular structure, and imply the same species exists in both physical states.

3.4.2 Complexation of *N*-picolyl substituted imidazolium precursors

Basset and Kühn have recently investigated the effect of NHC-to-pyridine ratio on electronic structure and redox behaviour of iron(II) metal centres.[32] Combining solution NMR studies with voltammetric analysis, the authors proved there to be a linear correlation between metal redox potential and NHC/pyridine ratio, which allows fine-tuning of electronic configuration. It was

therefore sought to expand our method by electrochemically preparing iron complexes of NHCs of various denticity.

Under analogous conditions to those described above, freshly prepared imidazolium **P3.3** underwent electrochemical conversion to afford iron(II) complex **3.3**, in 85 % yield (**Figure 3.7**).
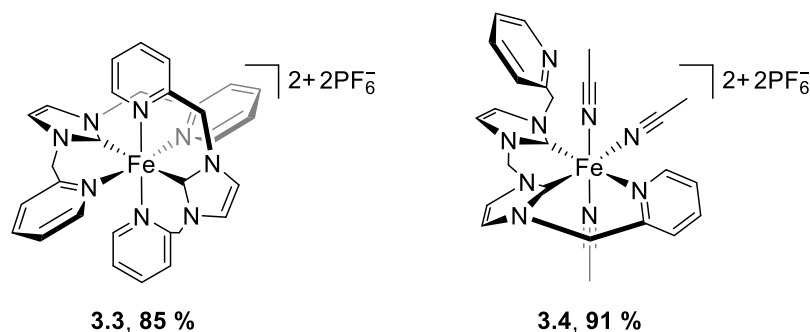
Figure 3.7 Representative iron(II) bis-NHC complexes, 3.3 and 3.4.

Formation of **3.3** was followed by high-resolution mass spectrometry, which after 90 minutes reaction time detected a significant relative quantity of an FeL_2 species. Positive mass peaks (*m/z*) 701.1422, 575.1771 and 278.0904 became evident in the ESI mass spectrum, indicative of 2:1 ligand/metal complex adducts in solution (representing $[ML_2 - PF_6]^+$, $[ML_2 - 2PF_6 + OH]^+$ and $[ML_2 - 2PF_6]^{2+}$ mass adducts, respectively).

Following work-up and isolation, **3.3** was analysed by multinuclear NMR spectroscopy. Recording the ^1H NMR spectrum in d_3-MeCN at room temperature illustrated clear absence of an imidazolium (NC*H*N) proton, as expected, alongside only five, well-resolved aromatic proton signals – suggestive of a low-spin octahedral iron(II) complex with significant molecular symmetry. Completing the spectrum, are a pair of well-separated doublet resonances at 5.62 and 4.17 ppm (500 MHz, CD$_3$CN), which present matching *J*-coupling constants (16.0 Hz) and arise from each set of diastereotopic protons attached to both methylene bridges of each ligand in **3.3**. A $^{13}C\{^1H\}$ NMR spectrum of **3.3** was also recorded under analogous conditions, showcasing a total of eight singlet resonances to include a diagnostic low-field Fe-C$_{carbene}$ signal at 209.4 ppm (125 MHz, CD$_3$CN), further supporting a high degree of molecular symmetry in solution.

Storing a sample of **3.3** in THF solution at -30 ˚C for 48 hours produced bright red needles of the complex, which were amenable to X-ray crystallographic study. Following structural authentication, the product was confirmed to be an [Fe(NHC)$_2$]2PF$_6$ complex, as shown in **Figure 3.8**.
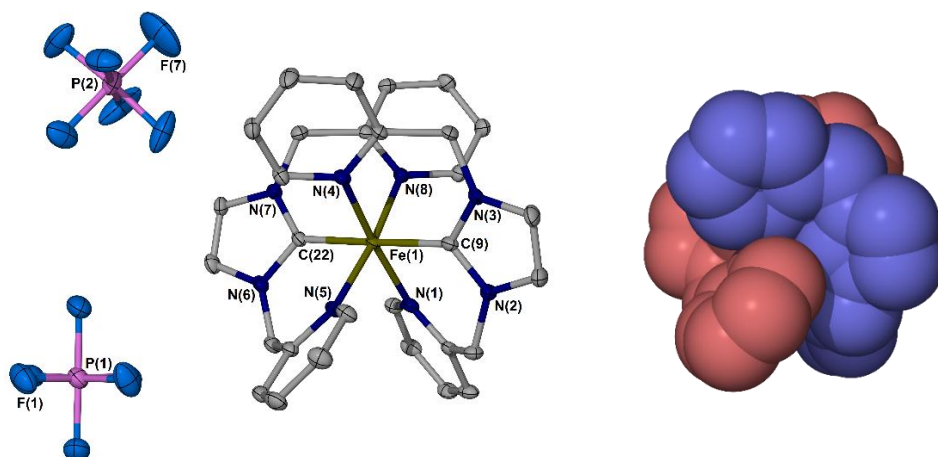
Figure 3.8 *Left: molecular structure of **3.3**. Atomic displacement parameters are drawn at the 50 % probability level, hydrogen atoms and two molecules of disordered THF solvent are omitted for clarity. Right: cationic portion of the asymmetric unit of **3.3**, displayed in space-filling mode, with each ligand distinguished by colour.*

|			
Fe(1)-C(9)	1.931(6)	C(9)-Fe(1)-N(1)	86.8(2)
Fe(1)-C(22)	1.930(5)	C(9)-Fe(1)-N(8)	93.39(19)
Fe(1)-N(1)	2.046(5)	C(9)-Fe(1)-C(22)	178.6(2)
Fe(1)-N(5)	2.036(5)	N(8)-Fe(1)-N(5)	173.24(17)

Table 3.4 *Selected bond lengths (Å) and angles (˚) from the crystal structure of **3.3**.*

The solid-state structure of **3.3** illustrates the expected 2:1 ligand/metal stoichiometry, with each NHC unit disposed mutually *trans* about the octahedron of an iron(II) centre, at an angle that only deviates from ideal linear geometry by 1.4˚. The two tridentate ligands of **3.3** are fully orthogonal, each occupying three positions on a meridian of the octahedron to coordinatively saturate the metal centre through κ^3 coordination. Two perpendicular lines of symmetry run through the plane of the metal, relating both halves of each equivalent ligand.

Displaying the molecular structure using a space-filling model (see **Figure 3.8**, right-hand image), it becomes clear that the surrounding ligands of **3.3** fully encase the metal centre, implying a significant level of steric protection of the iron(II) core. Using mass spectrometry, the stability of **3.3** towards hydrolysis was therefore examined. A positive ESI mass spectrum of pure **3.3** (5 mg) was recorded in MeCN solvent (2 mL), followed by subsequent analysis in the presence of deionised water (3 μL, 20 equiv. relative to **3.3**) over the course of 24 hours, as shown by the sequence of spectra given in **Figure 3.9**.
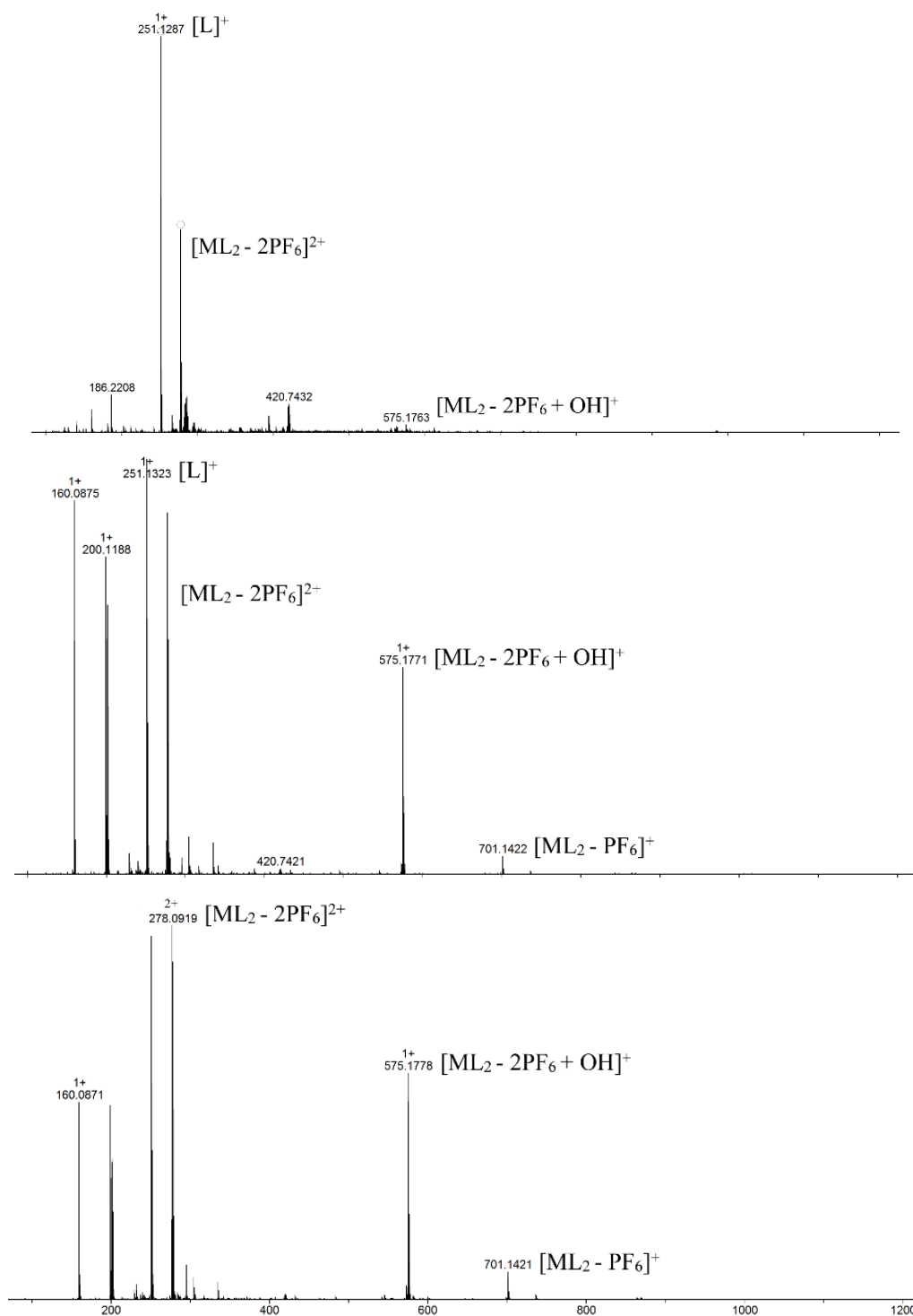
Figure 3.9 Interpreted HR-MS excerpts, from the water-sensitivity study of **3.3**. Bottom: ESI spectrum of pure **3.3** in neat MeCN solvent. Middle: ESI spectrum upon addition of H_2O (20 equiv.) after 1 hour. Top: ESI spectrum of the same sample after 24 hours.

Indeed, from **Figure 3.9** it can be seen that **3.3** slowly decomposes in the presence of water. After one hour (middle spectrum), no appreciable change is observed regarding relative peak ratio of **3.3** and free ligand. Following 24 hours however, all signals corroborating the iron-NHC complex have diminished (*m/z* 278.0919, 575.1771 and 701.1422), with free ligand now

dominating the spectrum (*m/z* 251.1287). Albeit slow, the hydrolysis of **3.3** is perhaps surprising given the level of steric encumbrance protecting the iron(II) centre, particularly when compared with Chen's water-stable iron-NHC complex which houses a pair of vacant coordination sites at iron.[13] Nevertheless, all solid-state analysis (including combustion) associate entirely with solution-state characterisation.

Following structural assignment of **3.3**, it was speculated that introduction of a methylene link between NHC units, as in precursor **P3.4**, may restrict their relative coordinative disposition mutually *cis*, opening access to the opposing face of the iron(II) centre which may be useful for further metal reactivity. Therefore, *bis*-imidazolium **P3.4** was electrochemically reduced and coordinated to iron, producing **3.4** as a microcrystalline red solid in 91 % yield (**Figure 3.7**).

Room temperature ^{1}H NMR spectroscopic analysis of **3.4** revealed broad signals for all methylene bridging protons between 5.20 – 6.40 ppm (500 MHz, CD_3CN), alongside twelve sharp, discrete aromatic resonances which point to a non C_2-symmetric ligand binding mode. Neither square-planar nor sawhorse-type coordination can explain these observations. The possibility of a conformational interconversion is not unrealistic, though would be expected to broaden all signals within the spectrum.

Variable temperature NMR spectroscopy (500 MHz, CD_3CN, 343 – 233K) was used to rationalise these observations. As anticipated, measuring the ^{1}H NMR spectrum of **3.4** at high temperatures (343K) led to significant broadening of all resonances, suggestive of increased rates of ligand fluxion on an NMR timescale. Recording the same spectrum at low temperature (233K) allows resolution of all signals, disclosing all six methylene protons as discrete diastereotopic doublets (see **Figure 3.10** for comparative ^{1}H NMR spectra between precursor **P3.4** and complex **3.4** at variable temperatures). It is therefore likely that rapid isomeric interconversion does indeed occur in acetonitrile solution, which is subdued at low temperature. At all temperatures, the major species of **3.4** in acetonitrile solution appears to be an unsymmetrical iron(II) complex, coordinating the ligand in a tridentate manner to leave one *N*-pyridyl group pendant. Recording a $^{13}C\{^1H\}$ NMR spectrum of the same sample supports this conclusion, as 19 distinct singlets are observed including two inequivalent and identifiable Fe-$C_{carbene}$ signals at 196.4 and 190.1 ppm (125 MHz, CD_3CN).

Notably, recording a room temperature ^{1}H NMR spectrum of the **3.4** in d_5-pyridine affords a full sequence of sharp resonances, including those pertaining to each methylene bridging proton (**Figure 3.10**, top spectrum, 500 MHz, C_5D_5N, 298K). Taking the measurement in this solvent brings about C_2 molecular symmetry, as evidenced by a 50 % loss in unique proton environments. The only ligand coordination geometry which can satisfy these findings must possess a plane of symmetry through both the central methylene link of the ligand and the metal atom itself.

Therefore, the *bis*-NHC ligand of **3.4** must adopt either κ^2 (through two NHCs only) or κ^4 (fully tetradentate) coordination to the iron(II) centre in the presence of strongly coordinating d_5-pyridine solvent, though this cannot be distinguished by NMR spectroscopy alone.
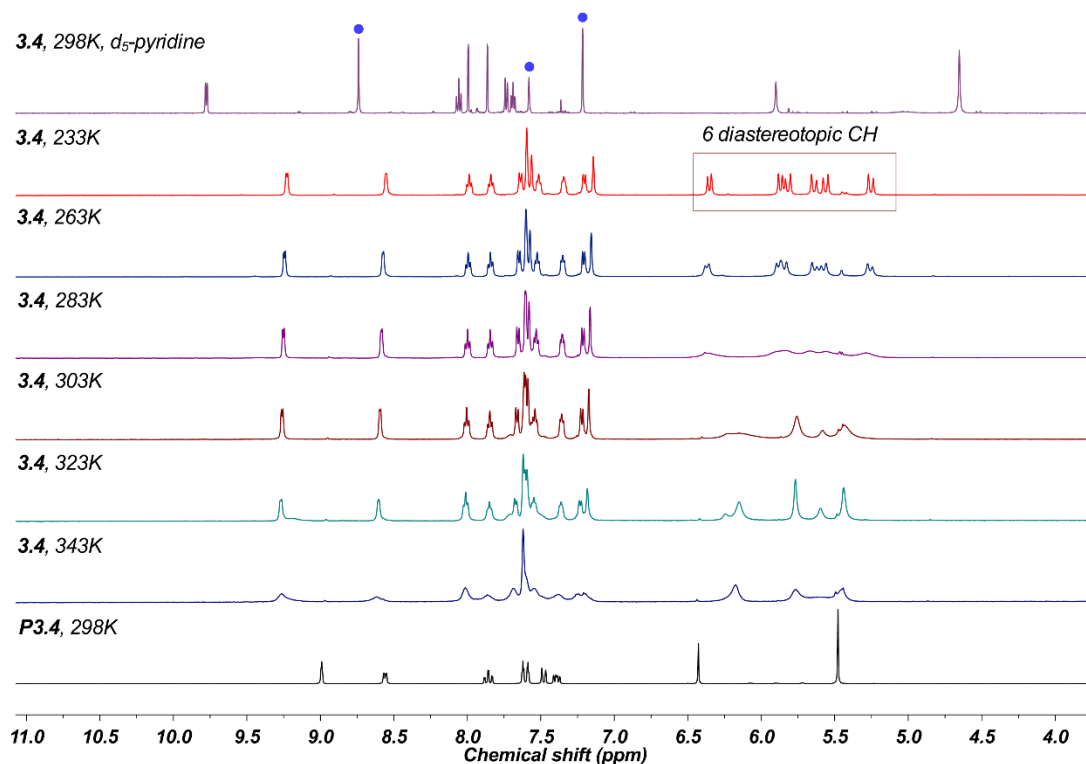
Figure 3.10 ^{1}*H NMR spectrum of azolium ligand precursor* **P3.4** *(black trace, 300 MHz, CD₃CN, 298K). Variable temperature* ^{1}*H NMR spectra (233 – 343K) of* **3.4** *(subsequent six traces, 500 MHz, CD₃CN), noting persistent diastereotopic doublet signals visible at 233K.* ^{1}*H NMR spectrum of* **3.4** *in d₅-pyridine (purple trace, 500 MHz, 298K), blue circles pertain to residual solvent peaks.*

Iron(II) *bis*-NHC complex **3.4** was further analysed through high-resolution mass spectrometry, featuring a prominent dicationic mass peak (*m/z*) 193.0477, attributable to a $[ML - 2PF_6]^{2+}$ molecular fragment which remains dominant regardless of solvent.

Diffusing vapours of diethyl ether into a concentrated acetonitrile solution of **3.4** allowed isolation of single, red crystals. Therefore, the solid-state structure of authentic **3.4** was elucidated through X-ray diffraction methods, which is presumed to be the original identity of the electrochemical product (**Figure 3.11**, left-hand image).
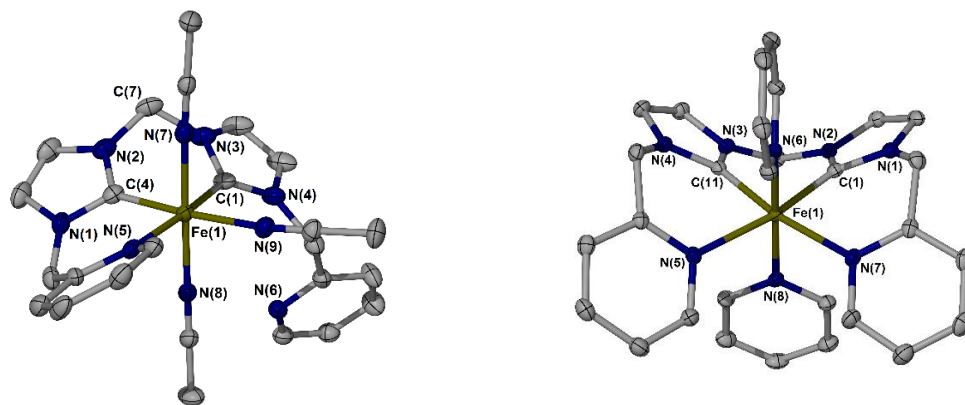
Figure 3.11 *Left: molecular structure of **3.4**, crystallised from MeCN solution. Right: molecular structure of **3.4**, crystallised from d₅-pyridine solution. Atomic displacement parameters are drawn at the 50 % probability level, hydrogen (and deuterium) atoms and two PF₆ counteranions are omitted from each structural solution for clarity.*

3.4·3MeCN	Fe(1)-C(1)	1.954(5)	C(1)-Fe(1)-C(4)	85.9(2)
3.4·3MeCN	Fe(1)-C(4)	1.891(5)	C(1)-Fe(1)-N(9)	93.0(2)
3.4·3MeCN	Fe(1)-N(5)	2.040(4)	C(4)-Fe(1)-N(9)	176.1(2)
3.4·3MeCN	Fe(1)-N(9)	1.987(4)	C(1)-Fe(1)-N(5)	173.1(2)
3.4·2C₅D₅N	Fe(1)-C(1)	1.921(3)	C(1)-Fe(1)-C(11)	85.00(13)
3.4·2C₅D₅N	Fe(1)-C(11)	1.909(3)	C(1)-Fe(1)-N(7)	86.28(12)
3.4·2C₅D₅N	Fe(1)-N(5)	2.150(3)	N(5)-Fe(1)-N(7)	103.90(10)
3.4·2C₅D₅N	Fe(1)-N(7)	2.137(3)	C(1)-Fe(1)-N(5)	169.76(12)

Table 3.5 *Selected bond lengths (Å) and angles (˚) from the crystal structure of **3.4**.*

Occupying the asymmetric unit of chiral **3.4**, are a pair of enantiomers which perhaps support the idea of isomeric interconversion in solution NMR studies. The potentially tetradentate ligand coordinates through only one hemilabile *N*-pyridyl group to the metal centre, vacating three meridional coordination sites which are occupied by solvating acetonitrile, whilst disrupting the overall symmetry of the molecule. Bond metrics are generally unremarkable, although a noticeable *trans*-influence is observed when comparing each Fe-C$_{carbene}$ bond length, which reside opposite either a coordinating pyridine ring or acetonitrile unit (Fe(1)-C(1) = 1.954(5) Å *versus* Fe(1)-C(4) = 1.891(5) Å, respectively). The solid-state structure retrofits agreeably with all solution-state analysis of **3.4** in acetonitrile solvent.

Following vacuum drying, bulk sample composition of **3.4** was assessed by elemental analysis, which consistently supported the incorporation of only two acetonitrile ligands into the complex assembly, implying one is removed *in vacuo* (similar findings have been reported by Kühn *et al.*).[32]

To investigate the apparent increase in molecular symmetry of **3.4** when dissolved in d_5-pyridine solution, crystals were obtained from this solvent by slowly diffusing diethyl ether vapours into the sample, and subsequently analysed by X-ray crystallography (**Figure 3.11**, right-hand image). The molecular structure displays an octahedral iron(II) complex which matches expectation based on solution NMR results. Answering a previous question regarding denticity that could not be concluded from solution NMR spectroscopy, the ligand coordinates to iron through a tetradentate κ^4 binding mode, placing two solvating molecules of pyridine in each axial position of the octahedron, with full substitution of all three previously-bound acetonitrile ligands.

In terms of the spectrochemical series, MeCN and C_5H_5N are similarly matched and neither are considered particularly strong high- or low-field ligands. However, C_5H_5N would be expected to impose a greater steric influence than MeCN when coordinated to iron, and from the X-ray crystal structure of **3.4**·$2C_5D_5N$ it can be seen that each orthogonal pyridine ring is well-suited to fit into each puckered cavity of the *bis*-NHC ligand. However, the lack of ligand fluxion in a C_5D_5N solution of **3.4** remains unresolved.

Unsymmetrical imidazolium precursor **P3.5** comprises a potentially reactive *N*-ester group, which are known to be susceptible to deprotonation in the presence of strong Brønsted bases, such as $[Fe\{N(SiMe_3)_2\}_2]$ or NaH. Consequently, completely chemoselective methods of metalating the C2 position of the imidazolium ring are scarce. Electrochemical reduction and subsequent metalation of **P3.5** was therefore performed using the electrochemical protocol, affording an isomeric mixture of chiral iron(II) *bis*-NHC complex, **3.5**, as a red powder in 76 % yield (**Scheme 3.9**).
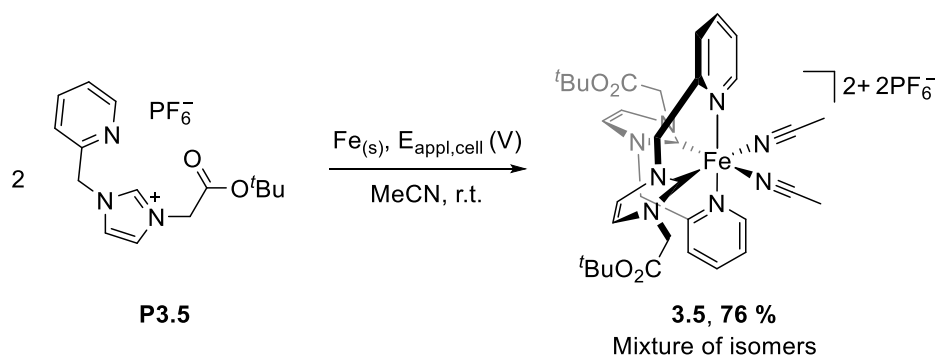
Scheme 3.9 *Electrochemical synthetic route to iron(II) bis-NHC complex, 3.5.*

From the outset, **3.5** was dissolved in d_3-MeCN and examined by ^{1}H NMR spectroscopy. Immediately evident, was a spectrum pertaining to multiple related species in solution in a similar relative ratio (as judged by solution integration measurement). All signals in the spectrum were sharp, with discrete multiplicity – suggestive of iron(II) ligated species of the same electronic structure to those described above. Interestingly, ^{13}C{^{1}H} NMR spectroscopic analysis of the

same sample provided a simplified spectrum of singlets which occur in distinct multiples of three, none of which corroborate with free ligand, though sum to a total of 39 unique carbon atoms which corroborate with that of three full, inequivalent ligands. Moreover, three low-field singlets are clearly presented within this spectrum at 194.8, 193.5 and 192.5 ppm, highly suggestive of three Fe-$C_{carbene}$ environments (a comparison between $^{13}C\{^{1}H\}$ NMR spectra of precursor **P3.5** and **3.5** is provided in **Figure 3.12**). It was therefore deemed likely, that more than one geometric isomer of **3.5** is produced upon complexation with iron, though based on these NMR data alone it is impossible to state their absolute molecular structure (in fact, very little structural information can be confidently taken from these spectra). Attempts were made to measure the proton NMR spectrum of this mixture at various temperatures, however no clear change in signal shift nor relative ratio was observed from 343 – 233K, implying these isomers are unable to interconvert on an NMR timescale. Interestingly, despite the synthesis of **3.5** in acetonitrile solvent, all d_3-MeCN NMR samples (sealed in a J. Young NMR tube) showed significant decomposition after as little as 12 hours at room temperature, with fine precipitate forming in each tube and resulting NMR signals diminishing into the baseline, perhaps suggestive of a ligand-assisted disproportionation mechanism (*i.e.* $3Fe^{2+} \rightarrow Fe^{0}_{(s)} + 2Fe^{3+}_{(sol)}$).
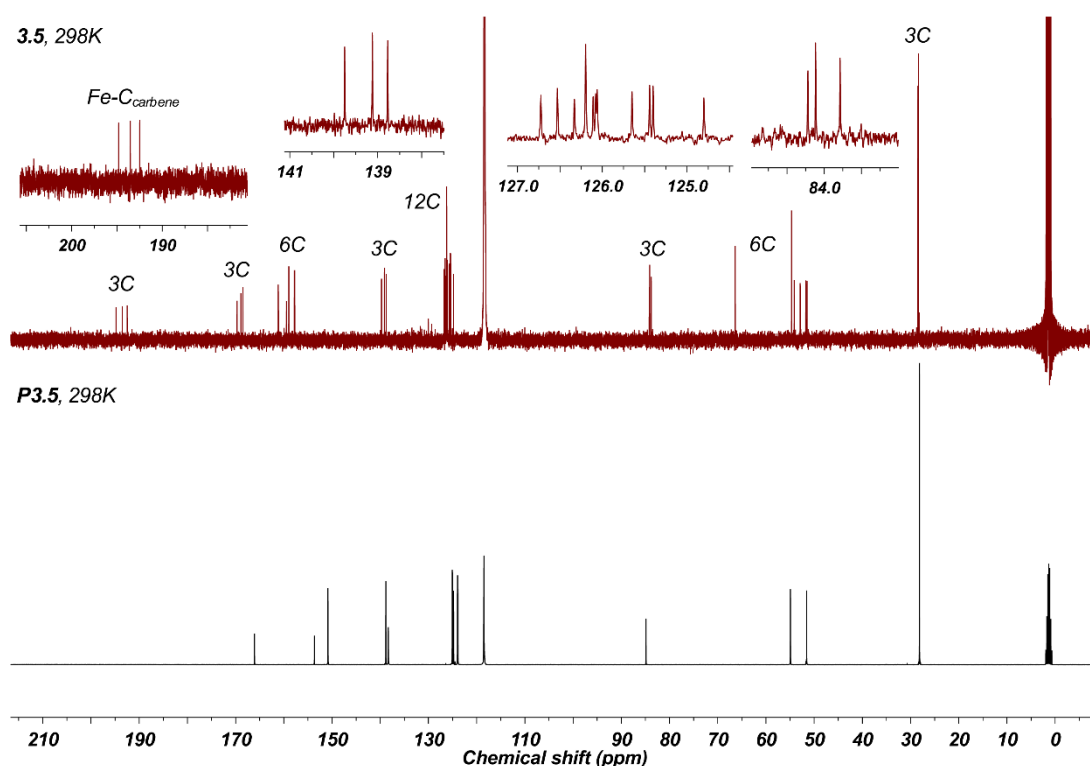
Figure 3.12 *$^{13}C\{^{1}H\}$ NMR spectrum of authentic ligand precursor **P3.5** (black trace, 125 MHz, CD₃CN, 298K), featuring 13 signals. $^{13}C\{^{1}H\}$ NMR spectrum of mixture of Fe-NHC **3.5** isomers (red trace, 125 MHz, CD₃CN, 298K), featuring 39 signals.*

Combustion analysis of the bulk material confirmed the expected elemental ratio of carbon, hydrogen and nitrogen, supporting the formation of mixed isomers of **3.5**. Further solid-state analysis was procured in the form of X-ray diffraction analysis, using single crystals obtained through the slow diffusion of diethyl ether vapours into an acetonitrile solution of **3.5** (**Figure 3.13**).
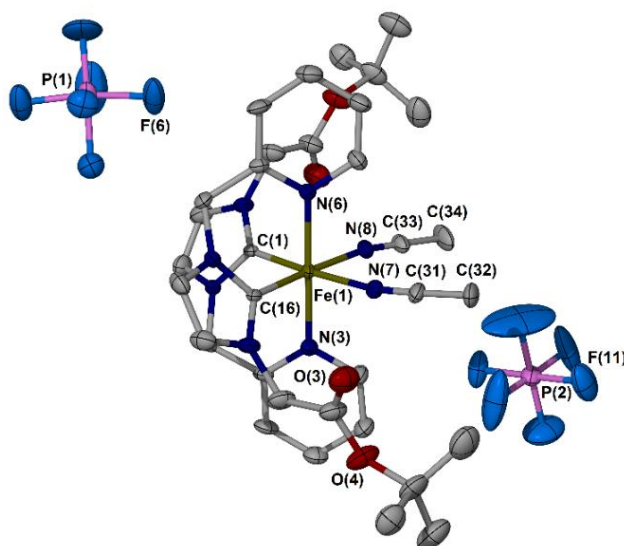

Figure 3.13 *Molecular structure of **3.5**. Atomic displacement parameters are drawn at the 50 % probability level, hydrogen atoms are omitted for clarity.*

Fe(1)-C(1)	1.958(6)	C(1)-Fe(1)-C(16)	96.0(2)
Fe(1)-C(16)	1.951(6)	C(1)-Fe(1)-N(6)	92.6(2)
Fe(1)-N(6)	2.013(6)	C(16)-Fe(1)-N(3)	93.1(2)
Fe(1)-N(3)	2.006(6)	C(1)-Fe(1)-N(7)	174.7(2)
Fe(1)-N(7)	1.990(6)	C(16)-Fe(1)-N(8)	175.5(2)
Fe(1)-N(8)	1.985(6)	N(3)-Fe(1)-N(6)	179.4(2)

Table 3.6 *Selected bond lengths (Å) and angles (°) from the crystal structure of **3.5**.*

The structural solution obtained displays one enantiomer of a C_2-symmetric octahedral iron(II) *bis*-NHC complex. Clear from the structure, are a pair of fully intact *N*-ester substituents attached to each ligand which remain pendant and related by symmetry. Each *N*-picolyl donor group occupies an opposing apical position at a near-ideal angle of 179.4(2)°, whilst two mutually *cis* NHC units remain *trans* to a pair of coordinating MeCN ligands.

The observed molecular structure given in **Figure 3.13** is arguably the most symmetrical isomer of **3.5** possible, therefore the isolation of an X-ray quality single crystal of **3.5** in this conformation is not surprising. It is likely that one sequence of signals in the solution NMR experiments described above are attributable to this conformer.

A number of different crystals from the same batch were also examined by X-ray crystallography. Serendipitously, two additional datasets were collected whose structural refinement each disclosed a different isomer of **3.5** to that above, with both being stereoisomers (Δ and Λ) of the same geometric isomer, as shown in **Figure 3.14**.
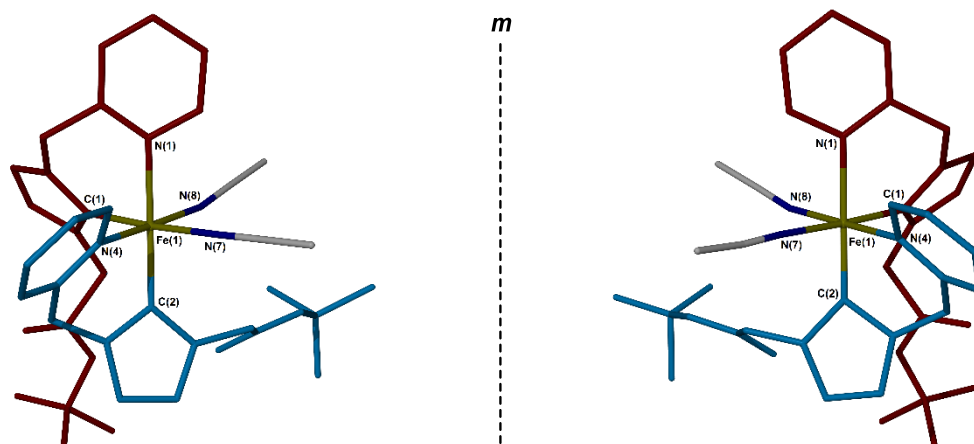
Figure 3.14 *Stick diagram representations of an alternative geometric isomer of **3.5**. Left: Δ-stereoisomer. Right: Λ-stereoisomer. All hydrogen atoms two PF$_6$ counteranions are omitted for clarity, and each identical ligand is distinguished by colour.*

Mechanical yet random separation of crystals within the batch allowed elucidation of both Δ- and Λ-stereoisomeric forms of a non C_2-symmetric geometric isomer of **3.5**, which appear to spontaneously crystallise in enantiopure form. Indeed, the formation of an unsymmetrical isomer alongside the fully symmetric variation (shown in **Figure 3.13**) supports the presence of three ligand environments in solution NMR spectroscopic measurements. However, reconciling the correct isomers with their corresponding solution data would require their separation and authentication, which has not yet been performed.

3.4.3   Complexation of *N*-allyl, *N'*-pyridyl substituted imidazolium precursors

Research conducted within our laboratory has shown *N*-allyl, *N'*-pyridyl substituted NHCs to be an interesting class of ancillary ligand, particularly in the presence of coordinating halides which appear to stabilise metals in multiple oxidation states.[14] Furthermore, the use of NHCs bearing terminal alkenic tethers is rare, due to alkene isomerisation under basic conditions (see Chapter 1). Therefore, imidazolium bromides **P3.6** and **P3.7** were targeted as electrochemical substrates.

Electrolysing an acetonitrile solution of azolium bromide **P3.6** (33 mM) with a pair of iron electrodes provided a noticeable increase in registered current under the standard electrochemical conditions, when compared with typical hexafluorophosphate salts (in the order of four-fold). Therefore, a reduced electrical potential was required (14 V) to maintain 50 mA current under

steady-state conditions. Following 90 minutes reaction time, the dark red solution was filtered and iron(II) *bis*-NHC **3.6** isolated upon addition of diethyl ether, in 64 % yield (**Scheme 3.10**).

P3.6: X = Br
P3.6.1: X = PF$_6$

3.6: X = Y = Br, Z = NCMe*
O3.6: X = Y = Z = Br*
3.6.1: Y = Z = NCMe, X = 2PF$_6$**
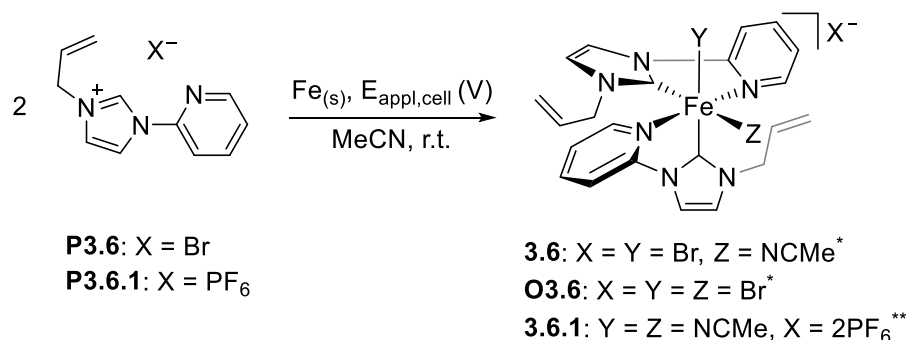
Scheme 3.10 *Electrochemical synthetic route to iron(II) bis-NHC complexes, 3.6 and 3.6.1.*
*Monocationic complex, **dicationic complex. Subsequent aerobic oxidation of isolated 3.6*
produces O3.6.

Following isolation, **3.6** was analysed by NMR spectroscopy, which displayed a sequence of uninformative broad resonances to represent two inequivalent ligand environments. However, electrospray mass spectrometry of the sample afforded a dominant dication at (*m/z*) 213.0658, attributable to a $[ML_2 - 2Br]^{2+}$ mass fragment, along with a molecular ion peak of (*m/z*) 505.0436, corroborating a $[ML_2 - Br]^+$ cationic species (see **Figure 3.15** for full ESI mass spectrum). The charge states observed for these masses confer with fragmentation of an original iron(II) complex, implying that observed broadening of NMR signals is not due to the production of a paramagnetic iron(III) complex.
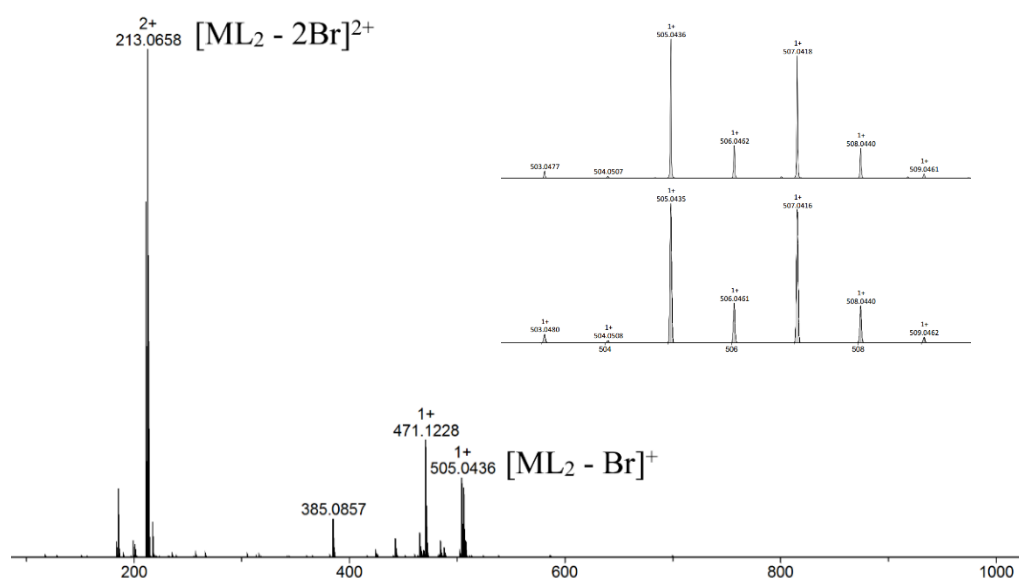
Figure 3.15 *Interpreted electrospray mass spectrum of 3.6 recorded in MeCN solvent.*
Inset image: simulated (bottom) vs observed (top) mass envelope for [3.6 − Br]$^+$ mass fragment, noting diagnostic isotopic distribution.

Dark red, block crystals were produced from the diffusion of diethyl ether vapours into an acetonitrile solution of **3.6**, and structurally elucidated using X-ray diffraction analysis (**Figure 3.16**).
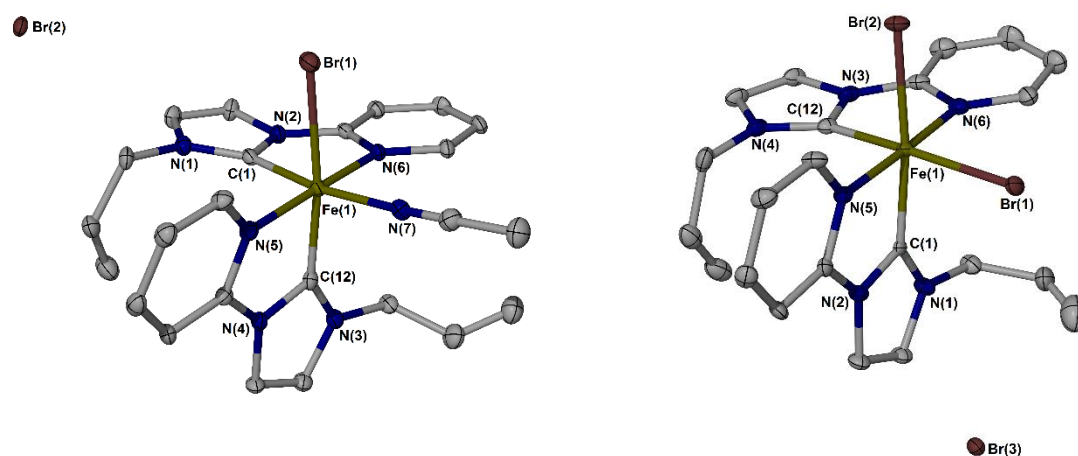
Figure 3.16 *Left: molecular structure of **3.6**. Right: molecular structure of **O3.6**, formed from the aerobic oxidation of **3.6**. Atomic displacement parameters are drawn at the 50 % probability level, hydrogen atoms are omitted from each structural solution for clarity.*

3.6	Fe(1)-C(1)	1.913(5)	C(1)-Fe(1)-C(12)	90.5(2)
3.6	Fe(1)-C(12)	1.928(5)	C(1)-Fe(1)-N(5)	96.80(19)
3.6	Fe(1)-N(5)	2.002(4)	C(12)-Fe(1)-Br(1)	172.40(14)
3.6	Fe(1)-Br(1)	2.5433(9)	C(1)-Fe(1)-N(7)	171.59(19)
O3.6	Fe(1)-C(1)	1.953(5)	C(1)-Fe(1)-C(12)	88.6(2)
O3.6	Fe(1)-C(12)	1.949(6)	C(1)-Fe(1)-N(5)	80.1(2)
O3.6	Fe(1)-N(5)	2.005(5)	C(12)-Fe(1)-Br(1)	174.26(17)
O3.6	Fe(1)-Br(1)	2.4302(11)	C(1)-Fe(1)-Br(2)	173.11(17)
O3.6	Fe(1)-Br(2)	2.4362(10)	Br(1)-Fe(1)-Br(2)	96.28(4)

Table 3.7 *Selected bond lengths (Å) and angles (°) from the crystal structures of **3.6** and **O3.6**.*

The structural solution of **3.6** displays the expected 2:1 NHC/metal combination, which supports the ESI mass spectrum above. Central, is an iron(II) atom in distorted octahedral geometry which also coordinates one bromide ligand and one molecule of solvating acetonitrile, providing an overall non C_2-symmetric coordination sphere which similarly supports solution NMR spectroscopic measurements. In general, all bond metrics are in keeping with those documented within, however it is clear that each alkene remains terminal in the product (average terminal C=C bond length = 1.31 Å).

Dissolution of single crystals of **3.6** into hydrous acetonitrile, followed by slow evaporation of the solvent under an atmosphere of air afforded a collection of dark red needles (**O3.6**). All spectroscopic measurements (^{1}H and ^{13}C{^{1}H} NMR, d_3-MeCN) displayed significantly broad, unassignable resonances, suggestive of a paramagnetic ferric sample. X-ray crystallographic analysis of the crystals provided a structural solution, which confirmed the formation of an iron(III) *bis*-NHC complex, **O3.6**, as shown in **Figure 3.16** (right-hand image). Interestingly, upon exposure to air **3.6** is oxidised to its iron(III) counterpart, which acquires an additional bromide counteranion to balance overall charge. It is speculated that this redox process takes place in solution, and is limited to a 50 % maximum yield of **O3.6**, though the mechanism of ligand-displacement remains unclear (similar findings have been observed for palladium(II)-NHCs of this ligand class, which will be discussed through Chapter 5).

Upon direct oxidation of **3.6**, each NHC ligand remains firmly bound to the metal centre in producing C_2-symmetric **O3.6**. A direct comparison between the bond metrics of **3.6** and **O3.6** is given in **Table 3.7**, and illustrates subtle lengthening of each Fe-C$_{carbene}$ bond upon oxidation of the ferrous centre (average Fe^{II}-C$_{carbene}$ = 1.92 Å, Fe^{III}-C$_{carbene}$ = 1.95 Å), which is a likely consequence of an additional coordinating bromide ligand within the sphere of **O3.6**. Aside from these lengths, all bond metrics of **3.6** and **O3.6** are highly comparable.

It was speculated that the observed poor quality NMR spectroscopic analysis of **3.6** may be due to rapid coordinative fluxion about the iron(II) centre, by both solvating acetonitrile and associated bromide anions. Therefore, the hexafluorophosphate analogue of **P3.6** was also prepared, through reaction of **P3.6** with two equivalents of aqueous NH_4PF_6 (**P3.6.1**), and coordinated to iron using the electrochemical procedure, affording iron(II) *bis*-NHC **3.6.1** in 84 % yield (**Scheme 3.10**).

Following isolation, **3.6.1** was examined using ^{1}H NMR spectroscopy, which illustrated a series of broad, yet assignable resonances. Clear from the spectrum, is a C_2-symmetric ligand environment which lacks an imidazolium C2 proton (NC*H*N signal) – indicative of complex formation (a comparison between the ^{1}H NMR spectra of **P3.6.1** and **3.6.1** is provided in **Figure 3.17**). In addition, a relatively up-field singlet is observed at 2.26 ppm (400 MHz, CD$_3$CN, 298K), attributable to two molecules of ligated MeCN at the iron centre. Analysis by ^{13}C{^{1}H} NMR spectroscopy provided only 11 singlets (*i.e.* one full ligand), including a low-field Fe-C$_{carbene}$ resonance at 199.2 ppm (100 MHz, CD$_3$CN, 298K) which further supports a C_2-symmetric ligand environment. Aside from these conclusions, no further structural information of **3.6.1** can be confidently deduced from these spectra.

3.6.1, 298K

6 aromatic signals

coordinated MeCN

P3.6.1, 298K

NCHN
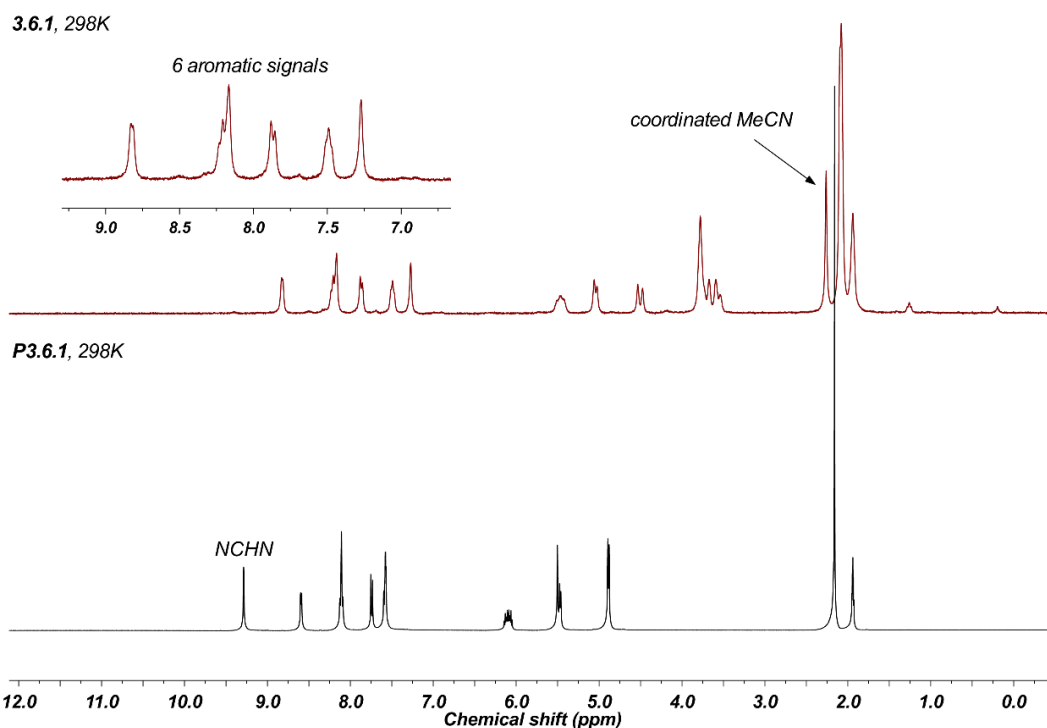
Figure 3.17 *^{1}H NMR spectrum of authentic ligand precursor **P3.6.1** (black trace, 400 MHz, CD$_3$CN, 298K), noting loss of original imidazolium signal at 9.23 ppm. ^{1}H NMR spectrum of Fe-NHC complex **3.6.1** (red trace, 500 MHz, CD$_3$CN, 298K).*

Analysis of **3.6.1** by high-resolution mass spectrometry afforded an intense parent cation at (*m/z*) 445.1254, attributable to a [ML$_2$ – 2PF$_6$ + OH]$^+$ mass fragment, alongside a similarly intense dicationic peak at (*m/z*) 213.0638 to corroborate a [ML$_2$ – 2PF$_6$]$^+$ molecular species.

The absolute molecular structure of **3.6.1** was confirmed through X-ray diffraction methods, using single crystals obtained from the slow diffusion of diethyl ether vapours into an acetonitrile solution of the complex (see **Figure 3.18** for the structural authentication). The solid-state structure of **3.6.1** illustrates the expected C_2-symmetric, octahedral iron(II) *bis*-NHC complex, which retrofits all solution-state analysis.
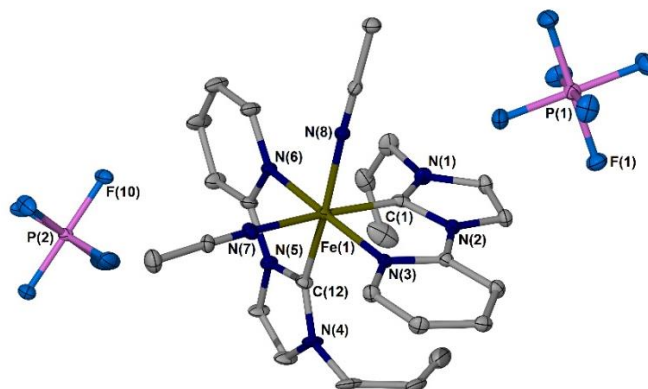
Figure 3.18 *Molecular structure of **3.6.1**. Atomic displacement parameters are drawn at the 40 % probability level, hydrogen atoms are omitted for clarity.*

Fe(1)-C(1)	1.936(7)	C(1)-Fe(1)-C(12)	89.8(3)
Fe(1)-C(12)	1.947(7)	C(1)-Fe(1)-N(3)	80.7(3)
Fe(1)-N(3)	2.000(6)	C(1)-Fe(1)-N(7)	172.6(3)
Fe(1)-N(6)	2.005(6)	N(3)-Fe(1)-N(6)	177.5(3)

Table 3.8 Selected bond lengths (Å) and angles (°) from the crystal structure of 3.6.1.

It has also been shown within our laboratory, that varying the electronic properties of NHCs bearing *N*-substituted pyridyl rings can yield a significant effect upon the reactivity of their subsequent complexes, and will be discussed further in Chapter 6 of this thesis. It was therefore decided to electrochemically produce 4-DMAP substituted iron(II) analogue, **3.7**, with a view to form a highly electron-rich iron(II)-NHC complex. Reaction of an acetonitrile solution of **P3.7** in the same manner as **P3.6** afforded iron(II) *bis*-NHC congener, **3.7**, as the major product of reaction (**Scheme 3.11**).

3.7: Y = Z = NCMe, X = 2Br[*]
O3.7: X = Y = Z = Br[**]
A3.7: Y = NCMe, Z = NH₃, X = 2Br[**]
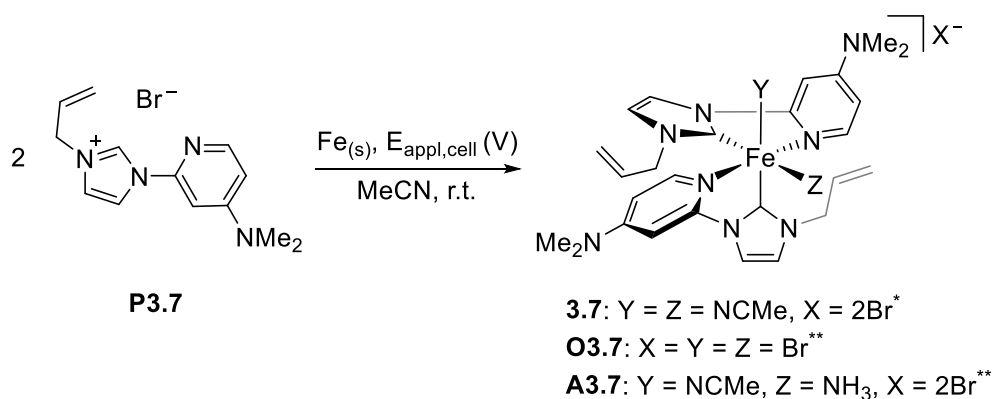
Scheme 3.11 Electrochemical synthetic route to iron(II) bis-NHC complex, 3.7. [**]Monocationic complex, [*]dicationic complex. Subsequent aerobic oxidation of isolated 3.7 produces O3.7.

Following reaction and work-up, a deep red powder was obtained of similar physical appearance to all analogues documented within. However, analysis of the bulk sample by ^{1}H NMR spectroscopy indicated a mixture of products in solution, which proved difficult to distinguish and identify.

In contrast, the electrospray mass spectrum of the bulk powder featured a single mass peak at (*m/z*) 256.1063 (recorded in MeCN solvent), attributable to an $[FeL_2]^{2+}$ molecular fragment (where L = [**P3.7** – HBr]), with no other mass adducts detected. An observed spectrum of this type implies the mixture of products illustrated within the solution ^{1}H NMR spectrum are not impurities, and are more likely to be conformational isomers of **3.7**.

Single crystals of **3.7** were grown from the slow diffusion of diethyl ether vapours into an acetonitrile solution of the product, and subsequently analysed by X-ray crystallography. The solid-state molecular structure is provided in **Figure 3.19** (left-hand image).
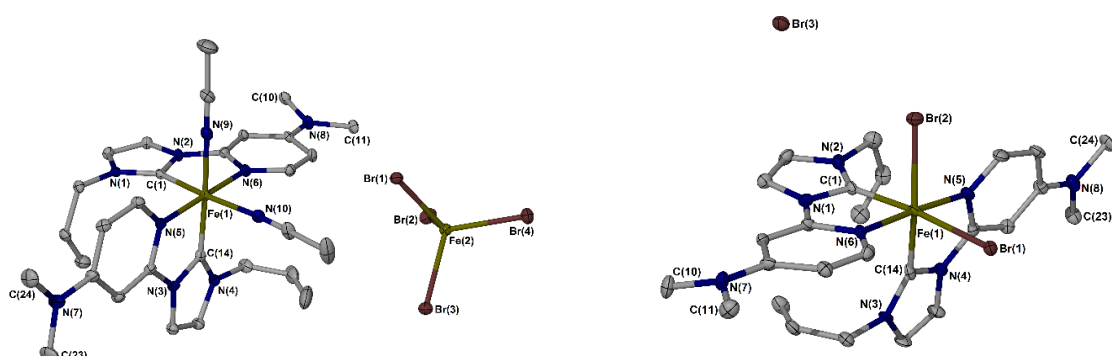
Figure 3.19 *Left: molecular structure of **3.7**. Right: molecular structure of **O3.7**, formed from the aerobic oxidation of **3.7**. Atomic displacement parameters are drawn at the 50 % probability level, hydrogen atoms are omitted from each structural solution for clarity.*

3.7	Fe(1)-C(1)	1.917(5)	C(1)-Fe(1)-C(14)	90.79(19)
3.7	Fe(1)-C(14)	1.926(5)	C(1)-Fe(1)-N(5)	96.96(17)
3.7	Fe(1)-N(5)	1.997(4)	C(1)-Fe(1)-N(10)	174.32(17)
3.7	Fe(1)-N(9)	1.975(4)	N(5)-Fe(1)-N(6)	176.88(16)
O3.7	Fe(1)-C(1)	1.955(8)	C(1)-Fe(1)-C(14)	86.6(3)
O3.7	Fe(1)-C(14)	1.976(8)	C(1)-Fe(1)-N(5)	102.3(3)
O3.7	Fe(1)-N(5)	2.031(7)	C(14)-Fe(1)-Br(2)	164.9(2)
O3.7	Fe(1)-Br(1)	2.4529(14)	C(1)-Fe(1)-Br(1)	172.3(2)
O3.7	Fe(1)-Br(2)	2.4545(13)	Br(1)-Fe(1)-Br(2)	99.54(5)

Table 3.9 *Selected bond lengths (Å) and angles (°) from the crystal structures of **3.7** and **O3.7**.*

The crystal structure of **3.7** displays the expected $[Fe(NHC)_2(MeCN)_2]^{2+}$ coordination sphere, though surprisingly adopts a $FeBr_4^{2-}$ counteranion. As the electrochemical protocol is thought to be restricted by the principle of electroneutrality, it is anticipated that the presence of a $FeBr_4^{2-}$ counteranion is a net product of crystallisation, and not a 'true' product of reaction (*i.e.* electrochemical reduction of ($2 \times$ **P3.7**) generates ($2 \times$ NHC and $1 \times Fe^{2+}$ ion) in an exact stoichiometric ratio only). Growing crystals of **3.7** from a pyridine solution provided a molecular structure whereby one acetonitrile ligand is displaced by a molecule of coordinating pyridine, and two bromide counteranions balance the $[Fe(NHC)_2]^{2+}$ charge – supporting this conclusion (see Experimental). Nevertheless, the structural solution features an iron(II) *bis*-NHC complex, with analogous geometry to **3.6**. In general, all bond lengths and angles pertaining to the inner coordination sphere of **3.7** align well with **3.6**, despite the presence of a strongly activating NMe$_2$

group attached to each pyridyl ring (**3.6** *versus* **3.7** Fe-N$_{pyridyl}$ = 2.002(4) and 1.997(4) Å, respectively).

Slowly evaporating an acetonitrile solution of **3.7** whilst exposed to an atmosphere of air produced red needle crystals (**O3.7**), which were also subject to X-ray diffraction analysis (**Figure 3.19**, right-hand image). The observed structural solution displays an iron(III) *bis*-NHC complex, **O3.7**, which is the oxidised product of **3.7**. **O3.7** occupies an analogous coordination mode and ligand environment as **O3.6**, and is presumed to have formed through a similar oxidative mechanism.

Closer examination of the crystal batch allowed division of a morphologically distinct set of red blocks, of which a variety were studied directly by X-ray diffraction analysis. Surprisingly, a consistent structural solution was obtained which features an identical ferrous coordination sphere to **3.7**, though locates one coordinating molecule of ammonia in substitution of an acetonitrile ligand (**A3.7**). The SCXRD structural solution is provided below (**Figure 3.20**).
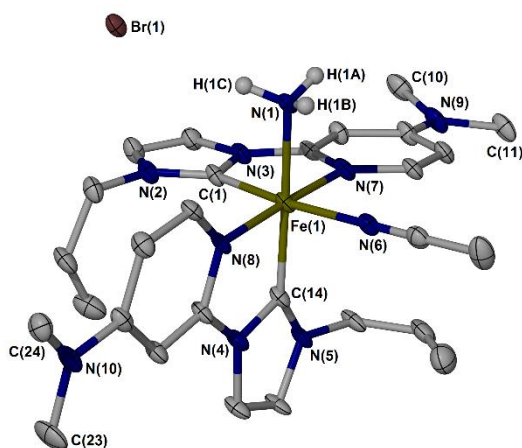
Figure 3.20 *Molecular structure of **A3.7**. Atomic displacement parameters are drawn at the 40 % probability level, hydrogen atoms (except those bound to N(1)) and one Br counteranion are omitted for clarity.*

Fe(1)-C(1)	1.931(10)	C(1)-Fe(1)-C(14)	91.1(4)
Fe(1)-C(14)	1.927(9)	C(1)-Fe(1)-N(8)	98.5(3)
Fe(1)-N(1)	2.059(7)	C(1)-Fe(1)-N(6)	172.5(3)
Fe(1)-N(8)	2.024(7)	C(14)-Fe(1)-N(1)	172.6(3)
Fe(1)-N(7)	2.021(8)	C(1)-Fe(1)-N(1)	92.7(4)
Fe(1)-N(6)	1.963(8)	N(7)-Fe(1)-N(8)	176.6(3)

Table 3.10 *Selected bond lengths (Å) and angles (˚) from the crystal structure of **A3.7**.*

All metal-ligand bond lengths and angles of **A3.7** measure well alongside those of **3.7**. However, a clear difference is observed between the Fe-N_{NH3} and Fe-N_{NCMe} bond lengths (2.059(7) *versus* 1.963(8), respectively), which suggests that the two nitrogen-donating ligands are indeed different (*i.e.* this is not likely to be a case of absent electron density within the structural refinement process). Examination of the bulk sample composition of **3.7** (presumably containing a proportion of **A3.7**) by infrared spectroscopy illustrated strong C=C and C=C-<u>H</u> bond stretches at 1621 and 2919 cm^{-1}, respectively, characteristic of each ligand allyl group. Two relatively strong, broad bands are also observed at 3369 and 3066 cm^{-1}, which would be expected for 'free' unsymmetrical and symmetrical N-H stretches of an unsubstituted amine, such as coordinated ammonia.

From these data alone, it is currently impossible to confidently state whether (i) a molecule of ammonia is truly bound to **3.7** in the X-ray crystal structure of **A3.7**, or the location of atoms (particularly hydrogen) are artefacts of data solution, and (ii) if the previous statement is true, where these hydrogen (and nitrogen) atoms originated.

The electrochemical reduction of imidazolium ions inherently produces hydrogen gas. Indeed, the prospect of an *in situ* forted iron(II) species utilising this gas to reduce dinitrogen to ammonia is improbable, albeit one explanation. The N≡N bond dissociation energy is approximately 945 kJmol^{-1}, and it is generally accepted that iron-mediated dinitrogen reduction requires an iron(0) starting material,[33] making this an unlikely interpretation. Another option is reduction of coordinated acetonitrile at the iron(II) centre, though this is equally as speculative. Current research remains ongoing to verify the identity of **A3.7**, and if successful, deconvolute its formation.

3.5 Synthesis and characterisation of pyridyl-bridged iron(II) *bis*-NHC complexes

An acetonitrile solution of **P3.8** was subject to an applied electrical potential using a pair of metallic iron electrodes, under analogous conditions to those described above (**Scheme 3.12**).
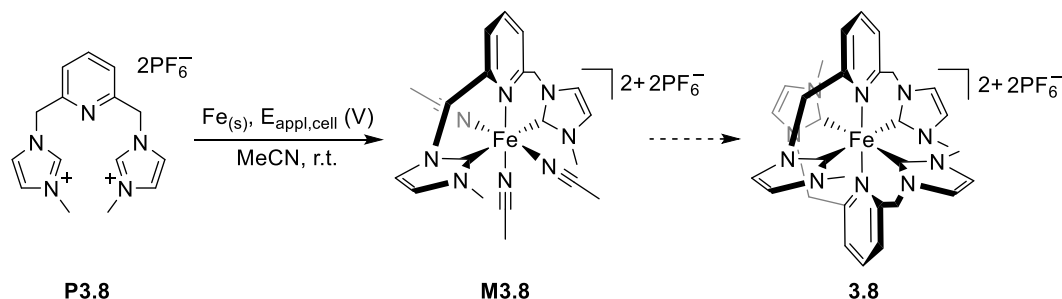
Scheme 3.12 *Electrochemical synthetic route to iron(II) tetra-NHC pincer complex, **3.8**.*

Following the reaction progress by high-resolution mass spectrometry, two dominant cationic mass peaks became evident at (*m/z*) 295.1167 and 735.1960, befitting the calculated masses of $[FeL_2 - 2PF_6]^{2+}$ and $[FeL_2 - PF_6]^+$ molecular species. These detections are somewhat unexpected, as each Fe^{2+} centre is associated with four NHC units – breaking the rule of electroneutrality.

The reaction contents were filtered and the red, homogenous solution layered with diethyl ether under an inert atmosphere to produce a batch of high quality pale red needles. Examination of the crystals by X-ray crystallography provided a structural solution, corroborating the expected $[FeL(MeCN)_3]2PF_6$ pincer complex, **M3.8** (see **Figure 3.21**, left-hand image).
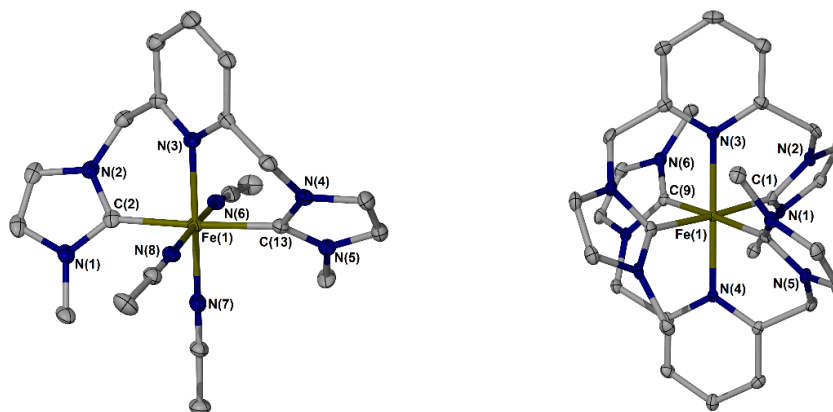
Figure 3.21 *Left: molecular structure of **M3.8**. Right: molecular structure of **3.8**. Atomic displacement parameters are drawn at the 50 % probability level, hydrogen atoms and two PF_6 counteranions are omitted from each structural solution for clarity.*

M3.8	Fe(1)-C(2)	2.010(5)	C(2)-Fe(1)-C(13)	176.89(19)
M3.8	Fe(1)-C(13)	2.010(5)	C(2)-Fe(1)-N(3)	88.80(17)
M3.8	Fe(1)-N(3)	2.061(4)	C(2)-Fe(1)-N(7)	91.68(18)
M3.8	Fe(1)-N(7)	1.927(4)	N(3)-Fe(1)-N(7)	177.99(16)
3.8	Fe(1)-C(1)	1.978(3)	C(1)-Fe(1)-C(9)	94.21(14)
3.8	Fe(1)-C(9)	1.969(3)	C(1)-Fe(1)-N(3)	88.15(11)
3.8	Fe(1)-N(3)	2.061(4)	C(1)-Fe(1)-N(4)	91.85(11)
3.8	Fe(1)-N(4)	2.043(4)	N(3)-Fe(1)-N(4)	180.000(1)

Table 3.11 *Selected bond lengths (Å) and angles (˚) from the crystal structures of **M3.8** and **3.8**.*

The crystal structure of **M3.8** displays an octahedral iron(II) centre, coordinating one ligand of **P3.8** through the anticipated C,N,C-pincer interaction. Three molecules of solvating acetonitrile occupy the remaining meridian of coordination sites, overall producing a metal centre with low steric encumbrance. Each NHC ring adopts *trans* disposition (at a near-linear angle of 176.89(19)˚), to produce a comfortable pincer ligand bite angle of *ca.* 89˚. Altogether, these bond geometries are within the expected range of a low-spin, octahedral iron(II) centre.

Unexpectedly, removal of layered anti-solvent from the crystals of **M3.8** led to their rapid and immediate physical decomposition, affording a dark brown oil. Subsequent analysis of the sample by ^{1}H NMR spectroscopy did indeed feature signals attributable to a significant quantity of free ligand, amongst a relatively negligible amount of **M3.8**. It was therefore speculated that such voluntary decomposition may be associated with the low steric protection offered by ligand **P3.8**, in combination with three weakly coordinated solvent ligands.

Modifying the original work-up procedure, pyridine (2 mL) was added to the crystals whilst blanketed under a layer of diethyl ether, which could be separated to give a homogenous deep red solution. After stirring the solution at room temperature for 15 minutes, the sample was layered with diethyl ether once more and allowed to stand overnight, producing bright red block crystals which were examined by X-ray crystallography. Unexpectedly, the *tris*-pyridine adduct of **M3.8** was not obtained; instead, an FeL₂ *bis*-pincer complex (**3.8**) was observed (**Figure 3.21**, right-hand image). Removal of layered solvent from these crystals saw no physical decomposition, allowing for good quality multinuclear NMR spectroscopic analysis (a comparison between the ^{1}H NMR spectra of **P3.8** with iron(II) complex **3.8** is provided in **Figure 3.22**).
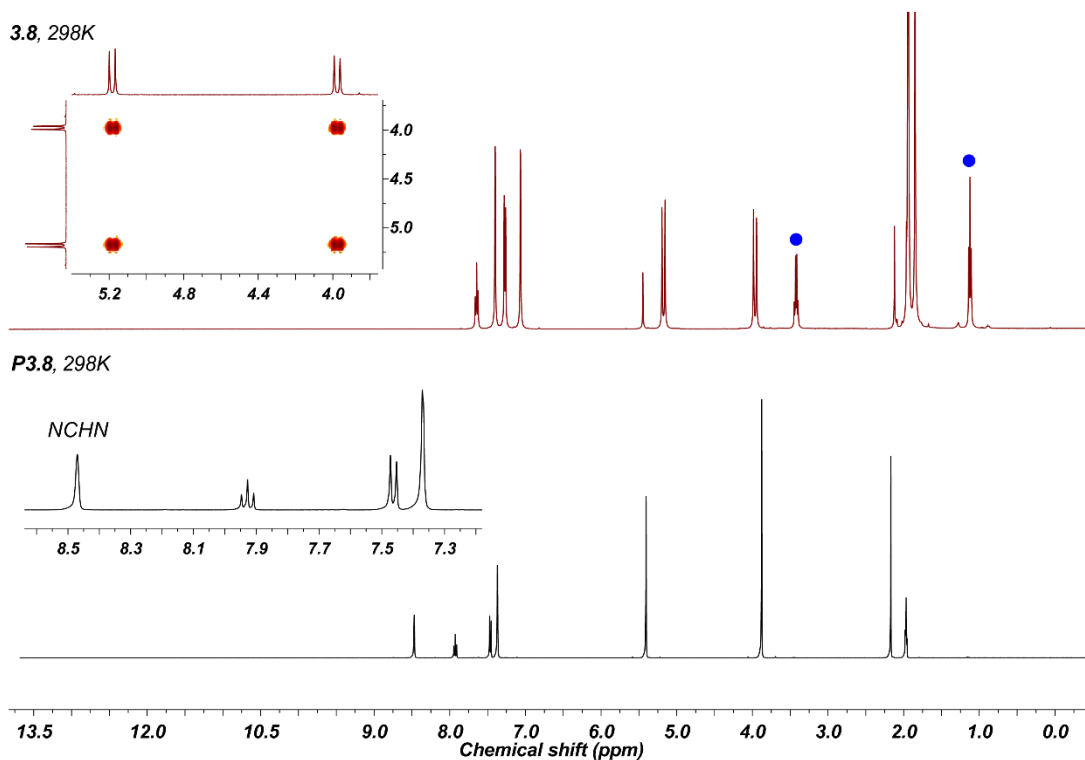
Figure 3.22 *^{1}H NMR spectrum of azolium ligand precursor **P3.8** (black trace, 500 MHz, CD$_3$CN, 298K), noting loss of original imidazolium signal at 8.47 ppm. ^{1}H NMR spectrum of Fe-NHC complex **3.8** (red trace, 500 MHz, CD$_3$CN, 298K). Inset image: excerpt taken from ^{1}H-^{1}H COSY NMR spectrum of **3.8**, under analogous conditions. Blue circles represent residual diethyl ether solvent.*

The solution ^{1}H NMR spectrum of **3.8** illustrates a C_2-symmetric ligand environment which retrofits exactly with the solid-state structure given in **Figure 3.21**. Sharp, discrete signals are observed which imply a low-spin d^6 iron(II) metal complex. Notable, are a pair of diastereotopic doublet resonances at 5.19 and 3.95 ppm ($J = 19.5$ Hz), which show strongly related cross peaks in their ^{1}H-^{1}H COSY NMR spectrum – each corroborating with four magnetically equivalent methylene-bridging protons of **3.8**. Recording the ^{13}C{^{1}H} NMR spectrum of the same sample provided a further simplified sequence of eight singlet resonances only, with one diagnostic Fe-C$_{carbene}$ signal at 200.8 ppm (125 MHz, CD$_3$CN, 298K), fully supportive of the solid-state structure.

The solution ESI mass spectrum of **3.8** displays two cationic signals only, at (*m/z*) 295.1194 and 735.2012, attributable to [**3.8** – 2PF$_6$]$^{2+}$ and [**3.8** – PF$_6$]$^+$, respectively. The same dominant molecular fragments were consistently detected in the crude mass spectra of **M3.8**, perhaps implying iron(II) *tetra*-NHC complex **3.8** is the most stable product in solution.

To obey electroneutrality, the reduction of **P3.8** must produce Fe^{2+} ions in a precise stoichiometric ratio. Formation of **3.8** must therefore take place *via* an effective transmetalation between two molecules of **M3.8**, to by-produce one equivalent of [Fe(S)$_x$(PF$_6$)$_2$] (where S = pyridine), and limit overall yield to 50 % (a simplified mechanism is postulated in **Scheme 3.13**). Aside from the

94

presumption that **3.8** may be the thermodynamically most stable product, research remains ongoing to rationalise its formation.

$$2[FeL(MeCN)_3]2PF_6 \xrightarrow[- 6MeCN]{Pyr\ (xs.)} [FeL_2]2PF_6 + [Fe(pyr)_6]2PF_6$$

M3.8 **3.8**, 50 %   **Byprod.**, 50 %
crystallise   solution
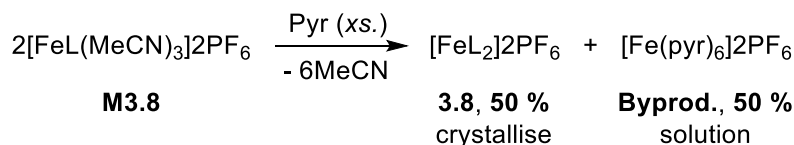
***Scheme 3.13** Proposed transmetalation reaction to produce **3.8**.*

It was envisaged that substitution of the relatively small *N*-methyl group of **P3.8** with a sterically larger motif may suppress the speculated transmetalation reaction described above, by enhanced stabilisation of the iron(II) centre. With this in mind, a solution of *N*-allyl substituted *bis*-imidazolium, **P3.9**, was electrolysed under identical reaction conditions, producing **3.9** as sole isolated product in 39 % yield (**Scheme 3.14**).

P3.9: R = allyl
P3.10: R = (2-OMe)Ph

3.9, 39 %

3.10, 46 %
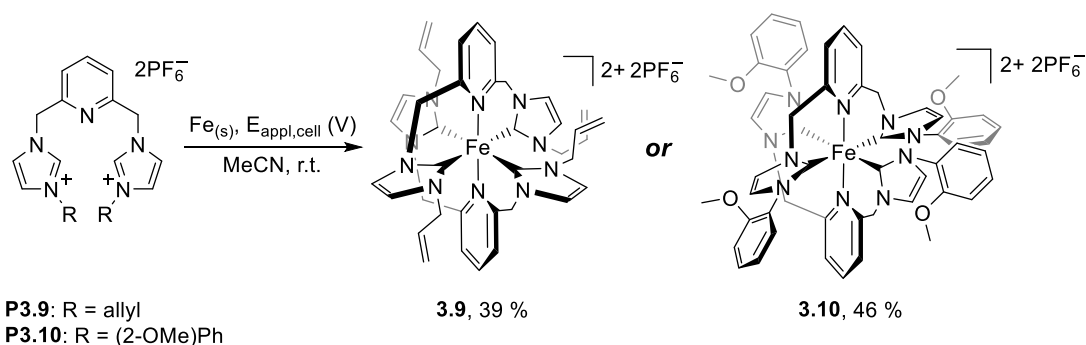
***Scheme 3.14** Electrochemical route to iron(II) tetra-NHC pincer complexes, **3.9** and **3.10**.*

Following recrystallisation, **3.9** was originally obtained as a deep red oil which solidifies upon addition of THF solvent. Analysis by ^{1}H NMR spectroscopy demonstrated a collection of sharp signals, fully attributable to a C_2-symmetric ligand environment. The observed ESI mass spectrum of **3.9** provided a dominant dication at (*m/z*) 347.1491, attributable to a $[FeL_2]^{2+}$ mass cluster. However, single crystals of **3.9** were obtained through slow diffusion of diethyl ether vapours into an acetonitrile solution of the product, and analysed by X-ray diffraction methods (**Figure 3.23**).
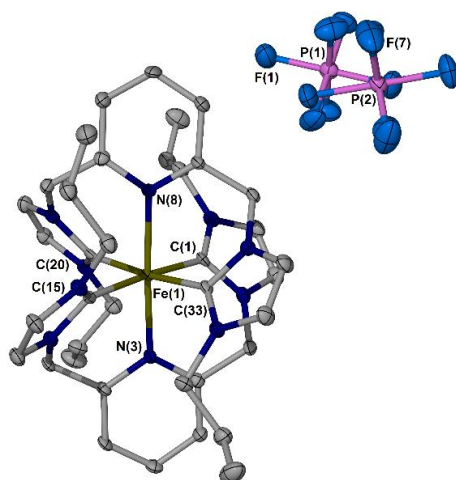
Figure 3.23 *Molecular structure of* **3.9**. *Atomic displacement parameters are drawn at the 50 % probability level, hydrogen atoms are omitted for clarity.*

Fe(1)-C(1)	1.981(4)	C(1)-Fe(1)-C(20)	87.52(18)
Fe(1)-C(15)	1.991(4)	C(1)-Fe(1)-C(33)	92.52(19)
Fe(1)-N(3)	2.064(4)	N(8)-Fe(1)-N(3)	177.10(15)
Fe(1)-N(8)	2.082(4)	C(1)-Fe(1)-C(15)	175.67(18)

Table 3.12 *Selected bond lengths (Å) and angles (˚) from the crystal structure of* **3.9**.

Surprisingly, the observed solid-state structure of **3.9** illustrates an [FeL$_2$]2PF$_6$-type *bis*-pincer complex, analogous to **3.8** – without use of pyridine solvent during work-up. All molecular bond metrics align well with those of **3.8**, though do indicate some octahedral distortion about the iron(II) centre. Indeed, these findings are altogether unexpected and reasons for sole isolation of an Fe^{II}(NHC)$_4$-type complex are not clear from these data alone.

Hoyt, Turner and Chirik recently reported the synthesis of a five-coordinate, iron(II) dibromide complex comprising a 2,6-*bis*(carbene)pyridine pincer ligand, topologically similar to those documented within.[28] The complex was prepared by reaction of the corresponding *bis*-imidazolium dibromide with one equivalent [Fe{N(SiMe$_3$)$_2$}$_2$], furnishing the trigonal bipyramidal complex in 93 % yield (**Scheme 3.15**, left-hand route). On account of this, it was speculated that removal of each 2,6-methylene bridge of **P3.9**, alongside employment of competing bromide counteranions, may allow entrapment of the corresponding [FeL(Br)$_2$]-type complex using the electrochemical methodology. Therefore, *bis*-imidazolium dibromide, **P3.9.1**, was electrochemically reduced and coordinated to an iron(II) centre, delivering **3.9.1** as an air- and moisture-stable orange powder in 37 % yield (right-hand route).
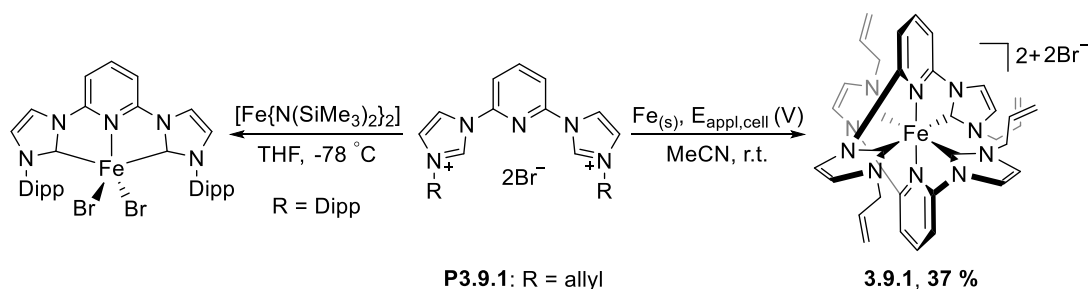
Scheme 3.15 *Left route: Chirik's chemical synthesis of iron(II) C,N,C-pincer complex.[28] Right route: electrochemical synthesis of iron(II) bis-C,N,C-pincer complex, 3.9.1.*

Analysis of the bulk powder by ^{1}H NMR spectroscopy displayed a sequence of sharp signals, absent of the original NC*H*N imidazolium proton of **P3.9.1** (featured at 11.34 ppm, 400 MHz, CD$_3$CN, 298K). Clear from the remainder of the spectrum, are four aromatic signals alongside five unique allylic resonances, indicative of a C_2-symmetric C,N,C-pincer interaction. Recording a ^{13}C{^{1}H} NMR spectrum of the same sample provided a total of nine signals, including only one low-field Fe-C$_{carbene}$ singlet at 201.2 ppm (125 MHz, CD$_3$CN, 298K), supportive of a C_2-symmetric ligand environment about an iron(II) metal centre (a comparison between the proton NMR spectra of **P3.9.1** with iron(II) complex **3.9.1** is provided in **Figure 3.24**).
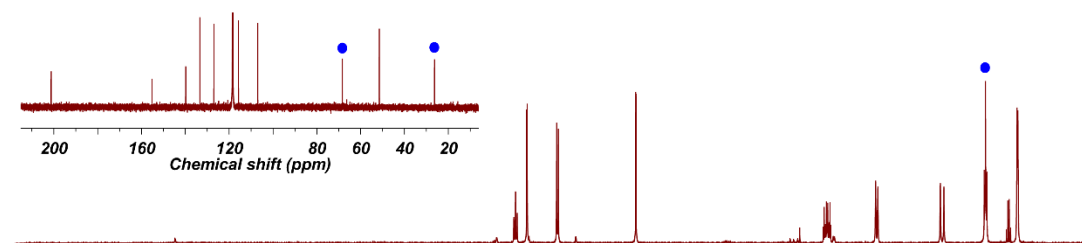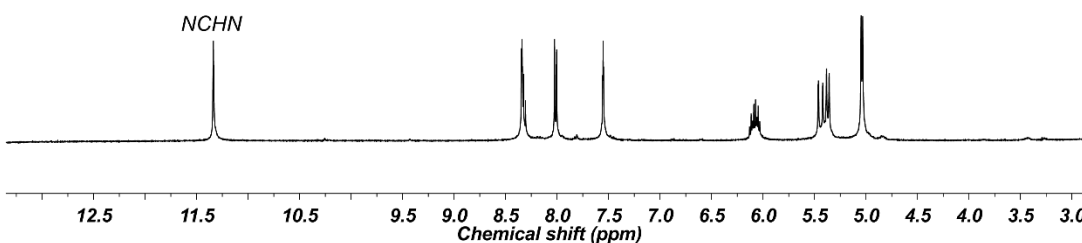
Figure 3.24 *^{1}H NMR spectrum of authentic ligand precursor P3.9.1 (black trace, 400 MHz, CD$_3$CN, 298K), noting loss of original imidazolium signal at 11.34 ppm. ^{1}H NMR spectrum of Fe-NHC complex 3.9.1 (red trace, 500 MHz, CD$_3$CN, 298K). Inset image: excerpt taken from ^{13}C{^{1}H} NMR spectrum of 3.9.1, under analogous conditions. Blue circles represent residual THF solvent.*

The electrospray mass spectrum of **3.9.1** afforded a strong mass peak at (*m/z*) 319.1186, corroborating an $[FeL_2 - 2Br]^{2+}$ dication. From these solution data, it is not possible to confidently identify the metal/ligand ratio, nor describe the absolute coordination environment around the metal centre of **3.9.1**.

Slowly diffusing diethyl ether vapours into a concentrated THF solution of **3.9.1** allowed isolation of single crystals of the complex. The pale orange blocks were subject to X-ray crystallographic analysis, which confirmed the molecular structure of **3.9.1** to be an [FeL_2]2Br-type complex − akin to both **3.8** and **3.9** (a structural solution is provided in **Figure 3.25**).
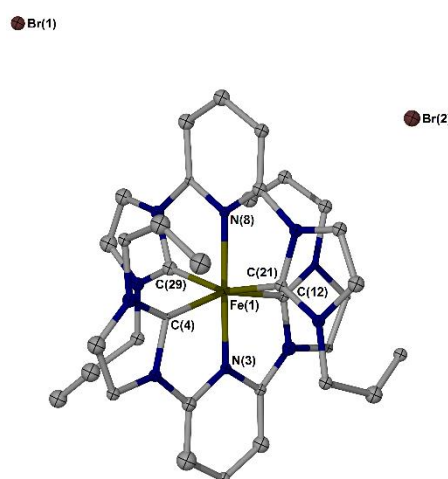
Figure 3.25 *Molecular structure of **3.9.1**. Atomic displacement parameters are drawn at the 40 % probability level, hydrogen atoms are omitted for clarity.*

Fe(1)-C(4)	1.964(15)	C(4)-Fe(1)-C(12)	159.4(6)
Fe(1)-C(12)	1.992(16)	C(4)-Fe(1)-N(3)	80.6(6)
Fe(1)-N(3)	1.903(13)	C(21)-Fe(1)-C(29)	158.7(7)
Fe(1)-N(8)	1.922(13)	N(3)-Fe(1)-N(8)	178.3(6)

Table 3.13 *Selected bond lengths (Å) and angles (˚) from the crystal structure of **3.9.1**.*

The asymmetric unit of **3.9.1** features a coordinatively saturated iron(II) *tetra*-NHC complex, adopting significantly distorted octahedral geometry. Each C,N,C-pincer ligand coordinates to the metal through the expected κ^3 binding mode, with a contracted pincer bite angle of *ca.* 80˚. Contrary to the findings of Chirik *et al.*, neither bromide anion coordinates to the iron(II) centre. However, taking the postulated mechanism in **Scheme 3.13** to be true, formation of **3.9.1** must by-produce a stoichiometric quantity of $FeBr_2$, which may act to drive transmetalation. Nonetheless, all solution-state data are in agreement with both elemental and crystallographic analysis of **3.9.1**.

In an attempt to sterically congest the initially formed iron(II) *bis*-NHC complex, 2-methoxyphenyl substituted *bis*-imidazolium, **P3.10**, was employed as electrochemical substrate (**Scheme 3.14**). Monitoring reaction progress by high-resolution mass spectrometry, a molecular ion of (*m/z*) 1103.3008 became apparent, alongside an intense dicationic mass fragment of 479.1705, attributable to $[FeL_2 - PF_6]^+$ and $[FeL_2 - 2PF_6]^{2+}$, respectively. Following 90 minutes reaction time, the pale red solution was filtered, diluted with diethyl ether and allowed to stand for 48 hours, upon which a microcrystalline orange solid was obtained (**3.10**).

Upon isolation, diamagnet **3.10** was examined by ^{1}H NMR spectroscopy, which illustrated a sum of thirty discrete aromatic protons to represent two full, magnetically unique ligands (recorded in d_3-MeCN solvent). Further up-field, are four diastereotopic doublet resonances which integrate to eight hydrogen atoms (6.30, 5.31, 4.79 and 4.38 ppm), owning a pair of matching *J*-coupling constants and unambiguously show correlation through 2D NMR analysis – attributable to each symmetry related pair of methylene-bridging protons of **3.10** (see **Figure 3.26** for a direct comparison between the proton NMR spectra of **P3.10** and **3.10**).
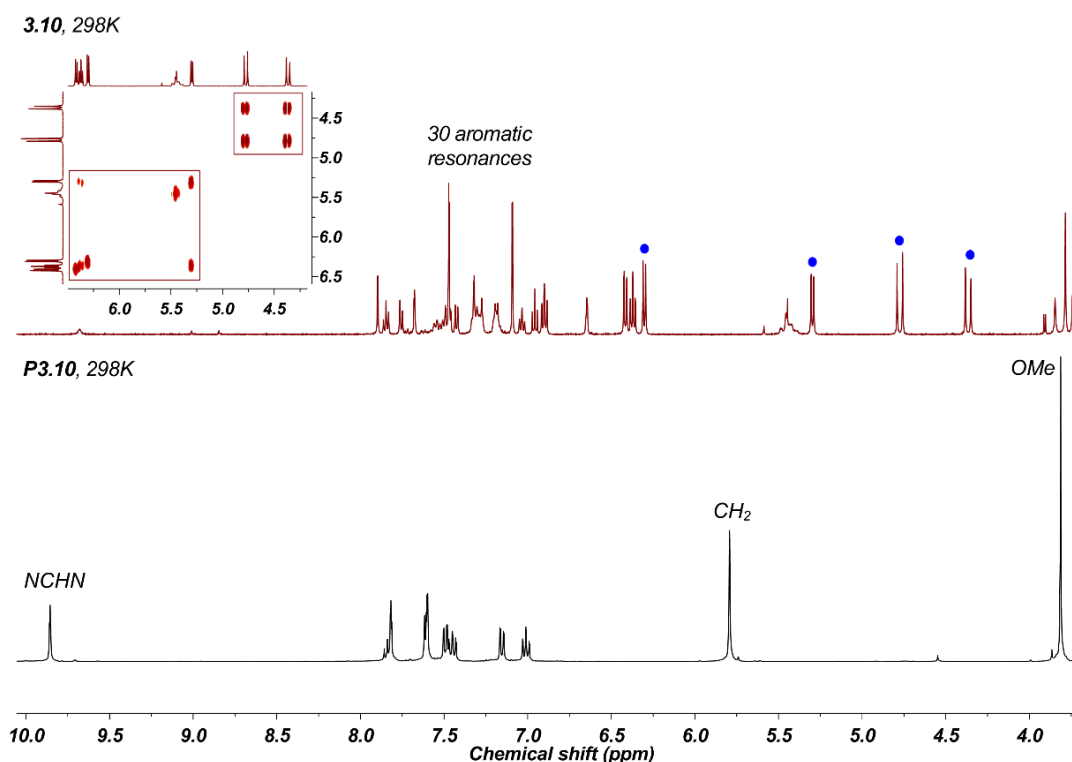
Figure 3.26 *^{1}H NMR spectrum of authentic ligand precursor* ***P3.10*** *(black trace, 400 MHz, CD₃CN, 298K), noting loss of original imidazolium signal at 9.86 ppm. ^{1}H NMR spectrum of Fe-NHC complex* ***3.10*** *(red trace, 500 MHz, CD₃CN, 298K). Inset image: excerpt taken from ^{1}H-^{1}H COSY NMR spectrum of* ***3.10****, under analogous conditions. Blue circles represent diastereotopic methylene-bridging protons.*

Interestingly, the $^{13}C\{^1H\}$ NMR spectrum of the same sample details only fourteen unique singlet resonances, including one characteristic low-field Fe-$C_{carbene}$ signal at 200.8 ppm (125 MHz, CD$_3$CN, 298K), which contradicts the apparent non C_2-symmetric ligand environment evidenced by ^1H NMR spectroscopy.

Single crystals of **3.10** were obtained in the form of pale orange blocks, through the slow diffusion of diethyl ether vapours into a THF solution of the sample at room temperature. In line with previous examples, structural authentication of **3.10** illustrates an iron(II) metal centre coordinating two tridentate ligands of **P3.10** (see **Figure 3.27** for a structural solution).
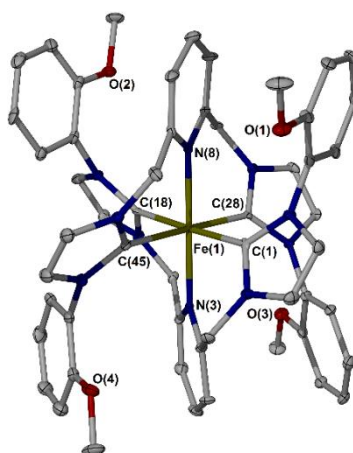
Figure 3.27 Molecular structure of **3.10**. Atomic displacement parameters are drawn at the 50 % probability level, hydrogen atoms and two PF$_6$ counteranions are omitted for clarity.

Fe(1)-C(1)	1.994(8)	C(1)-Fe(1)-C(28)	88.2(3)
Fe(1)-C(18)	1.985(8)	C(1)-Fe(1)-C(18)	178.0(3)
Fe(1)-N(8)	2.045(6)	N(8)-Fe(1)-N(3)	179.9(3)
Fe(1)-N(3)	2.036(6)	N(3)-Fe(1)-C(1)	90.8(3)

Table 3.14 Selected bond lengths (Å) and angles (˚) from the crystal structure of **3.10**.

Despite employment of sterically bulky, *ortho*-substituted *N*-phenyl rings within the ligand template, **3.10** forms as an [FeL$_2$]2PF$_6$-type *bis*-pincer complex of similar conformation to **3.8**, **3.9** and **3.9.1**. Within **3.10**, four NHC units are situated about the meridian in 'propeller' fashion, whilst each 2,6-pyridyl bridge occupies both apical positions. In fact, all bond angles about the octahedron approach ideal, with all lengths comparing well with those documented above.

Closer inspection of the solid-state structure of **3.10** reveals two perpendicular mirror planes running through the molecule, with one defined through all Fe-C$_{NHC}$ bonds. Though each ligand is undoubtedly related by symmetry in the crystal structure, two magnetically inequivalent ligand environments are clearly observed in the ^1H NMR spectrum, whilst signals pertaining to only one ligand arise in the $^{13}C\{^1H\}$ NMR spectrum. In terms of rationale, strong π-π interactions appear

present between both phenyl rings of one ligand, with the only pyridyl ring of the opposing ligand, which may act to restrict the geometrical conformation of **3.10**. A similar conformational lock was observed regarding *N*-mesityl, *N'*-pyridyl substituted iron(II) complex **3.2**, which provided an explanation for inequivalent (yet apparently symmetrical) hydrogen atoms within NMR experiments based on the position of aromatic ring currents (see above). However, all ten ring currents of **3.10** are entirely symmetrical in the solid-state, with no ^{1}H environment of one ligand appearing unique to the other. It is therefore difficult to reconcile the observed solution data with the observed molecular structure of **3.10** at this stage.

As a final example, a solution of C_2-symmetric *bis*-picolyl substituted analogue, **P3.11**, underwent electrochemical reduction in the same manner to those described throughout, and was subsequently coordinated to iron (**Scheme 3.16**). Upon complex formation, the colourless solution was replaced by a red reaction mixture which was followed by ESI mass spectrometry, detecting an intense [FeL – 2PF$_6$]$^{2+}$ mass peak at (*m/z*) 238.5702 which grew over the course of reaction. The product was purified by recrystallisation and obtained as a red solid in 83 % isolated yield.
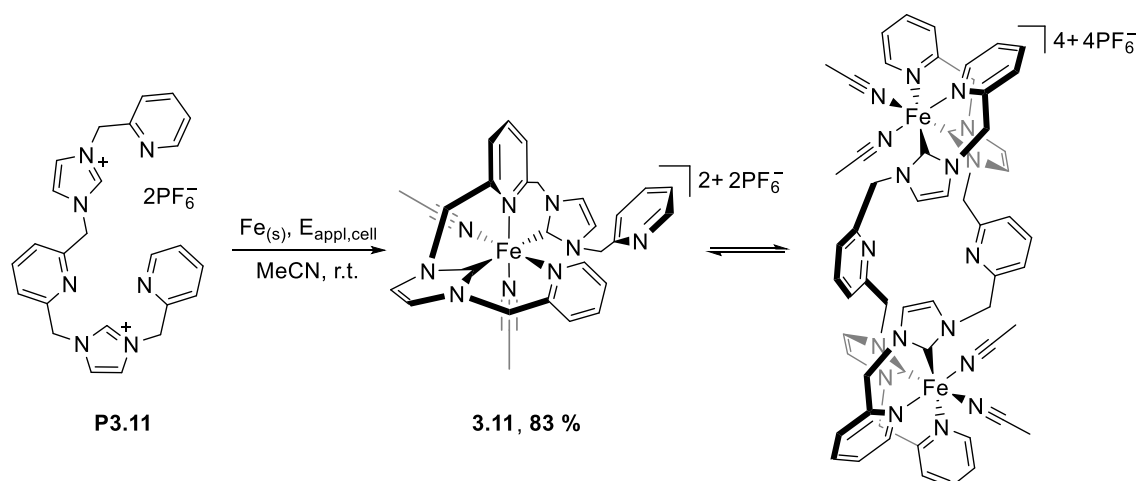
Scheme 3.16 *Electrochemical synthetic route to mononuclear **3.11**, which is proposed to exist in equilibrium with a dinuclear iron(II) helicate.*

Following isolation, **3.11** was dissolved in d_3-MeCN and a ^{1}H NMR spectrum recorded at ambient temperature. Clear, was absence of an NC*H*N signal, alongside the presence of fifteen discrete aromatic proton resonances, resembling the calculated number of aromatic protons within one full ligand. Completing the spectrum, are eight unique doublet resonances (6.29, 6.03, 5.41, 5.28, 5.07, 4.89, 4.33 and 3.60 ppm) which pertain to all eight diastereotopic methylenic protons of one ligand, and show strong through-bond correlation by ^{1}H-^{1}H COSY NMR spectroscopy (see **Figure 3.28** for a comparison between NMR spectra of **P3.11** and **3.11**). As a first approximation, a spectrum of 23 protons would imply a non C_2-symmetric, κ^4 coordinated ligand

binding mode, leaving one pyridyl ring pendant. Revisiting the ^{1}H NMR spectrum of **3.4**, hemilabile picolyl donor groups of this type tend to undergo rapid ligand fluxion in d_3-MeCN solvent, leading to extremely broad methylenic resonances which are not observed for **3.11** – suggestive of a static iron(II) coordination sphere. Analysis of the ^{13}C{^{1}H} NMR spectrum (d_3-MeCN) provided a total of 25 singlet resonances, with two remote low-field signals at 194.6 and 193.4 ppm (125 MHz, 298K), attributable to two unique Fe-C$_{carbene}$ environments.
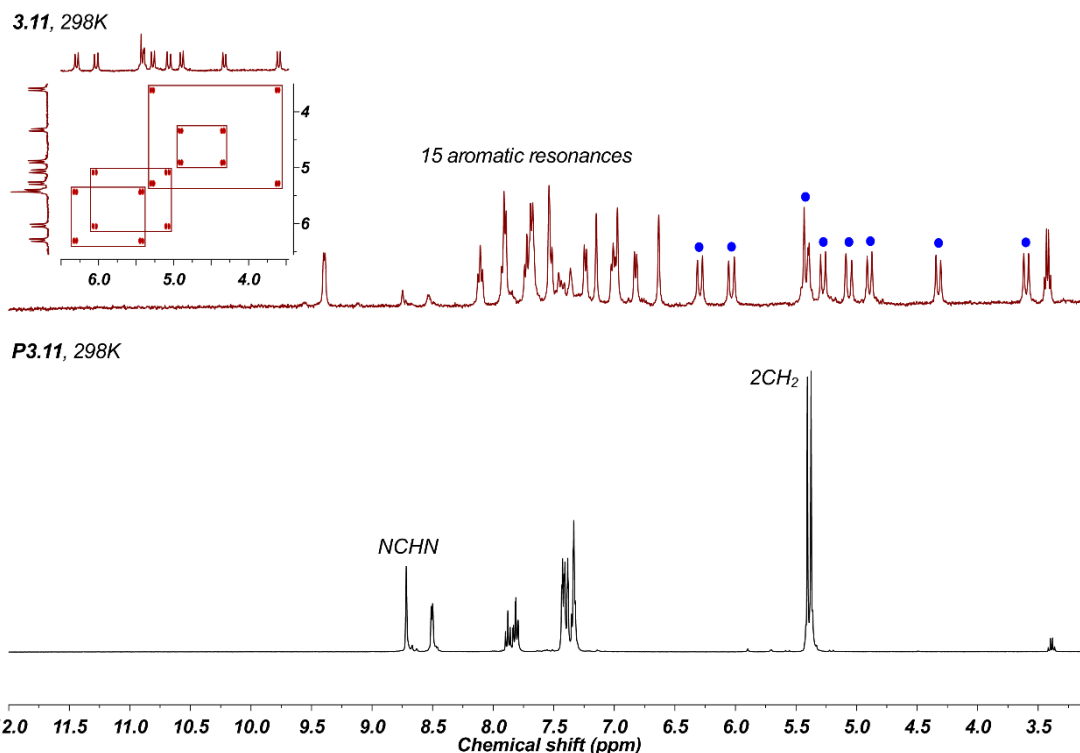
Figure 3.28 *^{1}H NMR spectrum of ligand precursor **P3.11** (black trace, 400 MHz, CD$_3$CN, 298K), noting loss of original imidazolium signal at 8.72 ppm. ^{1}H NMR spectrum of Fe-NHC complex **3.11** (red trace, 500 MHz, CD$_3$CN, 298K). Inset image: excerpt taken from ^{1}H-^{1}H COSY NMR spectrum of **3.11**, under analogous conditions. Blue circles represent diastereotopic methylene-bridging protons.*

A sample of **3.11** was dissolved into acetonitrile solvent, layered with diethyl ether and allowed to stand for 48 hours. Following, bright red needles were obtained which were analysed by single crystal X-ray diffraction methods. Surprisingly, **3.11** was structurally elucidated as a dinuclear [Fe$_2$L$_2$]4PF$_6$ helicate (see **Figure 3.29** for a structural solution).
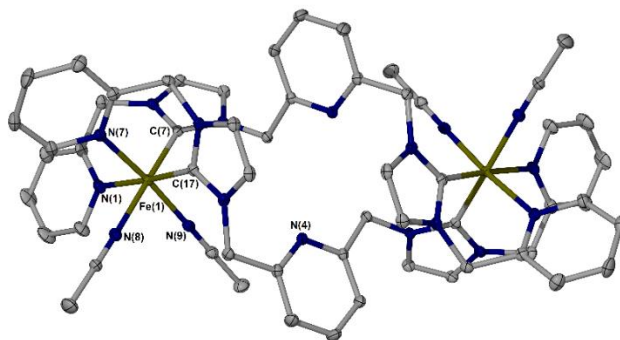
Figure 3.29 *Molecular structure of **3.11**. Atomic displacement parameters are drawn at the 40 % probability level, hydrogen atoms and four PF₆ counteranions are omitted for clarity.*

Fe(1)-C(7)	1.961(4)	C(7)-Fe(1)-C(17)	93.02(16)
Fe(1)-C(17)	1.933(4)	C(17)-Fe(1)-N(1)	175.87(16)
Fe(1)-N(1)	2.065(4)	C(7)-Fe(1)-N(8)	176.18(15)
Fe(1)-N(7)	2.031(4)	N(7)-Fe(1)-N(9)	174.82(14)

Table 3.15 *Selected bond lengths (Å) and angles (°) from the crystal structure of **3.11**.*

Unexpectedly, the molecular structure of **3.11** solves as a dinuclear iron(II) complex, whereby each metal coordinates through one pyridyl donor and one NHC group of two independent ligands. Previously unobserved, each 2,6-pyridyl bridge does not coordinate to a metal centre, and instead acts to link a pair of iron atoms into two strands of an overall *P* helical twist. The two iron(II) centres lie on a two-fold rotational axis which defines the crystallographically unique unit as half of the $[Fe_2L_2]^{4+}$ cation. Therefore, each metal centre is equivalent by symmetry, and exhibits an intrahelical Fe···Fe distance of 9.383(3) Å in the solid-state.

By virtue of each iron centre adopting a Δ configuration, the complex-cation is a homochiral Δ-Δ pair, inherently giving rise to a screw coordination arrangement of the two ligands around iron. Only the Δ-Δ isomer is located within the sample, naturally producing an optically pure double helicate crystal of **3.11** (a space-filling model of each Δ-Δ pair is given in **Figure 3.30**).
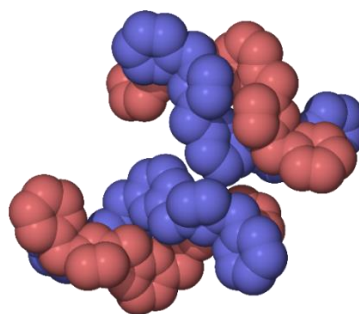
Figure 3.30 *Space-filling representation of two homochiral Δ-Δ pairs, found in the crystal structure of **3.11**. Each coordinated MeCN ligand, hydrogen atoms and four PF₆ counteranions are omitted for clarity.*

In a comparative study, Skelton, Simpson and Brown recently reported on the synthesis of NHC-pincer ligands of both 2,6-pyridyl and 2,6-aminotriazine cores, which were coordinated to silver(I), gold(I) and palladium(II) metal centres.[34] Upon metallation, all 2,6-pyridyl bridged examples (structurally similar to those above) afforded linear complexes, where triazinyl derivatives adopted a helical twist. Computationally, the authors found that the twisted conformation is generally most stable for these metal complexes. Teng and Huynh have also connected NHCs to 2,6-pyridine-dicarboxamides, and subsequently produced stable helicate architectures of cobalt.[35] However, to the author's knowledge, no dinuclear iron(II) helicates comprising NHC ligands are known.

Combustion analysis of the bulk sample supports formation of an $[Fe_2L_2]4PF_6$ helicate, though would equally match the calculated elemental values for a mononuclear $[FeL]2PF_6$ complex. The room temperature PXRD pattern of the same sample provided good agreement with a simulated version from SCXRD (120K). These data imply that the original product batch exists as a dinuclear iron(II) complex in the solid-state (see Experimental).

Indeed, a challenging question regarding **3.11**, is whether the observed solid-state identity holds true for that in solution. Closer inspection of the original crude electrospray mass spectrum does in fact, detail a molecular ion peak of (*m/z*) 1263.1993, which matches the calculated mass of a $[M_{helicate} + H_2O - 2PF_6]^{2+}$ molecular fragment. However, the most intense mass peak observed in all ESI spectra is detected at (*m/z*) 238.5702, attributable to a mononuclear $[FeL - 2PF_6]^{2+}$ molecular ion. The isotopic envelope for this fragment is clearly separated by 0.5 Da, confirming the dicationic charge to rule out the possibility of a larger (4+) molecular structure, comprising two iron centres linked by two ligands.

In an attempt to observe through-space correlations across the cavity of dinuclear **3.11** (*ca.* 2.4 Å, in the solid-state), 2D nuclear Overhauser effect spectroscopy (NOESY) was employed (*d₃*-MeCN solvent). The bidimensional spectrum obtained did not illustrate any strong nOe signals to support helicate existence in solution, though may be a result of the symmetry relation between each helical strand. Perhaps useful, may be to compare DOSY NMR spectra of pure **P3.11** and the product batch of **3.11**, with the expectation being a very similar diffusion coefficient value for a mononuclear complex, *versus* a much greater discrepancy for that of a dinuclear form (expected in the order of *ca.* two-fold), though this has yet to be performed.

Interestingly, the cyclic voltammogram of **3.11** in MeCN solution provided only one reversible redox event, with a half-wave potential recorded at +0.80 V (analogous conditions were applied to those of section **3.6**). A peak-to-peak separation of 100 mV was observed for this band, demonstrative of a truly reversible electrochemical redox couple (attributable to the $Fe^{2+} \leftrightarrow Fe^{3+}$ couple). Given that all solution NMR (*d₃*-MeCN) spectra of **3.11** illustrate a non C_2-symmetric

ligand binding mode, this would generate two non-equivalent iron(II) centres if bound as a dinuclear helicate, which may be expected to show two different redox events in the voltammogram (see Experimental for a cyclic voltammogram of **3.11**).

At present, it is therefore proposed that **3.11** predominantly exists as a mononuclear [FeL]2PF$_6$-type complex in MeCN solution, though preferentially forms a dinuclear [Fe$_2$L$_2$]4PF$_6$-type structure in the solid-state. Multinuclear NMR spectroscopy, high-resolution mass spectrometry, cyclic voltammetry, single crystal and powder XRD support these conclusions, though current research remains ongoing to further rationalise these observations.

3.6 Redox behaviour of *N*-donor substituted iron(II) *bis*-NHC complexes

Prompted by the accessible redox properties of both **3.6** and **3.7**, as evidenced by their spontaneous oxidation, it was decided evaluate iron(II) *bis*-NHC complexes (**3.1** – **3.7**) by cyclic voltammetry. Applying conditions outlined by Herrmann and Kühn, all measurements were carried out under an atmosphere of argon using acetonitrile solutions of ^{n}Bu$_4$NPF$_6$ as supporting electrolyte (0.10 M), scanning at 0.10 Vs^{-1} from -0.2 to +1.8 V.[36] Cyclic voltammograms of **3.1** – **3.5** are charted in **Figure 3.31**.
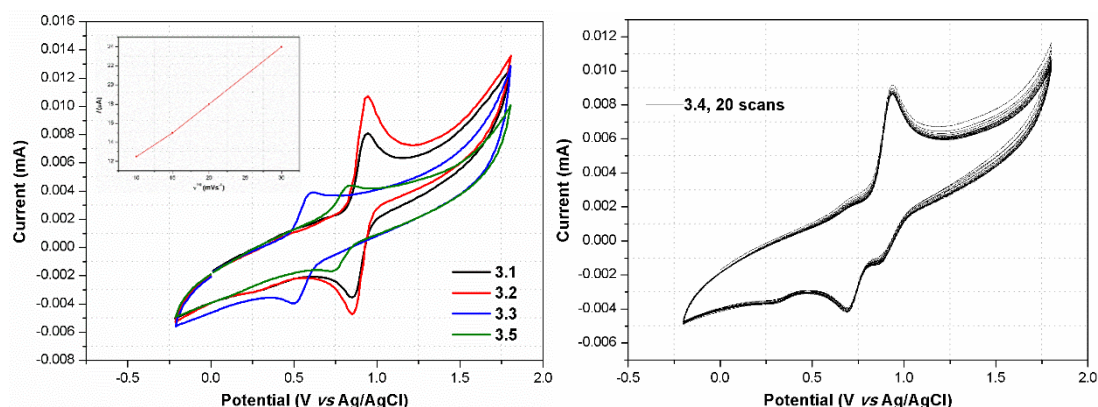
Figure 3.31 *Left: superimposed cyclic voltammogram charts (anodic portion) of iron(II) bis-NHC complexes, **3.1** – **3.3** and **3.5**, illustrating their respective reversible Fe$^{II/III}$ redox couple in MeCN solvent; inset image: linearly-dependent plot of anodic peak current (**3.1**) upon the square root of scan rate (10 – 30 Vs^{-1}). Right: cyclic voltammogram chart of **3.4**, illustrating multiple redox events which remain consistent over 20 cycles. Conditions: [Fe] = 1.0 mM, media = (MeCN/[^{n}Bu$_4$N]PF$_6$ 0.10 M), scan rate (v) = 100 mVs^{-1} (left), 400 mVs^{-1} (right), T = 298K.*

Voltammetric analysis of **3.1** displays a one-electron redox event at E^{ox} = +0.95 V *versus* the Ag/AgCl reference, assignable to the [FeL]$^{2+}$/[FeL]$^{3+}$ couple. Plotting the intensity of this current peak against the square root of sweep rate generates a straight line, indicative of a truly reversible electrochemical process. The peak-to-peak separation (ΔE) for **3.1** is measured at 100 mV, which is above the theoretical value of a one-electron process (*ca.* 60 mV), though is typical for related

iron complexes (**Figure 3.31**, left-hand image, black trace). The half-wave potential for **3.1** ($E_{1/2}$ = +0.90 V) is in good agreement with those previously reported for [FeL(MeCN)$_2$]$^{2+}$-type complexes (~ +1.1 V).[36–40]

Substitution of the *N*-pyridyl group of **3.1** with a non-donating *N*-mesityl function (**3.2**) provides no significant change in the electrochemical properties of the complex (red trace). However, coordinatively saturated *bis-N*-picolyl substituted example, **3.3**, gave the most negative one-electron Fe$^{II/III}$ redox band, with a relative $E_{1/2}$ value recorded at +0.55 V (blue trace). As referenced above, Basset and Kühn have loosely outlined a number of rules which appear to regulate the redox potentials of iron(II) NHC/pyridine hybrids.[36] The authors demonstrate that (i) a stepwise increase in NHC:pyridine ratio linearly decreases $E_{1/2}$ by ~0.2 V, (ii) reduced octahedral distortion lowers $E_{1/2}$ and (iii) *trans*-standing NHC groups increase $E_{1/2}$. Iron(II) complex **3.3** possesses a 1:2 NHC/pyridine ratio, with each NHC group disposed *trans* about the metal centre. Under the rules summarised above, these properties should act to increase the observed $E_{1/2}$ of **3.3**; however it appears that the more structurally fluid ligand environment about the octahedron overrides both factors to significantly reduce $E_{1/2}$.

These rules can similarly be employed to rationalise the intermediate $E_{1/2}$ value obtained regarding **3.5** (+0.79 V, green trace). It is presumed that **3.5** exists in solution as lowly interconvertible geometric isomers, therefore the relative disposition of NHC groups cannot be considered constant. Nonetheless, combustion analysis determines the NHC/pyridine ratio to be binary and each picolyl group coordinates to iron with little octahedral distortion, producing a half-wave potential centred within the spread obtained for **3.1/3.2** (geometry distorted, 1:1 NHC/pyridine, *cis*-NHC groups, $E_{1/2}$ = +0.90 V) and **3.3** (geometry undistorted, 1:2 NHC/pyridine, *trans*-NHC groups, $E_{1/2}$ = +0.55 V).

A more complicated sequence of redox events are observed within the CV of **3.4** (**Figure 3.31**, right-hand image). Scanning at 100 mVs^{-1}, a single oxidation peak at +0.90 V and reduction band at +0.63 V are observed, producing a ΔE of 270 mV; such a peak-to-peak separation is too large to indicate a truly reversible redox step. Increasing scan rate to 400 mVs^{-1} reveals an additional reduction (+0.81 V) and oxidation (+0.65 V) band (consistently *pseudo-reversible* over 20 scans), which have been assigned to an *in situ* conformational change of **3.4** from an [Fe(κ^3L)]^{II} → [Fe(κ^4L)]^{III} ligand binding mode upon oxidation of the metal centre, independently by Basset and Kühn at the time of these findings.[36]

Iron(II) dibromides **3.6** and **3.7** were analysed by similar methods (**Figure 3.32**, left-hand image). Each cyclic voltammogram illustrates a reversible Fe$^{II/III}$ half-wave potential within the expected region (**3.6** = +0.88 V, **3.7** = +0.89 V), both of which show peak-to-peak separations of 100 mV and remain consistent over 20 continuous cycles – indicative of stable and reversible one-electron

transfer. Interestingly, both plots display a second reversible redox couple with matching $E_{1/2}$ values (+0.56 V), attributable to the presence of bromide within each coordination sphere. This redox wave is entirely absent within the voltammogram of dihexafluorophosphate analogue, **3.6.1**, at both relatively slow (100 mVs^{-1}) and fast (400 mVs^{-1}) scan rates, supporting this conclusion (**Figure 3.32**, right-hand image). Moreover, there are almost insignificant changes to the electrochemical properties of the cationic portion of **3.6** upon substitution of bromide with hexafluorophosphate (**3.6.1** = +0.90 V), suggesting that the electronic structure of this complex is dominated by the [FeL$_2$] section of the core. For interest, observed values of $E_{1/2}$ for **3.1 – 3.7** are listed in **Table 3.15**, alongside a simplified formula of each respective ligand.
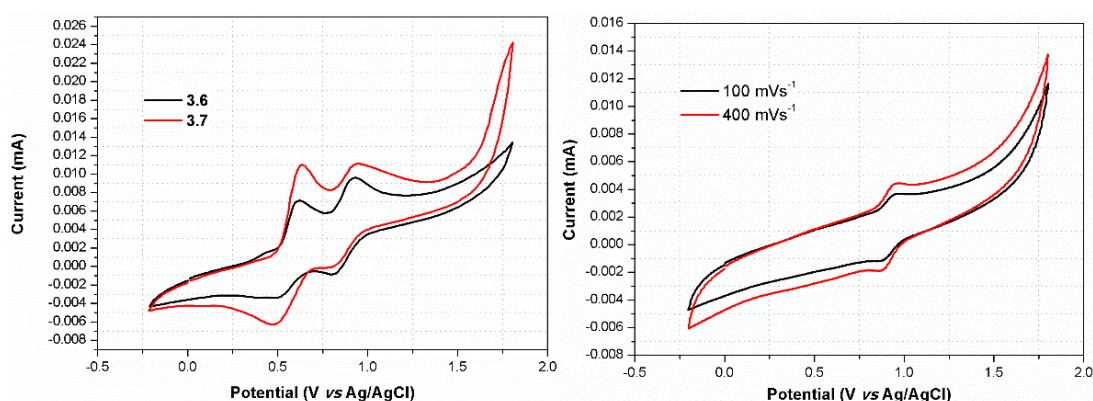
Figure 3.32 *Left: superimposed cyclic voltammogram charts (anodic portion) of iron(II) bis-NHC complexes,* **3.6** *and* **3.7***, illustrating their respective reversible Fe$^{II/III}$ redox couple in MeCN solvent. Right: superimposed cyclic voltammogram charts of* **3.6.1** *at 100/400 mVs^{-1}. Analogous conditions to those of* **Figure 3.31***.*

Complex	Ligand	$E_{1/2}$ (V)	ΔE (mV)
3.1	$2 \times$ N-C-pyr	0.90	100
3.2	$2 \times$ N-C-mes	0.90	100
3.3	$2 \times$ N^C^N	0.55	110
3.4[a,b]	$1 \times$ N^C^C^N	0.77[a], 0.73[b]	270[a], 160[b]
3.5	$2 \times$ N^C-ester	0.79	100
3.6[c] (**3.6.1**)	$2 \times$ N-C-allyl	0.88 (0.90)	100 (100)
3.7[c]	$2 \times$ N$_{DMAP}$-C-allyl	0.89	100

Table 3.16 *Dependence of $E_{1/2}$ of* **3.1 – 3.7** *on coordination environment.* [a]*Assumed κ^3-coordination,* [b]*assumed κ^4-coordination,* [c]*two bromide counteranions.* ^ = *CH$_2$.*

3.7   Conclusions and future work

A family of pyridyl-substituted imidazolium salts have been prepared and coordinated to iron using a synthetically clean electrochemical protocol, which represents a mild alternative to the commonly employed $[Fe\{N(SiMe_3)_2\}_2]$ route. Scope and generality of the method were realised by its tolerance towards various reactive *N*-substituents at the heterocyclic ring, allowing chemoselective and predictable C2-metallation of all examples in good to high yield. A combination of solid- and solution-state analyses have been employed to rationalise both dynamic and static complex behaviour, with a view to fine-tune metal coordination sphere by simple pro-ligand modification.

N-Allyl, *N'*-pyridyl-substituted NHC ligands have been shown to stabilise both iron(II) and iron(III) metal centres in the solid-state, with cyclic voltammetry supportive of $Fe^{2+} \leftrightarrow Fe^{3+}$ reversibility for these complexes in solution, suggestive of complexes which should be suitable for one-electron-transfer (catalytic) reactions. Installation of a strong electron-donating group to the *N*-pyridyl ring of **3.6** produces **3.7**, amongst an unexpected ammonia-bound adduct (**A3.7**) which was observed through crystallographic study. Both the identity and origin of **A3.7** remain under investigation, though current SCXRD and infrared spectroscopy data strongly support its formation. To the author's knowledge, this represents the only example of an iron(II)-NHC complex coordinated to ammonia.

Various 2,6-pyridyl bridged imidazolium salts were electrochemically reduced and coordinated to iron(II). For all examples, $[Fe(NHC)_4]2PF_6$-type complexes were obtained. To obey the principle of electroneutrality, these complexes must form by way of their $[Fe(NHC)_2]2PF_6$ counterparts, and current research aims to employ theoretical calculations to rationalise their formation.

The effect of polydenticity within the 2,6-pyridyl bridged NHC scaffold was also examined. Electrochemical conversion of *bis*-picolyl substituted analogue, **P3.11**, to its iron(II) complex (**3.11**) occurs smoothly in 83 % yield. All solution-state analysis of the product support formation of a mononuclear, non C_2-symmetric $[FeL]2PF_6$-type complex. However, single crystal XRD of the sample solves for a dinuclear $[Fe_2L_2]4PF_6$ helicate, for which powder diffraction of the bulk solid provides agreement. Based upon this evidence, it is hypothesised that a state-dependent equilibrium exists between $[FeL] \leftrightarrow [Fe_2L_2]$ versions of **3.11**. Nonetheless, the solid-state molecular structure of **3.11** represents the only known example of a helical iron(II)-NHC complex.

In brief, this chapter demonstrates the application of one electrochemical reaction to prepare a variety of iron(II)-NHC complexes, which are summarised below (**Scheme 3.17**). The method represents a valuable alternative to those pre-existing, presents no requirement on ligand functionality, and occurs under mild conditions.
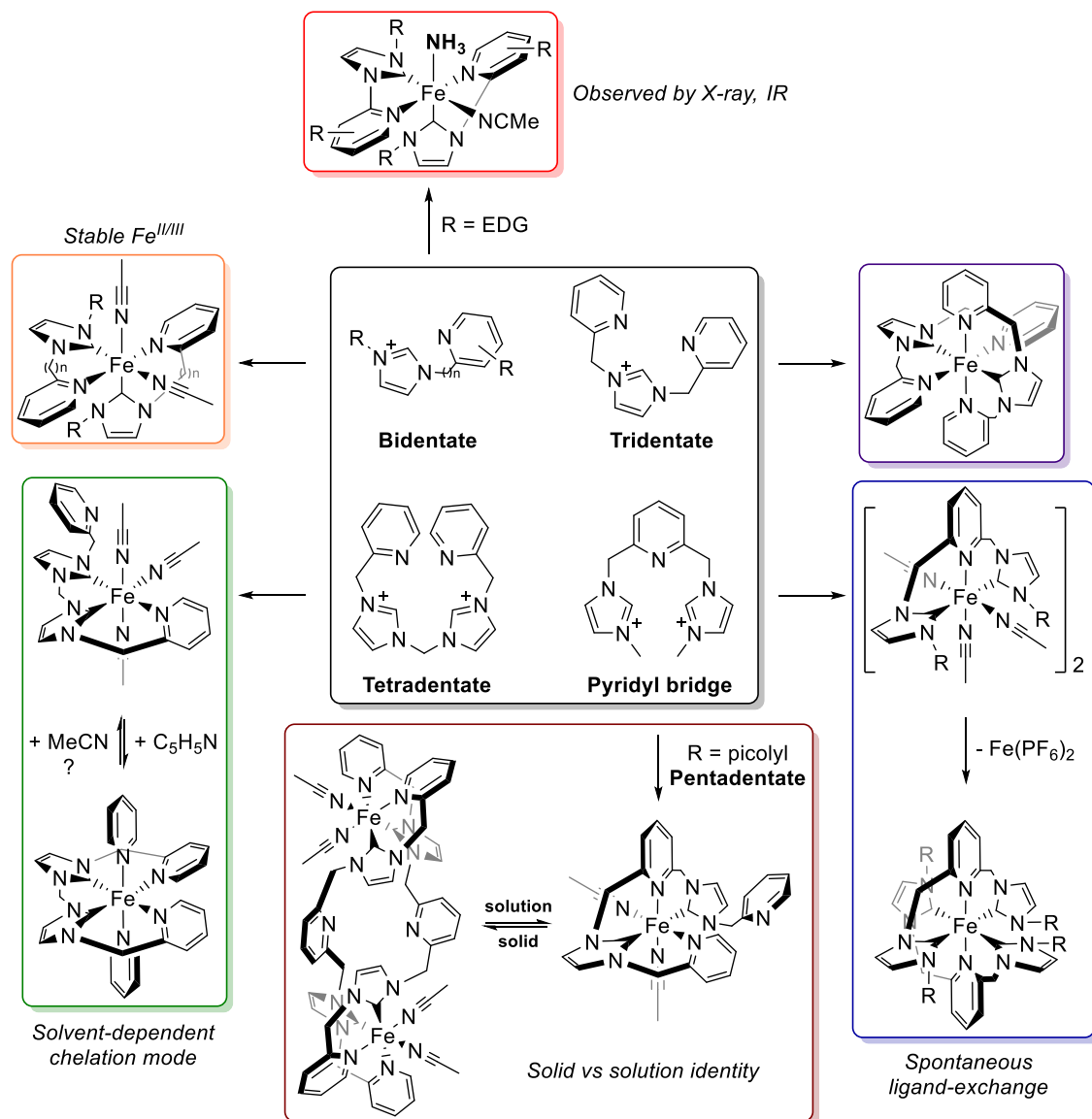
Scheme 3.17 *Summary of iron(II)-NHC complexes produced within this study.*
All counteranions are omitted for clarity.

The results presented within this chapter represent those most recently obtained within this thesis. At present, patterns are emerging with respect to pro-ligand denticity and metal-NHC produced *via* this route. However, **Scheme 3.17** provides only a guideline to the type of iron complex to be expected from a particular ligand scaffold. Further work in this area should look to exploit these design principles to rationally produce iron complexes bearing synthetically useful functional groups, which are not easily tolerated by conventional methods. Moreover, all iron(II) complexes reported here occupy octahedral geometry, pertaining to a d^6, low-spin electronic configuration.

It should be possible to design azolium precursors which equally stabilise (or trap) high-spin iron(II) compounds, opening the scope of this protocol to diverse and unusual iron-NHCs.

Future work should also be focussed on translation of the electrochemical method into a continuous-flow protocol, in a similar manner to copper(I)-NHC complexes, as described in Chapter 1. For this purpose, the use of in-line and quantitative ESI mass spectrometry would be beneficial, as a simple means of monitoring formation of sensitive iron compounds. Producing iron(II)-NHC complexes in this fashion would represent a significant milestone, as current synthetic protocols require harsh reagents and tedious purification techniques.

Despite the uncertainty surrounding the observation of iron(II)-NH$_3$ adduct **A3.7**, efforts should be placed towards confirming or denying its formation. As it stands, both **3.7** and **A3.7** are observed as a mixture of products from the electrolysis of **P3.7**. Considering both the lack of hydrogen source and that **A3.7** is presumed to form through reduction of either fixated N$_2$ or MeCN solvent, the concentration of **A3.7** should be much lower than that of **3.7**. Therefore, instead of attempting to isolate **A3.7** from this mixture, it may be possible to drive its formation through addition of a suitable hydrogen source. Doing so in the presence of ^{15}N labelled solvent or dinitrogen gas, may provide insight into the formation of **A3.7**.

A longstanding aim of this research rests in the post-synthetic application of iron(II)-NHC complexes, particularly with respect to catalysis. Preliminary findings which are not presented here, have shown octahedral iron(II)-NHC complexes of the type [Fe(NHC)$_2$(S)$_n$]2PF$_6$ (where S = labile solvent, n = 2 or 3) listed above to be active in the oxidative hydroxylation of C(sp^3)-H bonds. Taking p-cymene as an example of substrate comprising multiple C-H bonds, it has been found that these complexes selectively oxidise the least hindered C(sp^3)-H bond (see **Figure 3.18**, blue circle). This preference is in contrast to the majority iron(II) C-H hydroxylation catalysts within modern literature, which are often highly electrophilic and target the most electron-rich C-H bond (red circle).[18,20,41–44]
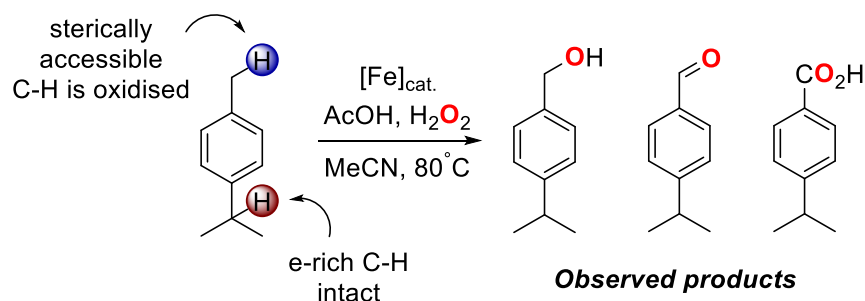
Scheme 3.18 Iron(II)-NHC catalysed C-H oxidation of p-cymene.

Activating bonds of this type is known to be challenging, especially using cheap and abundant first row transition metal complexes – therefore future work should aim to explore this reactivity.

3.8 Experimental

Where stated, manipulations were performed under an atmosphere of dry nitrogen by means of standard Schlenk line or glovebox techniques. Anhydrous solvents were prepared by passing the solvent over activated alumina to remove water, copper catalyst to remove oxygen and molecular sieves to remove any remaining water, *via* the Dow-Grubbs solvent system. Deuterated CD_3CN, $CDCl_3$ and C_5D_5N were dried over CaH_2, cannula filtered or distilled, and then freeze-pump-thaw degassed prior to use. All other chemicals were obtained from commercial sources and used as received. Fe foil (99.5 % purity) was used as electrode surface directly without further purification (purchased from Goodfellow Cambridge Ltd).

N-Pyridylimidazole (**I3.1**),[45] *N*-mesitylimidazole (**I3.2**),[46] *N*-(2-methylpyridyl)imidazole (**I3.3**),[45] 2-(imidazole-1-yl)-4-(dimethylamino)pyridine (**I3.7**),[47] 2,6-*bis*(bromomethyl)pyridine,[48] 1-methoxy-2-(imidazol-1-yl)benzene[49] and 2,6-*bis*(1-imidazolyl)pyridine[50] were prepared in reference to literature procedures. All other chemicals were obtained from commercial sources and used as received.

A PSD 30/3B high performance digital power supply was used in constant voltage mode (CV), with current measurements recorded by a 15XP-B Amprobe digital multimeter, at a milliampere scale.

3.8.1 Instrumentation

^1H and ^{13}C NMR spectra were recorded by automated procedures on either a Bruker Avance (500/125 MHz), Bruker Ascend (400/100 MHz) or DPX (300/75 MHz) NMR spectrometer, using the residual solvent as an internal standard. High resolution NOESY and variable temperature ^1H NMR spectra were recorded in collaboration with Mr Simon Barrett of the University of Leeds. The values of chemical shift are reported in parts per million (ppm) with the multiplicities of the spectra assigned as follows: singlet (s), doublet (d), triplet (t), quartet (q), multiplet (m) and broad (br), values for coupling constants (*J*) are assigned in Hz. High-resolution electrospray mass spectra (ESI-MS) were measured on an open-access Bruker Daltonics (micro TOF) instrument operating in the electrospray mode. Samples for microanalysis were dried under vacuum prior to analysis and the elemental composition determined by either Ms. Tanya Marinko-Covell of the University of Leeds Microanalytical Service using a Carlo Erba elemental analyser MOD 1106 spectrometer, or Mr Stephen Boyer of the London Metropolitan University, School of Human Sciences.

Electrochemical measurements were conducted using an Autolab PGSTAT204 voltammetric analyser under an argon atmosphere, solvated in pre-dried CH_3CN containing 0.10 M [$^nBu_4N$]PF_6 as supporting electrolyte. Voltammetric experiments utilised a Pt disk working electrode, a Pt rod

auxiliary electrode and an Ag/AgCl reference electrode. Due to the nature of each iron(II) complex, $E_{1/2}$ values could not be calibrated against the ferrocene/ferrocenium standard couple as peak overlap becomes problematic, and are quoted as measured with reference to Ag/AgCl.

X-ray powder diffraction measurements were obtained from a Bruker D2 Phaser diffractometer, using Cu Kα radiation (λ = 1.5418 Å). SCXRD datasets were used to simulate powder patterns using Mercury Crystal Structure Visualisation software and compared with those obtained directly from PXRD.

Single crystal X-ray diffraction data were collected on an Agilent SuperNova diffractometer fitted with an Atlas CCD detector with Mo Kα radiation (λ = 0.7107 Å) or Cu Kα radiation (λ = 1.5418 Å). Crystals were mounted under oil on nylon fibres. Data sets were corrected for absorption using a multiscan method, and the structures were solved by direct methods using SHELXS-97 or SHELXT and refined by full-matrix least squares on F^2 using ShelXL-97, interfaced through the program Olex2.[51] Molecular graphics for all structures were generated using POV-RAY in the X-Seed program.

3.8.2   Preparation of imidazolium salt precursors

Synthesis of 1,3-*bis*(2-pyridyl)imidazolium hexafluorophosphate (P3.1). Following a modified literature procedure,[52] *N*-methylimidazole (1.00 g, 12.2 mmol) and 2-bromopyridine (2.32 mL, 24.4 mmol) were added to a sealed round-bottomed flask and stirred vigorously at 190 ˚C for 12 hours. Dissolution of the resulting dark brown residue with methanol (10 mL) followed by slow addition of acetone (10 mL) led to precipitation of a pale yellow solid (imidazolium bromide intermediate). The solid was re-dissolved with deionised water (30 mL) and stirred vigorously with ammonium hexafluorophosphate (3.98 g, 24.4 mmol) for 2 hours. The resulting off-white precipitate was collected by vacuum filtration, rinsed with deionised water (3 × 30 mL) followed by diethyl ether (3 × 30 mL) and dried under vacuum to deliver the title compound as an off-white powder. Yield: 3.00 g, 8.10 mmol, 66 %. ^{1}H NMR (300 MHz, CD$_3$CN) δ (ppm) 9.89 (s, 1H, NC*H*N), 8.54 (d, *J* = 4.2 Hz, 2H, py*H*), 8.20 (s, 2H, im*H*), 8.04 (t, *J* = 8.1 Hz, 2H, py*H*), 7.80 (d, *J* = 8.1 Hz, 2H, py*H*), 7.52 (t, *J* = 8.1 Hz, 2H, py*H*). ^{13}C{^{1}H} NMR (75 MHz, CD$_3$CN) δ (ppm) 150.7, 147.2, 141.6, 133.3, 126.9, 121.5, 115.6. HR-MS (ESI$^+$): *m/z* 223.0988 [C$_{13}$H$_{11}$N$_4$]$^+$, calcd. [M − PF$_6$]$^+$ 223.0978. Anal. calcd. (%) for C$_{13}$H$_{11}$N$_4$F$_6$P: C 42.40, H 3.01, N 15.22; found C 42.70, H 3.15, N 15.20.

Synthesis of 1-mesityl-3-(2-pyridyl)imidazolium hexafluorophosphate (P3.2). Freshly prepared *N*-mesitylimidazole[46] (1.10 g, 5.80 mmol) and 2-bromopyridine (0.58 mL, 6.00 mmol) were charged to a sealed round-bottomed flask and stirred vigorously at 160 ˚C for 12 hours. Dissolution of the resulting dark brown residue with chloroform (10 mL) followed by slow

addition of cold diethyl ether (50 mL) led to formation of a pale brown precipitate (imidazolium bromide intermediate). The solid was re-dissolved with deionised water (30 mL) and stirred vigorously with ammonium hexafluorophosphate (1.90 g, 11.6 mmol) for 2 hours. The resulting off-white precipitate was collected by vacuum filtration, washed with deionised water (3×30 mL) followed by diethyl ether (3×30 mL) and dried under vacuum to afford the product as a microcrystalline, off-white solid. Yield: 1.52 g, 3.71 mmol, 64 %. ^{1}H NMR (300 MHz, CD$_3$CN) δ (ppm) 9.41 (t, J = 3.3 Hz, 1H, NCHN), 8.63 (d, J = 4.8 Hz, 1H, im$H$), 8.35 (t, J = 3.3 Hz, 1H, im$H$), 8.15 (td, J = 15.9, 8.1, 3.3 Hz, 1H, py$H$), 7.84 (d, J = 8.1 Hz, 1H, py$H$), 7.65 − 7.60 (m, 2H, py$H$), 7.16 (s, 2H, mes ar$H$), 2.38 (s, 3H, mes p-CH_3), 2.12 (s, 6H, mes (o-CH_3)$_2$). ^{13}C{^{1}H} NMR (100 MHz, CD$_3$CN) δ (ppm) 150.3, 147.6, 142.5, 141.4, 136.4, 135.8, 132.0, 130.6, 126.5, 125.8, 121.1, 115.8, 21.2, 17.7. HR-MS (ESI$^+$): m/z 264.1507 [C$_{17}$H$_{18}$N$_3$]$^+$, calcd. [M − PF$_6$]$^+$ 264.1495. Anal. calcd. (%) for C$_{17}$H$_{18}$N$_3$F$_6$P($^1/_5$H$_2$O): C 49.45, H 4.49, N 10.18; found C 49.30, H 4.30, N 9.90.

Synthesis of 1,3-*bis*(2-methylpyridyl)imidazolium hexafluorophosphate (P3.3). 2-(Bromomethyl)pyridine hydrobromide (1.20 g, 4.74 mmol), imidazole (0.21 g, 3.10 mmol), potassium carbonate (1.65 g, 11.9 mmol) and acetonitrile (40 mL) were charged to a round-bottomed flask and stirred vigorously at 60 ˚C for 18 hours, upon which a red colouration dissipated to leave a pale brown suspension. The resulting mixture was filtered and concentrated to *ca*. 10 % volume, to which diethyl ether (50 mL) was added to produce a brown oil (imidazolium bromide intermediate). Solvent was decanted and the oil re-dissolved in deionised water (30 mL) and stirred with ammonium hexafluorophosphate (0.78 g, 4.74 mmol) for 2 hours. The resulting precipitate was collected by vacuum filtration, washed with deionised water (3×30 mL), followed by diethyl ether (3×30 mL) and dried under vacuum to afford the title compound as a spectroscopically pure pale brown solid. Yield: 0.55 g, 1.40 mmol, 59 %. ^{1}H NMR (400 MHz, CD$_3$CN) δ (ppm) 8.78 (br s, 1H, NCHN), 8.56 (br d, J = 4.5 Hz, 2H, im$H$), 7.84 (td, J = 15.3, 7.8, 1.5 Hz, 2H, py$H$), 7.48 − 7.35 (m, 6H, py$H$), 5.44 (s, 4H, (CH_2)$_2$). ^{13}C{^{1}H} NMR (125 MHz, CDCl$_3$) δ (ppm) 152.4, 150.0, 137.8, 137.6, 124.2, 124.1, 122.5, 54.2. HR-MS (ESI$^+$): m/z 251.1304 [C$_{15}$H$_{15}$N$_4$]$^+$, calcd. [M − PF$_6$]$^+$ 251.1291. All data are consistent with the literature.[45]

Synthesis of 1,1'-methylene-*bis*(3-(2-methylpyridyl))imidazolium dihexafluorophosphate (P3.4). Freshly prepared N-(2-methylpyridyl)imidazole[15] (0.65 g, 4.40 mmol) and dibromomethane (3.10 mL, 44.0 mmol) were stirred vigorously in a round-bottomed flask at 80 ˚C for 18 hours. After this time, excess dibromomethane was removed *in vacuo* and the remaining residue washed with THF (3×50 mL) to leave a hygroscopic white solid (imidazolium bromide intermediate), which was subsequently dissolved in deionised water (30 mL) and stirred vigorously with ammonium hexafluorophosphate (1.43 g, 8.80 mmol) for 2 hours. The resulting pale brown precipitate was collected by vacuum filtration, rinsed with deionised water

(3 × 30 mL), followed by diethyl ether (3 × 30 mL) and dried under vacuum to deliver the desired product as a pale brown solid. Yield: 1.10 g, 1.76 mmol, 80 %. ^{1}H NMR (300 MHz, CD$_3$CN) δ (ppm) 8.99 (br s, 2H, NCHN), 8.57 (d, J = 4.5 Hz, 2H, im$H$), 7.86 (td, J = 15.3, 7.5, 1.5 Hz, 2H, py$H$), 7.62 (t, J = 3.9, 2.1 Hz, 2H, py$H$), 7.59 (t, J = 3.9, 2.1 Hz, 2H, py$H$), 7.49 (d, J = 7.5 Hz, 2H, py$H$), 7.40 (dd, J = 7.5, 4.5 Hz, 2H, im$H$), 6.43 (s, 2H, NCH_2N), 5.48 (s, 4H, (NCH_2C)$_2$). ^{13}C{^{1}H} NMR (100 MHz, CD$_3$CN) δ (ppm) 153.0, 150.9, 138.8, 138.6, 125.5, 125.1, 124.2, 123.0, 60.0, 55.2. HR-MS (ESI$^+$): m/z 477.1414 [C$_{19}$H$_{20}$N$_6$F$_6$P]$^+$, calcd. [M − PF$_6$]$^+$ 477.1391. Anal. calcd. (%) for C$_{19}$H$_{20}$N$_6$F$_{12}$P$_2$: C 36.60, H 3.24, N 13.50; found C 36.20, H 3.15, N 13.10.

Synthesis of 1-(2-methylpyridyl)-3-(*tert*-butylacetate)imidazolium hexafluorophosphate (P3.5). Freshly prepared *N*-(2-methylpyridyl)imidazole[15] (1.00 g, 6.25 mmol) and *tert*-butyl chloroacetate (1.34 mL, 9.40 mmol) were stirred vigorously in refluxing acetonitrile (30 mL) for 16 hours. Following, diethyl ether (50 mL) was slowly added to the reaction mixture to precipitate a pale brown solid. The precipitate was collected by vacuum filtration, rinsed with cold diethyl ether (3 × 30 mL) and dried under vacuum to afford the chloride salt intermediate of the desired product as a microcrystalline pale brown solid. (Yield: 1.93 g, 6.25 mmol, quant.). The solid was further dissolved in deionised water (30 mL) and stirred vigorously with ammonium hexafluorophosphate (2.00 g, 12.5 mmol) for 2 hours. The resulting brown residue was rinsed with deionised water (3 × 30 mL), followed by diethyl ether (3 × 30 mL) and dried under vacuum to deliver the desired product as a pale yellow oil. Yield: 1.62 g, 3.90 mmol, 62 %. ^{1}H NMR (400 MHz, CD$_3$CN) δ (ppm) 8.68 (s, 1H, NCHN), 8.56 (d, J = 4.8 Hz, 1H, im$H$), 7.85 (td, J = 7.7, 1.8 Hz, 1H, py$H$), 7.49 (t, J = 1.8 Hz, 1H, py$H$), 7.47 (d, J = 4.8 Hz, 1H, im$H$), 7.44 (t, J = 1.8 Hz, 1H, py$H$), 7.38 (m, 1H, py$H$), 5.48 (s, 2H, CH_2CO$_2$), 4.90 (s, 2H, NCCH_2), 1.47 (s, 9H, C(CH_3)$_3$). ^{13}C{^{1}H} NMR (100 MHz, CD$_3$CN) δ (ppm) 166.1, 153.7, 150.8, 138.8, 138.3, 125.1, 124.8, 124.0, 123.9, 84.9, 54.9, 51.6, 28.1. HR-MS (ESI$^+$): m/z 274.1562 [C$_{15}$H$_{20}$N$_3$O$_2$]$^+$, calcd. [M − PF$_6$]$^+$ 274.1550.

Synthesis of 1-allyl-3-(2-pyridyl)imidazolium bromide (P3.6). 2-(Imidazole-1-yl)pyridine (0.72 g, 5.0 mmol) and allyl bromide (2.0 mL, 23.0 mmol) were stirred vigorously in refluxing acetonitrile (40 mL) for 16 hours. After this time, the mixture was cooled to room temperature and the volume of solvent reduced to *ca.* 10 mL. Slow addition of diethyl ether (35 mL) to the stirring solution led to precipitation of the product as an off-white microcrystalline solid. Yield: 1.18 g, 4.45 mmol, 89 %. ^{1}H NMR (300 MHz, CDCl$_3$) δ (ppm) 11.74 (s, 1H, NCHN), 8.57 − 8.47 (m, 2H, py$H$), 8.32 (t, J = 1.7 Hz, 1H, im$H$), 8.08 − 7.98 (m, 1H, py$H$), 7.52 (t, J = 1.7 Hz, 1H, im$H$), 7.48 − 7.42 (m, 1H, py$H$), 6.12 (ddt, J = 16.8, 10.1, 6.5 Hz, 1H, CH=CH$_2$), 5.57 (d, J = 16.8 Hz, 1H, HC=CHH_{trans}), 5.51 (dd, J = 10.1, 0.6 Hz, 1H, HC=CHH_{cis}), 5.24 (d, J = 6.5 Hz, 2H, NCH_2). ^{13}C{^{1}H} NMR (75 MHz, CDCl$_3$) δ (ppm) 149.1, 146.1, 140.8, 136.0,

129.7, 125.3, 123.5, 122.0, 119.1, 115.2, 52.8. HR-MS (ESI⁺): m/z 186.1030 $[C_{11}H_{12}N_3]^+$, calcd. $[M - Br]^+$ 186.1026. All data are consistent with the literature.[14]

Synthesis of 1-allyl-3-(2-pyridyl)imidazolium hexafluorophosphate (P3.6.1). **P3.6** (1.10 g, 4.40 mmol) was dissolved into deionised water (30 mL) and stirred vigorously with ammonium hexafluorophosphate (1.63 g, 10.0 mmol) for 2 hours. The resulting off-white precipitate was collected by vacuum filtration, rinsed with deionised water (3 × 30 mL), followed by diethyl ether (3 × 30 mL) and dried under vacuum to deliver the desired product as an off-white solid. Yield: 0.75 g, 2.26 mmol, quant.. ¹H NMR (400 MHz, CD₃CN) δ (ppm) 9.29 (s, 1H, NC*H*N), 8.60 (d, J = 4.0 Hz, 1H, py*H*), 8.13 – 8.09 (m, 2H, im*H* and py*H*), 7.75 (d, J = 8.4 Hz, 1H, im*H*), 7.60 – 7.57 (m, 2H, py*H*), 6.11 (ddt, J = 17.7, 9.3, 4.8 Hz, 1H, C*H*=CH₂), 5.50 – 5.46 (m, 2H, HC=C*HH*$_{cis/trans}$), 4.90 (d, J = 6.4 Hz, 2H, NC*H₂*). ¹³C{¹H} NMR (100 MHz, CD₃CN) δ (ppm) 150.5, 147.5, 141.5, 135.1, 131.2, 126.5, 124.5, 122.6, 120.7, 115.1, 53.2. HR-MS (ESI⁺): m/z 186.1026 $[C_{11}H_{12}N_3]^+$, calcd. $[M - PF_6]^+$ 186.1026. Anal. calcd. (%) for $C_{11}H_{12}N_3F_6P$: C 39.89, H 3.65, N 12.69; found C 39.87, H 3.79, N 12.53.

Synthesis of 1-allyl-3-(2-(4-dimethylamino)pyridyl)imidazolium bromide (P3.7). 2-(Imidazole-1-yl)-4-(dimethylamino)pyridine[47] (0.94 g, 5.0 mmol) and allyl bromide (2.0 mL, 23 mmol) were stirred vigorously in refluxing acetonitrile (40 mL) for 16 hours. After this time, the mixture was cooled to room temperature and the volume of solvent reduced to *ca.* 10 mL. Slow addition of diethyl ether (35 mL) to the stirring solution led to precipitation of the product as an off-yellow microcrystalline solid, which was collected by vacuum filtration, washed with diethyl ether (2 × 20 mL) and dried under vacuum to provide the title compound as a pale yellow solid. Yield: 1.31 g, 4.25 mmol, 85 %. ¹H NMR (300 MHz, CDCl₃) δ (ppm) 11.97 (s, 1H, NC*H*N), 8.23 (t, J = 3.6, 1.8 Hz, 1H, im*H*), 8.03 (d, J = 6.3 Hz, 1H, *o*-py*H*), 7.62 (d, J = 2.1 Hz, *m*-py*H*), 7.27 (t, J = 3.6, 1.8 Hz, 1H, im*H*), 6.53 (dd, J = 6.3, 2.1 Hz, 1H, *p*-py*H*), 6.11 (ddt, J = 16.8, 10.1, 6.5 Hz, 1H, C*H*=CH₂), 5.53 (d, J = 16.8 Hz, 1H, HC=CH*H*$_{trans}$), 5.49 (dd, J = 10.1, 0.6 Hz, 1H, HC=CH*H*$_{cis}$), 5.15 (d, J = 6.5 Hz, 2H, NC*H₂*), 3.20 (s, 6H, N(C*H₃*)₂). ¹³C{¹H} NMR (75 MHz, CDCl₃) δ (ppm) 156.7, 148.2, 147.1, 135.3, 129.8, 122.9, 121.6, 119.3, 107.5, 96.7, 52.3, 40.2. HR-MS (ESI⁺): m/z 229.1453 $[C_{13}H_{17}N_4]^+$, calcd. $[M - Br]^+$ 229.1448. Anal. calcd. (%) for $C_{13}H_{17}N_4Br$: C 49.30, H 5.54, N 18.12; found C 48.90, H 5.75, N 17.90.

Synthesis of 1,1'-(*bis*(methylene)-2,6-pyridyl)-3,3'-methyldiimidazolium dihexafluorophosphate (P3.8). 2,6-*Bis*(bromomethyl)pyridine (0.82 g, 3.10 mmol) and *N*-methylimidazole (0.57 mL, 7.11 mmol) were stirred vigorously in acetonitrile (40 mL) at 70 ˚C for 12 hours. After this time, the solution was cooled slowly to room temperature, allowing a microcrystalline white solid to form which proved extremely hygroscopic when exposed to air (*bis*-imidazolium dibromide intermediate). The solid was re-dissolved in deionised water (30 mL) and ammonium hexafluorophosphate (1.63 g, 10 mmol) added portionwise, rapidly precipitating

a white powder which was collected by vacuum filtration, washed with deionised water (2×20 mL), followed by diethyl ether (2×20 mL) and dried under vacuum to deliver the title compound as a microcrystalline white solid. Yield: 1.23 g, 2.20 mmol, 71 %. ^{1}H NMR (400 MHz, CD$_3$CN) δ (ppm) 8.44 (br s, 2H, NC*H*N), 7.90 (t, *J* = 15.6, 7.6 Hz, 1H, *p*-py*H*), 7.44 (d, *J* = 7.6 Hz, 2H, *m*-py*H*), 7.34 (s, 4H, im*H*), 5.38 (s, 4H, (C*H*$_2$)$_2$), 3.85 (s, 6H, (C*H*$_3$)$_2$). ^{13}C{^{1}H} NMR (100 MHz, CD$_3$CN) δ (ppm) 154.2, 140.0, 137.6, 124.5, 124.2, 123.6, 54.2, 37.0. HR-MS (ESI$^+$): *m/z* 414.1294 [C$_{15}$H$_{19}$N$_5$F$_6$P]$^+$, calcd. [M − PF$_6$]$^+$ 414.1277. Anal. calcd. (%) for C$_{15}$H$_{19}$N$_5$F$_{12}$P$_2$: C 32.21, H 3.42, N 12.52; found C 32.30, H 3.35, N 12.30.

Synthesis of 1,1'-(*bis*(methylene)-2,6-pyridyl)-3,3'-allyldiimidazolium dihexafluorophosphate (P3.9). 2,6-(Dibromomethyl)pyridine (0.50 g, 1.89 mmol) and 1-allylimidazole (0.25 mL, 2.30 mmol) were stirred vigorously in refluxing acetonitrile (30 mL) for 16 hours. After this time, the mixture was cooled to room temperature and the volume of solvent reduced to *ca.* 10 mL. Slow addition of diethyl ether (35 mL) to the stirring solution led to precipitation of a highly hygroscopic off-white solid (*bis*-imidazolium dibromide intermediate). The solid was re-dissolved in deionised water (30 mL) and ammonium hexafluorophosphate (0.40 g, 2.50 mmol) added portionwise, rapidly precipitating a white powder which was collected by vacuum filtration, washed with deionised water (2×20 mL), followed by diethyl ether (2×20 mL) and dried under vacuum to deliver the title compound as a microcrystalline white solid. Yield: 0.40 g, 1.25 mmol, 66 %. ^{1}H NMR (400 MHz, CD$_3$CN) δ (ppm) 8.25 (s, 2H, NC*H*N), 7.91 (t, *J* = 7.8 Hz, 1H, *p*-py*H*), 7.45 (d, *J* = 7.8 Hz, 2H, *m*-py*H*), 7.38 (d, *J* = 6.4 Hz, 4H, im*H*), 6.03 (ddt, 16.6, 10.3, 6.2 Hz, 2H, C*H*=CH$_2$), 5.44 (d, *J* = 10.3 Hz, 2H, HC=CH*H*$_{trans}$), 5.38 (m, 6H, C*H*$_2$ and HC=CH*H*$_{cis}$), 4.77 (d, *J* = 6.2 Hz, 4H, NC*H*$_2$). ^{13}C{^{1}H} NMR (100 MHz, CD$_3$CN) δ (ppm) 154.2, 140.1, 137.1, 131.7, 124.6, 123.8, 123.3, 122.0, 54.4, 52.7. HR-MS (ESI$^+$): *m/z* 160.5971 [C$_{19}$H$_{23}$N$_5$]$^{2+}$, calcd. [M − 2PF$_6$]$^{2+}$ 160.5971.

Synthesis of 1,1'-(2,6-pyridyl)-3,3'-allyldiimidazolium dibromide (P3.9.1). 2,6-*Bis*(1-imidazolyl)pyridine (0.27 g, 1.3 mmol) and allyl bromide (0.24 mL, 2.7 mmol) were stirred vigorously in refluxing acetonitrile (40 mL) for 16 hours. After this time, the mixture was cooled to room temperature and the volume of solvent reduced to *ca.* 10 mL. Slow addition of diethyl ether (35 mL) to the stirring solution led to precipitation of the product as an off-white microcrystalline solid, which was collected by vacuum filtration, washed with diethyl ether (2×20 mL) and dried under vacuum to provide the title compound as an off-white solid. Yield: 0.33 g, 0.73 mmol, 57 %. ^{1}H NMR (400 MHz, CD$_3$CN) δ (ppm) 11.43 (s, 2H, NC*H*N), 8.43 − 8.39 (m, 3H, *p*-py*H* and im*H*), 8.11 (dd, *J* = 8.0, 0.8 Hz, 2H, im*H*), 7.64 (t, *J* = 3.6 Hz, 2H, py*H*), 6.19 (ddt, *J* = 27.4, 16.8, 10.4 Hz, 2H, C*H*=CH$_2$), 5.60 (d, *J* = 16.8 Hz, 2H, HC=CH*H*$_{trans}$), 5.47 (d, *J* = 10.4, Hz, 2H, HC=CH*H*$_{cis}$), 5.14 (d, *J* = 6.4 Hz, 4H, NC*H*$_2$). ^{13}C{^{1}H} NMR (100 MHz, CD$_3$CN) δ (ppm) 146.7, 145.9, 137.6, 131.7, 124.6, 122.3, 120.5, 115.2, 52.9. HR-MS (ESI$^+$):

m/z 146.5814 [$C_{17}H_{19}N_5$]$^{2+}$, calcd. [M − 2Br]$^{2+}$ 146.5815. All data are consistent with the literature.[16]

Synthesis of 1,1'-(*bis*(methylene)-2,6-pyridyl)-3,3'-(2-methoxyphenyl)diimidazolium dihexafluorophosphate (P3.10). 1-Methoxy-2-(imidazol-1-yl)benzene (0.50 g, 2.87 mmol) and 2,6-(dibromomethyl)pyridine (0.38 g, 1.44 mmol) were stirred vigorously in refluxing acetonitrile (50 mL) for 16 hours. Upon cooling, diethyl ether (100 mL) was slowly added to the mixture to precipitate an off-white solid. The solid was re-dissolved in deionised water (30 mL) and ammonium hexafluorophosphate (0.30 g, 1.84 mmol) added portionwise, rapidly precipitating a white powder which was collected by vacuum filtration, washed with deionised water (2 × 20 mL), followed by diethyl ether (2 × 20 mL) and dried under vacuum to deliver the title compound as a microcrystalline white solid. Yield: 0.64 g, 0.86 mmol, 60 %. ^{1}H NMR (400 MHz, CD$_3$CN) δ (ppm) 10.05 (s, 2H, NC*H*N), 8.05 (m, 1H, *p*-py*H*), 8.01 (t, *J* = 3.2, 1.2 Hz, 2H, ph*H*), 7.81 (d, *J* = 3.6 Hz, 2H, im*H*), 7.79 (d, *J* = 2.0 Hz, 2H, *m*-py*H*), 7.67 (dd, *J* = 8.0, 1.6 Hz, 2H, ph*H*), 7.66 (m, 2H, ph*H*), 7.35 (d, *J* = 3.6 Hz, 2H, im*H*), 7.20 (td, *J* = 15.2, 8.0, 1.6 Hz, 2H, ph*H*), 5.98 (s, 4H, (C*H*$_2$)$_2$), 4.00 (s, 6H, (OC*H*$_3$)$_2$). ^{13}C{^{1}H} NMR (100 MHz, CD$_3$CN) δ (ppm) 154.2, 152.9, 139.6, 138.5, 132.5, 126.5, 124.2, 124.0, 123.8, 122.2, 114.1, 57.2, 54.0. HR-MS (ESI$^+$): *m/z* 227.1103 [$C_{27}H_{27}N_5O_2$]$^{2+}$, calcd. [M − 2PF$_6$]$^{2+}$ 227.1094. Anal. calcd. (%) for $C_{27}H_{27}N_5O_2F_{12}P_2$: C 43.62, H 3.66, N 9.42; found C 43.90, H 3.60, N 9.80.

Synthesis of 1,1'-(*bis*(methylene)-2,6-pyridyl)-3,3'-(2-methylpyridyl)diimidazolium dihexafluorophosphate (P3.11). Freshly prepared *N*-(2-methylpyridyl)imidazole (1.00 g, 6.25 mmol) and 2,6-(dibromomethyl)pyridine (0.83 g, 3.13 mmol) were stirred vigorously in refluxing acetonitrile (50 mL) for 16 hours. Upon cooling, diethyl ether (50 mL) was slowly added to the mixture to produce a pale orange oil (*bis*-imidazolium dibromide intermediate). The oil was re-dissolved in deionised water (30 mL) and ammonium hexafluorophosphate (1.14 g, 7.0 mmol) added portionwise, rapidly precipitating an off-white powder which was collected by vacuum filtration, washed with deionised water (2 × 20 mL), followed by diethyl ether (2 × 20 mL) and dried under vacuum to deliver the title compound as a microcrystalline white solid. Single crystals suitable for X-ray crystallographic analysis (colourless, diffuse blocks) were obtained upon slow diffusion of Et$_2$O vapours into an MeCN solution of the compound at room temperature. Yield: 1.43 g, 2.00 mmol, 64 %. ^{1}H NMR (400 MHz, CD$_3$CN) δ (ppm) 8.75 (br s, 2H, NC*H*N), 8.54 (br d, *J* = 4.8 Hz, 2H, im*H*), 7.91 (t, *J* = 7.8 Hz, 1H, *p*-py*H*), 7.85 (td, *J* = 7.7, 1.7 Hz, 2H, py*H*), 7.47 − 7.35 (m, 10H, im*H* and py*H*), 5.44 (s, 4H, C*H*$_2$), 5.41 (s, 4H, C*H*$_2$). ^{13}C{^{1}H} NMR (100 MHz, CD$_3$CN) δ (ppm) 154.1, 153.7, 150.9, 140.0, 138.7, 137.9, 125.0, 124.3, 124.0, 123.9, 123.6, 54.8, 54.3. HR-MS (ESI$^+$): *m/z* 568.1852 [$C_{25}H_{25}N_7PF_6$]$^+$, calcd. [M − PF$_6$]$^+$ 568.1808. All data are consistent with the literature.[49]

3.8.3 Preparation of iron(II) *N*-heterocyclic carbene complexes

General procedure. A flame-dried three-necked round-bottomed flask equipped with a magnetic stirrer bar was charged with ligand precursor (**P3.1** – **P3.11**, 1.0 mmol) and the solid was further dried under high vacuum for 30 minutes. Anhydrous/degassed acetonitrile (30 mL) was added to the flask *via* cannula. Two oven-dried iron foil electrodes (99.5 % purity, 13 × 10 × 1 mm) were connected to an external power supply (positive and negative terminals), introduced to the solution and a potential range applied (25 – 27 V) to maintain a constant current of 50 mA (measured by an in-series ammeter) for 90 minutes. Following, the solution was filtered through a short path of Celite® (under an atmosphere of $N_{2 (g)}$) and solvent reduced to *ca.* 10 % volume under vacuum, to which anhydrous/degassed diethyl ether (20 mL) was added. The resulting red/orange precipitate was collected and further recrystallised from MeCN/Et$_2$O, washed with diethyl ether (3 × 30 mL) and collected by filtration under $N_{2 (g)}$ to afford the title iron(II) complexes as microcrystalline red or orange powders. Unless otherwise stated, all complexes were treated as air-sensitive samples.

Synthesis of *bis*[1,3-*bis*(2-pyridyl)imidazole-2-ylidene]iron(II) *bis*-acetonitrile dihexafluorophosphate (3.1). Ligand precursor **P3.1** was reacted according to the general procedure, affording the [Fe^{II}(NHC)$_2$(CH$_3$CN)$_2$]2PF$_6$ complex as an air- and moisture-stable light red powder. Single crystals **3.3** (suitable for X-ray crystallographic analysis) were isolated by slow diffusion of Et$_2$O vapours into a concentrated MeCN solution of the complex at room temperature. Yield: 0.36 g, 0.41 mmol, 82 %. ^{1}H NMR (500 MHz, CD$_3$CN) δ (ppm) 8.35 (ddd, J = 6.0, 1.5, 1.0 Hz, 2H, py*H*), 8.11 (ddd, J = 6.0, 1.5, 1.0 Hz, 2H, py*H*), 8.06 (d, J = 2.0 Hz, 2H, im*H*), 7.74 (ddd, J = 8.3, 7.5, 1.5 Hz, 2H, py*H*), 7.49 (td, J = 8.3, 1.5 Hz, 2H, py*H*), 7.43 (d, J = 2.0 Hz, 2H, im*H*), 7.39 (dt, J = 7.5, 1.5, 1.0 Hz, 2H, py*H*), 7.15 (ddd, J = 12.5, 6.0, 1.0 Hz, 2H, py*H*), 7.06 (ddd, J = 12.5, 6.0, 1.0 Hz, 2H, py*H*), 6.89 (dt, J = 7.5, 1.5, 1.0 Hz, 2H, py*H*), 1.96 (s, 6H, coord. (C*H$_3$*CN)$_2$). ^{13}C{^{1}H} NMR (125 MHz, CD$_3$CN) δ (ppm) 200.1, 155.6, 155.2, 150.9, 150.3, 140.5, 139.8, 131.3, 128.0, 125.7, 122.8, 121.2, 118.8, 112.0. HR-MS (ESI$^+$): *m/z* 250.0574 [C$_{26}$H$_{20}$N$_8$Fe]$^{2+}$, calcd. [M − 2CH$_3$CN − 2PF$_6$]$^{2+}$ 250.0575. Anal. calcd. (%) for C$_{30}$H$_{26}$N$_{10}$F$_{12}$P$_2$Fe: C 41.26, H 3.12, N 16.04; found C 41.30, H 3.00, N 16.10.

Synthesis of *bis*[1-(2-pyridyl)-3-mesitylimidazole-2-ylidene]iron(II) *bis*-acetonitrile dihexafluorophosphate (3.2). Ligand precursor **3.2** was reacted according to the general procedure, affording the [Fe^{II}(NHC)$_2$(CH$_3$CN)$_2$]2PF$_6$ complex as an air- and moisture-stable light red powder. Single crystals of **3.2** (suitable for X-ray crystallographic analysis) were isolated upon standing of a weak Et$_2$O solution of the compound at room temperature over 48 hours. Yield: 0.35 g, 0.37 mmol, 74 %. ^{1}H NMR (500 MHz, CD$_3$CN) δ (ppm) 8.19 (d, J = 2.0 Hz, 2H, im*H*), 8.15 (d, J = 5.3 Hz, 2H, py*H*), 7.76 (t, J = 7.2 Hz, 2H, py*H*), 7.43 (d, J = 7.2 Hz, 2H, py*H*),

7.15 (d, J = 2.0 Hz, 2H, im$H$), 6.86 (t, J = 7.2 Hz, 2H, py$H$), 6.68 (s, 2H, mesityl ar$H$), 6.53 (s, 2H, mesityl ar$H$), 2.18 (s, 6H, mes p-CH_3), 1.97 (s, 6H, inequiv. mesityl o-CH_3), 1.96 (s, 6H, inequiv. mesityl o-CH_3), 1.44 (s, 6H, coord. (CH_3CN)$_2$). ^{13}C{^{1}H} NMR (125 MHz, CD$_3$CN) δ (ppm) 200.3, 199.0, 155.4, 154.4, 140.5, 139.5, 136.2, 134.7, 134.6, 131.6, 130.5, 130.1, 128.9, 122.9, 119.5, 111.5, 20.9, 17.7, 17.4, 1.7. HR-MS (ESI$^+$): m/z 809.2360 [C$_{38}$H$_{40}$N$_8$FeF$_6$P]$^+$, calcd. [M − PF$_6$]$^+$ 809.2362. Anal. calcd. (%) for C$_{38}$H$_{40}$N$_8$F$_{12}$P$_2$Fe: C 47.81, H 4.22, N 11.74; found C 47.45, H 4.20, N 11.40.

Synthesis of *bis*[1,3-(2-methylpyridyl)imidazole-2-ylidene]iron(II) dihexafluorophosphate (3.3). Ligand precursor **P3.3** was reacted according to the general procedure, affording the initial [Fe^{II}(NHC)$_2$]2PF$_6$ complex as a dark red oil, which solidifies immediately upon standing in THF. Single crystals of **3.3** (suitable for X-ray crystallographic analysis) were isolated upon standing of a concentrated THF solution of the compound at − 30 ˚C over 48 hours. Yield: 0.36 g, 0.43 mmol, 85 %. ^{1}H NMR (400 MHz, CD$_3$CN) δ 8.01 (s, 4H, im$H$), 7.55 (td, J = 7.6, 2.0 Hz, 4H, py$H$), 7.33 (d, J = 7.6 Hz, 4H, py$H$), 7.08 (d, J = 7.6 Hz, 4H, py$H$), 6.60 (td, J = 7.6, 2.0 Hz, 4H, py$H$), 5.61 (d, J = 16.0 Hz, 4H, diastereo. (CH_2)$_2$), 4.16 (d, J = 16.0 Hz, 4H, diastereo. (CH_2)$_2$). ^{13}C{^{1}H} NMR (100 MHz, CD$_3$CN) δ (ppm) 209.4, 163.0, 160.1, 138.5, 126.6, 124.9, 124.8, 54.2. HR-MS (ESI$^+$): m/z 701.1421 [C$_{30}$H$_{28}$N$_8$FeF$_6$P]$^+$, calcd. [M − PF$_6$]$^+$ 701.1423. Anal. calcd. (%) for C$_{30}$H$_{28}$N$_8$F$_{12}$P$_2$Fe.^{2}/$_3$CH$_3$CN: C 43.10, H 3.47, N 13.93; found C 43.50, H 3.70, N 13.80.

Synthesis of [1,1'-methylene-*bis*(3-(2-methylpyridyl))imidazole-2-ylidene]iron(II) *tris*-acetonitrile dihexafluorophosphate (3.4). Ligand precursor **P3.4** was reacted according to the general procedure, affording the [Fe^{II}(NHC)$_2$(CH$_3$CN)$_3$]2PF$_6$ complex as a dark red powder. Single crystals of **3.4** (suitable for X-ray crystallographic analysis) were isolated by slow diffusion of Et$_2$O vapours into a concentrated MeCN solution of the complex at room temperature. Yield: 0.36 g, 0.46 mmol, 91 %. ^{1}H NMR (500 MHz, CD$_3$CN, 233 K) δ (ppm) 9.23 (d, J = 6.0 Hz, 1H, im$H$), 8.56 (d, J = 3.5 Hz, 1H, py$H$), 7.99 (t, J = 15.0, 7.5 Hz, 1H, py$H$), 7.84 (t, J = 15.0, 7.5 Hz, 1H, py$H$), 7.65 (d, J = 8.0 Hz, 1H, py$H$), 7.60 (s, 2H, py$H$), 7.56 (s, 1H, im$H$), 7.51 (t, J = 15.0, 7.5 Hz, 1H, py$H$), 7.34 (t, J = 15.0, 7.5 Hz, 1H, py$H$), 7.21 (d, J = 6.0 Hz, 1H, im$H$), 7.14 (s, 1H, im$H$), 6.37 (d, J = 13.0 Hz, 1H, NCH_2N), 5.88 (d, J = 13.0 Hz, 1H, NCH_2N), 5.84 (d, J = 16.5 Hz, 1H, α-CH_2 coord. py), 5.66 (d, J = 16.5 Hz, 1H, α-CH_2 coord. py), 5.58 (d, J = 16.0 Hz, 1H, α-CH_2 uncoord. py), 5.27 (d, J = 16.0 Hz, 1H, α-CH_2 uncoord. py), 1.96 (br s, 9H, coord. (CH_3CN)$_3$). ^{13}C{^{1}H} NMR (125 MHz, CD$_3$CN, 298 K) δ (ppm) 196.4, 190.1, 159.0, 158.2, 157.1, 150.6, 139.2, 138.3, 126.3, 125.8, 125.5, 125.1, 124.8, 124.0, 123.5, 122.8, 62.7, 55.4, 53.8, 1.8. HR-MS (ESI$^+$): m/z 193.0474 [C$_{19}$H$_{18}$N$_6$Fe]$^{2+}$, calcd. [M − 3CH$_3$CN − 2PF$_6$]$^{2+}$ 193.0466. Anal. calcd. (%) for C$_{23}$H$_{23}$N$_9$F$_{12}$P$_2$Fe: C 36.43, H 3.19, N 14.78; found C 36.20, H 3.20, N 14.70 (microanalysis corroborates with one molecule of coordinating MeCN removed upon vacuum-drying sample).

Synthesis of *bis*[1-(2-methylpyridyl)-3-(*tert*-butylacetato)imidazole-2-ylidene]iron(II) *bis*-acetonitrile dihexafluorophosphate (3.5). Ligand precursor **P3.5** was reacted according to the general procedure, affording the [Fe^{II}(NHC)$_2$(CH$_3$CN)$_2$]2PF$_6$ complex (mixture of geometric isomers) as a light red powder. A batch of single crystals of **3.5** (suitable for X-ray crystallographic analysis) were isolated by slow diffusion of Et$_2$O vapours into a concentrated MeCN solution of the complex at room temperature, from which three independent datasets were collected and solved to illustrate three geometric isomers of **3.5**. Yield: 0.37 g, 0.38 mmol, 76 %. Due to the inherent formation of multiple geometric isomers of **3.5**, multinuclear NMR spectroscopy does not present clear or assignable structural information. HR-MS (ESI$^+$): *m/z* 301.1159 [C$_{30}$H$_{38}$N$_6$O$_4$Fe]$^{2+}$, calcd. [M − 2CH$_3$CN − 2PF$_6$]$^{2+}$ 301.1147. Anal. calcd. (%) for C$_{34}$H$_{44}$N$_8$O$_4$F$_{12}$P$_2$Fe: C 41.90, H 4.55, N 11.50; found C 41.87, H 4.41, N 11.39.

Synthesis of *bis*[1-(2-pyridyl)-3-allylimidazole-2-ylidene]iron(II) *mono*-acetonitrile dibromide (3.6). Ligand precursor **P3.6** was reacted according to the general procedure, affording the [Fe^{II}(NHC)$_2$(CH$_3$CN)Br]Br complex (mixture of geometric isomers) as a dark red powder. Single crystals of **3.6** (suitable for X-ray crystallographic analysis) were isolated by slow diffusion of Et$_2$O vapours into a concentrated MeCN solution of the complex at room temperature. (Dissolution of these crystals into MeCN, followed by slow evaporation of the solvent gave single red needles of **O3.6**). Yield: 0.21 g, 0.32 mmol, 64 %. ^{1}H NMR (500 MHz, CD$_3$CN) δ (ppm) 8.75 − 7.14 (br m, 12H, py*H* and im*H*), 6.13 (br m, 1H, alkenyl *H*), 5.50 − 4.72 (br m, 5H, alkenyl *H*), 4.36 (br m, 1H, alkenyl *H*), 3.62 − 3.29 (br m, 3H, alkenyl *H*). HR-MS (ESI$^+$): *m/z* 505.0436 [C$_{22}$H$_{22}$N$_8$BrFe]$^+$, calcd. [M − CH$_3$CN − Br]$^+$ 505.0433.

Synthesis of *bis*[1-(2-pyridyl)-3-allylimidazole-2-ylidene]iron(II) *bis*-acetonitrile dihexafluorophosphate (3.6.1). Ligand precursor **3.6.1** was reacted according to the general procedure, affording the [Fe^{II}(NHC)$_2$(CH$_3$CN)$_2$]2PF$_6$ complex as a light red powder. Single crystals of **3.6.1** (suitable for X-ray crystallographic analysis) were isolated by slow diffusion of Et$_2$O vapours into a concentrated MeCN solution of the complex at room temperature. Yield: 0.34 g, 0.42 mmol, 84 %. ^{1}H NMR (400 MHz, CD$_3$CN) δ (ppm) 8.83 (d, *J* = 8.8 Hz, 2H, im*H*), 8.23 − 8.17 (m, 4H, py*H*), 7.88 (d, *J* = 8.8 Hz, 2H, im*H*), 7.49 (t, *J* = 16.0, 8.8 Hz, 2H, py*H*), 7.27 (br s, 2H, py*H*), 5.52 − 5.41 (m, 2H, C*H*=CH$_2$), 5.06 (d, *J* = 13.2 Hz, 2H, CH=C*H*$_{cis}$), 4.53 (d, *J* = 21.6 Hz, 2H, CH=C*H*$_{trans}$), 3.78 (s, 6H, coord (C*H$_3$*CN)$_2$), 3.67 − 3.54 (m, 4H, NC*H$_2$*). ^{13}C{^{1}H} NMR (100 MHz, CD$_3$CN) δ (ppm) 199.2, 156.5, 155.4, 140.9, 134.0, 127.8, 122.9, 119.1, 116.2, 112.4, 51.4. HR-MS (ESI$^+$): *m/z* 213.0638 [C$_{22}$H$_{22}$N$_6$Fe]$^{2+}$, calcd. [M − 2CH$_3$CN − 2PF$_6$]$^{2+}$ 213.0622. Anal. calcd. (%) for C$_{26}$H$_{28}$N$_8$F$_{12}$P$_2$Fe: C 39.12, H 3.54, N 14.04; found C 39.04, H 3.31, N 13.79.

Synthesis of *bis*[1-(2-(4-dimethylamino)pyridyl)-3-allylimidazole-2-ylidene]iron(II) *bis*-acetonitrile dibromide (3.7). Ligand precursor **3.7** was reacted according to the general procedure, affording the $[Fe^{II}(NHC)_2(CH_3CN)_2]2Br$ complex as the major product of reaction, as a deep red powder. Single crystals of **3.7** (suitable for X-ray crystallographic analysis) were isolated by slow diffusion of Et_2O vapours into a concentrated MeCN solution of the complex at room temperature. (Dissolution of these crystals into MeCN, followed by slow evaporation of the solvent gave single red needles of **O3.7**). Yield (based on the assumption that pure **3.7** must form as the original product of reaction): 0.34 g, 0.38 mmol, 76 %. Due to the inherent formation of multiple geometric isomers of **3.7**, multinuclear NMR spectroscopy does not present clear or assignable structural information. HR-MS (ESI$^+$): m/z 256.1063 $[C_{26}H_{32}N_8Fe]^{2+}$, calcd. $[M - 2CH_3CN - 2Br]^{2+}$ 256.1044. Infrared analysis (FT-IR, cm^{-1}) 3369, 3066, 2919, 1621, 1570, 1418, 1390.

Synthesis of *bis*[1,1'-(*bis*(methylene)-2,6-pyridyl)-3,3'-methyldiimidazole-2-ylidene]iron(II) dihexafluorophosphate (3.8). Ligand precursor **P3.8** was reacted according to the general procedure, affording the initial $[Fe(NHC)_2(CH_3CN)_3]2PF_6$ complex (**M3.8**) as a light red powder, which quickly decomposes to a dark red oil upon desolvation/vacuum (though remains stable under a blanket of Et_2O solvent). Initial mass yield (based on solvent subtraction): 0.67 g, 0.91 mmol, 91 %. HR-MS (ESI$^+$): m/z 295.1167 $[C_{30}H_{34}N_{10}Fe]^{2+}$, calcd. $[M - 3CH_3CN - 2PF_6]^{2+}$ 295.1153. At this stage, single crystals of **M3.8** (suitable for X-ray crystallographic analysis) may be isolated by slow diffusion of Et_2O vapours into a concentrated MeCN solution of the complex. However, crystal desolvation or vacuum-drying the original material leads to rapid sample decomposition, which was confirmed by a number of free ligand signals in the ^1H and $^{13}C\{^1H\}$ NMR spectra. Following electrochemical formation, **M3.8** was therefore immediately re-dissolved in anhydrous/degassed pyridine (2 mL) and stirred at room temperature for 15 minutes. Excess pyridine/MeCN were removed *in vacuo* and the resulting residue washed with a small quantity of dichloromethane (2×5 mL), furnishing a dark red solid. Recrystallisation of the solid from MeCN/Et_2O delivered the corresponding $[Fe(NHC)_4]2PF_6$ complex (**3.8**) as a vacuum-stable red powder. Single crystals of **3.8** (suitable for X-ray crystallographic analysis) were isolated by slow diffusion of Et_2O vapours into a concentrated MeCN solution of the complex at room temperature. Yield: 0.30 g, 0.34 mmol, 34 %. ^1H NMR (400 MHz, CD$_3$CN) δ (ppm) 7.64 (t, $J = 7.6$ Hz, 2H, p-py$H$), 7.40 (d, $J = 1.2$ Hz, 4H, im$H$), 7.27 (d, $J = 7.6$ Hz, 4H, m-py$H$), 7.07 (d, $J = 1.2$ Hz, 4H, im$H$), 5.17 (d, $J = 15.9$ Hz, 4H, diastereo. CH_2), 3.97 (d, $J = 15.9$ Hz, 4H, diastereo. CH_2), 1.85 (s, 12H, (CH_3)$_4$). $^{13}C\{^1H\}$ NMR (100 MHz, CD$_3$CN) δ (ppm) 200.8, 162.8, 137.2, 125.8, 125.5, 123.5, 55.3, 34.7. HR-MS (ESI$^+$): m/z 295.1194 $[C_{30}H_{34}N_{10}Fe]^{2+}$, calcd. $[M - 2PF_6]^{2+}$ 295.1153.

Synthesis of *bis*[1,1'-(*bis*(methylene)-2,6-pyridyl)-3,3'-allyldiimidazole-2-ylidene]iron(II) dihexafluorophosphate (3.9). Ligand precursor **P3.9** was reacted according to the general procedure, affording the [Fe(NHC)$_4$]2PF$_6$ complex as a red oil which solidifies upon standing in Et$_2$O solvent. Single crystals of **3.9** (suitable for X-ray crystallographic analysis) were isolated by slow diffusion of Et$_2$O vapours into a concentrated THF solution of the complex at room temperature. Yield: 0.38 g, 0.39 mmol, 39 %.^{1}H NMR (300 MHz, CD$_3$CN) δ (ppm) 7.67 (t, J = 7.5 Hz, 2H, *p*-py*H*), 7.50 (d, J = 1.8 Hz, 4H, im*H*), 7.33 (d, J = 7.5 Hz, 4H, *m*-py*H*), 7.18 (d, J = 1.8 Hz, 4H, im*H*), 5.47 (m, 4H, alkenyl *H*), 5.25 (d, J = 15.9 Hz, 4H, diastereo. C*H*$_2$), 5.16 (m, 4H, alkenyl *H*), 4.99 (m, 4H, alkenyl *H*), 2.89 (m, 8H, alkenyl *H*). Anal. calcd. (%) for C$_{38}$H$_{42}$N$_{10}$P$_2$F$_{12}$Fe.CH$_3$CN: C 46.84, H 4.42, N 15.02; found C 46.61, H 3.82, N 15.21.

Synthesis of *bis*[1,1'-(2,6-pyridyl)-3,3'-allyldiimidazole-2-ylidene]iron(II) dibromide (3.9.1). Ligand precursor **P3.9.1** was reacted according to the general procedure, affording the [Fe(NHC)$_4$]2Br complex as an air- and moisture-stable orange powder. The orange solid was further purified by suspending in hot chloroform, followed by hot filtration. Single crystals of **3.9.1** (suitable for X-ray crystallographic analysis) were isolated by slow diffusion of Et$_2$O vapours into a concentrated THF solution of the complex at room temperature. Yield: 0.30 g, 0.37 mmol, 37 %. ^{1}H NMR (500 MHz, CD$_3$CN) δ (ppm) 8.21 (t, J = 8.1 Hz, 2H, *p*-py*H*), 8.10 (d, J = 2.2 Hz, 4H, im*H*), 7.80 (d, J = 8.1 Hz, 4H, *m*-py*H*), 7.04 (d, J = 2.2 Hz, 4H, im*H*), 5.18 (ddt, J = 17.6, 10.7, 4.3 Hz, 4H, C*H*=CH$_2$), 4.70 (dt, J = 4.3, 1.5 Hz, 4H, CH=C*H*$_{cis}$), 4.07 (dtd, J = 17.6, 1.5, 0.7 Hz, 4H, CH=C*H*$_{trans}$), 3.33 (dt, J = 4.3, 1.5 Hz, 8H, NC*H*$_2$). ^{13}C{^{1}H} NMR (125 MHz, CD$_3$CN) δ (ppm) 201.1, 155.1, 139.8, 133.3, 126.9, 118.4, 115.7, 106.9, 51.4. HR-MS (ESI$^+$): *m/z* 319.1186 [C$_{34}$H$_{34}$N$_{10}$Fe]$^{2+}$, calcd. [M − 2Br]$^{2+}$ 319.1153. Anal. calcd. (%) for C$_{34}$H$_{34}$N$_{10}$Br$_2$Fe.1^1/$_4$CHCl$_3$: C 44.68, H 3.75, N 14.78; found C 44.74, H 3.57, N 14.96.

Synthesis of *bis*[1,1'-(*bis*(methylene)-2,6-pyridyl)-3,3'-(2-methoxyphenyl)diimidazol-2-ylidene]iron(II) dihexafluorophosphate (3.10). Ligand precursor **P3.10** was reacted according to the general procedure, affording the [Fe(NHC)$_4$]2PF$_6$ complex as an air- and moisture-stable light orange powder. Single crystals of **3.10** (suitable for X-ray crystallographic analysis) were isolated by slow diffusion of Et$_2$O vapours into a concentrated THF solution of the complex at room temperature. Yield: 0.37 g, 0.46 mmol, 46 %. ^{1}H NMR (500 MHz, CD$_3$CN) δ (ppm) 7.90 (d, J = 1.9 Hz, 1H, im*H*), 7.85 (t, J = 7.7 Hz, 1H, *p*-py*H*), 7.76 (d, J = 7.7 Hz, 1H, *m*-py*H*), 7.68 (br s, 1H, *m*-py*H*), 7.56 − 7.46 (m, 5H, 3ar*H* and 2im*H*), 7.42 (d, J = 7.7 Hz, 1H, *m*-py*H*), 7.33 − 7.27 (m, 5H, 3ar*H* and 2 im*H*), 7.19 (m containing d, J = 7.7 Hz, 2H, *m*-py*H* and im*H*), 7.09 (d, J = 1.9 Hz, 2H, im*H*), 7.03 (t, J = 7.7 Hz, 1H, *p*-py*H*), 6.96 (t, J = 7.5 Hz, 1H, ar*H*), 6.93 (td, J = 7.5, 1.1 Hz, 2H, ar*H*), 6.65 (br s, 1H, ar*H*), 6.42 (d, J = 7.5 Hz, 2H, ar*H*), 6.37 (td, J = 7.5, 1.1 Hz, 2H, ar*H*), 6.30 (d, J = 7.6 Hz, 2H, C*H*$_2$), 5.46 (m, 2H, C*H*$_2$), 5.30 (dd, J = 7.5, 1.1 Hz, 2H, ar*H*), 4.77 (d, J = 16.4 Hz, 2H, C*H*$_2$), 4.37 (d, J = 16.4 Hz, 2H, C*H*$_2$), 3.79 (s, 3H, OC*H*$_3$),

3.72 (s, 3H, OCH_3), 3.54 (s, 6H, OCH_3). ^{13}C{^{1}H} NMR (125 MHz, CD$_3$CN) δ (ppm) 200.8, 160.5, 153.8, 136.5, 130.4, 129.0, 128.5, 127.4, 123.6, 123.5, 120.1, 113.0, 55.5, 55.1. HR-MS (ESI$^+$): *m/z* 1103.3008 [C$_{54}$H$_{50}$N$_{10}$FeO$_4$F$_6$P]$^+$, calcd. [M − PF$_6$]$^+$ 1103.3002.

Synthesis of [1,1'-(*bis*(methylene)-2,6-pyridyl)-3,3'-(2-methpyridyl)diimidazol-2-ylidene]iron(II) dihexafluorophosphate (3.11). Ligand precursor **P3.11** was reacted according to the general procedure, affording the [Fe$_2$(NHC)$_4$(CH$_3$CN)$_4$]4PF$_6$ complex as an air- and moisture-stable dark red powder, which decomposes to free ligand in hydrous solvent over a period of 4 weeks. Single crystals of **3.11** (suitable for X-ray crystallographic analysis) were isolated by slow diffusion of Et$_2$O vapours into a concentrated MeCN solution of the complex at room temperature. Yield: 0.73 g, 0.42 mmol, 83 %. ^{1}H NMR (500 MHz, CD$_3$CN) δ (ppm) 9.40 (d, *J* = 6.5 Hz, 1H, py*H*), 8.11 (t, *J* = 6.5 Hz, 1H, py*H*), 7.93 − 7.89 (m, 2H, im*H* and py*H*), 7.74 − 7.63 (m, 3H, py*H*), 7.54 − 7.51 (m, 2H, py*H*), 7.25 (d, *J* = 9.5 Hz, 1H, py*H*), 7.15 (s, 1H, im*H*), 7.01 (t, *J* = 9.0 Hz, 1H, py*H*), 6.97 (s, 1H, im*H*), 6.83 (d, *J* = 9.5 Hz, 1H, py*H*), 6.63 (s, 1H, im*H*), 6.31 (d, *J* = 20.5 Hz, 1H, diastereo. C*H$_2$*), 6.06 (d, *J* = 23.5 Hz, 1H, diastereo. C*H$_2$*), 5.43 (d, *J* = 20.5 Hz, 1H, diastereo. C*H$_2$*), 5.30 (d, *J* = 20.5 Hz, 1H, diastereo. C*H$_2$*), 5.08 (d, *J* = 23.5 Hz, 1H, diastereo. C*H$_2$*), 4.91 (d, *J* = 20.0 Hz, 1H, diastereo. C*H$_2$*), 4.34 (d, *J* = 20.0 Hz, 1H, diastereo. C*H$_2$*), 3.62 (d, *J* = 20.5 Hz, 1H, diastereo. C*H$_2$*). ^{13}C{^{1}H} NMR (125 MHz, CD$_3$CN) δ (ppm) 194.6, 193.4, 160.9, 159.8, 158.6, 157.8, 157.6, 139.7, 138.8, 138.7, 136.4, 131.9, 126.8, 126.6, 126.3, 126.0, 125.5, 125.1, 124.9, 124.6, 122.8, 55.6, 55.3, 54.9, 54.4. HR-MS (ESI$^+$): *m/z* 238.5702 [C$_{25}$H$_{23}$N$_7$Fe]$^{2+}$, calcd. [M − 2MeCN − 2PF$_6$]$^+$ 238.5677.
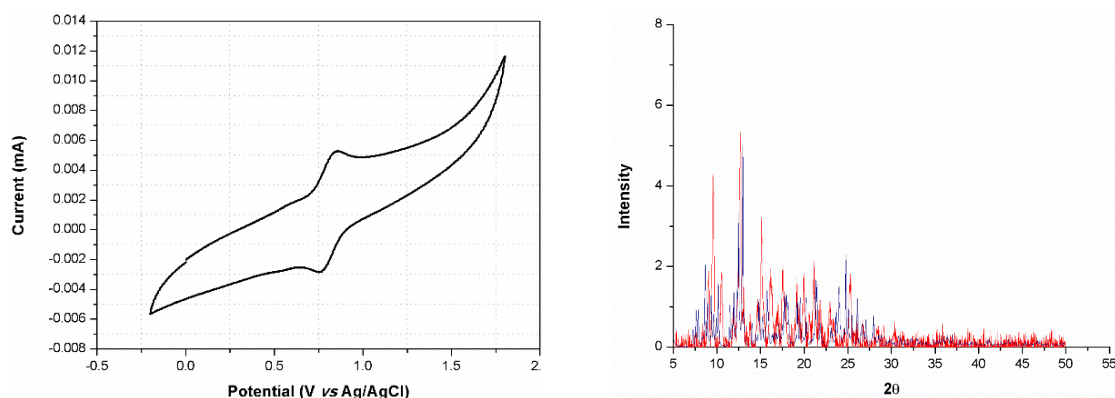
Figure 3.33 *Left: cyclic voltammogram (anodic portion) of **3.11**, illustrating a reversible Fe$^{II/III}$ redox couple in MeCN solvent (E$_{1/2}$ = +0.80 V). Conditions: [Fe] = 1.0 mM, media = (MeCN/[^{n}Bu$_4$N]PF$_6$ 0.10 M), scan rate (v) = 100 mVs^{-1}, T = 298K. Right: superimposed SCXRD (red) versus PXRD (blue) patterns of **3.11**.*

3.9 Bibliography

1. K. Öfele, C. G. Kreiter, *Chem. Ber.* **1972**, *105*, 529–540.

2. (a) M. F. Lappert, P. L. Pye, *J. Chem. Soc. Dalton Trans.* **1977**, 2160–2172; (b) L. Bourget-Merie, M. F. Lappert, J. R. Severn, *Chem. Rev.* **2002**, *102*, 3031–3066; (c) J. Arnold, P. J. Brothers, P. Mountford, W. E. Piers, C. M. Thomas, T. D. Tilley, *Dalton Trans.* **2014**, *43*, 16553–16556; (d) D. J. Cardin, B. Cetinkaya, M. J. Doyle, M. F. Lappert, *Chem. Soc. Rev.* **1973**, *2*, 99–144.

3. M. J. Ingleson, R. A. Layfield, *Chem. Commun.* **2012**, *48*, 3579–3589.

4. (a) U. Kernbach, M. Ramm, P. Luger, W. P. Fehlhammer, *Angew. Chem. Int. Ed. Engl.* **1996**, *35*, 310–312; (b) U. Plaia, H. Stolzenberg, W. P. Fehlhammer, *J. Am. Chem. Soc.* **1985**, *107*, 2171–2172.

5. K. Riener, S. Haslinger, A. Raba, M. P. Högerl, M. Cokoja, W. A. Herrmann, F. E. Kühn, *Chem. Rev.* **2014**, *114*, 5215–5272.

6. I. Nieto, F. Cervantes-Lee, J. M. Smith, *Chem. Commun.* **2005**, *125*, 3811–3813.

7. B. Liu, Y. Zhang, D. Xu, W. Chen, *Chem. Commun.* **2011**, *47*, 2883–2885.

8. A. A. Danopoulos, K. Y. Monakhov, P. Braunstein, *Chem. Eur. J.* **2013**, *19*, 450–455.

9. (a) A. A. Danopoulos, N. Tsoureas, J. A. Wright, M. E. Light, *Organometallics* **2004**, *23*, 166–168; (b) S. A. Sulway, D. Collison, J. J. W. McDouall, F. Tuna, R. A. Layfield, *Inorg. Chem.* **2011**, *50*, 2521–2526.

10. R. A. Andersen, K. Faegri, J. C. Green, A. Haaland, M. F. Lappert, W. P. Leung, K. Rypdal, *Inorg. Chem.* **1988**, *27*, 1782–1786.

11. R. A. Layfield, J. J. W. McDouall, M. Scheer, C. Schwarzmaier, F. Tuna, *Chem. Commun.* **2011**, *47*, 10623–10625.

12. (a) B. M. Day, T. Pugh, D. Hendriks, C. F. Guerra, D. J. Evans, F. M. Bickelhaupt, R. A. Layfield, *J. Am. Chem. Soc.* **2013**, *135*, 13338–13341. For an example at cobalt, see: (b) B. M. Day, K. Pal, T. Pugh, J. Tuck, R. A. Layfield, *Inorg. Chem.* **2014**, *53*, 10578–10584.

13. B. Liu, Q. Xia, W. Chen, *Angew. Chem. Int. Ed.* **2009**, *48*, 5513–5516.

14. B. R. M. Lake, C. E. Willans, *Organometallics* **2014**, *33*, 2027–2038.

15. K. Riener, M. J. Bitzer, A. Pöthig, A. Raba, M. Cokoja, W. A. Herrmann, F. E. Kühn, *Inorg. Chem.* **2014**, 1524–1532.

16. B. R. M. Lake, A. Ariafard, C. E. Willans, *Chem. Eur. J.* **2014**, 12729–12733.

17. (a) G. Olivo, M. Nardi, D. Vìdal, A. Barbieri, A. Lapi, L. Gómez, O. Lanzalunga, M. Costas, S. Di Stefano, *Inorg. Chem.* **2015**, *54*, 10141–10152; (b) J. Xiang, H. Li, J.-S. Wu, *Z. Anorg. Allg. Chem.* **2014**, *640*, 1670–1674.

18. (a) L. Gómez, I. Garcia-Bosch, A. Company, J. Benet-Buchholz, A. Polo, X. Sala, X. Ribas, M. Costas, *Angew. Chem. Int. Ed. Engl.* **2009**, *48*, 5720–5723; (b) S. Chakraborty, P. Bhattacharya, H. Dai, H. Guan, *Acc. Chem. Res.* **2015**, *48*, 1995–2003.

19. X. Wang, S. Wang, L. Li, E. B. Sundberg, G. P. Gacho, *Inorg. Chem.* **2003**, *42*, 7799–7808.

20. (a) M. S. Chen, M. C. White, *Science* **2007**, *318*, 783–787; (b) T. J. Osberger, D. C. Rogness, J. T. Kohrt, A. F. Stepan, M. C. White, *Nature* **2016**, *537*, 214–219; (c) J. M. Howell, K. Feng, J. R. Clark, L. J. Trzepkowski, M. C. White, *J. Am. Chem. Soc.* **2015**, *137*, 14590–14593.

21. A. Raba, M. Cokoja, S. Ewald, K. Riener, E. Herdtweck, A. Pöthig, W. A. Herrmann, F. E. Kühn, *Organometallics* **2012**, *31*, 2793–2800.

22. B. R. M. Lake, C. E. Willans, *Chem. Eur. J.* **2013**, *19*, 16780–16790.

23. D. Pugh, A. A. Danopoulos, *Coord. Chem. Rev.* **2007**, *251*, 610–641.

24. M. Poyatos, J. A. Mata, E. Peris, *Chem. Rev.* **2009**, *109*, 3677–3707.

25. E. Peris, R. H. Crabtree, *Coord. Chem. Rev.* **2004**, *248*, 2239–2246.

26. D. Pugh, A. Boyle, A. A. Danopoulos, *Dalton Trans.* **2008**, *41*, 1087–1094.

27. D. S. McGuinness, V. C. Gibson, J. W. Steed, *Organometallics* **2004**, *23*, 6288–6292.

28. R. P. Yu, J. M. Darmon, J. M. Hoyt, G. W. Margulieux, Z. R. Turner, P. J. Chirik, *ACS Catal.* **2012**, *2*, 1760–1764.

29. R. Pony Yu, D. Hesk, N. Rivera, I. Pelczer, P. J. Chirik, *Nature* **2016**, *529*, 195–199.

30. T. C. B. Harlang, Y. Liu, O. Gordivska, L. A. Fredin, C. S. Ponseca, P. Huang, P. Chábera, K. S. Kjaer, H. Mateos, J. Uhlig, R. Lomoth, R. Wallenberg, S. Styring, P. Persson, V. Sundström, K. Wärnmark, *Nat. Chem.* **2015**, *7*, 883–889.

31. I. Klawitter, M. R. Anneser, S. Dechert, S. Meyer, S. Demeshko, S. Haslinger, A. Pöthig, F. E. Kühn, F. Meyer, *Organometallics* **2015**, *34*, 2819–2825.

32. D. T. Weiss, M. R. Anneser, S. Haslinger, A. Pöthig, M. Cokoja, J.-M. Basset, F. E. Kühn, *Organometallics* **2015**, *34*, 5155–5166.

33. N. Hazari, *Chem. Soc. Rev.* **2010**, *39*, 4044–4056.

34. J. Vaughan, D. J. Carter, A. L. Rohl, M. I. Ogden, B. W. Skelton, P. V Simpson, D. H. Brown, *Dalton Trans.* **2016**, *45*, 1484–1495.

35. Q. Teng, H. V. Huynh, *Chem. Commun.* **2014**, *50*, 971–974.

36. D. T. Weiss, M. R. Anneser, S. Haslinger, A. Pöthig, M. Cokoja, J.-M. Basset, F. E. Kühn, *Organometallics* **2015**, *34*, 5155–5166.

37. D. T. Weiss, P. J. Altmann, S. Haslinger, C. Jandl, A. Pöthig, M. Cokoja, F. E. Kühn, *Dalton Trans.* **2015**, *44*, 18329–18339.

38. I. Klawitter, M. R. Anneser, S. Dechert, S. Meyer, S. Demeshko, S. Haslinger, A. Pöthig, F. E. Kühn, F. Meyer, *Organometallics* **2015**, *34*, 2819–2825.

39. A. Raba, M. Cokoja, W. A. Herrmann, F. E. Kühn, *Chem. Commun.* **2014**, *50*, 11454–11457.

40. J. Rieb, A. Raba, S. Haslinger, M. Kaspar, A. Pöthig, M. Cokoja, J.-M. Basset, F. E. Kühn, *Inorg. Chem.* **2014**, *53*, 11447–11456.

41. C. J. Legacy, A. Wang, B. J. O'Day, M. H. Emmert, *Angew. Chem. Int. Ed. Engl.* **2015**, *54*, 14907–14910.

42. A. C. Lindhorst, S. Haslinger, F. E. Kühn, *Chem. Commun.* **2015**, *51*, 17193–17212.

43. M. Oszajca, A. Franke, M. Brindell, G. Stochel, R. van Eldik, *Coord. Chem. Rev.* **2016**, *306*, 483–509.

44. L. Gómez, I. Garcia-Bosch, A. Company, J. Benet-Buchholz, A. Polo, X. Sala, X. Ribas, M. Costas, *Angew. Chem. Int. Ed.* **2009**, *48*, 5720–5723.

45. M. R. Chapman, B. R. M. Lake, C. M. Pask, B. N. Nguyen, C. E. Willans, *Dalton Trans.* **2015**, *44*, 15938–15948.

46. B. J. Truscott, R. Klein, P. T. Kaye, *Tetrahedron Lett.* **2010**, *51*, 5041–5043.

47. M. Peters, R. Breinbauer, *Tetrahedron Lett.* **2010**, *51*, 6622–6625.

48. W. Chen, Y. Zhang, L. Zhu, J. Lan, R. Xie, J. You, *J. Am. Chem. Soc.* **2007**, *129*, 13879–13886.

49. Z. Xi, X. Zhang, W. Chen, S. Fu, D. Wang, *Organometallics* **2007**, *26*, 6636–6642.

50. F. Xue, J. Fang, S. L. Delker, H. Li, P. Martásek, L. J. Roman, T. L. Poulos, R. B. Silverman, *J. Med. Chem.* **2011**, *54*, 2039–2048.

51. H. Puschmann, O. V. Dolomanov, L. J. Bourhis, R. J. Gildea, J. A. K. Howard, *J. Appl. Crystallogr.* **2009**, *42*, 339–341.

52. D. S. McGuinness, K. J. Cavell, *Organometallics* **2000**, *19*, 741–748.

Chapter 4

A synthetically versatile electrochemical approach towards imine- and amine-*bis*(phenolate) base metal complexes

4.1   Introduction

Over 150 years ago, Hugo Schiff reported the condensation between an aldehyde and an amine to produce an "intensely coloured" compound, now commonly referred to as a Schiff base.[1] These compounds are able to coordinate metals through their imine nitrogen atoms along with another group, which is typically linked to the original aldehyde unit. Owed to their simple synthesis and modification, Schiff bases are considered 'privileged ligands' and can be readily adjusted to comprise stereogenic centres or other elements of chirality (*e.g.* planes and axes). These properties have led Schiff base ligands to the forefront of the most widely studied chelators in inorganic chemistry to date.[2–5]

Perhaps the most popular class of Schiff base ligand are formed from reaction of two equivalents of salicylaldehyde with a 1,2-diamine.[6] These so-called 'salen' ligands are [*O,N,N,O*] tetradentate *bis*-Schiff base ligands, and are able to provide four coordination sites to a metal centre whilst leaving two axial sites open to ancillary donors – very much resembling porphyrins,[7] though are often more easily prepared. In fact, landmark research by Hoveyda and Snapper has even allowed inclusion of common amino acids and peptides into this strategy, assembling salen-type ligand scaffolds from environmentally benign, inexpensive building blocks which are commercially available in optically pure form.[8]

In particular, salen-type ligands have been shown to coordinate to and stabilise a broad scope of metals occupying various oxidation states. On these grounds, metal-salen complexes have been applied broadly as catalysts and small-molecule carriers (**Figure 4.1**), alongside showing desirable properties in biomedicine and materials chemistry.[9–13]
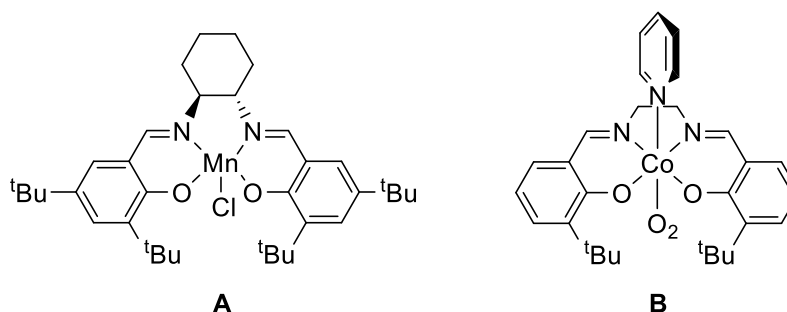
Figure 4.1 *Highly reactive Schiff base ligated metal complexes.* ***A:*** *Jacobsen's asymmetric manganese epoxidation catalyst.*[14,15] ***B:*** *Cobalt salcomine-derived dioxygen transporter, prepared by Schaefer.*[16]

4.1.1　Schiff base complexation

Synthetic methods to prepare Schiff base complexes are relatively diverse, and were succinctly organised into a concise review article by Cozzi in 2004.[2] Since this report there appear to have been no attempts to improve the synthesis of these compounds, and the summary presented by Cozzi remains accurate. In the context of catalysis, a common approach to deploy a metal-salen complex into reaction media is to generate the active species *in situ* from its constituent neutral ligand (*i.e.* H$_2$L) and an appropriate, well-defined metal source. Essentially, there are five widely adopted synthetic strategies to achieve this, which are summarised within **Scheme 4.1**.

Where Y = H
1. M(OR)$_n$
2. M(NR$_2$)$_n$
3. MR$_n$*
4. M(OAc)$_2$

Where Y = Na, K
5. MX$_n$**
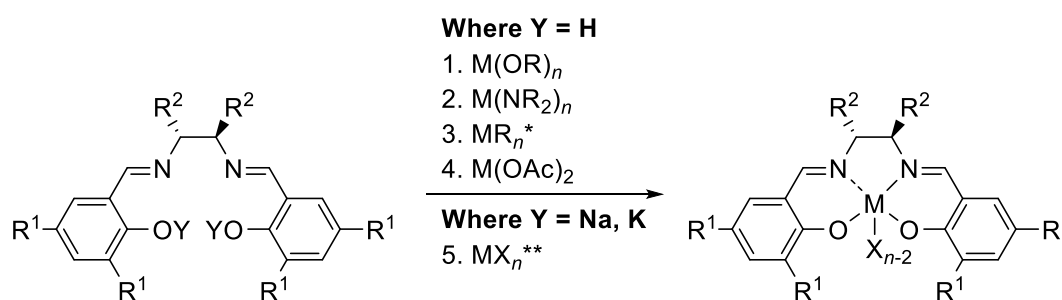
Scheme 4.1 Summarisation of the five common routes to prepare Schiff base complexes.
*R = alkyl, aryl, **X = Cl, Br.

Route 1 involves treatment of phenolic ligand precursor with a metal alkoxide (M(OR)$_n$). For early transition-metals, (*e.g.* Ti and Zr), their alkoxide derivatives are commercially available and relatively robust, however for the majority of metal alkoxides this is not the case. In addition to their sensitivity towards water, reaction of a Schiff base with a metal alkoxide leads to an equilibrium mixture, for which the 'true identity' of the major product is difficult to predict.

Similarly useful approaches to isolate these complexes are outlined within routes 2 and 3. Route 2 involves employment of a basic metal amide precursor (M(NR$_2$)$_n$), to eliminate the phenolic proton of the Schiff base ligand and generate volatile NHR$_2$, which subsequently drives the formation of the desired complex and can be removed *in vacuo*. Route 3 represents a complementary method, using metal alkyl precursors (MR$_n$) to perform a direct exchange reaction with a Schiff base to afford the corresponding complex.

Whilst suitable in their own right, routes 1 − 3 tend to produce complexes which are sensitive to low traces of water and often continue to form stable μ-oxo bridged species by reaction with moisture.[17–19] Where generation of the Schiff base complex is performed *in situ* (with respect to catalysis), the presence of water can be especially difficult to control and the persistence of μ-oxo complexes often leads to unreliable results.

Arguably the most widely adopted methods of synthesising Schiff base complexes, and in particular metal-salen complexes, are illustrated in routes 4 and 5. As shown in the former, treatment of a Schiff base precursor with an appropriate metal acetate ($M(OAc)_2$) at high temperature (typically solvent reflux temperature) provides access to their metal-coordinated complexes (*e.g.* M = Fe, Co, Ni, Cu).[20] Despite representing an operationally practical route, findings within our laboratory have shown, in certain cases, that this method does not guarantee full control over the metal oxidation state/coordination sphere of the final product, and will be discussed within this chapter.

As shown in route 5, using a deprotonated version of the Schiff base ligand, it is possible to bring about a direct exchange reaction with a suitable metal halide (MX_n). Deprotonation of the relatively acidic phenolic hydrogen atoms ($pK_a \approx 10$) may be realised using lithium bases, such as ^{n}BuLi or MeLi, though alkyl lithium reagents are known to attack imine groups and may lead to undesired side-products. Instead, it is typical to employ an excess of NaH or KH for proton abstraction, followed by addition of the soluble $Na_2/K_2(L)$ species to a tetrahydrofuranyl adduct of the metal halide ($ZrCl_4(THF)_2$ or $VCl_3(THF)_3$, for example).

Chapters 2 and 3 of this thesis are concerned with an electrochemical procedure for the synthesis of metal *N*-heterocyclic carbene (NHC) complexes. The route was found to be simple, efficient and versatile, and obviates the use of high temperatures or basic reaction conditions. Underpinning the reaction, an imidazolium ion (HL) is reduced at a cathodic metal surface, releasing hydrogen gas to produce a free carbene (L). Concomitantly, a 'sacrificial anode' is oxidised to liberate its own metal ions into solution – effectively dissolving the metal surface. These two electrogenerated species are able to combine, affording the desired metal-NHC complex with high atom economy. To complement these findings and extend the current state-of-the-art,[21–26] it was envisaged that a variety of 'HL-type' ligand precursors of appropriate reduction potential could be employed with a range of metals to electrochemically derive organometallic complexes in the same efficient manner, as shown in **Scheme 4.2**.

$$\textbf{a)} \quad H_nL \xrightarrow[-\,^n/_2\,H_2]{ne^-} L^{n-}$$

$$\xrightarrow{\textbf{c)}} ML$$

$$\textbf{b)} \quad M_{(s)} \xrightarrow{-\,ne^-} M^{n+}_{(sol)}$$
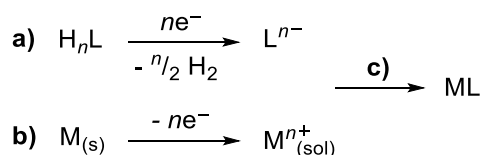
Scheme 4.2 *Electrochemical synthesis of metal-ligand (ML) complexes. Key: **a)** cathodic reduction of HL ligand; **b)** anodic oxidation of metal source, M; **c)** in situ combination of metal ion and ligand to form a complex, ML.*

4.2 Schiff base ligand synthesis

Reliable preparative routes to Schiff base compounds are well established within the literature from the simple condensation of aldehydes and amines, as exemplified in a recent publication by Clegg and Harrington.[27] As such, a library of salen ligand precursors incorporating unsubstituted (**P4.1** and **P4.4**), cyclohexyl (**P4.2** and **P4.5**) and phenylene (**P4.3**) bridged backbones were prepared, alongside an enantiomerically pure (*S,S*)-1,2-diphenyl ethyl bridged analogue (**P4.6**), by reaction of the appropriate 1,2-diamine with two equivalents of suitable aldehyde in refluxing ethanol solvent, as shown in **Scheme 4.3**. For each example, cooling the reaction mixture to 0 °C allowed the product to cleanly precipitate from solution as a brightly coloured, microcrystalline solid which could be collected by filtration, in good to quantitative yield.
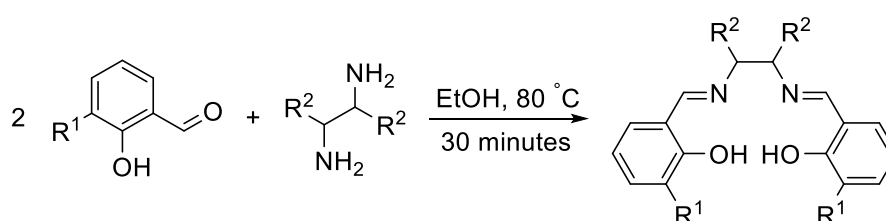
P4.1: $R^1 = R^2 = H$
P4.2: $R^1 = H$, R^2 backbone = cyclohexyl
P4.3: $R^1 = H$, R^2 backbone = phenylene
P4.4: $R^1 = OMe$, $R^2 = H$
P4.5: $R^1 = OMe$, R^2 backbone = cyclohexyl
P4.6: $R^1 = OMe$, R^2 backbone = (*S*)-Ph

Scheme 4.3 One-step synthesis of various salen ligand precursors.

As ligands, nitrogen-saturated aminophenolate versions of salen, often coined 'salan', tend to demonstrate additional flexibility and are able to provide more electron density to a metal centre than their unsaturated counterparts. With this in mind, salan derivatives **P4.7** and **P4.8** were prepared using procedures developed by Whitwood and Willans,[28] condensing *N*-methylethylenediamine with two equivalents of appropriate phenol in the presence of formaldehyde (**Scheme 4.4**).
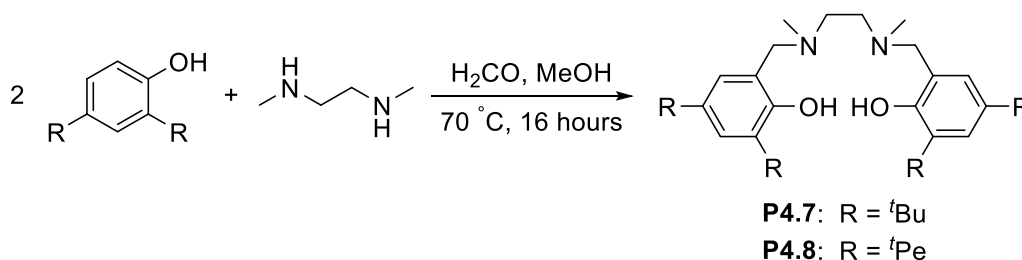
P4.7: R = ^{t}Bu
P4.8: R = ^{t}Pe

Scheme 4.4 One-step synthesis of two salan ligand precursors.

All pro-ligands (**P4.1** – **P4.8**) were fully characterised using multinuclear NMR spectroscopy and high-resolution mass spectrometry. Most notable resonances displayed in the ^{1}H NMR spectra of **P4.1** – **P4.6** include an unambiguous singlet between 8.24 – 8.53 ppm, attributable to each deshielded imine N=C*H* proton. Successful imine formation for these products was further supported by the presence of a diagnostic singlet in their ^{13}C NMR spectra, featured around 160 ppm, which provides good agreement with literature values quoted for a N=*C* nucleus.[27]

4.2.1 Redox behaviour of Schiff base ligand precursors

Phenols are facile one-electron reducing agents that have been involved in electrochemical, photochemical and radiation chemical electron-transfer reactions. The one-electron oxidation of phenolate (PhO$^-$) to produce phenoxyl radicals (PhO$^•$) is well-known, and these intermediates generally decay *via* rapid dimerisation.[29] Though this mechanism is well-understood, the oxidation of phenol involves loss of hydrogen and is therefore pH dependent. Consequently, numerous detailed studies have been performed to measure the redox properties of phenol under aqueous conditions, with reports from Hoffman and Xavier both proving cyclic voltammetry to be a convenient method for this purpose.[30,31]

The non-aqueous redox properties of Schiff base ligands using voltammetric analysis is poorly explored. To this end, Schiff base ligands **P4.1** – **P4.5** were further analysed by cyclic voltammetry, for which each relevant cathodic portion is illustrated in **Figure 4.2**. Each cyclic trace is calibrated with respect to the ferrocene/ferrocenium redox couple as an internal standard, and the observed reduction potential for each precursor is listed in **Table 4.1**.
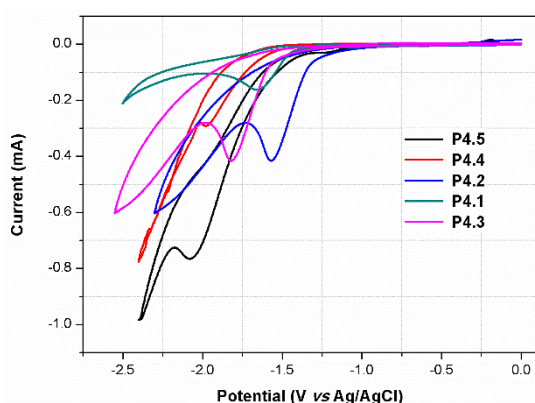
Entry	Ligand precursor	E_{red} *vs* Fc/Fc$^+$ (V)
1	**P4.1**	-2.12
2	**P4.2**	-2.04
3	**P4.3**	-2.13
4	**P4.4**	-2.45
5	**P4.5**	-2.55

Figure 4.2 *Superimposed cyclic voltammogram plots (displaying cathodic region) of salen ligand precursors **P4.1** – **P4.5**, illustrating their respective reduction potentials in MeCN solvent. Conditions: [salen ligand] = [Fc] = 1.0 mM, media = (MeCN/[^{n}Bu$_4$N]BF$_4$ 0.10 M), scan rate (v) = 400 mVs^{-1}, T = 298 K. Right: **Table 4.1**, listing observed reduction potentials of **P4.1** – **P4.5**, as calibrated against Fc/Fc$^+$.*

Cyclic voltammograms of compounds **P4.1** – **P4.5** each feature a broad and relatively short-lived reduction band between -2.0 and -2.6 V (referenced against the Fc/Fc$^+$ half-wave redox couple, which was recorded at +0.48 V under the specified conditions), which is attributable to the reduction of each phenolic proton to produce the corresponding phenolate ion. Expectedly, this cathodic peak shows no reversibility (nor *pseudo*-reversibility) at any scan rate – a feature which is characteristic of an unstable electrogenerated intermediate (for full experimental details, a full-sweep voltammogram of **P4.3** and data extrapolation, see Experimental).

The observed reduction potentials listed in **Table 4.1** align well with those measured for the electrochemical reduction of imidazolium ions, both within the literature and recorded in our laboratory (*i.e.* typical values fall within the range -2.4 to -2.10 V, see Chapter 2).[32] This alignment suggests that our electrochemical synthetic method to produce metal-NHC complexes may be extended towards similar products of phenolic ligand precursors.

4.3   Electrochemical synthesis of copper(II) salen/salan complexes

Cu^I and Cu^{II} complexes comprising salen-type ligands are well-documented within the literature and have been deployed as active catalysts for various bond-forming reactions, such as asymmetric alkylation, ring-opening polymerisation and the Henry reaction.[33–35] Although routes to these complexes have existed for decades, none occur without significant side-product formation, and in some cases require column chromatography to afford pure complex – albeit in low yield.[20]

Importantly, copper(II) salen complexes typically display air- and moisture-stability. Where reduction of an imidazolium ion furnishes a highly reactive free carbene which may be quenched by O$_2$ (*i.e.* imidazolinone formation, Chapter 2),[36] it was postulated that reduction of a neutral phenolic proton would produce a phenoxide intermediate which is not susceptible to the same termination mechanism, and use of aerobic conditions may be tolerated for this chemistry.

Comparing further, solutions of imidazolium salts are good electrical conductors on account of their ionic character, a property which enables high current flow through the system without addition of external electrolyte. However, in our hands it has been found that solutions of neutral salen precursors are weakly conducting, generating current values akin to those registered for solvent background. Consequently, all metal-salen complexes electrochemically prepared herein were done so in the presence of tetrabutylammonium tetrafluoroborate (^{n}Bu$_4$NBF$_4$, 0.6 mM, 3 mol% relative to substrate).

Using a modified procedure to that described by Tuck,[21] a pair of copper electrodes (99.9 % purity) were introduced to a hydrous acetonitrile solution of ligand precursors **P4.1** – **P4.6** in the presence of ^{n}Bu$_4$NBF$_4$ under an atmosphere of air, and a potential range applied across the

solution to maintain a constant current of 50 mA for 90 minutes reaction time (charge-redundancy of 1.4). Pleasingly, under these conditions the corresponding copper(II) complexes precipitated from solution, simplifying their isolation and purification to afford analytically pure copper(II) salen complexes, **4.1 – 4.6**, in good yield (**Scheme 4.5**).

4.1: $R^1 = R^2 = H$, **79 %**
4.2: $R^1 = H$, R^2 backbone = cyclohexyl, **54 %**
4.3: $R^1 = H$, R^2 backbone = phenylene, **81 %**
4.4: $R^1 = OMe$, $R^2 = H$, **86 %**
4.5: $R^1 = OMe$, R^2 backbone = cyclohexyl, **78 %**
4.6: $R^1 = OMe$, R^2 backbone = (*S*)-Ph, **58 %**
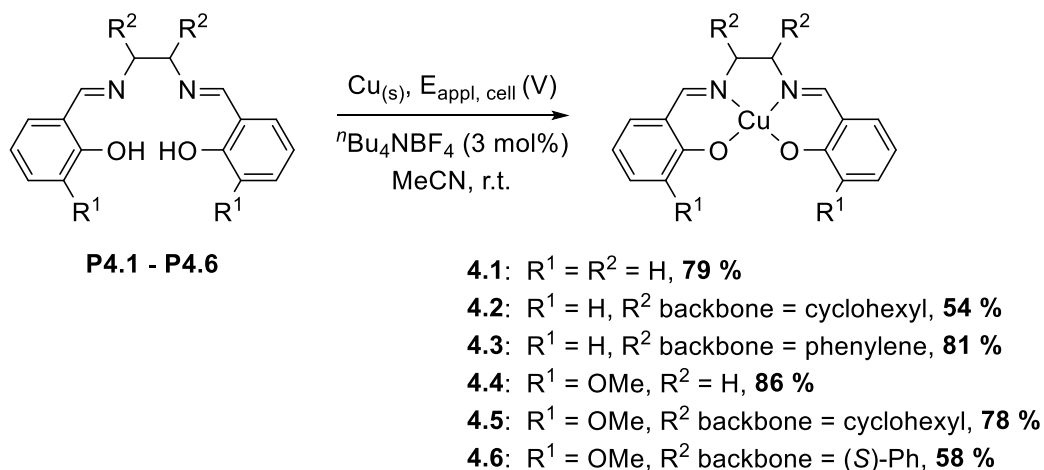
Scheme 4.5 *Electrochemical synthesis of Cu^{II}-salen complexes. Conditions: ligand precursor (1.0 mmol), ^{n}Bu$_4$NBF$_4$ (0.03 mmol), hydrous MeCN (50 mL), applied potential (22 – 25 V, maintaining 50 mA at steady-state), T = 298 K, 90 minutes reaction time. Quoted yield values are isolated.*

On account of their d^9 electronic configuration, NMR spectroscopic analysis presented little structural information for paramagnets, **4.1 – 4.6**. Instead, high-resolution mass spectrometry was employed as the primary tool to probe complex formation, with melting point determination and combustion analysis used to confirm sample purity and composition.

Notable with respect to all complexes, is the characteristic detection of multiple complex mass clusters within each electrospray ionised mass spectrum (positive mode). Each recording suggests that the metal complexes are monomeric in nature, and the metal to ligand ratio is 1:1. An exemplar electrospray mass spectrum of Cu^{II}-salen **4.4** is provided in **Figure 4.3**, highlighting the detection of [ML + H]$^+$, [2ML + H]$^+$ and [3ML + H$_2$O + H]$^+$, at (*m/z*) 390.0647, 781.1211 and 1187.2018, respectively.
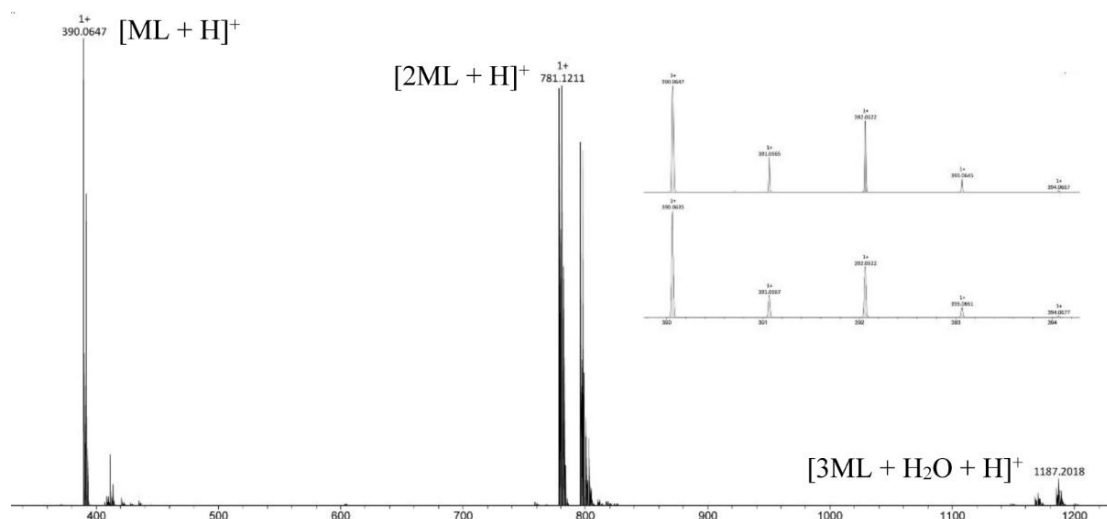
Figure 4.3 *Main image: interpreted electrospray mass spectrum of complex **4.4**, recorded in DCM solvent. Inset image: simulated (bottom) vs observed (top) mass envelope for monomeric [**4.4** + H]$^+$ mass fragment, noting diagnostic isotopic distribution.*

Whilst only colourless (d^{10}) Cu^I species are observed in the electrochemical synthesis of Cu-NHCs,[37] the overall two-electron reduction of salen ligand precursors leads to exclusive production of dark green Cu^{II} complexes. Sousa and co-workers have investigated the electrochemical formation of similar Schiff base ligated Cu^{II} complexes, using an inert Pt cathode with a dissolving Cu plate anode in acetonitrile solvent.[38] The authors found that for their system, the neutral Cu^{II} complexes were formed with an electrochemical efficiency of 1.0 molF^{-1} (E$_F$ = amount of metal dissolved per number of Faradays), which indicates that the anodic oxidation step originally produces a Cu^I compound. To explain the unambiguous observation of a Cu^{II} complex, Sousa proposes that dianionic ligands of this type are themselves capable of further oxidising Cu$^I \rightarrow$ Cu^{II} in solution, as soon as they are formed. The same authors have drawn this conclusion for related electrochemical systems, involving copper metal anodes and 2-pyridylsulfonamide ligand precursors.[39]

Reduction (often hydrogenation) of the salen ligand produces a new tetradentate ligand, termed 'salan'. Such ligands do not possess a C=N double bond, resulting in a more fluid framework around the metal centre which is more resistant to hydrolysis. Several metal-salan complexes have been reported, namely with copper, cobalt, nickel, vanadium and zinc.[40–46] However, common across their syntheses are use of refluxing temperatures and generation of acidic waste-streams, which require further neutralisation to allow the products to precipitate from the reaction mixture. To our knowledge, the electrochemical complexation of these ligands remains untapped.

N-Saturated aminophenolate salan precursors **P4.7** and **P4.8** underwent smooth electrochemical conversion in a similar manner to their unsaturated analogues, using two copper metal plates in hydrous acetonitrile solvent, under an atmosphere of air. Following 90 minutes reaction time, analytically pure copper(II)-salan complexes **4.7** and **4.8** were filtered from solution in 75 and 83 % isolated yield, respectively, following a simple rinse with reaction solvent (**Scheme 4.6**).

P4.7: $R^1 = {}^t$Bu
P4.8: $R^1 = {}^t$Pe

4.7: $R^1 = {}^t$Bu, **75 %**
4.8: $R^1 = {}^t$Pe, **83 %**
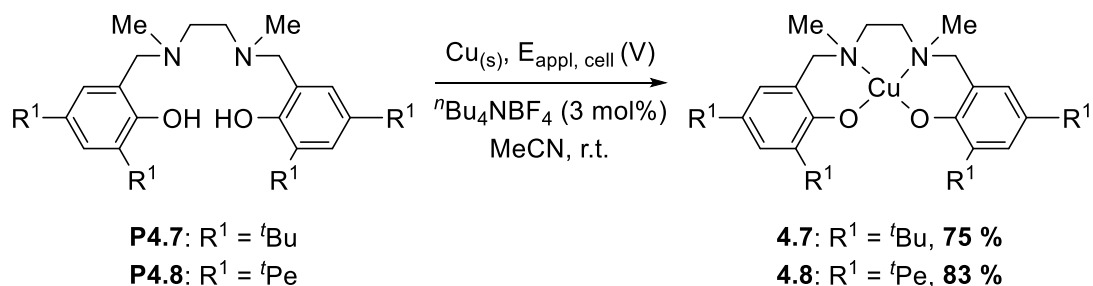
Scheme 4.6 *Electrochemical synthesis of two Cu^{II}-salan complexes. Conditions: ligand precursor (1.0 mmol), $^nBu_4NBF_4$ (0.03 mmol), hydrous MeCN (50 mL), applied potential (22 – 25 V, maintaining 50 mA at steady-state), T = 298 K, 90 minutes reaction time. Quoted yield values are isolated.*

Formation of **4.7** and **4.8** was monitored by high-resolution mass spectrometry, providing mass peaks (*m/z*) 586.3575 and 642.4202 respectively, corroborating with each [M + H]$^+$ mass fragment, and ultimately confirmed by microanalysis. Dark green needles of each complex were obtained from the slow evaporation of DCM solutions of each, and analysed by single crystal diffraction methods. Despite ligand-scrambling observed in solution by mass spectral data, the procured solid-state structures are supportive of [CuL] formation, and are given in **Figure 4.4**. Each C_2 symmetric complex adopts distorted square planar geometry about a copper(II) metal centre. A clear stepped conformation of each ligand around copper is evident, which is pronounced by the low rigidity of the aminophenolate ligand.
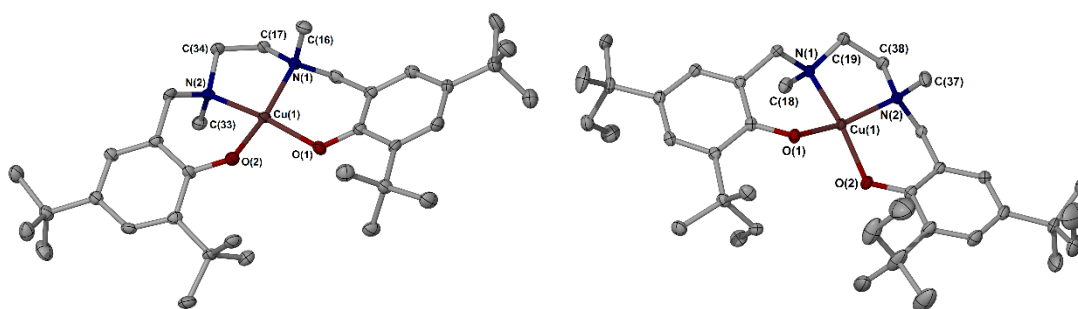
Figure 4.4 *Left: molecular structure of **4.7**. Right: molecular structure of **4.8**. Atomic displacement parameters are drawn at the 50 % probability level, hydrogen atoms are omitted for clarity.*

4.7	Cu(1)-N(1)	2.045(2)	N(1)-Cu(1)-N(2)	86.03(9)
4.7	Cu(1)-N(2)	2.031(2)	N(2)-Cu(1)-O(2)	93.38(9)
4.7	Cu(1)-O(1)	2.109(6)	O(1)-Cu(1)-O(2)	94.41(8)
4.7	Cu(1)-O(2)	1.9047(19)	N(2)-Cu(1)-O(1)	158.64(9)
4.8	Cu(1)-N(1)	2.037(3)	N(1)-Cu(1)-N(2)	86.45(14)
4.8	Cu(1)-N(2)	2.024(3)	N(2)-Cu(1)-O(2)	92.68(14)
4.8	Cu(1)-O(1)	1.898(3)	O(1)-Cu(1)-O(2)	91.88(13)
4.8	Cu(1)-O(2)	1.895(3)	N(2)-Cu(1)-O(1)	163.04(16)

Table 4.2 *Selected bond lengths (Å) and angles (˚) from the crystal structures of* **4.7** *and* **4.8**.

4.4 Electrochemical synthesis of nickel(II) salen complexes

Although group 10 complexes of salen have found relatively little use in catalysis when compared with their direct neighbours, nickel(II)-salen complexes have been identified as active catalysts for O_2 activation, olefin epoxidation and vinylic polymerisation reactions.[47–49] Sousa and Real have previously reported the electrochemical synthesis of a dinuclear nickel(II) complex of a tripodal *bis*(phenolato) ligand (H_2L), using a Pt wire cathode and a Ni plate dissolving anode.[38] Using electrode weight following the reaction, the authors found that the complex forms with an electrochemical efficiency of 0.50 $molF^{-1}$, compatible with the following reaction scheme (**Scheme 4.7**).

Cathode: $H_2L + 2e^- \longrightarrow H_2 + L^{2-}$

Anode: $L^{2-} + Ni \longrightarrow NiL + 2e^-$

= H_2L
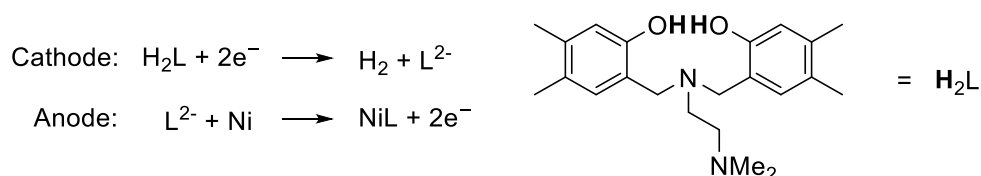
Scheme 4.7 *Half-reactions associated with the electrochemical synthesis of a Ni^{II}-bis(phenolato) complex, described by Sousa.*

Unlike their findings with copper electrodes, Sousa *et al.* suggest that solid nickel is dissolved at an effective rate of 0.50 moles per mole of electrons consumed, or in other words, only nickel(II) species are formed electrochemically. Very similar conclusions were also drawn by Maresca and Zubieta, who synthesised a number of nickel complexes of phosphinothiol ligands under the same electrochemical reaction conditions (E_F = 0.48 $molF^{-1}$), which the authors claim to precipitate from the reaction mixtures as pure, single crystals in high yield.[50]

It was therefore sought to extend our complex scope toward analogous Ni^{II}-salen complexes, *via* the electrochemical reduction of ligand precursors **P4.1 – P4.5**. Using a pair of nickel foil electrodes (99.5 % purity), under reaction conditions akin to those described for the synthesis of Cu^{II}-salen complexes (see above), the corresponding Ni^{II}-salen compounds were produced in high yield (**Scheme 4.8**). It is notable however, that employment of hydrous reaction solvent led to isolation of the crude products as hygroscopic oily solids, which could be further purified by sequential recrystallisation from DCM.
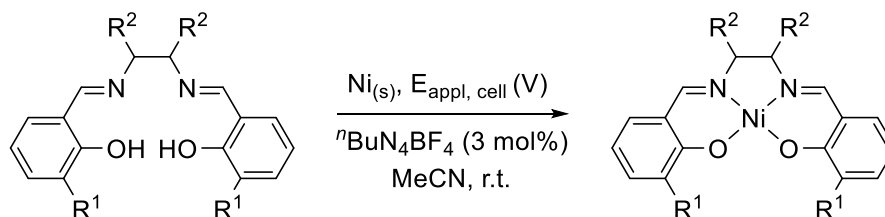
P4.1 - P4.5

4.9: $R^1 = R^2 = H$, **91 %**
4.10: $R^1 = H$, R^2 backbone = cyclohexyl, **84 %**
4.11: $R^1 = H$, R^2 backbone = phenylene, **80 %**
4.12: $R^1 = OMe$, $R^2 = H$, **77 %**
4.13: $R^1 = OMe$, R^2 backbone = cyclohexyl, **88 %**

Scheme 4.8 *Electrochemical synthesis of Ni^{II}-salen complexes. Conditions: ligand precursor (1.0 mmol), $^nBuN_4BF_4$ (0.03 mmol), hydrous MeCN (50 mL), applied potential (22 – 25 V, maintaining 50 mA at steady-state), T = 298 K, 90 minutes reaction time. Quoted yield values are isolated.*

All diamagnetic d^8 nickel(II) complexes (**4.9 – 4.13**) were probed by multinuclear NMR spectroscopy, with each ^1H NMR spectrum featuring complete absence of a phenolic O*H* proton resonance, alongside a diagnostic downfield shift of each coordinated imine NC*H* signal (an example is given in **Figure 4.5**). All NMR spectra presented well-resolved signals, with clear evidence of a C_2-symmetric ligand environment within the metal coordination sphere.
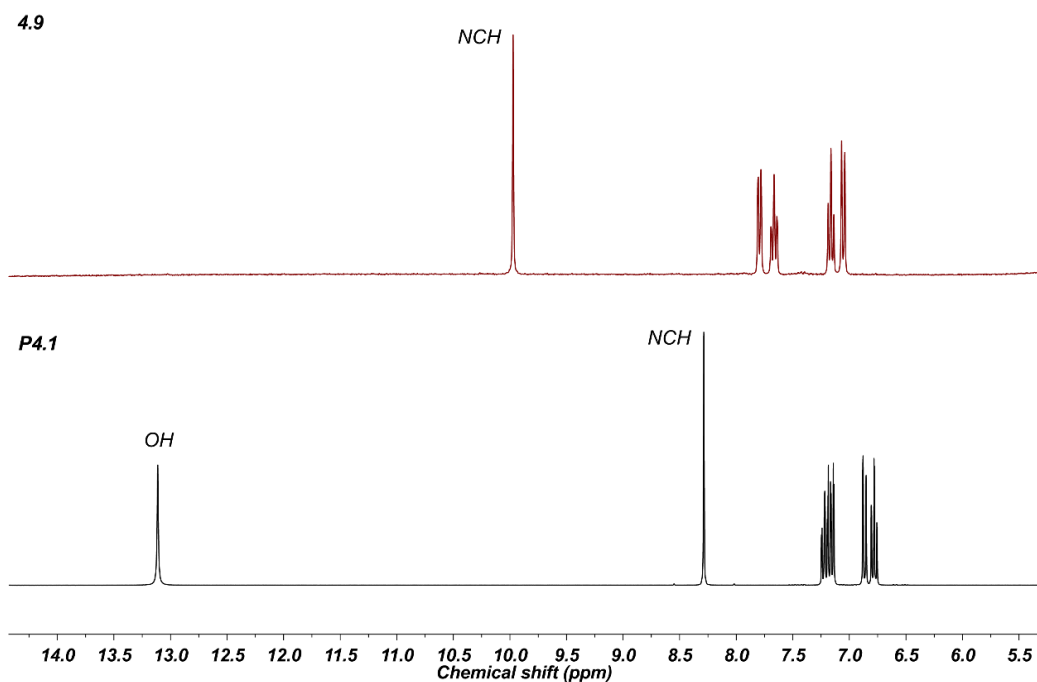
Figure 4.5 *¹H NMR spectrum of authentic ligand precursor **P4.1** (black trace, 300 MHz, CD₃CN, 298K), noting original phenolic singlet at 13.11 ppm. ¹H NMR spectrum of Niᴵᴵ-salen complex **4.9** (red trace, 300 MHz, CD₃CN, 298K).*

When subject to electrospray ionisation mass spectrometry, each nickel(II)-salen complex displayed a similar detection pattern to their copper(II) counterparts. Three distinct mass peaks were typically observed, attributable to each mass collection $[ML + H]^+$, $[2ML + H]^+$ and $[3ML + H]^+$ – all of which are supportive of a binary metal to ligand combination. The full electrospray mass spectrum of complex **4.10** is provided in **Figure 4.6**, demonstrating such a sequence with observed mass clusters at (*m/z*) 379.0940, 757.2212 and 1137.4369.
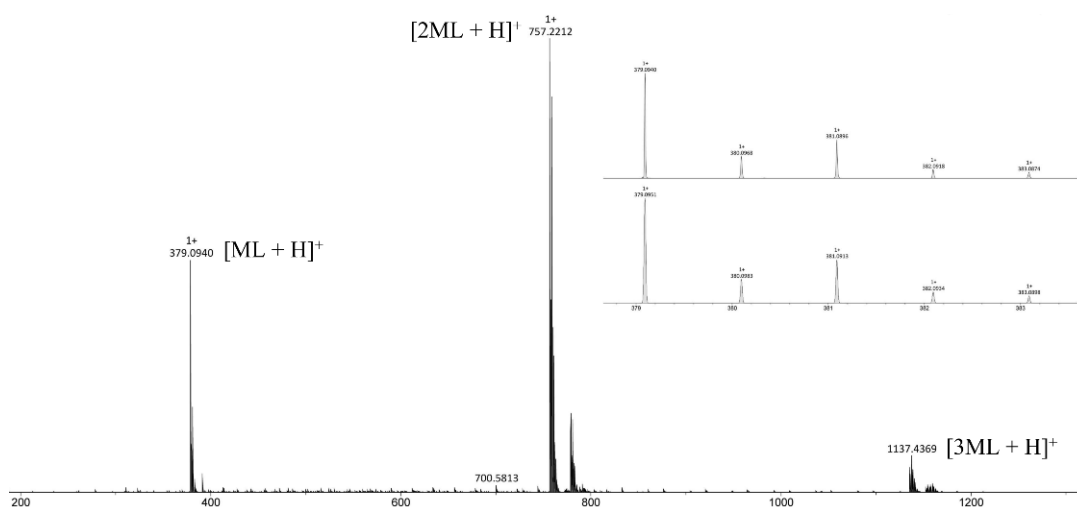

Figure 4.6 *Main image: interpreted electrospray mass spectrum of complex **4.10**, recorded in DCM solvent. Inset image: simulated (bottom) vs observed (top) mass envelope for monomeric $[4.10 + H]^+$ mass fragment, noting diagnostic isotopic distribution.*

Pale orange single crystals of **4.10** and **4.13** were isolated from the slow diffusion of Et$_2$O vapours into concentrated DCM solutions of each complex, which were suitable for X-ray crystallographic analysis (**Figure 4.7**).
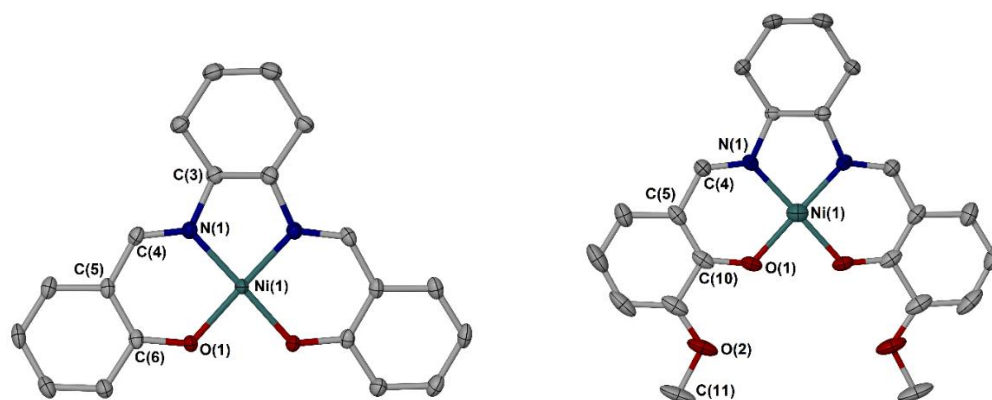
Figure 4.7 *Left: molecular structure of **4.10**. Right: molecular structure of **4.13**. Atomic displacement parameters are drawn at the 50 % probability level, hydrogen atoms are omitted for clarity.*

4.10	Ni(1)-N(1)	1.852(2)	N(1)-Ni(1)-O(1)	95.15(9)
4.10	Ni(1)-O(1)	1.8483(17)	N(1)-Ni(1)-N(1')	86.19(13)
4.13	Ni(1)-N(1)	1.848(3)	N(1)-Ni(1)-O(1)	94.99(15)
4.13	Ni(1)-O(1)	1.842(3)	N(1)-Ni(1)-N(1')	86.0(2)

Table 4.3 *Selected bond lengths (Å) and angles (˚) from the crystal structures of **4.10** and **4.13**.*

Analysis of the solid-state structures of complexes **4.10** and **4.13** each reveal a square-planar nickel(II) coordination sphere, comprising the expected tetradentate [N_2O_2] ligand binding mode which corroborates well with both spectroscopic and spectrometric measurements, and confirm neutral [NiL] molecular structures.

4.5   Electrochemical synthesis of zinc(II) salen complexes

Numerous reports describe the synthesis of zinc(II)-salen complexes from either Zn(OAc)$_2$ or ZnCl$_2$/NEt$_3$, though these strategies often create difficulty in isolating pure metalated product and in certain cases, inseparable mixtures of product and 'free salen' are obtained.[2] A more direct method involves treatment of a salen ligand precursor with a reactive dialkyl zinc derivative (*e.g.* ZnMe$_2$ or ZnEt$_2$), though isolation (and particularly, crystallisation) of the resulting zinc(II)-salen complex requires facilitation with pyridine in order to avoid unwanted polymerisation of the product, through each Schiff base ligand coordinating more than one zinc atom. This being said, Cozzi and Kozlowski have independently shown that the ability of zinc salen complexes to

coordinate metals and salts, even after chelation, can be used advantageously to catalyse the addition of $ZnEt_2$ to aldehydes.[51,52]

Our attention was therefore turned toward the electrochemical synthesis of Zn^{II}-salen complexes, as a mild and general alternative to those outlined above. **P4.1 – P4.5** were dissolved in hydrous acetonitrile solvent and electrolysed using a pair of zinc sticks (99.9 % purity, 30 mm length, 6 mm dia.). Rapidly, the corresponding zinc salen complexes each precipitated from the reaction mixture as off-white or pale yellow solids, which proved extremely insoluble in most common laboratory solvents. Following a simple filtration work-up procedure, the zinc(II) hydrate complexes, **4.14 – 4.18**, were obtained in good yield (**Scheme 4.6**).

4.14: $R^1 = R^2 = H$, **88 %**
4.15: $R^1 = H$, R^2 backbone = cyclohexyl, **79 %**
4.16: $R^1 = H$, R^2 backbone = phenylene, **83 %**
4.17: $R^1 = OMe$, $R^2 = H$, **77 %**
4.18: $R^1 = OMe$, R^2 backbone = cyclohexyl, **94 %**
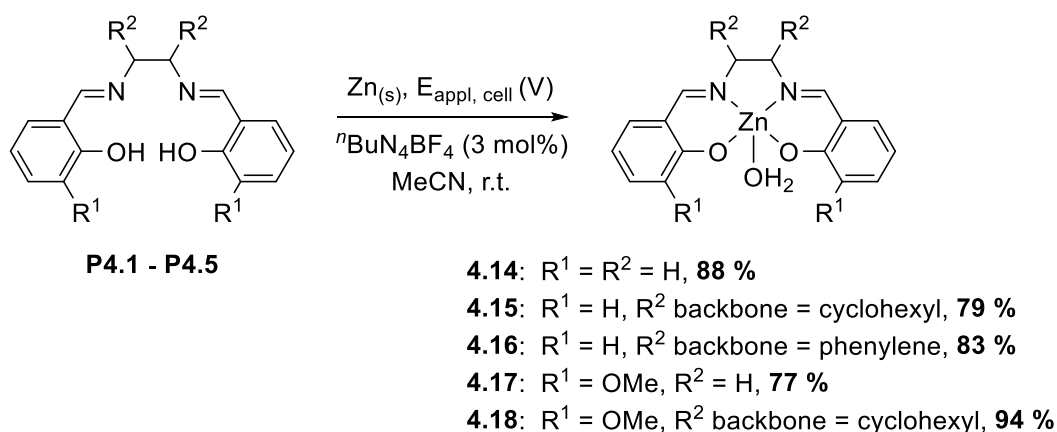
Scheme 4.9 *Electrochemical synthesis of Zn^{II}-salen complexes. Conditions: ligand precursor (1.0 mmol), $^nBuN_4BF_4$ (0.03 mmol), hydrous MeCN (50 mL), applied potential (22 – 25 V, maintaining 50 mA at steady-state), T = 298 K, 90 minutes reaction time. Quoted yield values are isolated.*

On account of their low solubility, acquisition of solution-state analysis was limited to the most polar solvents. Nevertheless, dissolution of each d^{10} configured zinc(II) complex using d_6-DMSO (at *ca.* 50 ˚C) allowed procurement of good quality NMR spectral data, an example of which is illustrated in **Figure 4.8**. In all cases, the original low-field phenolic O*H* singlet was removed and weak resonance broadening became evident.
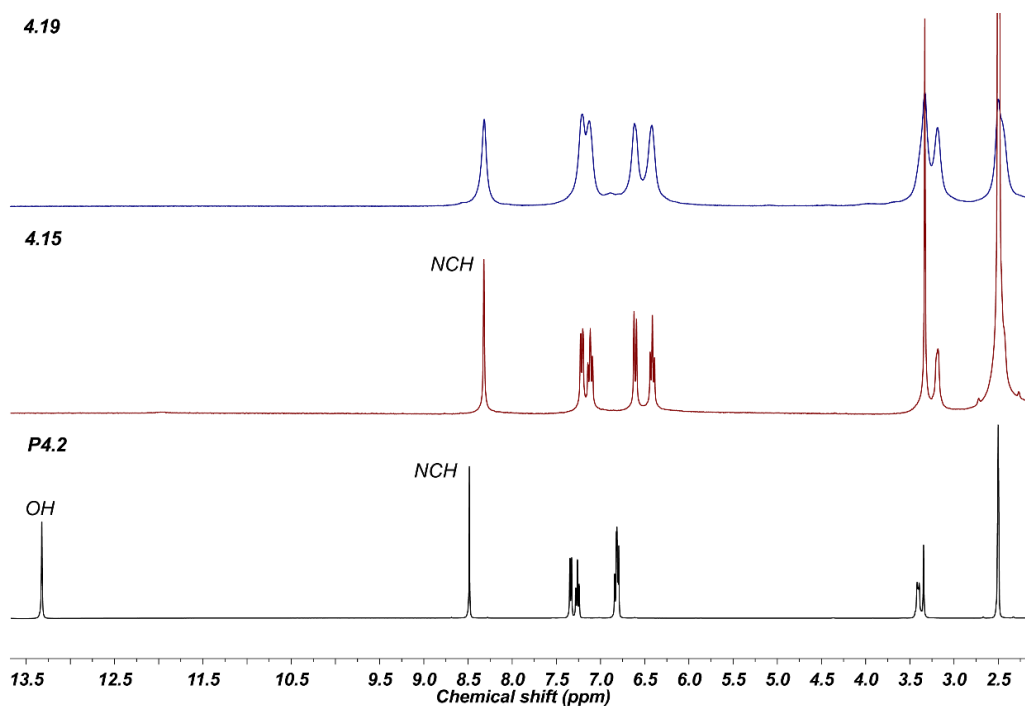
Figure 4.8 *^{1}H NMR spectrum of authentic ligand precursor **P4.2** (black trace, 400 MHz, (CD$_3$)SO, 298K), noting original phenolic singlet at 13.32 ppm. ^{1}H NMR spectra of Zn^{II}-salen complexes **4.15** (red trace) and **4.19** (blue trace, 500 MHz, (CD$_3$)SO, 298K).*

Analysis of complexes **4.14** – **4.18** using mass spectrometry also proved informative. For each example, a monomeric mass peak was detected which corresponds with each [ZnL] fragment (mass/charge ratios observed: **4.14** 331.0418, **4.15** 385.0887, **4.16** 379.0420, **4.17·DMSO** 469.0770 and **4.18** 445.1109, recorded in DMSO solvent). However, the general ESI fragmentation patterns of **4.14** – **4.18** were not dissimilar to their copper or nickel related analogues, with so-called ligand scrambling prominent in all spectra to generate protonated [ML], [ML$_2$] and [M$_2$L$_3$] mass adducts in solution (**Figure 4.9**, for example).
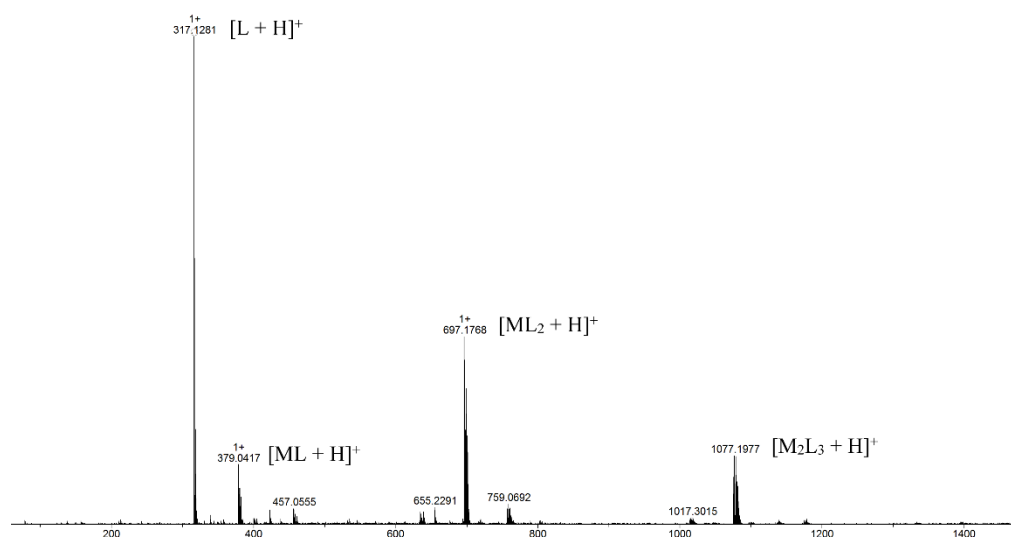
Figure 4.9 *Interpreted electrospray mass spectrum of complex **4.16**, recorded in DMSO solvent, indicating [ML], [ML$_2$] and [M$_2$L$_3$] mass adducts in solution.*

The purity of complexes **4.14** – **4.18** were further assessed by combustion analysis, which indicated each compound was formed as a monohydrate species. This result is perhaps unsurprising, as an early structural report by the group of Atwood showed that zinc salen complexes of this type typically undergo dimerisation (particularly in the solid-state) through axial coordination of one of the O-atoms of each ligand to the zinc(II) centre of a neighbouring unit. The authors claim that this dimerisation is generally suppressed by the presence of other donor ligands, such as H_2O or DMSO.[53]

Numerous attempts to isolate single crystals of **4.14** – **4.18** proved troublesome, on account of their poor solubility. In fact, zinc salen complexes are rarely structurally elucidated without use of pyridine for this reason.[54] Nonetheless, slowly cooling a DMSO solution of zinc complex **4.18** from 100 ˚C under solvothermal conditions allowed isolation of pale yellow blocks of the product, which were subsequently analysed by X-ray crystallography (**Figure 4.10**).
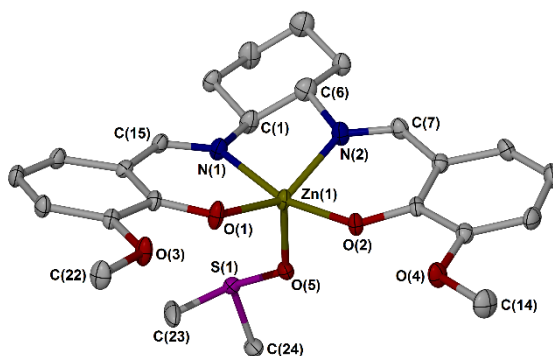
Figure 4.10 *Molecular structure of **4.18·DMSO**. Atomic displacement parameters are drawn at the 50 % probability level, hydrogen atoms are omitted for clarity. One sulphur atom from coordinated DMSO solvent displays molecular disorder, and is refined anisotropically over two equal positions, of which one is hidden for clarity.*

Zn(1)-N(1)	2.089(3)	N(1)-Zn(1)-N(2)	79.49(11)
Zn(1)-N(2)	2.080(3)	N(1)-Zn(1)-O(1)	88.69(10)
Zn(1)-O(1)	1.976(2)	N(2)-Zn(1)-O(2)	89.82(10)
Zn(1)-O(2)	1.981(2)	O(1)-Zn(1)-O(2)	92.77(9)
Zn(1)-O(5)	2.075(2)	O(1)-Zn(1)-O(5)	111.30(9)

Table 4.4 *Selected bond lengths (Å) and angles (˚) from the crystal structure of **4.18·DMSO**.*

The asymmetric unit comprises one **P4.5** ligand that coordinates one zinc(II) centre, through the anticipated [N_2O_2] chelating binding mode. The metal centre adopts square-based pyramidal geometry, through axial coordination to one molecule of solvating DMSO, which is presumed to have displaced a H_2O ligand during crystallisation. Under retrofit analysis, all solution-state measurements support the observed solid-state structure.

It is worth mentioning that within the efforts to obtain X-ray quality single crystals of the zinc salen complexes described above, a remote result was found in the form of zinc complex **4.19**. Dissolution of isolated **4.15** into DCM was facilitated by addition of a small portion of neat acetic acid (5 % $^v/_v$, DCM:AcOH 1.0:0.05 ratio), into which Et$_2$O vapours were slowly diffused over two days to produce pale yellow block crystals, amongst a vibrant yellow solution phase. Based on d^{10} electronically configured zinc complexes generally producing non-coloured compounds, the appearance of a brightly coloured solution phase within the crystallisation vial was indicative of re-protonation and subsequent complex-dissociation of ligand **P4.2**. The crystals were therefore collected, rinsed with acetone solvent and re-examined by proton NMR spectroscopy (see **Figure 4.8**, blue trace). The NMR spectrum displayed a sequence of broad resonances, which align well with signals of 'parent complex' **4.15**, in terms of chemical shift. However, aside from C_2 symmetry, no structural information could be taken from this spectrum. Instead, the crystals were subject to X-ray crystallographic analysis, which verified the absolute molecular structure of complex **4.19** as a trinuclear [M$_3$L$_2$] zinc cluster. A proposed schematic for the formation of **4.19** is provided in **Scheme 4.7**, with the solid-state X-ray structural solution given in **Figure 4.11**.

Scheme 4.10 *Proposed formation of trinuclear Zn cluster, **4.19**.*
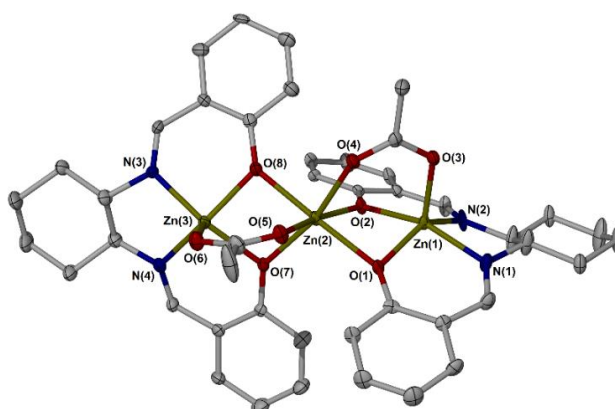
Figure 4.11 *Molecular structure of **4.19**. Atomic displacement parameters are drawn at the 50 % probability level, hydrogen atoms, four molecules of solvating DCM and one molecule of anti-solvating Et$_2$O are omitted for clarity.*

Zn(1)···Zn(2)	2.9937(16)	O(4)-Zn(2)-O(2)	90.4(3)
Zn(2)-O(1)	2.156(7)	O(5)-Zn(2)-O(2)	168.7(3)
Zn(2)-O(8)	2.145(8)	O(8)-Zn(2)-O(1)	177.4(3)
Zn(2)-O(5)	2.066(8)	Zn(1)-O(1)-Zn(2)	91.8(3)
Zn(2)-O(4)	2.105(8)	Zn(2)-O(8)-Zn(3)	93.4(3)
Zn(2)···Zn(3)	3.0206(16)	Zn(1)···Zn(2)···Zn(3)	161.42(6)

Table 4.5 *Selected bond lengths (Å) and angles (˚) from the crystal structure of **4.19**.*

Analysis of **4.19** in the solid-state reveals a pair of square pyramidal zinc atoms (Zn(1) and Zn(3)) which remain fully chelated to two independent salen ligands, themselves linked to a third zinc atom (Zn(2)) *via* four bridging μ-phenoxo O atoms. The average Zn···Zn separations of the Zn_3 framework were measured at 3.00 Å, comparable to the intermetallic distances of 3.04 Å recorded for a similar complex reported by Nabeshima and colleagues.[55] Though known, the synthesis of multinuclear $[Zn_3L_2(OAc)_2]$ complexes has been limited to more sophisticated parent ligands (*i.e.* H_2L) of salbn (*N,N'*-disalicylidene-1,4-diaminobutane) and salamo (1,2-*bis*(salicylideneaminooxy)ethane) only, with no examples of simple salen ligand precursors stabilising higher order zinc(II) complexes of this kind. Whilst difficult to conclusively state the exact mechanism for formation of **4.19**, it is assumed that incorporation of each μ-acetato bridging ligand sufficiently stabilises the structure by neutralising the overall charge of the molecule. However, as there appears to be no obvious entropic drive to form **4.19**, it is possible that under acidic conditions pentacoordinate complex **4.15** is simply no longer stable, and **4.19** becomes a thermodynamically favoured product. This postulation is perhaps supported by closer examination of the ESI mass spectrum of zinc compound **4.16**, which is supplied in **Figure 4.9**; it is clear that under the acidic spectrometric conditions of the experiment, a large abundance of fragmented free ligand is detected relative to the monomeric zinc complex, suggestive of some degree of protic sensitivity.

4.6 Selective electrochemical synthesis of iron(II)/(III) salen complexes

Iron-containing porphyrins have been found to effect a broad range of chemical transformations, holding a firm position within the fields of oxidation, reduction and isomerisation chemistry.[56,57] Given the topological similarity between porphyrin and salen, the focus of several reports has been centred upon exploiting iron-salen complexes as alternatives for comparable reactions.

In terms of organometallic synthesis, routes to both iron(II) and iron(III) complexes of salen are thought to be very well-established, and are generally unquestioned. Common iron precursors include FeX_n (where X = halide, n = oxidation number),[58] Fe_2Mes_4[59] and $Fe[(N(SiMe_3)_2]_2$.[60] However, while iron halides are commercially available, the remainder of this list require in-

house preparation and are challenging to handle due to their sensitivity toward air and moisture. The original metal oxidation state within these precursors is thought to be conserved when incorporated into the final iron salen product.

In spite of longstanding research, modern literature appears littered with inconsistencies regarding the physical properties of such pre-defined compounds, most notably with regard to iron(II)-salen complexes. For example, Woo and co-workers reported the reaction of $Fe(OAc)_2$ with *N,N'-bis*(salicylidene)-1,2-cyclohexanediamine (*i.e.* **P4.2** of this chapter) to produce the corresponding iron(II) complex as a purple powder,[61] where North and Steed later isolate the same complex as a bright orange solid,[20] but Lemos and Webster independently quote the product as a 'straw-yellow' microcrystalline solid.[62,63] Seemingly minor, the physical appearance of these iron-containing complexes provides insight into both the ligand field surrounding the metal centre and its oxidation state – both of which play important roles for these complexes during catalysis and are not trivial to acquire from standard spectroscopic, spectrometric or microanalytical methods.

Within their findings, North and co-workers noted that only their pre-defined iron(II) and manganese(II)-salen complexes were completely inactive in the catalytic synthesis of α-methyl α-amino acids, amongst a broad range of active metal(II)-salen complexes.[20] As these metals are well-known to occupy multiple oxidation states when complexed with salen ligands, it was speculated that perhaps these well-defined complexes were not purely pertaining to one single oxidation state.

Prompted by this, and the conflicting physical data within the literature, **P4.2** was treated with one equivalent of fresh $Fe(OAc)_2$ in refluxing anhydrous ethanol in our laboratory. Using this procedure described by North and Steed, a deep red/purple microcrystalline solid was obtained upon cooling of the reaction mixture (**4.20**). Following isolation, the compound displayed no remarkable signals in the proton NMR spectrum. However, the electrospray mass spectrum featured dominant mass peaks (*m/z*) 376.0893 and 436.1209, attributable to $[FeL + H]^+$ and $[FeL(OAc) + H]^+$ mass fragments. With solution measurements providing little structural information about the reaction product, other than the containment of both iron and ligand as judged by mass spectrometry, the whole sample was re-dissolved in ethanol and layered with anhydrous hexane, affording a large batch of dark red single crystalline needles (77 % yield, isolated as single crystals) which were amenable to X-ray structural analysis (**Figure 4.12**).
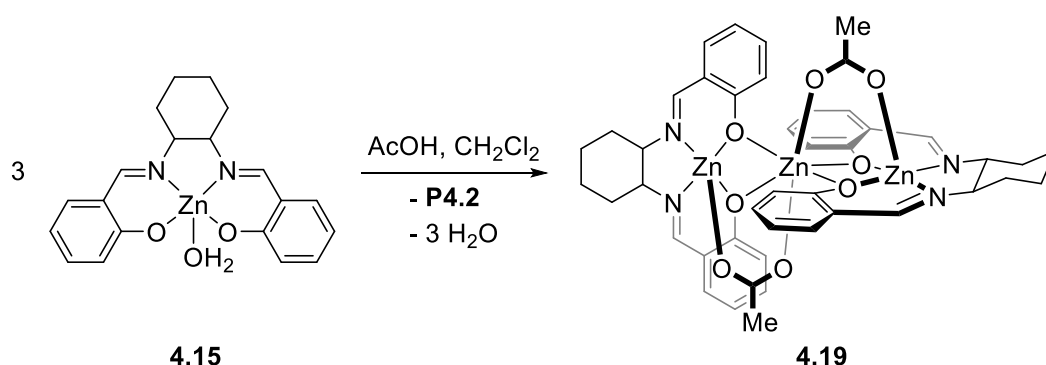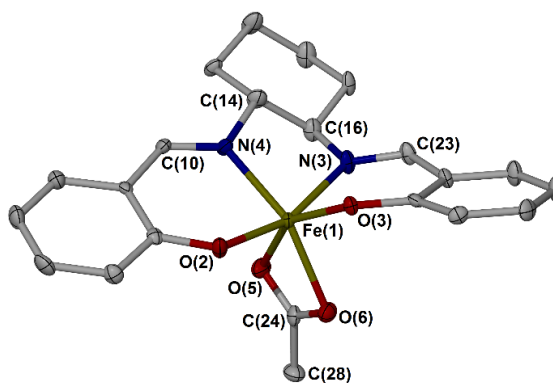
Figure 4.12 *Molecular structure of **4.20**. Atomic displacement parameters are drawn at the 50 % probability level, hydrogen atoms are omitted for clarity.*

Following structural refinement, it was uncovered that the product of this reaction is an Fe^{III}-salen complex. One molecule of acetate remains bound to the metal centre alongside a chelating salen ligand, generating an iron(III) coordination sphere which adopts heavily distorted octahedral geometry, with the usual C_2 symmetry. Sample composition was also assessed by combustion analysis, which further supports incorporation of the acetate ligand within the bulk material.

Indeed, these findings were not anticipated, as treatment of a salen precursor (*i.e.* H_2L) with an iron(II) source under inert conditions is expected to lead to the deprotonation of two phenolic hydrogen atoms (*i.e.* loss of two molecules of acetic acid byproduct), and preserve an iron(II) metal centre. As discussed within this chapter, the most common route to deploy these complexes as catalysts into reaction media is to generate them *in situ*, and contamination of what is thought to be pure, reactive iron(II) catalyst with its potentially unreactive iron(III) form presents a problem. Given that our electrochemical protocol to produce metal-salen complexes does not introduce any side-products into solution which may coordinate the product, it was surmised that it could be possible to control metal oxidation state simply based on availability of oxygen within the system.

Taking ligand precursors **P4.1** – **P4.5** forward with this idea, a pair of iron foil electrodes (99.5 % purity) were introduced to acetonitrile solutions of each compound, under hydrous and aerated conditions. Establishing a potential across this stirring solution (steady-state current of 50 mA), an obvious colour change was evident from which the original yellow reaction mixture was rapidly replaced by a bright red solution of each complex (**Figure 4.13**) – indicative of iron(III)-salen complex formation.[63]
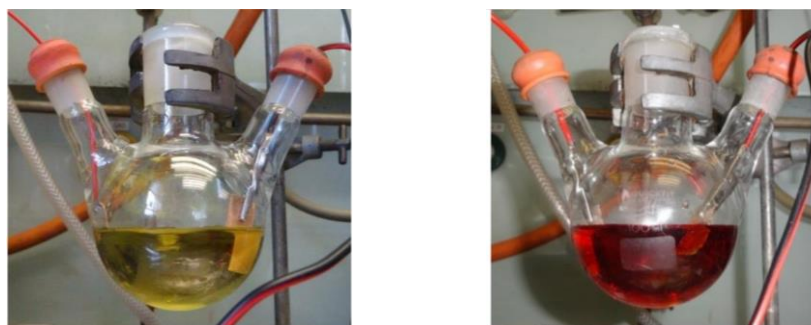
Figure 4.13 *Images of aerobic reaction vessel before electrical potential application (left) and during (right), illustrating the change in composition of the reaction mixture by colouration over time.*

Relative complex formation was monitored by high-resolution mass spectrometry, which in each case provided a handle on reaction progress. However, following completion the iron-salen products precipitated from solution with low reliability, and in some instances not at all. For these examples, product isolation was performed by recrystallisation of the crude product mixture from DCM, allowing access to five μ-oxo bridged iron(III) complexes (**4.21 – 4.25**) in reasonable yield (**Scheme 4.8**, right-hand path).

4.26: $R^1 = R^2 = H$, **88 %**
4.27: $R^1 = H$, R^2 backbone = cyclohexyl, **90 %**
4.28: $R^1 = OMe$, R^2 backbone = cyclohexyl, **93 %**

4.21: $R^1 = R^2 = H$, **59 %**
4.22: $R^1 = H$, R^2 backbone = cyclohexyl, **74 %**
4.23: $R^1 = H$, R^2 backbone = phenylene, **69 %**
4.24: $R^1 = OMe$, $R^2 = H$, **78 %**
4.25: $R^1 = OMe$, R^2 backbone = cyclohexyl, **64 %**
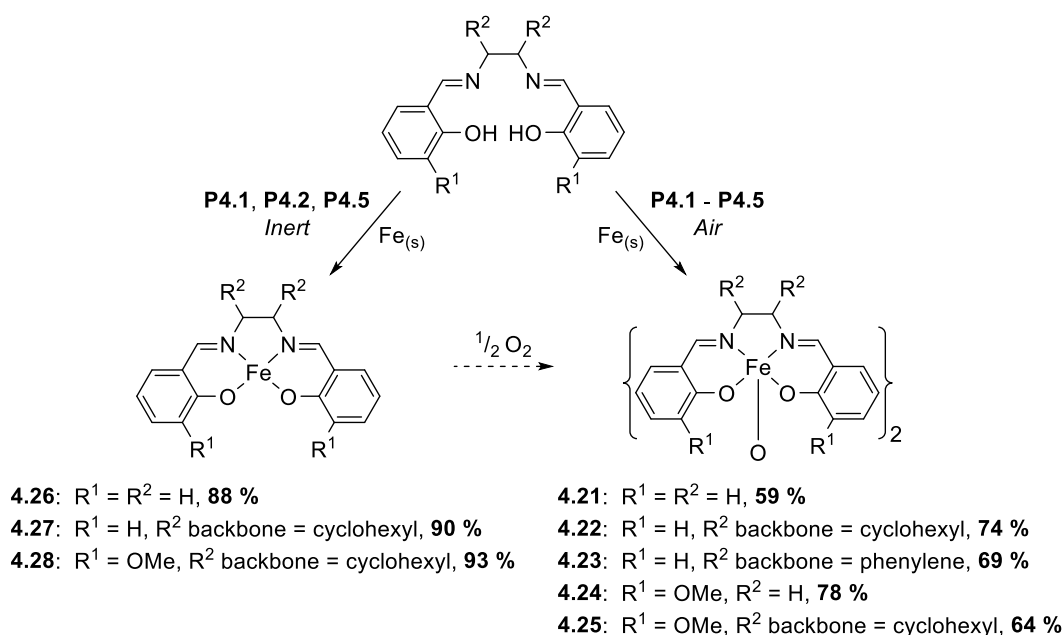
Scheme 4.11 *Selective electrochemical synthesis of Fe^{II}/Fe^{III}-salen complexes. Right-hand path conditions: ligand precursor (1.0 mmol), $^nBu_4NBF_4$ (0.03 mmol), hydrous MeCN (50 mL), applied potential (22 – 25 V, maintaining 50 mA at steady-state), T = 298 K, 90 minutes reaction time. Left-hand path conditions are analogous, except all solvents were freeze-pump-thaw-degassed prior to use, and the products were isolated under an inert atmosphere. Quoted yield values are isolated.*

Solution NMR spectroscopic analysis of **4.21** – **4.25** presented significantly broadened resonances, suggestive of paramagnetic samples. Electrospray mass spectrometry however, provided compelling evidence for complex formation in every case, an example of which is provided below in **Figure 4.13**. For each complex, the ESI mass spectrum featured a notable relative abundance of a mass collection attributed to the corresponding monomeric [FeL] species. However, it is generally accepted that such species are rapidly quenched by O_2, especially in solution, to form their more stable μ-oxo bridged iron(III) counterparts.[64] It is therefore probable that each [FeL] mass peak is an artefact of molecular fragmentation, from the higher order $[(FeL)_2(\mu\text{-}O)]$ electrochemical product.
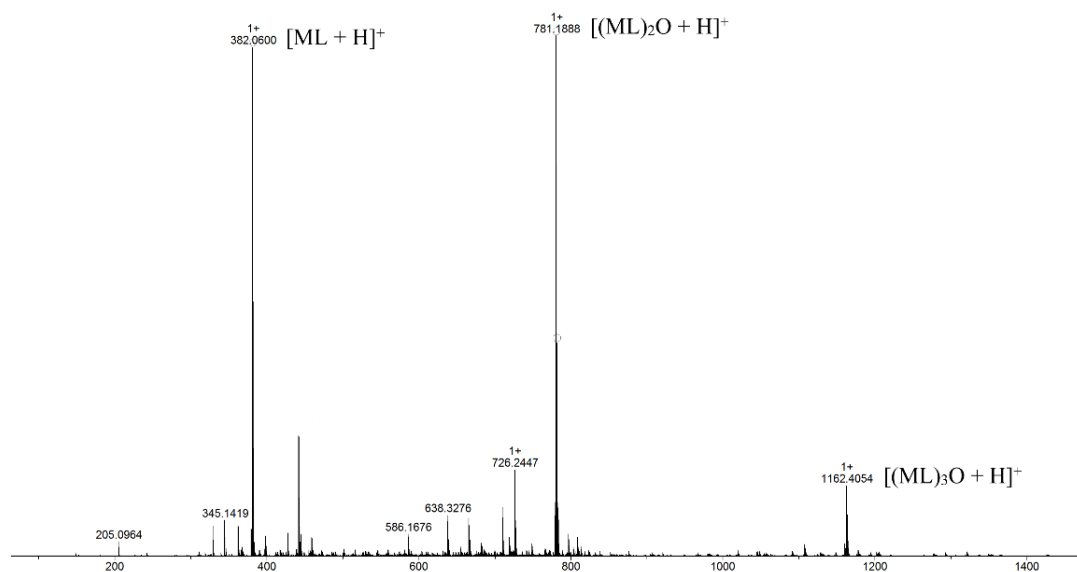
Figure 4.14 *Interpreted electrospray mass spectrum of complex **4.24**, recorded in DCM solvent, indicating [ML], [(ML)$_2$O] and [(ML)$_3$O] mass adducts in solution.*

Particularly diagnostic was infrared spectroscopy, which was employed to examine bulk sample composition, with each spectrum disclosing an asymmetric Fe-O-Fe stretching band between $760 - 820$ cm^{-1} – aligning well with those outlined in a review article by Murray.[65] Likewise, microanalytical data also supports formation of these dinuclear [Fe^{III}(salen)]$_2$O complexes under aerobic conditions, though is not dependable alone to conclusively state whether half of an oxygen atom is associated with an [FeL] fragment (in terms of molecular ratio). Instead, dark red crystals of complex **4.21** were isolated by slowly diffusing vapours of Et$_2$O into a DCM solution of the product, and analysed by X-ray diffraction methods to confirm the structure as the expected μ-oxo bridged iron(III) dimer (**Figure 4.14**).
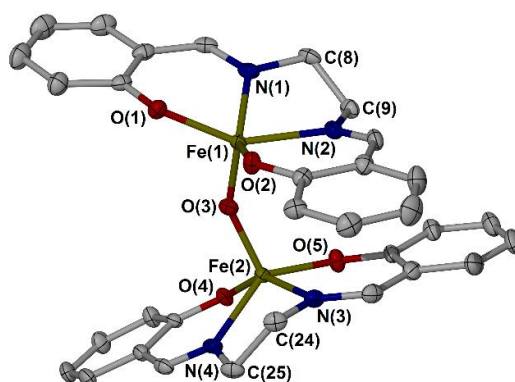
***Figure 4.15** Molecular structure of **4.21**. Atomic displacement parameters are drawn at the 50 % probability level, hydrogen atoms are omitted for clarity.*

Fe(1)-O(1)	1.935(2)	N(1)-Fe(1)-N(2)	76.29(10)
Fe(1)-O(2)	1.925(2)	Fe(1)-O(3)-Fe(2)	143.82(12)
Fe(1)-O(3)	1.784(2)	O(1)-Fe(1)-O(2)	93.43(9)
Fe(2)-O(3)	1.790(2)	O(3)-Fe(2)-O(5)	111.76(10)

***Table 4.6** Selected bond lengths (Å) and angles (°) from the crystal structure of **4.21**.*

One molecule of **4.21** occupies the asymmetric unit, which adopts a square-based pyramidal geometry about each iron(III) centre, both coordinating two phenoxide oxygen atoms, two imine donors and are linked by a bridging oxo group. Nguyen and co-workers have previously synthesised a series of dimeric iron(III)-salen complexes of this type, using $FeCl_3 \cdot 6H_2O$ as metal source.[66] The authors found that these air-stable complexes are efficient catalysts for the cyclopropanation of various olefins with ethyl diazoacetate, however, the synthesis of the authentic complexes must be performed in $Mg(OMe)_2$-distilled MeOH solvent, otherwise trace impurities are unavoidably produced which impede catalyst performance.

As considered above, the 'naked' mononuclear iron(II) equivalents of complexes **4.21** – **4.25** are well-known to be highly reactive towards molecular oxygen, making them difficult to handle and purify.[67] Webster and Gallagher have recently met with this challenge, and have found that their simplified synthesis, using $FeCl_2$ in refluxing THF to coordinate the salen ligand, provides access to the pure iron(II) product. Upon exposure to air, the authors note that O_2 activation takes place within seconds.[63]

It was envisaged that employment of our electrochemical method, which produces H_2 as the only byproduct, should allow entrapment of the 'naked', four-coordinate iron(II) salen complexes, provided no oxygen is present within the system. To this end, anhydrous, anoxic acetonitrile solutions of ligand precursors **P4.1**, **P4.2** and **P4.5** underwent the same electrochemical procedure

as described above, under an inert atmosphere. During electrolysis, the solution colour changed from bright yellow to orange/brown, until finally a deep purple colour persisted (**Figure 4.15**).

Figure 4.16 *Images of inert reaction vessel before electrical potential application (left), during (middle) and after (right), illustrating formation of a purple reaction product, which precipitates from solution over time.*

Following reaction, the solution phase was removed by cannula filtration and the resulting precipitate washed with reaction solvent, affording the desired iron(II)-salen complexes, **4.26** – **4.28** in high yield (**Scheme 4.8**, left-hand path). Of note, were the air-sensitivity of each complex whilst in solution, rapidly changing from deep purple to pale orange within seconds of exposure to the atmosphere (*i.e.* indicative of $Fe^{2+} \rightarrow Fe^{3+}$). NMR spectroscopic analysis of the solids was attempted in d_6-DMSO, $CDCl_3$ and C_6D_6 solvents, though no informative signals were observed to confidently discern between a mononuclear or higher order iron species. The poorly resolved proton NMR spectra do, however, imply a paramagnetic iron(II) metal centre which resides in a high-spin d^6 electronic configuration.

The Evans NMR method provides a means of measuring the susceptibility of a paramagnet such as this in solution.[68–70] By correlating the observed difference in chemical shift of a signal from an inert reference material (*i.e.* residual solvent), in the presence and absence of a paramagnetic solute, it is possible to calculate the number of unpaired electrons associated with the compound. To do so, a flame-sealed coaxial insert containing a deuterated reference solvent (C_6D_6/C_6H_6, 50:50) was placed into a J. Young's NMR tube under an inert atmosphere. Complex **4.26** was dissolved in C_6D_6 (100 %, 5.6 mg in 0.46 mL) and the paramagnetic solution added to the tube, and the $^1H\{^{13}C\}$ NMR spectrum recorded. Taking the spectral difference in residual solvent signals, the solution magnetic moment of this sample was calculated between 4.9 – 5.0 μ_B, corroborating with four unpaired electrons – supportive of a high-spin ($S = 2$) iron(II) metal centre. Likewise, the method was applied to complexes **4.27** and **4.28** to present similar results (4.8 and 5.1 μ_B, respectively) (for full experimental details and mathematical extrapolation, see Experimental).

One drawback of the Evans solution method, is a relatively high range of error (estimated to be between 5 – 10 %),[71] which is largely dependent on the concentration, and therefore solubility, of the paramagnetic solute. Along similar lines, only the bulk susceptibility of the sample is measured, and diamagnetic or paramagnetic impurities can lead to incorrect conclusions; this holds especially true for air-sensitive iron(II) compounds, according to Walker and Weber.[72] Nevertheless, the magnetometric measurements were recorded within this margin of error.

Complexes **4.26**, **4.27** and **4.28** were further analysed by microanalysis and ESI mass spectrometry, detecting the monomeric $[FeL + H]^+$ species within mass peaks (*m/z*) 323.1761, 376.0870 and 437.1160, respectively.

Violet needles of **4.28** were grown from the slow diffusion of Et_2O vapours into a weak DCM solution of the complex, under an inert atmosphere. Using X-ray crystallography, a solid-state structural solution of **4.28** was obtained, which authenticates the targeted 'naked' iron(II)-salen complex, as shown in **Figure 4.16**.
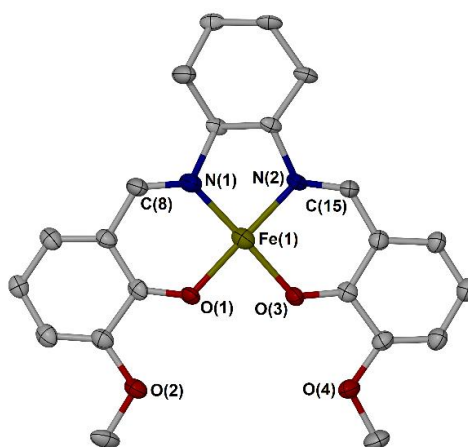
Figure 4.17 *Molecular structure of **4.28**. Crystals of the compound solved and refined as a twin. Atomic displacement parameters are drawn at the 40 % probability level, hydrogen atoms are omitted for clarity.*

Fe(1)-O(1)	1.868(8)	N(1)-Fe(1)-N(2)	87.0(5)
Fe(1)-O(3)	1.859(8)	N(1)-Fe(1)-O(1)	93.5(4)
Fe(1)-N(1)	1.829(11)	N(2)-Fe(1)-O(3)	94.8(4)
Fe(1)-N(2)	1.868(10)	O(1)-Fe(1)-O(3)	84.7(4)

Table 4.7 *Selected bond lengths (Å) and angles (°) from the crystal structure of **4.28**.*

The coordination environment around the iron(II) centre can be described as distorted square planar, with the smallest angle attributed to the O(1)-Fe(1)-O(3) connection of 84.7(4)°. Apparent, is the absence of any additional donor ligands situated at the apical positions of the metal, which forces the iron centre into a relatively unstable geometry.

Square planar iron(II) complexes are abundant and virtually all adopt an $S = 1$ intermediate spin-state, with the most common example being their porphyrins.[73] In stark contrast, are high-spin square planar iron(II) compounds, which are undoubtedly rare. To date, only four non-macrocyclic or sterically-driven examples exist, with the first only emerging in 2011 by Klüffers.[74] Since, three others have been published, though rely on an anionic FeO_4 core to stabilise the complex.[75–77] An elegant report by Chirik and colleagues details the isolation of an $S = 3/2$ square planar *bis*(imino)pyridine iron chloride, possessing an electronic structure which is best described by considering an $S = 2$ Fe^{II} centre, antiferromagnetically coupled to a ligand-based radical. However, the structural assignment was based solely on theoretical calculations.[78] The solid-state analysis of **4.28** certainly suggests a molecular iron(II) structure about a square plane, though would require additional experiments to verify this coordination mode in solution (*e.g.* frozen solution Mössbauer, or high-field EPR spectroscopies may provide this information).

4.7   Selective electrochemical synthesis of manganese(II)/(IV) salen complexes

Manganese complexes of salen have found widespread utility over recent years, though arguably the major breakthrough in this area was discovered independently by Jacobsen and Katsuki in 1990, of manganese(III) salen complexes which catalyse the asymmetric epoxidation of olefins with superb efficiency.[14,79] Although controversy still exists regarding the mechanism of oxidation, it is generally accepted that oxygen delivery is brought about by a Mn(O)salen species, which itself exists in equilibrium with other Mn-salen components in solution. Importantly, μ-oxo bridged manganese dimer species (*i.e.* $[MnL]_2O_2$) are catalytically inactive with respect to epoxidation, and coordinating axial ligands are often used (*e.g.* halides) to stabilise the active monomer form of the complex.[2] Therefore the ability to carefully control both metal oxidation state and coordination sphere of these complexes is essential.

Reconsidering North and Steed's list of highly active, *in situ*-generated metal(II)-salen catalysts for α-methyl α-amino acid synthesis, which deems those of iron and manganese to be inactive, it was sought to isolate and characterise the well-defined product of their reaction. **P4.1** was treated with one equivalent $Mn(OAc)_2$ in anhydrous ethanol, under uniform conditions to those outlined by North and colleagues. A dark brown solid precipitated from solution, which was subsequently collected and dried (**4.29**). Solution phase analysis of the product was limited to the most polar solvents, due to poor solubility in most common laboratory solvents. Nonetheless, recording the ESI mass spectrum in DMSO solvent presented the monomeric $[MnL + H]^+$ and $[MnL(DMSO) + H]^+$ solvated mass adducts, at (*m/z*) 321.0440 and 399.0571, respectively. Two additional mass peaks were also observed, at (*m/z*) 589.1643 and 675.0853, attributable to ligand-scrambled $[MnL_2 + H]^+$ and *bis* μ-oxo bridged $[(MnL)_2O_2 + H]^+$ species, respectively. Aside from

the incorporation of manganese and ligand within the sample, the mass spectrum confirmed little information of structure, nor metal/ligand ratio.

Upon standing of a DCM solution of **4.29**, single crystals of the complex were isolated and analysed by X-ray diffraction methods. The solid-state structural solution revealed a 2D acetate-bridged polymer, which is given in **Figure 4.17**.
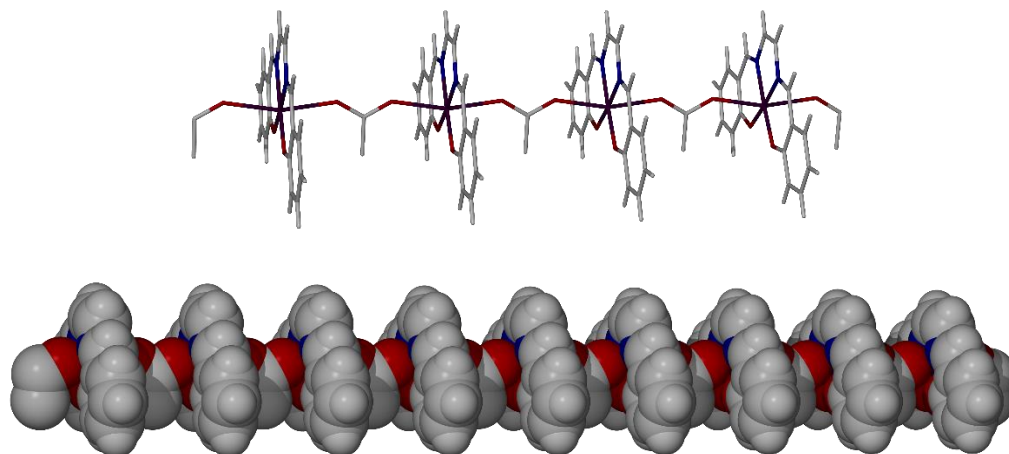
Figure 4.18 *Taken from the crystal structure of **4.29**. Top: stick model of polymeric repeating units, propagating a bidimensional framework. Bottom: space-filled model of the extended structure.*

The central unit of the polymer comprises a manganese(III) metal centre, which adopts octahedral geometry, and each unit is linked by a molecule of acetate. Admittedly, acetate within the coordination sphere was not observed by mass spectrometry, nor could the corresponding bonds be accurately distinguished by infrared spectroscopy. Albeit arguable, the crystallographic evidence still points to manganese(III) contaminants within a presumed manganese(II) bulk sample – similar to our findings regarding iron-salen synthesis, and may help explain why these two metal-salen species were catalytically inactive for North and Steed.

Following our selective synthesis of iron-salen complexes of various oxidation state, it was sought to extend the electrochemical methodology toward analogues of manganese. Despite representing an inexpensive and abundant transition metal, zero-valent manganese is a brittle material which is virtually impossible to machine into a robust electrode surface alone. One solution to this problem is to employ a mixed-metal alloy of manganese, many of which are known, to build an electrode surface with robust physical properties whilst maintaining a high concentration of metallic manganese. By judicious choice of alloy, it was hypothesised that selective metal ion liberation from this solid interface could be controlled by simply tuning electrical potential.

To this end, a bimetallic manganese/nickel (88 % Mn, 12 % Ni) metal alloy was selected as sacrificial anode. The standard potential required to liberate Mn^{2+} ions into solution is 0.90 V

more negative than that of Ni^{2+}, the upshot of which is that such a gap in potential should allow for selective Mn^{2+} ion release from the solid alloy before Ni^{2+}, providing a timeframe to trap pure complexes of manganese.

Pleasingly, employment of this anodic alloy under the same aerated conditions as described for copper, nickel, zinc and iron, allowed electrochemical conversion of **P4.1** – **P4.5** to their corresponding *bis*(μ-oxo)-bridged $[Mn^{IV}(salen)]_2O_2$ complexes, **4.30** – **4.34**, in high yield (**Scheme 4.9**, right-hand path).

4.35: $R^1 = R^2 = H$, **77 %**
4.36: $R^1 = H$, R^2 backbone = cyclohexyl, **71 %**
4.37: $R^1 = OMe$, R^2 backbone = cyclohexyl, **78 %**

4.30: $R^1 = R^2 = H$, **87 %**
4.31: $R^1 = H$, R^2 backbone = cyclohexyl, **90 %**
4.32: $R^1 = H$, R^2 backbone = phenylene, **95 %**
4.33: $R^1 = OMe$, $R^2 = H$, **98 %**
4.34: $R^1 = OMe$, R^2 backbone = cyclohexyl, **78 %**
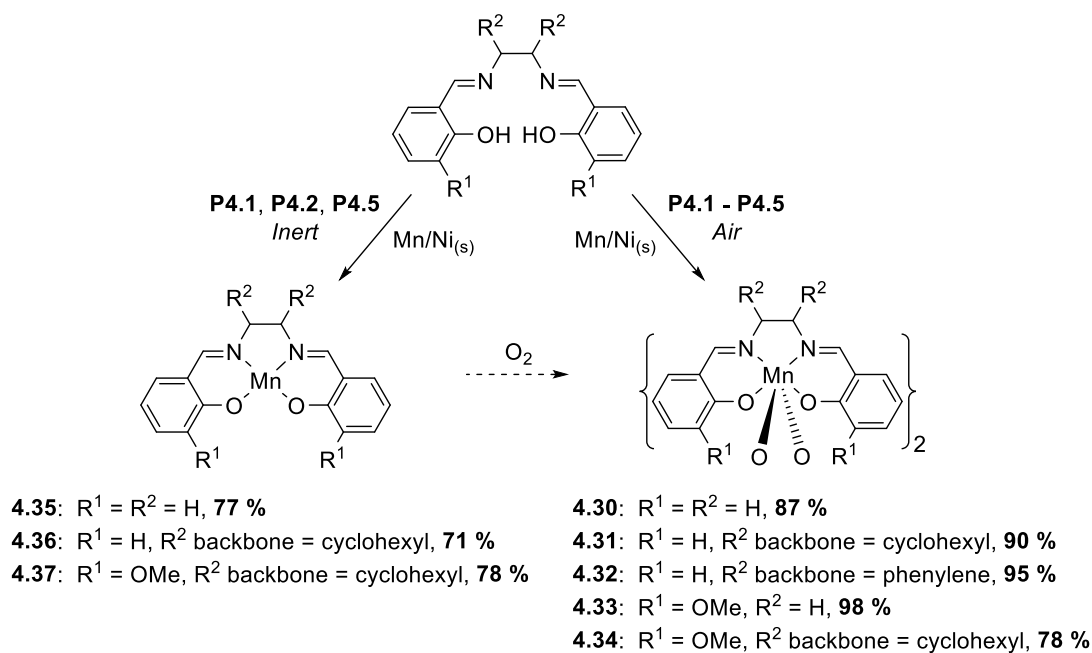
Scheme 4.12 *Selective electrochemical synthesis of Mn^{II}/Mn^{IV}-salen complexes, using a Mn/Ni (88:12) alloy. Right-hand path conditions: ligand precursor (1.0 mmol), $^nBu_4NBF_4$ (0.03 mmol), hydrous MeCN (50 mL), applied potential (22 – 25 V, maintaining 20 mA at steady-state), T = 298 K, 90 minutes reaction time. Left-hand path conditions are analogous, except all solvents were freeze-pump-thaw-degassed prior to use, and the products were isolated under an inert atmosphere. Quoted yield values are isolated.*

From the outset, applied potential was incrementally increased to produce steady-state current values of 2, 5, 10 and 20 mA, monitoring the reaction composition by high-resolution mass spectrometry at each interval. Clear, was the formation of manganese-salen complexes only, with no evidence to support the presence of any nickel-salen species in solution (to the detection limit of the mass spectrometer). By way of example, a 'timecourse' sequence of mass spectra are provided in **Figure 4.18**, demonstrating the detection of manganese-salen mass adducts (**4.30**) only, for each increment up to an applied potential of 20 V (to generate 20 mA current). These high-resolved mass spectra were particularly diagnostic, given the unique isotopic signatures of manganese and nickel. All manganese-salen complexes were therefore produced at this current limit.
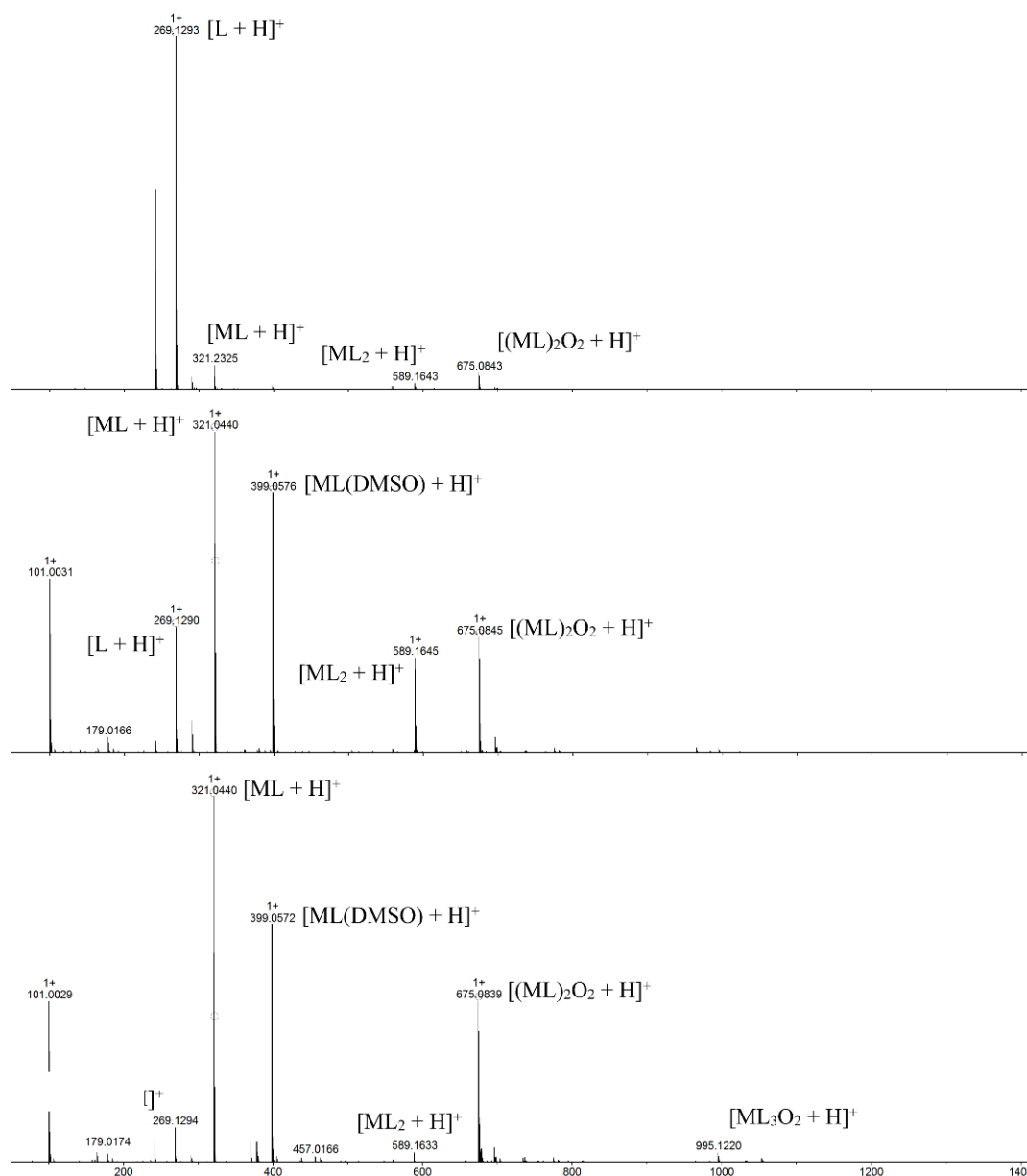
Figure 4.19 Interpreted 'timecourse' HR-MS excerpts, from the electrochemical conversion of precursor P4.1 using a Mn/Ni bimetallic alloy anode, highlighting the selective formation of manganese-salen adducts only (in all cases above, M = Mn). Top: 5 V applied, 5 minutes. Middle: 10 V applied, 20 minutes. Bottom: 20 V applied, 90 minutes; spectra recorded in DMSO solvent.

Following their formation, **4.30 – 4.34** precipitated from solution as dark brown powders, which were collected by filtration and dried. In terms of elemental analysis, the discrepancy between a manganese complex of salen and its corresponding nickel analogue fall within the range of error associated with analysing a sample by combustion. Therefore, atomic absorption spectroscopy (AAS) was used to confirm the absence of nickel within the bulk samples. **4.30**, **4.31** and **4.32** were dissolved in strongly acidic, aqueous solutions (30 % nitric acid/10 % hydrochloric acid) and examined by AAS, which indicated only trace quantities of nickel, consistent with amounts

observed in blank solvent. Increasing the concentration of each complex 10-fold did not lead to a linear response in nickel content, suggesting that the readings were within range of error of the instrument (*i.e.* no nickel above 1 ppm was accurately measured in any of the three samples. For further details, see Experimental).

Likewise, X-ray fluorescence spectroscopy (XRF) was employed as a solid-state analytical tool to probe the bulk samples for nickel content. Taking benzylmanganese(I) pentacarbonyl and nickel(II) nitrate as solid standards, the characteristic K_L and K_M lines of both Mn and Ni were recorded (BnMn(CO)$_5$ K_L 5.89, K_M 6.49 KeV; Ni(NO$_3$)$_2$ K_L 7.48, K_M 8.63 KeV). Subsequently, bulk samples **4.30**, **4.31** and **4.32** were analysed under the same conditions as for the reference samples. In total, six independent measurements of each sample were performed to ensure sample homogeneity. In all cases, manganese was the strongest element present and no nickel was detected (to the limits of detection, estimated *ca.* 10 ppm. For further details, see Experimental).

Multinuclear NMR spectroscopy of these products presented no interpretable signals. Following such, it was anticipated that further solution-state analysis would be challenging to procure, as all complexes showed poor general solubility, even in the most polar solvents (*e.g.* DMSO, DMF and MeNO$_2$).

X-ray quality single crystals of complexes **4.30** and **4.34** were grown (the former is discussed directly below, the latter is illustrated in **Figure 4.20**). It was found that single crystals of complex **4.30** could be obtained *via* two methods, to produce a pair of different solvent-dependent solid-state structures of the product. Originally, pale brown blocks of **4.30** were isolated by slowly diffusing Et$_2$O vapours into a binary DCM:DMSO solution of the complex (**4.30a**). Alternatively, standing of a weak MeCN solution of the compound also produced good quality pale brown needles, which were equally suitable for X-ray crystallographic analysis (**4.30b**). Each structural solution is provided in **Figure 4.19**, with distances and angles pertaining the inner coordination of Mn listed in **Table 4.8**.
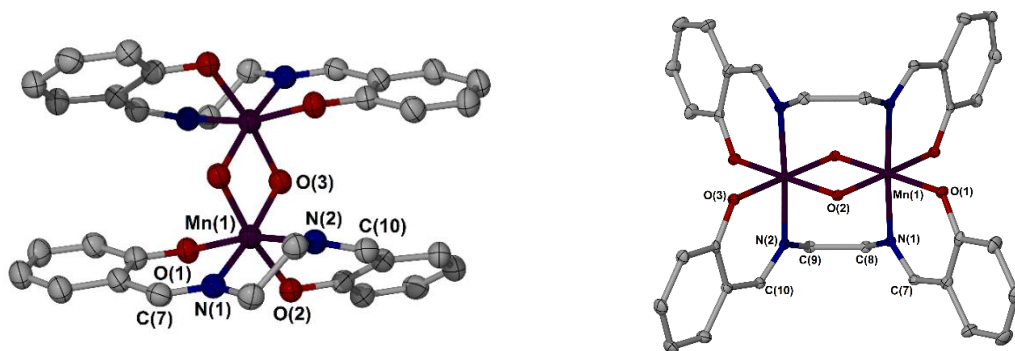
Figure 4.20 *Two method-dependent solid-state structures of **4.30**. Atomic displacement parameters are drawn at the 50 % probability level, hydrogen atoms are omitted for clarity. Left: crystallisation product of the slow diffusion method, involving three solvents (**4.30a**). Right: crystallisation product of still-standing method, involving one solvent (**4.30b**).*

4.30a	Mn(1)-N(1)	2.059(5)	N(1)-Mn(1)-N(2)	79.15(19)
4.30a	Mn(1)-N(2)	1.990(4)	N(1)-Mn(1)-O(1)	89.40(17)
4.30a	Mn(1)-O(1)	1.906(4)	N(2)-Mn(1)-O(3)	95.75(18)
4.30a	Mn(1)-O(3)	1.829(4)	O(1)-Mn(1)-O(3)	95.51(16)
4.30b	Mn(1)-O(1)	1.924(2)	N(1)-Mn(1)-O(1)	91.11(9)
4.30b	Mn(1)-O(2)	1.8124(19)	O(1)-Mn(1)-O(2)	92.54(9)
4.30b	Mn(1)-O(3)	1.925(2)	O(1)-Mn(1)-O(3)	92.56(9)
4.30b	Mn(1)-N(1)	2.014(2)	N(1)-Mn(1)-O(3)	86.99(9)

Table 4.8 *Selected bond lengths (Å) and angles (°) from the crystal structures of **4.30**.*

For each crystallisation environment, the solid-state structural solution of complex **4.30** displays a centrosymmetric dinuclear manganese(IV) salen complex. Common to both, is the presence of a *bis(μ-oxo)*-bridge connecting each metal centre, generating a pair of octahedral Mn^{IV} sites which are related by symmetry. For **4.30a**, each salen ligand coordinates one atom of manganese in the expected chelating fashion, distorting the octahedron around the metal and providing an average Mn···Mn separation of 2.74 Å. In contrast, the crystal structure of **4.30b** shows each salen ligand to coordinate two manganese atoms into a pair of oxo-bridged 7-membered rings, with a comparable Mn···Mn intermetallic distance of 2.71 Å. Bond metrics such as these are in agreement with those reported by Christou and Streib, for structurally related [Mn$_2$(μ-O)$_2$]-type complexes.[80]

On account of their sensitivity, manganese(II) salen complexes are not often isolated. In early work, Sousa and co-workers reported on the electrochemical synthesis of manganese(III) complexes of salicylaldiminates, which the authors propose form *via* their neutral manganese(II) counterparts. Taking note of our strategy to selectively prepare iron(II)-salen complexes, by removal of oxygen within the electrochemical procedure, it was assumed that this methodology

could be extended towards entrapment of manganese(II) salen products. In like manner, a Mn/Ni bimetallic anode was fitted to an electrochemical reactor under an atmosphere of argon, and precursors **P4.1**, **P4.2** and **P4.5** were each converted to their manganese(II)-salen complexes (**Scheme 4.9**, left-hand path). Following reaction, each product (**4.35 – 4.37**) formed as a highly air-sensitive pale orange/brown suspension which could be isolated by cannula filtration, in moderate yield.

All three samples were partially soluble in DMSO solvent at room temperature, allowing analysis by high-resolution mass spectrometry in the first instance. The electrospray mass spectrum of **4.35**, **4.36** and **4.37** each displayed the corresponding positive monomeric [MnL] molecular fragment, at (*m/z*) 321.0436, 375.0905 and 435.1194, respectively, though peaks were also present to represent the complexes in their oxidised form. Further solution evidence for complex formation was obtained in the form of NMR spectroscopy, which displayed virtually no information of molecular structure, though did provide a residual solvent difference in chemical shift *via* the Evans method to extract magnetic susceptibility measurements. Consistent across all, was an observed solution magnetic moment between 5.7 – 5.9 μ_B, supportive of a high-spin ($S = 5/2$) manganese(II) metal centre.

Bright yellow block crystals of the electrochemical product, **4.37**, were obtained from the slow diffusion of Et₂O vapours into a 1:1 (ᵛ/ᵥ) DCM:DMSO solution of the complex, and subsequently examined by X-ray diffraction methods to confirm the anticipated manganese(II)-salen complex (**Figure 4.20**, right).
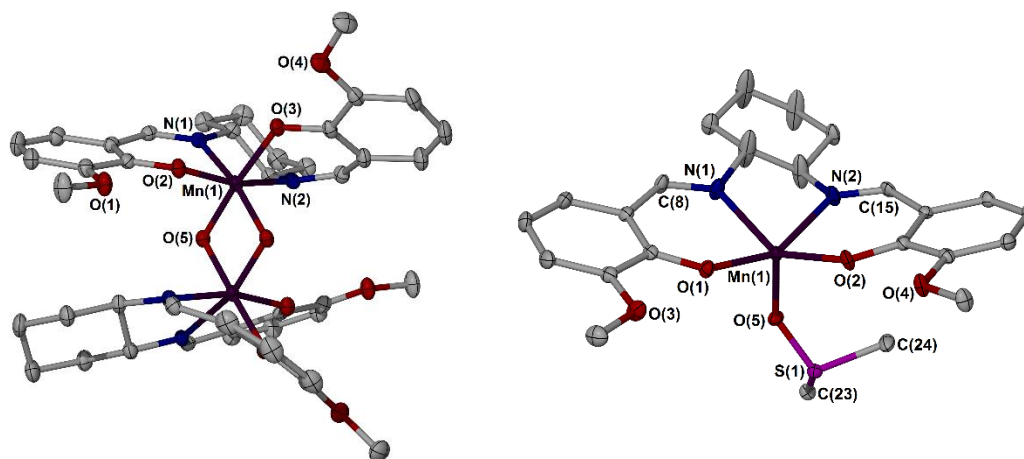
Figure 4.21 *Molecular structures of Mn^{IV} (**4.34**, left) and Mn^{II} (**4.37·DMSO**, right) complexes of ligand precursor **P4.5**. Atomic displacement parameters are drawn at the 50 % probability level, hydrogen atoms are omitted for clarity.*

4.34	Mn(1)-N(1)	2.045(3)	N(1)-Mn(1)-N(2)	79.70(13)
4.34	Mn(1)-N(2)	1.995(4)	N(1)-Mn(1)-O(2)	90.14(13)
4.34	Mn(1)-O(2)	1.897(3)	N(2)-Mn(1)-O(3)	85.14(12)
4.34	Mn(1)-O(5)	1.813(3)	Mn(1)-O(5)-Mn(1')	97.95(18)
4.37	Mn(1)-O(1)	2.047(3)	N(1)-Mn(1)-O(1)	85.48(13)
4.37	Mn(1)-O(2)	2.039(3)	O(1)-Mn(1)-O(2)	99.23(12)
4.37	Mn(1)-O(5)	2.152(3)	O(1)-Mn(1)-O(5)	110.41(12)
4.37	Mn(1)-N(1)	2.196(4)	N(1)-Mn(1)-O(2)	141.95(16)

Table 4.9 *Selected bond lengths (Å) and angles (˚) from the crystal structures of **4.34** and **4.37·DMSO**.*

Pleasingly, the crystal structure of **4.37** features a discrete, mononuclear manganese(II) metal centre, adopting square-based pyramidal geometry. About the square-base, is a tetradentate salen ligand, with one molecule of solvating DMSO binding through a fifth coordination site in the apical plane. For the benefit of comparison, the refined crystal structure of direct manganese(IV) analogue, **4.34**, is provided adjacent in **Figure 4.20**.

4.8   Conclusions and future work

A simple electrochemical protocol has been developed for the synthesis of various Schiff base metal complexes, which cleanly releases gaseous H_2 as the only side-product. The procedure is highly versatile, representing a 'one-size-fits-all' approach towards imine- and amine-*bis*(phenolate) base metal complexes which require minimal effort to isolate and purify. In doing so, broad application has been demonstrated through the preparation of 34 complexes under mild and ambient conditions.

Employment of metallic copper, nickel or zinc as sacrificial anode allowed access to a range of their corresponding metal(II) Schiff base complexes. Synthetic practicality was supplemented by the tolerance of hydrous solvents and an aerobic atmosphere within their syntheses. Once formed, the organometallic products were insoluble in the reaction solvent, allowing for straightforward isolation in synthetically useful yields.

Dissolution of an iron plate anode under analogous conditions led to the isolation of dinuclear iron(III) examples, which exist *via* a *μ*-oxo bridge between each metal centre. Deoxygenation of the reaction conditions allowed entrapment of the preceding iron(II) Schiff base complexes, which were unambiguously distinguished by single crystal X-ray diffraction analysis.

Extension of the synthetic model was demonstrated by the use of a bimetallic anodic alloy, comprising both elemental manganese and nickel. By tuning electrical potential, the selective liberation of manganese ions from this surface was achieved, to produce a variety of dimeric

manganese(IV)-salen adducts which are supported by *bis(μ-oxo)* bridging groups. Overlaying selective ion release with the removal of oxygen from the system, the corresponding manganese(II)-salen complexes were obtained exclusively.

To the authors knowledge, the concept of selectively dissolving mixed-metal materials in a manner which is restricted by both electrical potential and reaction stoichiometry is unprecedented. The expansion of this model towards the generation of organometallic molecules of various oxidation state, in a well-understood and fully controlled fashion, represents synthetic methodology which can be extended towards a broad array of metal/ligand combinations.

Future work in this area should involve an investigation into the isolation of metal complexes of unusual, or inaccessible oxidation states. For example, detailed within is a brief summary of Sousa's findings regarding the electrochemical efficiency associated with forming copper(II)-*bis*(phenolate) complexes. In turn, it should be feasible to modify the electrochemical reaction conditions such that copper(I) ligated complexes are isolated *en route* to their higher oxidation congeners. Subsequent deployment of these complexes as catalysts would be expected to attract a wide audience.

4.9   Experimental

Where stated, manipulations were performed under an atmosphere of dry nitrogen or argon by means of standard Schlenk line or glovebox techniques. Anhydrous solvents were prepared by passing the solvent over activated alumina to remove water, copper catalyst to remove oxygen and molecular sieves to remove any remaining water, *via* the Dow-Grubbs solvent system. Deuterated $CDCl_3$, CD_3CN and C_6D_6 were dried over CaH_2, cannula filtered or distilled, and then freeze-pump-thaw degassed prior to use

Cu foil (99.9 % purity), Ni foil (99.5 % purity), Zn sticks (99.9 % purity, complexometric standard), Fe foil (99.5 % purity) and Mn/Ni foil (Mn 88/Ni 12) were used as electrode surfaces directly without further purification (purchased from Goodfellow Cambridge Ltd).

Salan ligand precursors *N,N'-bis*(3,5-*tert*-butylsalicyl)-1,2-ethylenedimethylamine **P4.7** and *N,N'-bis*(3,5-*tert*-pentylsalicyl)-1,2-ethylenedimethylamine **P4.8** were synthesised according to literature procedures.[28] All other chemicals were obtained from commercial sources and used as received. Commercially available AAS standard solutions were purchased as 1000 $mgmL^{-1}$ stock and diluted as required using ultra-pure water.

A PSD 30/3B high performance digital power supply was used in constant voltage mode (CV), with current measurements recorded by a 15XP-B Amprobe digital multimeter, at a milliampere scale.

4.9.1 Instrumentation

^{1}H and ^{13}C NMR spectra were recorded by automated procedures on either a Bruker Avance (500/125 MHz) or DPX (300/75 MHz) NMR spectrometer, using the residual solvent as an internal standard. The values of chemical shift are reported in parts per million (ppm) with the multiplicities of the spectra assigned as follows: singlet (s), doublet (d), triplet (t), quartet (q), multiplet (m) and broad (br), values for coupling constants (J) are assigned in Hz. High-resolution electrospray mass spectra (ESI-MS) were measured on an open-access Bruker Daltonics (micro TOF) instrument operating in the electrospray mode. Samples for microanalysis were dried under vacuum prior to analysis and the elemental composition determined by Ms. Tanya Marinko-Covell of the University of Leeds Microanalytical Service using a Carlo Erba elemental analyser MOD 1106 spectrometer. Atomic absorption spectroscopy (AAS) measurements were performed using a Perkin-Elmer Atomic Absorption Spectrometer AAnalyst 400, operating with an air-acetylene flame, by Dr Alexander Kulak of the University of Leeds. X-ray fluorescence (XRF) analysis was obtained by Professor Ian Fairlamb at the University of York on a Horiba XGT7000 X-ray analytical microscope instrument using a partial vacuum.

Electrochemical measurements were conducted using an Autolab PGSTAT20 voltammetric analyser under an argon atmosphere, solvated in pre-dried CH_3CN containing 0.10 M [^{n}Bu$_4$N]BF$_4$ as supporting electrolyte. Voltammetric experiments utilised a Pt disk working electrode, a Pt rod auxiliary electrode and a Ag/AgCl reference electrode. All potentials quoted are referenced to an internal ferrocene/ferrocenium standard and were obtained at a scan rate (v) of 400 mVs^{-1}. The ferrocene/ferrocenium couple under these conditions was observed at +0.40 $\leq E_{1/2} \leq$ 0.55 V vs Ag/AgCl, providing observed reduction potentials of **P4.1 – P4.5** which are listed in **Table 4.1**.

X-ray diffraction data were collected on an Agilent SuperNova diffractometer fitted with an Atlas CCD detector with Mo Kα radiation (λ = 0.7107 Å) or Cu Kα radiation (λ = 1.5418 Å). Crystals were mounted under oil on nylon fibres. Data sets were corrected for absorption using a multiscan method, and the structures were solved by direct methods using SHELXS-97 or SHELXT and refined by full-matrix least squares on F^2 using ShelXL-97, interfaced through the program Olex2.[81] Molecular graphics for all structures were generated using POV-RAY in the X-Seed program.

4.9.2 Preparation of Schiff base ligands

Synthesis of *N,N'-bis*(salicylidene)ethylenediamine (P4.1). Salicylaldehyde (4.50 mL, 41.0 mmol) and ethylenediamine (1.40 mL, 20.5 mmol) were stirred vigorously in refluxing ethanol (50 mL) for 30 minutes. The resulting yellow solution was cooled to 0 ˚C, upon which a bright yellow precipitate formed which was collected by vacuum filtration, washed with cold ethanol (10 mL) followed by diethyl ether (3 × 30 mL) and dried under vacuum to deliver the title compound as a microcrystalline yellow solid. Yield: 3.45 g, 12.9 mmol, 63 %. ^{1}H NMR (300 MHz, CDCl$_3$) δ (ppm) 13.19 (br s, 2H, O*H*), 8.36 (s, 2H, C*H*=N), 7.32 – 7.22 (m, 4H, ar*H*), 6.96 – 6.83 (m, 4H, ar*H*), 3.94 (s, 4H, NC*H$_2$*C*H$_2$*N). ^{13}C{H} NMR (75 MHz, CDCl$_3$) δ (ppm) 166.7, 161.2, 132.5, 131.6, 118.8, 118.6, 117.1, 59.9. HR-MS (ESI$^+$): *m/z* 269.1274 [C$_{16}$H$_{17}$N$_2$O$_2$]$^+$, calcd. [M + H]$^+$ 269.1285. All data are consistent with the literature.[27]

Synthesis of *trans-N,N'-bis*(salicylidene)-1,2-cyclohexanediamine (P4.2). Salicylaldehyde (4.50 mL, 41.0 mmol) and (±)-*trans*-1,2-diaminocyclohexane (2.50 mL, 20.5 mmol) were stirred vigorously in refluxing ethanol (50 mL) for 30 minutes. The resulting yellow solution was cooled to 0 ˚C, upon which a bright yellow precipitate formed which was collected by vacuum filtration, washed with cold ethanol (10 mL) followed by diethyl ether (3 × 30 mL) and dried under vacuum to deliver the title compound as a microcrystalline yellow solid. Yield: 6.52 g, 20.2 mmol, 99 %. ^{1}H NMR (300 MHz, CDCl$_3$) δ (ppm) 13.30 (br s, 2H, O*H*), 8.26 (s, 2H, C*H*=N), 7.27 – 7.21 (m, 2H, ar*H*), 7.16 (d, *J* = 0.6 Hz, 1H, ar*H*), 7.13 (d, *J* = 0.6 Hz, 1H, ar*H*), 6.89 (m, 2H, ar*H*), 6.79 (td, *J* = 15.0, 7.5, 0.6 Hz, 2H, ar*H*), 3.36 – 3.27 (m, 2H, NC*H*), 1.97 – 1.44 (m, 8H, cy*H*). ^{13}C{H} NMR (75 MHz, CDCl$_3$) δ (ppm) 164.8, 161.1, 132.3, 131.6, 118.8, 118.7, 116.9, 72.8, 33.2, 24.3. HR-MS (ESI$^+$): *m/z* 323.1755 [C$_{20}$H$_{23}$N$_2$O$_2$]$^+$, calcd. [M + H]$^+$ 323.1754. All data are consistent with the literature.[27]

Synthesis of *N,N'-bis*(salicylidene)-1,2-phenylenediamine (P4.3). Salicylaldehyde (4.50 mL, 41.0 mmol) and *o*-phenylenediamine (2.18 g, 20.5 mmol) were stirred vigorously in refluxing ethanol (50 mL) for 15 minutes. The resulting orange suspension was cooled to 0 ˚C, upon which a bright orange precipitate formed which was collected by vacuum filtration, washed with cold ethanol (10 mL) followed by diethyl ether (3 × 30 mL) and dried under vacuum to deliver the title compound as a microcrystalline orange solid. Yield: 5.76 g, 18.2 mmol, 89 %. ^{1}H NMR (500 MHz, CDCl$_3$) δ (ppm) 12.91 (br s, 2H, O*H*), 8.53 (s, 2H, C*H*=N), 7.29 – 7.21 (m, 6H, ar*H*), 7.16 – 7.11 (m, 2H, ar*H*), 6.95 – 6.93 (m, 2H, ar*H*), 6.81 (td, *J* = 25.0, 12.5, 1.5 Hz, 2H, ar*H*). ^{13}C{H} NMR (75 MHz, CDCl$_3$) δ (ppm) 163.8, 161.4, 142.6, 133.4, 132.4, 127.8, 119.8, 119.3, 119.1, 117.6. HR-MS (ESI$^+$): *m/z* 317.1299 [C$_{20}$H$_{17}$N$_2$O$_2$]$^+$, calcd. [M + H]$^+$ 317.1285. All data are consistent with the literature.[27]

Figure 4.21 (see below) illustrates a full-sweep cyclic voltammogram of **P4.3**. All potentials quoted are referenced to an internal ferrocene/ferrocenium standard and were obtained at a scan rate (v) of 400 mVs^{-1}. The ferrocene/ferrocenium couple under these conditions was observed at $+0.40 \leq E_{1/2} \leq 0.55$ V vs Ag/AgCl, providing an observed reduction potential of **P4.3** at -2.13 V (vs Fc/Fc$^+$).
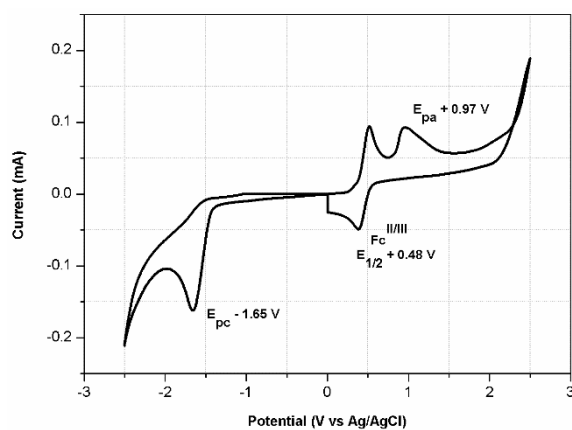
Figure 4.22 *Cyclic voltammogram of* ***P4.3*** *(1.0 mM) in non-aqueous media* *($CH_3CN/[^nBu_4N]BF_4$ 0.10 M), $v = 400$ mVs^{-1}, $T = 298$ K, [Fc] = 1.0 mM, E_{pa} ascribed to* *phenolate oxidation band.*

Synthesis of *N,N'-bis(o*-vanillidene)ethylenediamine (P4.4). *O*-Vanillin (3.00 g, 19.7 mmol) and ethylenediamine (0.66 mL, 9.86 mmol) were stirred vigorously in refluxing ethanol (50 mL) for 15 minutes. The resulting yellow solution was cooled to 0 ˚C, upon which a bright yellow precipitate formed which was collected by vacuum filtration, washed with cold ethanol (10 mL) followed by diethyl ether (3 × 30 mL) and dried under vacuum to deliver the title compound as a microcrystalline yellow solid. Yield: 2.90 g, 9.86 mmol, quant.. ^{1}H NMR (500 MHz, CDCl$_3$) δ (ppm) 13.22 (br s, 2H, O*H*), 8.30 (s, 2H, C*H*=N), 6.89 (dd, *J* = 7.5, 1.5 Hz, 2H, ar*H*), 6.83 (dd, *J* = 7.5, 1.5 Hz, 2H, ar*H*), 6.77 – 6.74 (m, 2H, ar*H*), 3.93 (s, 4H, NC*H*$_2$C*H*$_2$N), 3.86 (s, 6H, OC*H*$_3$). ^{13}C{H} NMR (75 MHz, CDCl$_3$) δ (ppm) 165.6, 150.4, 147.3, 122.1, 117.4, 117.0, 113.1, 58.4, 55.0. HR-MS (ESI$^+$): *m/z* 329.1400 [C$_{18}$H$_{21}$N$_2$O$_4$]$^+$, calcd. [M + H]$^+$ 329.1496. All data are consistent with the literature.[82]

Synthesis of *trans-N,N'-bis(o*-vanillidene)-1,2-cyclohexanediamine (P4.5). *O*-Vanillin (3.00 g, 19.7 mmol) and (±)-*trans*-1,2-diaminocyclohexane (1.20 mL, 9.86 mmol) were stirred vigorously in refluxing ethanol (50 mL) for 30 minutes. The resulting yellow solution was cooled to 0 ˚C, upon which a bright yellow precipitate formed which was collected by vacuum filtration, washed with cold ethanol (10 mL) followed by diethyl ether (3 × 30 mL) and dried under vacuum to deliver the title compound as a microcrystalline yellow solid. Yield: 2.79 g, 8.29 mmol, 84 %. ^{1}H NMR (300 MHz, CDCl$_3$) δ (ppm) 13.83 (br s, 2H, O*H*), 8.24 (s, 2H, C*H*=N), 6.86 (dd, *J* = 7.8, 1.8 Hz, 2H, ar*H*), 6.79 (dd, *J* = 7.8, 1.8 Hz, 2H, ar*H*), 6.74 − 6.69 (m, 2H, ar*H*), 3.86 (s, 6H,

OCH_3), 3.34 – 3.27 (m, 2H, NCH), 1.97 – 1.86 (m, 4H, cy$H$), 1.77 – 1.70 (m, 2H, cy$H$), 1.57 – 1.25 (m, 2H, cy$H$). ^{13}C{H} NMR (75 MHz, CDCl$_3$) δ (ppm) 164.9, 151.7, 148.4, 123.3, 118.5, 118.0, 114.0, 72.5, 56.1, 33.2, 24.2. HR-MS (ESI$^+$): m/z 383.1943 [C$_{22}$H$_{27}$N$_2$O$_4$]$^+$, calcd. [M + H]$^+$ 383.1965. All data are consistent with the literature.[82]

Synthesis of *N,N'-bis*(vanillidene)-1,2-diphenyl-1,2-ethylenediamine (P4.6). *O*-Vanillin (3.00 g, 19.7 mmol) and (1*S*,2*S*)-(-)-1,2-diphenylethylenediamine (2.09 g, 9.86 mmol) were stirred vigorously in refluxing ethanol (50 mL) for 16 hours. The resulting yellow solution was cooled to 0 ˚C, upon which a bright yellow precipitate formed which was collected by vacuum filtration, washed with hot ethanol (10 mL) followed by diethyl ether (3 × 30 mL) and dried under vacuum to deliver the title compound as a yellow solid. Yield: 1.43 g, 3.82 mmol, 39 %. ^{1}H NMR (300 MHz, CDCl$_3$) δ (ppm) 13.79 (br s, 2H, OH), 8.35 (s, 2H, CH=N), 7.20 – 7.12 (m, 12H, ar$H$), 6.89 – 6.65 (m, 4H, ar$H$), 3.88 (s, 2H, NCH), 2.16 (s, 6H, OCH_3). ^{13}C{H} NMR (75 MHz, CDCl$_3$) δ (ppm) 207.1, 166.1, 128.5, 128.3, 128.0, 127.8, 123.6, 118.5, 114.4, 80.5, 56.2, 31.0. HR-MS (ESI$^+$): m/z 481.2101 [C$_{30}$H$_{29}$N$_2$O$_4$]$^+$, calcd. [M + H]$^+$ 481.2122. All data are consistent with the literature.[83]

4.9.3   Preparation of copper(II) salen complexes

General procedure. A three-necked round bottomed flask equipped with stirrer bar was charged with salen ligand precursor (1.0 mmol), ^{n}Bu$_4$NBF$_4$ (0.03 mmol) and acetonitrile (50 mL). Two copper electrodes (30 × 10 × 1 mm) were introduced to the solution and a potential applied *via* an external power supply (22.0 – 25.0 V, operating in CV mode) to maintain a constant current of 50.0 mA for 90 minutes. The resulting precipitate was collected by vacuum filtration, washed with dichloromethane (2 × 10 mL), water (2 × 30 mL) diethyl ether (3 × 30 mL) and dried under vacuum to deliver the corresponding Cu^{II}-salen complex as a microcrystalline solid.

Synthesis of copper(II) salen complex (4.1). Salen precursor **P4.1** was reacted according to the general procedure, affording the product as a dark green solid. Yield: 0.26 g, 0.79 mmol, 79 %. Mp decomp. >170 ˚C. HR-MS (ESI$^+$): m/z 330.0461 [C$_{16}$H$_{15}$CuN$_2$O$_2$]$^+$, calcd. [M + H]$^+$ 330.0424. Anal. calcd. (%) for C$_{16}$H$_{14}$N$_2$O$_2$Cu.^{1}/$_3$CH$_2$Cl$_2$: C 54.14, H 4.10, N 7.80; found C 54.00, H 4.10, N 7.70.

Synthesis of copper(II) salen complex (4.2). Salen precursor **P4.2** was reacted according to the general procedure, affording the product as a purple solid. Yield: 0.21 g, 0.54 mmol, 54 %. Mp decomp. >150 ˚C. HR-MS (ESI$^+$): m/z 384.0909 [C$_{20}$H$_{21}$CuN$_2$O$_2$]$^+$, calcd. [M + H]$^+$ 384.0894. Anal. calcd. (%) for C$_{20}$H$_{20}$N$_2$O$_2$Cu.^{1}/$_3$H$_2$O: C 61.61, H 5.34, N 7.19; found C 61.21, H 5.20, N 7.00.

Synthesis of copper(II) salen complex (4.3). Salen precursor **P4.3** was reacted according to the general procedure, affording the product as a dark brown solid. Yield: 0.31 g, 0.81 mmol, 81 %. Mp decomp. >180 ˚C. HR-MS (ESI$^+$): m/z 378.0427 $[C_{20}H_{15}CuN_2O_2]^+$, calcd. $[M + H]^+$ 378.0424. Anal. calcd. (%) for $C_{20}H_{14}N_2O_2Cu$: C 63.57, H 3.73, N 7.41; found C 63.40, H 3.70, N 7.30.

Synthesis of copper(II) salen complex (4.4). Salen precursor **P4.4** was reacted according to the general procedure, affording the product as a dark green solid. Yield: 0.34 g, 0.86 mmol, 86 %. Mp decomp. >155 ˚C. HR-MS (ESI$^+$): m/z 390.0640 $[C_{18}H_{19}CuN_2O_4]^+$, calcd. $[M + H]^+$ 390.0635. Anal. calcd. (%) for $C_{18}H_{18}N_2O_4Cu.H_2O$: C 53.00, H 4.94, N 6.87; found C 52.60, H 4.90, N 6.80.

Synthesis of copper(II) salen complex (4.5). Salen precursor **P4.5** was reacted according to the general procedure, affording the product as a dark purple solid. Yield: 0.35 g, 0.78 mmol, 78 %. Mp decomp. >150 ˚C. HR-MS (ESI$^+$): m/z 444.1109 $[C_{22}H_{25}CuN_2O_4]^+$, calcd. $[M + H]^+$ 444.1105. Anal. calcd. (%) for $C_{22}H_{24}N_2O_4Cu.H_2O$: C 57.19, H 5.67, N 6.06; found C 57.00, H 5.65, N 6.00.

Synthesis of copper(II) salen complex (4.6). Salen precursor **P4.6** was reacted according to the general procedure, affording the product as a pale green solid. Yield: 0.31 g, 0.58 mmol, 58 %. Mp decomp. >180 ˚C. HR-MS (ESI$^+$): m/z 542.1276 $[C_{30}H_{27}CuN_2O_4]^+$, calcd. $[M + H]^+$ 542.1261. Anal. calcd. (%) for $C_{30}H_{26}N_2O_4Cu.^1/_3CH_2Cl_2$: C 63.90, H 4.71, N 4.91; found C 63.80, H 4.90, N 4.80.

4.9.4   Preparation of copper(II) salan complexes

General procedure. A three-necked round bottomed flask equipped with stirrer bar was charged with salan ligand precursor (1.0 mmol), $^nBu_4NBF_4$ (0.03 mmol), acetonitrile (50 mL) and heated to 40 ˚C until full dissolution was achieved, upon which the solution was allowed to cool to ambient temperature. Two copper electrodes (30 × 10 × 1 mm) were introduced to the solution and a potential applied *via* an external power supply (22.0 – 25.0 V, operating in CV mode) to maintain a constant current of 50.0 mA for 90 minutes. The resulting precipitate was collected by vacuum filtration, washed with dichloromethane (2 × 10 mL), water (2 × 30 mL) diethyl ether (3 × 30 mL) and dried under vacuum to deliver the corresponding Cu^{II}-salan complex as a microcrystalline solid.

Synthesis of copper(II) salan complex (4.7). Salan precursor **P4.7** was reacted according to the general procedure, affording the product as a dark green solid. Green needles suitable for X-ray crystallographic analysis were grown *via* slow evaporation of a concentrated CH_2Cl_2 solution of the complex. Yield: 0.44 g, 0.75 mmol, 75 %. Mp decomp. >180 ˚C. HR-MS (ESI$^+$): m/z 586.3575 $[C_{34}H_{55}CuN_2O_2]^+$, calcd. $[M + H]^+$ 586.3554. Anal. calcd. (%) for $C_{34}H_{54}N_2O_2Cu.^2/_3CH_2Cl_2$: C 64.80, H 8.68, N 4.36; found C 64.40, H 8.30, N 4.10.

Synthesis of copper(II) salan complex (4.8). Salan precursor **P4.8** was reacted according to the general procedure, affording the product as a dark green solid. Green needles suitable for X-ray crystallographic analysis were grown *via* slow evaporation of a concentrated CH_2Cl_2 solution of the complex. Yield: 0.53 g, 0.83 mmol, 83 %. Mp decomp. >150 ˚C. HR-MS (ESI⁺): *m/z* 642.4202 $[C_{38}H_{63}CuN_2O_2]^+$, calcd. $[M + H]^+$ 642.4180. Anal. calcd. (%) for $C_{38}H_{62}N_2O_2Cu.H_2O$: C 69.10, H 9.77, N 4.24; found C 69.00, H 9.80, N 4.15.

4.9.5 Preparation of nickel(II) salen complexes

General procedure. A three-necked round bottomed flask equipped with stirrer bar was charged with salen ligand precursor (1.0 mmol), $^nBu_4NBF_4$ (0.03 mmol) and acetonitrile (50 mL) [*N.B.* product yields were much improved by use of anhydrous solvent, whilst an atmosphere of N_2 *vs* air did not affect yield]. Two nickel electrodes (30 × 10 × 1 mm) were introduced to the solution and a potential applied *via* an external power supply (22.0 – 25.0 V, operating in CV mode) to maintain a constant current of 50.0 mA for 90 minutes. The resulting precipitate was collected by vacuum filtration, washed with dichloromethane (2 × 10 mL) followed by diethyl ether (3 × 30 mL) to give the crude product as a hygroscopic brown/red solid. Recrystallisation of the crude product from dichloromethane/diethyl ether delivered the corresponding Ni^{II}-salen complex as a microcrystalline solid.

Synthesis of nickel(II) salen complex (4.9). Salen precursor **P4.1** was reacted according to the general procedure, affording the product as a light brown solid. Yield: 0.30 g, 0.91 mmol, 91 %. Mp decomp. >300 ˚C. ^{1}H NMR (300 MHz, CD$_3$CN) δ (ppm) 9.66 (s, 2H, C*H*=N), 7.50 (d, *J* = 9.0 Hz, 2H, ar*H*), 7.35 (t, *J* = 16.8, 9.0 Hz, 2H, ar*H*), 6.85 (t, *J* = 16.8, 9.0 Hz, 2H, ar*H*), 6.76 (d, *J* = 9.0 Hz, 2H, ar*H*), 3.09 (s, 4H, NC*H₂*C*H₂*N). ^{13}C{H} NMR (75 MHz, CDCl₃) δ (ppm) 166.5, 162.0, 132.4, 131.5, 129.9, 118.8, 118.7, 59.8. HR-MS (ESI⁺): *m/z* 325.0483 $[C_{16}H_{15}NiN_2O_2]^+$, calcd. $[M + H]^+$ 325.0482. Anal. calcd. (%) for $C_{16}H_{14}N_2O_2Ni$: C 59.13, H 4.34, N 8.62; found C 59.10, H 4.20, N 8.40.

Synthesis of nickel(II) salen complex (4.10). Salen precursor **P4.2** was reacted according to the general procedure, affording the product as a light red solid. Pale orange needles suitable for X-ray crystallographic analysis were grown *via* the slow diffusion of Et₂O vapours into a concentrated CH_2Cl_2 solution of the complex. Yield: 0.32 g, 0.84 mmol, 84 %. Mp decomp. >300 ˚C. ^{1}H NMR (300 MHz, CDCl₃) δ (ppm) 7.32 (bs, 2H, C*H*=N), 7.19 (t, *J* = 12.9, 5.7 Hz, 2H, ar*H*), 7.02 – 6.99 (m, 4H, ar*H*), 6.51 (t, *J* = 12.9, 5.7 Hz, 2H, ar*H*), 3.24 – 3.19 (m, 2H, NC*H*), 2.44 – 2.38 (m, 2H, cy*H*), 1.96 – 1.89 (m, 2H, cy*H*), 1.39 – 1.27 (m, 4H, cy*H*). ^{13}C{H} NMR (75 MHz, CDCl₃) δ (ppm) 177.3, 168.6, 139.0, 132.7, 122.6, 119.4, 110.5, 64.5, 27.7, 23.9. HR-MS (ESI⁺): *m/z* 379.0940 $[C_{20}H_{21}NiN_2O_2]^+$, calcd. $[M + H]^+$ 379.0951. Anal. calcd. (%) for $C_{20}H_{20}N_2O_2Ni.^3/_4H_2O$: C 61.19, H 5.52, N 7.14; found C 61.20, H 5.20, N 7.00.

Synthesis of nickel(II) salen complex (4.11). Salen precursor **P4.3** was reacted according to the general procedure, affording the product as a light red solid. Yield: 0.30 g, 0.80 mmol, 80 %. Mp decomp. >300 ˚C. ^{1}H NMR (300 MHz, CDCl$_3$) δ (ppm) 8.27 (bs, 2H, C*H*=N), 7.75 − 7.71 (m, 2H, ar*H*), 7.35 − 7.32 (m, 4H, ar*H*), 7.20 − 7.18 (m, 4H, ar*H*), 6.67 (t, *J* = 14.1, 7.5 Hz, 2H, ar*H*). ^{13}C{H} NMR (75 MHz, CDCl$_3$) δ (ppm) 166.0, 161.8, 134.4, 131.2, 130.9, 126.9, 121.5, 119.4, 116.8, 112.0. HR-MS (ESI$^+$): *m/z* 373.0482 [C$_{20}$H$_{15}$NiN$_2$O$_2$]$^+$, calcd. [M + H]$^+$ 373.0482. Anal. calcd. (%) for C$_{20}$H$_{14}$N$_2$O$_2$Ni.H$_2$O: C 61.43, H 4.12, N 7.16; found C 61.20, H 3.80, N 6.95.

Synthesis of nickel(II) salen complex (4.12). Salen precursor **P4.4** was reacted according to the general procedure, affording the product as a light orange solid. Yield: 0.30 g, 0.77 mmol, 77 %. Mp decomp. >300 ˚C. ^{1}H NMR (500 MHz, CDCl$_3$) δ (ppm) 7.46 (s, 2H, C*H*=N), 6.67 − 6.65 (m, 4H, ar*H*), 6.44 (t, *J* = 15.0, 8.0 Hz, 2H, ar*H*), 3.79 (s, 6H, OC*H$_3$*), 3.42 (s, 4H, NC*H$_2$*C*H$_2$*N). ^{13}C{H} NMR (125 MHz, CDCl$_3$) δ (ppm) 161.6, 156.5, 151.3, 123.1, 119.5, 114.0, 112.4, 58.4, 55.3. HR-MS (ESI$^+$): *m/z* 385.0697 [C$_{18}$H$_{19}$NiN$_2$O$_4$]$^+$, calcd. [M + H]$^+$ 385.0693. Anal. calcd. (%) for C$_{18}$H$_{18}$N$_2$O$_4$Ni: C 56.15, H 4.71, N 7.28; found C 55.80, H 4.70, N 7.20.

Synthesis of nickel(II) salen complex (4.13). Salen precursor **P4.5** was reacted according to the general procedure, affording the product as a light brown solid. Pale brown needles suitable for X-ray crystallographic analysis were grown *via* the slow diffusion of Et$_2$O vapours into a concentrated CH$_2$Cl$_2$ solution of the complex. Yield: 0.39 g, 0.88 mmol, 88 %. Mp decomp. >300 ˚C. ^{1}H NMR (300 MHz, CDCl$_3$) δ (ppm) 7.12 (s, 2H, C*H*=N), 6.63 (dd, *J* = 7.5, 1.5 Hz, 2H, ar*H*), 6.49 (dd, *J* = 7.5, 1.5 Hz, 2H, ar*H*), 6.34 (m, 2H, ar*H*), 3.75 (s, 6H, OC*H$_3$*), 3.20 (m, 2H, NC*H*), 2.28 (m, 2H, cy*H*), 1.83 (m, 2H, cy*H*), 1.36 − 1.18 (m, 4H, cy*H*). ^{13}C{H} NMR (125 MHz, CDCl$_3$) δ (ppm) 168.2, 155.7, 144.1, 123.3, 120.2, 118.9, 111.0, 72.5, 55.5, 33.2, 20.2. HR-MS (ESI$^+$): *m/z* 439.1168 [C$_{22}$H$_{25}$NiN$_2$O$_4$]$^+$, calcd. [M + H]$^+$ 439.1162. Anal. calcd. (%) for C$_{22}$H$_{24}$N$_2$O$_4$Ni.H$_2$O: C 57.80, H 5.73, N 6.13; found C 57.90, H 5.50, N 5.75.

4.9.6   Preparation of zinc(II) salen complexes

General procedure. A three-necked round bottomed flask equipped with stirrer bar was charged with salen precursor (1.0 mmol), ^{n}Bu$_4$NBF$_4$ (0.03 mmol) and acetonitrile (50 mL). Two zinc electrodes (30 mm length, 6 mm dia.) were introduced to the solution and a potential applied *via* an external power supply (22.0 − 25.0 V, operating in CV mode) to maintain a constant current of 50.0 mA for 90 minutes. The resulting precipitate was collected by vacuum filtration, washed with acetonitrile (2 × 10 mL), water (2 × 30 mL) followed by diethyl ether (3 × 30 mL) and dried under vacuum to deliver the corresponding Zn^{II}-salen complex as a hygroscopic off-white solid.

Synthesis of zinc(II) salen complex (4.14). Salen precursor **P4.1** was reacted according to the general procedure, affording the product as a pale yellow solid. Yield: 0.29 g, 0.88 mmol, 88 %. ^{1}H NMR (500 MHz, d_6-DMSO) δ (ppm) 8.43 (s, 2H, CH=N), 7.15 - 7.10 (m, 4H, ar$H$), 6.62 (d, J = 14.0 Hz, 2H, ar$H$), 6.42 (t, J = 14.0 Hz, 2H, ar$H$), 3.72 (s, 4H, NCH_2CH_2N). ^{13}C{H} NMR (75 MHz, d_6-DMSO) δ (ppm) 171.0, 168.0, 134.8, 132.8, 122.7, 119.4, 112.2, 55.8. HR-MS (ESI$^+$): m/z 331.0418 [$C_{16}H_{15}ZnN_2O_2$]$^+$, calcd. [M + H]$^+$ 331.0420. Anal. calcd. (%) for $C_{16}H_{14}N_2O_2Zn$: C 57.94, H 4.25, N 8.45; found C 57.90, H 4.30, N 8.40.

Synthesis of zinc(II) salen complex (4.15). Salen precursor **P4.2** was reacted according to the general procedure, affording the product as an off-white solid. Yield: 0.30 g, 0.79 mmol, 79 %. ^{1}H NMR (500 MHz, d_6-DMSO) δ (ppm) 8.33 (s, 2H, CH=N), 7.23 (dd, J = 12.0, 2.5 Hz, 2H, ar$H$), 7.13 (td, J = 15.6, 12.0, 2.5 Hz, 2H, ar$H$), 6.63 (d, J = 15.6 Hz, 2H, ar$H$), 6.42 (t, J = 15.6 Hz, 2H, ar$H$), 3.19 (m, 2H, cy$H$), 2.45 (m, 2H, cy$H$), 1.91 (m, 2H, cy$H$), 1.38 (m, 4H, cy$H$). ^{13}C{H} NMR (75 MHz, d_6-DMSO) δ (ppm) 170.9, 164.6, 135.4, 132.7, 122.6, 119.3, 112.2, 64.5, 27.7, 23.9. HR-MS (ESI$^+$): m/z 385.0887 [$C_{20}H_{21}ZnN_2O_2$]$^+$, calcd. [M + H]$^+$ 385.0889. Anal. calcd. (%) for $C_{20}H_{22}N_2O_2Zn.^1/_2H_2O$: C 60.85, H 5.36, N 7.10; found C 61.00, H 5.20, N 7.00.

Synthesis of zinc(II) salen complex (4.16). Salen precursor **P4.3** was reacted according to the general procedure, affording the product as a pale yellow solid. Yield: 0.35 g, 0.93 mmol, 93 %. ^{1}H NMR (500 MHz, d_6-DMSO): δ (ppm) 9.01 (s, 2H, CH=N), 7.91 – 7.89 (m, 2H, ar$H$), 7.42 – 7.38 (m, 4H, ar$H$), 7.25 (td, J = 1.5, 6.5, 15.0 Hz, 2H, ar$H$), 6.72 (d, J = 15.0 Hz, 2H, ar$H$), 6.51 (t, J = 6.5, 15.0 Hz, 2H, ar$H$). ^{13}C{H} NMR (75 MHz, d_6-DMSO): δ (ppm) 172.2, 162.8, 139.3, 136.2, 134.3, 127.2, 123.1, 119.4, 116.4, 112.9. HR-MS (ESI$^+$): m/z 379.0420 [$C_{20}H_{15}ZnN_2O_2$]$^+$, calcd. [M + H]$^+$ 379.0417. Anal. calcd. (%) for $C_{20}H_{17}N_2O_3Zn$: C 60.30, H 4.05, N 7.04; found C 59.90, H 4.10, N 6.80.

Synthesis of zinc(II) salen complex (4.17). Salen precursor **P4.4** was reacted according to the general procedure, affording the product as a colourless solid. Yield: 0.30 g, 0.77 mmol, 77 %. ^{1}H NMR (500 MHz, d_6-DMSO) δ (ppm) 8.42 (s, 2H, CH=N), 6.78 – 6.76 (m, 4H, ar$H$), 6.36 – 6.33 (m, 2H, ar$H$), 3.72 (s, 6H, OCH_3), 3.71 (s, 4H, NCH_2CH_2N). ^{13}C{H} NMR (75 MHz, d_6-DMSO) δ (ppm) 168.0, 162.1, 152.5, 126.1, 118.5, 113.0, 110.9, 56.0, 55.0. HR-MS (ESI$^+$): m/z 469.0772 [$C_{18}H_{19}ZnN_2O_4$ + DMSO]$^+$, calcd. [M + H]$^+$ 469.0770. Anal. calcd. (%) for $C_{18}H_{20}N_2O_5Zn$: C 52.76, H 4.92, N 6.84; found C 52.40, H 4.90, N 6.70.

Synthesis of zinc(II) salen complex (4.18). Salen precursor **P4.5** was reacted according to the general procedure, affording the product as an off-white solid. Colourless blocks suitable for X-ray crystallographic analysis were grown upon standing of a concentrated DMSO solution of the complex. Yield: 0.42 g, 0.94 mmol, 94 %. ^{1}H NMR (500 MHz, d_6-DMSO) δ (ppm) 8.32 (s, 2H, CH=N), 6.84 (d, J = 8.0 Hz, 2H, ar$H$), 7.78 (d, J = 8.0 Hz, 2H, ar$H$), 6.34 (t, J = 8.0, 15.0 Hz, 2H,

ar$H$), 3.72 (s, 6H, OCH_3), 3.20 – 3.18 (m, 2H, cy$H$), 2.45 – 2.43 (m, 2H, cy$H$), 1.91 – 1.90 (m, 2H, cy$H$), 1.43 – 1.30 (m, 4H, cy$H$). ^{13}C{H} NMR (75 MHz, d_6-DMSO) δ (ppm) 164.7, 151.9, 126.5, 118.2, 114.8, 111.4, 64.9, 63.9, 27.8, 23.9, 14.6. HR-MS (ESI$^+$): m/z 445.1109 [$C_{22}H_{25}ZnN_2O_4$]$^+$, calcd. [M + H]$^+$ 445.1100. Anal. calcd. (%) for $C_{22}H_{26}N_2O_5$Zn.$^1/_4$H$_2$O: C 56.42, H 5.70, N 5.98; found C 56.20, H 5.90, N 5.60.

4.9.7   Preparation of iron(III) salen complexes

General procedure. A three-necked round bottomed flask equipped with stirrer bar was charged with salen precursor (1.0 mmol), ^{n}Bu$_4$NBF$_4$ (0.03 mmol) and acetonitrile (50 mL). Two iron electrodes (30 × 10 × 1 mm) were introduced to the solution and a potential applied *via* an external power supply (22.0 – 25.0 V, operating in CV mode) to maintain a constant current of 50.0 mA for 90 minutes. In cases where the products precipitated from solution, they were collected by vacuum filtration, washed with acetonitrile (2 × 10 mL) followed by diethyl ether (3 × 30 mL) and dried *in vacuo*. Where the solution remained homogenous, volatiles were removed *in vacuo* and the residue washed with water (2 × 10 mL). The residue was subsequently dissolved in dichloromethane (5 mL) and filtered over a short path of Celite, followed by recrystallisation from dichloromethane/diethyl ether to provide the Fe^{III}-salen complex as a microcrystalline dark red powder.

Synthesis of iron(III)(OAc) salen complex (4.20). Salen precursor **P4.2** (0.20 g, 0.62 mmol) and anhydrous Fe(OAc)$_2$ (0.11 g, 0.62 mmol) were charged to a flame-dried Schlenk flask and stirred in anhydrous ethanol (10 mL) at 75 ˚C for 1 hour under an inert atmosphere. Upon slow cooling to room temperature, a dark purple microcrystalline solid precipitated from solution, which was collected by filtration under N$_2$ and washed with anhydrous hexane (2 × 15 mL). The solid was further purified by suspension in refluxing ethanol under N$_2$, followed by filtration and washing with additional hexane (3 × 20 mL) to give the Fe^{III}(salen)(OAc) complex as a microcrystalline dark purple solid. The solid was further purified by dissolution in dichloromethane (5 mL), followed by layering with an excess of hexane to afford the product as deep red/purple needles, which were suitable for X-ray crystallographic study. Yield: 0.21 g, 0.48 mmol, 77 %. HR-MS (ESI$^+$): m/z 436.1080 [$C_{22}H_{24}FeN_2O_4$]$^+$, calcd. [M + H]$^+$ 436.1209. Anal. calcd. (%) for $C_{22}H_{23}N_2O_4$Fe: C 60.71, H 5.33, N 6.64; found C 60.80, H 5.15, N 7.00.

Synthesis of iron(III) salen complex (4.21). Salen precursor **P4.1** was reacted according to the general procedure, affording the product as a dark red solid. Dark red needles suitable for X-ray crystallographic analysis were grown *via* the slow diffusion of Et$_2$O vapours into a concentrated CH$_2$Cl$_2$ solution of the complex. Yield: 0.20 g, 0.30 mmol, 59 %. Mp decomp. >180 ˚C. HR-MS (ESI$^+$): m/z 661.0828 [$C_{32}H_{28}Fe_2N_4O_5$]$^+$, calcd. [M + H]$^+$ 661.0831. Anal. calcd. (%) for $C_{32}H_{29}N_4O_5$Fe$_2$: C 56.83, H 4.17, N 8.28; found C 56.80, H 4.20, N 8.10.

Synthesis of iron(III) salen complex (4.22). Salen precursor **P4.2** was reacted according to the general procedure, affording the product as a red solid. Yield: 0.28 g, 0.37 mmol, 74 %. Mp decomp. >200 ˚C. HR-MS (ESI$^+$): m/z 769.1777 [$C_{40}H_{41}Fe_2N_4O_5$]$^+$, calcd. [M + H]$^+$ 769.1770. Anal. calcd. (%) for $C_{40}H_{40}N_4O_5Fe_2 \cdot {}^1/_4 H_2O$: C 62.15, H 5.28, N 7.25; found C 61.85, H 5.20, N 7.20.

Synthesis of iron(III) salen complex (4.23). Salen precursor **P4.3** was reacted according to the general procedure, affording the product as a dark red/brown solid. Yield: 0.26 g, 0.35 mmol, 69 %. Mp decomp. >200 ˚C. HR-MS (ESI$^+$): m/z 757.1090 [$C_{40}H_{29}Fe_2N_4O_5$]$^+$, calcd. [M + H]$^+$ 757.0831. Anal. calcd. (%) for $C_{40}H_{28}N_4O_5Fe_2 \cdot H_2O$: C 59.43, H 3.99, N 6.93; found C 59.30, H 3.80, N 6.60.

Synthesis of iron(III) salen complex (4.24). Salen precursor **P4.4** was reacted according to the general procedure, affording the product as a red/brown solid. Yield: 0.30 g, 0.39 mmol, 78 %. Mp decomp. >180 ˚C. HR-MS (ESI$^+$): m/z 781.1888 [$C_{36}H_{37}Fe_2N_4O_9$]$^+$, calcd. [M + H]$^+$ 781.1254. Anal. calcd. (%) for $C_{36}H_{36}N_4O_9Fe_2 \cdot 1^1/_2 H_2O$: C 50.84, H 4.98, N 6.59; found C 50.80, H 4.90, N 6.50.

Synthesis of iron(III) salen complex (4.25). Salen precursor **P4.5** was reacted according to the general procedure, affording the product as a dark brown solid. Yield: 0.28 g, 0.32 mmol, 64 %. Mp decomp. >200 ˚C. HR-MS (ESI$^+$): m/z 889.2180 [$C_{44}H_{49}Fe_2N_4O_9$]$^+$, calcd. [M + H]$^+$ 889.2193. Anal. calcd. (%) for $C_{44}H_{48}N_4O_9Fe_2$: C 61.54, H 5.14, N 7.14; found C 61.85, H 5.20, N 7.20.

4.9.8 Preparation of iron(II) salen complexes

General procedure. A flame-dried three-necked round bottomed flask equipped with stirrer bar was charged with salen precursor (1.0 mmol), $^nBu_4NBF_4$ (0.03 mmol) and further dried *in vacuo*. Anhydrous (anoxic) acetonitrile (50 mL) was added *via* cannula and the solution further degassed by bubbling a stream of N_2 or Ar for *ca*. 30 minutes through the solution. Two iron electrodes (30 × 10 × 1 mm) were introduced to the solution and a potential applied *via* an external power supply (22.0 − 25.0 V, operating in CV mode) to maintain a constant current of 50.0 mA for 90 minutes. The suspended violet precipitate was isolated by cannula filtration and washed with anhydrous (anoxic) acetonitrile (2 × 15 mL), followed by rinsing with anhydrous (anoxic) diethyl ether (3 × 15 mL) before drying under vacuum to deliver the corresponding Fe^{II}-salen complex as a (highly air- and moisture-sensitive) light violet powder [*N. B.* upon exposure to an atmosphere of air, the products rapidly become an orange powder, which is likely due to oxidation of the Fe centre, see **Figure 4.21**].

Synthesis of iron(II) salen complex (4.26). Salen precursor **P4.1** was reacted according to the general procedure, affording the product as a light violet solid. Yield: 0.28 g, 0.88 mmol, 88 %. μ_{eff} = 5.0 μ_B. HR-MS (ESI$^+$): *m/z* 323.1761 [$C_{16}H_{15}FeN_2O_2$]$^+$, calcd. [M + H]$^+$ 323.0477. Anal. calcd. (%) for $C_{16}H_{14}N_2O_2Fe$: C 59.66, H 4.38, N 8.70; found C 59.90, H 4.30, N 8.60.

Synthesis of iron(II) salen complex (4.27). Salen precursor **P4.2** was reacted according to the general procedure, affording the product as a violet solid. Yield: 0.34 g, 0.90 mmol, 90 %. μ_{eff} = 4.9 μ_B. HR-MS (ESI$^+$): *m/z* 376.0870 [$C_{20}H_{21}FeN_2O_2$]$^+$, calcd. [M + H]$^+$ 376.0874. Anal. calcd. (%) for $C_{16}H_{14}N_2O_2Fe.^3/_4H_2O$: C 61.63, H 5.56, N 7.19; found C 61.50, H 5.20, N 7.10.

Synthesis of iron(II) salen complex (4.28). Salen precursor **P4.5** was reacted according to the general procedure, affording the product as a pale violet solid. Violet blocks suitable for X-ray crystallographic analysis were grown *via* slow diffusion of Et$_2$O vapours into a weak CH$_2$Cl$_2$ solution of the complex. Yield: 0.41 g, 0.93 mmol, 93 %. μ_{eff} = 4.9 μ_B. HR-MS (ESI$^+$): *m/z* 437.1160 [$C_{22}H_{25}FeN_2O_4$]$^+$, calcd. [M + H]$^+$ 437.1158. Anal. calcd. (%) for $C_{22}H_{24}N_2O_4Fe.^3/_4CH_3CN$: C 60.43, H 5.66, N 8.25; found C 60.50, H 5.40, N 8.30.

Figure 4.23 *Exemplar images of residual Fe^{II}-salen complexes in solution. Left: blanketed by an atmosphere of N$_2$, prior to oxidation. Right: the same sample following ca. 10 seconds exposure to air.*

4.9.9   Preparation of manganese(IV) salen complexes

General procedure. A three-necked round bottomed flask equipped with stirrer bar was charged with salen precursor (1.0 mmol), $^nBu_4NBF_4$ (0.03 mmol) and acetonitrile (50 mL). Two manganese/nickel (88:12 weight %) electrodes (25 × 10 × 0.25 mm) were introduced to the solution and a potential applied *via* an external power supply (22.0 – 25.0 V, operating in CV mode) to maintain a constant current of 20.0 mA for 90 minutes. The resulting precipitate was collected by vacuum filtration, washed with acetonitrile (2 × 10 mL) followed by diethyl ether (3 × 30 mL) and dried under vacuum to deliver the corresponding Mn^{IV}-salen complex as a brown powder.

Synthesis of manganese(III)(OAc) salen 2D polymer (4.29). Salen precursor **P4.1** (0.17 g, 0.62 mmol) and anhydrous $Mn(OAc)_2$ (0.11 g, 0.62 mmol) were charged to a flame-dried Schlenk flask and stirred in anhydrous ethanol (10 mL) at 75 ˚C for 1 hour under an inert atmosphere. Upon slow cooling to room temperature, a dark brown microcrystalline solid precipitated from solution, which was collected by filtration under N_2 and washed with anhydrous hexane (2×15 mL). The solid was further purified by suspending in refluxing ethanol under N_2, followed by filtration and washing with additional hexane (3×20 mL) to give the $[Mn^{III}(salen)(OAc)]_n$ 2D polymer as a microcrystalline dark brown solid. X-ray quality single crystals of the polymer were obtained upon standing of a weak DCM solution of the product. Anal. calcd. (%) for $C_{18}H_{17}N_2O_4Mn$: C 56.85, H 4.51, N 7.37; found C 56.50, H 4.50, N 7.20.

Synthesis of manganese(IV) salen complex (4.30). Salen precursor **P4.1** was reacted according to the general procedure, affording the product as a brown powder. Pale brown blocks suitable for X-ray crystallographic analysis were grown *via* either (i) slow diffusion of Et_2O vapours into a concentrated binary CH_2Cl_2/DMSO solution of the complex, or (ii) standing of a weak MeCN solution of the complex to give two different solvent-dependent solid-state structures of **4.30**. Yield: 0.30 g, 0.44 mmol, 87 %. Mp decomp. >300 ˚C. HR-MS (ESI$^+$): *m/z* 675.0845 $[C_{32}H_{29}Mn_2N_4O_6]^+$, calcd. $[M + H]^+$ 675.0843. Anal. calcd. (%) for $C_{32}H_{28}N_4O_6Mn_2$: C 57.99, H 4.18, N 8.31; found C 58.10, H 4.25, N 8.40.

Synthesis of manganese(IV) salen complex (4.31). Salen precursor **P4.2** was reacted according to the general procedure, affording the product as a brown powder. Yield: 0.39 g, 0.45 mmol, 90 %. Mp decomp. >300 ˚C. HR-MS (ESI$^+$): *m/z* 783.1780 $[C_{40}H_{41}Mn_2N_4O_6]^+$, calcd. $[M + H]^+$ 783.1782. Anal. calcd. (%) for $C_{40}H_{40}N_4O_6Mn_2$: C 61.39, H 5.15, N 7.16; found C 61.20, H 5.20, N 7.20.

Synthesis of manganese(IV) salen complex (4.32). Salen precursor **P4.3** was reacted according to the general procedure, affording the product as a brown powder. Yield: 0.38 g, 0.49 mmol, 95 %. Mp decomp. >300 ˚C. HR-MS (ESI$^+$): *m/z* 771.0840 $[C_{40}H_{29}Mn_2N_4O_6]^+$, calcd. $[M + H]^+$ 771.0843. Anal. calcd. (%) for $C_{40}H_{28}N_4O_6Mn_2$: C 62.35, H 3.66, N 7.27; found C 62.30, H 3.99, N 7.00.

Synthesis of manganese(IV) salen complex (4.33). Salen precursor **P4.4** was reacted according to the general procedure, affording the product as a brown powder. Yield: 0.39 g, 0.49 mmol, 98 %. Mp decomp. >300 ˚C. HR-MS (ESI$^+$): *m/z* 795.1271 $[C_{36}H_{37}Mn_2N_4O_{10}]^+$, calcd. $[M + H]^+$ 795.1265. Anal. calcd. (%) for $C_{36}H_{36}N_4O_{10}Mn_2 \cdot H_2O$: C 53.21, H 4.71, N 6.89; found C 53.30, H 4.61, N 6.95.

Synthesis of manganese(IV) salen complex (4.34). Salen precursor **P4.5** was reacted according to the general procedure, affording the product as a brown powder. Pale brown blocks suitable for X-ray crystallographic analysis were grown *via* slow diffusion of Et_2O vapours into a concentrated binary CH_2Cl_2/DMSO solution of the complex. Yield: 0.35 g, 0.39 mmol, 78 %. Mp decomp. >300 ˚C. HR-MS (ESI$^+$): *m/z* 903.2225 $[C_{44}H_{49}Mn_2N_4O_{10}]^+$, calcd. $[M + H]^+$ 903.2204. Anal. calcd. (%) for $C_{44}H_{48}N_4O_{10}Mn_2 \cdot 1/2 H_2O$: C 57.96, H 5.42, N 6.14; found C 57.65, H 5.20, N 6.10.

4.9.10 Preparation of manganese(II) salen complexes

General procedure. A flame-dried three-necked round bottomed flask equipped with stirrer bar was charged with salen precursor (1.0 mmol), $^nBu_4NBF_4$ (0.03 mmol) and further dried *in vacuo*. Anhydrous (anoxic) acetonitrile (50 mL) was added *via* cannula and the solution further degassed by bubbling a stream of N_2 or Ar for *ca*. 30 minutes through the solution. Two manganese/nickel (88:12 weight %) electrodes (25 × 10 × 0.25 mm) were introduced to the solution and a potential applied *via* an external power supply (22 – 25 V, operating in CV mode) to maintain a constant current of 20.0 mA for 90 minutes. The suspended pale orange precipitate was isolated by cannula filtration and washed with anhydrous (anoxic) acetonitrile (2 × 15 mL), followed by rinsing with anhydrous (anoxic) diethyl ether (3 × 15 mL) before drying under vacuum to deliver the corresponding Mn^{II}-salen complex as a (highly air- and moisture-sensitive) pale orange powder.

Synthesis of manganese(II) salen complex (4.35). Salen precursor **P4.1** was reacted according to the general procedure, affording the product as a pale orange microcrystalline powder. Yield: 0.25 g, 0.77 mmol, 77 %. μ_{eff} = 5.9 μ_B. HR-MS (ESI$^+$): *m/z* 321.0460 $[C_{16}H_{14}MnN_2O_2]^+$, calcd. $[M]^+$ 321.0436. Anal. calcd. (%) for $C_{16}H_{14}N_2O_2Mn$: C 59.82, H 4.39, N 8.72; found C 60.20, H 4.10, N 8.75.

Synthesis of manganese(II) salen complex (4.36). Salen precursor **P4.2** was reacted according to the general procedure, affording the product as a pale orange microcrystalline powder. Yield: 0.27 g, 0.71 mmol, 71 %. μ_{eff} = 5.7 μ_B. HR-MS (ESI$^+$): *m/z* 375.0903 $[C_{20}H_{20}MnN_2O_2]^+$, calcd. $[M]^+$ 375.0905. Anal. calcd. (%) for $C_{20}H_{20}N_2O_2Mn$: C 64.00, H 5.37, N 7.46; found C 64.22, H 5.00, N 7.75.

Synthesis of manganese(II) salen complex (4.37). Salen precursor **P4.5** was reacted according to the general procedure, affording the product as a pale orange microcrystalline powder. Bright orange/yellow blocks suitable for X-ray crystallographic analysis were grown *via* slow diffusion of Et_2O vapours into a concentrated binary CH_2Cl_2/DMSO solution of the complex. Yield: 0.33 g, 0.78 mmol, 78 %. μ_{eff} = 5.8 μ_B. HR-MS (ESI$^+$): *m/z* 429.0647 $[C_{22}H_{18}MnN_2O_4]^+$, calcd. $[M]^+$ 429.0647. Anal. calcd. (%) for $C_{22}H_{24}N_2O_4Mn$: C 60.69, H 5.56, N 6.43; found C 60.40, H 5.10, N 6.80.

4.10 Bibliography

1.   H. Schiff, *Ann. Suppl.* **1864**, *3*, 343–345.

2.   P. G. Cozzi, *Chem. Soc. Rev.* **2004**, *33*, 410–421.

3.   A. M. Abu-Dief, I. M. A. Mohamed, *Beni-Suef Univ. J. Basic Appl. Sci.* **2015**, *4*, 119–133.

4.   A. K. Shiryaev, *Curr. Org. Chem.* **2012**, *16*, 1788–1807.

5.   (a) T. Katsuki, *Chem. Soc. Rev.* **2004**, *33*, 437–444; (b) T. Katsuki, *Synlett.* **2003**, 281–297.

6.   P. Pfeiffer, E. Breith, E. Lübbe, T. Tsumaki, *Justus Liebig's Ann. der Chemie* **1933**, *503*, 84–130.

7.   M. Sono, M. P. Roach, E. D. Coulter, J. H. Dawson, *Chem. Rev.* **1996**, *96*, 2841–2888.

8.   B. M. Cole, K. D. Shimizu, C. A. Krueger, J. P. A. Harrity, M. L. Snapper, A. H. Hoveyda, *Angew. Chem. Int. Ed. Engl.* **1996**, *35*, 1668–1671.

9.   J. K.-H. Hui, Z. Yu, M. J. MacLachlan, *Angew. Chem. Int. Ed.* **2007**, *46*, 7980–7983.

10.   A. K. Crane, M. J. MacLachlan, *Eur. J. Inorg. Chem.* **2012**, *3*, 17–30.

11.   A. W. Kleij, *Dalton Trans.* **2009**, *28*, 4635–4639.

12.   S. Medina, A. S. Henderson, J. F. Bower, M. C. Galan, *Chem. Commun.* **2015**, *51*, 8939–8941.

13.   Y. Hitomi, Y. Iwamoto, A. Kashida, M. Kodera, *Chem. Commun.* **2015**, *51*, 8702–8704.

14.   W. Zhang, J. L. Loebach, S. R. Wilson, E. N. Jacobsen, *J. Am. Chem. Soc.* **1990**, *112*, 2801–2803.

15.   E. N. Jacobsen, W. Zhang, A. R. Muci, J. R. Ecker, L. Deng, *J. Am. Chem. Soc.* **1991**, *113*, 7063–7064.

16.   W. P. Schaefer, B. T. Huie, M. G. Kurilla, S. E. Ealick, *Inorg. Chem.* **1980**, *19*, 340–344.

17.   S. Matsunaga, M. Shibasaki, *Synthesis (Stuttg).* **2013**, *45*, 421–437.

18.   A. S. Kumbhar, S. G. Damle, S. T. Dasgupta, S. Y. Rane, A. S. Kumbhar, *J. Chem. Res.* **1999**, *8*, 98–99.

19.   C. J. Whiteoak, R. Torres Martin de Rosales, A. J. P. White, G. J. P. Britovsek, *Inorg. Chem.* **2010**, *49*, 11106–11117.

20.   Y. N. Belokon, J. Fuentes, M. North, J. W. Steed, *Tetrahedron* **2004**, *60*, 3191–3204.

21.   J. J. Habeeb, D. G. Tuck, F. H. Walters, *J. Coord. Chem.* **1978**, *8*, 27–33.

22.   N. Kumar, D. G. Tuck, *Can. J. Chem.* **1982**, *60*, 2579–2582.

23.   L. Bustos, J. H. Green, J. L. Hencher, M. A. Khan, D. G. Tuck, *Can. J. Chem.* **1983**, *61*, 2141–2146.

24.   L. Matassa, N. Kumar, D. G. Tuck, *Inorganica Chim. Acta* **1985**, *109*, 19–21.

25.   T. A. Annan, C. Peppe, D. G. Tuck, *Can. J. Chem.* **1990**, *68*, 423–430.

26.   N. Kumar, D. G. Tuck, K. D. Watson, *Can. J. Chem.* **1987**, *65*, 740–743.

27.   D. Nartop, W. Clegg, R. W. Harrington, R. A. Henderson, C. Y. Wills, *Dalton Trans.* **2014**, *43*, 3372–3382.

28.   F. M. Kerton, S. Holloway, A. Power, R. G. Soper, K. Sheridan, J. M. Lynam, A. C. Whitwood, C. E. Willans, *Can. J. Chem.* **2008**, *86*, 435–443.

29.   J. Lilie, *Chemical Kinetics of Small Organic Radicals*, CRC Publishing Co., Boca Raton, FL, **1988**, 1st edition.

30.   C. Li, M. Z. Hoffman, *J. Phys. Chem. B* **1999**, *103*, 6653–6656.

31. J. L. N. Xavier, E. Ortega, J. Z. Ferreira, A. M. Bernardes, V. Perez-Herranz, *Int. J. Electrochem. Sci.* **2011**, *6*, 622–636.

32. K. A. Ogawa, A. J. Boydston, *Chem. Lett.* **2014**, *43*, 907–909.

33. Y. N. Belokon, D. Bhave, D. D'Addario, E. Groaz, M. North, V. Tagliazucca, *Tetrahedron* **2004**, *60*, 1849–1861.

34. N. Ananthi, U. Balakrishnan, S. Velmathi, *Ark. Arch. Org. Chem.* **2010**, *11*, 370–379.

35. H. Yang, L. Zhang, W. Su, Q. Yang, C. Li, *J. Catal.* **2007**, *248*, 204–212.

36. S. S. Stahl, J. L. Thorman, R. C. Nelson, M. A. Kozee, *J. Am. Chem. Soc.* **2001**, *123*, 7188–7189.

37. B. R. M. Lake, E. K. Bullough, T. J. Williams, A. C. Whitwood, M. A. Little, C. E. Willans, *Chem. Commun.* **2012**, *48*, 4887–4889.

38. L. Rodríguez, E. Labisbal, A. Sousa, J. A. García-Vázquez, J. Romero, M. L. Durán, J. A. Real, A. Sousa, *Inorg. Chem.* **2006**, *45*, 7903–7914.

39. I. Beloso, J. Borrás, J. Castro, J. A. García-Vázquez, P. Pérez-Lourido, J. Romero, A. Sousa, *Eur. J. Inorg. Chem.* **2004**, 635–645.

40. M. Valko, R. Klement, P. Pelikan, R. Boca, L. Dlhan, A. Boettcher, H. Elias, L. Mueller, *Inorg. Chem.* **1993**, *32*, 4131–4138.

41. R. Klement, F. Stock, H. Elias, H. Paulus, P. Pelikán, M. Valko, M. Mazúr, *Polyhedron* **1999**, *18*, 3617–3628.

42. A. Boettcher, H. Elias, E. G. Jaeger, H. Langfelderova, M. Mazur, L. Mueller, H. Paulus, P. Pelikan, M. Rudolph, M. Valko, *Inorg. Chem.* **1993**, *32*, 4131–4138.

43. A. Böttcher, H. Elias, L. Müller, H. Paulus, *Angew. Chem. Int. Ed.* **1992**, *104*, 635–637.

44. I. Correia, J. Costa Pessoa, M. T. Duarte, R. T. Henriques, M. F. M. Piedade, L. F. Veiros, T. Jakusch, T. Kiss, Á. Dörnyei, M. M. C. A. Castro, C. F. G. C. Geraldes, F. Avecilla, *Chem. Eur. J.* **2004**, *10*, 2301–2317.

45. I. Correia, J. C. Pessoa, M. T. Duarte, M. F. M. da Piedade, T. Jackush, T. Kiss, M. M. C. A. Castro, C. F. G. C. Geraldes, F. Avecilla, *Eur. J. Inorg. Chem.* **2005**, 732–744.

46. I. Correia, A. Dornyei, F. Avecilla, T. Kiss, J. Costa Pessoa, *Eur. J. Inorg. Chem.* **2006**, 656–662.

47. G. Soto-Garrido, V. Salas-Reyes, *Transit. Met. Chem.* **2000**, *25*, 192–195.

48. M. Yamada, S. Ochi, H. Suzuki, A. Hisazumi, S. Kuroda, I. Shimao, K. Araki, *J. Mol. Catal.* **1994**, *87*, 195–202.

49. S. Borkar, P. K. Saxena, *Polym. Bull.* **2000**, *44*, 167–172.

50. P. Pérez-Lourido, J. Romero, J. García-Vázquez, A. Sousa, J. Zubieta, K. Maresca, *Polyhedron* **1998**, *17*, 4457–4464.

51. P. G. Cozzi, A. Papa, A. Umani-Ronchi, *Tetrahedron Lett.* **1996**, *37*, 4613–4616.

52. E. F. DiMauro, M. C. Kozlowski, *Org. Lett.* **2002**, *4*, 3781–3784.

53. D. Hall, F. H. Moore, *J. Chem. Soc. A* **1966**, 1822–1824.

54. J. Reglinski, S. Morris, D. E. Stevenson, *Polyhedron* **2002**, *21*, 2175–2182.

55. S. Akine, T. Taniguchi, T. Nabeshima, *Inorg. Chem.* **2004**, *43*, 6142–6144.

56. J. Barona-Castaño, C. Carmona-Vargas, T. Brocksom, K. de Oliveira, *Molecules* **2016**, *21*, 310.

57.   M. Oszajca, A. Franke, M. Brindell, G. Stochel, R. van Eldik, *Coord. Chem. Rev.* **2016**, *306*, 483–509.

58.   G. Hilt, C. Walter, P. Bolze, *Adv. Synth. Catal.* **2006**, *348*, 1241–1247.

59.   L. H. Do, S. J. Lippard, *Inorg. Chem.* **2009**, *48*, 10708–10719.

60.   C. Prinzisky, A. Jacob, M. Harrer, M. Elfferding, J. Sundermeyer, *Eur. J. Inorg. Chem.* **2016**, 477–489.

61.   C. G. Hamaker, G. A. Mirafzal, L. K. Woo, *Organometallics* **2001**, *20*, 5171–5176.

62.   F. C. D. Lemos, M. Muraro, J. Zukerman-Schpector, É. T. G. Cavalheiro, E. R. Dockal, *J. Therm. Anal. Calorim.* **2004**, *75*, 599–606.

63.   K. J. Gallagher, R. L. Webster, *Chem. Commun.* **2014**, *50*, 12109–12111.

64.   M. Gerloch, E. D. Mckenzie, A. D. C. Towl, *Nature* **1968**, *220*, 906–907.

65.   K. S. Murray, *Coord. Chem. Rev.* **1974**, *12*, 1–35.

66.   S. K. Edulji, S. T. Nguyen, *Organometallics* **2003**, *22*, 3374–3381.

67.   A. Jozwiuk, A. L. Ingram, D. R. Powell, B. Moubaraki, N. F. Chilton, K. S. Murray, R. P. Houser, *Dalton Trans.* **2014**, *43*, 9740–9753.

68.   D. F. J. Evans, *J. Chem. Soc.* **1959**, 2003–2005.

69.   D. H. Live, S. I. Chan, *Anal. Chem.* **1970**, *42*, 791–792.

70.   D. Ostfeld, I. A. Cohen, *J. Chem. Educ.* **1972**, *49*, 829.

71.   L. A. Yatsunyk, F. A. Walker, *Inorg. Chem.* **2004**, *43*, 757–777.

72.   B. Weber, F. A. Walker, *Inorg. Chem.* **2007**, *46*, 6794–6803.

73.   W. R. Scheidt, C. A. Reed, *Chem. Sci.* **2015**, *6*, 608–612.

74.   X. Wurzenberger, H. Piotrowski, P. Klüfers, *Angew. Chem. Int. Ed.* **2011**, *50*, 4974–4978.

75.   S. A. Cantalupo, S. R. Fiedler, M. P. Shores, A. L. Rheingold, L. H. Doerrer, *Angew. Chem. Int. Ed.* **2012**, *51*, 1000–1005.

76.   D. Pinkert, S. Demeshko, F. Schax, B. Braun, F. Meyer, C. Limberg, *Angew. Chem. Int. Ed.* **2013**, *52*, 5155–5158.

77.   M. E. Pascualini, N. V di Russo, A. Thuijs, A. Ozarowski, S. A. Stoian, K. A. Abboud, G. Christou, A. S. Veige, *Chem. Sci.* **2014**, *6*, 608–612.

78.   M. W. Bouwkamp, S. C. Bart, E. J. Hawrelak, R. J. Trovitch, E. Lobkovsky, P. J. Chirik, *Chem. Commun.* **2005**, *104*, 3406–3408.

79.   R. Irie, K. Noda, Y. Ito, N. Matsumoto, T. Katsuki, *Tetrahedron Lett.* **1990**, *31*, 7345–7348.

80.   S. Bhaduri, A. J. Tasiopoulos, M. A. Bolcar, K. A. Abboud, W. E. Streib, G. Christou, *Inorg. Chem.* **2003**, *42*, 1483–1492.

81.   H. Puschmann, O. V. Dolomanov, L. J. Bourhis, R. J. Gildea, J. A. K. Howard, *J. Appl. Crystallogr.* **2009**, *42*, 339–341.

82.   T. A. Immel, M. Grützke, E. Batroff, U. Groth, T. Huhn, *J. Inorg. Biochem.* **2012**, *106*, 68–75.

83.   D.-N. Lee, H. Kim, L. Mui, S.-W. Myung, J. Chin, H.-J. Kim, *J. Org. Chem.* **2009**, *74*, 3330–3334.

Chapter 5

Relating solid-state structure, solution-state behaviour and catalytic activity of C,N-chelating palladium(II) *N*-heterocyclic carbene complexes

5.1   Introduction

Palladium-catalysed cross-coupling represents an extremely powerful tool available to synthetic chemists in their endeavour to construct intricate molecular scaffolds.[1,2] The importance of connecting two organic fragments using relatively mild, catalytic conditions was recognised by the Nobel committee in 2010 by awarding Richard Heck, Ei-ichi Negishi and Akira Suzuki the Nobel prize in Chemistry for what was described as "artwork in a test-tube".[3] In these carbon-carbon and carbon-heteroatom bond-forming processes, which are mediated by two-electron M^n / M^{n+2} redox cycles, it is postulated that both the steric and electronic properties of *N*-heterocyclic carbene (NHC) ligands lead to enhancements at distinct steps in the proposed catalytic cycle (**Scheme 5.1**).[4] Primarily, the strong σ-donation from the NHC ligand generates a metal centre which is electron-rich, catalytically active and may readily undergo oxidative cleavage of carbon-(*pseudo*)halogen bonds – a ligand feature which is essential to allow challenging substrates to enter the catalytic cycle (*e.g.* aryl chlorides, which possess a relatively strong carbon-chlorine bond).[5] The large steric influence of NHC ligands around the metal site may also facilitate reductive elimination of the coupled organic product, closing the catalytic loop whilst stabilising an unsaturated, low oxidation state metal centre to re-enter the cycle.
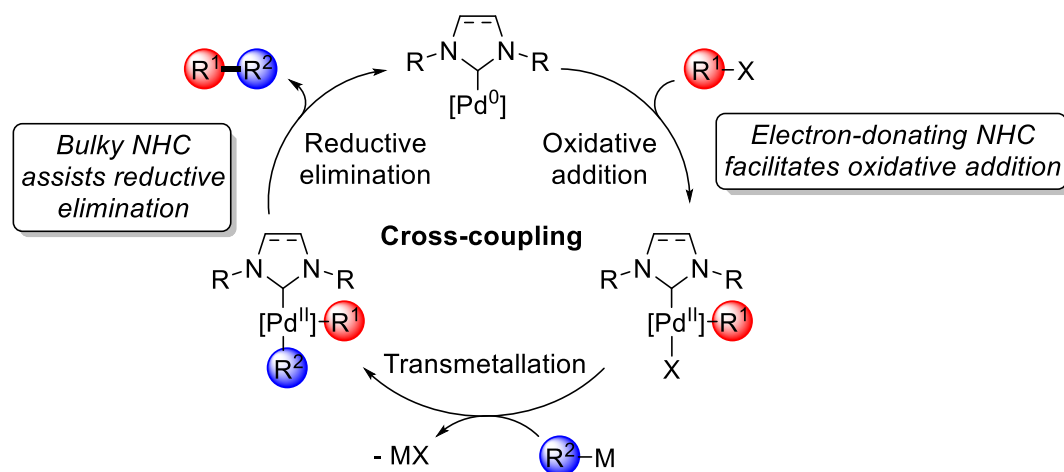
Scheme 5.1 *General mechanism of palladium-catalysed cross-coupling reactions. R^1, R^2 = aryl, heteroaryl, alkyl; X = (pseudo)halide; M = B(OR)$_2$ (Suzuki-Miyaura), SnR$_3$ (Stille), ZnR (Negishi) and heteroatom partners HNR$_2$ (Buchwald-Hartwig).[4]*

A wide variety of well-defined palladium-NHCs bearing ancillary nitrogen donor ligands have demonstrated significant activities in both carbon-carbon and carbon-heteroatom bond forming

reactions.[6–10] Examples include C,N-palladacycles,[11–13] [Pd(NHC)(Et$_3$N)Cl$_2$] described by Navarro[14] and [Pd(NHC)(im)Cl$_2$] (im = imidazole) developed by Shao.[15,16] Arguably at the forefront of such catalysts are Pd-PEPPSI complexes, pioneered by Organ and co-workers in 2005 (PEPPSI = pyridine-enhanced pre-catalyst preparation stabilisation and initiation).[17,18] Originally intended for the Negishi coupling of unactivated sp^3 centres,[19,20] the Pd-PEPPSI series emerged as a superior class of palladium-NHC catalyst to couple a broad range of sterically encumbered and heterocyclic substrates. In terms of catalyst design, the displaceable pyridine ligand of the PEPPSI pre-catalysts plays a pivotal role in the formation of the active species by both stabilising the complex and dissociating upon activation. Moreover, the steric topography around the metal centre is crucial, with bulky NHC *N*-substituents generally leading to enhanced catalytic activity (**Figure 5.1**).[21]
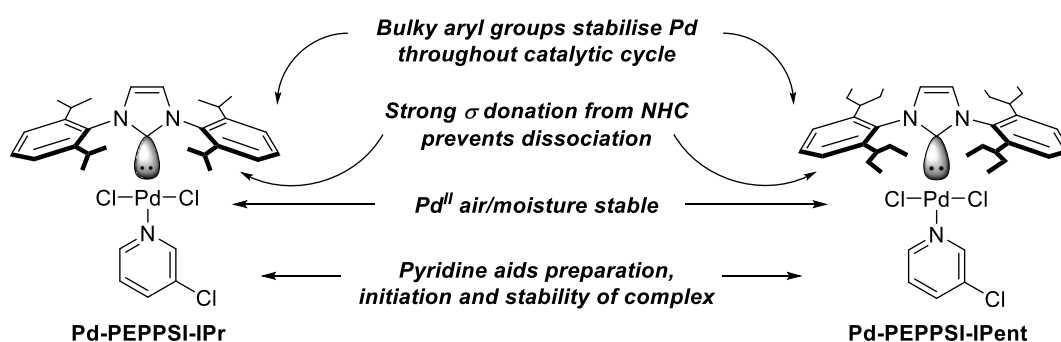
Figure 5.1 Key attributes of the most active cross-coupling Pd-PEPPSI complexes.[21]

In a seminal report by Fairlamb *et al.*,[22] it has been demonstrated that alkenic π-acid-coordinated 'spectator' ligands, for example, dibenzylideneacetone (dba), fumaronitrile[23] and *p*-fluorostyrene,[24] are able to play significant roles in Pd^0-mediated cross-coupling reactions – a ligand property which is arguably underutilised. In this study, synergistic effects (dπ-π* backbonding) appear able to control the rate of dissociation of the alkene from Pd^0, stabilising low oxidation state metal to prevent catalyst deactivation through cluster formation. However, the authors postulate that the alkene must not coordinate 'too strongly', as oxidative addition of substrate becomes problematic (*i.e.* the alkene must dissociate), and re-coordination of the alkene may assist the following reductive elimination step (**Scheme 5.2**).
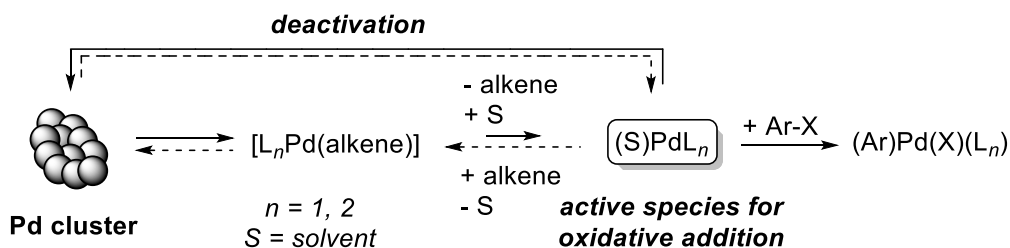
Scheme 5.2 Alkene-associated stabilisation/deactivation pathway of Pd versus alkene-dissociated oxidative addition pathway.[22]

In our laboratory, recent findings have shown that hemilabile NHC-appended pyridyl donor groups are able to significantly stabilise complexes of copper, both as well-defined complexes and as catalysts for cross-coupling reactions (Ullmann etherification, for example).[25] It was therefore envisaged that a suitable combination between the π-electron accepting ability of an alkene, tethered to a strongly σ-coordinating NHC which is also attached to a hemilabile pyridyl motif may exist, which meets the desired criteria to sufficiently stabilise a palladium metal centre throughout various steps of a cross-coupling catalytic cycle.

5.2   Ligand precursor synthesis

A commonly employed and efficient route to NHC-ligated complexes is *via* their corresponding imidazolium salt precursors, therefore azolium bromides **P5.1** and **P5.2** were prepared along a two-step synthetic procedure previously reported within our group.[25] Reaction of imidazole with (substituted) 2-bromopyridine in the presence of a catalytic quantity of copper iodide/*DL*-proline ((+/.)-pyrrolidine-2-carboxylic acid) under basic conditions led to the corresponding C,N-coupled 1-(2-pyridyl)imidazole products, **I5.1** and **I5.2**. Independent treatment of **I5.1** and **I5.2** with an excess of allyl bromide (4.6 equivalents) furnished the desired *N*-allylated imidazolium bromides, **P5.1** and **P5.2** in 89 and 93 % yield, respectively, following a simple recrystallisation work-up procedure (**Scheme 5.3**).
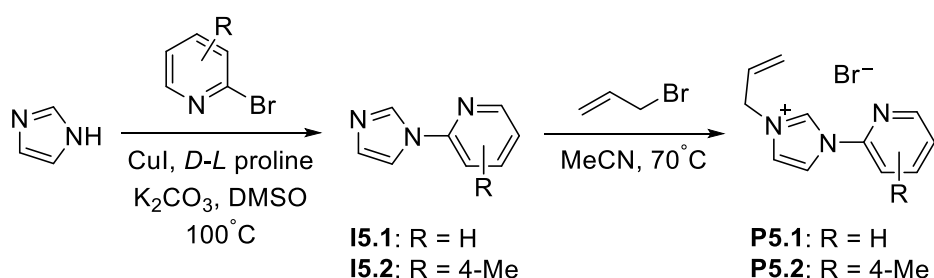
*Scheme 5.3 Two-step synthetic protocol to ligand precursors **P5.1** and **P5.2**.*

Following isolation, diagnostic low-field resonances are observed for each NC*H*N proton in the ^{1}H NMR spectra of both **P5.1** and **P5.2**, showcased at 11.74 and 11.34 ppm (300 MHz, CDCl$_3$) respectively, indicative of azolium ion formation. Moreover, mass peaks (*m/z*) 186.1030 and 200.1180 were observed in the mass spectra of **P5.1** and **P5.2**, respectively, corresponding to each [M – Br]$^+$ mass fragment.

In addition, ligand precursors **P5.3** and **P5.4** were prepared with a view to increase and decrease electron density, and subsequent nucleophilicity, of the adjoining pyridyl ring of the imidazolium core. Using a modified literature procedure, sodium imidazolide and 2-bromo-5-nitropyridine were reacted in a nucleophilic aromatic substitution to produce precursor, **I5.3**. Along a similar S$_N$Ar mechanism, 4-methoxypyridine *N*-oxide and 1,1'-sulfonyldiimidazole were combined and

heated in toluene to afford electronically converse precursor, **I5.4**. Successive treatment of **I5.3** and **I5.4** with allyl bromide, in an analogous protocol to that described for **I5.1** and **I5.2**, gave desired imidazolium bromides, **P5.3** and **P5.4**, in 86 and 84 % isolated yield, respectively (**Scheme 5.4**), which were similarly characterised using multinuclear NMR spectroscopy and high-resolution mass spectrometry.
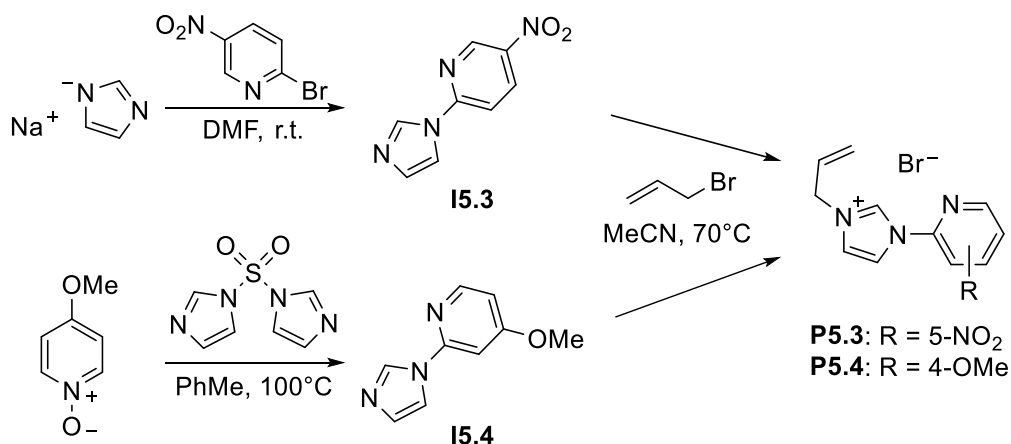
Scheme 5.4 Synthetic routes to electronically deactivating and activating ligand precursors, P5.3 and P5.4.

Key to the success of the Pd-PEPPSI series are a combination of topographically favourable sterics, and the presence of a displaceable pyridyl donor group at the metal centre. With this in mind, *N*-picolyl substituted imidazolium halides **P5.5** and **P5.6** were prepared, with intent to further facilitate conformational freedom of each *N*-substituted pyridyl donor moiety by use of a methylene linkage (**Scheme 5.5**). Carbene precursor **P5.5** was readily accessed from reaction of *N*-(methylpyridyl)imidazole (**I5.5**) with allyl bromide, and subsequently isolated as a pale orange oil in quantitative yield. In a separate reaction, addition of **I5.5** to one equivalent of 2-bromomethylpyridine hydrobromide under basic conditions led to smooth formation of 1,3-*bis*(2-methylpyridyl)imidazolium bromide, **P5.6**, in 84 % yield.
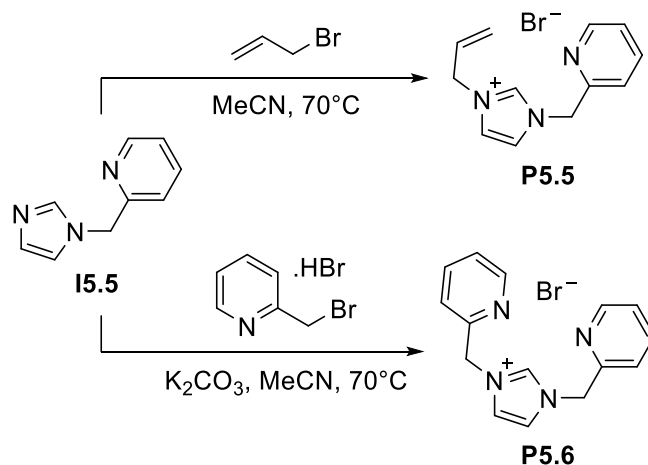
Scheme 5.5 Synthetic routes to N-picolyl substituted analogues, P5.5 and P5.6.

The ^{1}H NMR spectra of both **P5.5** and **P5.6** each illustrate a low-field, strongly deshielded proton resonance (*i.e.* NC*H*N signal) characteristic of azolium ion formation, and were each further analysed by ^{13}C{^{1}H} NMR spectroscopy, high-resolution mass spectrometry and microanalysis. In addition, colourless needles of ligand precursor **P5.6** suitable for X-ray crystallographic study were obtained from the slow diffusion of diethyl ether vapours into a concentrated acetonitrile solution of the compound (**Figure 5.2**).
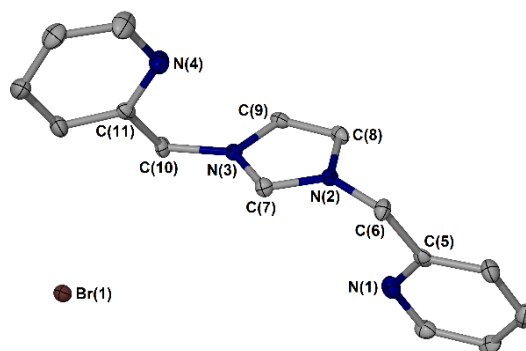
Figure 5.2 Molecular structure of ligand precursor, **P5.6**. Atomic displacement parameters are drawn at the 50 % probability level, hydrogen atoms are omitted for clarity.

N(3)-C(7)	1.334(4)	N(3)-C(7)-N(2)	108.0(3)
N(2)-C(7)	1.336(5)		
N(3)-C(10)	1.472(4)		
N(2)-C(6)	1.466(4)		

Table 5.1 Selected bond lengths (Å) and angles (˚) from the crystal structure of **P5.6**.

5.3 Synthesis of palladium(II) *N*-heterocyclic carbene complexes

A broad range of well-defined palladium-NHC cross-coupling pre-catalysts have been reported, which themselves may be prepared along a number of synthetic routes. From a thermodynamic viewpoint, the strength of the Pd-C$_{carbene}$ bond underlines 'ligand-exchange' as an attractive route to these complexes, by reaction of free carbene with Pd^{II} or Pd^0 complexes of alkenes,[26] phosphanes[7] or nitrogen donor ligands.[27] Another common synthetic approach involves use of an imidazolium salt precursor in the presence of base to form a free NHC *in situ*, which is intercepted by palladium. Although there have only been a limited number of studies into the aqueous thermodynamic pK_a values of azolium ions, Washabaugh and Jencks were able to use H/D exchange studies to estimate general pK_a values between 17 – 19 for various substituted imidazolium salts (in water).[28] Despite relatively strong bases such as potassium hexamethyldisilazide (pK_a = 26 – 27) proving effective in forming a free NHC,[29] weak bases such as cesium carbonate[30] or even sodium acetate[31] (pK_a = 10 and 5, respectively) may be used –

though the mechanism of generation and transfer of the carbenic fragment in the presence of such weak bases remains unclear.

Instead, employment of palladium(II) acetate as both deprotonation agent and Pd source provides an atom-economical synthetic alternative. Though the absolute mechanism of palladium-NHC formation *via* metal acetate remains ill-defined, Fagnou and Glorius have each postulated that a ligand-assisted C-H activation pathway occurs, whereby abstraction of the imidazolium (C2) proton is facilitated by an acetate ligand at the metal centre. This mechanism is thought to be both concerted and associative, with deprotonation occurring concomitantly with palladium-insertion, supported by an agostic interaction from the $C(sp^2)$-H σ-bond; product formation is overall redox-neutral and driven by the production of acetic acid to deliver a palladium(II)-NHC complex (**Scheme 5.6**).[32–36] Interestingly, computational results conducted within our research group suggest this transition state to be influenced significantly by the presence (or absence) of donor solvent molecules, and will be discussed in Chapter 6 of this thesis.
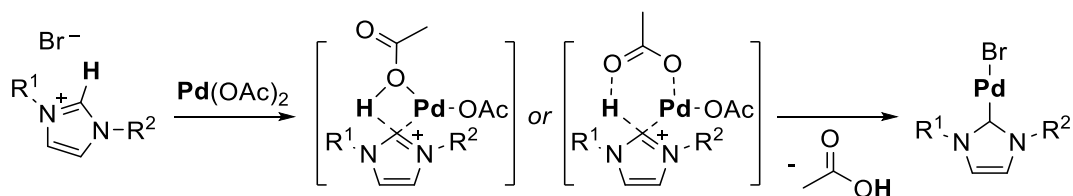
Scheme 5.6 Proposed acetate-facilitated C-H activation pathway to Pd-NHCs.

Therein a general synthetic protocol was adapted, whereby imidazolium bromides **P5.1 – P5.3** were treated with 0.5 equivalents of $Pd(OAc)_2$ in anhydrous acetonitrile, and stirred at reflux under an inert atmosphere. Following reaction, bench-stable palladium(II) *bis*-NHC complexes, **5.1 – 5.3**, were formed in 58, 77 and 50 % isolated yields, respectively (**Scheme 5.7**).
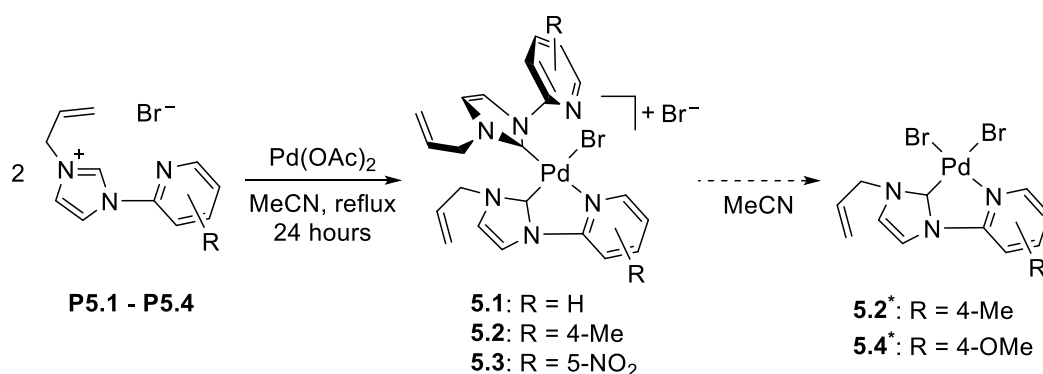
Scheme 5.7 General synthetic route to [Pd^{II}(NHC)_2(Br)]Br complexes.

The formation of complexes **5.1 – 5.3** were evidenced by NMR spectroscopy and mass spectrometry, with their purity and composition confirmed by combustion analysis.

It is speculated that complexes **5.1** and **5.2** undergo rapid isomerisation whilst in the solution-state, *via* interchange between both *cis/trans* geometrical conformers and also coordinative substitution from each independent pyridyl donor group/bromide anion. This fluxional activity is reflected on an NMR timescale by solution spectroscopic measurements, as the ^{1}H NMR spectra of complexes **5.1** and **5.2** display appreciable signal-broadening at ambient temperature, as exemplified in **Figure 5.3**.
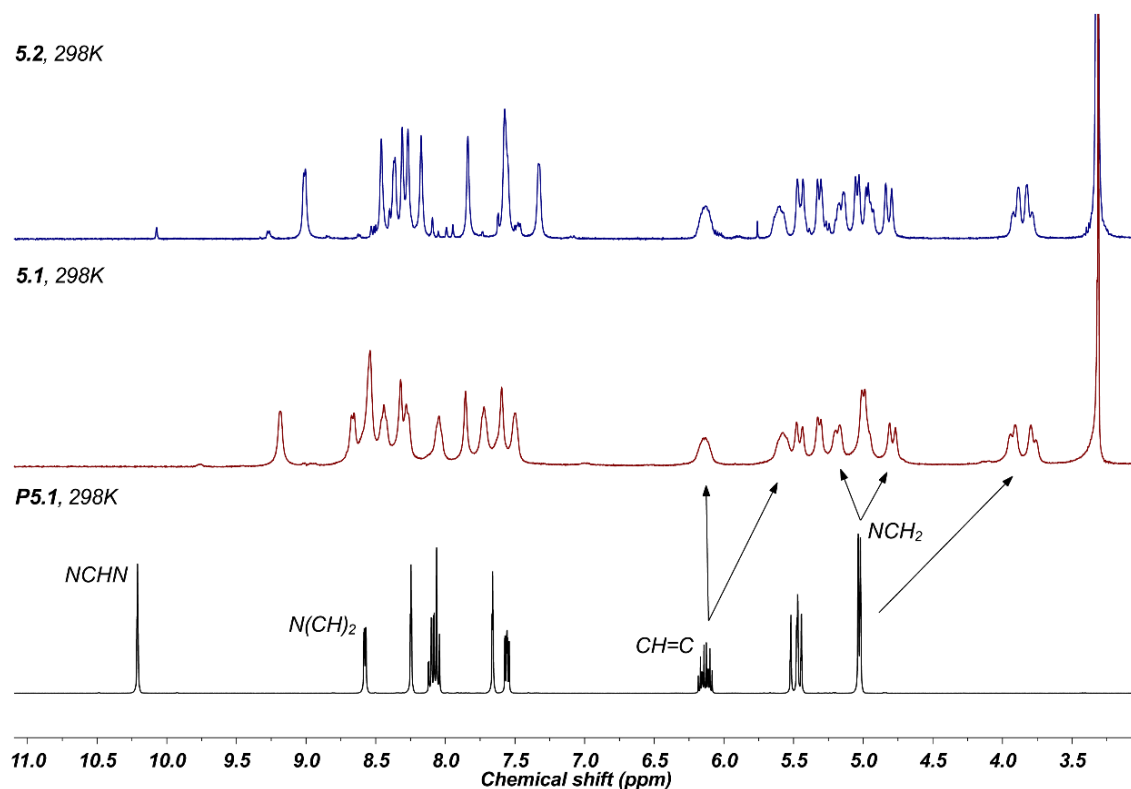
Figure 5.3 *^{1}H NMR spectrum of ligand precursor **P5.1** (black trace, 400 MHz, CD$_3$CN, 298K), noting original vinylic multiplet at 6.14 ppm, allylic NCH$_2$ doublet at 5.04 ppm and imidazolium NCHN singlet at 10.21 ppm, arrows represent their new chemical shift. ^{1}H NMR spectrum of Pd-NHC complex **5.1** (red trace, 500 MHz, (CD$_3$)$_2$SO, 298K), indicating loss of NCHN resonance and signal-broadening. ^{1}H NMR spectrum of related Pd-NHC **5.2** (blue trace, 500 MHz, (CD$_3$)$_2$SO, 298K) is also provided for comparison.*

For both **5.1** and **5.2**, two magnetically inequivalent ligand environments are clearly illustrated in their NMR spectra, representing both chelating and non-chelating binding modes of each ligand at the metal centre. Further interpretation is provided by homonuclear 2D correlation spectroscopy (^{1}H-^{1}H COSY), which allows distinction between vinylic and allylic proton signals of each ligand of **5.1**, further supporting an overall non C_2-symmetric Pd(NHC)$_2$-type complex (**Figure 5.4**).
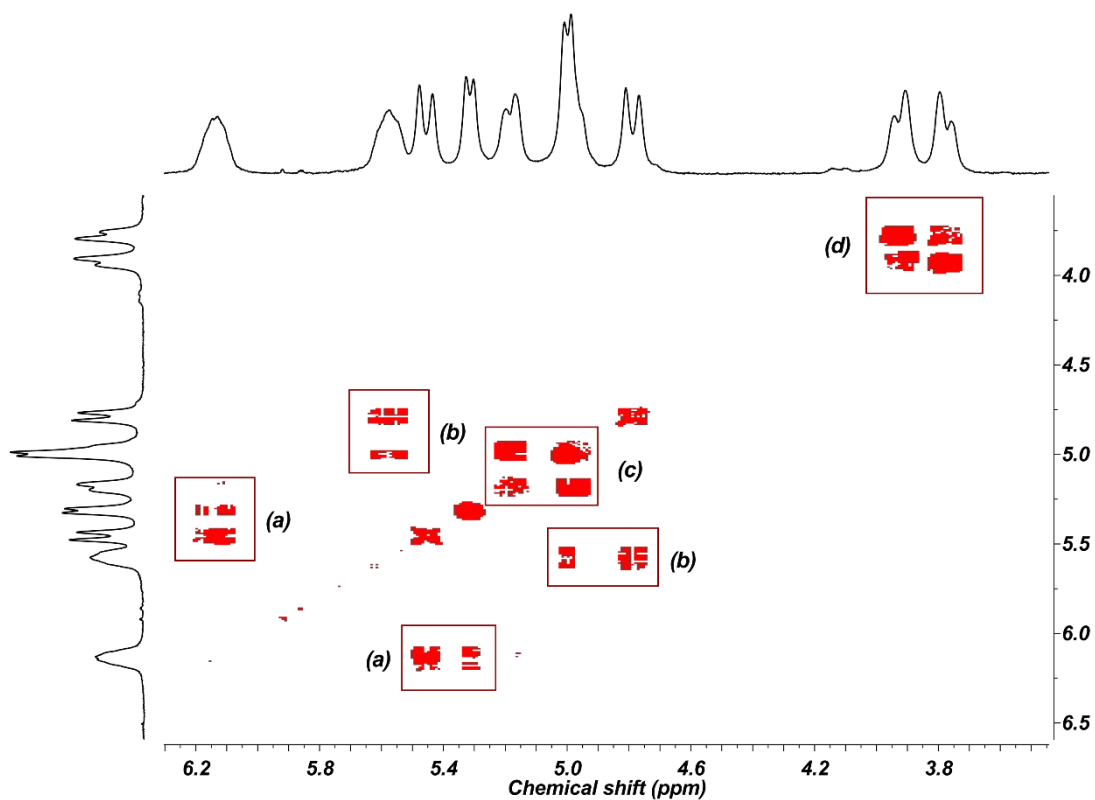
Figure 5.4 *Interpreted 2D ^{1}H-^{1}H COSY spectrum of Pd-NHC complex **5.1** (400 MHz, (CD$_3$)$_2$SO, 298K), 6.5 – 3.5 ppm region; (**a**) and (**b**) independent C=CH protons (6.13, 5.57 ppm) strongly couple to both cis (5.33, 5.01 ppm) and trans (5.48, 4.81 ppm) terminal vinyl protons, (**c**) and (**d**) newly formed diastereotopic NCH$_2$ doublet resonances (5.16, 5.00 ppm and 3.90, 3.80 ppm).*

Yellow needles of **5.1** and **5.2** suitable for X-ray crystallographic analysis were obtained upon slow evaporation of saturated, hydrous methanolic solutions of each complex, with both solid-state structures authenticating the expected [Pd(NHC)$_2$(Br)Br] coordination environment around the metal centre (**Figure 5.5**).
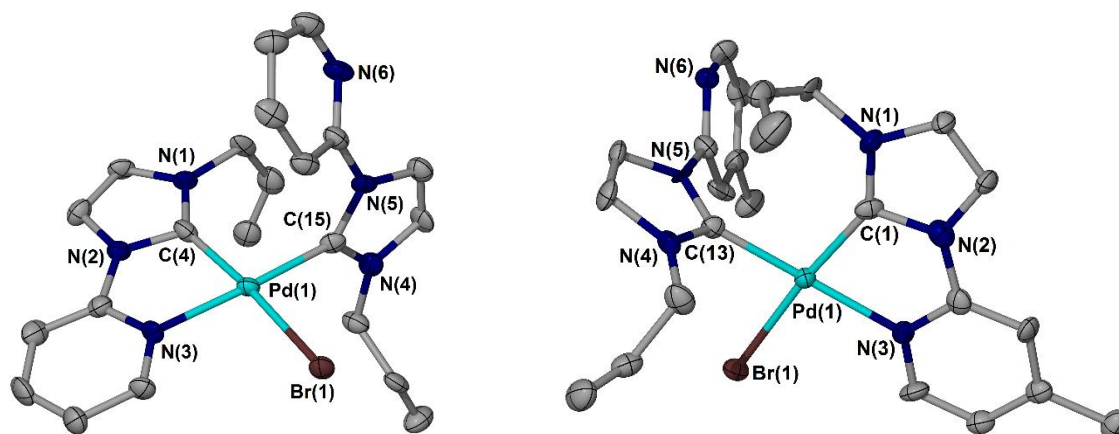
Figure 5.5 *Left: molecular structure of **5.1**. Right: molecular structure of **5.2**. Atomic displacement parameters are drawn at the 50 % probability level, hydrogen atoms and one Br counteranion are omitted from each for clarity.*

5.1	Pd(1)-C(4)	1.961(12)	C(4)-Pd(1)-N(3)	79.6(4)
5.1	Pd(1)-C(15)	1.968(10)	N(3)-Pd(1)-Br(1)	95.8(2)
5.1	Pd(1)-N(3)	2.091(8)	C(15)-Pd(1)-Br(1)	88.3(3)
5.1	Pd(1)-Br(1)	2.454(13)	C(4)-Pd(1)-Br(1)	175.1(3)
5.2	Pd(1)-C(1)	1.966(11)	C(1)-Pd(1)-C(13)	96.5(4)
5.2	Pd(1)-C(13)	1.986(11)	C(1)-Pd(1)-N(3)	80.3(4)
5.2	Pd(1)-N(3)	2.115(9)	N(3)-Pd(1)-Br(1)	94.7(3)
5.2	Pd(1)-Br(1)	2.4694(14)	C(1)-Pd(1)-Br(1)	174.6(3)

Table 5.2 *Selected bond lengths (Å) and angles (˚) from the crystal structures of **5.1** and **5.2**.*

Alongside the presence of two complex molecules per asymmetric unit, two molecules of methanol solvent were found to co-crystallise within the unit cell of **5.1**. The coordination environment around the metal centre can be described as mildly distorted square planar, with the smallest angle attributed to the C(4)-Pd(1)-N(3) intrachelate angle of 79.6(4)˚. In order to satisfy a square planar bonding mode, only one pyridyl-appended NHC ligand is able to fully chelate in the solid-state, whilst the opposing mutually *cis*-coordinated NHC resides relatively orthogonal to twist the adjoining pyridine ring out of the chelated plane. The coordinated pyridyl donor ligand is connected to the palladium centre at a contact distance of 2.091(8) Å (Pd(1)-N(3)), which is in agreement with those reported in the literature.[37] The molecular structure of **5.2** extends a similar discussion.

Under analogous reaction conditions, imidazolium bromide **P5.3** was combined in a 2:1 ratio with Pd(OAc)$_2$ to afford 5-nitropyridyl substituted congener, **5.3**, as a microcrystalline yellow solid. The electrospray mass spectrum of the complex supported palladium(II) *bis*-NHC formation, with a dominant mass peak (*m/z*) 644.9833 identified and attributed to the [Pd(NHC)$_2$Br]$^+$ molecular fragment.

The room temperature proton NMR spectrum of **5.3** was recorded in *d$_3$*-MeCN. Detailed within the spectrum, were a sequence of unremarkable broad signals attributed to the complex. Whilst fine-structural information could not be extrapolated, the spectrum clearly illustrated only one ligand environment implicative of a *C$_2$*-symmetric product. However, resonance-broadening could be subdued by recording the spectrum at low temperatures (*i.e.* 238K allowed for good quality signal resolution), revealing a pair of distinct ligand signals which corroborate a similar coordination geometry to those of **5.1** and **5.2** (variable temperature NMR measurements are provided in **Figure 5.6**).
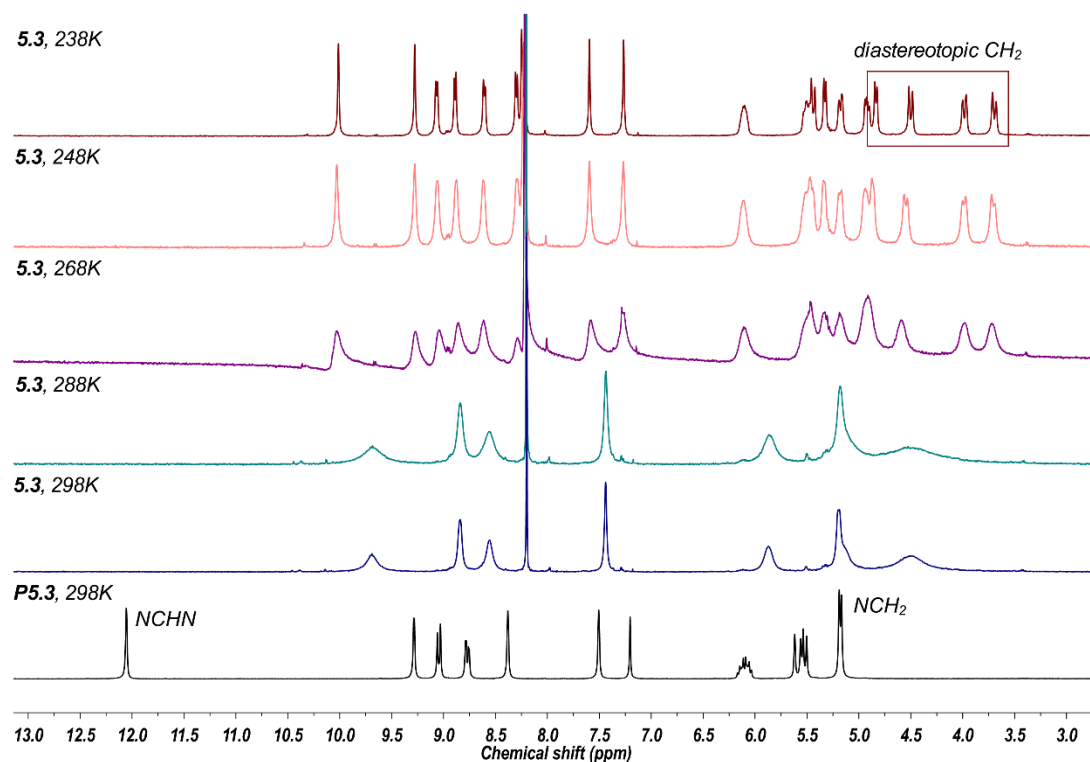
Figure 5.6 *^{1}H NMR spectrum of ligand precursor **P5.3** (black trace, 500 MHz, CDCl$_3$, 298K), noting original allylic NCH$_2$ doublet at 5.20 ppm and imidazolium NCHN singlet at 12.10 ppm. ^{1}H NMR spectrum of Pd-NHC complex **5.3** (blue trace, 500 MHz, CD$_3$CN, 298K), indicating loss of NCHN resonance and severe signal-broadening. Variable temperature ^{1}H NMR spectra of **5.3** (subsequent traces, 500 MHz, CD$_3$CN, 288 – 238K).*

Upon cooling, a well-resolved ^{1}H NMR spectrum of **5.3** was obtained which highlights a clearly unsymmetrical ligand binding mode around the metal centre, with full absence of the original imidazolium C2 proton signal. Four, mildly broadened singlet resonances at 10.01, 9.28, 8.25 and 8.21 ppm are observed, attributed to each distinct proton attached to both NHC backbones. Four additional, well-separated doublet (9.08, 8.88, 8.62 and 8.31 ppm) as well as two singlet signals (7.60, 7.27 ppm) are also displayed, which correspond to each inequivalent proton attached to both coordinated and non-coordinated pyridyl rings. Overall, ten magnetically inequivalent allylic/vinylic resonances are also presented between 6.2 – 3.6 ppm, with all four allylic NC*H$_2$* signals appearing as diastereotopic doublets on account of complexation.

X-ray quality crystals of **5.3** were obtained by the slow diffusion of diethyl ether vapours into a concentrated solution of the complex in a binary mixture of methanol/dimethyl sulfoxide, and subsequently authenticated using crystallographic analysis (a structural solution is supplied in **Figure 5.7**).
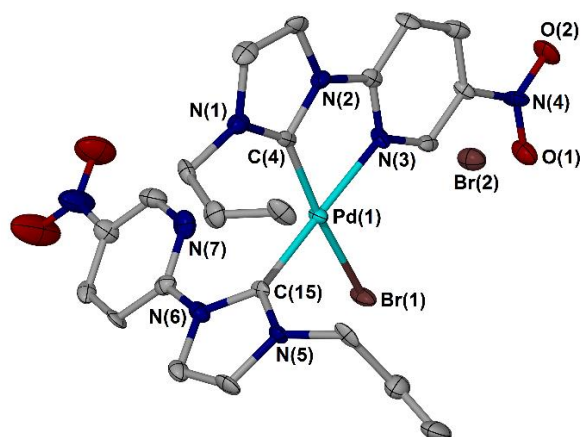
Figure 5.7 *Molecular structure of **5.3**. Atomic displacement parameters are drawn at the 50 % probability level, hydrogen atoms and one molecule of co-crystallised MeOH are omitted for clarity.*

Pd(1)-C(4)	1.994(9)	C(4)-Pd(1)-N(3)	79.0(3)
Pd(1)-C(15)	1.978(8)	C(4)-Pd(1)-C(15)	98.4(4)
Pd(1)-N(3)	2.090(7)	C(15)-Pd(1)-Br(1)	87.5(2)
Pd(1)-Br(1)	2.4508(12)	C(4)-Pd(1)-Br(1)	174.1(3)

Table 5.3 *Selected bond lengths (Å) and angles (˚) from the crystal structure of **5.3**.*

The crystal structure of **5.3** depicts a coordination sphere around the palladium(II) centre comprising two mutually *cis* NHC ligands, a chelating pyridyl donor group and one bromide ligand. The geometry around the metal is distorted square planar, with an intrachelate angle highly similar to that of **5.1**, at 79.0(3)˚ (C(4)-Pd(1)-N(3)). Interestingly, both Pd-C$_{carbene}$ bond lengths are equivalent (within error) at 1.99(9) and 1.98(8) Å, (Pd(1)-C(4) and Pd(1)-C(15), respectively); such close values may be surprising considering that one NHC chelates to afford a 5-membered ring where the other NHC does not. Further, each NHC is disposed *trans* to markedly different donor substituents at Pd (C(4) to bromide, C(15) to pyridyl), which may be expected to exhibit contrasting *trans* influences. The solid-state structure supports NMR spectroscopic measurements, implying an overall unsymmetrical Pd(NHC)$_2$ complex also exists in solution.

So-called ligand-scrambling studies were conducted in solution on complexes **5.1** – **5.3** using high-resolution mass spectrometry. A 5 mg sample of each complex was dissolved separately in MeCN solution, and directly subject to electrospray ionisation mass spectrometry; positive ions of [**5.1** – Br]$^+$ 557.0109, [**5.2** – Br]$^+$ 585.0401 and [**5.3** – Br]$^+$ 646.9797 were observed. Three further MeCN solutions were prepared of {**5.1** + **5.2**}, {**5.1** + **5.3**} and {**5.2** + **5.3**} in equal masses and analysed by ESI-MS. Only original homoleptic complex mass peaks were detected, with no evidence for cross-ligand metal species – indicative that fluxional solution-state behaviour is

caused solely by coordination/de-coordination of each pyridyl group, and that the NHC ligands remain firmly bound to Pd in solution.

Reaction of imidazolium bromide **P5.2** with half an equivalent of Pd(OAc)$_2$ delivered the expected 2:1 (NHC:Pd) stoichiometric complex, **5.2**. As shown in **Figure 5.3** (blue trace), the ^{1}H NMR spectrum of **5.2** features broad, yet assignable resonances which point toward palladium(II) *bis*-NHC complex formation, with complete absence of an azolium NC*H*N proton. Moreover, the mass spectrum collected in acetonitrile solvent features a dominant mass peak (*m/z*) 585.0465, attributable to the [Pd(NHC)$_2$Br]$^+$ molecular fragment with loss of one bromide anion upon ionisation, for which the calculated *versus* observed mass envelopes are given in **Figure 5.8**.
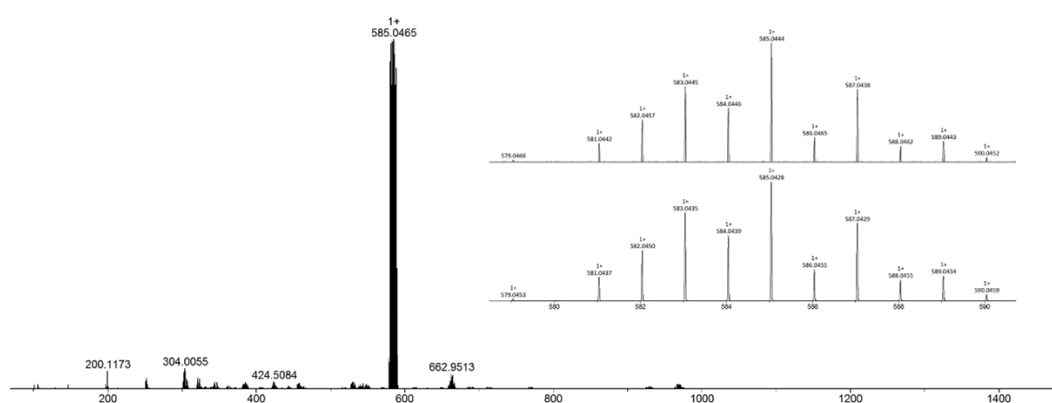
Figure 5.8 *Main image: electrospray mass spectrum of complex **5.2** recorded in MeCN solvent. Inset image: simulated (bottom) vs observed (top) mass envelope for [**5.2** – Br]$^+$ mass fragment, noting diagnostic isotopic distribution.*

Despite microanalytical data also implicative of a palladium(II) *bis*-NHC dibromide complex, crystallisation of **5.2** led to formation and isolation of the overall neutral [Pd(NHC)Br$_2$] complex, **5.2***. Broad, low quality ^{1}H NMR spectra of **5.2*** were procured, on account of poor solubility of the complex in common deuterated (including highly polar) solvents. However, electrospray mass spectrometry afforded the mass peak (*m/z*) 383.9333 corresponding with a [Pd(NHC)Br]$^+$ ion, and subsequent combustion analysis supports formation of a [Pd(NHC)Br$_2$] stoichiometric complex. With the only structural alteration between ligands **P5.1** (R = H)/**P5.3** (R = 5-NO$_2$) and **P5.2** being the presence of a mildly electron-donating 4-methyl group on the pyridyl ring, it was speculated that mild electronic activation may occur at Pd *via* this N-donor in complex **5.2** to evict one NHC ligand from the coordination sphere in forming **5.2***.

To judge this hypothesis, 4-methoxypyridyl substituted ligand precursor **P5.4** was similarly treated with Pd(OAc)$_2$ under analogous conditions to those outlined above. Supporting the idea of an electronically-driven ligand displacement pathway to [Pd(NHC)Br$_2$]-type complexes, **5.4*** was isolated as sole product and characterised using multinuclear NMR spectroscopy, high-resolution mass spectrometry and combustion analysis. Single crystals of **5.2*** and **5.4*** were

grown from the vapour diffusion of diethyl ether into a dichloromethane/dimethylsulfoxide (1:1, $^v/_v$) solution of each complex, and both were structurally elucidated using X-ray diffraction methods (**Figure 5.9**).
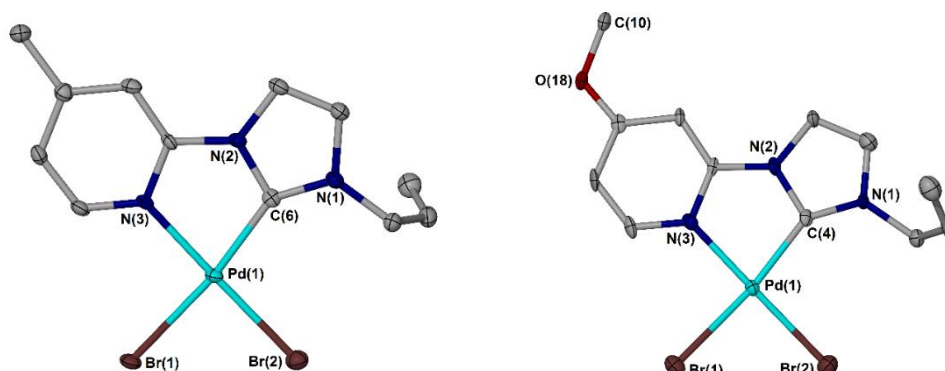
Figure 5.9 *Left: molecular structure of **5.2***. Right: molecular structure of **5.4***. Atomic displacement parameters are drawn at the 50 % probability level, hydrogen atoms are omitted for clarity.*

5.2*	Pd(1)-C(6)	1.982(4)	C(6)-Pd(1)-N(3)	79.8(14)
5.2*	Pd(1)-N(3)	2.065(3)	C(6)-Pd(1)-Br(1)	172.5(11)
5.2*	Pd(1)-Br(1)	2.482(5)		
5.2*	Pd(1)-Br(2)	2.427(5)		
5.4*	Pd(1)-C(4)	1.998(8)	C(4)-Pd(1)-N(3)	80.3(3)
5.4*	Pd(1)-N(3)	2.057(7)	C(4)-Pd(1)-Br(1)	171.9(2)
5.4*	Pd(1)-Br(1)	2.470(10)		
5.4*	Pd(1)-Br(2)	2.418(11)		

Table 5.4 *Selected bond lengths (Å) and angles (°) from the crystal structures of **5.2*** and **5.4***.*

The solid-state structures of Pd(NHC)Br$_2$ complexes **5.2*** and **5.4*** are highly similar, both displaying distorted square planar geometry about a palladium(II) metal centre. Despite bearing a strongly electron donating methoxy substituent at the *para* position of the pyridyl ring in **5.4***, the Pd-N$_{pyridyl}$ bond length is maintained at 2.057(7) Å – a value in keeping with *meta*-nitro substituted analogue, **5.3** (2.090(7) Å) and *para*-methyl substituted direct analogue, **5.2*** (2.065(3) Å), implying little electronic influence upon pyridyl basicity.

Crabtree, Albrecht and Faller have studied the effect of nucleophilic outer sphere anions on pyridyl substituted, chelating carbene complexes of palladium.[38] The authors found that in the presence of weakly coordinating anions (*e.g.* tosylate), square planar complexes of palladium(II) undergo intramolecular coordinative fluxion, which involves only the ligand and does not change the coordination number of the metal. However, strongly coordinating anions are shown to de-coordinate pyridyl donor groups at Pd, opening up an additional site at the metal that would

otherwise not be considered possible. In view of these findings, a proposed mechanism for Pd(NHC)Br$_2$ formation is provided in **Scheme 5.8**.

It is postulated that complexes **5.2**[*] and **5.4**[*] form *via* a solution-state ligand displacement process, whereby the initially-formed 2:1 ligand:metal [Pd(NHC)$_2$(Br)Br] complex (**5.2** or **5.4**) dissociates one hemilabile pyridyl donor group to vacate a coordination site at Pd. Following reversible de-coordination, a vicinal bromide counterion is able to occupy a coordination site at Pd, with subsequent displacement of an NHC ligand by a strongly activated and chelating pyridyl wingtip group. It is proposed that in the presence of aerated solvent, the free NHC is oxidised to a neutral imidazolinone which is irreversible and drives the displacement reaction, as illustrated in **Scheme 5.8**.

5.2: R = 4-Me
5.4: R = 4-OMe

5.2[*]: R = 4-Me
5.4[*]: R = 4-OMe
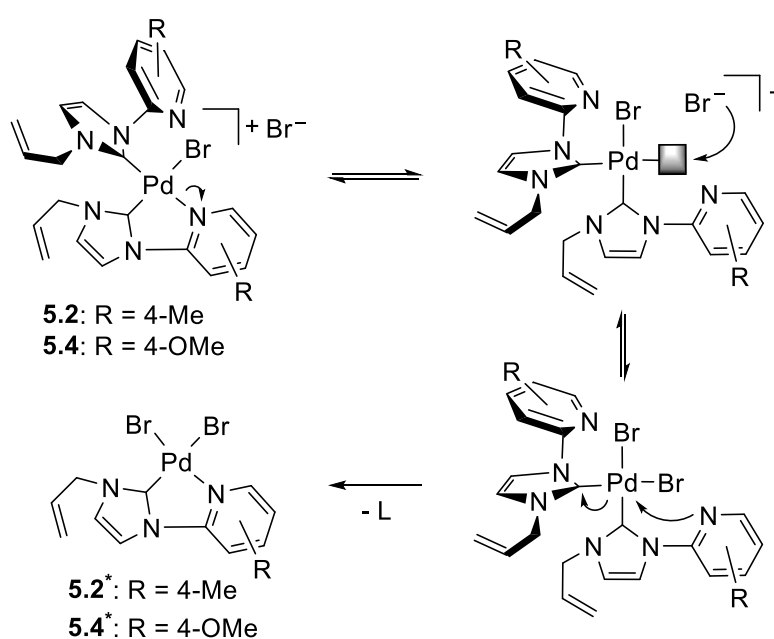
Scheme 5.8 Proposed mechanism of Pd(NHC)Br$_2$ complex formation.

In general, palladium-catalysed cross-coupling reactions involve a truly homogenous palladium complex which mediates the mechanism through distinct catalytic steps. With this in mind, it was sought to improve the solubility of complexes **5.1 – 5.4** by preparing their corresponding acetonitrile adducts. The direct halide abstraction from a metal centre offers a convenient route to their solvent-coordinated versions, which is typically driven by the formation of an insoluble silver(I) halide salt, and has been well-exemplified in the literature.[39,40] However, as complexes **5.2** and **5.4** appear to undergo an unusual ligand displacement reaction in solution, it was instead decided to abstract bromide from parent ligand precursors **P5.1 – P5.4**, by treatment with two equivalents of ammonium hexafluorophosphate under aqueous conditions to deliver their hexafluorophosphate analogues, **P5.1.1 – P5.4.1**. Subsequent treatment of **P5.1.1 – P5.4.1** with 0.5 equivalents Pd(OAc)$_2$ in anhydrous acetonitrile allowed isolation of palladium(II) *bis*-NHC dihexafluorophosphate complexes, **5.1.1 – 5.4.1** (**Scheme 5.9**).
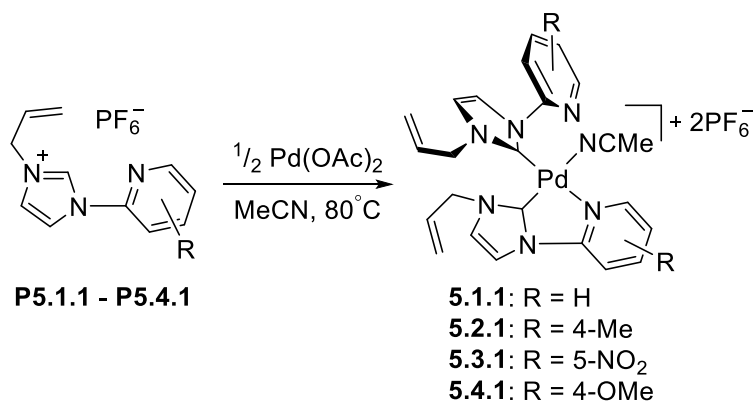
Scheme 5.9 General synthetic route to [Pd^{II}(NHC)$_2$(NCMe)]2PF$_6$ complexes.

Dihexafluorophosphate complexes **5.1.1** – **5.4.1** were characterised using multinuclear NMR spectroscopy, high-resolution mass spectrometry and elemental analysis. From the outset, the ^{1}H NMR spectra of complexes **5.1.1** and **5.2.1** were recorded in d_3-MeCN – for which each proved highly soluble at room temperature. Each spectrum displayed a sequence of sharp resonances, both corroborating two distinct ligand environments around the metal centre with no evidence of C_2-symmetry. Importantly, the spectra suggest little, if any ligand fluxion occurs in solution on an NMR timescale where bromide is not present within the coordination sphere. Room temperature proton NMR spectra of **5.1.1** and **5.2.1** are reproduced in **Figure 5.10**.
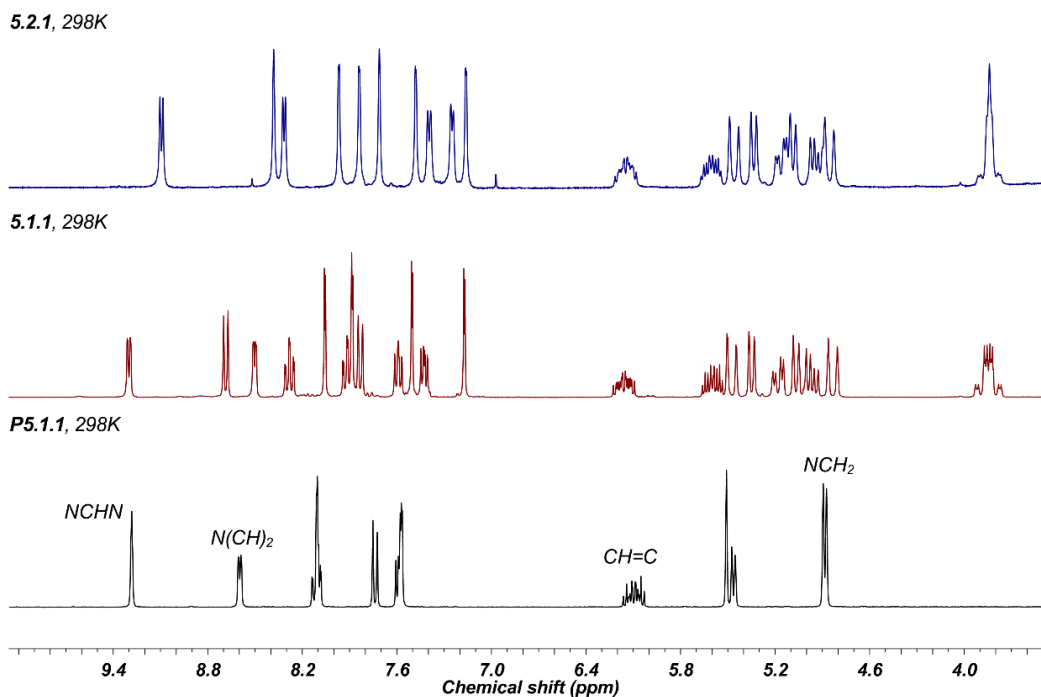
Figure 5.10 ^{1}H NMR spectrum of ligand precursor **P5.1.1** (black trace, 400 MHz, CD$_3$CN, 298K), noting original vinylic multiplet at 6.09 ppm, allylic NCH$_2$ doublet at 4.89 ppm and imidazolium NCHN singlet at 9.28 ppm. ^{1}H NMR spectrum of Pd-NHC complex **5.1.1** (red trace, 500 MHz, CD$_3$CN, 298K), indicating loss of NCHN signal. ^{1}H NMR spectrum of related Pd-NHC **5.2.1** (blue trace, 500 MHz, CD$_3$CN, 298K) is provided for comparison.

The positive mass peaks (*m/z*) 238.0471, 289.9902, and 331.0185 noted in the mass spectrum of **5.1.1** were attributable to $[\{M - MeCN\} - 2PF_6]^{2+}$, $[\{M - L - MeCN\} - 2PF_6]^{+}$ and $[\{M - L\} - 2PF_6]^{+}$, respectively, displaying that the species loses weakly coordinating PF_6 anions prior to detection (a similar fragmentation pattern was observed for **5.2.1**).

The proton NMR spectrum of complex **5.3.1** is given in **Figure 5.11**. Notably, recording the spectrum at room temperature provides a sequence of relatively sharp, well-defined signals, which compare well with those found for **5.1.1** and **5.2.1** (red trace). Contrary to expectation, procurement of the same spectrum at elevated temperature (333K) leads to further resonance resolution, to overall distinguish twenty magnetically inequivalent proton signals with discrete multiplicity (blue trace). The electrospray mass spectrum featured dominant peaks (*m/z*) 283.0336 and 583.0664, corroborating with molecular fragments $[\{M - MeCN\} - 2PF_6]^{2+}$ and $[\{M - MeCN + OH\} - 2PF_6]^{+}$, respectively.

5.3.1, 333K

5.3.1, 298K

P5.3.1, 298K
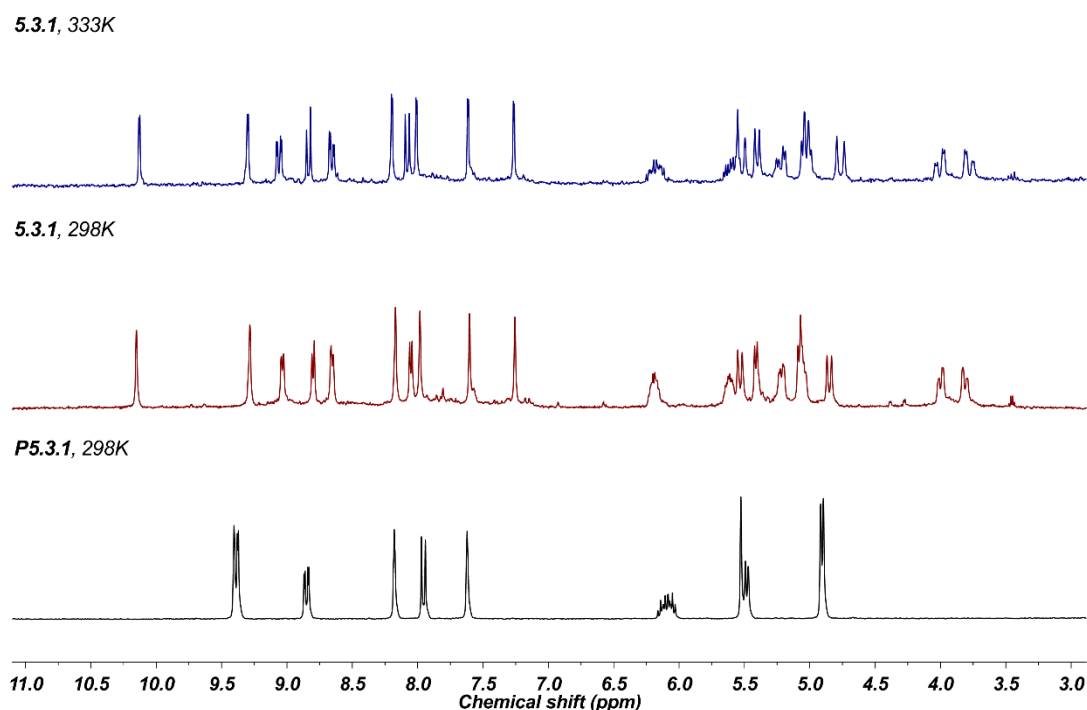
Figure 5.11 ^{1}H NMR spectrum of ligand precursor P5.3.1 (black trace, 400 MHz, CD$_3$CN, 298K). ^{1}H NMR spectrum of Pd-NHC complex 5.3.1 (red trace, 500 MHz, CD$_3$CN, 298K), (blue trace, 500 MHz, CD$_3$CN, 333K).

Single crystals of **5.3.1** were grown from the slow evaporation of a concentrated acetonitrile solution of the complex, and isolated as pale yellow blocks which were analysed by X-ray crystallography (**Figure 5.12**). Structural solution of **5.3.1** in the solid-state reveals the expected [Pd(NHC)$_2$(NCMe)]2PF$_6$ complex, whereby a molecule of acetonitrile solvent occupies a vacant coordination site at palladium. As observed for previously described complexes within, **5.3.1** exhibits distorted square planar geometry, with one NHC ligand forming a 5-membered chelate

ring. The Pd-C$_{carbene}$ bond length (1.962(3) Å, Pd(1)-C(4)) is refined to a value surprisingly similar to that of analogue **5.3** (1.994(9) Å, Pd(1)-C(4)), considering a *trans* bromide ligand is substituted for a molecule of acetonitrile.

Full characterisation, including single crystal X-ray diffraction analysis, was also conducted on palladium(II) *bis*-NHC complex **5.4.1** and will be discussed within Chapter 6.
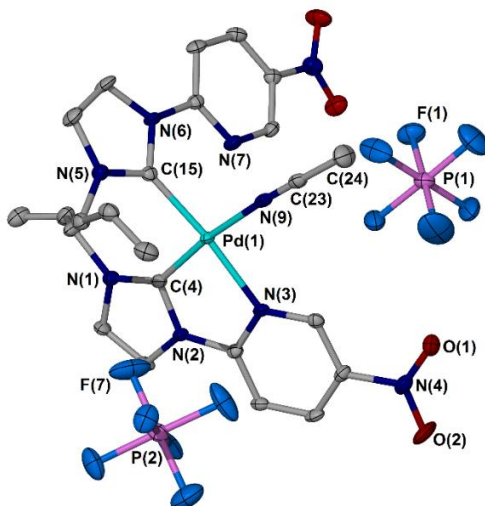
Figure 5.12 *Molecular structure of* ***5.3.1***. *Atomic displacement parameters are drawn at the 50 % probability level, hydrogen atoms are omitted for clarity.*

Pd(1)-C(4)	1.962(3)	N(3)-Pd(1)-C(4)	80.25(10)
Pd(1)-C(15)	1.978(3)	N(9)-Pd(1)-C(4)	172.81(10)
Pd(1)-N(9)	2.055(2)		
Pd(1)-N(3)	2.092(2)		

Table 5.5 *Selected bond lengths (Å) and angles (˚) from the crystal structure of* ***5.3.1***.

A clear observation regarding the palladium(II) complexes of *N*-pyridyl appended NHC ligands outlined within, is the extent of coordinative restriction around the distorted square plane of the metal centre – as evidenced by the inability for both NHC ligands to fully chelate within each palladium *bis*-NHC assembly. To improve conformational flexibility about the coordination sphere, *N*-picolyl substituted NHC precursors **P5.5**, **P5.6** and hexafluorophosphate congener **P5.6.1** were treated with Pd(OAc)$_2$ under standard conditions, furnishing palladium(II) *bis*-NHC complexes **5.5.1**, **5.6** and **5.6.1** (**Scheme 5.10**).
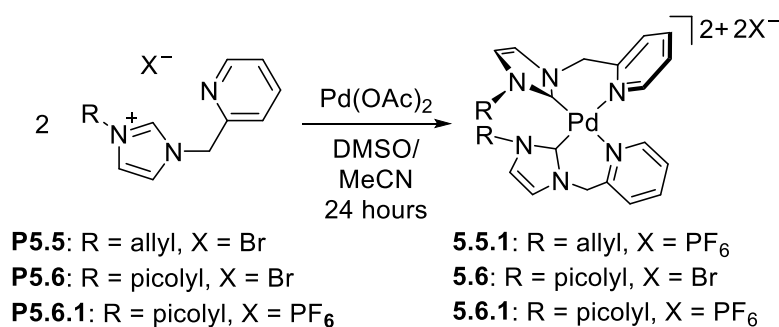
Scheme 5.10 *General synthetic route to N-picolyl substituted Pd^{II}-NHC complexes.*

Initial reaction of two equivalents of imidazolium salt **P5.5** with Pd(OAc)$_2$ delivered the corresponding Pd(NHC)$_2$Br$_2$ complex, which proved to be extremely hygroscopic and difficult to handle under an atmosphere of air. Consequently, the resulting residue was dissolved in deionised water and reacted immediately with an excess of NH$_4$PF$_6$, providing the air- and moisture-stable [Pd(NHC)$_2$]2PF$_6$ complex, **5.5.1**, as a microanalytically pure pale yellow solid.

Recording the proton NMR spectrum of **5.5.1** in *d$_3$*-MeCN solution at room temperature provided a sequence of well-defined signals, with some broad resonances attributed to hydrogen atoms attached to each conformationally 'unlocked' *N*-allyl group which could be further resolved by their measurement at low temperature (233K), allowing identification of their structural environments (**Figure 5.13**, dark red circles). Upon complexation, two doublet resonances appear clearly in the ^{1}H NMR spectrum at 5.28 and 5.22 ppm, corroborating with each diastereotopic proton attached to the methylene bridge of the ligand (blue circles). These signals appear sharp throughout all variable temperature measurements (233 – 323K), indicating that both *N*-picolyl nitrogen donors are fully coordinated to the Pd centre at all times. Notable is a strongly deshielded proton environment signalling at 9.26 ppm in the same spectrum, which is attributable to hydrogen atoms in the *ortho* position of each coordinated pyridyl ring – as confirmed by bidimensional NMR spectroscopy.
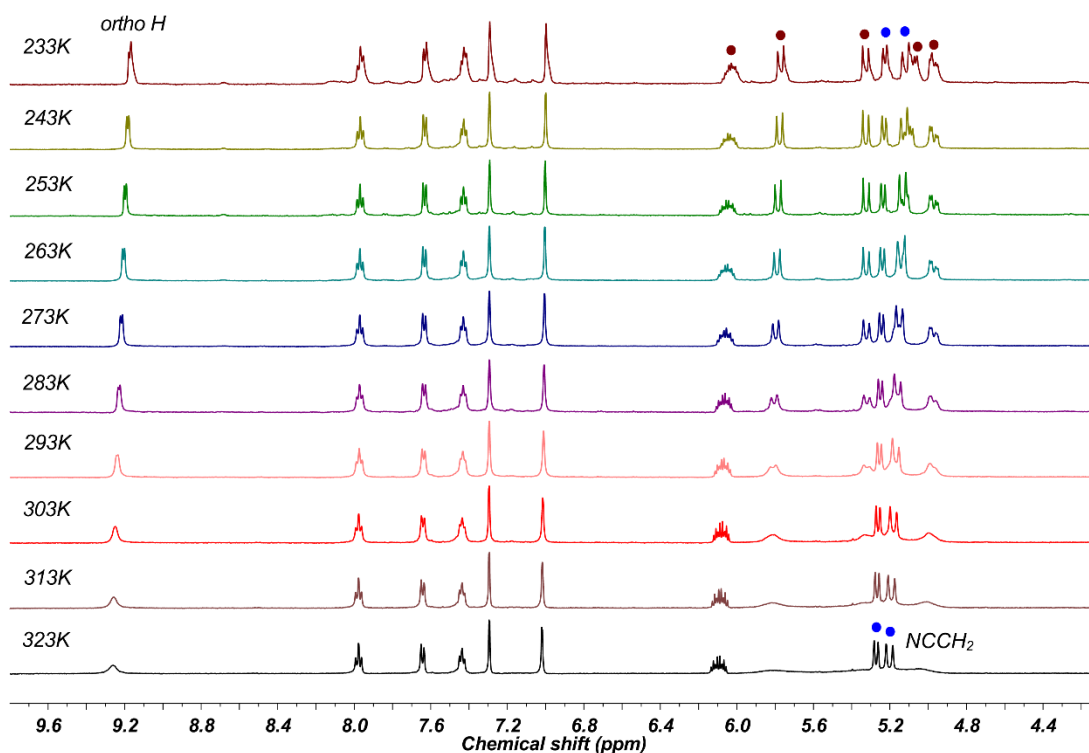
Figure 5.13 *Variable temperature ^{1}H NMR spectra (233 – 323K) of **5.5.1** (500 MHz, CD$_3$CN), noting persistent diastereotopic doublet signals at 5.28 and 5.22 ppm (blue circles), and fully resolved allylic resonances (dark red circles).*

Slow diffusion of diethyl ether vapours into an acetonitrile solution of **5.5.1** allowed isolation of pale yellow needles, which were amenable to X-ray crystallographic analysis (given in **Figure 5.14**). Analysis of the solid-state structure disclosed comfortable square planar geometry around the Pd centre, with the smallest intrachelate angle of 85.97(10)°, attributed to C(4)-Pd(1)-N(3), and a C(4)-Pd(1)-C(16) angle of 95.25(11)° between the mutually *cis*-coordinated NHC ligands. As a result of additional conformational relief from each methylene-bridged ligand, each hemilabile 6-membered C,N-palladacycle adopts boat-like geometry, allowing each independent NHC unit to reside relatively orthogonal, generating a pair of 5,6,6-fused tricyclic ring scaffolds within the full assembly.

Visually, it is possible to retrofit the presence of persistent doublet resonances in the solution-state ^{1}H NMR spectrum of **5.5.1** based on the partial crystal structure depicted in **Figure 5.14** (right image). Despite the difficulty associated with accurately locating hydrogen atoms by X-ray diffraction, the partial crystal structure of **5.5.1** clearly illustrates two boat-shaped rings which are interlocked at the Pd metal centre, with each housing one sp^3-hybridised carbon atom. For this reason, it is possible to consider the locations of H(7A,B) and H(19A,B) to be true, in that one pair of protons (H(7A) and H(19A)) are equivalently located in the 'flag-pole' position, whilst the remaining pair (H(7B) and H(19B)) are positioned equatorial. This conformational lock is the origin of nuclear magnetic inequivalence.

195
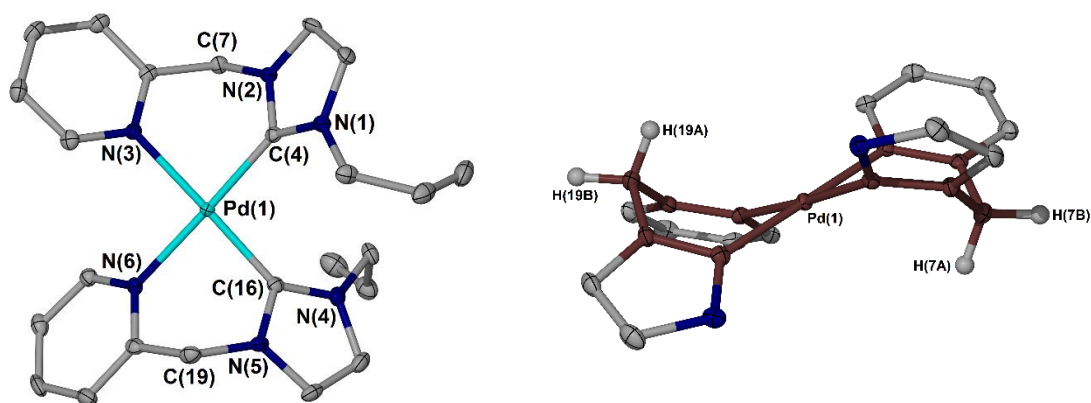
Figure 5.14 *Left: cationic portion of the asymmetric unit of **5.5.1**. Right: partial molecular structure of **5.5.1**, highlighting two 6-membered boat motifs interlocked at Pd (bonds highlighted in dark red). Atomic displacement parameters are drawn at the 50 % probability level, hydrogen atoms (except (H7A, B) and H(19A, B)) and two PF_6 counteranions are omitted for clarity.*

Pd(1)-C(4)	1.979(3)	N(3)-Pd(1)-C(4)	85.97(10)
Pd(1)-C(16)	1.977(3)	N(6)-Pd(1)-C(16)	86.22(10)
Pd(1)-N(3)	2.101(2)	C(4)-Pd(1)-C(16)	95.25(11)
Pd(1)-N(6)	2.091(2)	C(4)-Pd(1)-N(6)	176.83(10)

Table 5.6 *Selected bond lengths (Å) and angles (˚) from the crystal structure of **5.5.1**.*

Similar independent treatment of ligand precursors **P5.6** and **P5.6.1** with 0.5 equivalents $Pd(OAc)_2$ led to formation of their corresponding $Pd(NHC)_2(Br)_2$ and $Pd(NHC)_2(PF_6)_2$ complexes, **5.6** and **5.6.1**, respectively. The identity of each complex was confirmed by multinuclear NMR spectroscopy, high-resolution mass spectrometry and combustion analysis. Electrospray mass spectrometry of **5.6** detected only two mass peaks (*m/z*) 303.0761 and 687.0666, appertaining to $[M - 2Br]^{2+}$ and $[M - Br]^+$ fragments, whereas only a single ion peak was observed for **5.6.1** at (*m/z*) 751.1138, attributable to $[M - PF_6]^+$ - implying that one weakly coordinating PF_6^- anion remains associated with the complex prior to detection.

X-ray quality crystals of **5.6** and **5.6.1** were obtained *via* diffusion of diethyl ether vapours into either a binary mixture of dimethylsulfoxide/dichloromethane (**5.6**) or acetonitrile (**5.6.1**), and structurally elucidated (**Figure 5.15**).
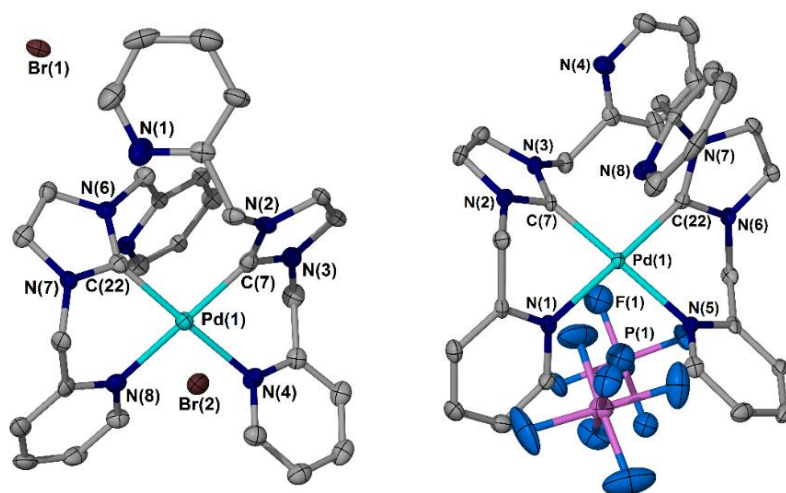
Figure 5.15 *Left: molecular structure of **5.6**. Right: molecular structure of **5.6.1**. Atomic displacement parameters are drawn at the 50 % probability level, hydrogen atoms are omitted for clarity.*

6.12	Pd(1)-C(7)	1.964(8)	N(4)-Pd(1)-C(7)	85.1(3)
6.12	Pd(1)-C(22)	1.980(7)	N(8)-Pd(1)-C(22)	85.4(3)
6.12	Pd(1)-N(4)	2.109(6)	C(7)-Pd(1)-N(8)	179.5(3)
6.12	Pd(1)-N(8)	2.103(7)	C(22)-Pd(1)-N(4)	175.5(3)
6.12.1	Pd(1)-C(7)	1.950(5)	N(1)-Pd(1)-C(7)	84.85(19)
6.12.1	Pd(1)-C(22)	1.969(5)	N(5)-Pd(1)-C(22)	85.71(19)
6.12.1	Pd(1)-N(1)	2.093(4)	C(7)-Pd(1)-N(5)	178.39(19)
6.12.1	Pd(1)-N(5)	2.097(4)	C(22)-Pd(1)-N(1)	176.79(19)

Table 5.7 *Selected bond lengths (Å) and angles (˚) from the crystal structures of **5.6** and **5.6.1**.*

Solid-state structural analysis revealed highly comparable geometrical settings between **5.6** and **5.6.1**, with each independent NHC ligand coordinating to the metal in a bidentate manner. Whilst both crystal structures of **5.6** and **5.6.1** are highly similar in terms of coordination environment, with very closely matched bond angles about the square plane of Pd, their ligand-metal bond distances differ notably. The presence of bromide within the outer coordination sphere of complex **5.6** appears to cause all metal-ligand bonds to contract significantly in comparison to those of dihexafluorophosphate analogue, **5.6.1** (refer to **Table 5.7**).

Moreover, the extended crystal structure of **5.6** is arranged to comprise a series of solvent-accessible channels running along the crystallographic *c* axis, with an approximate internal diameter of 14 Å, in which DMSO solvent molecules remain situated in the solid-state (**Figure 5.16**).
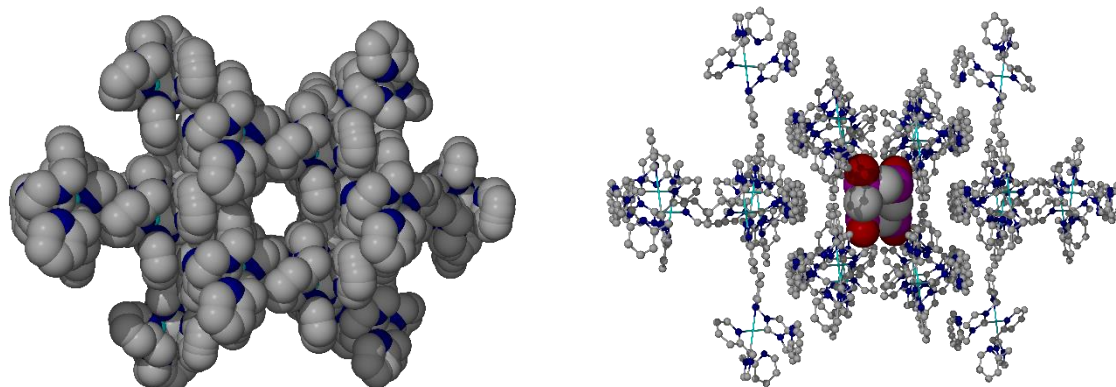
Figure 5.16 *Left: space-filling diagram revealing solvent-accessible pore running parallel to the crystallographic c axis. Right: ball-and-stick diagram with space-filled model of four DMSO molecules occupying one accessible channel.*

5.4 Palladium-catalysed cross-coupling reactions

Since its independent discovery in the early 1970's by Richard Heck[41] and Tsutomo Mizoroki,[42] the Heck-Mizoroki reaction (most commonly referred to as the "Heck reaction") has been widely employed as a tool for the direct attachment of olefenic groups to aromatic rings.[43–45] Numerous palladium-based catalysts with various ligand-types (*e.g.* phosphines,[46,47] amines[48] and thiolates[49]) have been published which mediate Heck cross-coupling, though high temperatures (*i.e.* 100 – 180 ˚C) are often required,[50–53] with few catalytic systems reported which affect the reaction below 100 ˚C with adequate efficiency.[26,54]

In general, metal complexes of NHCs tend to display high stability toward heat, oxygen and moisture, and have long been the subject of catalytic study. Herrmann and co-workers reported the first example of a palladium-NHC catalysed Heck cross-coupling of aryl bromides (and even activated aryl chlorides) in 1995.[55] Since, a range of palladium-NHC complexes have been evaluated in these reactions using a variety of coupling partners, with the overall rate of reaction dependent upon a number of parameters, such as temperature, solvent, base and catalyst loading. With these in mind, it was sought to examine the overall effect on catalysis of a flexible pyridyl donor group tethered together with a proximal alkene, framed around a strongly bound NHC ligand at Pd. The cross-coupling between bromobenzene and *n*-butyl acrylate was selected as a benchmark arylation reaction, using adapted conditions to those independently reported by Fairlamb[22] and Fu[46] (**Scheme 5.11**).

Using a high-throughput carousel reactor, a sequence of Radley tubes were each charged under the standard conditions, which are provided below **Table 5.8**. From the outset, it was found that a small quantity of boronic acid additive (2 equivalents relative to catalyst) was required to initiate the Pd pre-catalysts, without such low conversion to *n*-butyl cinnamate was observed (entry 1^a, 5%); therefore an incubation period (5 minutes) was employed to generate the low-valent Pd^0 source to trigger the catalytic cycle. Similarly, a control experiment in which Cs_2CO_3 was omitted led to comparably low product formation (entry 1^b, 5%), implying the presence of base is essential. However, employment of both boronic acid (0.06 equivalents) and base (1.1 equivalents) provided arylated product in much higher yield (entry 1, 28%), with a 4.5-fold greater catalyst turnover number.

In general, palladium-NHC complexes incorporating bromide counterions within the coordination sphere (entries 1 – 6) led to low consumption of starting materials, relative to their hexafluorophosphate analogues. It is postulated that the reduced solubility of these complexes acts to lower their effective solution concentration, with coordinative saturation inhibiting substrate binding at the metal centre. Use of non-coordinating hexafluorophosphate anions (entries 7 – 12) increased conversion to coupled product, with topmost conversion achieved using *N*-allyl-*N'*-picolyl substituted Pd-NHC, **5.5.1** (entry 11, TON = 12). Notably, no clear electronic trend was observed to relate complexes of 4-Me (entry 8, TON = 11), 5-NO_2 (entry 9, TON = 11) and 4-OMe (entry 10, TON = 10) pyridyl substituted NHC ligands with catalytic activity.
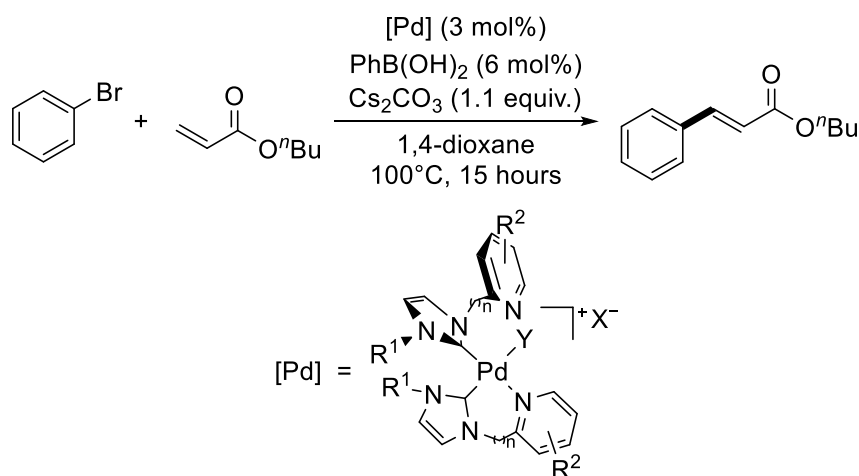
Scheme 5.11 *Archetypal intermolecular Heck arylation reaction.*

Entry	Catalyst (R^1, R^2, n)	X	Y	Conv. (%)[d]	TON
1[a]	**5.1** (allyl, H, 0)	Br	Br	5	2
1[b]	**5.2** (allyl, H, 0)	Br	Br	5	2
1	**5.1** (allyl, H, 0)	Br	Br	28	9
2	**5.2** (allyl, 4-Me, 0)	Br	Br	34	11
3	**5.2**[*] (allyl, 4-Me, 0)	Neutral[c]	2Br	14	5
4	**5.3** (allyl, 5-NO_2, 0)	Br	Br	23	8
5	**5.4**[*] (allyl, 4-OMe, 0)	Neutral[c]	2Br	9	3
6	**5.6** (picolyl, H, 1)	2Br	picolyl	27	9
7	**5.1.1** (allyl, H, 0)	$2PF_6$	MeCN	35	12
8	**5.2.1** (allyl, 4-Me, 0)	$2PF_6$	MeCN	34	11
9	**5.3.1** (allyl, 5-NO_2, 0)	$2PF_6$	MeCN	34	11
10	**5.4.1** (allyl, 4-OMe, 0)	$2PF_6$	MeCN	31	10
11	**5.5.1** (allyl, H, 1)	$2PF_6$	picolyl	37	12
12	**5.6.1** (picolyl, H, 1)	$2PF_6$	picolyl	33	11

Table 5.8 *Evaluation of Pd-NHCs in Heck cross-coupling reaction. Conditions: bromobenzene (1.9 mmol), n-butyl acrylate (3.6 mmol), Pd pre-catalyst (0.057 mmol), $PhB(OH)_2$ (0.11 mmol), Cs_2CO_3 (2.1 mmol), 1,4-dioxane solvent (3 mL, anhydrous). [a]$PhB(OH_2)$ omitted; [b]Cs_2CO_3 omitted; [c]two bromide anions are coordinated to Pd; [d]conversion (%) analysed by GC and are recorded as the average of three consecutive runs.*

On the whole, poor catalyst turnover numbers and modest product conversions were observed using palladium(II) *bis*-NHC complexes in the Heck arylation of *n*-butyl acrylate. Given that each palladium(II) pre-catalyst requires an additional activation step through homocoupling of a boronic acid additive to form an active Pd^0 species, it was hypothesised that the family of palladium *bis*-NHC complexes outlined within may better suit a Suzuki-Miyaura cross-coupling reaction, whereby a boronic acid may play a role to both activate the pre-catalyst and act as coupling partner.

In the first instance, a simple cross-coupling reaction between phenylboronic acid and bromobenzene was considered, using Cs_2CO_3 as source of base and 1,4-dioxane solvent (**Scheme 5.12**), the results of which are summarised in **Table 5.9**.
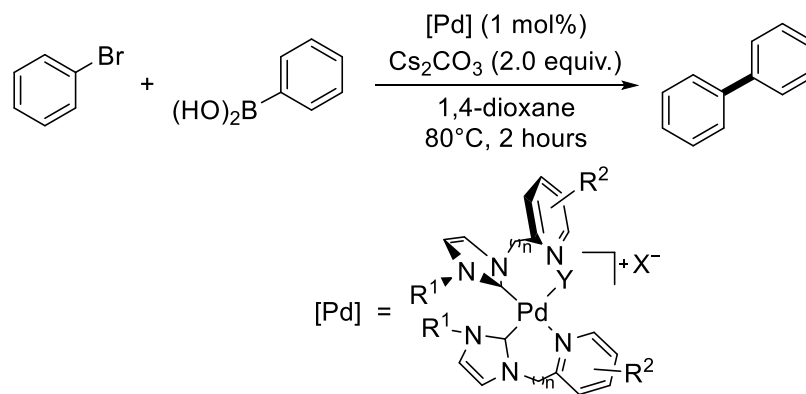
Scheme 5.12 *Benchmark Suzuki-Miyaura cross-coupling reaction.*

Entry	Catalyst (R^1, R^2, n)	X	Y	Conv. (%)^d	TON/TOF (h^{-1})
1^a	**5.1** (allyl, H, 0)	Br	Br	3	3/1.5
1	**5.1** (allyl, H, 0)	Br	Br	83	83/42
2	**5.2** (allyl, 4-Me, 0)	Br	Br	86	86/43
3	**5.2*** (allyl, 4-Me, 0)	Neutral^c	2Br	56	56/28
4	**5.3** (allyl, 5-NO$_2$, 0)	Br	Br	78	78/39
5	**5.4*** (allyl, 4-OMe, 0)	Neutral^c	2Br	68	68/34
6	**5.6** (picolyl, H, 1)	2Br	picolyl	94	94/47
7	**5.1.1** (allyl, H, 0)	2PF$_6$	MeCN	86	86/43
8	**5.2.1** (allyl, 4-Me, 0)	2PF$_6$	MeCN	84	84/43
9	**5.3.1** (allyl, 5-NO$_2$, 0)	2PF$_6$	MeCN	81	81/41
10	**5.4.1** (allyl, 4-OMe, 0)	2PF$_6$	MeCN	88	88/44
11	**5.5.1** (allyl, H, 1)	2PF$_6$	picolyl	92	92/46
12	**5.6.1** (picolyl, H, 1)	2PF$_6$	picolyl	94	94/47
13^b	**5.6.1** (picolyl, H, 1)	2PF$_6$	picolyl	>99	66/33

Table 5.9 *Evaluation of Pd-NHCs in Suzuki-Miyaura cross-coupling reaction. Conditions: bromobenzene (1.0 mmol), PhB(OH)$_2$ (1.5 mmol), Pd pre-catalyst (0.01 mmol), Cs$_2$CO$_3$ (2.0 mmol), 1,4-dioxane solvent (5 mL, anhydrous). ^{a}Cs$_2$CO$_3$ omitted; ^{b}catalyst loading increased to 0.015 mmol (1.5 mol%); ^{c}two bromide anions are coordinated to Pd; ^{d}conversion (%) analysed by GC and are recorded as the average of three consecutive runs.*

As anticipated, a clear increase in catalytic activity is observed on deployment of palladium(II) *bis*-NHC complexes in a Suzuki-Miyaura cross-coupling reaction, when compared with a Heck-type arylation reaction. A more noticeable trend is now apparent between electronically diverse pyridyl donor wingtip groups; a subtle increase in conversion as an electron-withdrawing nitro substituent (entry 9, 81%) is replaced by a mildy electron-donating methyl (entry 8, 84%) or strongly electron-rich methoxy group (entry 10, 88%) on the hemilabile pyridyl ring. This pattern may be interpreted such that electron-dense proximal pyridyl donor groups act to enhance

catalytic turnover. In contrast, overall neutral palladium(II) *mono*-NHC dibromide complexes perform poorly in the coupling transformation (entries 3 and 5), providing lowest recorded conversions to biphenyl (56 and 68%, respectively). Hexafluorophosphate analogues (entries 7 – 13) afforded turnover numbers comparable to their dibromide counterparts, implying little influence of coordinating counterion on the catalytically active Pd species. Taking from these, it is plausible that the presence of two pyridyl donor groups within the coordination sphere of Pd enables constant (or close-to) occupancy of vacant coordination sites upon removal of bromide, stabilising the presumably low-valent palladium metal throughout the cycle whilst able to dissociate for substrate binding.

Highest conversions were achieved using *N*-picolyl tethered NHC ligated Pd complexes (entries 11 – 13), with *bis*-picolyl substituted palladium-NHC complex **5.6.1** displaying upmost turnover number (entry 12, TON = 94). For this system, a 50% increase in catalyst loading (entry 13, 1.5 mol% Pd) led to only trace quantities of bromobenzene detectable by GC analysis after 2 hours reaction time. In all cases, relatively low catalyst turnover numbers (and therefore, frequencies) were observed. Nevertheless, these results imply that additional geometrical freedom of each hemilabile pyridyl donor provides greater stabilisation of Pd throughout catalysis; such a conclusion has been previously drawn for analogous complexes of Cu, Ir, Ru and Fe.[14,15,17]

With respect to the cross-coupling of organoboron reagents with organic electrophiles, one of the most challenging couplings remains the formation of *tetra-ortho*-substituted biaryl compounds, particularly under mild reaction conditions. In an initial report produced by Johnson and Foglesong in 1997, a combination of [Pd(PPh$_3$)$_4$] and Na$_2$CO$_3$ was found to furnish an unsymmetrical *tetra-ortho*-substituted biaryl in 12% overall yield (no temperature was given).[56] These findings spurred Buchwald and co-workers to refine a system using hindered biarylphosphine ligands in combination with [Pd$_2$(dba)$_3$] at 110 ˚C to access similar biphenyl products.[57,58] In 2004, Glorius *et al.* prepared analogous biaryl compounds *via* coupling of substituted aryl chlorides with boronic acids, catalysed by a bioxazoline-derived ligand (coined IBiox12.HOTf) with Pd(OAc)$_2$ at 110 ˚C,[59] with a further report by Hoshi and Hagiwara forming the same products by use of a ruthenocenylphosphine/[Pd$_2$(dba)$_3$] system at 100 ˚C.[60] The requirement for high reaction temperatures places limitation on this synthetic methodology, and the development of a catalytic system which can affect the formation of sterically congested/functionalised biaryls at relatively low temperatures would constitute a significant landmark.

The Pd-PEPPSI series have been evaluated against the catalytic coupling of 2,6-dimethylphenylboronic acid and 1-bromo-2-methoxynaphthalene, using KOH as source of base and 1,4-dioxane as solvent (**Scheme 5.13**).[17] Therefore, it was decided to use these conditions as

a model reaction to directly compare the most active palladium-NHC catalysts enclosed within, the results of which are summarised in **Table 5.10**.
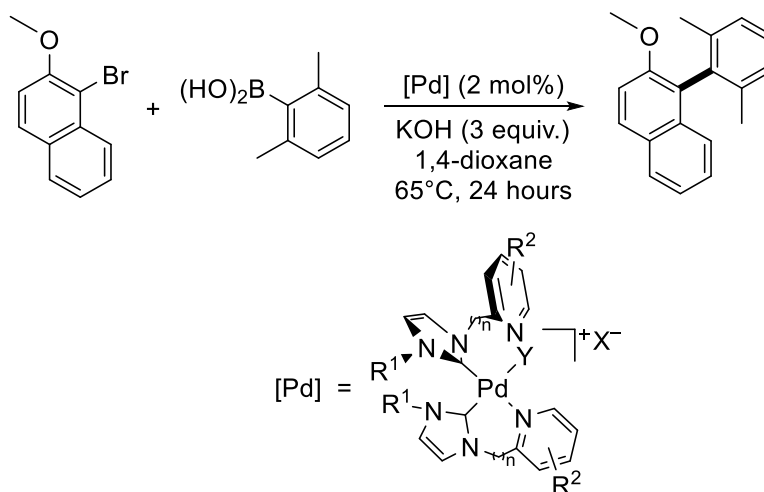
Scheme 5.13 *Model Suzuki-Miyaura cross-coupling reaction to sterically congested biaryls.*

Entry	Catalyst (R^1, R^2, n)	X	Y	Conv. (%)[a]	TON
1	**5.1.1** (allyl, H, 0)	$2PF_6$	MeCN	36	18
2	**5.2.1** (allyl, 4-Me, 0)	$2PF_6$	MeCN	33	17
3	**5.3.1** (allyl, 5-NO$_2$, 0)	$2PF_6$	MeCN	32	16
4	**5.5.1** (allyl, H, 1)	$2PF_6$	picolyl	39	20
5	**5.6.1** (picolyl, H, 1)	$2PF_6$	picolyl	48	24

Table 5.10. *Conditions: 1-bromo-2-methoxynaphthalene (1.0 mmol), 2,6-dimethylphenylboronic acid (1.2 mmol), Pd pre-catalyst (0.02 mmol), KOH (3.0 mmol), 1,4-dioxane solvent (3 mL, anhydrous). [a]Conversion (%) analysed by GC and are recorded as the average of three consecutive runs.*

It was found that *N*-allyl *N'*-pyridyl substituted NHC complexes (entries 1 – 3) furnished biaryl product in similar overall yield (36, 33 and 32%, respectively), despite housing pyridyl donors of varying basicity. Further, addition of a methylene link between NHC and pyridine ring in direct analogue **5.5.1** leads to slight enhancement in product formation (entry 4, 39%). Complete replacement of *N*-allylic tether with an additional *N*-picolyl donor group leads to further increase in catalytic turnover (entry 5, 48%, TON = 24), implying a negligible positive effect of a proximal alkene around the metal centre on catalysis.

In a comparative study, Pd-PEPPSI complexes furnished conversions of 4% (Pd-PEPPSI-IBu), 9% (Pd-PEPPSI-cPent), 41% (Pd-PEPPSI-IPr) and 91% (Pd-PEPPSI-IPent), with the authors concluding that the steric bulk around the Pd centre must be "conformationally fluid" to exert a positive influence on the cross-coupling reaction. Values for conversion obtained in this study correlate well with the sterically crowded catalyst, Pd-PEPPSI-IPr, with topographically most flexible *bis*-picolyl substituted Pd-NHC (**5.6.1**) providing highest conversion.

5.5   Conclusions and future work

A family of novel palladium(II) *bis*-NHC complexes bearing electronically diverse pyridyl or picolyl wingtip substituents have been prepared in a single step *via* their corresponding imidazolium salt precursors. A combination of spectroscopic and crystallographic analyses have been employed to both rationalise and affiliate the dynamic solution-state behaviour with solid-state structure of these complexes, with an overarching view to design robust catalysts capable of mediating challenging cross-coupling reactions, whilst maintaining low susceptibility to thermal degradation.

In general, presence of coordinating bromide anions within the coordination sphere of such complexes provides a competitive ligand environment which acts to increase rates of fluxion around the metal centre, and in specific cases leads to overall ligand displacement from the metal itself. This fluctuation is primarily reflected in solution-state spectroscopic measurements, and can be suppressed at low temperatures or by replacement of bromide with non-competitive hexafluorophosphate counteranions.

A basic functional principle in homogenous catalysis is that ligands must provide a balance between protecting a low-valent metal from aggregation (*i.e.* stabilisation), whilst creating open coordination sites in "dissociation equilibria" at which elementary catalytic steps may proceed (*i.e.* activation).[61] In this regard, a basic palladium(II)-NHC template has been sought, which combines the use of hemilabile *N*-donor functions with strongly bound carbene ligands, as summarised in **Figure 5.17**. The template enables coordinative protection of the metal centre, whilst simultaneously allowing neutral donor tethers to dissociate and open access to reactive palladium. The model is tuneable, and produces complexes which are catalytically active (see below).
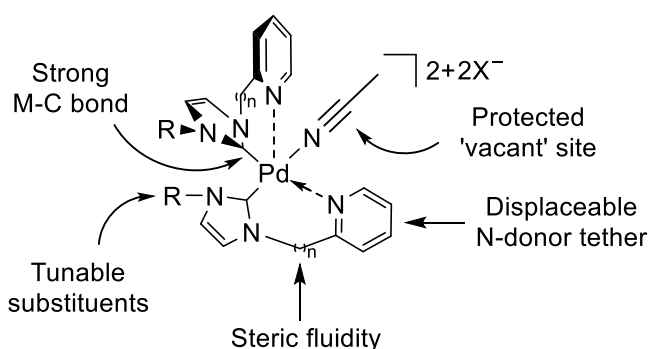
Figure 5.17 Basic palladium(II)-NHC template derived from solid/solution-state studies.

The palladium(II) complexes were initially trialled as catalysts in a classical Heck-Mizoroki cross-coupling reaction to produce *n*-butyl cinnamate. Poor catalyst turnover numbers were generally observed for this transformation, with an additional 'pre-activation/incubation' step

required *via* homocoupling of a boronic acid additive in all cases (highest TON = 12, 3 mol% Pd). Instead, deployment of the complexes in an organoboron Suzuki-Miyaura coupling reaction led to a significant increase in catalyst activity (highest TON = 94, TOF = 47 h^{-1}, 1 mol% Pd), by use of conformationally flexible *N*-picolyl NHC *N*-substituents. Five of the most promising complexes were examined in a more challenging cross-coupling reaction, generating a sterically congested *tetra-ortho* substituted biaryl compound. In this setting, a direct comparison may be drawn between the complexes described within and the well-established Pd-PEPPSI series, developed by Organ *et al*. It was found that *bis-N*-picolyl substituted Pd-NHC complex **5.6.1** (48%, TON = 24), is able to catalyse the coupling reaction with higher efficiency than that of Pd-PEPPSI-IBu (4%), Pd-PEPPSI-cPent (9%) and Pd-PEPPSI-IPr (41%), and to the best of the author's knowledge, the only Pd-NHC complex to offer improvement on this activity is Pd-PEPPSI-IPent (91%). In line with conclusions derived by Organ and co-workers, a topographically "fluid" environment around the Pd centre does indeed provide a positive effect on the cross-coupling process, with the availability of hemilabile pyridyl *N*-donor groups acting to stabilise oxidation state changes at the metal centre throughout the catalytic cycle.

Future work is to be focussed toward further ligand modification to vary the steric profile of the NHC unit, as electronic factors appear to play a minor role during turnover. However, underlined within this chapter – and complementary to literature precedent – is a clear positive influence of a strong hemilabile *N*-donor ligand within the inner sphere of Pd upon catalysis, with additional flexibility further enhancing turnover number. It should therefore be sought to evaluate the effect of tether-length between NHC and donor on catalysis; as the Pd-PEPPSI complexes are void of a tether entirely, a longer linkage than methylene may prove beneficial.

5.6   Experimental

Where stated, manipulations were performed under an atmosphere of dry nitrogen by means of standard Schlenk line or glovebox techniques. Anhydrous solvents were prepared by passing the solvent over activated alumina to remove water, copper catalyst to remove oxygen and molecular sieves to remove any remaining water, *via* the Dow-Grubbs solvent system. Deuterated CD_3CN, $(CD_3)_2SO$ and $CDCl_3$ were dried over CaH_2, cannula filtered or distilled, and then freeze-pump-thaw degassed prior to use.

2-(Imidazole-1-yl)pyridine (**I5.1**),[62] 2-(imidazole-1-yl)-4-methylpyridine (**I5.2**),[63] 2-(imidazole-1-yl)-5-nitropyridine (**I5.3**)[64] and 2-(imidazole-1-yl)-4-methoxypyridine (**I5.4**)[65] were synthesised using literature protocols. For the synthesis of **5.4.1**, see Chapter 6.

For the purpose of calibrating a gas chromatograph to plot a linear response *versus* concentration map, 1-(2,6-dimethylphenyl)-2-methoxynaphthalene[66] was synthesised according to a modified literature procedure (*n*-butyl cinnamate and 1,1'-biphenyl were purchased from Sigma-Aldrich and used directly for the same purpose). All other chemicals were obtained from commercial sources and used as received.

5.6.1   Instrumentation

^1H and ^{13}C NMR spectra were recorded by automated procedures on either a Bruker Avance (500/125 MHz), Bruker Ascend (400/100 MHz) or DPX (300/75 MHz) NMR spectrometer, using the residual solvent as an internal standard. Variable temperature ^1H NMR spectra were recorded in collaboration with Mr Simon Barrett of the University of Leeds. The values of chemical shift are reported in parts per million (ppm) with the multiplicities of the spectra assigned as follows: singlet (s), doublet (d), triplet (t), quartet (q), multiplet (m) and broad (br), values for coupling constants (*J*) are assigned in Hz. High-resolution electrospray mass spectra (ESI-MS) were measured on an open-access Bruker Daltonics (micro TOF) instrument operating in the electrospray mode. Samples for microanalysis were dried under vacuum prior to analysis and the elemental composition determined by Ms. Tanya Marinko-Covell of the University of Leeds Microanalytical Service using a Carlo Erba elemental analyser MOD 1106 spectrometer. FT-IR spectra were recorded as solid phase samples on a Perkin-Elmer Spectrum One spectrophotometer.

X-ray diffraction data were collected on an Agilent SuperNova diffractometer fitted with an Atlas CCD detector with Mo Kα radiation (λ = 0.7107 Å) or Cu Kα radiation (λ = 1.5418 Å). Crystals were mounted under oil on nylon fibres. Data sets were corrected for absorption using a multiscan method, and the structures were solved by direct methods using SHELXS-97 or SHELXT and refined by full-matrix least squares on F^2 using ShelXL-97, interfaced through the program

Olex2.[67] Molecular graphics for all structures were generated using POV-RAY in the X-Seed program.

GC analyses were performed using a Bruker 430-GC equipped with a CP-8400 autosampler and a BR-5 column (30 m × 0.25 mm (ID) × 0.25 μm film thickness) with carrier gas flow rate of 2.0 mLmin^{-1} and a temperature ramp from 50 → 310 ˚C at 20 ˚Cmin^{-1}. The injection volume was 1.0 μL with a split ratio of 10. The response factors for the internal standard (*p*-cymene), substrate and authentic product were calculated using an appropriate calibration for this GC, method and column.

5.6.2 Preparation of imidazolium salt precursors

General allylation protocol. 2-(1-Imidazol)-pyridine derivative (**I5.1** – **I5.5**, 5.0 mmol), allyl bromide (2.0 mL, 23 mmol) and acetonitrile (40 mL) were added to a round-bottomed flask and heated at reflux for 16 hours. Following, the mixture was cooled to ambient temperature and the volume of solvent reduced *in vacuo* (to approx. 10 mL). Slow addition of diethyl ether (*ca.* 35 mL) to the stirring acetonitrile solution allowed the precipitation of the product as an off-white microcrystalline solid, which was collected by vacuum filtration, washed repeatedly with diethyl ether and dried *in vacuo*.

General salt metathesis protocol. 1-Allyl-3-(2-pyridyl)imidazolium bromide derivative (**P5.1** – **P5.6**, 2.00 mmol), ammonium hexafluorophosphate (0.98 g, 6.0 mmol) and deionised water (40 mL) were added to a round-bottomed flask and stirred at room temperature for 2 hours. Following, an off-white microcrystalline solid had developed which was collected by vacuum filtration, rinsed with deionised water (3 × 30 mL) followed by aliquots of diethyl ether (3 × 30 mL) and dried *in vacuo*.

Synthesis of 1-allyl-3-(2-pyridyl)imidazolium bromide (P5.1). 2-(Imidazole-1-yl)pyridine (0.72 g, 5.0 mmol) was reacted according to the general allylation procedure (*vide supra*). Yield: 1.18 g, 4.45 mmol, 89 %. ^{1}H NMR (300 MHz, CDCl$_3$) δ (ppm) 11.74 (s, 1H, NC*H*N), 8.57 – 8.47 (m, 2H, py*H*), 8.32 (t, *J* = 1.7 Hz, 1H, im*H*), 8.08 – 7.98 (m, 1H, py*H*), 7.52 (t, *J* = 1.7 Hz, 1H, im*H*), 7.48 – 7.42 (m, 1H, py*H*), 6.12 (ddt, *J* = 16.8, 10.1, 6.5 Hz, 1H, C*H*=CH$_2$), 5.57 (d, *J* = 16.8 Hz, 1H, HC=CH*H*$_{trans}$), 5.51 (dd, *J* = 10.1, 0.6 Hz, 1H, HC=CH*H*$_{cis}$), 5.24 (d, *J* = 6.5 Hz, 2H, NC*H*$_2$). ^{13}C{^{1}H} NMR (75 MHz, CDCl$_3$) δ (ppm) 149.1, 146.1, 140.8, 136.0, 129.7, 125.3, 123.5, 122.0, 119.1, 115.2, 52.8. HR-MS (ESI$^+$): *m/z* 186.1030 [C$_{11}$H$_{12}$N$_3$]$^+$, calcd. [M − Br]$^+$ 186.1026. All data are consistent with the literature.[25]

Synthesis of 1-allyl-3-(2-(4-methyl)pyridyl)imidazolium bromide (P5.2). 2-(Imidazole-1-yl)-4-methylpyridine (0.80 g, 5.0 mmol) was reacted according to the general allylation procedure (*vide supra*). Yield: 1.25 g, 4.46 mmol, 89 %. ^{1}H NMR (300 MHz, CDCl$_3$) δ (ppm) 11.34 (s, 1H, NC*H*N), 8.42 − 8.21 (m, 3H, py*H*, im*H*), 7.67 (s, 1H, im*H*), 7.20 (d, J = 4.9 Hz, 1H, py*H*), 6.09 (ddt, J = 16.9, 10.1, 6.5 Hz, 1H, C*H*=CH$_2$), 5.56 (d, J = 16.9 Hz, 1H, C*H*=CH*H*$_{trans}$), 5.44 (d, J = 10.1 Hz, 1H, C*H*=CH*H*$_{cis}$), 5.21 (d, J = 6.5 Hz, 2H, NC*H*$_2$), 2.48 (s, 3H, C*H*$_3$). ^{13}C{^{1}H} NMR (75 MHz, CDCl$_3$) δ (ppm) 152.9, 148.6, 146.1, 135.2, 129.8, 126.2, 123.2, 122.5, 119.2, 115.5, 52.6, 21.3. HR-MS (ESI$^+$): *m/z* 200.1180 [C$_{12}$H$_{14}$N$_3$]$^+$, calcd. [M − Br]$^+$ 200.1182. All data are consistent with the literature.[25]

Synthesis of 1-allyl-3-(2-(5-nitro)pyridyl)imidazolium bromide (P5.3). 2-(Imidazole-1-yl)-5-nitropyridine (0.95 g, 5.0 mmol) was reacted according to the general allylation procedure (*vide supra*). Yield: 1.37 g, 4.43 mmol, 86 %. ^{1}H NMR (300 MHz, CDCl$_3$) δ (ppm) 12.22 (s, 1H, NC*H*N), 9.34 (d, J = 2.4 Hz, 1H, py*H*), 9.12 (d, J = 9.0 Hz, 1H, py*H*), 8.84 (dd, J = 9.0, 2.4 Hz, 1H, py*H*), 8.42 (t, J = 1.8 Hz, 1H, im*H*), 7.51 (t, J = 1.8 Hz, 1H, im*H*), 6.15 (m, 1H, C*H*=CH$_2$), 5.64 (d, J = 16.7 Hz, 1H, CH=CH*H*$_{trans}$), 5.58 (d, J = 10.2 Hz, 1H, CH=CH*H*$_{cis}$), 5.22 (d, J = 6.6 Hz, 2H, NC*H*$_2$). ^{13}C{^{1}H} NMR (75 MHz, CDCl$_3$) δ (ppm) 149.2, 145.1, 144.6, 137.0, 136.3, 129.3, 124.1, 123.0, 119.6, 116.2, 53.1. HR-MS (ESI$^+$): *m/z* 231.0880 [C$_{11}$H$_{11}$N$_4$O$_2$]$^+$, calcd. [M − Br]$^+$ 231.0877. All data are consistent with the literature.[25]

Synthesis of 1-allyl-3-(2-(4-methoxy)pyridyl)imidazolium bromide (P5.4). 2-(Imidazole-1-yl)-4-methoxypyridine (0.88 g, 5.0 mmol) was reacted according to the general allylation procedure (*vide supra*). Yield: 1.24 g, 4.20 mmol, 84 %. ^{1}H NMR (300 MHz, CDCl$_3$) δ (ppm) 11.81 (s, 1H, NC*H*N), 8.29 (s, 1H, im*H*), 8.22 (d, J = 5.8 Hz, 1H, py*H*), 8.19 (d, J = 3.0 Hz, 1H, py*H*), 7.51 (s, 1H, im*H*), 6.90 (dd, J = 5.8, 3.0 Hz, 1H, py*H*), 6.14 (ddt, J = 16.8, 10.1, 6.5 Hz, 1H, C*H*=CH$_2$), 5.66 (d, J = 16.8 Hz, 1H, CH=CH*H*$_{trans}$), 5.55 (d, J = 10.1 Hz, 1H, CH=CH*H*$_{cis}$), 5.14 (d, J = 6.5 Hz, 2H, NC*H*$_2$), 4.10 (s, 3H, OC*H*$_3$). ^{13}C{^{1}H} NMR (75 MHz, CDCl$_3$) δ (ppm) 169.3, 150.0, 147.8, 136.1, 129.7, 123.3, 121.7, 119.4, 113.9, 100.1, 58.0, 52.9. HR-MS (ESI$^+$): *m/z* 216.1161 [C$_{12}$H$_{14}$N$_3$O]$^+$, calcd. [M − Br]$^+$ 216.1131. All data are consistent with the literature.[25]

Synthesis of 1-allyl-3-(2-methylpyridyl)imidazolium bromide (P5.5). 2-Bromomethylpyridine hydrobromide (0.51 g, 2.00 mmol), 1-allylimidazole (0.23 g, 2.1 mmol) and potassium carbonate (1.40 g, 10.00 mmol) were charged to a round-bottomed flask and stirred vigorously in acetonitrile (30 mL) at 60 ˚C for 18 hours. After this time, the mixture was filtered and solvents removed *in vacuo* to furnish a pale orange oil. Dissolution in acetonitrile (20 mL) followed by reprecipitation with diethyl ether (50 mL) (twice) delivered the pure product as a pale yellow oil. Yield: 0.25 g, 2.00 mmol, quantitative. ^{1}H NMR (400 MHz, CDCl$_3$) δ (ppm) 10.92 (s, 1H, NC*H*N), 8.55 (d, J = 4.0 Hz, 1H, im*H*), 7.87 (d, J = 8.0 Hz, 1H, *meta*-C*H*), 7.76 (td, J = 8.0 Hz,

1H, *para*-C*H*), 7.63 (d, J = 4.0 Hz, 1H, im*H*), 7.30 (td, J = 8.0 Hz, 1H, *meta'*-C*H*), 7.16 (d, J = 8.0 Hz, 1H, *ortho*-C*H*), 6.02 (m, 1H, CH$_2$=C*H*C), 5.79 (s, 2H, C*H*$_2$), 5.49 (d, J = 12.0 Hz, 2H, C*H*$_2$=CH), 4.92 (d, J = 3.0 Hz, 2H, NC*H*$_2$). ^{13}C{^{1}H} NMR (100 MHz, CDCl$_3$) δ (ppm) 152.5, 150.0, 137.9, 137.6, 129.6, 124.3, 124.2, 123.1, 121.3, 110.1, 54.2, 52.4. HR-MS (ESI$^+$): *m/z* 200.1202 [C$_{12}$H$_{14}$N$_3$]$^+$, calcd. [M − Br]$^+$ 200.1182. All data are consistent with the literature.[25]

Synthesis of 1,3-*bis*(2-methylpyridyl)imidazolium bromide (P5.6). 2-Bromomethylpyridine (1.20 g, 4.74 mmol), imidazole (0.21 g, 3.10 mmol) and potassium carbonate (1.65 g, 11.9 mmol) were charged to a round-bottomed flask and stirred vigorously in acetonitrile (50 mL) at 60 ˚C for 24 hours. After this time, the mixture was filtered and solvents removed *in vacuo* to give a crude brown oil. The residue was dissolved in acetonitrile (30 mL) followed by reprecipitation with diethyl ether (60 mL) (twice) to furnish a light brown oil, which was further washed with diethyl ether (3 × 30 mL) and dried *in vacuo* to afford spectroscopically pure product as a light-brown solid. Yield: 0.64 g, 2.00 mmol, 84 %. ^{1}H NMR (300 MHz, CDCl$_3$) δ (ppm) 10.95 (br s, 1H, NC*H*N), 8.56 (d, J = 3.0 Hz, 2H, im*H*), 7.78 − 7.75 (m, 4H, pyC*H*), 7.54 (br s, 2H, im*H*), 7.31 (td, J = 6.0 Hz, 2H, *meta*-C*H*), 5.67 (s, 4H, C*H*$_2$). ^{13}C{^{1}H} NMR (100 MHz, CDCl$_3$) δ (ppm) 152.3, 149.9, 137.8, 137.5, 124.1, 124.0, 122.4, 54.2. HR-MS (ESI$^+$): *m/z* 251.1297 [C$_{15}$H$_{15}$N$_4$]$^+$, calcd. [M − Br]$^+$ 251.1291. Anal. calcd. (%) for C$_{15}$H$_{15}$N$_4$Br: C 54.39, H 4.61, N 16.92; found C 54.00, H 5.00, N 16.90.

Synthesis of 1-allyl-3-(2-pyridyl)imidazolium hexafluorophosphate (P5.1.1). 1-Allyl-3-(2-pyridyl)imidazolium bromide (0.53 g, 2.0 mmol) was reacted according to the general salt metathesis reaction (*vide supra*). Yield: 0.66 g, 2.00 mmol, quantitative. ^{1}H NMR (300 MHz, CD$_3$CN) δ (ppm) 9.28 (s, 1H, NC*H*N), 8.61 (d, J = 4.8 Hz, 1H, im*H*), 8.34 − 8.08 (m, 2H, py*H*), 7.75 (d, J = 9.0 Hz, 1H, py*H*), 7.07 (d, J = 4.8 Hz, 1H, im*H*), 7.58 − 7.56 (m, 1H, py*H*), 6.16 (ddt, J = 15.9, 9.0, 1.5 Hz, 1H, C*H*=CH$_2$), 5.51 (d, J = 15.9 Hz, 1H, HC=CH*H*$_{trans}$), 5.47 (dd, J = 6.6, 0.9 Hz, 1H, HC=CH*H*$_{cis}$), 4.89 (d, J = 6.5 Hz, 2H, NC*H*$_2$). ^{13}C{^{1}H} NMR (75 MHz, CD$_3$CN) δ (ppm) 150.7, 148.1, 142.3, 136.0, 128.1, 125.2, 123.3, 120.9, 118.8, 115.1, 52.3. HR-MS (ESI$^+$): *m/z* 186.1020 [C$_{11}$H$_{12}$N$_3$]$^+$, calcd. [M − PF$_6$]$^+$ 186.1026. Anal. calcd. (%) for C$_{11}$H$_{12}$N$_3$PF$_6$: C 35.97, H 3.46, N 10.80; found C 35.70, H 3.20, N 11.20.

Synthesis of 1-allyl-3-(2-(4-methyl)pyridyl)imidazolium hexafluorophosphate (P5.2.1). 1-Allyl-3-(2-(4-methyl)pyridyl)imidazolium bromide (0.56 g, 2.0 mmol) was reacted according to the general salt metathesis reaction (*vide supra*). Yield: 0.65 g, 1.88 mmol, 94 %. ^{1}H NMR (300 MHz, CD$_3$CN) δ (ppm) 9.26 (br s, 1H, NC*H*N), 8.44 (d, J = 5.1 Hz, 1H, py*H*), 8.07 (br t, J = 1.5 Hz, 1H, im*H*), 7.61 (br s, 1H, py*H*), 7.57 (br t, J = 1.5 Hz, 1H, im*H*), 7.42 (br d, J = 5.1 Hz, 1H, py*H*), 6.08 (ddt, J = 18.1, 10.1, 6.5 Hz, 1H, C*H*=CH$_2$), 5.47 (d, J = 18.1 Hz, 1H, C*H*=CH*H*$_{trans}$), 4.89 (d, J = 10.1 Hz, 1H, C*H*=CH*H*$_{cis}$), 2.50 (s, 3H, C*H*$_3$). ^{13}C{^{1}H} NMR (75 MHz, CD$_3$CN) δ (ppm) 149.9, 148.0, 135.0, 131.3, 127.2, 124.4, 122.5, 120.5, 118.6, 115.5,

53.1, 21.2. HR-MS (ESI$^+$): m/z 200.1163 [C$_{12}$H$_{14}$N$_3$]$^+$, calcd. [M − PF$_6$]$^+$ 200.1182. Anal. calcd. (%) for C$_{12}$H$_{14}$N$_3$PF$_6$·CH$_2$Cl$_2$: C 36.30, H 3.75, N 9.91; found C 36.25, H 3.50, N 10.10.

Synthesis of 1-allyl-3-(2-(5-nitro)pyridyl)imidazolium hexafluorophosphate (P5.3.1). 1-Allyl-3-(2-(5-nitro)pyridyl)imidazolium bromide (0.62 g, 2.0 mmol) was reacted according to the general salt metathesis reaction (*vide supra*). Yield: 0.74 g, 1.96 mmol, 98 %. ^{1}H NMR (300 MHz, CD$_3$CN) δ (ppm) 9.23 (br s, 1H, NC*H*N), 9.22 (br s, 1H, py*H*), 8.72 (d, J = 8.1 Hz, 1H, im*H*), 8.07 (s, 1H, py*H*), 7.87 (d, J = 8.1 Hz, 1H, im*H*), 7.51 (br s, 1H, py*H*), 6.08 − 5.91 (m, 1H, C*H*=CH$_2$), 5.41 (d, J = 6.3 Hz, 1H, CH=CH*H*$_{trans}$), 5.35 (br s, 1H, CH=CH*H*$_{cis}$), 4.81 (br d, J = 5.7 Hz, 2H, NC*H*$_2$). ^{13}C{^{1}H} NMR (75 MHz, CD$_3$CN) δ (ppm) 150.4, 146.3, 145.9, 137.2, 136.1, 130.9, 125.0, 123.0, 121.0, 115.8, 53.5. HR-MS (ESI$^+$): m/z 231.0888 [C$_{11}$H$_{11}$N$_4$O$_2$]$^+$, calcd. [M − PF$_6$]$^+$ 231.0877. Anal. calcd. (%) for C$_{11}$H$_{11}$N$_4$O$_2$PF$_6$·^{1}/$_2$H$_2$O: C 34.30, H 3.14, N 14.54; found C 34.15, H 2.80, N 14.20.

Synthesis of 1-allyl-3-(2-(4-methoxy)pyridyl)imidazolium hexafluorophosphate (P5.4.1). 1-Allyl-3-(2-(4-methoxy)pyridyl)imidazolium bromide (0.56 g, 2.00 mmol) was reacted according to the general salt metathesis reaction (*vide supra*). Yield: 0.72 g, 2.00 mmol, quantitative. ^{1}H NMR (300 MHz, CD$_3$CN) δ (ppm) 9.28 (s, 1H, NC*H*N), 8.39 (d, J = 6.0 Hz, 1H, py*H*), 8.10 (br t, J = 1.8 Hz, 1H, im*H*), 7.56 (br t, J = 1.8 Hz, 1H, im*H*), 7.26 (d, J = 2.1 Hz, 1H, py*H*), 7.11 (dd, J = 5.7, 2.1 Hz, 1H, py*H*), 6.16 − 6.02 (ddt, J = 17.7, 12.6, 6.3 Hz, 1H, C*H*=CH$_2$), 5.50 (d, J = 17.7 Hz, 1H, CH=CH*H*$_{trans}$), 5.45 (d, J = 12.6 Hz, 1H, CH=CH*H*$_{cis}$), 4.88 (d, J = 6.3 Hz, 2H, NC*H*$_2$), 3.98 (s, 3H, OC*H*$_3$). ^{13}C{^{1}H} NMR (75 MHz, CD$_3$CN) δ (ppm) 169.7, 151.3, 149.0, 135.4, 131.4, 124.2, 122.5, 120.6, 112.6, 101.4, 57.5, 53.3. HR-MS (ESI$^+$): m/z 216.1149 [C$_{12}$H$_{14}$N$_3$O]$^+$, calcd. [M − PF$_6$]$^+$ 216.1131.

Synthesis of 1,3-*bis*(2-methylpyridyl)imidazolium hexafluorophosphate (P5.6.1). 1,3-*Bis*(2-methylpyridyl)imidazolium bromide (0.66 g, 2.0 mmol) was reacted according to the general salt metathesis reaction (*vide supra*). Yield: 0.75 g, 1.90 mmol, 95 %. ^{1}H NMR (300 MHz, CD$_3$CN) δ (ppm) 8.82 (br s, 1H, NC*H*N), 8.62 (dd, J = 5.7, 1.8 Hz, 2H, im*H*), 8.06 (td, J = 15.6, 7.8, 1.8 Hz, 2H, py*H*), 7.59 − 7.55 (m, 4H, py*H*), 7.52 (d, J = 1.8 Hz, 2H, py*H*), 5.55 (s, 4H, C*H*$_2$). ^{13}C{^{1}H} NMR (100 MHz, CD$_3$CN) δ (ppm) 152.3, 149.0, 141.5, 138.4, 126.0, 125.0, 124.5, 53.7. HR-MS (ESI$^+$): m/z 251.1288 [C$_{15}$H$_{15}$N$_4$]$^+$, calcd. [M − PF$_6$]$^+$ 251.1291. All data are consistent with the literature.[68]

5.6.3 Preparation of palladium(II) *N*-heterocyclic carbene complexes

Synthesis of *bis*[1-allyl-3-(2-pyridyl)imidazole-2-ylidene]palladium(II) dibromide (5.1). 1-Allyl-3-(2-pyridyl)imidazolium bromide **P5.1** (0.19 g, 0.70 mmol) and Pd(OAc)$_2$ (79 mg, 0.35 mmol) were added to a flame-dried Schlenk tube and dried *in vacuo*. Anhydrous acetonitrile (20 mL) was added using an oven-dried cannula, and the homogeneous mixture stirred at 70 °C for 18 hours. Following, the mixture was cooled to room temperature and diethyl ether (*ca.* 50 mL) added slowly, precipitating a yellow solid. The product was collected onto a glass frit by vacuum filtration, rinsed with diethyl ether (2 × 20 mL) and dried *in vacuo*, affording the pure title compound as a microcrystalline yellow solid. Single crystals of the product were obtained through slow evaporation of a MeOH solution of the complex at room temperature. Yield: 0.13 g, 0.20 mmol, 58 %. Mp decomp. >222 °C. ^{1}H NMR (500 MHz, (CD$_3$)$_2$SO, 298K) δ (ppm) 9.18 (br s, 1H, py*H*), 8.66 (br s, 1H, im*H*), 8.53 (br m, 2H, py*H*), 8.44 (br s, 1H, im*H*), 8.27 (br m, 2H, py*H*), 8.04 (br m, 1H, py*H*), 7.85 (s, 1H, im*H*), 7.72 (m, 1H, py*H*), 7.59 (s, 1H, im*H*), 7.50 (br s, 1H, py*H*), 6.19 (br m, 1H, C*H*=CH$_2$), 5.58 (br m, 1H, C*H'*=CH$_2$), 5.45 (br d, *J* = 23.5 Hz, 1H, alkenyl *H*), 5.32 (br d, *J* = 14.0 Hz, 1H, alkenyl *H*), 5.19 (br d, *J* = 14.0 Hz, 1H, alkenyl *H*), 5.04 − 4.95 (br m, 2H, NC*H$_2$*), 4.79 (br d, *J* = 23.5 Hz, 1H, alkenyl *H*), 3.93 (br d, *J* = 19.5 Hz, 1H, NC*H'*), 3.78 (br d, *J* = 19.5 Hz, 1H, NC*H'*). On account of significant resonance broadening, a satisfactory ^{13}C{^{1}H} NMR spectrum could not be obtained for unambiguous signal assignment. HR-MS (ESI$^+$): *m/z* 555.0120 [C$_{22}$H$_{22}$N$_6$BrPd]$^+$, calcd. [M − Br]$^+$ 555.0119. Anal. calcd. (%) for C$_{22}$H$_{22}$N$_6$Br$_2$Pd·^{2}/$_3$MeCN: C 40.73, H 3.63, N 12.96; found C 40.50, H 3.35, N 12.75.

Synthesis of *bis*[1-allyl-3-(2-(4-methyl)pyridyl)imidazole-2-ylidene]palladium(II) dibromide (5.2). 1-Allyl-3-(2-(4-methyl)pyridyl)imidazolium bromide **P5.2** (0.21 g, 0.75 mmol) and Pd(OAc)$_2$ (84 mg, 0.38 mmol) were added to a flame-dried Schlenk tube and dried *in vacuo*. Anhydrous dimethyl sulfoxide (8 mL) was added using an oven-dried cannula, and the homogeneous mixture stirred at 100 °C for 18 hours. Following, the crude black mixture was filtered through a short path of Celite, which was rinsed with dichloromethane (*ca.* 10 mL) to provide a golden solution. Diethyl ether (50 mL) was added to this solution with moderate stirring, precipitating a yellow solid which was collected onto a glass frit by vacuum filtration, rinsed with diethyl ether (2 × 20 mL) and dried *in vacuo*, affording the title compound as a yellow solid. Single crystals of the product were obtained through slow diffusion of diethyl ether vapours into a MeOH solution of the complex at room temperature. Yield: 0.20 g, 0.30 mmol, 77 %. Mp decomp. >222 °C. ^{1}H NMR (500 MHz, (CD$_3$)$_2$SO, 298K) δ (ppm) 9.01 (br d, *J* = 5.5 Hz, 1H, py*H*), 8.45 (br s, 1H, im*H*), 8.37 (br d, *J* = 5.5. Hz, 1H, py*H*), 8.30 (br s, 1H, im*H*), 8.26 (br s, 1H, py*H*), 8.17 (br s, 1H, im*H*), 7.83 (br s, 1H, im*H*), 7.57 (br s, 2H, py*H*), 7.32 (br s, 1H, py*H*), 6.13 (br m, 1H, C*H*=CH$_2$), 5.59 (br m, 1H, C*H'*=CH$_2$), 5.47 (br d, *J* = 19.5 Hz, 1H, alkenyl *H*),

5.32 (br d, J = 13.0 Hz, 1H, alkenyl H), 5.17 – 5.13 (br m, 1H, alkenyl H), 5.02 (br d, J = 13.0 Hz, 1H, alkenyl H), 4.96 – 4.92 (br m, 1H, alkenyl H), 4.83 (br d, J = 19.5 Hz, 1H, alkenyl H), 3.91 (br d, J = 19.5 Hz, 1H, NCH'), 3.82 (br d, J = 19.5 Hz, 1H, NCH'). On account of significant resonance broadening, a satisfactory $^{13}C\{^1H\}$ NMR spectrum could not be obtained for unambiguous signal assignment. HR-MS (ESI$^+$): m/z 585.0650 [$C_{24}H_{26}N_6BrPd$]$^+$, calcd. [M – Br]$^+$ 585.0417. Anal. calcd. (%) for $C_{22}H_{22}N_6Br_2Pd$: C 43.36, H 3.94, N 12.64; found C 40.70, H 3.69, N 11.60.

Neutral palladium(II) dibromide complex **5.2**** was formed from dissolution of **5.2** into hot, hydrous acetonitrile (50 mg, 0.075 mmol, dissolved in 10 mL) and filtered through a short path of SiO$_2$. Following, diethyl ether (*ca.* 30 mL) was added to the filtrate to precipitate a bright yellow solid, which was subsequently collected onto a glass frit by vacuum filtration, rinsed with diethyl ether (2 × 20 mL) and dried *in vacuo* to afford **5.2****. Single crystals of the product were obtained through slow diffusion of diethyl ether vapours into a 1:1 ($^v/_v$) MeOH/DMSO solution of the complex at room temperature. Yield: 8 mg, 0.017 mmol, 23 %. ^1H NMR (500 MHz, CD$_3$CN, 298K) δ (ppm) ^1H NMR (400 MHz, CD$_3$CN, 298K) δ (ppm) 9.39 (br d, J = 8.0 Hz, 1H, im$H$), 8.67 (br d, J = 8.0 Hz, 1H, im$H$), 7.80 (br d, J = 2.8 Hz, 1H, py$H$), 7.77 (br d, J = 2.8 Hz, 1H, py$H$), 7.62 (br s, 1H, py$H$), 6.14 – 6.01 (m, 1H, C=CH), 5.49 (br d, J = 7.6 Hz, 2H, NCH_2), 5.31 – 5.22 (m, 2H, alkenyl H), 2.51 (s, 3H, CH_3). $^{13}C\{^1H\}$ NMR (125 MHz, (CD$_3$)$_2$SO, 298K) δ (ppm) 181.4, 155.3, 153.8, 149.6, 133.6, 128.2, 121.5, 112.7, 111.5, 98.5, 54.4, 52.3. HR-MS (ESI$^+$): m/z 383.9333 [$C_{12}H_{13}N_3BrPd$]$^+$, calcd. [M – Br]$^+$ 383.9322. Anal. calcd. (%) for $C_{12}H_{13}N_3Br_2Pd \cdot H_2O$: C 29.80, H 3.10, N 8.69; found C 29.40, H 2.70, N 8.70.

Synthesis of *bis*[1-allyl-3-(2-(5-nitro)pyridyl)imidazole-2-ylidene]palladium(II) dibromide (5.3). 1-Allyl-3-(2-(5-nitro)pyridyl)imidazolium bromide **P5.3** (0.47 g, 1.51 mmol) and Pd(OAc)$_2$ (0.17 g, 0.75 mmol) were added to a flame-dried Schlenk tube and dried *in vacuo*. Anhydrous acetonitrile (35 mL) was added using an oven-dried cannula, and the homogeneous mixture stirred at 70 ˚C for 18 hours. Following, the mixture was cooled to room temperature and diethyl ether (*ca.* 50 mL) added slowly, precipitating a yellow solid. The product was collected onto a glass frit by vacuum filtration, rinsed with diethyl ether (2 × 20 mL) and dried *in vacuo*, affording the pure title compound as a microcrystalline yellow solid. Single crystals of the product were obtained through slow diffusion of diethyl ether vapours into a 1:1 ($^v/_v$) MeOH/DMSO solution of the complex at room temperature. Yield: 0.27 g, 0.38 mmol, 50 %. Mp decomp. >229 ˚C. ^1H NMR (500 MHz, CD$_3$CN, 238K) δ (ppm) 10.01 (s, 1H, im$H$), 9.28 (s, 1H, im$H$), 9.08 (d, J = 8.5 Hz, 1H, py$H$), 8.90 (d, J = 8.5 Hz, 1H, py$H$), 8.62 (d, J = 8.5 Hz, 1H, py$H$), 8.31 (d, J = 8.5 Hz, 1H, py$H$), 8.25 (s, 1H, im$H$), 8.21 (s, 1H, im$H$), 7.60 (s, 1H, py$H$), 7.27 (s, 1H, py$H$), 6.11 (m, 1H, C=CH), 5.50 (m, 1H, C=C'H), 5.46 (d, J = 17.0 Hz, 1H, alkenyl H), 5.34 (d, J = 10.0 Hz, 1H, alkenyl H), 5.19 (m, 1H, alkenyl H), 4.94 (m, 1H, alkenyl H),

4.85 (d, J = 10.0 Hz, 1H, NCH), 3.71 (d, J = 17.0 Hz, 1H, NCH'). ^{13}C{^{1}H} NMR (125 MHz, CD$_3$CN, 298K) δ (ppm) 155.9, 154.0, 146.4, 144.9, 138.6, 132.0, 126.7, 121.9, 120.0, 115.3, 55.0. HR-MS (ESI$^+$): m/z 644.9833 [C$_{22}$H$_{20}$N$_8$O$_4$BrPd]$^+$, calcd. [M − Br]$^+$ 644.9823. Anal. calcd. (%) for C$_{22}$H$_{20}$N$_8$O$_4$Br$_2$Pd: C 36.36, H 2.77, N 15.42; found C 36.40, H 2.70, N 15.30.

Synthesis of [1-allyl-3-(2-(4-methoxy)pyridyl)imidazole-2-ylidene]palladium(II) dibromide (5.4*). 1-Allyl-3-(2-(4-methoxy)pyridyl)imidazolium bromide **P5.4** (0.10 g, 0.39 mmol) and Pd(OAc)$_2$ (88 mg, 0.39 mmol) were added to a flame-dried Schlenk tube and dried *in vacuo*. Anhydrous acetonitrile (20 mL) was added using an oven-dried cannula, and the homogeneous mixture stirred at 80 ˚C for 48 hours. Following, the mixture was cooled to room temperature and filtered through a short path of Celite. Solvents were removed under reduced pressure to give a crude yellow residue. The residue was dissolved in acetonitrile (*ca.* 5 mL) and filtered through a SiO$_2$-packed pipette directly into an excess of diethyl ether, precipitating a bright yellow solid. The product was collected onto a glass frit by vacuum filtration, rinsed with diethyl ether (2 × 10 mL) and dried *in vacuo*, affording the title compound as a yellow solid. Single crystals of the product were obtained through slow diffusion of diethyl ether vapours into a 1:1 ($^v/_v$) MeOH/DMSO solution of the complex at room temperature. Yield: 43 mg, 0.089 mmol, 26 %. ^{1}H NMR (400 MHz, CD$_3$CN, 298K) δ (ppm) 9.35 (br d, J = 2.0 Hz, 1H, py$H$), 7.83 (br d, J = 6.5 Hz, 1H, im$H$), 7.24 (br d, J = 2.0 Hz, 1H, py$H$), 7.19 (br d, J = 2.0 Hz, 1H, py$H$), 6.98 (br dd, J = 6.5, 2.0 Hz, 1H, py$H$), 6.12 − 6.04 (m, 1H, alkenyl H), 5.49 (br d, J = 5.5 Hz, 2H, NCH_2), 5.31 − 5.23 (m, 2H, alkenyl H), 4.02 (s, 3H, OCH_3). ^{13}C{^{1}H} NMR (125 MHz, (CD$_3$)$_2$SO, 298K) δ (ppm) 169.6, 152.7, 142.0, 133.6, 124.5, 118.3, 117.4, 109.6, 98.7, 98.2, 57.4, 52.3. HR-MS (ESI$^+$): m/z 379.0381 [C$_{14}$H$_{17}$N$_4$O$_2$Pd]$^+$, calcd. [M + MeCN + OH − Br]$^+$ 379.0381. Anal. calcd. (%) for C$_{12}$H$_{13}$N$_3$OBr$_2$Pd: C 29.93, H 2.72, N 8.73; found C 29.65, H 2.70, N 8.50.

Synthesis of *bis*[1-allyl-3-(2-pyridyl)imidazole-2-ylidene]palladium(II) dihexafluorophosphate (5.1.1). 1-Allyl-3-(2-pyridyl)imidazolium hexafluorophosphate **P5.1.1** (0.30 g, 0.91 mmol) and Pd(OAc)$_2$ (0.11 g, 0.50 mmol) were added to a flame-dried Schlenk tube and dried *in vacuo*. Anhydrous acetonitrile (20 mL) was added using an oven-dried cannula, and the homogeneous mixture stirred at 70 ˚C for 48 hours. Following, the mixture was cooled to room temperature and filtered through a short path of Celite. Solvents were removed under reduced pressure, and the resultant residue recrystallised from acetone/pentane to afford a pale yellow solid. The solid was rinsed with cold chloroform (2 × 5 mL) and dried *in vacuo*, providing the title compound as a pale yellow solid. Yield: 0.18 g, 0.23 mmol, 50 %. Mp decomp. >215 ˚C. ^{1}H NMR (500 MHz, CD$_3$CN, 298K) δ (ppm) 9.30 (d, J = 5.4 Hz, 1H, py$H$), 8.69 (d, J = 8.2 Hz, 1H, im$H$), 8.50 (d, J = 3.8 Hz, 1H, py$H$), 8.28 (t, J = 8.2 Hz, 1H, im$H$), 8.06 (d, J = 3.8 Hz, 1H, py$H$), 8.00 − 7.77 (m, 3H, py$H$ and im$H$), 7.65 − 7.54 (m, 1H, im$H$), 7.50 (d, J = 3.8 Hz, 1H, py$H$), 7.43 (dd, J = 8.2, 3.8 Hz, 1H, py$H$), 7.17 (d, J = 2.0 Hz, 1H, py$H$), 6.30 − 6.01 (m, 1H,

C=C*H*), 5.60 (ddd, *J* = 22.1, 10.2, 5.0 Hz, 1H, C=C*H'*), 5.48 (d, *J* = 17.1 Hz, 1H, alkenyl *H*), 5.35 (d, *J* = 10.2 Hz, 1H, alkenyl *H*), 5.18 (dd, *J* = 10.2, 5.0 Hz, 1H, alkenyl *H*), 5.07 (d, *J* = 10.2 Hz, 1H, alkenyl *H*), 4.96 (dd, *J* = 17.1, 5.0 Hz, 1H, NC*H*), 4.83 (d, *J* = 17.1 Hz, 1H, NC*H'*), 3.97 − 3.71 (m, 2H, NC*H*$_2$). ^{13}C{^{1}H} NMR (125 MHz, CD$_3$CN, 298K) δ (ppm) 162.9, 156.5, 152.7, 151.1, 151.0, 150.0, 144.3, 140.2, 132.7, 132.2, 125.2, 124.9, 124.7, 124.6, 123.9, 121.8, 119.1, 113.1, 55.9, 53.0 (neither C$_{carbene}$ resonances were observed). HR-MS (ESI$^+$): *m/z* 238.0471 [C$_{22}$H$_{22}$N$_6$Pd]$^{2+}$, calcd. [M − MeCN − 2PF$_6$]$^{2+}$ 238.0465. Anal. calcd. (%) for C$_{22}$H$_{22}$N$_6$P$_2$F$_{12}$Pd·CHCl$_3$: C 31.17, H 2.62, N 9.99; found C 31.55, H 2.70, N 10.50.

Synthesis of *bis*[1-allyl-3-(2-(4-methyl)pyridyl)imidazole-2-ylidene]palladium(II) dihexafluorophosphate (5.2.1). 1-Allyl-3-(2-(4-methyl)pyridyl)imidazolium hexafluorophosphate **P5.2.1** (0.18 g, 0.52 mmol) and Pd(OAc)$_2$ (59 mg, 0.26 mmol) were added to a flame-dried Schlenk tube and dried *in vacuo*. Anhydrous acetonitrile (20 mL) was added using an oven-dried cannula, and the homogeneous mixture stirred at 70 ˚C for 48 hours. Following, the mixture was cooled to room temperature and filtered through a short path of Celite. Solvents were removed under reduced pressure, and the resultant residue recrystallised from acetone/pentane to afford a pale yellow solid. The solid was rinsed with cold chloroform (2 × 5 mL) and dried *in vacuo*, providing the title compound as a pale yellow solid. Yield: 0.13 g, 0.15 mmol, 56 %. Mp decomp. >211 ˚C. ^{1}H NMR (500 MHz, CD$_3$CN, 298K) δ (ppm) 9.09 (d, *J* = 5.7 Hz, 1H, py*H*), 8.38 (s, 1H, py*H*), 8.32 (d, *J* = 4.9 Hz, 1H, im*H*), 7.97 (s, 1H, im*H*), 7.84 (s, 1H, py*H*), 7.71 (s, 1H, im*H*), 7.48 (s, 1H, im*H*), 7.39 (d, *J* = 5.7 Hz, 1H, py*H*), 7.25 (d, *J* = 4.9 Hz, 1H, py*H*), 7.16 (s, 1H, py*H*), 6.15 (dt, *J* = 17.0, 7.6 Hz, 1H, C=C*H*), 5.61 (dt, *J* = 17.0, 7.7 Hz, 1H, C=C*H'*), 5.46 (d, *J* = 17.0 Hz, 1H, alkenyl *H*), 5.34 (d, *J* = 10.1 Hz, 1H, alkenyl *H*), 5.26 − 5.02 (m, 2H, alkenyl *H*), 5.03 − 4.76 (m, 2H, NC*H*), 3.84 (s, 2H, NC*H'*), 2.55 (s, 3H, C*H*$_3$), 2.35 (s, 3H, C*H*$_3$'). ^{13}C{^{1}H} NMR (125 MHz, CD$_3$CN, 298K) δ (ppm) 153.7, 150.0, 147.5, 134.9, 131.1, 127.2, 124.4, 122.5, 120.5, 118.3, 115.6, 53.1, 21.2. HR-MS (ESI$^+$): *m/z* 252.0623 [C$_{24}$H$_{26}$N$_6$Pd]$^{2+}$, calcd. [M − MeCN − 2PF$_6$]$^{2+}$ 252.0621. Anal. calcd. (%) for C$_{26}$H$_{29}$N$_7$P$_2$F$_{12}$Pd·^{3}/$_4$CHCl$_3$: C 34.72, H 3.24, N 10.59; found C 34.80, H 3.30, N 10.30.

Synthesis of *bis*[1-allyl-3-(2-(5-nitro)pyridyl)imidazole-2-ylidene]palladium(II) dihexafluorophosphate (5.3.1). 1-Allyl-3-(2-(5-nitro)pyridyl)imidazolium hexafluorophosphate **P5.3.1** (0.45 g, 1.20 mmol) and Pd(OAc)$_2$ (0.13 g, 0.60 mmol) were added to a flame-dried Schlenk tube and dried *in vacuo*. Anhydrous acetonitrile (20 mL) was added using an oven-dried cannula, and the homogeneous mixture stirred at 70 ˚C for 48 hours. Following, the mixture was cooled to room temperature and filtered through a short path of Celite. Solvents were removed under reduced pressure, and the resultant residue recrystallised from acetonitrile/diethyl ether to afford a pale yellow solid which was collected onto a glass frit by vacuum filtration, rinsed with diethyl ether (2 × 10 mL) and dried *in vacuo*, providing the pure product as a pale yellow solid.

Single crystals of the product were obtained through slow evaporation of a concentrated acetonitrile solution of the complex at room temperature. Yield: 0.43 g, 0.47 mmol, 79 %. Mp decomp. >212 °C. ^{1}H NMR (500 MHz, CD$_3$CN, 333K) δ (ppm) 10.15 (s, 1H, im*H*), 9.28 (s, 1H, im*H*), 9.04 (d, *J* = 8.5 Hz, 1H, py*H*), 8.81 (d, *J* = 9.0 Hz, 1H, py*H*), 8.67 (d, *J* = 9.0 Hz, 1H, py*H*), 8.17 (s, 1H, im*H*), 8.06 (d, *J* = 8.5 Hz, 1H, py*H*), 7.98 (s, 1H, im*H*), 7.60 (s, 1H, py*H*), 7.26 (s, 1H, py*H*), 6.18 (m, 1H, C=C*H*), 5.61 (m, 1H, C=C*H'*), 5.55 (d, *J* = 17.0 Hz, 1H, C=C*H*), 5.42 (d, *J* = 10.5 Hz, 1H, C=C*H'*), 5.22 (m, 1H, C=C*H*), 5.07 (m, 2H, C=C*H'*), 4.87 (d, *J* = 17.0 Hz, 1H, NC*H*), 4.01 (d, *J* = 10.0 Hz, 1H, NC*H*), 3.83 (d, *J* = 10.0 Hz, 1H, NC*H*), 1.97 (s, 3H, coord. C*H*$_3$CN). ^{13}C{^{1}H} NMR (125 MHz, CD$_3$CN, 298K) δ (ppm) 155.9, 154.0, 146.4, 144.9, 138.6, 132.0, 126.7, 121.9, 120.0, 115.3, 66.3, 55.0, 15.7. HR-MS (ESI$^+$): *m/z* 585.0634 [C$_{22}$H$_{21}$N$_8$O$_5$Pd]$^+$, calcd. [M − MeCN − 2PF$_6$ + OH]$^+$ 585.0668. Anal. calcd. (%) for C$_{24}$H$_{23}$N$_9$P$_2$F$_{12}$O$_4$Pd·^{1}/$_3$H$_2$O: C 31.89, H 2.64, N 13.95; found C 31.60, H 2.50, N 13.60.

Synthesis of *bis*[1-allyl-3-(2-methylpyridyl)imidazole-2-ylidene]palladium(II) dihexafluorophosphate (5.5.1). 1-Allyl-3-(2-methylpyridyl)imidazolium bromide **P5.5** (0.50 g, 1.79 mmol) and Pd(OAc)$_2$ (0.20 g, 0.89 mmol) were added to a flame-dried Schlenk tube and dried *in vacuo*. Anhydrous dimethyl sulfoxide (8 mL) was added using an oven-dried cannula, and the homogeneous mixture stirred at 70 °C for 2 hours, 90 °C for 6 hours and 120 °C for a further 12 hours. Following, the mixture was cooled to room temperature and filtered through a short path of Celite, which was rinsed with dichloromethane (*ca*. 10 mL). To the combined solvents, diethyl ether (20 mL) was added slowly, precipitating an off-white solid which proved extremely hygroscopic when exposed to air. Subsequently, the solid was dissolved in deionised water (*ca*. 20 mL) and ammonium hexafluorophosphate (0.70 g, 5.26 mmol) added in excess. The resulting off-white suspension was filtered onto a glass frit, rinsed with water (2 × 10 mL) and dried *in vacuo* for several hours, providing the title compound as an off-white solid. Single crystals of the product were obtained through slow diffusion of diethyl ether vapours into a concentrated acetonitrile solution of the complex at room temperature. Yield: 0.25 g, 0.31 mmol, 35 %. Mp decomp. >243 °C. ^{1}H NMR (500 MHz, CD$_3$CN, 233K) δ (ppm) 9.18 (d, *J* = 5.5 Hz, 2H, im*H*), 7.97 (t, *J* = 15.0, 7.5 Hz, 2H, py*H*), 7.64 (d, *J* = 7.5 Hz, 2H, py*H*), 7.43 (t, *J* = 12.5, 7.5 Hz, 2H, py*H*), 7.30 (s, 2H, im*H*), 7.00 (s, 2H, py*H*), 6.02 (m, 2H, C=C*H*), 5.79 (d, *J* = 15.0 Hz, 2H, C*H*$_2$), 5.34 (d, *J* = 15.0 Hz, 2H, C*H*$_2$), 5.24 (d, *J* = 10.0 Hz, 2H, C=C*H*$_{cis}$), 5.14 (d, *J* = 21.0 Hz, 2H, C=C*H*$_{trans}$), 5.09 (m, 2H, NC*H*), 5.06 (m, 2H, NC*H*). ^{13}C{^{1}H} NMR (100 MHz, CD$_3$CN) δ (ppm) 207.6, 157.1, 154.6, 153.5, 142.6, 133.1, 127.1, 126.8, 124.7, 123.7, 119.9, 56.3, 53.8. HR-MS (ESI$^+$): *m/z* 649.0903 [C$_{24}$H$_{26}$N$_6$F$_6$PPd]$^+$, calcd. [M − PF$_6$]$^+$ 649.0902. Anal. calcd. (%) for C$_{24}$H$_{26}$N$_6$P$_2$F$_{12}$Pd: C 36.30, H 3.30, N 10.59; found C 36.50, H 3.30, N 10.65.

Synthesis of *bis*[1,3-(2-methylpyridyl)imidazol-2-ylidene]palladium(II) dibromide (5.6). 1,3-*Bis*(2-methylpyridyl)imidazolium bromide **P5.6** (0.50 g, 1.51 mmol) and Pd(OAc)$_2$ (0.17 g, 0.76 mmol) were added to a flame-dried Schlenk tube and dried *in vacuo*. Anhydrous dimethyl sulfoxide (8 mL) was added using an oven-dried cannula, and the homogeneous mixture stirred at 80 °C for 2 hours, followed by further reaction at 100 °C for 16 hours. Following, the mixture was cooled to room temperature and filtered through a short path of Celite, which was rinsed with dichloromethane (*ca*. 10 mL). To the combined solvents, diethyl ether (20 mL) was added slowly, precipitating a pale yellow solid which was collected onto a glass frit by vacuum filtration and rinsed with cold chloroform (2 × 5 mL), followed by diethyl ether (2 × 5 mL), providing the product as a pale yellow solid. Single crystals of the product were obtained through slow diffusion of diethyl ether vapours into a concentrated solution of the complex in dichloromethane/dimethyl sulfoxide (1:1). Yield: 0.24 g, 0.31 mmol, 41 %. Mp decomp. >248°C. ^{1}H NMR (400 MHz, (CD$_3$)$_2$SO) δ (ppm) 9.56 (br s, 1H, im*H*), 9.37 (br s, 1H, im*H*), 8.53 – 8.40 (br m, 2H, im*H*), 8.24 – 7.17 (br m, 16H, pyr*H*), 5.74 (br s, 4H, NC*H*$_2$), 5.47 (br s, 4H, N'C*H*$_2$). ^{13}C{^{1}H} NMR (100 MHz, CD$_3$CN) δ (ppm) 118.6, 118.0, 116.1, 114.7, 113.8, 103.1, 102.1, 92.5, 88.5, 87.1, 86.7, 86.3, 83.4, 80.9, 16.5, 15.5, 14.5. HR-MS (ESI$^+$): *m/z* 687.0652 [C$_{30}$H$_{28}$N$_8$BrPd]$^+$, calcd. [M − Br]$^+$ 687.0629. Anal. calcd. (%) for C$_{30}$H$_{28}$N$_8$Br$_2$Pd·CHCl$_3$: C 41.02, H 3.50, N 12.64; found C 41.20, H 3.80, N 12.70.

Synthesis of *bis*[1,3-(2-methylpyridyl)imidazol-2-ylidene]palladium(II) dihexafluorophosphate (5.6.1). 1,3-*Bis*(2-methylpyridyl)imidazolium hexafluorophosphate **P5.6.1** (1.25 g, 3.16 mmol) and Pd(OAc)$_2$ (0.35 g, 1.58 mmol) were added to a flame-dried Schlenk tube and dried *in vacuo*. Anhydrous dimethyl sulfoxide (8 mL) was added using an oven-dried cannula, and the homogeneous mixture stirred at 100 °C for 24 hours, Following, the mixture was cooled to room temperature and filtered through a short path of Celite, which was rinsed with dichloromethane (*ca*. 10 mL). To the combined solvents, diethyl ether (20 mL) was added slowly, precipitating a pale brown solid which was collected onto a glass frit by vacuum filtration and rinsed with diethyl ether (2 × 10 mL), providing the product as a pale brown solid. Single crystals of the product were obtained through slow diffusion of diethyl ether vapours into a concentrated solution of the complex in acetonitrile. Yield: 1.10 g, 1.23 mmol, 39 %. Mp decomp. >231 °C. ^{1}H NMR (400 MHz, CD$_3$CN, 298K) δ (ppm) 8.71 – 8.51 (m, 4H, im*H*), 8.12 – 7.08 (m, 16H, py*H*), 5.87 (d, *J* = 20.0 Hz, 2H, NC*H*$_2$), 5.51 (d, *J* = 20.0 Hz, 2H, NC*H*$_2$), 5.06 (d, *J* = 21.2 Hz, 2H, NC*H*$_2$), 4.73 (d, *J* = 21.2 Hz, 2H, NC*H*$_2$). ^{13}C{^{1}H} NMR (100 MHz, CD$_3$CN, 298K) δ (ppm) 199.4, 160.9, 158.0, 155.0, 154.6, 154.2, 153.9, 153.1, 150.5, 150.4, 142.3, 142.0, 138.2, 136.2, 132.7, 126.9, 126.8, 126.7, 126.6, 124.7, 124.5, 123.9, 123.4, 122.9, 56.2, 56.0, 55.6, 54.0. HR-MS (ESI$^+$): *m/z* 751.1138 [C$_{30}$H$_{28}$N$_8$F$_6$PPd]$^+$, calcd. [M − PF$_6$]$^+$

751.1108. Anal. calcd. (%) for $C_{30}H_{28}N_8P_2F_{12}Pd \cdot {}^1/_2H_2O$: C 39.00, H 3.38, N 12.13; found C 38.95, H 3.00, N 12.00.

General procedure for cross-coupling reactions.

Cross-coupling reaction 1. Phenylboronic acid (0.18 g, 1.5 mmol), bromobenzene (0.16 g, 1.0 mmol), Pd 'catalyst' (see **Table 5.9**) and Cs_2CO_3 (0.65 g, 2.0 mmol) were charged to a Radley tube and briefly dried *in vacuo*. To these was added anhydrous dioxane (5 mL) *via* syringe. The resulting mixture was stirred at 80 ˚C for 2 hours. After this time, the mixture was cooled and a 100 μL aliquot was withdrawn and quenched into a CH_2Cl_2 solution of *p*-cymene (2 mL, 9.52 mM). The resulting solution was filtered through Celite and subsequently analysed by GC.

Cross-coupling reaction 2. 2,6-Dimethylphenylboronic acid (0.18 g, 1.2 mmol), 1-bromo-2-methoxynaphthalene (0.24 g, 1.0 mmol), Pd 'catalyst' (see **Table 5.10**) and KOH (0.17 g, 3.0 mmol) were charged to a Radley tube and briefly dried *in vacuo*. To these was added anhydrous dioxane (3 mL) *via* syringe. The resulting mixture was stirred at 65 ˚C for 24 hours. After this time, the mixture was cooled and a 100 μL aliquot was withdrawn and quenched into a CH_2Cl_2 solution of *p*-cymene (2 mL, 17.5 mM). The resulting solution was filtered through Celite and subsequently analysed by GC.

5.7   Bibliography

1. (a) J.-P. Corbet, G. Mignani, *Chem. Rev.* **2006**, *106*, 2651–2710; (b) A. Littke, G. Fu, *Angew. Chem. Int. Ed.* **2002**, *41*, 4176–4211; (c) R. Heck, *Org. React.* **1982**, *27*, 345–390.

2. (a) C. C. C. Johansson Seechurn, M. O. Kitching, T. J. Colacot, V. Snieckus, *Angew. Chem. Int. Ed. Engl.* **2012**, *51*, 5062–5085; (b) T. Jeffrey, *Adv. Met.-Org. Chem.* **1996**, *5*, 153–260; (c) M. Shnibasaki, E. Vogl, *J. Organomet. Chem.* **1999**, *576*, 1–15.

3. G. C. Fortman, S. P. Nolan, *Chem. Soc. Rev.* **2011**, *40*, 5151–5169.

4. M. N. Hopkinson, C. Richter, M. Schedler, F. Glorius, *Nature* **2014**, *510*, 485–496.

5. E. V Vinogradova, B. P. Fors, S. L. Buchwald, *J. Am. Chem. Soc.* **2012**, *134*, 11132–11135.

6. P. L. Arnold, F. G. N. Cloke, T. Geldbach, P. B. Hitchcock, *Organometallics* **1999**, *18*, 3228–3233.

7. C. W. K. Gstöttmayr, V. P. W. Böhm, E. Herdtweck, M. Grosche, W. A. Herrmann, *Angew. Chem. Int. Ed.* **2002**, *41*, 1363–1365.

8. Z. Liu, T. Zhang, M. Shi, *Organometallics* **2008**, *27*, 2668–2671.

9. Z. Lu, S. A. Cramer, D. M. Jenkins, *Chem. Sci.* **2012**, *3*, 3081–3087.

10. F. E. Hahn, M. C. Jahnke, T. Pape, *Organometallics* **2006**, *25*, 5927–5936.

11. T. Samanta, S. K. Seth, S. K. Chattopadhyay, P. Mitra, V. Kushwah, J. Dinda, *Inorganica Chim. Acta* **2014**, *411*, 165–171.

12. A. R. Chianese, P. T. Bremer, C. Wong, R. J. Reynes, *Organometallics* **2009**, *28*, 5244–5252.

13. V. César, S. Bellemin-Laponnaz, L. H. Gade, *Organometallics* **2002**, *21*, 5204–5208.

14. M.-T. Chen, D. A. Vicic, M. L. Turner, O. Navarro, *Organometallics* **2011**, *30*, 5052–5056.

15. Y.-Q. Tang, J.-M. Lu, L.-X. Shao, *J. Organomet. Chem.* **2011**, *696*, 3741–3744.

16. Z.-Y. Wang, G.-Q. Chen, L.-X. Shao, *J. Org. Chem.* **2012**, *77*, 6608–6614.

17. C. Valente, S. Calimsiz, K. H. Hoi, D. Mallik, M. Sayah, M. G. Organ, *Angew. Chem. Int. Ed. Engl.* **2012**, *51*, 3314–3332.

18. M. G. Organ, S. Avola, I. Dubovyk, N. Hadei, E. A. B. Kantchev, C. J. O'Brien, C. Valente, *Chem. Eur. J.* **2006**, *12*, 4749–4755.

19. N. Hadei, E. A. B. Kantchev, C. J. O'Brien, M. G. Organ, *Org. Lett.* **2005**, *7*, 3805–3807.

20. N. Hadei, E. A. B. Kantchev, C. J. O'Brien, M. G. Organ, *J. Org. Chem.* **2005**, *70*, 8503–8507.

21. C. Valente, M. E. Belowich, N. Hadei, M. G. Organ, *Eur. J. Org. Chem.* **2010**, *23*, 4343–4354.

22. I. J. S. Fairlamb, A. R. Kapdi, A. F. Lee, G. P. McGlacken, F. Weissburger, A. H. M. de Vries, L. Schmieder-van de Vondervoort, *Chem. Eur. J.* **2006**, *12*, 8750–8761.

23. R. Sustmann, J. Lau, M. Zipp, *Tetrahedron Lett.* **1986**, *27*, 5207–5210.

24. A. E. Jensen, P. Knochel, *J. Org. Chem.* **2002**, *67*, 79–85.

25. B. R. M. Lake, C. E. Willans, *Organometallics* **2014**, *33*, 2027–2038.

26. K. Selvakumar, A. Zapf, A. Spannenberg, M. Beller, *Chem. Eur. J.* **2002**, *8*, 3901–3906.

27. L. G. Bonnet, R. E. Douthwaite, R. Hodgson, *Organometallics* **2003**, *22*, 4384–4386.

28. M. W. Washabaugh, W. P. Jencks, *Biochemistry* **1988**, *27*, 5044–5053.

29. K. S. Coleman, S. Turberville, S. I. Pascu, M. L. H. Green, *J. Organomet. Chem.* **2005**, *690*, 653–658.

30. H. Lebel, M. K. Janes, A. B. Charette, S. P. Nolan, *J. Am. Chem. Soc.* **2004**, *126*, 5046–5047.

31. H. M. Lee, P. L. Chiu, J. Y. Zeng, *Inorganica Chim. Acta* **2004**, *357*, 4313–4321.

32. J. Wencel-Delord, T. Dröge, F. Liu, F. Glorius, *Chem. Soc. Rev.* **2011**, *40*, 4740–4761.

33. A. Maleckis, J. W. Kampf, M. S. Sanford, *J. Am. Chem. Soc.* **2013**, *135*, 6618–6625.

34. M. Anand, R. B. Sunoj, H. F. Schaefer, *J. Am. Chem. Soc.* **2014**, *136*, 5535–5538.

35. K. M. Engle, D.-H. Wang, J.-Q. Yu, *J. Am. Chem. Soc.* **2010**, *132*, 14137–14151.

36. L.-C. Campeau, D. R. Stuart, J.-P. Leclerc, M. Bertrand-Laperle, E. Villemure, H.-Y. Sun, S. Lasserre, N. Guimond, M. Lecavallier, K. Fagnou, *J. Am. Chem. Soc.* **2009**, *131*, 3291–3306.

37. V. J. Catalano, A. O. Etogo, *Inorg. Chem.* **2007**, *46*, 5608–5615.

38. J. R. Miecznikowski, S. Gründemann, M. Albrecht, C. Mégret, E. Clot, J. W. Faller, O. Eisenstein, R. H. Crabtree, *Dalton Trans.* **2003**, 831–838.

39. T. G. Larocque, A. C. Badaj, G. G. Lavoie, *Dalton Trans.* **2013**, *42*, 14955–14958.

40. B. M. Mattson, W. A. G. Graham, *Inorg. Chem.* **1981**, *20*, 3186–3189.

41. R. F. Heck, J. P. Nolley, *J. Org. Chem.* **1972**, *37*, 2320–2322.

42. T. Mizoroki, K. Mori, A. Ozaki, *Bull. Chem. Soc. Jpn.* **1971**, *44*, 581–582.

43. K. Sakoda, J. Mihara, J. Ichikawa, *Chem. Commun.* **2005**, *41*, 4684–4686.

44. A. B. Dounay, L. E. Overman, A. D. Wrobleski, *J. Am. Chem. Soc.* **2005**, *127*, 10186–10187.

45. A. de Meijere, F. E. Meyer, *Angew. Chem. Int. Ed. Engl.* **1995**, *33*, 2379–2411.

46. (a) A. F. Littke, G. C. Fu, *J. Org. Chem.* **1999**, *64*, 10–11; (b) M. Shibasaki, E. Vogl, T. Ohshima, *Compr. Asymmetric Catal. Suppl.* **2004**, *1*, 217–218.

47. K. H. Shaughnessy, P. Kim, J. F. Hartwig, *J. Am. Chem. Soc.* **1999**, *121*, 2123–2132.

48. R. B. Bedford, *Chem. Commun.* **2003**, 1787–1796.

49. D. E. Bergbreiter, P. L. Osburn, Y.-S. Liu, *J. Am. Chem. Soc.* **1999**, *121*, 9531–9538.

50. E. A. B. Kantchev, C. J. O'Brien, M. G. Organ, *Angew. Chem. Int. Ed. Engl.* **2007**, *46*, 2768–2813.

51. T. Iwasawa, T. Komano, A. Tajima, M. Tokunaga, Y. Obora, T. Fujihara, Y. Tsuji, *Organometallics* **2006**, *25*, 4665–4669.

52. J.-P. Ebran, A. L. Hansen, T. M. Gøgsig, T. Skrydstrup, *J. Am. Chem. Soc.* **2007**, *129*, 6931–6942.

53. M. Feuerstein, H. Doucet, M. Santelli, *J. Org. Chem.* **2001**, *66*, 5923–5925.

54. S. K. Yen, L. L. Koh, F. E. Hahn, H. V. Huynh, T. S. A. Hor, *Organometallics* **2006**, *25*, 5105–5112.

55. W. A. Herrmann, M. Elison, J. Fischer, C. Köcher, G. R. J. Artus, *Angew. Chem. Int. Ed. Engl.* **1995**, *34*, 2371–2374.

56. M. G. Johnson, R. J. Foglesong, *Tetrahedron Lett.* **1997**, *38*, 7001–7002.

57. S. D. Walker, T. E. Barder, J. R. Martinelli, S. L. Buchwald, *Angew. Chem. Int. Ed. Engl.* **2004**, *43*, 1871–1876.

58. T. E. Barder, S. D. Walker, J. R. Martinelli, S. L. Buchwald, *J. Am. Chem. Soc.* **2005**, *127*, 4685–4696.

59. G. Altenhoff, R. Goddard, C. W. Lehmann, F. Glorius, *J. Am. Chem. Soc.* **2004**, *126*, 15195–15201.

60. T. Hoshi, T. Nakazawa, I. Saitoh, A. Mori, T. Suzuki, J. Sakai, H. Hagiwara, *Org. Lett.* **2008**, *10*, 2063–2066.

61. M. G. Organ, S. Calimsiz, M. Sayah, K. H. Hoi, A. J. Lough, *Angew. Chem. Int. Ed. Engl.* **2009**, *48*, 2383–2387.

62. Z. Xi, F. Liu, Y. Zhou, W. Chen, *Tetrahedron* **2008**, *64*, 4254–4259.

63. A. Raba, M. R. Anneser, D. Jantke, M. Cokoja, W. A. Herrmann, F. E. Kühn, *Tetrahedron Lett.* **2013**, *54*, 3384–3387.

64. M. J. McPhillie, R. Trowbridge, K. R. Mariner, A. J. O'Neill, A. P. Johnson, I. Chopra, C. W. G. Fishwick, *ACS Med. Chem. Lett.* **2011**, *2*, 729–734.

65. J. M. Keith, *J. Org. Chem.* **2008**, *73*, 327–330.

66. T. Tu, Z. Sun, W. Fang, M. Xu, Y. Zhou, *Org. Lett.* **2012**, *14*, 4250–4253.

67. H. Puschmann, O. V. Dolomanov, L. J. Bourhis, R. J. Gildea, J. A. K. Howard, *J. Appl. Crystallogr.* **2009**, *42*, 339–341.

68. J.-R. Hu, L.-H. Liu, X. Hu, H.-D. Ye, *Tetrahedron* **2014**, *70*, 5815–5819.

Chapter 6

Experimental and theoretical approach to rationalise a rare cyclometalation at palladium

6.1   Introduction

Over five decades ago, Kleinman and Dubeck described the treatment of azobenzene with nickelocene ($Ni(\eta^5-C_5H_5)_2$) to obtain a five-membered nickelacycle, which represents the first example of a cyclometalation reaction.[1] Soon after, their approach was extended to neighbouring group 10 transition metals, with Cope, Siekman and Friedrich reacting azobenzene and benzylamines with suitable palladium sources (*e.g.* $PdCl_2$ or Li_2PdCl_4) to afford the first isolated, well-characterised family of palladacycles (**Scheme 6.1**).[2,3]
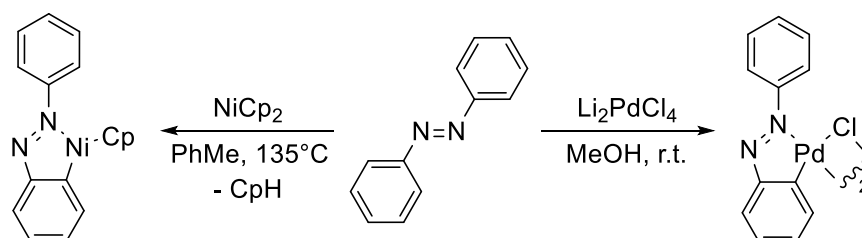
Scheme 6.1 *Cyclometalation approach to metallacycles of azobenzene. Left route: Kleinman and Dubeck's original nickelacycle.[1] Right route: exemplar palladacycle, prepared by Cope.[2]*

The physical properties of these compounds, notably their high thermal stability in the solid-state, spurred the group of Herrmann towards the discovery of a cyclopalladated tri-*o*-tolyl-phosphine complex, which is a highly active catalyst precursor for cross-coupling reactions (the crystal structure of which is illustrated in **Figure 6.1**).[4] These findings raised high expectations for this class of compound, as Herrmann showed his example to activate more economic and challenging substrates than those previously required (*i.e.* aryl iodides and triflates), such as aryl chlorides.
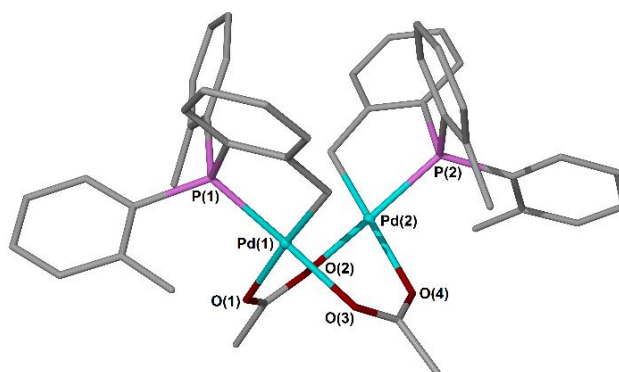
Figure 6.1 *Taken from the crystal structure of Herrmann's robust palladacyclic catalyst.[4]*

From a retrosynthetic standpoint, cyclometalation offers a convenient route to metallacycles by way of C-H activation chemistry. As such, numerous palladacyclic scaffolds have been derived from a metal-induced C-H activation process paralleled by coordination of pendant heteroatom donors (for example, imines,[5] amines,[6] phosphines,[7] oximes,[8] thioethers[9] and oxazolines)[10] to the metal centre. The absolute position of the C-H bond to be activated with respect to the donor atoms(s), along with the degree of hybridisation of the related carbon atom, regulate the ease of cyclometalation. Due to the intrinsic number of variables, the predictability of metalation is poor, though formal energetic calculations regarding the strength of aromatic *versus* aliphatic C-H bonds have been performed.[11,12] Nonetheless, it is generally accepted that for the majority of known complexes the metalated carbon atom is an aromatic sp^2 centre (**Figure 6.2**, **a**),[13] or less commonly an sp^3 aliphatic[14] or benzylic carbon centre (**Figure 6.2**, **b**).[15]

Undoubtedly rare, is cyclometalation at an alkenyl sp^2 carbon atom. An isolated example was communicated by Dupont and Konrath, whereby reaction of propargyl amines or thioethers with Li_2PdCl_4 in methanol produces air-stable, five-membered palladacyclic products, brought about by nucleophilic addition of chloride to the C≡C bond.[16] By employing a high concentration of chloride, the authors were able to trap the σ-vinyl palladium(II) intermediate for full characterisation (**Figure 6.2**, **c**).
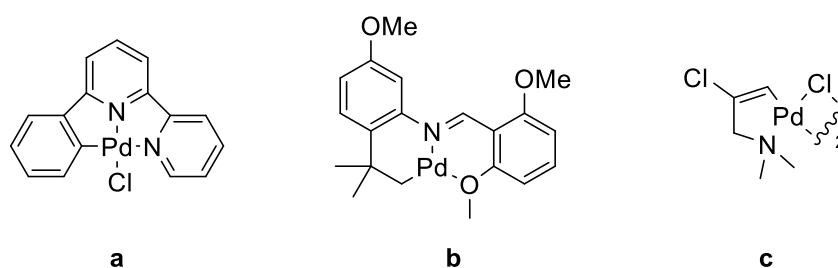
Figure 6.2 *Representative palladacycles formed via aromatic C(sp²)-H (**a**)[13] or aliphatic C(sp³)-H (**b**) activation.[15] Illustration **c** represents Dupont's rare σ-alkenyl palladacycle, produced by a nucleophilic trapping experiment.[16]*

As demonstrated within this thesis, work conducted in our laboratory largely pivots around the reactivity and applications of *N*-heterocyclic carbenes as ancillary donor ligands to facilitate chemical transformations. Known for producing complexes which are thermally robust, NHCs bind securely to metal centres *via* strong carbenic σ-donation, whilst imposing an equally strong influence on the coordination sphere through their tuneable steric profile. NHCs however, have seldom been employed as supporting ligands for palladium metallacycles, despite their suitability for the role. Few examples do exist, which are typically produced through coordination of a free carbene to a pre-existing palladacyclic framework,[17] or oxidative addition of a heteroaryl precursor to palladium(0).[18]

Chapter 5 describes the logical preparation of various palladium(II) *bis*-NHC complexes, which aimed to balance steric fluidity with hemilabile chelation of an NHC unit, to create a useful catalyst for challenging cross-coupling reactions. In doing so, all synthetic examples reported within Chapter 5 represent palladium complexes of true spectator NHC ligands, which do not partake in reactivity at the metal centre. Less commonly, however, NHC ligands have been seen to undergo 'non-innocent' behaviour (*i.e.* experience reactivity themselves) within various well-defined metal complexes, shaping the subject of a recent review article by Willans and Lake.[19]

Amongst the palladium compounds surveyed in Chapter 5, reaction of Pd(OAc)$_2$ with 4-methoxypyridyl substituted imidazolium salt, **5.4.1**, produced the expected palladium(II) *bis*-NHC complex, **5.10.1**, amongst a significant quantity of one other product. During this investigation, it became apparent that this side-product is formed by virtue of a non-innocent ligand pathway. Accordingly, it was sought to delineate this reactivity.

6.2   Synthesis of palladium-NHC complexes

Reaction of freshly prepared 4-methoxypyridylimidazole (**P5.4**) with an excess of allyl bromide furnished imidazolium salt **5.4** in 84 % isolated yield. The associated bromide anion was further exchanged through treatment of the bromide salt with three equivalents of ammonium hexafluorophosphate in water, providing imidazolium hexafluorophosphate **5.4.1** in quantitative yield, as described in Chapter 5. Subsequent reaction of **5.4.1** with half an equivalent of Pd(OAc)$_2$ in refluxing acetonitrile delivered the expected palladium(II) *bis*-NHC complex, **5.10.1** as the major product of reaction (**Scheme 6.1**).
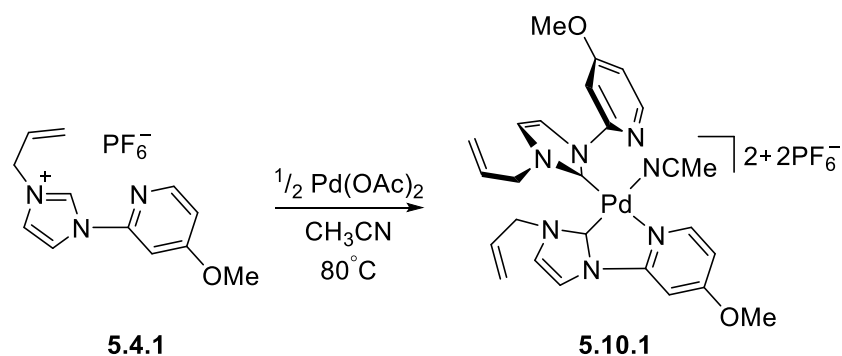
***Scheme 6.2** Formation of palladium(II) bis-NHC complex, **5.10.1**.*

The product batch was originally analysed by proton NMR spectroscopy, recorded in d_3-MeCN. Evident, were a sequence of sharp signals attributed to the target [Pd(NHC)$_2$(MeCN)]2PF$_6$ complex (confirmed by additional ^{1}H-^{1}H correlation spectroscopy), accompanied by a second set of well-resolved resonances at neighbouring chemical shift. As shown in Chapter 5, all *bis*-(*N*-pyridyl)-appended NHC ligated complexes of palladium are chelated only through one ligand,

producing an overall unsymmetrical coordination sphere which is often reflected in their solution NMR spectra. It should therefore be of no surprise to observe paired-signals corroborating two ligand environments in the ^{1}H NMR spectrum. However, the two sets of signals are observed in a 69:31 average ratio (major belonging to **5.10.1**), as judged by solution integration measurement, which remains independent of temperature. If all resonances pertained to a single species undergoing ligand fluxion in solution, as is common to this family of complex, some signal coalescence would be expected under high temperature NMR conditions. It was therefore speculated that alongside **5.10.1**, a competing side-product is generated.

Indeed, performing the reaction with a 1:1 stoichiometric ratio of Pd(OAc)$_2$ to ligand precursor **5.4.1** (*i.e.* doubling the concentration of palladium source), led to a two-fold increase in observed side-product formation (39:61 observed ratio of **5.10.1** to side-product, respectively), following a crystallisation work-up procedure. Conversely, conducting the reaction with a 4:1 stoichiometric quantity of **5.4.1** to Pd(OAc)$_2$ (*i.e.* doubling the concentration of ligand source), reduced side-product formation by one half (84:16, **5.10.1** to side-product, respectively). These findings not only verify the production of two discrete compounds, but also highlight a linear dependence of product formation on reaction stoichiometry. A comparison between the ^{1}H NMR spectra of the product mixtures on varying reactant stoichiometry is provided in **Figure 6.3**.
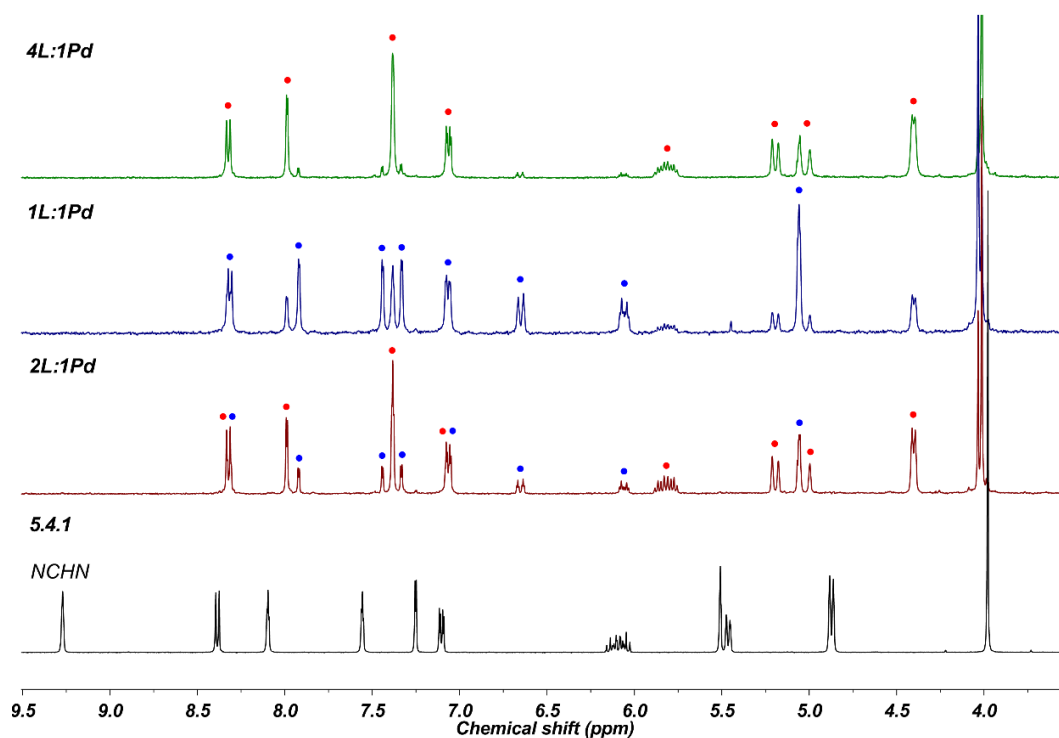
Figure 6.3 *^{1}H NMR spectrum of authentic ligand precursor **5.4.1** (black trace, 300 MHz, CD$_3$CN, 298K), noting complete loss of imidazolium NCHN signal at 9.27 ppm. Subsequent ^{1}H NMR spectra were recorded following a change in palladium concentration (red trace = 0.5 equiv. Pd, blue trace = 1.0 equiv. Pd, green trace = 0.25 equiv. Pd). Red circles indicate signals attributed to **5.10.1**, blue circles represent those pertaining to side-product.*

Analysis of the impure reaction mixture by high-resolution mass spectrometry further supported the presence of **5.10.1** as the major product of reaction. Dominant mass peaks were observed at (m/z) 268.0581 and 581.1134, attributable to both dicationic $[(ML_2) - MeCN - 2PF_6]^{2+}$ and monocationic $[(ML_2 + HCO_2) - MeCN - 2PF_6]^+$ molecular fragments of the palladium(II) *bis*-NHC complex, as shown in **Figure 6.4**.

$[(ML_2) - MeCN - 2PF_6]^{2+}$

$[(ML) - MeCN - 2PF_6 - H]^+$

$[(ML_2 + HCO_2) - MeCN - 2PF_6]^+$
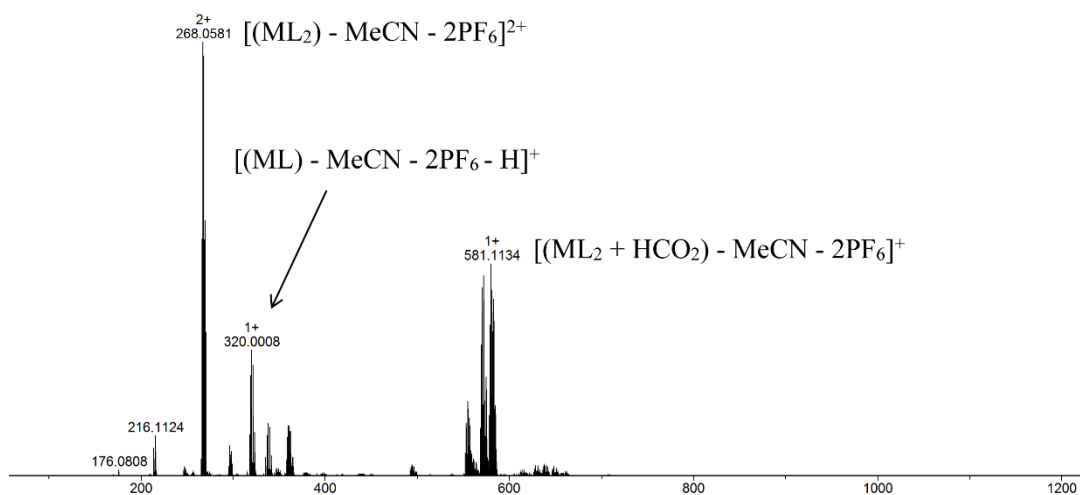
*Figure 6.4 Interpreted electrospray mass spectrum of original reaction mixture, predominantly comprising **5.10.1**, recorded in MeCN solvent.*

Palladium(II) *bis*-NHC complex **5.10.1** could be purified by flash chromatography (SiO$_2$, using a saturated acetone solution of NH$_4$PF$_6$ as eluent), affording the pure product as a pale yellow solid in 50 % yield. Multinuclear NMR spectroscopic analysis of the complex, recorded at ambient temperature in d_3-MeCN, suggested an overall C_2-symmetric ligand environment around the metal centre. This observation is unremarkable, given that low temperature spectroscopic measurements (around 233K) were required to fully resolve each unsymmetrically-bound ligand environment for analogous complexes of Chapter 5. Electrospray mass spectrometry and combustion analysis further supported a 1:2 metal/ligand ratio, with X-ray diffraction analysis ultimately confirming the absolute structure of complex **5.10.1**. For this purpose, Et$_2$O vapours were slowly diffused into an MeCN solution of the complex, producing pale yellow block crystals of the compound which were suitable for crystallographic study. The structural authentication of **5.10.1** is provided in **Figure 6.5**.
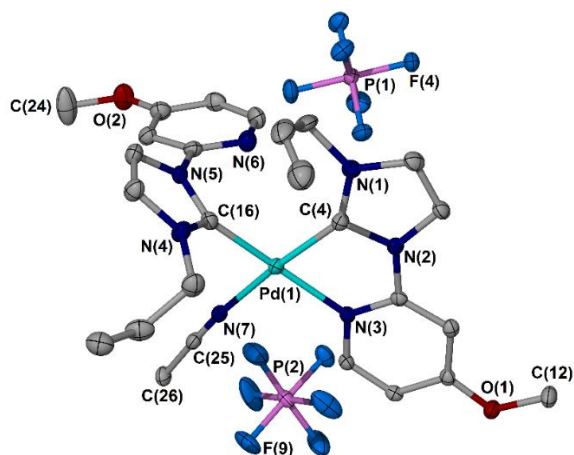
Figure 6.5 *Molecular structure of **5.10.1**. Atomic displacement parameters are drawn at the 50 % probability level, hydrogen atoms are omitted for clarity.*

Pd(1)-C(4)	1.964(4)	C(4)-Pd(1)-N(3)	79.63(14)
Pd(1)-C(16)	1.989(4)	C(16)-Pd(1)-C(4)	95.71(16)
Pd(1)-N(3)	2.078(3)	C(16)-Pd(1)-N(7)	91.24(15)
Pd(1)-N(7)	2.059(4)	N(7)-Pd(1)-N(3)	93.81(12)

Table 6.1 *Selected bond lengths (Å) and angles (˚) from the crystal structure of **5.10.1**.*

The asymmetric unit of **5.10.1** displays one molecule of the expected palladium(II) *bis*-NHC complex. As was observed for analogues of the previous chapter, one NHC ligand is able to chelate to palladium through a neutral *N*-substituted pyridyl ring, distorting an 'ideal' angle around the square plane by over 10˚. This contraction prevents the *cis*-coordinated NHC ligand from chelating in the same manner, allowing a solvating molecule of acetonitrile to occupy a fourth coordination site at the metal centre. Overall the molecule does not demonstrate C_2 symmetry in the solid-state, suggesting a single ligand environment observed in the room temperature proton NMR spectrum is an outcome of coordinative fluxion at palladium.

Following chromatographic separation and isolation of **5.10.1**, the remaining fractions were combined and allowed to slowly evaporate. Resulting were a small collection of low quality single crystals of the original side-product, which could be structurally elucidated using X-ray crystallography. Therein, it was confirmed that an unusual NHC-ligated palladium(II) pincer complex was formed, through cyclometalation of a pendant allyl tether with the metal centre, affording an endocyclic σ-alkenyl palladacycle, **6.1** (**Figure 6.6**).
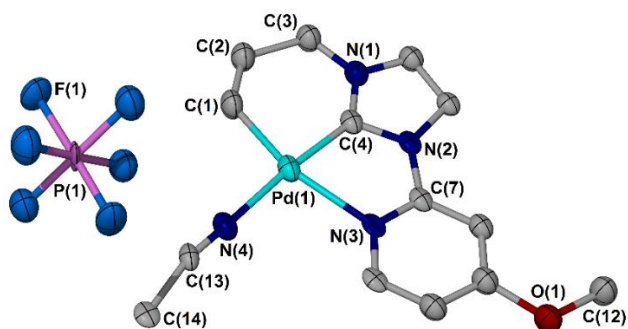
Figure 6.6 *Molecular structure of **6.1**. Atomic displacement parameters are drawn at the 30 % probability level, hydrogen atoms are omitted for clarity.*

A number of crystals were examined by X-ray diffraction methods, all of which were weakly diffracting and resulted in limited high angle data. In addition, the entire molecule is found to lie on a crystallographic mirror plane, leading to nonsensical atomic displacement parameters which could be improved through the use of restraints. Nevertheless, the structural solution clearly depicts a palladium(II) metal core which is coordinated to an allyl group through a terminal η^1 binding mode. The 1-allyl-3-(2-(4-methoxy)pyridyl)imidazol-2-ylidene ligand is unprecedentedly tridentate, forming a C,C,N pincer interaction to assemble a 6,5,5,6-fused palladacycle. Though restrained, the C(1)-C(2) bond length refines to a distance close to 1.30 Å, in keeping with a typical C=C double bond. The C(3)-C(2)-C(1)-Pd(1) torsion angle is close to 28.90°, which partially puckers the σ-vinyl group out of the ligand plane, and overall the palladium(II) centre adopts heavily distorted square planar geometry.

Under retrofit analysis, a low intensity mass peak at (*m/z*) 320.0008 was detected in the mass spectrum of the original product mixture, illustrated in **Figure 6.4**, which corroborates strongly with the simulated mass of **6.1** (calculated mass/charge of 320.0009). Likewise, closer inspection of the side-product enriched ^{1}H NMR spectrum given in **Figure 6.3** (blue trace), shows one allylic proton resonance is absent from the non-aromatic region (three signals present in a 1:1:2 ratio, integrating four protons altogether). The two remaining alkenic signals (displayed at 6.67 and 6.07 ppm) are shifted significantly downfield when compared with similar complexes of this type (*i.e.* **Figure 6.3**, green trace). It was therefore concluded, that **6.1** is the true identity of the original side-product.

Given that the pK_a of an unconjugated vinylic proton far exceeds that of the conjugate acid of acetate (*ca*. 43 *versus* 5),[20] it was proposed that an intramolecular $C(sp^2)$-H activation mechanism governs palladacycle formation. Taking account of the linear dependence of product distribution on palladium concentration, it was speculated that **6.1** could be produced selectively by controlling reactant stoichiometry to promote an intramolecular mechanism at palladium, whilst suppressing an intermolecular reaction with excess ligand. To do so, a high dilution strategy was

employed whereby a 30 mM solution of imidazolium salt **5.4.1** in MeCN was added dropwise to a stirring solution of Pd(OAc)$_2$ (110 mM) in uniform solvent at 80 ˚C. Following recrystallisation, σ-alkenyl palladacycle **6.1** was isolated exclusively as a pale yellow solid in 74 % yield, with competitive palladium(II) *bis*-NHC **5.10.1** undetectable by NMR spectroscopy (a ^{1}H NMR spectrum of **6.1** is given in **Figure 6.7**, red trace).
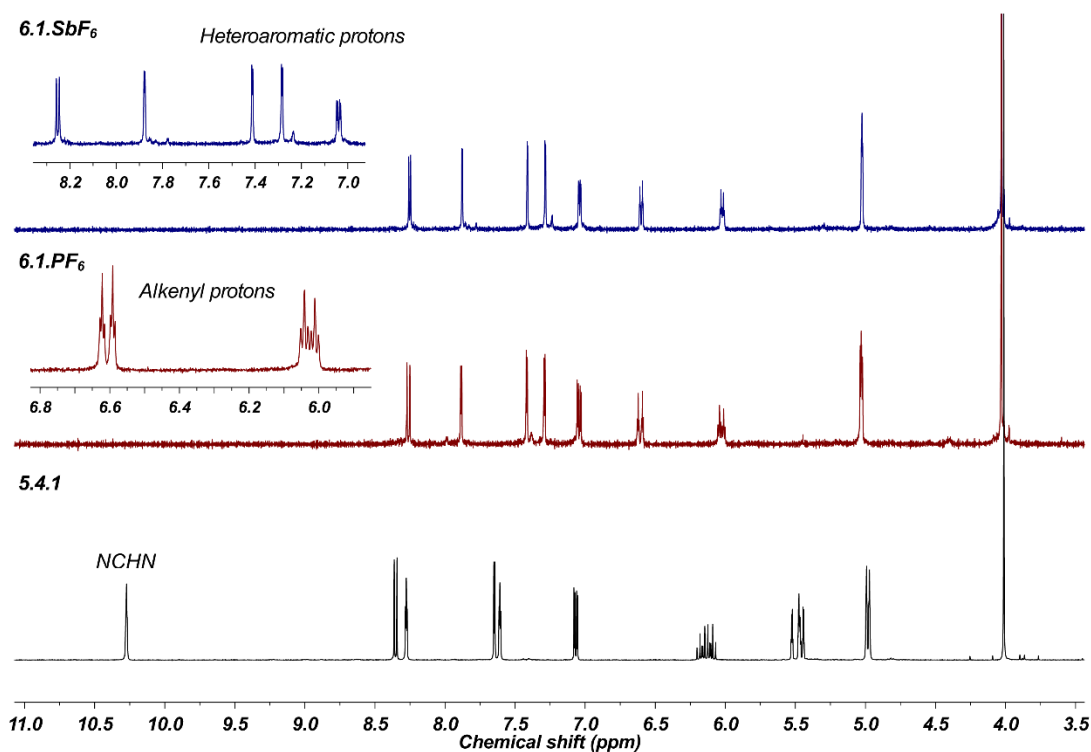
Figure 6.7 *^{1}H NMR spectrum of authentic ligand precursor **5.4.1** (black trace, 300 MHz, CD$_3$CN, 298K), noting complete loss of imidazolium NCHN signal at 9.27 ppm. ^{1}H NMR spectrum of **6.1** (red trace, 300 MHz, CD$_3$CN, 298K), highlighting downfield shift of σ-alkenyl protons to 6.67 and 6.07 ppm. ^{1}H NMR spectrum of hexafluoroantimonate salt of **6.1** (blue trace, 300 MHz, CD$_3$CN, 298K).*

The electrospray mass spectrum of **6.1** featured an intense signal at (*m/z*) 320.0019, attributed to a [M − PF$_6$]$^+$ monocation, comprising an isotopic envelope which overlays well with its simulated partner. The purity and composition of **6.1** were confirmed by combustion analysis and infrared spectroscopy, the latter displaying both C=C and C≡N bond stretches at 1642 and 2330 cm^{-1}, respectively.

An identical reaction using the hexafluoroantimonate salt of **5.4.1** yielded a palladacycle with indistinguishable spectroscopic (**Figure 6.7**, blue trace) and crystallographic data. This level of reproducibility suggests that a non-coordinating counteranion plays no role in the cyclometalation step. However, as seen in the formation of **5.4***, employment of a bromide counteranion leads to its coordination to the metal centre, shutting down cyclometalation entirely.

Modifying the electronic properties of the pyridyl ring connected to the NHC ligand, as illustrated in the preceding chapter, affords their palladium(II) *bis*-NHC complexes only. Amongst this list, includes a 4-(dimethylaminopyridyl)imidazolium analogue, which would be expected to accentuate palladacycle formation if cyclometalation were directly dependent on electronic activation. Moreover, no cyclometalation was observed when chain-length between alkene and NHC unit was increased by one carbon atom. These observations imply that ligand **5.4.1**, which bears both a 4-methoxypyridyl substituent and allyl tether, is a unique case in palladacycle formation, for which a narrow, unobvious electronic balance exists to promote $C(sp^2)$-H activation.

6.3   Theoretical calculations

The notion of synthesising **6.1** by way of vinylic $C(sp^2)$-H bond activation is not unreasonable, though reasons for the confinement of this reaction pathway to ligand **5.4.1** are not obvious. In fact, it is not possible to offer a satisfactory explanation for this unique reactivity from the experimental results presented within.

In an attempt to rationalise these findings, density functional theory (DFT) was applied. Calculations were performed by Dr Alireza Ariafard of the University of Tasmania, using Gaussian 09 at the M06 level of theory, in MeCN using the CPCM solvation model (for further details, see Experimental). From the outset, deprotonation of the first imidazolium NC*H*N hydrogen atom was considered, as illustrated in **Figure 6.8**. The DFT computation presents the most stable palladium(II) acetate adduct in MeCN solvent to exist as a square planar *cis*-MeCN complex (**4**), in terms of their respective free energies (ΔG, kcalmol^{-1}). It is important to note however, that for a prediction such as this, whereby three reactant molecules combine into a single product (*i.e.* Pd(OAc)$_2$ and two molecules of MeCN, to create **4**), the Gibbs free energy change is typically overestimated due to error in entropic contributions. For this model, the deficiency has been corrected using methodology developed by Whitesides and co-workers.[21]

Following the introduction of imidazolium ion **5.4.1**, the ligand initially binds favourably to palladium *via* its pyridyl nitrogen atom to form intermediate **8** (-3.1 kcalmol^{-1}). Latterly, a metalation-deprotonation sequence occurs, by way of an unexpected trigonal bipyramidal transition state structure (**1TS**), whereby a molecule of coordinating MeCN acts to lower the associated activation energy (23.1 kcalmol^{-1}). To the author's knowledge, a five-coordinate palladium(II) transition structure is unprecedented for this type of process. Generally accepted within the 'conventional' mechanism outlined independently by Houk and Schaefer,[22,23] is the requirement of a vacant coordination site at palladium prior to deprotonation, shown at the foot of **Figure 6.8** (**2TS**). The stepwise isomerisation of an η^2-acetate ligand to its η^1 form is thought to supply this, to subsequently allow deprotonation of the C-H bond by a pendant carbonyl group.

The four-coordinate transition state is thermodynamically favoured in the absence of MeCN (*i.e.* **1TS** *versus* **2TS**, 23.1 *versus* 25.1 kcalmol^{-1} activation barriers, respectively), however, these studies suggest that a five-coordinate transition structure may be more general in the presence of strongly coordinating solvents. More specifically, the presence of MeCN enables C-H deprotonation and substitution of pyridyl with carbene to occur simultaneously, producing **13** as the most thermodynamically stable species through loss of acetic acid from intermediate **11**.
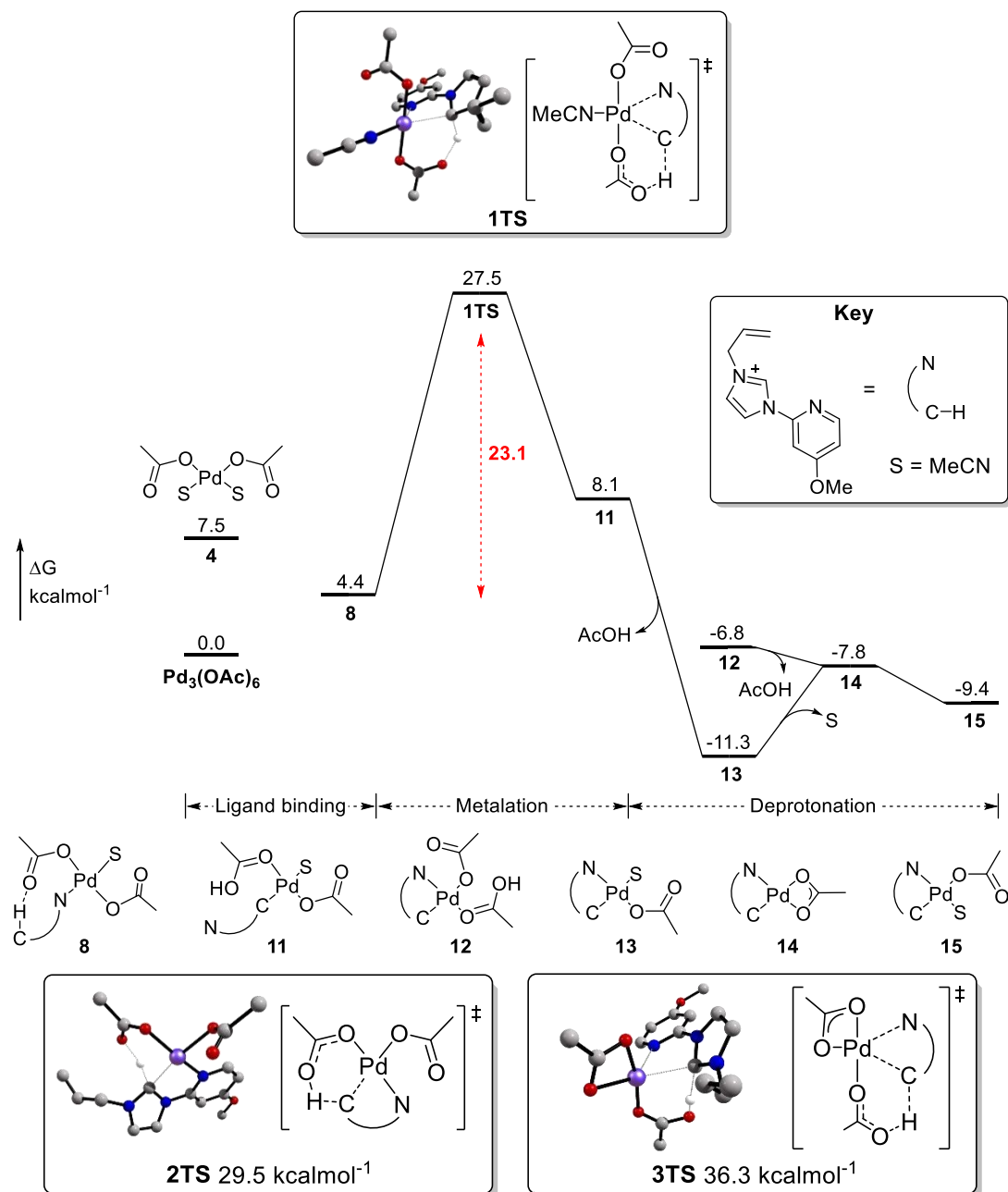
Figure 6.8 *Free energy profile in MeCN for the deprotonation of imidazolium salt **5.4.1** by Pd(OAc)$_2$. Step one describes elementary ligand binding, steps two and three illustrate a concerted metalation-deprotonation sequence. ΔG values are calculated in kcalmol^{-1}. All structures (including simulated) are cationic, and include only a simulation of one relevant hydrogen atom, with all others omitted for clarity.*

Taking **13** as the most stable product of initial deprotonation, further calculations were performed to assess the addition of a second NHC group to palladium in forming complex **5.10.1**. The free energy profile illustrated in **Figure 6.9** begins with substitution of coordinated MeCN in **13** by a pyridyl group of a second NHC unit, costing 2.6 kcalmol^{-1} with no overall change in entropy to produce intermediate **21**. Formation of this species allows entry to a five-coordinate trigonal bipyramidal transition state (**4TS**), whose structure is not entirely divorced with **1TS**, though no vacant sites exist at palladium to permit solvent-facilitated stabilisation (23.2 kcalmol^{-1} activation barrier to form **22**). Following formation, computation suggests that *trans* species **22** is able to reorient into its *cis* isomer **19**, which is thermodynamically favoured by 9.8 kcalmol^{-1}. However, the activation energy for interconversion *via* trigonal **5TS** is significant (33.8 kcalmol^{-1}), and is predicted not to occur. Instead, the actual outcome of these calculations is product **24** (palladium(II) *bis*-NHC geometrical isomer of **5.10.1**). The overall transformation is therefore endergonic by 5.7 kcalmol^{-1}, which implies that the addition of a second NHC never occurs from intermediate **12**; even if it is to be assumed that **23** is generated at some stage of the reaction, computation predicts that its conversion back to **13** is probable, as formation of **23** ultimately leads to a 'dead end'.
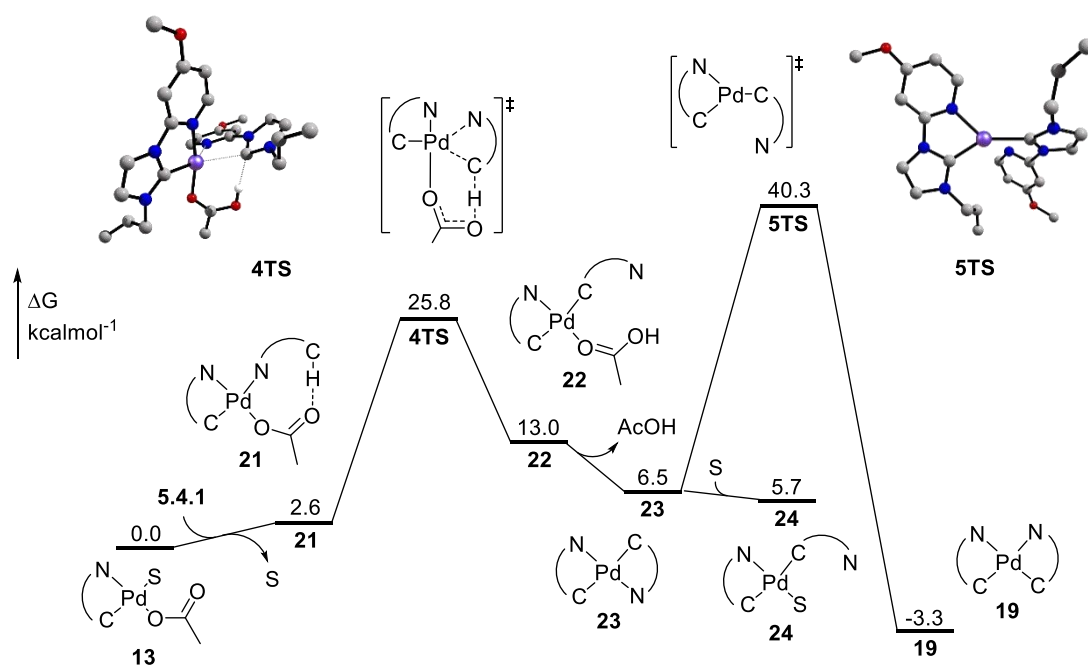
Figure 6.9 *Free energy profile in MeCN for the addition of a second NHC group to* **13**. *ΔG values are calculated in kcalmol^{-1}. All structures (including simulated) are cationic, and include only a simulation of one relevant hydrogen atom, with all others omitted for clarity.*

The energetic impasse calculated where a second NHC group is added to **13** suggests that this pathway takes place *via* its geometrical isomer, **15**, whereby the activation barrier for NHC addition is reduced. Building on these calculations, the origin of palladacyclisation was evaluated against competitive *bis*-NHC complexation, using **15** as a common starting point. A combined free energy profile to describe both intramolecular cyclometalation and intermolecular *bis*-NHC complex formation is provided below in **Figure 6.10**.
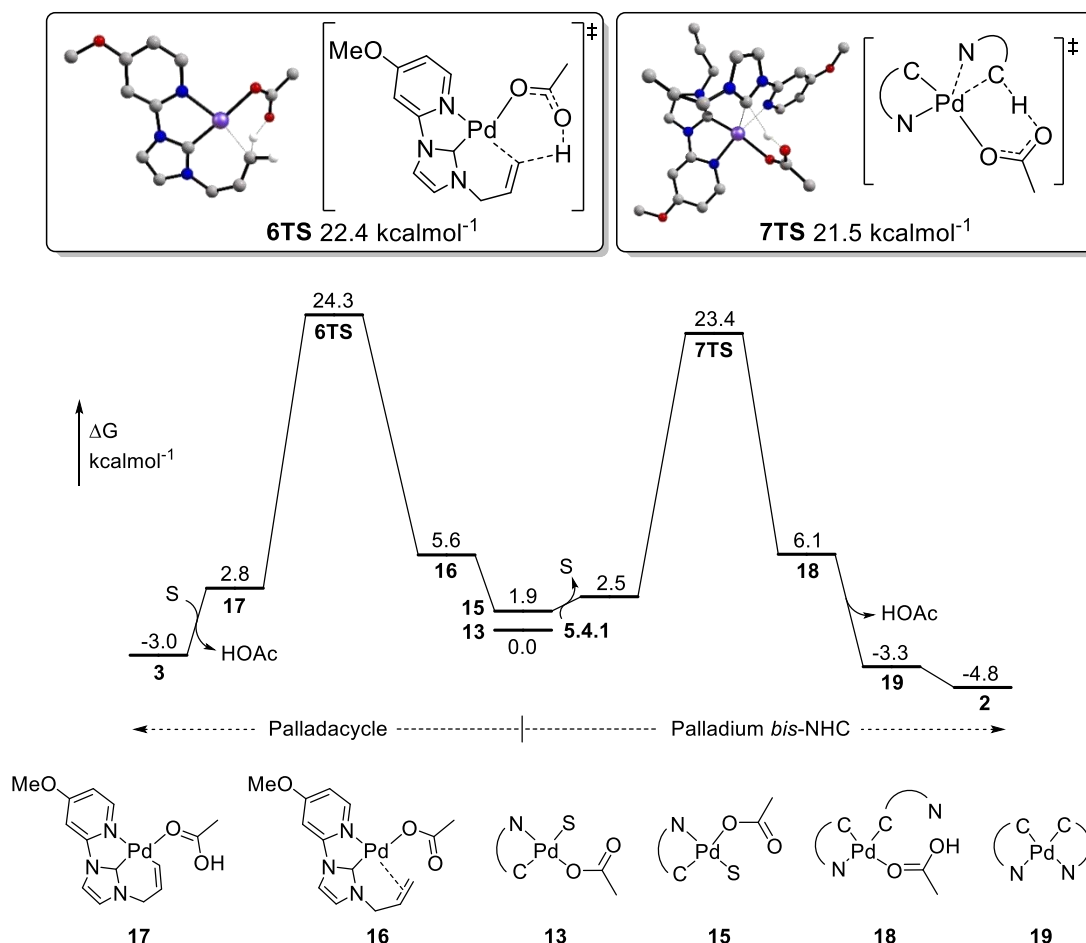
Figure 6.10 Overall free energy profile in MeCN for the formation of both bis-NHC complex 2 and palladacycle 3. ΔG values are calculated in kcalmol⁻¹. All structures are cationic, and include only a simulation of one relevant hydrogen atom, with all others omitted for clarity.

Considering the former, computation suggests that an η^2-alkene association step occurs at palladium to generate **16** through removal of coordinated MeCN (3.7 kcalmol⁻¹). Within this atomic arrangement, it may be possible that π-backbonding from the alkene to the metal centre facilitates the activation of one alkenyl C(sp²)-H bond. The mechanism proceeds through a four-coordinate transition state structure (**6TS**, 22.4 kcalmol⁻¹), creating a 6-membered envelope between palladium, acetate and η^1-alkene to deprotonate a terminal vinyl hydrogen atom and produce **17**, which is further stabilised by 5.8 kcalmol⁻¹ by a coordinating MeCN molecule to produce palladacycle **3** (**6.1**) as the outcome of reaction. Indeed, this prediction of metal-insertion

at the least substituted end of the alkene is consistent with the apparent regiospecificity observed through experiment, and can be rationalised by both a stable 6-membered transition state structure alongside Baldwin's rules for ring-closing reactions.[24,25]

In the case of the latter, a lower activation energy is calculated to reach the most stable transition state *en route* to a palladium(II) *bis*-NHC complex (**7TS**, 21.5 kcalmol^{-1}). Interestingly, this transition structure displays the same unusual five-coordinate trigonal bipyramidal coordination geometry as observed for **1TS**, though no vacant site exists for solvent-assisted stabilisation. Subsequent stepwise displacement of acetic acid from **18** with MeCN ultimately travels through a downhill energy pathway to *bis*-NHC complex **2** (**5.10.1**).

Clear from these calculations, are the remarkably close energetic penalties for each reaction pathway (0.9 kcalmol^{-1} difference in free energy barriers, **6TS** *versus* **7TS**). It is also notable that both routes are not exceedingly exergonic, which is thought to be largely attributed to steric factors, as evidenced by the distorted square planar geometry of each product. These findings are very much level with experimental results, as controlling reaction stoichiometry and order of reagent addition allows selective formation of either product. Disappointingly, these DFT calculations are not able to justify the absence of palladacycle formation under kinetic control when the 4-methoxypyridyl group is substituted for various electronically (de)activating pyridyl donors (*i.e.* those of Chapter 5, including a 4-dimethylaminopyridyl analogue). Supplementary calculations have been performed for these related analogues, which indicate that the free energies of the theorised palladacycle and *bis*-NHC complexes are comparable in every example, as are their respective activation barriers. It is possible that this discrepancy is related to entropic error associated with the calculation. Perhaps more likely, is the presence of a currently unknown reaction condition which is able to 'switch off' cyclometalation in favour of *bis*-NHC complex formation, which can only be speculated at this stage.

According to the model, addition of the first NHC group to palladium (**1TS**, 27.5 kcalmol^{-1}) is calculated to be much slower than addition of the second NHC (**7TS**, 23.4 kcalmol^{-1}), as the particularly stable Pd$_3$(OAc)$_6$ cluster renders the initial step highly energy consuming. The first addition being the rate-determining step is consistent with laboratory findings, as the *mono*-NHC palladium(II) complex (**13** or **15**) is never observed spectroscopically. The computational model also predicts that cyclometalation should be supressed in the absence of MeCN solvent, which plays a vital role to stabilise the transition state. Indeed, this prediction falls in-line with experimental observations; attempts to form **6.1** in THF, DMSO and DMF were unsuccessful.

6.4 Conclusions and future work

Chapter 5 discusses the synthesis of various electronically diverse pyridyl- and picolyl-substituted imidazolium salts, and their subsequent coordination to palladium to produce a family of palladium(II) *bis*-NHC complexes. Included within this scope, is the synthesis of a palladium(II) *bis*-NHC complex comprising a 4-methoxypyridyl wingtip donor group (**5.10.1**). Confined to this single example, was the observation of significant side-product contamination which could be amplified by adjusting reaction stoichiometry. Subsequent separation of this side-product allowed for its characterisation in both the solid- and solution-state, confirming its identity as a unique σ-alkenyl *endo*-palladacycle (**6.1**). To the author's knowledge, no NHC-ligated pincer complexes which house a stable σ-alkenyl palladacyclic motif are known, with the formation of **6.1** also representing a rare example of vinylic $C(sp^2)$-H bond activation at palladium.

Employing density functional theory, attempts were made to rationalise the confinement of cyclometalation to this single example (*i.e.* where the pyridyl substituent = H, 4-Me, 5-NO$_2$ or 4-NMe$_2$, cyclometalation appears shut down). These calculations proved particularly insightful, with especial regards to Pd(OAc)$_2$-mediated deprotonations, which hold a firm position within current methodology to synthesise palladium-NHC complexes and are not well-understood. Along these lines, an unprecedented five-coordinate palladium(II) transition state structure is favoured upon deprotonation of each imidazolium ion in the presence of coordinating solvent, which contests the traditional four-coordinate structure currently hypothesised in the literature. Overall, the model predicts remarkably close free energy barriers for both palladacycle and palladium *bis*-NHC complex formation, with a discrepancy of only 0.9 kcalmol^{-1}. Taking account of each energy-minimised pathway, and the metal/ligand stoichiometry of each product (1:2 in *bis*-NHC complex, 1:1 in palladacycle), simple tuning of reaction conditions allows for selective isolation of either complex – mapping well with computation. However, this theoretical model is not able to provide a satisfactory reason as to why cyclometalation is restricted to ligand precursor **5.4.1** (and its SbF$_6$ analogue). In fact, computation suggests that replacement of 4-methoxypyridyl with its unsubstituted analogue (*i.e.* R = H) should similarly afford a palladacyclic product of a comparable free energy barrier to those disclosed within, implying the 4-OMe group has no effect on cyclometalation.

Future work in this area should look to extend the synthetic methodology to different transition metals. For example, the cyclometalation chemistry of nickel is relatively well-documented, and being a direct group 10 neighbour, would be expected to form similar complexes of NHCs to those of palladium. However, a longstanding goal in this area should be to better understand the conditions of C-H activation, with a view to delineate the apparent 'hidden condition' for cyclometalation of **5.4.1** over all other examples.

6.5 Experimental

Where stated, manipulations were performed under an atmosphere of dry nitrogen by means of standard Schlenk line or glovebox techniques. Anhydrous solvents were prepared by passing the solvent over activated alumina to remove water, copper catalyst to remove oxygen and molecular sieves to remove any remaining water, *via* the Dow-Grubbs solvent system. Deuterated CD_3CN and $CDCl_3$ were dried over CaH_2, cannula filtered or distilled, and then freeze-pump-thaw degassed prior to use.

2-(Imidazole-1-yl)-4-methoxypyridine (**P5.4**) was synthesised according to procedures described in Chapter 5. All other chemicals were obtained from commercial sources and used as received.

6.5.1 Instrumentation

^1H and ^{13}C NMR spectra were recorded by automated procedures on either a Bruker Avance (500/125 MHz) or DPX (300/75 MHz) NMR spectrometer, using the residual solvent as an internal standard. The values of chemical shift are reported in parts per million (ppm) with the multiplicities of the spectra assigned as follows: singlet (s), doublet (d), triplet (t), quartet (q), multiplet (m) and broad (br), values for coupling constants (J) are assigned in Hz. High-resolution electrospray mass spectra (ESI-MS) were measured on an open-access Bruker Daltonics (micro TOF) instrument operating in the electrospray mode. Samples for microanalysis were dried under vacuum prior to analysis and the elemental composition determined by Ms. Tanya Marinko-Covell of the University of Leeds Microanalytical Service using a Carlo Erba elemental analyser MOD 1106 spectrometer. FT-IR spectra were recorded as solid phase samples on a Perkin-Elmer Spectrum One spectrophotometer.

X-ray diffraction data were collected on an Agilent SuperNova diffractometer fitted with an Atlas CCD detector with Mo Kα radiation (λ = 0.7107 Å) or Cu Kα radiation (λ = 1.5418 Å). Crystals were mounted under oil on nylon fibres. Data sets were corrected for absorption using a multiscan method, and the structures were solved by direct methods using SHELXS-97 or SHELXT and refined by full-matrix least squares on F^2 using ShelXL-97, interfaced through the program Olex2.[26] Molecular graphics for all structures were generated using POV-RAY in the X-Seed program.

All density functional theoretical calculations were performed by Dr Alireza Ariafard of the University of Tasmania, Australia. Gaussian 09[27] was used to fully optimise all the structures reported in this chapter at the M06 level of density functional theory (DFT)[28] in MeCN using the CPCM solvation model.[29–31] The effective-core potential of Hay and Wadt with a double-ξ valence basis set (LANL2DZ)[32,33] was chosen to describe Pd. The 6-31G(d) basis set was used for other atoms.[34] A polarisation function was also added for Pd (ξf = 1.472).[35] This basis set

combination will be referred to as BS1. Frequency calculations were carried out at the same level of theory as those for the structural optimisation. Transition structures were located using the Berny algorithm. Intrinsic reaction coordinate (IRC)[36] calculations were used to confirm the connectivity between transition structures and minima. To further refine the energies obtained from the M06/BS1 calculations, we carried out single-point energy calculations for all of the structures with a larger basis set (BS2) in MeCN using the CPCM solvation model at M06 level. To estimate the corresponding Gibbs energies, ΔG, the entropy corrections were calculated at the M06/BS1 level, adjusted by the method proposed by Whitesides *et al.*[21] and finally added to the single-point energies. BS2 utilises the def2-QZVP basis set on all atoms. We have used the Gibbs free energies obtained from the M06/BS2//M06/BS1 calculations in MeCN throughout the chapter unless otherwise stated.

Reaction coordinate files (.xyz) were generated through the program Avogadro and used to produce theoretical molecular graphics by way of the software package, Chemcraft. All raw computational data, including original Cartesian coordinates and total energies for all structures obtained through DFT calculations can be found on the supplementary compact disk.

6.5.2 Preparation of imidazolium salt precursors

Synthesis of 1-allyl-3-(2-(4-methoxy)pyridyl)imidazolium bromide (5.4). 2-(Imidazole-1-yl)-4-methoxypyridine (0.88 g, 5.0 mmol), allyl bromide (2.0 mL, 23 mmol) and acetonitrile (40 mL) were added to a small round-bottomed flask and heated to reflux for 16 hours. After this time, the mixture was cooled to room temperature and the volume of solvent reduced *in vacuo* (to approx. 10 mL). Slow addition of diethyl ether (35 mL) to the stirring acetonitrile solution led to the precipitation of the imidazolium bromide intermediate as an off-white crystalline solid, which was collected by vacuum filtration, washed repeatedly with diethyl ether and dried under vacuum. Yield: 1.24 g, 4.20 mmol, 84 %. ^{1}H NMR (300 MHz, CDCl$_3$) δ (ppm) 11.81 (s, 1H, NC*H*N), 8.29 (s, 1H, im*H*), 8.22 (d, J = 5.8 Hz, 1H, py*H*), 8.19 (d, J = 3.0 Hz, 1H, py*H*), 7.51 (s, 1H, im*H*), 6.90 (dd, J = 5.8, 3.0 Hz, 1H, py*H*), 6.14 (ddt, J = 16.8, 10.1, 6.5 Hz, 1H, C*H*=CH$_2$), 5.66 (d, J = 16.8 Hz, 1H, CH=CH*H*$_{trans}$), 5.55 (d, J = 10.1 Hz, 1H, CH=CH*H*$_{cis}$), 5.14 (d, J = 6.5 Hz, 2H, NC*H*$_2$), 4.10 (s, 3H, OC*H*$_3$). ^{13}C{^{1}H} NMR (75 MHz, CDCl$_3$) δ (ppm) 169.3, 150.0, 147.8, 136.1, 129.7, 123.3, 121.7, 119.4, 113.9, 100.1, 58.0, 52.9. HR-MS (ESI$^+$): *m/z* 216.1161 [C$_{12}$H$_{14}$N$_3$O]$^+$, calcd. [M − Br]$^+$ 216.1131.

Synthesis of 1-allyl-3-(2-(4-methoxy)pyridyl)imidazolium hexafluorophosphate (5.4.1). Imidazolium bromide **5.4** (0.60 g, 2.00 mmol), ammonium hexafluorophosphate (0.98 g, 6.0 mmol) and water (40 mL) were added to a round-bottomed flask and stirred at room temperature for 2 hours. After this time, an off-white crystalline solid had developed which was isolated by vacuum filtration and washed with water (3 × 30 mL) followed by aliquots of cold

diethyl ether (3 × 30 mL) and dried under vacuum. Yield: 0.72 g, 2.00 mmol, quantitative. ^{1}H NMR (300 MHz, CD$_3$CN) δ (ppm) 9.28 (s, 1H, NC*H*N), 8.39 (d, J = 6.0 Hz, 1H, py*H*), 8.10 (br t, J = 1.8 Hz, 1H, im*H*), 7.56 (br t, J = 1.8 Hz, 1H, im*H*), 7.26 (d, J = 2.1 Hz, 1H, py*H*), 7.11 (dd, J = 5.7, 2.1 Hz, 1H, py*H*), 6.16 – 6.02 (ddt, J = 17.7, 12.6, 6.3 Hz, 1H, C*H*=CH$_2$), 5.50 (d, J = 17.7 Hz, 1H, CH=CH*H*$_{trans}$), 5.45 (d, J = 12.6 Hz, 1H, CH=CH*H*$_{cis}$), 4.88 (d, J = 6.3 Hz, 2H, NC*H*$_2$), 3.98 (s, 3H, OC*H*$_3$). ^{13}C{^{1}H} NMR (75 MHz, CD$_3$CN) δ (ppm) 169.7, 151.3, 149.0, 135.4, 131.4, 124.2, 122.5, 120.6, 112.6, 101.4, 57.5, 53.3. HR-MS (ESI$^+$): m/z 216.1149 [C$_{12}$H$_{14}$N$_3$O]$^+$, calcd. [M – PF$_6$]$^+$ 216.1131. Note: employment of the ammonium hexafluoroantimonate salt in place of hexafluorophosphate affords the corresponding imidazolium hexafluoroantimonate salt in quantitative yield, with indistinguishable spectroscopic properties to **5.4.1**. All data are consistent with the literature.[37]

6.5.3   Preparation of palladium(II) *N*-heterocyclic carbene complexes

Synthesis of *bis*[1-allyl-3-(2-(4-methoxy)pyridyl)imidazol-2-ylidene]palladium(II) dihexafluorophosphate (5.10.1). 1-Allyl-3-(4-methoxy)pyridyl imidazolium hexafluorophosphate **5.4.1** (0.25 g, 0.69 mmol) and Pd(OAc)$_2$ (77.7 mg, 0.35 mmol) were charged to a flame-dried ampoule under an inert atmosphere and stirred in anhydrous acetonitrile (20 mL) at 80 ˚C for 48 hours. After this time, the mixture was cooled to room temperature, filtered through a path of Celite and solvents removed *in vacuo* to give a crude yellow residue. The crude product was dissolved in acetone and purified by flash chromatography on SiO$_2$ (saturated acetone solution of NH$_4$PF$_6$ as eluent) to afford a pale yellow residue. Dissolution of the residue in acetonitrile followed by dropwise addition to cold diethyl ether delivered the pure title compound as a pale yellow solid. Yield: 0.32 g, 0.35 mmol, 50 %. Mp decomp. >209 ˚C. ^{1}H NMR (300 MHz, CD$_3$CN) δ (ppm) 7.95 (br d, J = 2.1 Hz, 1H, im*H*), 7.82 (br d, J = 2.1 Hz, 1H, im*H*), 7.77 (br d, J = 16.5 Hz, 2H, py*H*), 7.76 (br d, J = 16.5 Hz, 2H, py*H*), 7.26 (d, J = 2.1 Hz, 1H, im*H*), 7.25 (d, J = 2.1 Hz, 1H, im*H*), 7.19 (d, J = 2.7 Hz, 1H, py*H*), 7.08 (d, J = 2.7 Hz, 1H, py*H*), 6.64 (br m, 2H, C*H*CH$_2$), 5.91 (br d, J = 9.0 Hz, 2H, CH=C*H*$_{cis}$), 5.47 (br dd, J = 9.0, 3.3 Hz, 2H, CH=C*H*$_{trans}$), 4.58 (br d, J = 2.7 Hz, 4H, NC*H*$_2$), 3.47 (br s, 6H, OC*H*$_3$). ^{13}C{^{1}H} NMR (75 MHz, CD$_3$CN) δ (ppm) 170.8, 152.7, 151.1, 151.0, 132.5, 125.4, 121.8, 119.8, 111.5, 101.6, 57.8, 54.6. HR-MS (ESI$^+$): m/z 573.0836 [C$_{24}$H$_{26}$N$_6$O$_2$ClPd]$^+$, calcd. [M – 2PF$_6$ + Cl]$^+$ 573.0836. Anal. calcd. (%) for C$_{24}$H$_{26}$N$_6$O$_2$P$_2$F$_{12}$Pd: C 34.86, H 3.17, N 10.29; found C 34.90, H 3.15, N 10.65.

Synthesis of palladacycle (6.1). To a stirring solution of Pd(OAc)$_2$ (0.25 g, 1.10 mmol, 0.11M) in anhydrous acetonitrile (10 mL) at 80 ˚C was added 1-allyl-3-(4-methoxy)pyridyl imidazolium hexafluorophosphate (**5.4.1**) (0.22 g, 0.60 mmol, 0.03M) in anhydrous acetonitrile (20 mL) dropwise, over a period of 1 hour under an inert atmosphere. The reaction mixture was maintained at 80 ˚C for 24 hours. After this time, cold diethyl ether (40 mL) was added to the mixture in a single portion, upon which a pale yellow solid precipitated from solution which was collected by vacuum filtration. Reprecipitation of the crude solid from acetonitrile (20 mL) with cold diethyl ether (50 mL), followed by repeated washing with cold pentane (3 × 20 mL) delivered the pure cyclometalated compound as an pale yellow solid. Yield: 0.25 g, 0.49 mmol, 82 %. Mp decomp. >284 ˚C. ^{1}H NMR (300 MHz, CD$_3$CN) δ (ppm) 8.27 (d, J = 6.3 Hz, 1H, im*H*), 7.89 (d, J = 2.1 Hz, 1H, py*H*), 7.42 (d, J = 2.1 Hz, 1H, py*H*), 7.23 (d, J = 2.1 Hz, 1H, py*H*), 7.07 (dd, J = 9.3, 6.3 Hz, 1H, im*H*), 6.63 (dt, J = 9.0, 3.9, 1.8 Hz, 1H, CH$_2$CHC*H*$_{cis}$), 6.02 (dt, J = 9.0, 3.9, 1.8 Hz, 1H, CH$_2$C*H*$_{cis}$CH), 5.03 (m, 2H, C*H*$_2$), 4.03 (s, 3H, OC*H*$_3$). ^{13}C{^{1}H} NMR (75 MHz, CD$_3$CN) δ (ppm) 171.1, 155.8, 152.7, 152.5, 126.3, 124.6, 122.7, 118.8, 110.9, 98.6, 58.0, 56.2. HR-MS (ESI$^+$): m/z 320.0016 [C$_{12}$H$_{12}$N$_3$OPd]$^+$, calcd. [M − MeCN − PF$_6$]$^+$ 320.0015. Anal. calcd (%) for C$_{14}$H$_{15}$N$_4$OPF$_6$Pd($^1/_3$C$_5$H$_{12}$): C 35.24, H 3.55, N 10.60; found C 35.50, H 3.20, N 11.00.

1-Allyl-3-(2-(4-methoxy)pyridyl)imidazolium hexafluoroantimonate is converted into its corresponding palladacycle (**6.1.SbF$_6$**) under analogous conditions. Yield: 0.26 g, 0.44 mmol, 74 %. ^{1}H NMR (500 MHz, CD$_3$CN) δ (ppm) 8.26 (d, J = 6.5 Hz, 1H, im*H*), 7.88 (d, J = 2.0 Hz, 1H, py*H*), 7.41 (d, J = 2.0 Hz, 1H, py*H*), 7.29 (d, J = 2.0 Hz, 1H, py*H*), 7.10 (dd, J = 6.5, 2.5 Hz, 1H, im*H*), 6.61 (dt, J = 8.5, 3.5, 1.5 Hz, 1H, CH$_2$CHC*H*$_{cis}$), 6.03 (dt, J = 8.5, 3.5, 1.5 Hz, 1H, CH$_2$C*H*$_{cis}$CH), 5.03 (m, 2H, C*H*$_2$), 4.03 (s, 3H, OC*H*$_3$). ^{13}C{^{1}H} NMR (125 MHz, CD$_3$CN) δ (ppm) 171.0, 155.8, 152.9, 152.5, 126.3, 124.6, 122.8, 118.5, 110.9, 98.6, 58.1, 56.2. HR-MS (ESI$^+$): m/z 320.0024 [C$_{12}$H$_{12}$N$_3$OPd]$^+$, calcd. [M − MeCN − SbF$_6$]$^+$ 320.0015. These data are consistent with those of **6.1**.

6.6 Bibliography

1. J. P. Kleiman, M. Dubeck, *J. Am. Chem. Soc.* **1963**, *85*, 1544–1545.

2. A. C. Cope, R. W. Siekman, *J. Am. Chem. Soc.* **1965**, *87*, 3272–3273.

3. A. C. Cope, E. C. Friedrich, *J. Am. Chem. Soc.* **1968**, *90*, 909–913.

4. W. A. Herrmann, C. Brossmer, K. Öfele, C.-P. Reisinger, T. Priermeier, M. Beller, H. Fischer, *Angew. Chem. Int. Ed. Engl.* **1995**, *34*, 1844–1848.

5. J. L. Serrano, L. García, J. Pérez, E. Pérez, J. García, G. Sánchez, P. Sehnal, S. De Ornellas, T. J. Williams, I. J. S. Fairlamb, *Organometallics* **2011**, *30*, 5095–5109.

6. Y. Ding, Y. Li, Y. Zhang, S. A. Pullarkat, P.-H. Leung, *Eur. J. Inorg. Chem.* **2008**, 1880–1891.

7. G. R. Rosa, D. S. Rosa, *RSC Adv.* **2012**, *2*, 5080–5083.

8. J. F. Cívicos, D. A. Alonso, C. Nájera, *Eur. J. Org. Chem.* **2012**, 3670–3676.

9. G. K. Rao, A. Kumar, S. Kumar, U. B. Dupare, A. K. Singh, *Organometallics* **2013**, *32*, 2452–2458.

10. S. F. Kirsch, L. E. Overman, M. P. Watson, *J. Org. Chem.* **2004**, *69*, 8101–8104.

11. A. J. Cheney, B. L. Shaw, *J. Chem. Soc. Dalton Trans.* **1972**, 860–865.

12. B. L. Shaw, M. M. Truelock, *J. Organomet. Chem.* **1975**, *102*, 517–525.

13. S.-W. Lai, T.-C. Cheung, M. C. W. Chan, K.-K. Cheung, S.-M. Peng, C.-M. Che, *Inorg. Chem.* **2000**, *39*, 255–262.

14. K. J. Keuseman, I. P. Smoliakova, V. V. Dunina, *Organometallics* **2005**, *24*, 4159–4169.

15. B. D. Dangel, K. Godula, S. W. Youn, B. Sezen, D. Sames, *J. Am. Chem. Soc.* **2002**, *124*, 11856–11857.

16. J. Dupont, N. R. Basso, M. R. Meneghetti, R. A. Konrath, R. Burrow, M. Horner, *Organometallics* **1997**, *16*, 2386–2391.

17. O. Navarro, R. A. Kelly, S. P. Nolan, *J. Am. Chem. Soc.* **2003**, *125*, 16194–16195.

18. S. Gründemann, M. Albrecht, J. A. Loch, J. W. Faller, R. H. Crabtree, *Organometallics* **2001**, *20*, 5485–5488.

19. B. R. M. Lake, M. R. Chapman, C. E. Willans, *RSC Organomet. Chem.* **2015**, *40*, 107–139.

20. D. D. Perrin, B. Dempsey, E. P. Serjeant, *pK$_a$ Prediction for Organic Acids and Bases*, Springer, Netherlands, Dordrecht, **1981**, 1st edition.

21. Y. Okuno, *Chem. Eur. J.* **1997**, *3*, 212–218.

22. G.-J. Cheng, Y.-F. Yang, P. Liu, P. Chen, T.-Y. Sun, G. Li, X. Zhang, K. N. Houk, J.-Q. Yu, Y.-D. Wu, *J. Am. Chem. Soc.* **2014**, *136*, 894–897.

23. M. Anand, R. B. Sunoj, H. F. Schaefer, *J. Am. Chem. Soc.* **2014**, *136*, 5535–5538.

24. I. V. Alabugin, K. Gilmore, *Chem. Commun.* **2013**, *49*, 11246–11250.

25. K. Gilmore, I. V. Alabugin, *Chem. Rev.* **2011**, *111*, 6513–6556.

26. H. Puschmann, O. V. Dolomanov, L. J. Bourhis, R. J. Gildea, J. A. K. Howard, *J. Appl. Crystallogr.* **2009**, *42*, 339–341.

27. M. J. Frisch, G. W. Trucks, H. B. Schlegel, G. E. Scuseria, M. A. Robb, J. R. Cheeseman, G. Scalmani, V. Barone, B. Mennucci, G. A. Petersson, H. Nakatsuji, M. Caricato, X. Li, H. P. Hratchian, A. F. Izmaylov, J. Bloino, G. Zheng, J. L. Sonnenberg, M. Hada, M. Ehara, K. Toyota, R. Fukuda, J. Hasegawa, M. Ishida, T. Nakajima, Y. Honda, O. Kitao, H. Nakai, T. Vreven, Jr, J. E. Peralta, F. Ogliaro, M. Bearpark, J. J. Heyd, E. Brothers, K. N. Kudin, V. N. Staroverov, R. Kobayashi, J. Normand, K. Raghavachari, A. Rendell, J. C. Burant, S. S. Iyengar, J. Tomasi, M. Cossi, N. Rega, J. M. Millam, M. Klene, J. E. Knox, J. B. Cross, V. Bakken, C. Adamo, J. Jaramillo, R. Gomperts, R. E. Stratmann, O. Yazyev, A. J. Austin, R. Cammi, C. Pomelli, J. W. Ochterski, R. L Martin, K. Morokuma, V. G. Zakrzewski, G. A. Voth, P. Salvador, J. J. Dannenberg, S. Dapprich, A. D. Daniels, O. Farkas, J. B. Foresman, J. V. Ortiz, J. Cioslowski, D. J. Fox, *Gaussian 09 Revision* A.02, Gaussian Inc. Wallingford CT **2009**.

28. Y. Zhao, D. G. Truhlar, *Acc. Chem. Res.* **2008**, *41*, 157–167.

29. A. D. Becke, *J. Chem. Phys.* **1993**, *98*, 5648–5652.

30. B. Miehlich, A. Savin, H. Stoll, H. Preuss, *Chem. Phys. Lett.* **1989**, *157*, 200–206.

31. C. Lee, W. Yang, R. G. Parr, *Phys. Rev. B* **1988**, *37*, 785–789.

32. P. J. Hay, W. R. Wadt, *J. Chem. Phys.* **1985**, *82*, 270–283.

33. W. R. Wadt, P. J. Hay, *J. Chem. Phys.* **1985**, *82*, 284–298.

34. P. C. Hariharan, J. A. Pople, *Theor. Chim. Acta* **1973**, *28*, 213–222.

35. A. W. Ehlers, M. Böhme, S. Dapprich, A. Gobbi, A. Höllwarth, V. Jonas, K. F. Köhler, R. Stegmann, A. Veldkamp, G. Frenking, *Chem. Phys. Lett.* **1993**, *208*, 111–114.

36. K. Fukui, *Acc. Chem. Res.* **1981**, *14*, 363–368.

37. B. R. M. Lake, C. E. Willans, *Chem. Eur. J.* **2013**, *19*, 16780–16790.